Sediment Transport in European Estuarine Environments

Proceedings of the STRAEE Workshop

Guest Editors: Paolo Ciavola and Mike Collins

Special Issue 41

Journal of Coastal Research

JOURNAL OF COASTAL RESEARCH

An international Forum for the Littoral Sciences

SPECIAL ISSUE NO. 41 **WINTER 2004**

Sediment Transport in European Estuarine Environments

Proceedings of the STRAEE Workshop

Guest Editors: Paolo Ciavola and Mike Collins

Special Issue 41

Ferrara, Italy

December 2004

ISSN 0749-0208

Cover Photo by P. Ciavola (Saltmarsh in the Thames Estuary, UK)

Finito di stampare nel mese di dicembre 2004
Printed in Bologna (Italy) in December 2004
Industrie Grafiche Labanti e Nanni

Journal of Coastal Research

SPECIAL ISSUE NO. 41 WINTER 2004

CONTENTS

PREFACE TO THE VOLUME

Historically, estuaries have been the focal point of extensive industrial activity for maritime nations. Similarly, it is well established that such marginal marine environments are particularly sensitive to both long- and short-term external factors. In particular, estuaries are subject to diverse anthropogenic influences, such as: maritime transport (port construction, navigational dredging and dumping, maritime traffic congestion), industrial development (both onshore and offshore), mineral and aggregate extraction, changes in hinterland agricultural practices, residential development and increased water- and sediment-based pollution. In future, these areas will be placed under enhanced environmental pressure.

All of the activities outlined will place this inherently unstable environment under excessive strain in terms of coastline evolution, intertidal saltmarsh development, and sediment contamination. In addition, superimposed upon these anthropogenic factors are the systems response to more globally-driven changes i.e. sea level rise. As the need for a coordinated and responsible approach to the effective management of these morphological systems becomes apparent, as seen by the development of national and international legislation for estuarine management plans, an improved understanding of the physical dynamics of these systems becomes imperative. Within this context, modern sediment processes require investigation whilst, at the same time, the development of the adjacent coastline should be established. Investigation of these data sets, representing different time-scales, will provide the essential scientific background to management decisions.

The research described in this Special Issue address these problems, through the application of a wide range of approaches (sedimentological, geological, physical and engineering-based); these, in turn, lead to an overall interdisciplinary investigation of estuaries. The research undertaken has involved the deployment of instrumentation at a number of differing localities within various estuaries, measuring processes using both established and newly-developed (state-of-the-art) techniques. Such measurements have been extended, within an historical and recent geological time-scale, to develop a conceptual understanding of the evolution of the estuarine systems. At the same time, interpretation of the interdisciplinary data sets has been placed within the context of coastal engineering and management.

Estuarine environments form a significant part of the tidally-influenced coastlines of Europe. Sedimentological research undertaken in such environments has been either specialised and/or not in any great detail – in terms of processes. An interdisciplinary approach is required, based upon established and innovative research methods.

The specific research objectives of the SWAMIEE (Sediment and Water Movement in Industrialised Estuarine Environments) TMR Network (EU Contract No ERBFMRX-CT97-0111) were as follows:

i. to further the scientific understanding, at specific industrialised and non-industrialised locations, of the movement of water and sediment, at a variety of time scales, through an integrated programme of established and innovative field and laboratory work;

ii. to integrate the various data sets (geological, geomorphological, physicochemical and sedimentological) into predictive (forecasting-hindcasting) numerical models, for use in the establishment of regional patterns of water and sediment movement and their sensitivity to changes in the controlling mechanisms;

iii. to transfer experience and expertise between European research groups working in different research disciplines and to foster the development of an applied approach to those concerned with environmental problems;

iv. to disseminate the results of the research to various end-users of estuarine environments.

The participants in SWAMIEE included: University of Southampton, U.K. (Co-ordinator); Université de Bordeaux I, France; Centre National de la Recherche Scientifique (ER 109 – Laboratoire de Géologie, Rouen),

France; Universidade do Algarve, Portugal; Universitá di Ferrara, Italy; University College Dublin, Ireland; University of Plymouth, U.K.; University of Oxford, U.K.; and Danish Hydraulic Institute, Denmark.

Within the context of a Work Plan, various research themes were established (including Key and Associated Participants): long-term estuarine evolution, incorporating the analysis of historical and existing data sets, together with the sedimentological and geochemical analysis of cores from marginal environments, to establish the long-term (10-100 year time-scale) evolution and impact of industrialisation; medium-term estuarine evolution, incorporating analysis of high-resolution morphological data sets (annual to decadal time-scales) and *in situ* measurements of patterns of sediment movement – with emphasis placed on the development of estuary mouth mud/sand banks; estuary bed process studies, incorporating dynamic processes at the sediment-water interface and the quantification of material exchange through an estuary, using high-frequency *in-situ* measurements and laboratory-based flume experiments (with emphasis placed upon fine-grained sediments); and the development of 3D models for fine-grained sediment transport in estuarine environments – similarly, the use of predictive models for medium and coarse-grained sedimentary environments, under variable boundary conditions. Within the context of the research themes, different emphasis was placed upon the fieldwork measurements (water column, water column – sea bed interface, and sea bed) for non-cohesive and cohesive sediments.

A series of European estuaries were selected for investigation, including: the Loire, Seine and Gironde, France; Teignmouth, U.K.; Venice Lagoon, Italy; and Guadiana, Portugal. Interdisciplinary research cruises (SWAMGIR1 and SWAMGIR2) were organised to investigate upstream and downstream hydrodynamics and sediment dynamics in the Gironde estuary.

Water/sediment interface studies required detailed information on nearbed flow structure and its effect on the entrainment and subsequent movement of sedimentary material. Taking into account the nature of turbulent flow in the benthic boundary layer, high frequency measurements of both the velocity structure and SPM concentration have been performed in-situ by the SWAMIEE partners in the Gironde Estuary. Specialised in-situ devices such as INSEV (In Situ SEttling Velocity instrument), were also used to obtain an improved understanding of the influence of particular environmental parameters (such as biological stabilisation/destabilisation, formation of aggregates, etc.) on the resuspension mechanisms. Finally, The SWAMIEE project has integrated field observation into numerical modelling, using a standard commercial 2-d model (Mike 21-DHI).

The ultimate objective of estuarine researchers is to identify the processes and predict the evolution of these environments at different temporal scales. In industrialised estuaries, the anthropogenic impact is such that the natural processes have been contaminated by considerable “noise”. Therefore, there is a need for establishing a “base-line” which is the natural evolution of these environments. Certain stratigraphic and geochemical methods can provide valuable information on sedimentary patterns. In SWAMIEE, radionuclide dating was used to identify horizons related to specific exceptional events in Venice and to study sedimentation patterns in the Gironde.

The STRAEE workshop was born as the final product of the SWAMIEE Project and took place in Ferrara during September 2002. The STRAEE workshop has provided an overview on aspects of estuarine research, taking advantage of the participation of young scientists from several parts of Europe and Australia. The enlargement of the audience outside of the SWAMIEE group has offered the possibility to debate the results, strengthen existing research links and create new ones. Last but not least, some attention was given to the management of estuarine areas, with the contribution of coastal managers charged with the management of the Lagoon of Venice. This site is peculiar for the Mediterranean area because of its tidal regime, but it concentrates a whole range of issues (historical monuments, conservation interests, navigation, industrial sites, tourism) which are common to many parts of the world. A fieldtrip was run in the lagoon to address the main environmental aspects of this site and the measures undertaken by local authorities to counteract pollution, saltmarsh erosion and Relative Sea Level Rise.

This special issue includes a series of publications which represent the research activities outlined above and similar investigations throughout the world. As one may expect, the main contribution comes from the Gironde Estuary, with four papers describing studies on flocculation through laboratory and field measurements (Manning; Gratiot and Manning; Manning *et al.*) and two papers on large scale sediment dynamics (Kapsimalis *et al.*). Of specialist's interest is the application of radionuclides as a tracer of water movement (Smith *et al.*) and the study of estuarine beaches (Gonzales *et al.*). A consistent contribution is presented by Lobo *et al.* on bedload transport at the second field site, the Guadiana Estuary at the border between Portugal and Spain. The flocculation issue is also examined by Mikes *et al.* after their field experiments in the Seine Estuary, in France.

The contributions from the other estuaries were varied. Large-scale and long-term perspectives are provided by the papers of Burningham and Cooper (Ireland). Lower energy environments were studied by Mitchell *et al.* in a macrotidal context (English Channel) and by Covelli *et al.* in the microtidal northern Adriatic Sea. Malvarez *et al.* manage to apply classic beach morphodynamic theories to sandy tidal flats inside an Irish lough. Finally, modelling is used by Lumborg in the Danish Wadden Sea while Schacht and Lemckert propose a new methodology for measuring suspended sediment characteristics.

Unfortunately not all the contributions presented at the workshop in Ferrara were selected for publication. Unlike other conference Special Issues, this volume has undergone a strict selection and refereeing process, employing scientists for all over the world, with many members of the JCR Editorial Board. We hope that all the contributions that were refused may benefit from the referees' comments and be published elsewhere.

A project like SWAMIEE involves a great deal of administration and the hard work of Justin Dix is greatly acknowledged. He has gone through a huge amount of paper work and science planning trying to keep together such an heterogeneous group that would manage to use during meetings most of the languages spoken in the European Union.

Instrument deployment, sample collection and surveying requires a capable Captain and crew onboard. Operations in the Gironde were successful thanks to the Captain and crew of the Cote d'Aquitaine.

A main contribution to the organisation of the STRAEE workshop in Ferrara was that of Corinne Corbau, a former project's post-doc. She helped in preparing all the divulgation material and in starting the process of paper submission. Unfortunately she was not able to complete the editorial job due to new work commitments, but she fully deserves the title of "Editorial Assistant".

Finally, we are grateful to the Consorzio Venezia Nuova for sponsoring the fieldtrip in the Lagoon of Venice at the end of the final workshop.

Paolo Ciavola
Michael Collins

Ferrara, December, 2004

Journal of Coastal Research	SI 41	1-11	STRAEE 2002	Ferrara, Italy	ISSN 0749-0208

Tidal impact on modern sedimentary facies in the Gironde Estuary, southwestern France

V. Kapsimalis†, L. Massé‡ and J.P. Tastet‡

† Institute of Oceanography, Hellenic Centre for Marine Research, P.O. Box 712, 190 13 Anavyssos, Attica, Greece
Email: kapsim@ncmr.gr

‡ Département de Géologie et Océanographie, UMR CNRS 5805, Université de Bordeaux- 1, 33405 Talence cedex, France

ABSTRACT

KAPSIMALIS, V.; MASSÉ, L. and TASTET, J.P., 2004. Tidal impact on modern sedimentary facies in the Gironde Estuary, southwestern France. *Journal of Coastal Research*, SI 41, 1-11. Ferrara (Italy), ISSN 0749-0208

Surficial sediment distribution patterns within the Gironde Estuary are investigated, through the grain size and statistical analysis of 642 surface samples. Sub-surface tidal facies are determined in 73 sediment cores, from various estuarine sub-environments (using radiographic methods). The study of the surficial sediments shows that the bed is composed of sediments derived from two different sources: (a) the adjacent Atlantic coasts and shore zone; and (b) the Garonne and Dordogne Rivers. The texture varies from gravel to mud and the nature of the sedimentary material is mainly terrigenous, with some biogenic debris; this is especially characteristic of the marine-dominated part of the estuary and over the mudflats. The surficial sediment distribution reveals a downstream decrease in grain size, up to the lower part of the mid-estuary; this is followed by a seaward increase. Comparison between the distribution of the present-day estuarine deposits and those described by Allen (1972) shows marked differences over the upper parts of the estuary; these are considered to be caused by natural processes and human interferences. The sub-surface sedimentary facies of the inner estuary mouth consist of clean sand, with scattered gravel and shell fragments. The intertidal facies contain laminated mud and decayed organic debris. In the mid-estuary, fluid mud with abundant coarse silt laminae and clay drapes are the dominant subtidal facies. Within the associated intertidal flats, structureless muds include peat lenses and layers. Upstream from the confluence point of the Garonne and Dordogne Rivers, the deposits lose gradually their typical tidally-induced features, until the uppermost limit of the estuary.

ADDITIONAL INDEX WORDS: *Macrotidal estuary, geomorphology, sedimentation, subenvironments, facies.*

INTRODUCTION

Estuaries have been the subject of intense and multidisciplinary investigations during past decades. From a sedimentological perspective, present-day estuaries are ephemeral environments acting as highly effective sediment traps (MEADE, 1972; BIGGS and HOWELL, 1984; and NICHOLS and BIGGS, 1985).

The interplay between marine and fluvial processes and the residual sediment transport patterns determine, to a large extent, the morphology and the distribution of sedimentary facies in estuaries. Any modification to the hydrological regime (tide, wave and river discharge), or sediment supply, affects the estuarine evolution and alters the previously-achieved equilibrium in the system (JOUANNEAU and LATOUCHE, 1981).

The last fall in sea level, during the late Pleistocene (ca. 18,000 years Before Present (B.P.)), resulted in the formation of deeply-incised fluvial valleys, which converted subsequently into estuaries during sea level rise. Since the post-Holocene stillstand, at about 6,000 yr B.P., most estuaries have been filled with sediments derived both from fluvial and marine sources (KNEBEL et al., 1988; ALLEN and POSAMENTIER, 1993; and DALRYMPLE and ZAITLIN, 1994).

The objective of this paper is to identify the present-day sediment distribution patterns, together with the tidal imprints, in the subsurface sediments of the Gironde estuary. Furthermore, comparison of the new data set with that presented by ALLEN (1972) aims to provide information on changes which have taken place in the sediment transport and accumulation mechanisms, over the last 30 years.

The studied site

The Gironde Estuary is the marine-influenced part of the hydrological system that drains the Aquitaine Basin, in southwestern France. The geomorphological pattern of the estuary reveals a well-developed tripartite, longitudinal zonation (ALLEN, 1991): (a) a deep tidal inlet with barriers, shoals and moving spits; (b) a funnel-shaped central basin with tidal channels, braided bars and islands; and (c) the upper riverine channels, with point bars (Figure 1). The estuary decreases in width to landward, from a maximum of 11 km near its mouth to less than 3 km at the confluence of the Garonne and Dordonge rivers, some 80 km upstream.

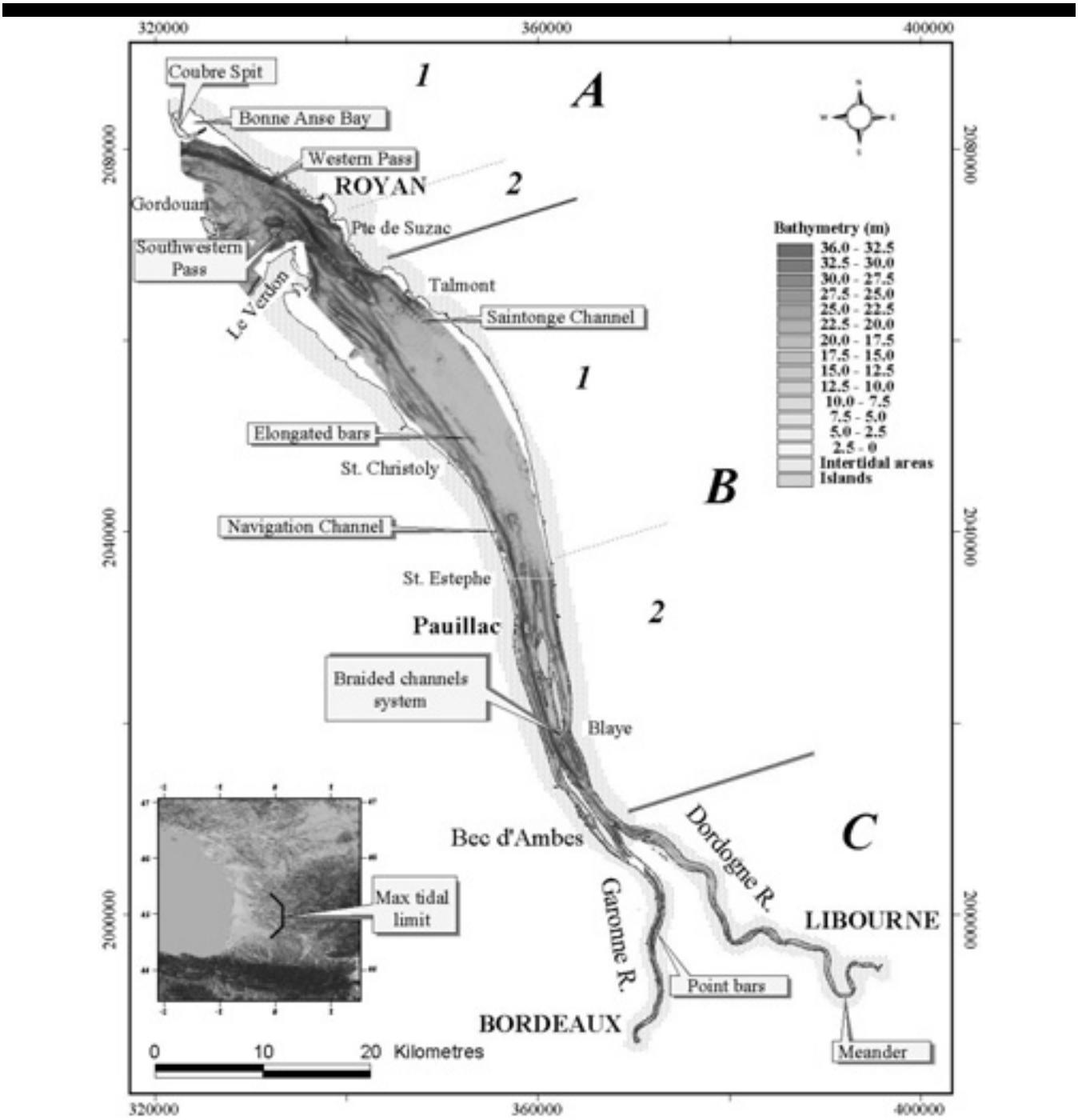

Figure 1. Digitised map of the Gironde estuary, based upon 10 bathymetric maps (scale 1:20,000), published between 1995 and 1998, obtained from the Port Autonome de Bordeaux (P.A.B.). The projection system used is the Lambert (Zone 2, ellipsoid Clark 1880), as applied more generally in France. The coordinates are in metres, whilst the zero level is the lowest spring tide, as defined by the P.A.B. Three distinct geomorphological areas can be detected: the inlet (A), which is separated into outer (A1) and inner (A2) sections; the mid-estuary (B), which is separated into the downstream (B1) and upstream (B2) sections; and the riverine estuary (C). The uppermost end of the estuary coincides with the maximum limit of the tidal influence, which is located some 20 km upstream from Bordeaux (see inset)

The estuary is characterised by a macrotidal regime, with semidiurnal tides; their amplitude ranges from 2.5 m during neap tides to > 5.5 m during spring tides, near Le Verdon (Figure 1). The tidal wave is deformed by friction and becomes asymmetrical, as it propagates landward into the upper estuary (CASTAING and ALLEN, 1981).

The average freshwater discharge into the estuary ranges between 500 and 1,000 m^3/sec. During low river flow, the estuary

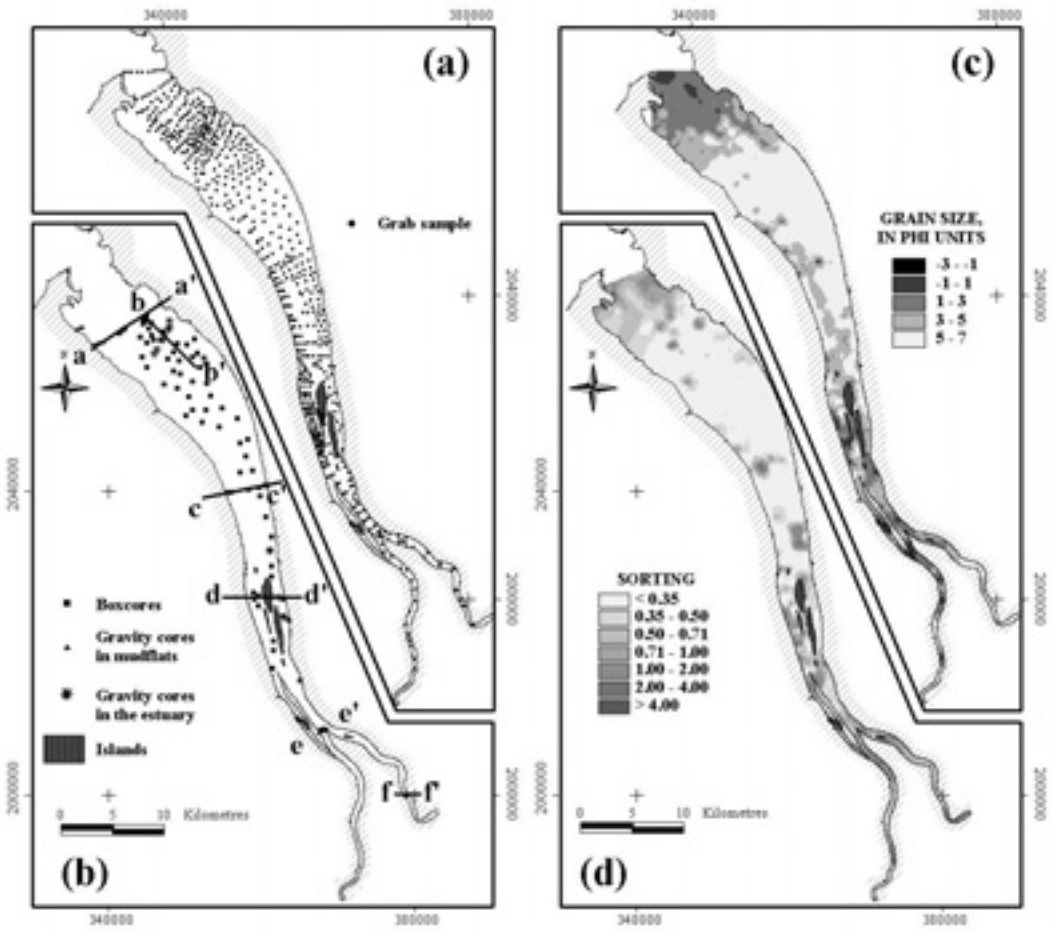

Figure 2. Location maps showing the sampling positions of the surficial sediment (a) and cores (b) as well as the bathymetric cross sections presented in Figures 6, 7 and 8. Likewise, sedimentary maps, showing the distribution of the mean grain size (c) and sorting (d) on the bed of the Gironde Estuary.

is well mixed and the tidal currents can be detected some 130 km upstream from the mouth. In comparison, the salinity intrusion extends 100-115 km upstream. In contrast, during river floods, the estuary is stratified, with the brackish water being restricted within the mid-estuarine funnel and up to a distance of 40 – 50 km from the inlet (ALLEN, 1991).

The bed of the estuary is supplied by two main sediment sources: the Garonne and Dordogne rivers; and the adjacent oceanic beaches and shore zone. All the fluvial sand transported as bedload remains within the estuary, as indicated by its absence within the inlet (CASTAING and ALLEN, 1981). However, a large volume of the fluvial suspended matter escapes out of the inlet, during the ebb tide; then it is deposited on the Aquitaine shelf (CASTAING, 1989; WEBER et al., 1991). To seaward, in response to coastal erosion, coarse-grained sediment is produced from Pleistocene alluvial outcrops; this is transported into the estuary inlet, by littoral drift and tidal currents. These reworked marine sand and gravel deposits penetrate into the mouth, approximately 20 km landward; they are molded into wide-scale bedforms (ALLEN and POSAMENTIER, 1993). The maximum thickness of this landward-thinning wedge is likely to be up to 25 m, including various sedimentary structures, such as parallel bedding, bi-directional cross-stratification and erosion surfaces. The sandy wedge is separated from the underlying tidal-estuarine sediments by a tidal ravinement surface (ALLEN and POSAMENTIER, 1994). Fluvial sand and mud accounts for about the 80 % of the total sediment input to the estuarine system (JOUANNEAU and LATOUCHE, 1981), whilst marine sand constitutes the remaining 20 % (HOWA, 1987).

As the Gironde is one of the largest estuaries in Europe and is of high economical importance, a large number of studies have been undertaken during the past 70 years. Of these, one of the most important early sedimentological studies was the description of the estuarine turbidity maximum, by GLANGEAUD and BONNICHON (1939). Further, the sedimentary patterns and facies have been investigated by a number of scientists, e.g. ALLEN (1972), CASTAING (1981), ALLEN (1991) and MALLET (1998). The internal stratigraphy of the estuary valley fill has been described by ALLEN and TRUILHE (1988), ALLEN and POSAMENTIER (1993, 1994) and LERICOLAIS et al. (2001).

METHODS

Sediment distribution patterns and facies characteristics of the Gironde Estuary were investigated, in this study, using 642 surficial samples, 61 box cores, 10 gravity cores and 8 cores from the intertidal flat area (Figure 2). The fieldwork was carried out during the GIROSED (May – June 1998) and SWAMGIR-1 (June

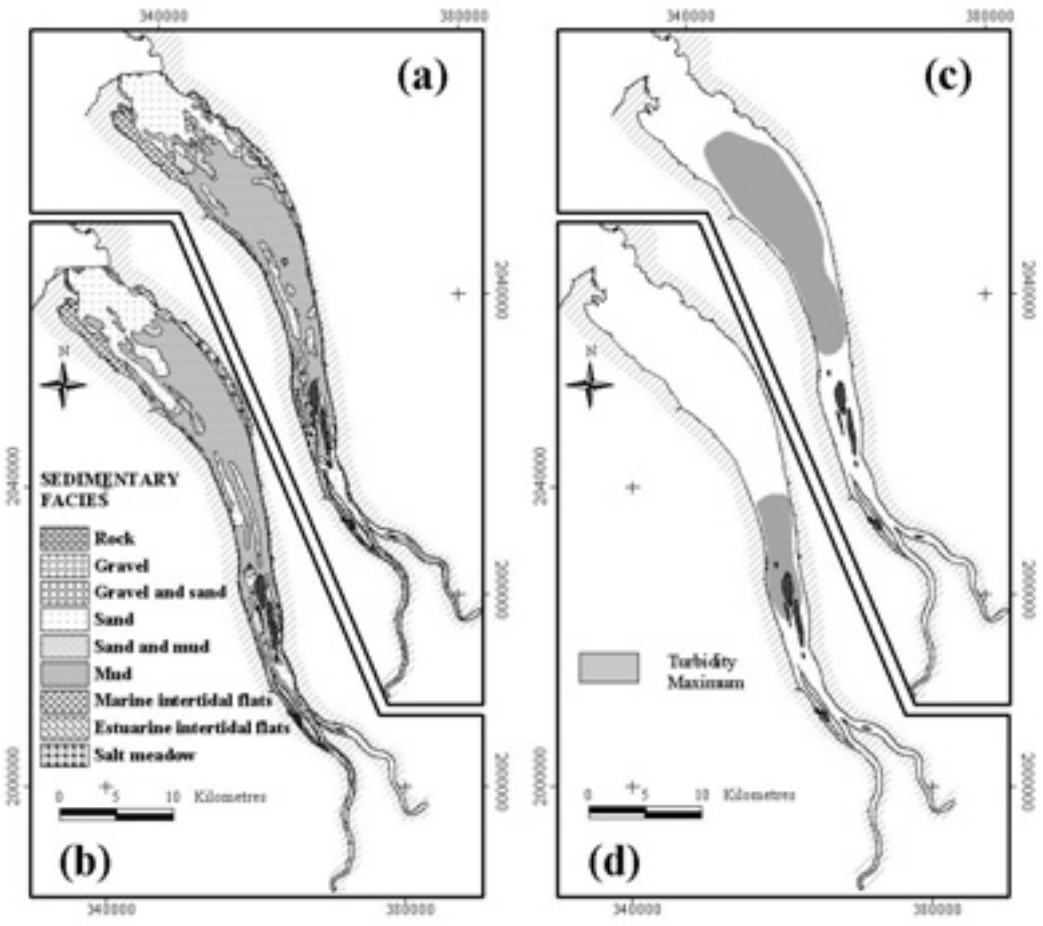

Figure 3. Surface sediment distribution patterns of the Gironde Estuary during Spring 1998 (a), and in the 1960's (after ALLEN, 1972) (b). Location of the turbidity maximum in May 1998 (c) and June 1998 (d) (for details, see text).

1999) surveys, with locations established using a Differential Global Positioning System.

Grain-size analysis was carried out in the laboratories of the University Bordeaux I, using: sieving for the coarse fractions (gravel and sand); and a Malvern 3600E laser-scattering particle size analyzer for the silt and clay (mud) fractions. Based upon these results, the mean size, sorting, skewness, porosity and density were calculated, according to moment procedures for grain-size statistics. Data were processed with the ArcView GIS and digitised maps were created (Figure 2).

In order to identify alterations in the surficial sedimentary facies during the last 30 years, the sedimentological map published by ALLEN (1972) was digitized and compared with the new version (Figure 3), where observations on displacement of the turbidity maximum are also shown (see below).

The classification of the sedimentary facies used (Figure 3) was that defined by ALLEN (1972) and is the same for both of the maps shown: mud, when the silt and clay content is more than 80%; sand and mud, when the sand fraction exceeds 20% and the finer material ranges between 20% and 80%; sand, when the sand exceeds 80%; gravel and sand, when both coarse-grained fractions vary between 20% and 80%; gravel and mud when these fractions are not lower than 20%; and gravel, when the gravel fraction is more than 80%. The map of ALLEN was created on the basis of numerous samples collected between 1960 and 1969, under differing hydrodynamic conditions. Although this approach does not incorporate seasonal variability within the system, it provides an adequate outline of the distribution of the surficial sediments during the 1960's. In contrast, the new map is taken to be more representative of a period of high river flow and spring tides, since sampling was accomplished during these specific conditions. The comparison between the two maps provides an indication of textural changes in the sedimentary bed of the estuary.

All the cores were opened, logged visually and photographed at the University of Bordeaux I. Sections were removed for radiographic analysis, for the identification of lithological characteristics and sedimentary structures, using the SCOPIX (a new digital X-ray imaging system for core analysis (MIGEON *et al*., 1999)).

RESULTS AND DISCUSSION

Hydrodynamic Regime

The GIROSED survey (21 May – 12 June 1998) was undertaken during equinox spring tides. The tidal range at the mouth of the estuary varied between 4.2 m (23th May) and 5.2 m (12th June). The upstream deformation of the tidal curves, caused

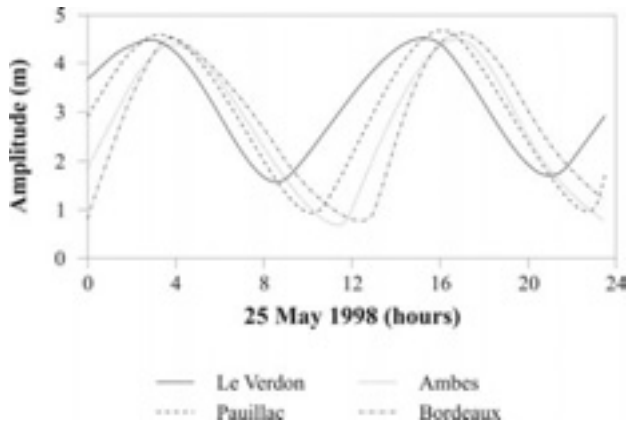

Figure 4. Tidal curves observed for 25th May 1998, showing their asymmetric deformation towards the inner part of the system (for tide gauge locations, see Figure 1). Data obtained from the P.A.B.

by the narrowing of the estuary, resulted in higher tidal amplitudes and a shorter lasting flood tide (Figure 4), in the riverine part of the estuary (C, in Figure 1). This tidal asymmetry increases the peak flood current velocity on the ebb, inducing increased sediment resuspension and landward transport during the flood tide, than during the ebb (CASTAING and ALLEN, 1981).

Variations in the freshwater discharge within the Gironde Estuary, for the first half of 1998, are illustrated in Figure 5. The Garonne River supplies 70% of the total freshwater volume of the estuary, whilst the Dordogne River provides the remaining (30%). Within the estuary, the maximum discharge reached was 3243 m^3/sec, whilst the minimum was 304 m^3/sec; the mean value was 1237 m^3/sec. The survey period (21 May – 12 June) was characterized by high river flows, but with a decreasing trend. Extreme values were recorded on 25th May (maximum) and 12th June (minimum), whilst the average value for this 23-day period was 1433 m^3/sec.

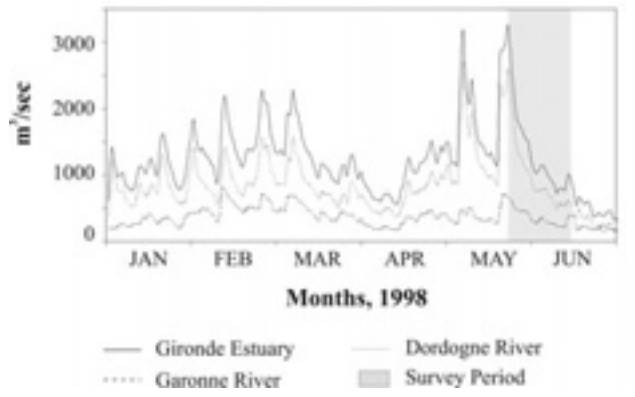

Figure 5. Freshwater discharges of the Gironde Estuary, the Garonne River and the Dordogne River, during the first half of 1998. The shaded section indicates the survey' period, over which a significant decrease in the river flow occured.

Interaction between tidally- and density-induced processes is the fundamental factor controlling the accumulation of suspended sediments in macrotidal estuaries (ALLEN *et al*., 1980). During high river flows, the density circulation becomes the main process; stratification occurs in the water column, and the turbidity maximum is located in the upper parts of the estuary. In contrast, when the river flow is low, tidal processes play the most important role; a well-mixed hydrological regime is established in the estuary, and the turbidity maximum migrates to seaward (CASTAING and ALLEN, 1981).

The displacements of the maximum turbidity zone, in May and June 1998, were established on the basis of plotting all the fluid mud samples ("crème de vase") collected from the estuary bed, in accordance with their sampling date. The resulting maps are illustrated in Figure 3. The data show an upstream shift in the turbidity maximum, caused by the significant reduction in the river discharge and the strengthening of the tides (see above). ALLEN (1972) has presented previously the seasonal locations of the turbidity maximum; these coincide with those identified within the present study.

Sedimentary Facies Distribution Patterns

The uppermost estuary inlet

The inner mouth is the outermost portion of the estuary funnel (A1, in Figure 1), which is affected by oceanic processes. The main morphological feature of this area is the ebb-dominated central channel, with a maximum depth of 35 m. At the upward limit of the inlet, the deep tidal channel shallows and is separated into two individual channels: the Médoc or Navigation Channel, in the west; and the Saintonge Channel, in the east. Over this section, the intertidal areas extend broadly, reaching a maximum width of 1.2 km along the western bank.

The sediments over this area are mainly coarse-grained in texture (Figure 2). The mean grain size decreases towards the inner estuary, from a maximum of 4 mm (–2 Φ) in the central channel, near Pointe de Suzac, to 0.125 mm (+3 Φ) about 20 km upstream. Poorly-sorted gravel and coarse sand cover the deep central channel, the eastern flank of the Banc des Marguerites, and the Saintonge Channel, near Meschers. The shallower areas are dominated by fine–medium sand with shell debris, whilst the bed of the Médoc Channel consists of moderately–well sorted fine sand. Such marine sediments enter the inner inlet during flood tides or storms; then create a 'tongue-like' sandy body, extending up to the maximum limit of wave action. Mud deposition is restricted to the shallow channels located amongst the elongated banks, on the western side of the estuary.

Over the intertidal flat of Le Verdon, fine sand and silt are the dominant grain-size fractions; their mean grain size shows an inland-fining trend, caused by the gradual weakening of the hydrodynamic processes. Biogenic debris is abundant throughout all these samples, whilst the organic matter (plant litter and roots) increases in an onshore direction.

On the basis of a comparison undertaken between the recently established sedimentological map, with that of ALLEN (1972), it is evident that the texture and distribution of the surficial sediments have not changed significantly over the past 30 years (Figure 3). Thus, within the inner inlet, sediment supply and hydrodynamic conditions appear to be relatively unaltered.

The sub-surface sedimentary facies in the upstream estuary inlet can be classified into two groups: (a) the subtidal facies: and (b) the intertidal flat facies.

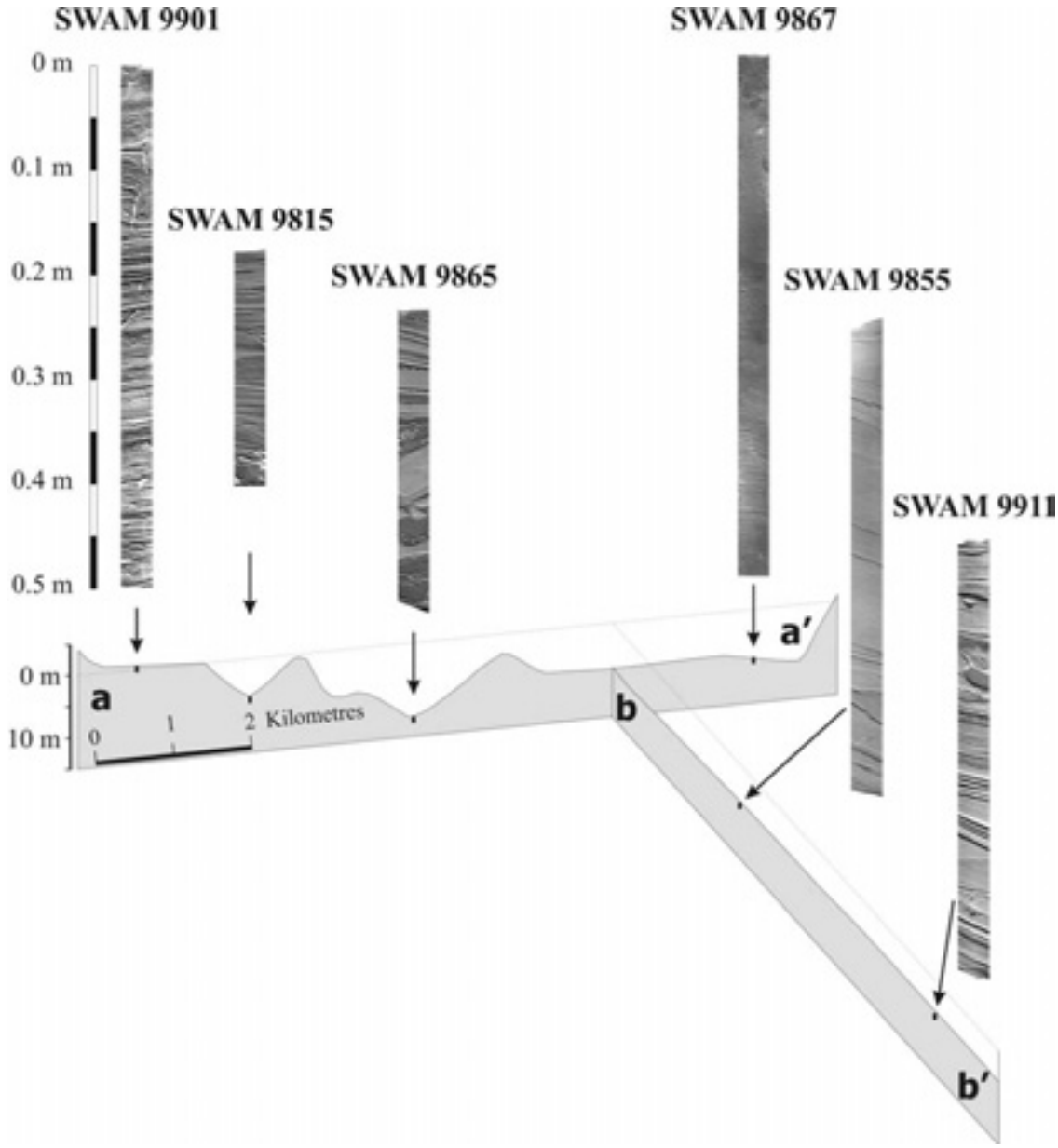

Figure 6. Core radiographs showing the distribution of the sub-surface sedimentary facies along the bathymetric cross-sections a–a′ and b–b′, in the lower estuary funnel (for locations, see Figure 2). Core SWAM9867 represents the subtidal channel facies of the inner inlet, whilst core SWAM9901 shows the laminated structure of the sediment within the adjacent intertidal flat. Cores SWAM9865 and SWAM9815, obtained from the Médoc Channel and the secondary channels of the western side of the estuary, respectively, indicate the transitional facies of marine/estuarine sediments. Cores SWAM9855 and SWAM9911, consisting of estuarine mud with an upstream increasing number of laminae, display the sub-tidal facies of the downstream mid-estuary.

The facies in the subtidal area consist of a thick body of fine–coarse sand, with abundant shell fragments. The sediment is moderately–well sorted and non-bioturbated (Figure 6, core SWAM 9867). At the uppermost limit of the inlet, sedimentary structures are almost absent from this sandy wedge. For comparison, BRAUD (1986) has identified many structures (e.g. cross-bedding, parallel stratification and wave ripples) in cores from the outer inlet. Such a reduction in the development of sedimentary structures, from the outer to the inner inlet, could be attributed to a gradual reduction in the marine processes, due to upstream attenuation of wave action.

The lithology of the intertidal flat facies varies, according to the intensity of the incoming waves and the sediment supply. The sediment can consist of estuarine silt and fine–medium sand, of marine origin. Such deposits consist of parallel laminae; these are a few mm or cm in thickness and can be disturbed by roots and annelids. The burrows are filled often with very fine sand (Figure 6, core SWAM 9901). Biogenic remains are usually scattered

within the mudflat sediments and, in some places, shell aggregations have been observed.

Transition zone

The transition from the marine-influenced inlet and the inner parts of the estuary (A2, in Figure 1) is undulating, separating the marine and estuarine facies. Over this area, the short-term (diurnal, daily or weekly) alternations of marine or estuarine processes result in the deposition of mixed sediments, such as sand and mud, with a mean grain size ranging between +1.5 Φ and +5.5 Φ (Figure 2). Wave action and the morphological complexity of the estuary inlet are the major factors controlling the transport and dispersion of the marine sand. However, during seasons of high freshwater discharge, the turbidity maximum reaches the inner part of the mouth, causing deposition of estuarine mud (CASTAING, 1981). In some places, well-sorted sand is in contact with the mud, indicating an abrupt and well-defined marine/fluvial interface.

Comparison between the two sedimentological maps reveals that some striking changes in the transition zone have taken place, over the last 30 years (Figure 3). Thus, the transition zone has moved: (i) upstream along the west bank, where marine sand has spread through the shallow Saintonge Channel; and (ii) downstream along the right bank, where estuarine mud has progradated through the deep Médoc Channel. This long-term change is likely to be related to an alteration in the local hydrodynamic regime, caused by small morphological changes of the estuary bed (e.g. deepening of the central channel, erosion of the Banc des Marguerites), and/or fluctuations in the freshwater discharge. Apart from these natural processes, human activities (dredging, construction of artificial bars, etc.) could also have affected the sediment transport patterns.

Within the vertical, the facies in the marine/fluvial transition zone contain alternating layers (1–20 cm thick) of well-sorted, very fine–fine sand, and massive brown mud (cores SWAM9865 and SWAM9815, in Figure 6). The thickness of these layers reflects the intensity and/or duration of the marine or fluvial dominance. When prevent, the contact between the sandy and muddy beds is abrupt and non-parallel; this is related to the rapid and abrupt changes in the hydrodynamic processes.

The mid-estuary

This segment comprises the mixed energy central zone of the estuary (B, in Figure 1), where tidal and riverine processes act together. The mid-estuary is funnel-shaped, with a maximum width of 11 km to seaward, reducing to less than 3 km at the confluence of the Garonne and Dordonge rivers (Figure 1). The area is effectively unaffected by waves, with only tidal and density currents controlling the sediment transport. The principal source of sediment supply to the mid-estuary is the aforementioned rivers.

The average annual fluvial sediment load has been evaluated by MIGNIOT (1971) and CASTAING (1981), to be 2.2×10^6 tons of suspended particulate matter (silt and clay), together with approximately 0.7×10^6 tons as bedload (sand and gravel). Although a significant fraction of the suspended load (about 60%) is carried to seaward onto the shelf, its temporary settling out in the downstream part of the mid-estuary creates a surface layer of fluid mud; this is devoid of any fluvial sand. The absence of any riverborne sand, near the mouth of the system, means that all the coarse-grained material remains within the estuary in response to tidal pumping and residual (water) circulation (ALLEN, 1991). The funnel can be sub-divided into two portions comprising particular sedimentary facies:

The downstream mid-estuary zone

The downstream zone extends from the uppermost limit of the mouth area, to St. Estéphe (B1, in Figure 1). In this part of the 'funnel', tides play a more significant role on the sediment dynamics, than the fluvial processes. The morphology is uncomplicated, with the Médoc and Saintonge Channels running along the left and right banks, respectively. Between the channels, there are some elongated tidal (or estuarine) bars, formed by the residual circulation. Massive estuarine muds have accumulated into the distal part of the 'funnel' and the main channels. The mean grain size is almost uniform, with only a small range (between +5.5 Φ and +6.5 Φ), whilst the median size is less than +0.1 Φ. (Figure 2) On the elongated bars, estuarine sand is the dominant grain size fraction; on the flanks, it decreases and becomes a less important component.

During the last 30 years, no significant change would appear to have occurred over this part of the estuary, with the exception of some sand shifting along the tidal bars (Figure 3).

The sub-surface sedimentary facies in the subtidal channel, near the marine/fluvial transition zone, consists of estuarine mud; this is uniform in character, but is interrupted occasionally by coarse silt laminae (core SWAM9855, in Figure 6). The creation of these deposits indicates that clay and fine silt have settled into the downstream mid-estuary zone. However, during periods of high river discharge, coarse silt enters and remains in the area. Upstream, the frequency of the coarse silt interbedding is higher, because the fluvial processes become more active and carry more coarse-grained material (core SWAM9911, in Figure 6; cores SWAM9825 and SWAM9870, in Figure 7).

The sub-surface facies of the lower intertidal areas, on the sides of the estuary, consist of brownish mud with abundant organic matter (core SWAM9827, in Figure 7). Decayed plant remains (i.e. roots, leaves and reed stems) are scattered throughout the sediments, as black spots or lenses; locally, they create independent layers of a few mm or cm in thickness. The intertidal mud is more cohesive than the subtidal mud; this is related to compaction, resulting from dewatering and decomposition of the organic matter.

The upstream mid-estuary zone

The upstream zone extends from St. Estéphe to Bec d'Ambés (IB2, in Figure 1). In this area, the fluvial impact becomes more important than the tidal influence. The morphology is complex, with the presence of elongated tidal bars and vegetated islands; these are separated by a system of secondary braided channels. In the Médoc Channel, the sediment consists generally of mud and sand, coarser than that in the channels along the eastern bank (Figure 2). The braided system of channels consists of sand and gravel, although fluid mud deposition occurs during the ebb tide.

The surficial sediment distribution pattern here was different during the 1960's (Figure 3). The Médoc Channel, the area between the islands, and the uppermost part of this zone (near the confluence of the rivers) were covered then by finer-grained sediments (mud and fine sand), compared with present-day conditions. This change may be the result of the downstream movement of the turbidity maximum (see above), dredging activities, or the continuous erosion of the estuary bed, from Bec d'Ambés to Pauilliac (as ALLEN (1972) ascertained, on the basis of the study of various historical bathymetric charts.

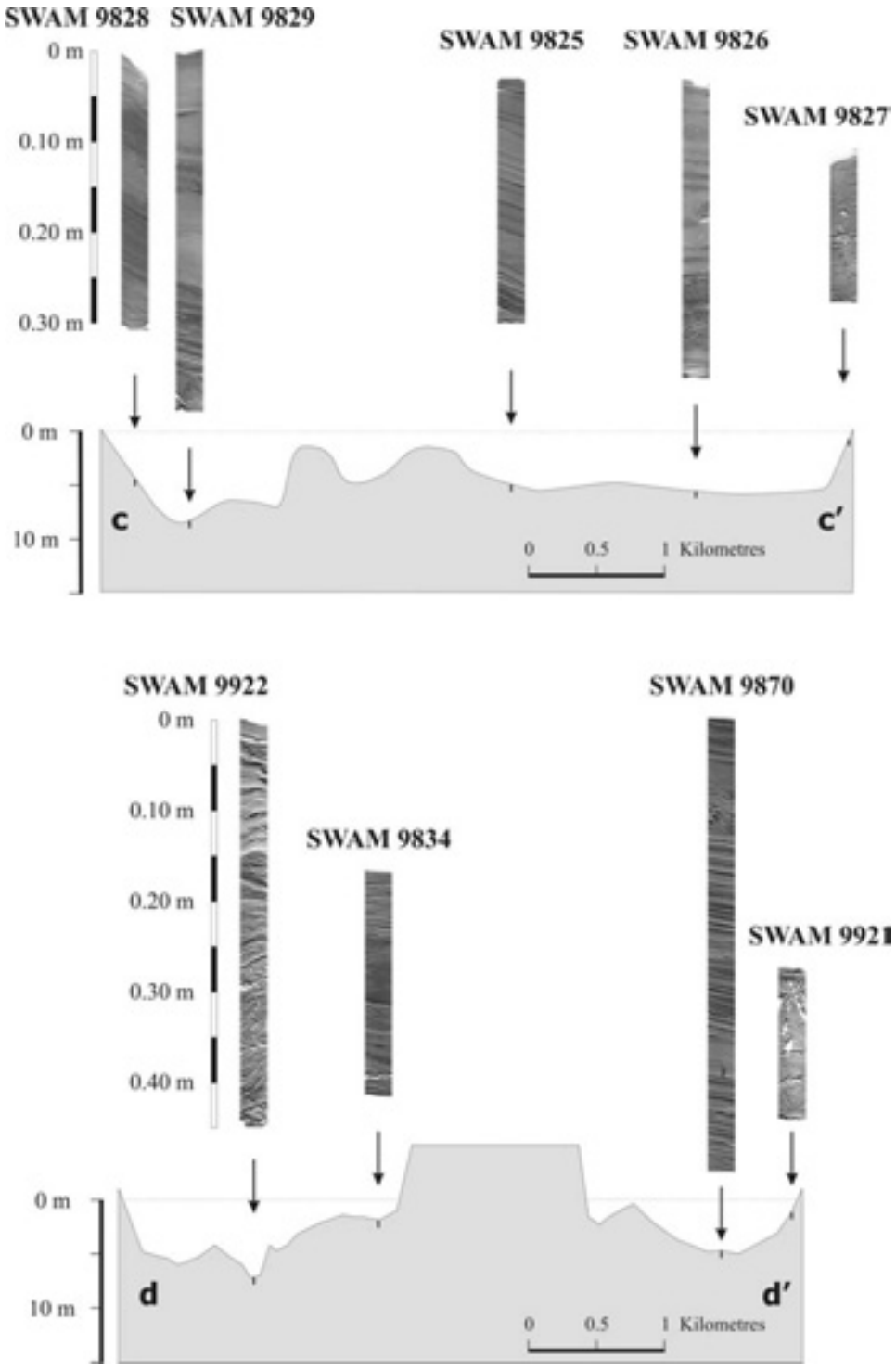

Figure 7. Core radiographs showing the distribution of the sub-surface sedimentary facies along the bathymetric cross-sections c–c′ and d–d′, in the mid-estuary (for locations, see Figure 2). Core SWAM9828 represents the sub-tidal facies on the western side of the estuary, whilst core SWAM9829 reveals the sedimentary sequence of the Médoc Channel. Cores SWAM9825 and SWAM9826 show the structure of the deposits in the central area of the mid-estuary, whilst core SWAM9827 displays the bioturbated features of the low intertidal mud, on the eastern side of the mid-estuary. The destruction of the internal structure, by dredging activities in the Médoc Channel, can be detected in the lower half of core SWAM99922. Core SWAM9834, obtained from the margin of the bars/islands within the mid-estuary, comprises alternations of sandy and muddy layers. Core SWAM9870 reveals tidal imprints within the shallow Saintonge Channel. Finally, core SWAM9921 shows the cohesive mud of the low intertidal areas, of the upstream part of the mid-estuary.

A variety of sedimentary facies covers the upper mid-estuary segment. In the Médoc Channel, medium–coarse silt is interbedded with sandy layers of variable thickness, whilst numerous clay-drape couplets are present (core SWAM9922, in Figure 7). Although the upper facies have an undisturbed internal structure, the lower facies appear to be totally deformed and destructed. As bioturbation is essentially absent, such chaotic structure could be attributed to the intense dredging activity, which would have taken place on a regular basis for navigation purposes. The tidal bars and islands have a complex internal structure, as studied elsewhere by TASTET *et al*. (1986), and FÉNIÈS and TASTET (1998). At the island margins, very fine sand alternates with laminae of medium–coarse silt, with a variety of small-scale structures; these consist of parallel or sub-parallel layers, wavy-bedding, isolated sandy lenses and erosional contacts (core SWAM 9834, in Figure 7).

Over the intertidal zone, intertidal flats and salt marshes are developed, which border the upstream mid-estuary. A thin (< 2 cm) surface layer of medium sand covers the mudflat sequence, containing olive grey mud and scattered vascular plants (core SWAM9921, in Figure 7). The sand is derived from adjacent tributaries, whilst the mud originates from the estuary. Bed-sedimentary structures are almost absent, because of severe bioturbation.

The riverine estuary

At Bec d'Ambés, the funnel shape of the mid-estuary narrows and is separated into two independent sinuous channels, representing the lower course of the Garonne and Dordogne rivers and comprising the riverine estuary (C, in Figure 1). These fluvial-dominated channels present all the features of meanders, i.e. a single thalweg winding between alternating depositional convex and erosive concave banks. Point bars are attached temporarily to the banks, but their shape and position change, over time, as the channel migrates. The sediment in the point bars near the confluence consists of a wide spectrum of mean grain size (from -2 Φ to +5 Φ). Farther upstream, the point bars are formed of coarse-grained fluvial sediments. In the thalwegs of the rivers, silt is the common grain-size fraction but, in some places, sand or gravel is the dominant material (Figure 2).

In the Garonne River, near its confluence with the Dordogne River, the sedimentary sequence comprises medium - coarse silt and very fine sand. The vertical structure is not well defined and its tidal character is not distinguishable (core SWAM9929, in Figure 8). In the Dordogne, 15 km upstream from Bec d'Ambés, the deposits consist of silt and very fine sand, without any tidal features. Thus, the gradual disappearance of tidal facies takes place, from the lower riverine part to upper limit of the estuary

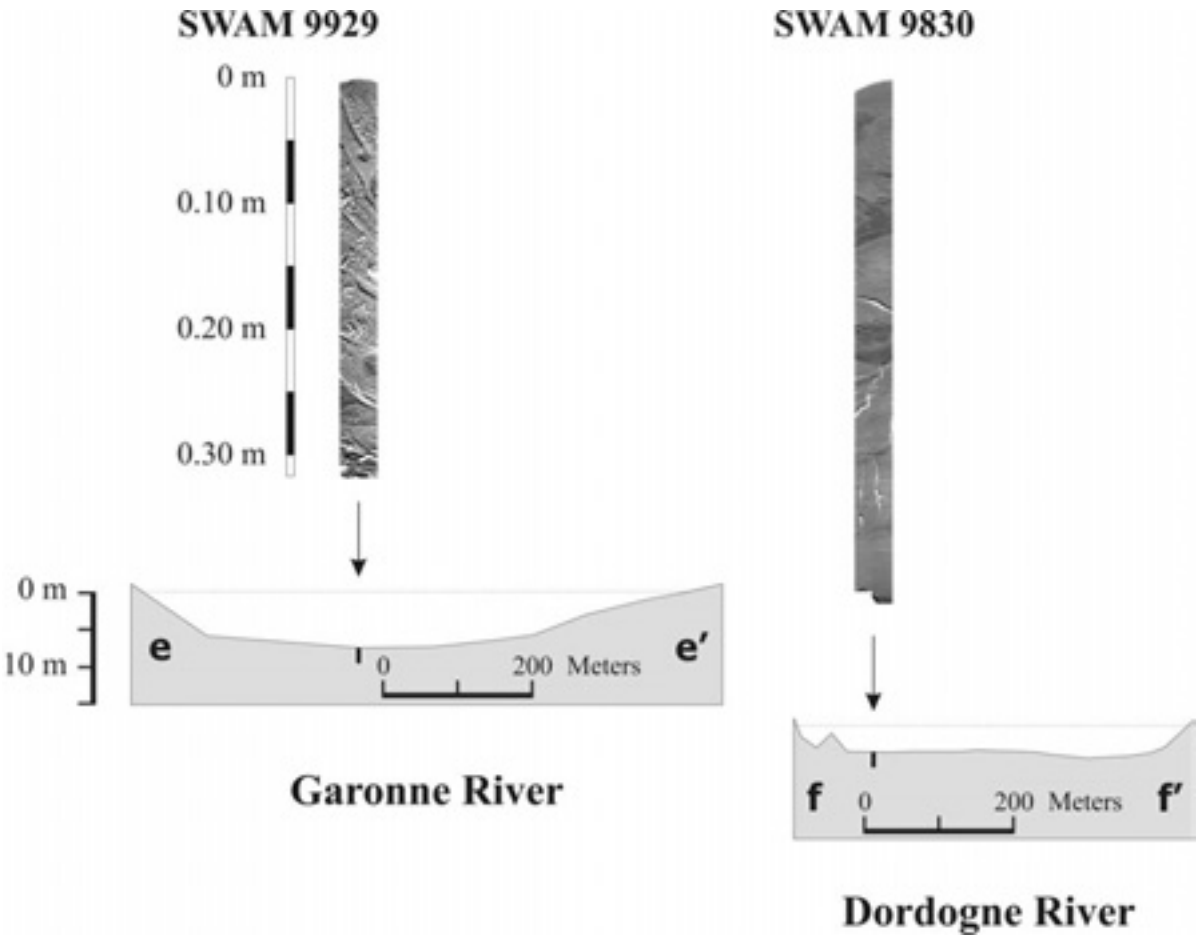

Figure 8. Core radiographs showing the distribution of the subsurface sedimentary facies along bathymetric cross-sections e–e′ and f–f′, within the riverine part of the estuary (for locations, see Figure 2). Core SWAM9929 represents the fine-grained deposits from the thalweg of the Garonne River. Core SWAM9830, obtained from the Dordogne River, shows estuarine sediment with a few tidal features.

(core SWAM9830, in Figure 8), where no trace of tidal estuarine sedimentation can be identified (ALLEN and TRUILHE, 1987). Within this zone, the tidal currents lose their ability to create distinct estuarine facies, due to the gradual dominance of the fluvial currents.
for old photographs and it is very difficult to quantify them when planning a new flight, especially if the monitored area is wide. To avoid errors coming from the seasonal beach profile changes, a solution is to compare flights done during summer when weather conditions are usually calm. But the most important cause of error is due to the tidal cycle. When analyzing an image, it is fundamental to evaluate the range of variation of the HWL due tidal oscillations. If predicted high tide levels are extracted from tide tables, max High Water Springs of +0.65 above m.s.l., the boundary between wet/dry sand has an horizontal variability of about 10 m near the groin (slope 0.08-0.10 m), 14 m in the central part of the beach (slope of 0.04) and of 30 m in the part close to the Bevano river (slope of 0.02). The influence of the swash is believed not to be so relevant, since close to high tide wave shoaling becomes less evident and the flights were done during summer, under moderate wave regimes.

CONCLUSIONS

The sedimentary patterns of the Gironde estuary are typical of mixed wave- and tidally-dominated estuaries (DALRYMPLE et al., 1992). The sediment facies identified within the estuary can be classified into two groups: (a) marine sand and gravel, which forms the tidal inlet prism; and (b) estuarine mud and sand, which are entrapped in the wave-sheltered upper sinuous channels and mid-estuary funnel.

The marine sediments, extending approximately 20 km upstream from the Pointe de Suzac, consist of gravels and sands, with abundant biogenic debris. On the adjacent intertidal flats, sand dominates in the lower areas, whilst mud (together with organic matter) prevails inland. The boundary of the inlet and the mid-estuary is a transition zone, which consists of mixed marine/estuarine material. Fine-grained sediment of estuarine origin comprises the bottom of the downstream mid-estuary. During periods of high freshwater discharge, the turbidity maximum is located in the lower part of the estuary funnel, where fluid mud) covers its bed. When the river flow is low, the turbidity maximum shifts upstream and incorporates the inner parts of the estuary. At the confluence of the rivers and the point bars, gravel and sand cover the subtidal areas, whilst the thalweg of the rivers is coated by more fine-grained sediment (fine sand and mud).

Some 30 years ago, the distribution of the surface sedimentary facies was somewhat different. The most significant changes, since that time, can be identified within the transition zone between marine sand and estuarine mud, and the upstream mid-estuary. In relation to its present-day position, the transition zone was located more downstream, in the past, along the eastern side of the estuary, and more upstream along the western side. Such displacements may be attributed to long-term changes in the main hydrodynamic factors, i.e. waves, river discharge and the turbidity maximum. In the 1960's, the upstream mid-estuary and lower course of the Garonne and Dordogne Rivers were covered by more fine-grained sediment, possibly as the result of the longer retention time of the turbidity maximum over this area. In contrast, some parts of the estuary, such as the inner mouth, the downstream mid-estuary and the uppermost estuary do not show any significant changes in their surficial sedimentary patterns.

The sub-surface sedimentary facies in the inner inlet consist of non-bioturbated marine sediment, with abundant shell fragments. Up to the uppermost limit of the mouth, the sandy body becomes more fine-grained and loses its structures; presumably, this is related to the upstream reduction in the marine processes. Over the adjoining intertidal flat, muds, with parallel laminae of coarse silt or fine sand, are highly disturbed by worms and plants. The vertical alternation of marine sand and estuarine mud characterizes the transition zone, whilst the thickness of these beds reveals the intensity and/or duration and dominance of the marine or fluvial processes over the area. The sub-tidal mud in the lower part of the mid-estuary is uniform in character; however it is interrupted occasionally by laminae of medium silt. Farther upstream, the presence of the coarse-grained interbedding increases gradually, due to the strengthening of the fluvial processes. Dredging activities disturb and destroy the internal structure of those sediments located within the navigation channels. The low intertidal flats of the mid-estuary are composed of cohesive mud, with a high organic content. Sand and gravel dominate in the riverine part of the system, whilst tidally-induced sedimentary structures become less frequent towards the uppermost limit of the tidal current effect.

ACKNOWLEDGEMENTS

This study was supported by the European Commission T.M.R. project " Sediment and Water Movement in Industrialised Estuarine Environments" (No: ERBFMRXCT970111). The authors wish to thank the Captain and crew of the R.V. *Côte d'Aquitqine* (C.N.R.S./I.N.S.U.), for their assistance in data acquisition. We appreciate also the help of J. Saint-Paul and O. Weber in producing the radiographs, and D. Poirier and G. Chabaud (all of the University of Bordeaux I) for analyzing the sediment grain size. Finally, Professor Michael Collins (School of Ocean and Earth Science, University of Southampton, U.K.) is thanked for his comments on an early draft of the manuscript.

LITERATURE CITED

ALLEN, G.P., 1972. Etude des processus sédimentaires dans l'estuaire de la Gironde. Bordeaux, France: University of Bordeaux I, Ph.D. thesis, 314p.

ALLEN, G.P., SALOMON, J.C., BASSOULLET, P., DU PENHOAT, Y. and DE GRANDPRÉ, C., 1980. Effects of tides on mixing and suspended sediment transport in macrotidal estuaries. *Sedimentary Geology*, 26, 69-90.

ALLEN, G.P., 1991. Sedimentary processes and facies in the Gironde Estuary: a recent model for macrotidal estuarine systems. *In*: SMITH, D.G., REINSON, G.E., ZAITLIN, B.A. and RAHMANI, R.A. (eds.), *Clasic Tidal Sedimentology*. Canadian Socciety of Pertoleum Geologists Memoir, 16, pp. 29-40.

ALLEN, G.P. and POSAMENTIER, H.W., 1993. Sequence stratigraphy and facies model of an incised valley fill: the Gironde Estuary, France. *Journal of Sedimentary Petrology*, 63(3), 378-391.

ALLEN, G.P. and POSAMENTIER, H.W., 1994. Transgressive facies and sequence architecture in mixed tide and wave-dominated incised valleys: example from the Gironde Estuary. *In*: DALRYMPLE, R.W., BOYD, R.J. and ZAITLIN B.A. (eds.), *Incised valley systems: origin and sedimentary sequences.* SEPM (Soc. Sediment. Geol.), Special Publication No. 51, pp. 225-240.

ALLEN, G.P. and TRUILHE, G., 1987. Stratigraphic and facies model of a transgressive estuarine valley fill in the Gironde

estuary (France). *In*: JAMES, D.P. and LECKIE, D.A. (eds), Sequences, Stratigraphy, Sedimentology, Surface and Subsurface. Canadian Society of Petroleum Geologist Memoir, 15, pp. 575.

BIGGS, R.B. and HOWELL, B.A., 1984. The estuary as a sediment trap; alternate approaches to estimating its filtering efficiency. *In*: KENNEDY, V.S. (ed.), The estuary as a filter. Academic Press, New York, pp. 107-129.

BRAUD, F., 1986. La dynamique sedimentaire a l'embouchure d'un estuaire. Bordeaux, France: University of Bordeaux I, Ph.D. thesis, 215p.

CASTAING, P., 1981. Le transfer à l'océan des suspensions estuariennes; cas de la Gironde. Bordeaux, France: University of Bordeaux I, Ph.D. thesis, 530p.

CASTAING, P., 1989. Co-oscillating tide controls long-term sedimentation in the Gironde Estuary, France. *Marine Geology*, 89, 1-9.

CASTAING, P. and ALLEN, G.P., 1981. Mechanisms controlling seaward escape of suspended sediment from the Gironde, a macrotidal estuary in France. *Marine Geology*, 40, 101-118.

DALRYMPLE R.W., ZAITLIN B. and BOYD R., 1992. Estuarine facies models: conceptual basis and stratigraphic implications. *Journal of Sedimentary Petrology*, 62, 1130–1146.

DALRYMPLE, R.W. and ZAITLIN B.A., 1994. High-resolution sequence stratigraphy of a complex, incised valley succession, Cobequid Bay – Salmon River estuary, Bay of Fundy, Canada. *Sedimentology,* 41, 1069-1091.

FÉNIÈS, H. and TASTET, J.P., 1998. Facies and architecture of an estuarine tidal bar (the Trompeloup bar, Gironde estuary, SW France). *Marine Geology*, 150, 149-169.

GLANGEAUD, L and BONNICHON, Y., 1939. Sur les causes dynamiques des variation de la turbidité et du débit solide dans la Gironde et la Garonne au cours des marées. *Compte Rendu de l'Académie des Sciences*, Paris, 208, 1072.

HOWA, H., 1987. Le littoral du Nord Médoc (Gironde): évolution d'une côte sableuse en érosion. Bordeaux, France: University of Bordeaux I, Ph.D. thesis, 258p.

JOUANNEAU, J.M. and LATOUCHE, C., 1981. The Gironde Estuary. E. Schw. Verlagchh., Stuttgart, pp. 115.

KNEBEL, H.J., FLETCHER, C.H., III and KRAFT, J.C., 1988. Late Wisconsinan – Holocene paleogeography of Delaware Bay: a large coastal plain estuary. *Marine Geology*, 83, 115-133.

LERICOLAIS, G., BERNÉ, S. and FÉNIÈS, H., 2001. Seaward pinching out and internal stratigraphy of the Gironde incised valley on the shelf (Bay of Biscay). *Marine Geology*, 175, 183-197.

MALLET, C., 1998. Etude de la dynamique des sédiments non cohésifs de l'embouchure de la Gironde. Bordeaux, France: University of Bordeaux I, Ph.D. thesis, 184p.

MEADE, R.H., 1972. Transport and deposition of sediments in estuaries. *In*: NELSON, B.W. (ed.), Environmental Framework of Coastal plain Estuaries. *Geological Society of Amer. Memoir*, 133, 91-120.

MIGEON, S., WEBER, O., FAUGERES, J.-C. and SAINT-PAUL, J., 1999. SCOPIX: a new X-ray imaging system for core analysis. *Geo-Marine Letters*, 18, 251-255.

MIGNIOT, C., 1971. L'évolution de la Gironde au cours des temps. *Bulletin de l'Institut de Géologie du Bassin d'Aquitaine*, 11, 221-281.

NICHOLS, M.M. and BIGGS, R.B., 1985. Estuaries. *In*: DAVIS R.A. (ed.), *Coastal Sedimentary environments*. Springer-Verlag, New York, pp. 77-125

TASTET J.P., FÉNIÈS, H. and ALLEN, G.P., 1986. Facies, sequences et géométrie d'une barre tidale estuarienne; le banc de Trompeloup dans léestuaire de la Gironde. *Bulletin de l'Institut de Géologie du Bassin d'Aquitaine*, 39, 165-184.

WEBER, O., JOUANNEAU, J.M., RUCH, P. and MIRMAND, M., 1991. Grain-size relationship between suspended matter originating in the Gironde Estuary and shelf mud-patch deposits. *Marine Geology*, 96, 159-165.

Journal of Coastal Research	SI 41	12-26	STRAEE 2002	Ferrara, Italy	ISSN 0749-0208

Estimations of bedload sediment transport in the Guadiana Estuary (SW Iberian Peninsula) during low river discharge periods

F.J. Lobo*, F. Plaza†, R. González†, J.M.A. Dias†, V. Kapsimalis‡, I. Mendes† and V. Díaz del Río∞

*Instituto Andaluz de Ciencias de la Tierra (IACT)
Universidad de Granada
Faculdad de Ciencias
Campus de Fuentenueva, s/n
18002 Granada, Spain
Email: pacolobo@ugr.es

†CIACOMAR/CIMA,
Universidade do Algarve
Avenidas 16 de Junho s/n
8700 - 311 Olhão, Portuga

‡National Centre for Marine Research (NCMR), Agios Kosmas, 166 04 Hellinikon, Greece

∞ Instituto Español de Oceanografía (IEO), Centro Oceanográfico de Málaga, Puerto Pesquero s/n, 29640 Fuengirola, Spain

ABSTRACT

LOBO, F.J.; PLAZA, F.; GONZÁLEZ, R.; DIAS, J.M.A.; KAPSIMALIS, V.; MENDES, I. and DÍAZ DEL RÍO, V., 2004. Estimations of bedload sediment transport in the Guadiana Estuary (SW Iberian Peninsula) during low river discharge periods. *Journal of Coastal Research*, SI 41, 12-26. Ferrara (Italy), ISSN 0749-0208

The Guadiana estuary, located in the south-western part of the Iberian Peninsula, is a narrow, bedrock-controlled estuary, characterized by a seasonal fluvial regime and mesotidal conditions. Bathymetric surveys, geophysical records (Side Scan Sonar, high-resolution seismics), surficial sediment sampling, fluvial discharge data, salinity and velocity measurements were integrated to decipher the influence of tidal currents on bedload sediment transport patterns during low fluvial discharge periods. Results evidence a landward change of dominant tidal transport direction, from ebb- to flood-current dominance. The southern (seaward) estuarine stretch shows mostly seaward-directed bedload transport patterns, related to ebb-current dominance close to the river mouth. Further upstream, morphological and hydrological evidences suggest a higher influence of flood currents. The estuarine stratification seems to control the observed flood-ebb asymmetry, as higher flood dominance during neap tides is related with the establishment of stratified conditions. However, the prevailing tidal pattern is not able to produce a reversal of estuarine dune asymmetry in widespread zones of the southern estuarine stretch. In contrast, intense, landward-directed sediment transport is evidenced in the northern estuarine stretch. Flood-current enhancement in the northern stretch is probably related with channel narrowing and, consequently, with channel section decrease.

ADDITIONAL INDEX WORDS: *Estuarine dunes, bathymetry, tidal currents, fluvial discharge, estuarine morphology.*

INTRODUCTION

The influence of estuarine flows on bedload transport patterns in narrow (< 1 km wide), confined bedrock-controlled estuaries is highly controlled by the particular estuarine morphology, as general patterns of dune orientation change according to channel geometry (FENSTER and FITZGERALD, 1996; FITZGERALD et al., 2000). The influence of hydrodynamic agents in sediment transport patterns is variable. While seaward-directed transport is dominant during periods of high fresh-water discharge, landward-directed transport can prevail during periods of low fresh-water discharge (FENSTER and FITZGERALD, 1996). Strong tidal currents (above 0.4 m/s) can be associated with estuarine narrowing, usually causing a local enhancement of bottom currents by the topography (KNEBEL et al., 1999; KNEBEL and POPPE, 2000). The current enhancement may lead to intense coarse-grained bedload transport, as evidenced by bedforms (VITAL et al., 1998). Other typical geomorphological indicators of strong bottom flows are steeply incised channels (GINSBERG and PERILLO, 1999; VITAL and STATTEGGER, 2000).

The Guadiana estuary (Fig. 1), located in the southwest of the Iberian Peninsula, is characterized by a narrow valley morphology controlled by underlying Paleozoic and Mesozoic strata (BOSKI *et al.*, 2002). The river discharge is highly seasonal, with episodic flood events occurring during winter months (LOUREIRO *et al.*, 1986). The morphological configuration should have a large influence on estuarine bottom-flow patterns, especially during low-discharge periods, when tidal currents dominate the estuarine hydrology. Under those considerations, the main goals of this study are to depict the main bedload sediment transport pathways in the Guadiana estuary during low river discharge periods, and to discern the relative significance of river freshets and tidal flows as controlling factors of such transport pathways.

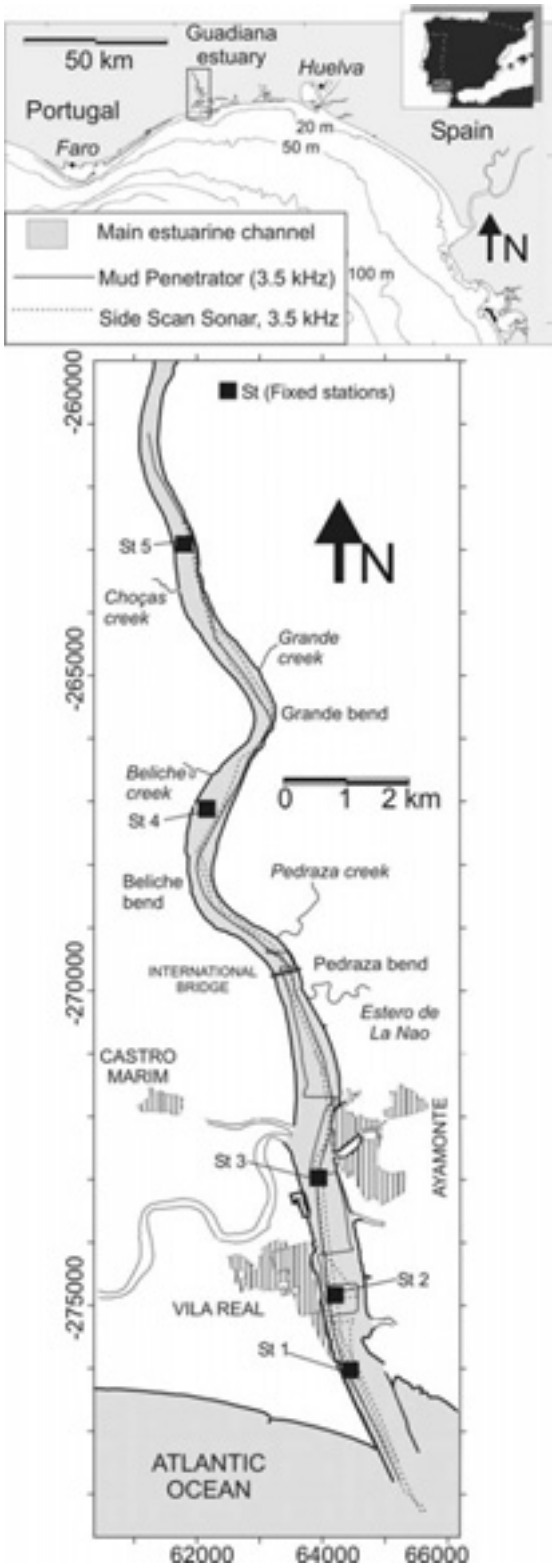

Figure 1. Geographic location of the Guadiana estuary, showing the position of geophysical records (Side Scan Sonar and Mud Penetrator) and fixed stations (St). St 6 is off the map, as it is located 35 km northward from the river mouth.

STUDY AREA

Hydrologic Characterization of the Guadiana Estuary

Fluvial Discharge

The Guadiana river is 810 km long, and its basin covers an area of 66.960 km^2, the fourth in size of the Iberian Peninsula. The flow volume is marked by changes associated with dry and wet years, as well as by large seasonal changes (LOUREIRO *et al.*, 1986). The regional climate is classified as semi-arid, with the exception of July and August (arid) and November to January (temperate-humid) (MORALES, 1993).

Fluvial discharge data are available for the period 1946-47 to 1998-99 at the hydrometric station of Pulo do Lobo, located 95 km landward from the river mouth. Values for the annually-averaged river discharge range between 170-190 m^3/s, although inter-annual variability is high. Thus, wet years show average values higher than 400 m^3/s, whereas dry years show average values ranging between 8-63 m^3/s.

Monthly-averaged river discharges show higher values in winter months (January to March), with values around 400 m^3/s, and lower values in summer months (July and August), with values around 40 m^3/s. However, inter-annual variability of monthly-averaged values is also high, as discharge values can be as high as 2000 m^3/s in winter months.

Tidal Regime

The tidal regime of the Guadiana estuary is mesotidal, with a mean amplitude of around 2 m and tidal ranges of 1.3 m for neap tides and of 3.5 m for spring tides (tide gauge in Vila Real, near the river mouth). A semidiurnal periodicity also characterizes the estuary. The tidal wave propagates following a synchronic mode, generating currents higher than 0.5 m/s (MORALES, 1997). Scarce velocity values document the occurrence of ebb dominance close to the river mouth (MORALES, 1993).

Estuarine Geology and Surficial Sediment Distribution

For most of its length the Guadiana estuarine valley cuts into the Carboniferous Lower Alentejo Flysch Group, composed of several formations characterized by thick sequences (>5000m) of pelitic shists and greywackes, with local occurrences of volcanoclastic series and conglomerates (e.g. OLIVEIRA *et al.*, 1979; OLIVEIRA, 1983). The river valley only crosses a band of

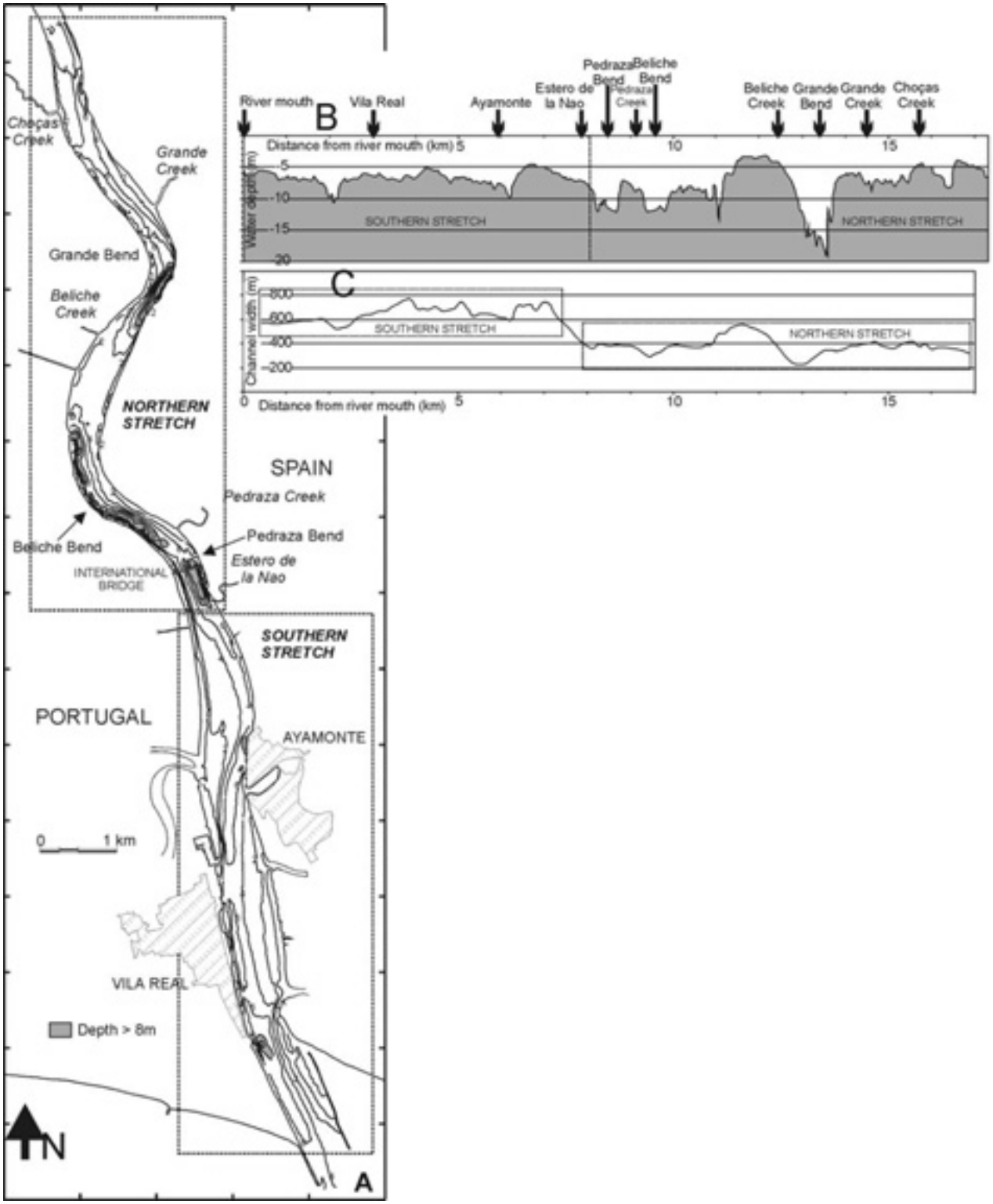

Figure 2. Physiographic characterization of the Guadiana estuary: (a) bathymetric chart of the Guadiana river estuary; (b) bathymetric profile along the estuarine thalweg; (c) channel width variation along the main estuarine channel.

Table 1: Summary of morphological and hydrological measurements conducted in the Guadiana estuary, with indication of tidal stage and fluvial discharge when available.

Dates	Equipment	Measurements	Fluvial discharge (Average daily values, m^3/s)	Tidal range (predicted, m)
September 2000	Petit Ponar dredge	surficial sediments	variable	variable
9 October 2000	echo-sounder	bathymetry	7.6	1.8
16 October 2000	echo-sounder	bathymetry	7.3	2.7
15 to 25 November 2000	ADCP	velocity	variable	variable
19 November 2000	SSS, 3.5 kHz	estuarine bottom features	5.3	1.8
20 November 2000	SSS, 3.5 kHz	estuarine bottom features	6	1.9
23 May 2001	RCM9	salinity, velocity	not available	2.7 (spring tide)
29 May 2001	RCM9	salinity, velocity	not available	1.6 (neap tide)
11 September 2001	RCM9	velocity	9.3	1.2
18 September 2001	RCM9	velocity	8.0	3.5
18 October 2001	RCM9	salinity, velocity	not available	3.2 (spring tide)
24 October 2001	RCM9	salinity, velocity	not available	1.1 (neap tide)

Mesozoic sediments of about 3-4 km width about 10 km from its mouth. These sediments are composed of arenites of fluvial semi-arid origin, evaporites, a volcano-sedimentary complex, and carbonates (e.g. MANUPELLA, 1992). South of this the river valley merges into an about 7 km wide coastal plain, composed mostly of unconsolidated sand of Quaternary and recent age. The seaward portion and areas near the main river channel of the coastal plain are dominated by marsh systems formed by the river (MORALES, 1997). The mouth of the estuary is a highly dynamic area, with considerable movement of sediments and associated morphological changes. The coastline only reached a position close to the present one about 200 years ago (MORALES, 1997; GONZÁLEZ *et al.*, 2001).

The Guadiana estuarine channel connects the fluvial channel with the open littoral domain. Fluvial sediments are transported through this channel, although they are mixed with marine sediments during tidal cycles. The deepest part of the channel is a bypassing channel, as sediments are exclusively sandy. Lateral tidal bars are composed of medium-sized fluvial sands alternating with muds (MORALES, 1997).

MATERIAL AND METHODS

The bulk of the data sets were obtained during intervals of low fluvial discharge (Table 1) and, consequently, the discussion and conclusions apply to periods with similar hydrodynamic conditions.

A bathymetric chart was elaborated from the integration of bathymetric measurements obtained in October (days 5, 6, 9, 11, 16 and 31) and in November (days 6 and 8) 2000 covering 15 km of the lower Guadiana estuary (Figure 1). Water depth was determined by means of a JMC-840 bathymetric sounder, with continuous analog recording, digital output and sub-decimetric precision. Positioning was achieved with a real-time DGPS with sub-metric precision. Bathymetric transects were executed perpendicular and parallel to the channel margins, with a mean separation of 50 m between adjacent lines.

Daily values of river discharge in m^3/s were obtained from INAG (Instituto da Agua, Portugal), covering the river volumes from January 2000 to October 2001 at Rocha da Galé, located about 80 km landward from the river mouth.

Information about salt stratification and near-bottom current velocity was obtained in November 2000 and in low river discharge periods in 2001, at several fixed stations along the estuarine valley (St 1 to St 6 at increasing distances from the river mouth). The salinity structure was defined from conductivity data obtained with several Aanderaa RCM9 current meters recording at 30 s intervals. The current meters were lowered from the surface to the near-bottom (up to 30 cm above the bottom) by means of cables marked at 1 m intervals, for sampling during 5 minutes at every depth.

An ADCP profiler was settled at St 1 (Figure 1). Data were acquired from 16:05 GMT on 14 November 2000 to 11:00 GMT on 25 November 2000. The ADCP profiler was the 'Work horse' manufactured by RD Instruments operating at 600 kHz frequency. The ADCP profiler was equipped with temperature and pressure sensors and was deployed in the self-contained mode facing upwards from the estuary bottom. The vertical resolution was 0.5 m (Depth Cell Size) and the sample interval was 5 minutes. For the purposes of this study, only near-bottom velocity values (at about 1 m above the estuarine bottom) were considered.

As limited current measurements were obtained during November 2000, additional near-bottom velocity data were collected during semidiurnal tidal cycles at St 2, St 3 and St 5 with Aanderaa RCM9 current meters during several surveys between spring and autumn 2001, in order to use them as a proxy for near-bottom tidal current behaviour under conditions of low river discharge (Table 1).

Geophysical data included bathymetric transepts collected parallel to the channel margins in October 2000, and Side Scan Sonar (SSS) records and high-resolution seismic profiling collected during 19 and 20 November 2000 between Choças creek and the Guadiana river mouth (Figure 1 and Table 1). The SSS source was a double frequency Klein system (model 422S-101HF) recording a lateral width of 75 m. The seismic source was a Mud Penetrator ORE transceptor (3.5 kHz), model 140, with a 100 ms recording interval.

Bedform analysis was executed using geophysical data collected in November 2000. Subaqueous dunes can be descriptively classified according to their height (H), which is used as an approximation to dune size (DALRYMPLE and RHODES, 1995). Thus, dunes are classified into small ($0.05 < H < 0.25$ m),

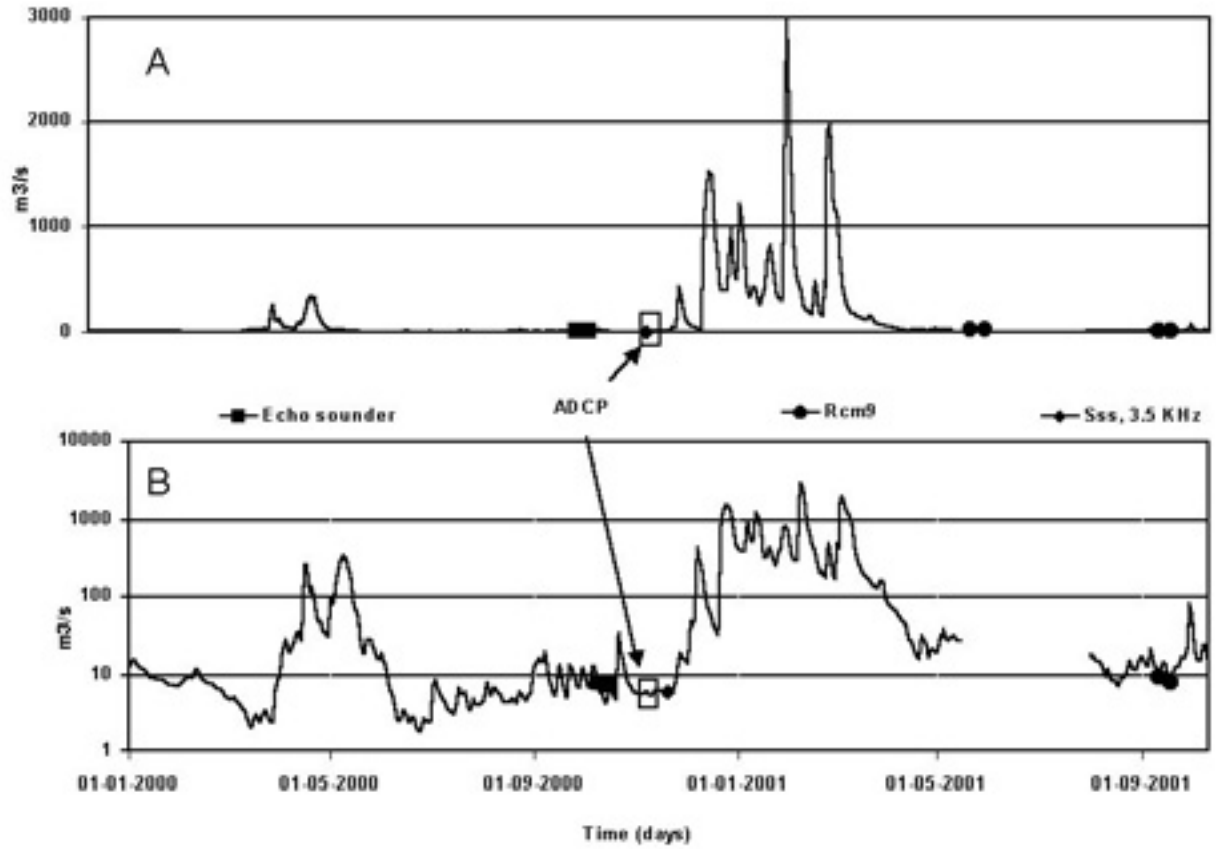

Figure 3. Summary of the Guadiana river volume at Rocha da Galé (80 km landward from the river mouth) from January 2000 to October 2001: (a) river volume in normal scale contrasting periods of flooding in winter and spring with periods of low volume in summer; (b) river volume in logarithmic scale, emphasizing variations during periods of low river discharge.

medium (0.25 < H < 0.5 m), large (0.5 < H < 3 m) and very large (H > 3 m) (ASHLEY, 1990).

The vertical profile of estuarine dunes is usually asymmetric, with a gentler stoss side and a steeper lee side. The steeper side faces in the direction of net sediment transport (BERNÉ *et al.*, 1993; VITAL and STATTEGGER, 2000), whereas symmetrical forms exist in areas where there is no net transport (HARRIS, 1988; BERNÉ *et al.*, 1993). It is assumed that asymmetrical forms generally retain a consistent facing direction over a tidal cycle, as the subordinate current does not transport sufficient sediment to reverse the profile (DALRYMPLE and RHODES, 1995). Medium and large dunes have a long response time and the reversal of asymmetry requires a long-period process (BERNÉ *et al.*, 1993; FENSTER and FITZGERALD, 1996). Consequently, the analysis of medium and large dune asymmetry enabled us to infer bedload sediment transport pathways which were representative of the dominant tidal currents, as most data were collected during periods of very low river discharge.

Two situations of bedload sediment transport were inferred. The first situation integrated along-channel echo-sounder measurements taken during 9 and 16 October 2000. Although 2-dimensional views of echo-sounder profiles only provide information about apparent dune orientation, they can be considered as good indicators of true dune orientation, as the main flow direction tends to prevail, and secondary flows only play a minor role due to the estuary narrowness. The second situation was inferred from the analysis of SSS records and high-resolution seismic profiling collected during 19 and 20 November 2000. The plan view obtained with the SSS records enabled us to confidently map the orientation of transport trends. It was observed that most of the transport patterns were parallel and sub-parallel to the estuarine margins, as documented in other estuarine channels (ALIOTTA and PERILLO, 1987; FENSTER and FITZGERALD, 1996). Another limitation was imposed by the narrowness of the deep estuarine channel, as navigation was very limited above lateral sand banks. Consequently, our investigations mainly refer to along-estuary variations of bedload sediment transport.

Surficial sediment samples were collected during September 2000 in the Guadiana estuary from Choças creek to the river mouth. These samples were collected with a Petit Ponar dredge along estuarine transepts (at least three samples for every transept) separated 150 m one from each other.

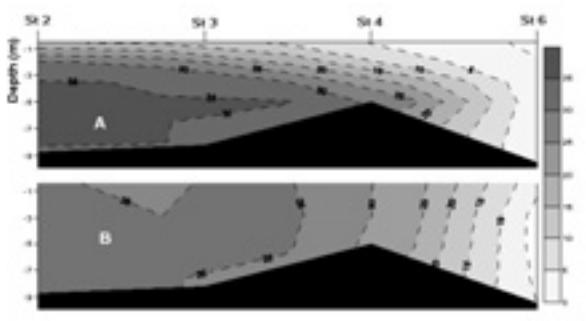

Figure 4. Salinity stratification along the Guadiana estuary an hour after the high tide during (a) neap and (b) spring tide conditions. As the main purpose of this figure is to show the vertical stratification, the horizontal axis has no scale due to the different separation between stations, particularly with regard to St 6.

RESULTS

Bathymetric Measurements

The general geological setup has strong influence on the morphological and physiographical characteristics of the main river valley (Figure 2). The river and its main tributaries have cut relatively narrow and in many places steep valleys into the terrain. While elevations in the vicinity of the main river valley do not exceed about 200-300 m, the main estuarine valley and the lower course of its main tributaries are generally well below 10 m above mean sea level. The main estuarine channel within the study area is narrow, with an average width of 540 m, and an average depth of 7.4 m.

Where the estuarine valley cuts through Paleozoic rocks north of Estero de la Nao, it shows a meandering-like pattern in plan view featuring three main river bends (Figure 2A). Also the path of the valley thalweg shows a net meandering pattern, approximating the outer margins at channel bends. The thalweg is characterized by significant along-channel depth changes, as several scour holes with depths of 7-18 m are evidenced (Figure 2B), except in the zone south of Beliche creek where depth shallows to less than 4 m. Cross-section profiles show V-shaped valleys, with high and uniformly steep valley walls between 3-10°, reaching locally more than 25°, although south of Beliche creek a symmetrical, U-shaped profile is identified (Figure 2A). The most common width of the northern estuarine stretch is about 400 m, and in some locations reaching as little as 200 m. Southwards of Beliche creek the estuarine channel reaches its maximum width (570 m) in the upper stretch, maintaining an average width higher than 450 m along 1.2 km (Figure 2C).

The southern 8.5 km long estuarine stretch between Estero de la Nao and the river mouth crosses through Mesozoic and Quaternary sediments and is less sinuous than the northern stretch. Maximum depths are less than 10 m, generally about 6 m and locally over 8 m in some small scour holes (Figure 2B). Cross-section profiles are mainly V-shaped, but with strongly asymmetric valley walls of relatively low steepness (lower than 1.5° for the gentler and higher than 2° for the more abrupt walls, except in the scour holes, where values higher than 10° can be observed) (Figure 2A). The average width of this stretch is 600 m (Figure 2C). The main estuarine channel is 500-600 m wide at the estuarine mouth, and channel width increases to more than 750 m 2.5 km upstream. The main channel remains about 700 m wide up to 6.5 km upstream from the river mouth, and its width decreases rapidly to less than 400 m close to Estero de la Nao.

River Discharge Data

The seasonality of the Guadiana river is exemplarity shown on Figure 3, covering the river discharge volumes (daily averages) from January 2000 to October 2001. There was hardly any rainfall during summer months (June to August) in 2000, when monthly-averaged values were of about 5 m^3/s, and from September to November – the period coinciding with bathymetric and geophysical surveys – where monthly-averaged values were below 10 m^3/s. The only exception was a low peak of about 30 m^3/s that occurred on 21 and 22 October (Figure 3). Therefore, it was assumed that the hydrologic regime during field surveys corresponded to summer conditions. An additional set of hydrologic measurements carried out between May and October 2001 do also fit in this pattern of low river discharge periods. No river discharge data were recovered between 15 May and 31 July, but, as no significant rainfall occurred during this interval, it was assumed that discharges corresponded to summer values.

Two main periods of increased fluvial discharge occurred during the reported interval (Figure 3): 1) Spring 2000, when the monthly-averaged value was 110 m^3/s in May and the river volume reached daily peak values of 400 m^3/s. 2) Winter 2000-2001, when strong regional rains led to river basin flooding. Monthly-averaged values ranged between 435-665 m^3/s, and the river volume reached peak values of up to 3000 m^3/s.

Estuarine Stratification

Surveys carried out on 18 (Figure 4A) and 24 October 2001 (Figure 4B) provided a synoptic view of the estuarine salinity structure during periods of low river discharge. Figure 4 shows two longitudinal salinity contours an hour after the high tide. Runoff conditions were weak enough to allow the entrance of sea-water into the estuary. On 18 October (neap tide) a salt wedge penetrated up to St 4 within the estuary and a strong halocline developed, allowing the upper layer of fresh water to extend out of the proximity of the estuarine mouth with little mixing. The

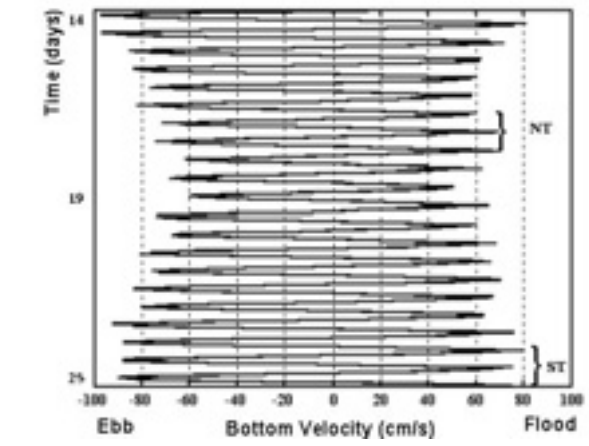

Figure 5. Near-bottom velocities obtained by ADCP from 14 to 25 November 2000 at St 1. The velocity values are projected on the estuarine longitudinal axis. NT: neap tide; ST: spring tide.

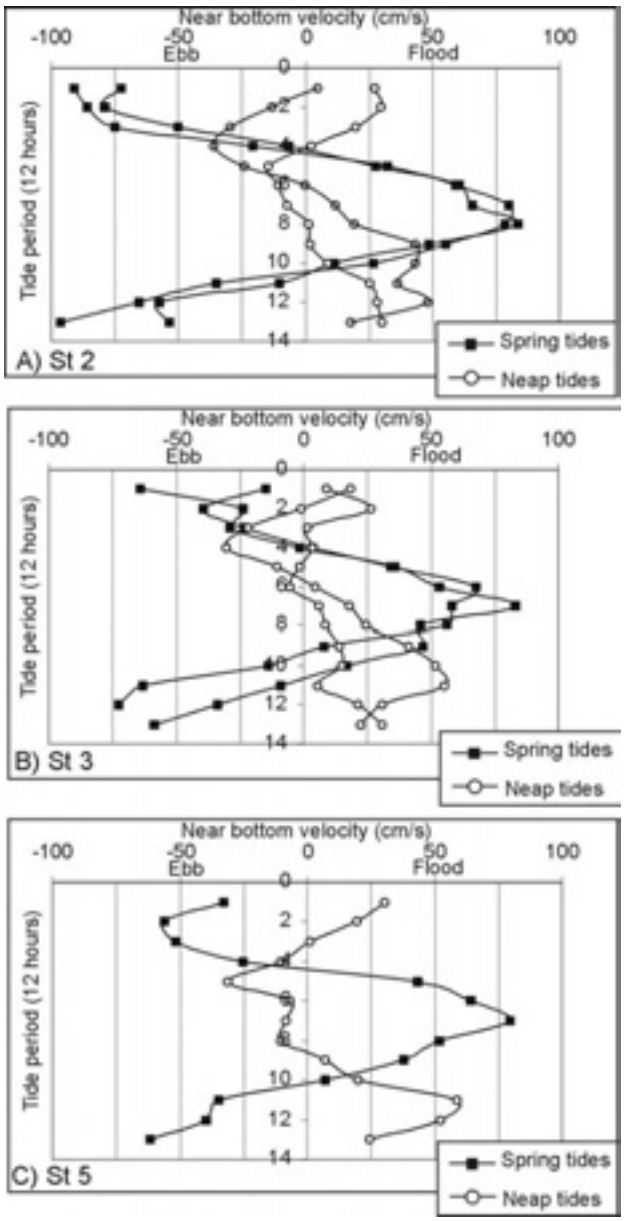

Figure 6. Near bottom velocities during semidiurnal tidal cycles at several fixed stations under conditions of low river discharge in 2001.

stratification due to the buoyancy of the fluvial input imposed an advective regime, and the fresh-water surface layer flowed over the lower layer as a gravity current. Tidal action did not break the estuarine stratification, in spite of the low fresh-water runoff (Figure 4A). On 24th October (spring tide) no vertical stratification was observed, and tidal mixing combined with low fresh-water input generated well-mixed conditions, evidenced by the vertical pattern of the isohalines up to 30 (Figure 4B).

ADCP Measurements

ADCP measurements provided current velocity data at St 1 during the period of geophysical surveying (second half of November 2000). The harmonic analysis of tidal currents (FOREMAN, 1978) determined a higher significance of the semidiurnal component M2 over the diurnal component K1. Near-bottom velocity data showed that this location was ebb dominated during the different tidal stages (Figure 5).

The first measurement days were characterized by relatively large tidal amplitudes, and ebb currents, with values close to 100 cm/s, were considerably larger than flood currents, below 80 cm/s. The transition to neap tides witnessed decreasing ebb-current values, but they remained above 70 cm/s. In contrast, flood currents decreased to values below 60 cm/s. During neap tides (18th November), ebb and flood currents were characterized by similar values ranging between 60-70 cm/s. Ebb currents increased to values around 80 cm/s during the transition from neap to spring tides, whereas flood currents were lower than 70 cm/s. The last measurement days were characterized by spring tides, when the ebb dominance was again evident, as ebb currents increased to around 90 cm/s, whereas peak flood current values were lower than 80 cm/s. Thus, ebb dominance was particularly significant during spring tide and relatively large tidal range conditions, when the difference between ebb- and flood-related velocities ranged between 10-20 cm/s (Figure 5).

Near-Bottom Current Measurements during Semidiurnal Tidal Cycles

Near-bottom current measurements were carried out at several fixed stations during periods of low river discharge and neap/spring tides in 2001 (Figure 6 and Table 1).

During spring tide conditions, St 2, located near the river mouth, was ebb dominated. There, ebb peak values were higher than 90 cm/s, whereas flood peak values were higher than 80 cm/s. In contrast, St 3 and St 5, located further up-river, were flood dominated during spring conditions. The flood-ebb asymmetry increased from St 3 (difference between peak values of about 10 cm/s) to St 5 (difference between peak values of about 20 cm/s).

During neap conditions, the three stations were flood dominated. The flood-ebb asymmetry also increased landward, from St 2 (difference between peak values of about 10 cm/s) to St 5 (difference between peak values of about 30 cm/s).

Estuarine Dunes

Dune size and shape

More than 570 medium and large dunes of H ≥ 0.25 m were identified. Many other small dunes could be distinguished on SSS records (Figure 7). However, as they were not identified in high-resolution seismic records, their H distribution could not be studied. According to the distribution of estuarine medium and large dunes, it was found useful to characterize them in both southern and northern estuarine stretches (Figure 8 and Table 2).
In the southern stretch, seaward-directed (49%) and symmetric dunes (46.5%) were much more abundant than landward-directed dunes (4.5%). Seaward-directed dunes were higher (average value of 0.6 m) than symmetric dunes (average value of 0.4 m). In the northern stretch, landward-directed (44%) and symmetric dunes (41.8%) were more abundant than seaward-directed dunes (14%). Landward-directed dunes showed the highest proportion of large dunes (about 47%) in the northern stretch, although seaward-directed dunes showed the highest average H (0.8 m) (Figures 8A, 8B and Table 2).

Table 2: Descriptive dune size and shape morphological parameters of Guadiana estuarine dunes, based on geophysical records collected from 19 to 20 November 2000.

	SOUTHERN STRETCH			NORTHERN STRETCH		
	Seaward-directed	Symmetric	Landward-directed	Seaward-directed	Symmetric	Landward-directed
Number	98 (49%)	93 (46.5%)	9 (4.5%)	50 (14%)	149 (41.8%)	157 (44%)
Medium dunes	69 (70.4%)	87 (93.6%)	7 (77.8%)	29 (58%)	101 (67.8%)	83 (52.9%)
Large dunes	29 (29.6%)	6 (6.4%)	2 (22.2%)	21 (42%)	48 (32.2%)	74 (47.1%)
Dune height characteristics (m)						
Mean value	0.6	0.4	0.6	0.8	0.6	0.7
Max. Value	2	1.5	2	2.75	2	2
Mode	0.5	0.25	0.25	0.5	0.5	0.5
Dune wavelength characteristics (m)						
Mean value	17.8	12.4	17.2	20.7	15	17.5
Max. Value	60	50	35	50	45	45
Mode	15	10	5	20	10	15
Lee slopes (degrees)						
Min. Value	2.4	Not applicable	2.3	3.6	Not applicable	2.9
Max. Value	26.6		14.0	20.6		14.0
Average value	8.4		9.9	8.8		7.3
Stoss slopes (degrees)						
Min. Value	0.6	Not applicable	1.3	0.9	Not applicable	1.1
Max. Value	5.7		5.2	5.7		7.9
Average value	2.6		3	3.1		3.5

Wavelength (L) distribution showed similar patterns to H distribution. In the southern stretch, seaward-directed and landward-directed dunes showed similar average L values, ranging between 17-18 m. In the northern stretch, the average L value was higher than 20 m for seaward-directed dunes, whereas landward-directed and symmetric dunes showed lower L values (Figures 8C, 8D and Table 2).

The relation between dune L and H followed a similar pattern in both stretches. Although a high scattering was observed, higher Hs correlated with higher Ls, and the relationship was found to be limited by the equation $H_{max}=0.16L^{0.84}$ (after FLEMMING, 1988) (Figures 8E, 8F and Table 2).

H distribution according to water depth (h) was equally scattered, although dunes with H larger than 1 m were related to h larger or equal to 8 m. A maximum H value was associated with each specific h, suggesting that h only represents an upper boundary for H (cf. BOKUNIEWICZ *et al.*, 1977). However, in the northern stretch few dunes were located above the boundary given by the equation H=0.2h (after FLEMMING, 1988) (Figures 8G, 8H and Table 2).

The analysis of lee and stoss slopes showed that, in the southern stretch, landward-directed dunes displayed higher lee and stoss gradients than seaward-directed dunes, and therefore presented a more cuspate profile. In the northern stretch, seaward-directed dunes showed higher lee slopes but lower stoss slopes than landward-directed dunes (Table 2).

Asymmetry distribution maps

Asymmetry distribution maps were used to estimate near-bottom sediment transport paths during two specific intervals. The first situation was inferred from echo-sounding data collected during the first half of October 2000 (Figure 9), whereas the second situation was inferred from geophysical data (SSS and high-resolution seismics) collected during the second half of November 2000 (Figures 7, 10 and Table 1). Therefore, the time interval between both situations was a month. We assumed that in some zones the bedforms could be the result of previous river freshets, whereas in other zones they reflected the control of tidal flows when river discharge was low.

The first half of October 2000 showed a clear dominance of seaward-directed dunes in the southern stretch (Figures 9A and 11A), although a small zone characterized by symmetric dunes or even by landward-directed dunes was identified close to Ayamonte. The poor quality of echo-sounding records did not allow a correct identification of dune asymmetries between Vila Real and the estuarine mouth.

The northern stretch showed contrasting asymmetry patterns. Landward-directed dunes prevailed to the north of Beliche creek (Figures 9B and 11A), although zones with symmetric dunes existed. In contrast, seaward-directed dunes dominated to the south of Beliche creek (Figures 9C and 11A), although landward-directed dunes were detected between Beliche and Pedraza bends.

During the second half of November 2000 the southern stretch showed relatively weak near-bottom transport trends, but with a clear seaward-directed dominance (Figures 7A, 10A and 11B). Large seaward-directed dunes were observed in front of Vila Real. Besides, the zone between Estero de la Nao and Ayamonte was dominated by medium seaward-directed dunes. The zone between Ayamonte and Vila Real showed medium symmetric dunes or even medium landward-directed dunes, with some large dunes close to Ayamonte. Medium symmetric dunes were also found

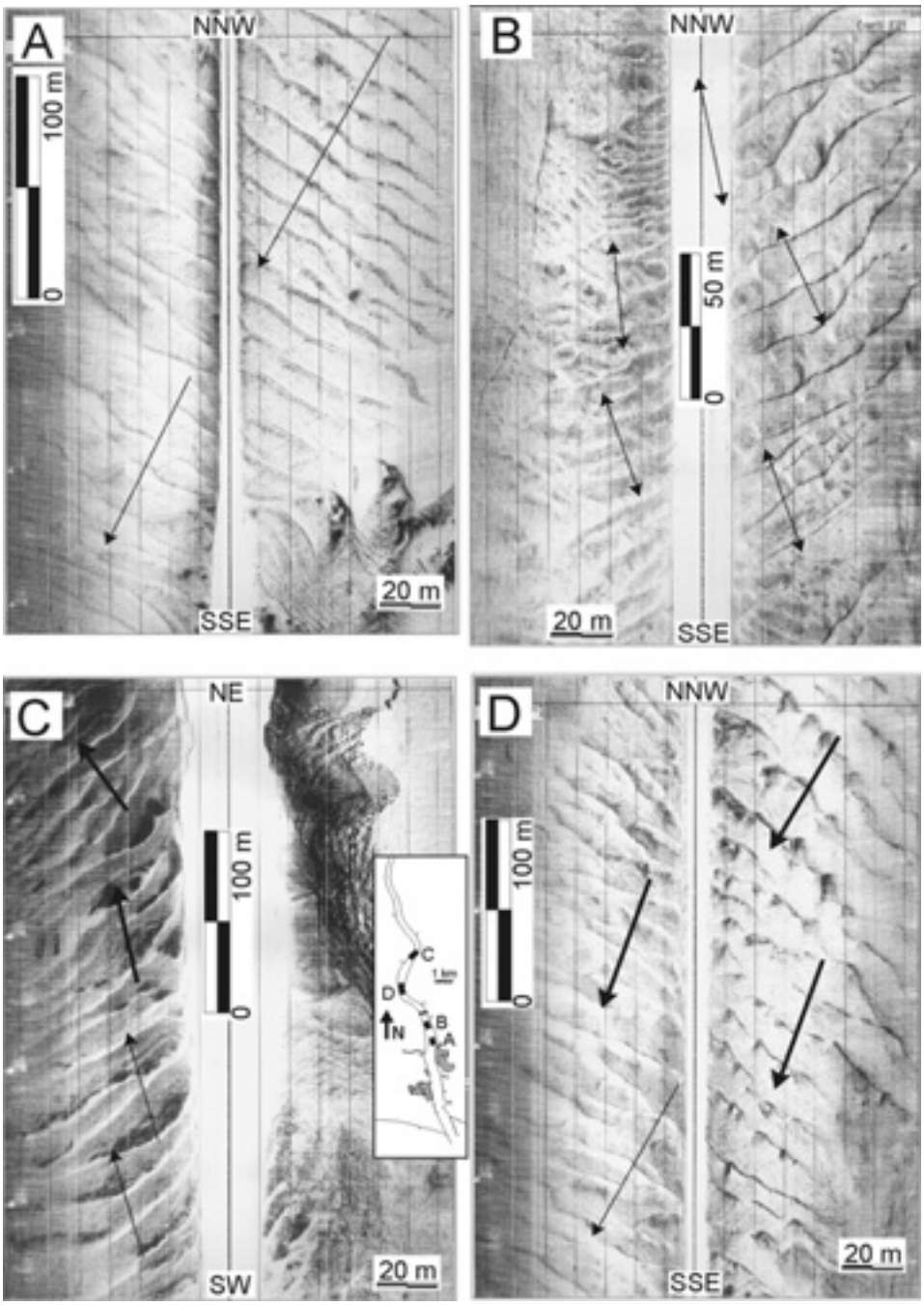

Figure 7. Examples of side scan sonar (SSS) records collected from 19 to 20 November 2000: (a) seaward-directed medium dunes in the southern stretch; (b) symmetric medium dunes with some small dunes observed to the north (in the southern stretch); (c) landward-directed dunes in the northern stretch, evolving northward from medium to large; (d) seaward-directed dunes in the northern stretch, evolving southward from large to medium.

close to the estuary mouth (Figures 7B and 11B).

The northern stretch was characterized by stronger transport trends. There, landward-directed dunes were dominant (Figures 7C, 10B and 11B), especially in four zones: 1) to the north of Grande creek; 2) between Grande bend and Beliche creek; 3) between Beliche creek and Beliche bend; 4) close to Pedraza bend. Seaward-directed dunes were only identified to the south of Beliche creek and between Beliche bend and Pedraza creek (Figures 7D, 10C and 11B). Transitional zones of symmetric dunes were identified associated with estuarine bends, such as Grande and Beliche bends (Figure 11B).

Surficial Sediment Cover

Sediments along the thalweg of the lower Guadiana estuary were dominated by sand. Exceptions generally occured where

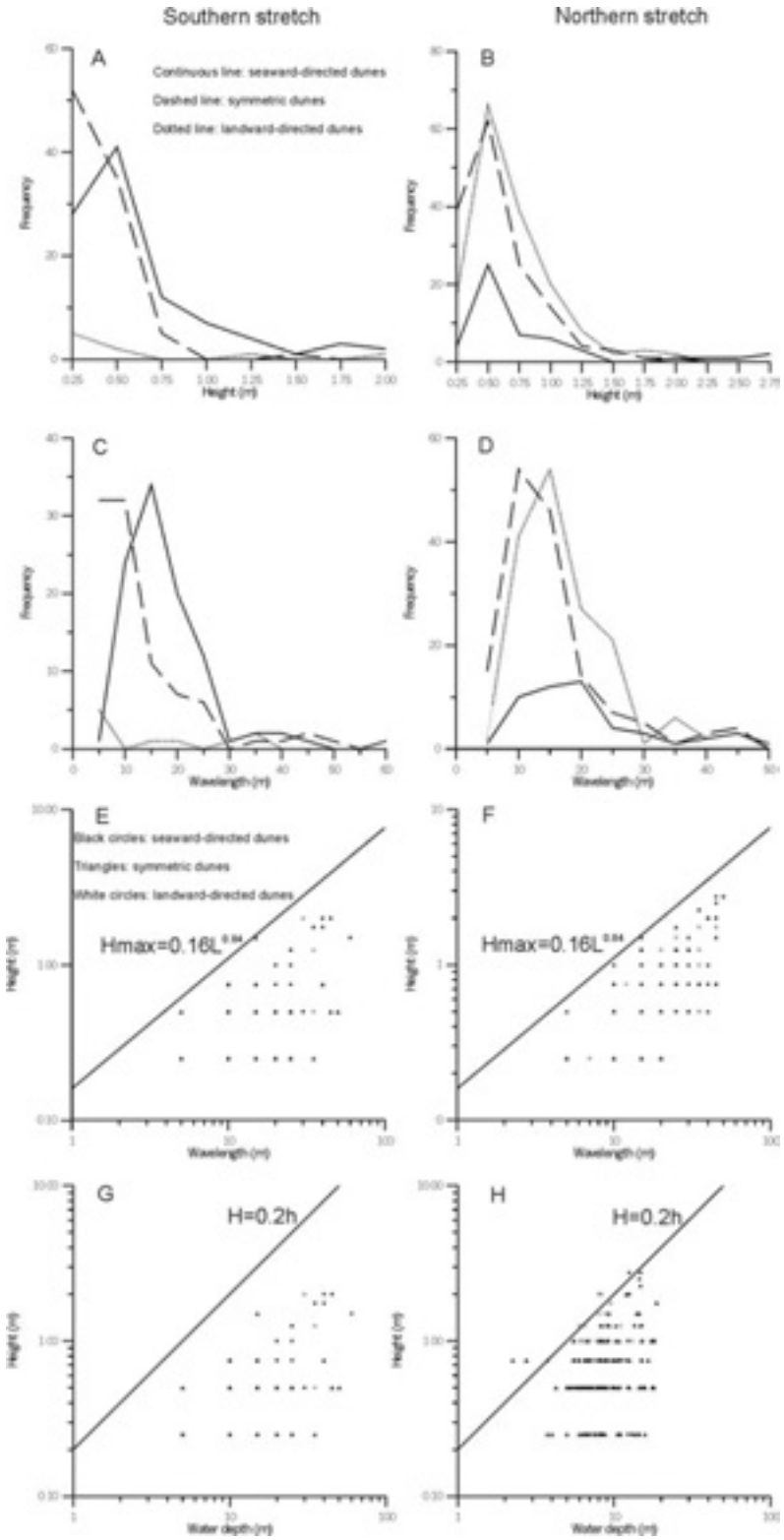

Figure 8. Morphological characterisation of subaqueous dunes in the Guadiana estuary: (a) frequency histogram of height (H) distribution in the southern stretch; (b) frequency histogram of H distribution in the northern stretch; (c) frequency histogram of wavelength (L) distribution in the southern stretch; (d) frequency histogram of L distribution in the northern stretch; (e) plot of L against H in the southern stretch; (f) plot of L against H in the northern stretch; (g) plot of water depth (h) against H in the southern stretch; (h) plot of h against H in the northern stretch.

unusually deep locations of the thalweg are located in the vicinity of creeks, for instance near the mouth of Beliche creek. In these cases fine-grained sediments <63 μm dominated. The immediate vicinity of the western jetty was dominated by gravely deposits.

The sand fraction of sediments in the study area was composed of quartz, feldspar, bioclasts, lithic components of diverse origin, with provenance primarily from Mesozoic outcrops (sandstones and vulcanites, as well as shallow marine carbonates), and shist and greywacke fragments, originating from a thick series of paleozoic turbidites, which make up large part of the interior of the south-western Iberian Peninsula.

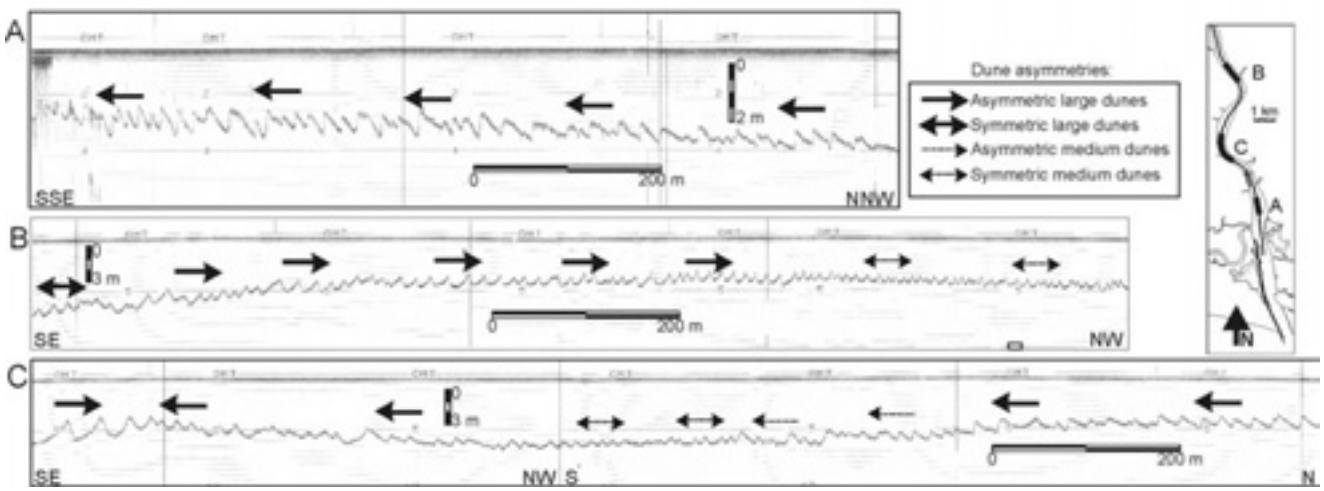

Figure 9. Echo-sounding records of estuarine dunes observed in the Guadiana estuary in October 2000: (a) seaward-oriented dunes in the southern stretch; (b) landward-oriented dunes in the northern stretch; (c) seaward-oriented dunes are locally significant in the northern stretch, as well as symmetric dunes.

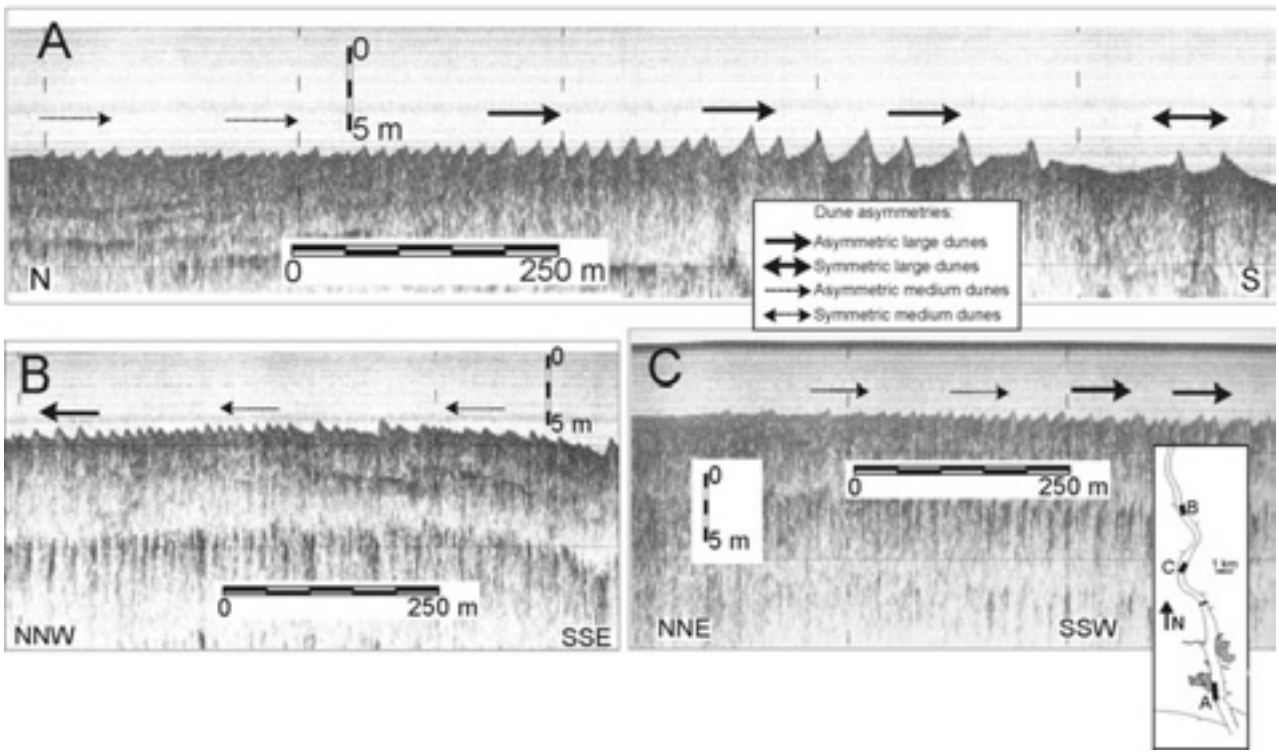

Figure 10. Examples of high-resolution seismic profiles (3.5 kHz) collected from 19 to 20 November 2000: (a) dune field in the southern stretch where seaward-oriented dunes evolve downstream from medium to large; (b) dune field in the northern stretch where landward-oriented dunes evolve upstream from medium to large; (c) dune field in the northern stretch where seaward-oriented dunes evolving downstream from medium to large.

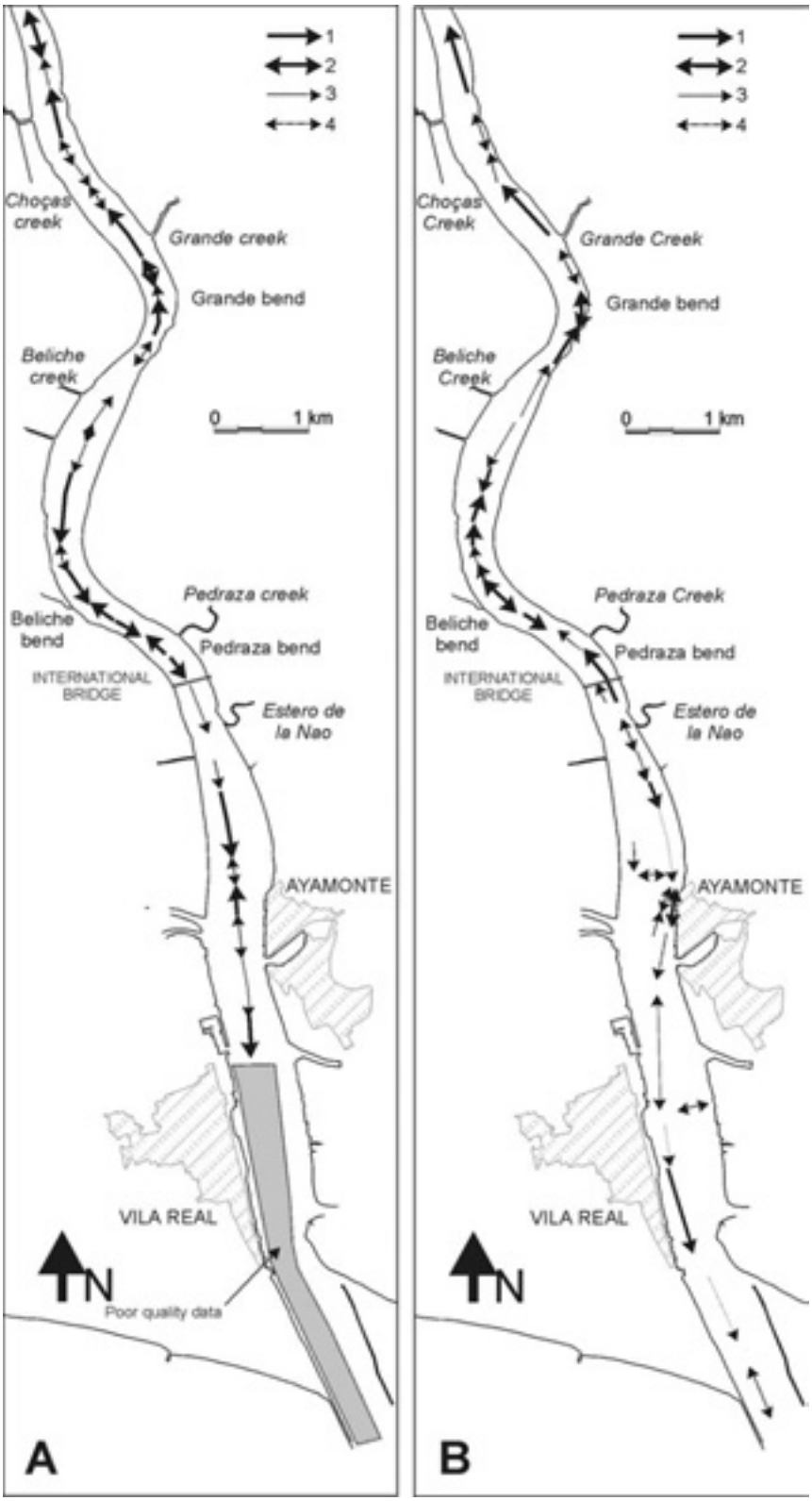

Figure 11. Estimation of near bottom sediment transport patterns deduced from dune asymmetries, from data collected in: (a) October 2000 and (b) November 2000. Legend: (1) sediment transport trends inferred from asymmetric large dunes; (2) sediment transport trends inferred from symmetric large dunes; (3) sediment transport trends inferred from asymmetric medium dunes; (4) sediment transport trends inferred from symmetric medium dunes.

DISCUSSION

Dune asymmetry distributions observed in the Guadiana estuary during two specific intervals were used to estimate trends of bedload sediment transport during periods of low river discharge, as the study of bottom bedforms in estuarine settings may provide estimates of dominant bedload transport patterns (VAN DEN BERG, 1987; PARK and YOO, 1997). Medium and large dunes are considered to be relatively stable features which only undergo major changes in response to highly energetic events (BOKUNIEWICZ *et al.*, 1977; FENSTER *et al.*, 1990), as net dune movement is unaffected by diurnal flow regime changes (FENSTER and FITZGERALD, 1996).

The differences between the two observed situations in the Guadiana estuary can be attributed to the dominant hydrodynamic regime, supposedly highly influenced by tidal currents. The transport trends were compared with limited near-bottom current velocity measurements, in order to discern the relative significance of tidal currents and fluvial freshets, as evidenced in other estuarine environments (e.g. COOPER, 1993; BERNÉ *et al.*, 1993; FENSTER and FITZGERALD, 1996). The relative narrowness of the estuarine channel probably prevented the existence of lateral reversing currents, as more intense currents tend to be conducted trough the deeper estuarine channel (cf. DALRYMPLE *et al.*, 1990).

The high proportion of medium dunes observed in the southern (seaward) stretch reflects either moderate hydrologic conditions or dune smoothing by the dominant tidal current pattern (cf. DALRYMPLE and RHODES, 1995). The dominance of seaward-oriented bedforms could be related either to ebb dominance or to the imprint of previous high fresh-water discharge events (cf. COOPER, 1993). In the zone close to Vila Real, the identified seaward-directed bedload transport could be confidently related to near-bottom ebb dominance observed in ADCP records (Figure 5). Particularly during spring tide conditions, the difference between ebb and flood currents may be as high as 20 cm/s, possibly due to the establishment of vertically homogeneous conditions. This pattern is in good agreement with the reported seaward export of sediments in the zone close to the river mouth (MORALES, 1997; MORALES *et al.*, 1997). Few data were available in the southernmost zone close to the river mouth, but the prevalence of symmetric, medium dunes indicates a low-energy hydrodynamic regime (cf. VITAL *et al.*, 1998), probably balanced between moderate tidal currents and the influence of wave action (Figure 11).

To the north of Vila Real, the interaction between bedload transport trends and near-bottom flows was more complex. Although seaward-directed dunes were still more frequent, symmetric dunes were also abundant, and local landward-directed transport also occurred. Morphological data indicate that the dominant seaward-directed transport become less evident from October to November 2000 (Figure 11). Hydrological data collected during intervals with similar hydrodynamic regime revealed a landward change from ebb to flood dominance during spring tides (Figure 6), similarly to the situation identified in other estuaries (BERNÉ *et al.*, 1993). The landward increase of flood dominance was even higher during neap conditions. The salinity structure of the estuary seems to influence the observed flood-ebb asymmetry, as the higher flood dominance during neap tides was associated with estuarine stratification. The increased flood dominance during stratified conditions could be related to a mass balance deficit of saltwater caused by its entrainment with overlying seaward-flowing fresh-water (DYER, 1973). In contrast, equal dominance of flood and ebb currents or slight flood dominance during spring tides could be related to the development of a vertically homogeneous estuary (Figure 4).

As the seaward-directed dunes identified in the northern zone of the southern stretch did not seem to be in equilibrium with the dominant tidal current pattern, it is suggested that they could reflect the influence of a previous high fresh-water discharge event (e.g, spring floods), which would increase ebb tidal flows (cf. FENSTER and FITZGERALD, 1996). The higher landward influence of flood currents during the low river discharge period might have caused a reduction of seaward asymmetry north of Ayamonte, but not a reversal of dune asymmetry. In this sense, the reversal of asymmetry during tidal dominance on sedimentation only has been reported in estuaries with very high tidal currents, such as the Gironde estuary (BERNÉ *et al.*, 1993).

The bedforms were larger in the northern estuarine stretch, indicative of a highly energetic hydrodynamic regime (cf. VITAL and STATTEGGER, 2000). The dominance of landward-directed bedload transport indicates enhanced flood currents during low river flow periods (COOPER, 1993; FENSTER and FITZGERALD, 1996). as dune migration is related with unequal flood and ebb tidal flows (cf. BOKUNIEWICZ *et al.*, 1977). According to the morphological data, the flood dominance increased landward, as no significant downstream-directed transport was identified to the north of Grande bend. The dominance of landward-directed dunes increased from October to November 2000, suggesting that the northern estuarine stretch is flood dominated during low river discharge periods. Limited hydrological data collected in the northern stretch agreed with morphological observations, as St 4 was flood dominated during spring and neap tides under conditions of low river discharge. In St 4, the flood dominance was higher than in stations located in the southern stretch. But, similarly to the situation observed in the southern stretch, the development of estuarine stratification during neap tides also led to higher flood dominance (Figures 4 and 6).

The particular estuarine morphology of the northern stretch may influence the intensity of estuarine flows, and consequently the bedload sediment transport patterns, as the bottom flow is enhanced by, and interacts with, the bottom topography (cf. KNEBEL and POPPE, 2000). This influence is presumed to be higher over tidal currents (cf. KNEBEL *et al.*, 1999). Our observations are in agreement with those statements, as the flood dominance seems to have been higher in zones where the estuarine valley becomes narrower, such as Pedraza and Grande bends (Figure 11). Thus, those narrow passages seem to cause the flood-ebb flow asymmetry.

However, the signature of local, intense seaward-directed bedload sediment transport was also evidenced in some locations, especially south of Beliche creek. The persistence of this transport pattern could indicate either the imprint of a previous high-discharge fluvial freshet (cf. FENSTER and FITZGERALD, 1996) or locally enhanced ebb tidal currents. As the seaward-directed dunes and most of the symmetrical dunes occurred in channel bends, it is suggested that seaward-directed flows accelerated when the main flow was deviated. As a result, equal influence of flood and ebb flows or even some local ebb dominance between Beliche bend and Pedraza creek occurred in relation with channel deviation.

CONCLUSIONS

Bedload transport patterns observed in the Guadiana estuary during low river discharge periods are highly complex, and probably influenced by the combined action of both tidal currents and fluvial flows. As in other estuaries characterized by a narrow, bedrock-controlled morphology, the imprints of high-energy, high

fresh-water discharge events are recorded in the estuarine bottom, even under the clear dominance of tidal currents. Two estuarine stretches (southern and northern) presented contrasting patterns of bedload sediment transport.

The higher abundance of medium dunes in the southern estuarine stretch was attributed to a less intense hydrodynamic regime. The meridional zone of the southern stretch was characterized by seaward-directed bedload sediment transport, which was related to ebb dominance evidenced in ADCP recording. The seaward-directed asymmetry become less evident northward. Current measurements indicated a higher landward influence of flood currents. The higher flood dominance, especially during neap tides, was related with the establishment of estuarine stratification. Consequently, it is suggested that the dominant seaward-directed asymmetry was a remnant of a previous high-discharge fluvial event. It is noteworthy to indicate that the dominant current pattern during periods of low fluvial discharge was not able to produce a reversal of asymmetry, supporting the idea that high-discharge, fresh-water flows can be significantly imprinted in bottom morphologies of narrow estuaries.

Bedload transport patterns were mainly landward-directed in the northern estuarine stretch, indicating flood dominance that increased landward. Limited current measurements indicated enhanced flood dominance in relation to the southern stretch. Flood current enhancement especially occurred where the estuarine channel become narrower. The local identification of seaward-directed or transitional transport trends in relation with estuarine bends probably indicates seaward-directed flow enhancement by channel deviation.

ACKNOWLEDGEMENTS

This work was completed under the framework of the EMERGE project (ODIANA program). F.J. Lobo was funded by a Post-Doctoral FCT Research Grant (Reference SFRH/BPD/5616/2001) and by a Marie Curie Individual Fellowship (contract nº HPMF-CT-2001-01494, between the Universidade do Algarve and the European Commission). Bathymetric and sediment sampling surveys were carried out by Sandra Fachin and Alexandre Braga Coli. The Instituto Español de Oceanografia (IEO) provided seismic equipment for the Wadi Ana 2000 survey. F. González, L. Godoy, M. García and J. Miranda took a very active part in the survey. Some hydrological data were provided by A. Jorge da Silva (Instituto Hidrográfico de Portugal) and by Miguel Saldanha (GEOSUB).

LITERATURE CITED

ALIOTTA, S. and PERILLO, G.M.E., 1987. A sand wave field in the entrance to Bahia Blanca Estuary, Argentina. *Marine Geology*, 76, 1-14.

ASHLEY, G.H., 1990. Classification of large-scale subaqueous bedforms: a new look at an old problem. SEPM Bedforms and Bedding Structures Research Symposium. *Journal of Sedimentary Petrology*, 60, 160-172.

BERNÉ, S.; CASTAING, P.; LE DREZEN, E., and LERICOLAIS, G., 1993. Morphology, internal structure, and reversal of assymetry of large subtidal dunes in the entrance to Gironde Estuary (France). *Journal of Sedimentary Petrology*, 63, 780-793.

BOKUNIEWICZ, H.J.; GORDON, R.B., and KASTENS, K.A., 1977. Form and migration of sand waves in a large estuary, Long Island Sound. *Marine Geology*, 24, 185-199.

BOSKI, T.; MOURA, D.; VEIGA-PIRES, C.; CAMACHO, S.; DUARTE, D; SCOTT, D.B., and FERNANDES, S.G., 2002. Postglacial sea-level rise and sedimentary response in the Guadiana Estuary, Portugal/Spain border. *Sedimentary Geology*, 150, 103-122.

COOPER, J.A.G., 1993. Sedimentation in the cliff-bound, microtidal Mtamvuna Estuary, South Africa. *Marine Geology*, 112, 237-256.

DALRYMPLE, R.W. and RHODES, R.N., 1995. Estuarine dunes and bars. *In*: PERILLO, G.M.E. (ed.), *Geomorphology and Sedimentology of Estuaries*. Developments in Sedimentology, 53, pp. 359-422.

DALRYMPLE, R.W.; KNIGHT, R.J.; ZAITLIN, B.A., and MIDDLETON, G.V., 1990. Dynamics and facies model of a macrotidal sand-bar complex, Cobequid Bay-Salmon River Estuary (Bay of Fundy). *Sedimentology*, 37, 577-612.

DYER, K.R., 1973. *Estuaries: A Physical Introduction*. Wiley, London, 140 p.

FENSTER, M.S. and FITZGERALD, D.M., 1996. Morphodynamics, stratigraphy, and sediment transport patterns of the Kennebec River estuary, Maine, USA. *Sedimentary Geology*, 107, 99-120.

FENSTER, M.S.; FITZGERALD, D.M.; BOHLEN, W.F.; LEWIS, R.S., and BALDWIN, C.T., 1990. Stability of Giant Sand Waves in Eastern Long Island Sound, U.S.A. *Marine Geology*, 91, 207-225.

FITZGERALD, D.M.; BUYNEVICH, I.V.; FENSTER, M.S., and MCKINLAY, P.A., 2000. Sand dynamics at the mouth of a rock-bound, tide-dominated estuary. *Sedimentary Geology*, 131, 25-49.

FLEMMING, B.W., 1988. Zur klassifikation subaquatischer, strömungstransversaler Transportkörper. *Bochum Geol. U. Geotechn. Arb.*, 29, 44-47.

FOREMAN, M.G.G., 1988. *Manual for tidal currents analysis and prediction*. Pacific Marine Science Report 78-6, Institute of Ocean Sciences, Patricia Bay, 70 p.

GINSBERG, S.S. and PERILLO, G.M.E., 1999. Deep-scour holes at tidal channel junctions, Bahia Blanca Estuary, Argentina. *Marine Geology*, 160, 171-182.

GONZÁLEZ, R.; ALVEIRINHO DIAS, J.M., and FERREIRA, O., 2001. Recent Rapid Evolution of the Guadiana Estuary Mouth (Southwestern Iberian Peninsula). *In*: Healy, T.R. (ed.), *ICS 2000 (Proceedings)*, Journal of Coastal Research Special Issue, 34, pp. 516-527.

HARRIS, P.T., 1988. Large-scale bedforms as indicators of mutually evasive sand transport and the sequential infilling of wide-mouthed estuaries. *Sedimentary Geology*, 57, 273-298.

KNEBEL, H.J. and POPPE, L.J., 2000. Sea-Floor Environments Within Long Island Sound: A Regional Overview. *Journal of Coastal Research*, 16, 533-550.

KNEBEL, H.J.; SIGNELL, R.P.; RENDIGS, R.R.; POPPE, L.J., and LIST, J.H., 1999. Seafloor environments in the Long Island Sound estuarine system. *Marine Geology*, 155, 277-318.

LOUREIRO, J.J.M.; NUNES, M.N., and MACHADO, M., 1986. Bacia hidrográfica do rio Guadiana. *Monografías Hidrológicas dos Principais Cursos de Água de Portugal Continental*, M.P.A.T., S.E.A.R.N. Direcção Geral dos Recursos e Aproveitamentos Hidráulicos, pp. 341-407.

MANUPELLA, G., 1992. *Carta Geológica da Região do Algarve*, Escala 1:100 000, nota explicativa. Serviços Geológicos de Portugal, 15 p.

MORALES, J.A., 1993. *Sedimentología del estuario del Guadiana (S.W. España-Portugal). Sevilla, Spain*. University of Sevilla, Ph.D. Thesis, 274 p.

MORALES, J.A., 1997. Evolution and facies architecture of the mesotidal Guadiana River delta (S.W. Spain-Portugal). *Marine Geology*, 138, 127-148.

MORALES, J.A.; RUIZ, F., and JIMÉNEZ, I., 1997. Papel de la sedimentación estuarina en el intercambio sedimentario entre el continente y el litoral: el estuario del río Guadiana (SO de España-Portugal). *Revista de la Sociedad Geológica de España*, 10, 309-325.

OLIVEIRA, J.T., 1983. The marine Carboniferous of South Portugal: a stratigraphic and sedimentological approach. *In*: Sousa, M.J.L. and Oliveira J.T. (eds.), *The Carboniferous of Portugal*. Memorias do Serviço Geologico de Portugal, 29, pp. 3-33.

OLIVEIRA, J.T.; HORN, M. AND PAPROTH, E.P., 1979. Preliminary note on the stratigraphy of the Baixo Alentejo Flysch Group, Carboniferous of Portugal and on the paleogeographic development compared to corresponding units in Northwest Germany. *Communicações do Serviço Geologico do Portugal*, 65, 151-168.

PARK, S.C. and YOO, D.G., 1997. Bedform Distribution and Sand Transport Trend on a Subtidal Sand Ridge in a Macrotidal Bay, West Coast of Korea. *Journal of the Korean Society of Oceanography*, 32, 181-190.

VAN DEN BERG, J.H., 1987. Bedform migration and bed-load transport in some rivers and tidal environments. *Sedimentology*, 34, 681-698.

VITAL, H. and STATTEGGER, K., 2000. Sediment Dynamics in the Lowermost Amazon. *Journal of Coastal Research*, 16, 316-328.

VITAL, H., STATTEGGER, K., POSEWANG, J. and THEILEN, F., 1998. Lowermost Amazon River: morphology and shallow seismic characteristics. *Marine Geology*, 152, 277-294.

SUMMARY

O estuário do rio Guadiana localiza-se no sudoeste da Península Ibérica e apresenta uma morfologia estreita, controlada pelos afloramentos rochosos. Este estuário é também caracterizado por um regime fluvial sazonal e por condições mesotidales. Inúmeras medições geológicas e hidrológicas, incluindo batimetrias, registos geofisicos (sónar de varredura lateral, sísmica de alta resolução), amostras de sedimento superficial, escoamentos fluviais, medições de salinidade e velocidade foram integradas com o objectivo de revelar a influência das correntes de maré sobre as tendências de transporte sedimentar de fundo durante períodos de baixos escoamentos fluviais.

Os resultados evidenciam uma direcção dominante do transporte tidal de correntes de vazante no sector meridional que sofre uma mudança à montante para correntes de enchente. A dominância de transporte sedimentar de fundo dirigido a jusante no troço estuarino meridional está relacionada com uma maior influência das correntes de vazante na zona mais próxima à foz do estuário. A montante, as evidencias morfológicas e hidrológicas sugerem uma maior influência das correntes de enchente. No entanto, este regime de marés não é capaz de produzir uma reversão da assimetria das dunas estuarinas em extensas zonas do troço estuarino meridional. Pelo contrario, um intenso, transporte sedimentar de fundo dirigido a montante é dominante no troço estuarino setentrional. A maior importância das correntes de enchente neste troço superior está possivelmente relacionada com os estreitamentos do canal estuarino.

Journal of Coastal Research	SI 41	27-42	STRAEE 2002	Ferrara, Italy	ISSN 0749-0208

Formation and growth of an estuarine sandbank: Saint-Georges Bank, Gironde Estuary (France)

V. Kapsimalis†, L. Massé‡, A. Velegrakis∞, J.P. Tastet‡, M.H. Lagasquie‡, and O. Paireau⁋

† Institute of Oceanography, Hellenic Centre for Marine Research, P.O. Box 712, 190 13 Anavyssos, Attica, Greece
Email: kapsim@ncmr.gr

‡ Département de Géologie et Océanographie, UMR CNRS 5805, Université de Bordeaux-1, 33405 Talence Cedex, France

∞ Department of Marine Sciences, University of the Aegean, University Hill, Mytilene, 81100, Lesbos, Greece

⁋ SOGREAH Consultants, 6 Rue de Lorraine, 38 130 Evhirolles, France

ABSTRACT

KAPSIMALIS, V.; MASSÉ, L.; VELEGRAKIS, A.; TASTET, J.P.; LAGASQUIE, M.-H.; and PAIREAU, O., 2004. Formation and growth of an estuarine sandbank: Saint-Georges Bank, Gironde Estuary (France). *Journal of Coastal Research*, SI 41, 27-42. Ferrara (Italy), ISSN 0749-0208

The formation and long-term evolution of an estuarine bank of the Gironde mouth, SW France (the Saint-Georges Bank) is studied through the comparison of nine historical bathymetric maps (1677, 1723, 1825, 1874, 1892, 1920, 1940, 1960, and 1992) and information obtained during a recent bathymetric survey (1999). The data show that the initial formation of Saint-Georges Bank occurred at the end of the 17th or the beginning of the 18th century and it could be related to the other morphological changes which took place at the estuarine inlet and particularly to the gradual destruction of the downstream estuarine shoal of Grande Barre, which (a) changed the inshore hydrodynamic regime, (b) allowed large quantities of marine sediments to move further upstream along the coast and (c) made large quantities of sand-sized sediments available. The Saint Georges Bank growth during the past centuries can be differentiated into 3 stages: Stage I (1723-1892), which has been characterized by a vertical and lateral (downstream) bank growth (with an average rate of accretion of about 0.3 x 10^6 m^3 yr^{-1}); Stage II (1892-1960), which is characterized by a relatively slow development (with an average growth rate of about 0.15 x 10^6 m^3 yr^{-1}); and Stage III (1960-1999), which is characterized by a rapid bank growth (with an accretion rate of about 0.7 x 10^6 m^3 yr^{-1}) and a anticlockwise rotation of the crest. The morphological and sedimentological data (side-scan sonar and sub-bottom profiling data and surficial sediment samples) which were collected during the present investigation suggest that Saint Georges Bank is likely to be maintained by a complex hydrodynamic/sediment dynamic regime consisting of a clockwise residual tidal circulation, headland associated secondary flows and trapping of sediments in a zone contained between mutually evasive sediment transport paths.

ADDITIONAL INDEX WORDS: *Sandbanks, historical bathymetry, macro-tidal estuaries, Gironde Inlet.*

INTRODUCTION

Sandbanks in macro-tidal estuaries (DALRYMPLE and RHODES, 1995; DYER and HUNTLEY, 1999) are both widespread and dynamic sedimentary structures. They form large sedimentary stores over 15 m in height with lengths and widths which may exceed 15 and 4 km, respectively. Most field observations and model simulations show that their formation and development are promoted by (DALRYMPLE and ZAITLIN, 1989; DALRYMPLE and RHODES, 1995): (i) suitable residual circulation patterns resulting from flow-seabed interactions, (ii) sufficient sediment supply from the adjacent sea floor and/or the coast and (iii) the presence of suitable sediment traps. There have been many suggestions with regard to the mechanisms which control the formation, growth and maintenance of sedimentary banks in coastal and continental shelf environments (DYER and HUNTLEY 1999), including secondary flow effects (e.g. spiral flows (e.g. HOUBOLT, 1968) or vorticity generated by coastal irregularities (e.g. PINGREE, 1978; ROBINSON, 1981, 1983; SIGNELL and GEYER, 1991; SIGNELL and HARRIS, 2000; BASTOS *et al*., 2002, 2003), flow-seabed interactions (e.g. SMITH, 1969; SWIFT and FIELD, 1981; HUTHNANCE, 1982a, 1982b; TROWBRIDGE, 1995; HULSCHER, 1996; HULSCHER and VAN DEN BRINK, 2001), edge waves (DOLAN *et al*., 1979) and instabilities of long period swell, infragravity and internal waves (BOCZAR-KARAKIEWICZ *et al*., 1990, DE VRIEND, 1990).

Elongated banks are frequently found close to estuarine inlets, particularly in cases where the tidal energy is dominant compared to the fluvial and/or wave energy (DALRYMPLE and ZAITLIN, 1989; DALRYMPLE *et al*., 1992). It has been suggested that such banks form mostly between channels with opposing directions of residual tidal flow (DALRYMPLE and RHODES, 1995); these areas have a large sediment trapping potential as they are often sandwiched between mutually evasive sediment transport pathways (HARRIS, 1988; HARRIS and COLLINS, 1991). Coastal irregularities (e.g. protruding headlands) can also promote the formation of nearshore estuarine banks; these banks (Type 3A banks or 'banner banks' (DYER and HUNTLEY (1999)) are often asymmetric and pear-shaped, with their landward ends being generally shallower and broader than their offshore extremities. Their long axes are directed parallel or obliquely to the coast as

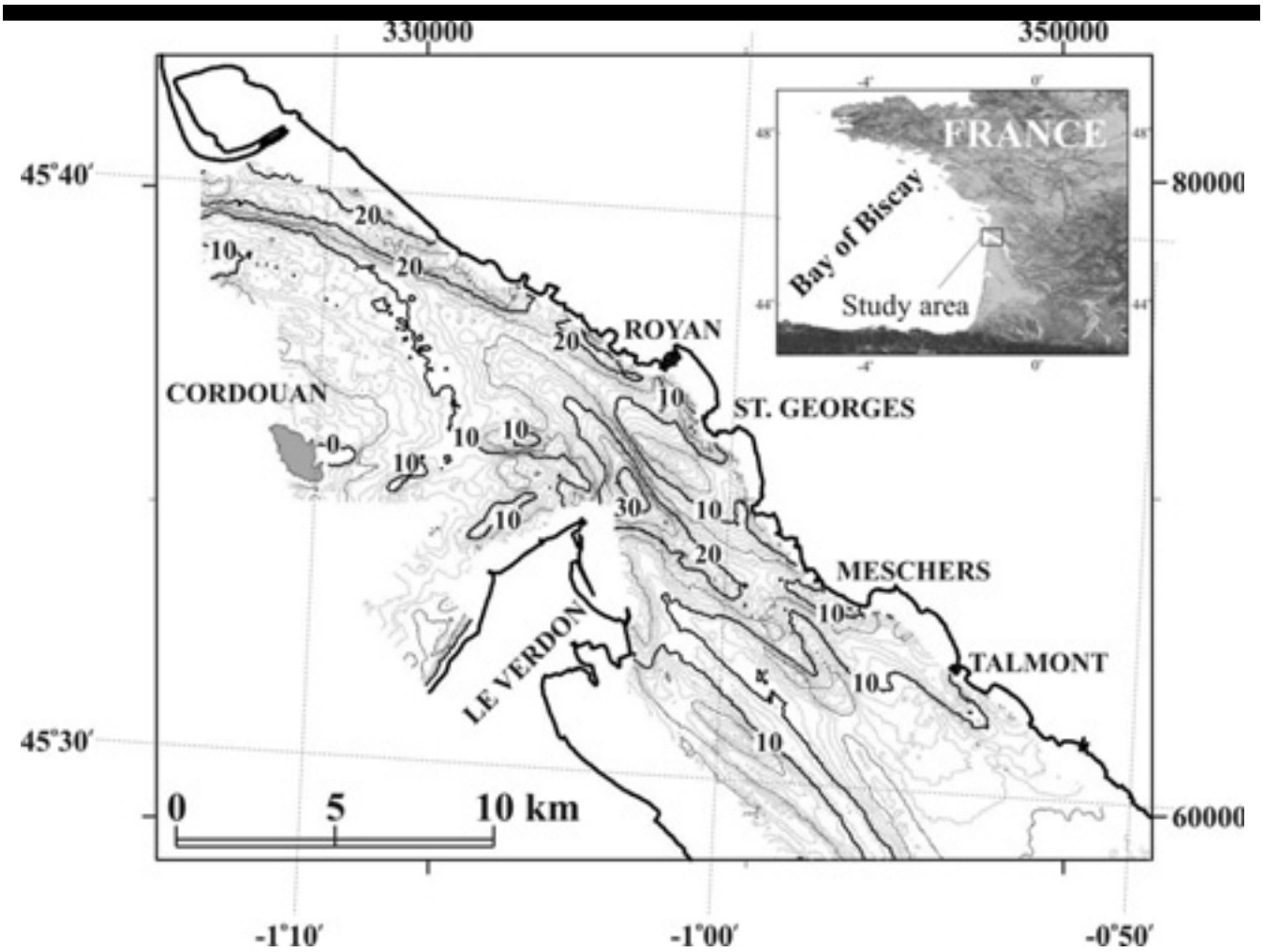

Figure 1. Bathymetry (in metres) of the mouth of Gironde Estuary. Coordinates in metres.

well as to the dominant tidal flow and their flanks are usually bounded by two sub-parallel tidal channels characterized by residual flows with opposing directions (e.g. PATTIARATCHI and COLLINS, 1987).

Active tidal banks are very dynamic features (e.g. AMOS and KING, 1984; HARRIS et al., 1992; LANCKNEUS and DE MOOR, 1995). This is particularly true for banks/shoals of coastal macrotidal environments, as has been shown by studies in the Bristol Channel (e.g. BRITTON and BRITTON, 1980), the English Channel (PINGREE, 1978; BASTOS *et al*., 2002), the Bahia Blanca estuary (GOMEZ and PERILLO, 1992; CUADRADO and PERILLO, 1997) and the Kennebec River estuary in Maine (FITZGERALD *et al*., 2000). The banks' morphological and sedimentological changes occur in different temporal and spatial scales (e.g. DE MOOR, 1989; HOUTHUYS *et al*., 1994). These changes can be impressive, ranging from (temporal) changes in grain-size distributions (TRENTESAUX *et al*., 1994) and the distribution, dimensions and asymmetry of the banks' bedforms (HARRIS and COLLINS, 1984) to changes in the dimensions, asymmetry and even position of the banks themselves (e.g. PATTIARACHI, 1985; BERNE *et al*., 1994).

Of particular importance to the study of the formation, growth and maintenance of banks are the changes of the highest order (i.e. changes in position, dimensions and asymmetry of the banks themselves), as these do not only integrate the smaller spatial morphological and sedimentological changes but also provide information on the dominant mechanisms responsible for the bank genesis and growth. Unfortunately, it is very rare that sufficiently long time series of morphological and/or sedimentological information on banks are available to allow a detailed study of their historical evolution.

The objective of the present contribution is to present and discuss the long-term morphological evolution of Saint-Georges Bank, a sandbank located close to the mouth of the Gironde Estuary, France (Figure 1), an area for which a plethora of good quality, long-term bathymetric data is available. Towards this objective, sequential bathymetric information obtained during the past 320 years, has been analyzed and compared and supplemented by newly acquired morphological and sedimentological observations

Estuaries have been the subject of intense and multidisciplinary investigations during past decades. From a sedimentological perspective, present-day estuaries are ephemeral environments acting as highly effective sediment traps (MEADE, 1972; BIGGS and HOWELL, 1984; and NICHOLS and BIGGS, 1985).

The interplay between marine and fluvial processes and the residual sediment transport patterns determine, to a large extent, the morphology and the distribution of sedimentary facies in estuaries. Any modification to the hydrological regime (tide, wave

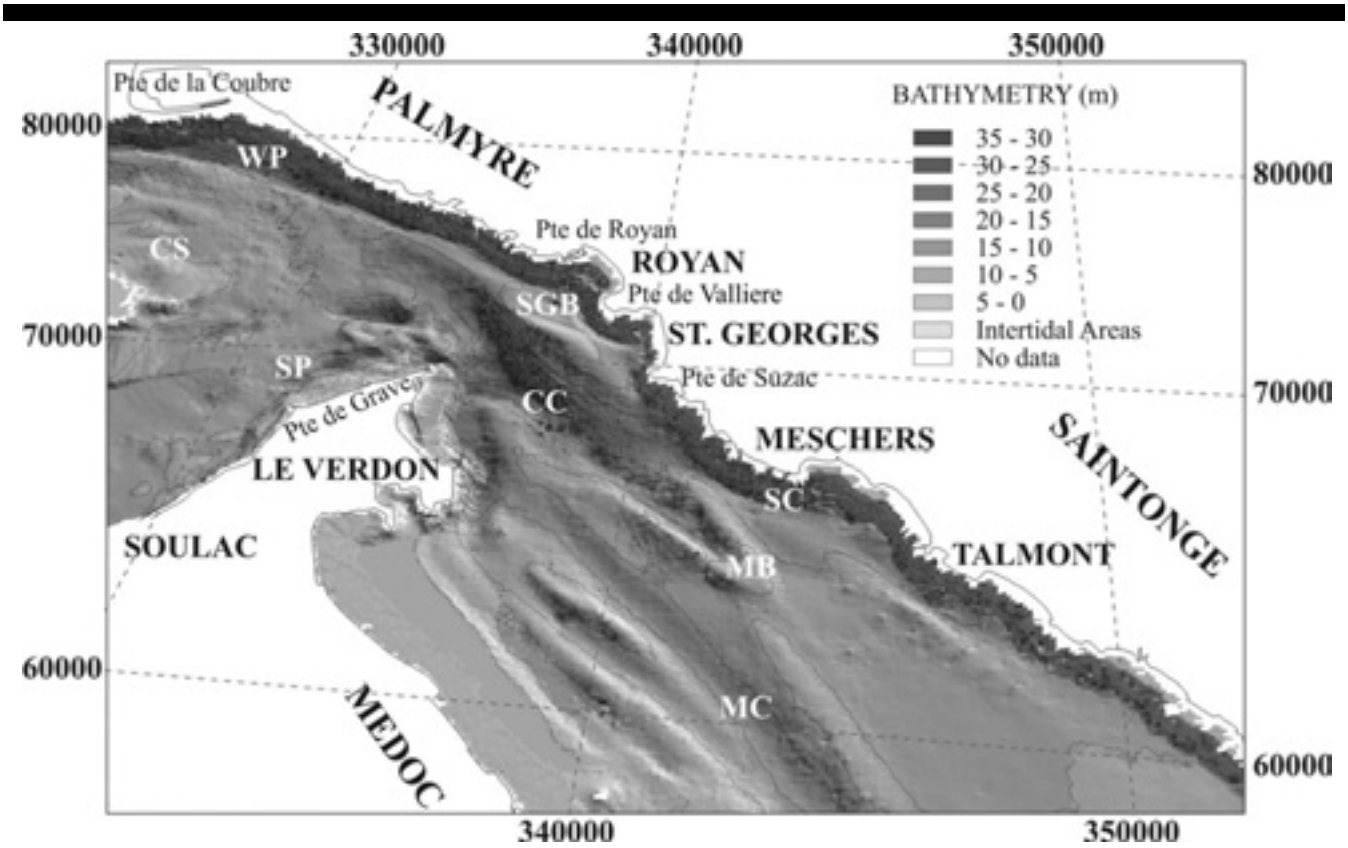

Figure 2. 3D morphological map of the Gironde Estuary inlet showing the major morphological features: WP, Western Pass (Passe de l' Ouest); SP, Southwestern Pass (Passe Sud); CS, Cordouan Shoals; SGB, Saint-Georges Bank; CC, Central Channel; SC, Saintonge Channel; MC, Médoc Channel; and MB, Banc des Marguerites.

and river discharge), or sediment supply, affects the estuarine evolution and alters the previously-achieved equilibrium in the system (JOUANNEAU and LATOUCHE, 1981).

The last fall in sea level, during the late Pleistocene (ca. 18,000 years Before Present (B.P.)), resulted in the formation of deeply-incised fluvial valleys, which converted subsequently into estuaries during sea level rise. Since the post-Holocene stillstand, at about 6,000 yr B.P., most estuaries have been filled with sediments derived both from fluvial and marine sources (KNEBEL et al., 1988; ALLEN and POSAMENTIER, 1993; and DALRYMPLE and ZAITLIN, 1994).

The objective of this paper is to identify the present-day sediment distribution patterns, together with the tidal imprints, in the subsurface sediments of the Gironde estuary. Furthermore, comparison of the new data set with that presented by ALLEN (1972) aims to provide information on changes which have taken place in the sediment transport and accumulation mechanisms, over the last 30 years.

REGIONAL SETTING

The Gironde Estuary mouth is formed by the rocky Saintonge coast to the north and the Médoc peninsula to the south (Figure 2); its geological substrate consists of Upper Cretaceous and Eocene calcareous sediments and Plio-Quaternary deposits (CASTAING *et al*., 1974, ALLEN, 1991; ALLEN and POSAMENTIER, 1993; LERICOLAIS *et al*., 2001). The access to the sea is guarded by the Cordouan shallows (formed by numerous sand banks/shoals and Pleistocene outcrops), which shield the inner estuarine mouth from the intensive wave activity of the Bay of Biscay (5 m high waves during 10% of the year) (ALLEN, 1971; CASTAING, 1981; MALLET, 1998). Thus, the average wave height and period at the inner estuarine mouth is about 1 m and 5-6 s, respectively (HOWA, 1993).

Presently, there are two channels (Passe de l' Ouest (WP) and Passe Sud (SP)) at the estuarine mouth (Figure 2). At the inlet narrows, between Pointe de Grave and Royan, these channels join to form the main channel of the inlet (the Central Channel (CC)), which further upstream separates again forming the Saintonge (SC) and Médoc (MC) Channels. The channel bed is mostly paved by coarse sands and gravels and is scoured in many areas by the inlet's strong tidal currents (ALLEN, 1972; ALLEN and POSAMENTIER, 1993).

The tides are semi-diurnal in character with amplitudes ranging from 2 m (on neaps) to more than 5 m (on springs) at the inlet (CASTAING, 1981). The estuary is regarded as a hypersynchronous, macro-tidal system (CASTAING and ALLEN, 1981; CASTAING, 1989), as the tidal wave, which is almost symmetrical at the downstream part of the estuary, increases its amplitude and becomes asymmetrical upstream having shorter duration and higher velocity during flood (SALOMON and ALLEN, 1983). The main estuarine channel at the inlet is ebb-dominated, with near-bed current velocities exceeding 0.5 m s^{-1} (LESUEUR and TASTET, 1994). The annual freshwater discharge of the estuary varies between 500 and 1000 m^3 s^{-1}, with

the average being 900 m^3 s^{-1} (MALLET *et al*., 2000). There is a strong, southerly littoral drift along the adjacent Atlantic coast, which introduces large quantities of coarse-grained material (about 0.7 x 10^6 tons yr^{-1}) into the estuarine mouth (HOWA, 1987); in contrast, large quantities of suspended particulate material (about 1.3 x 10^6 tons yr^{-1}) are evacuated from the estuary onto the adjacent continental shelf (CASTAING, 1981; ALLEN, 1991).

Saint-Georges Bank is located at the inner estuarine mouth (Figure 2). It is over 5 km long, 1.2 km wide, and its crown lies 1.7 m above the level of the Lowest Astronomical Tide (LAT); its broad, landward end is connected to the shoreface of Saint-George Beach, which forms between the Pointe de Suzac and Pointe de Vallière promontories**.** The bank is bounded by the ebb-dominated Central Channel and the flood-dominated, marginal Saint-Georges Channel (CASTAING and FROIDEFOND, 1978; MALLET *et al*., 2000). Saint George Bank is asymmetrical in cross-section; its steeper (lee) flank, which faces the Central Channel to the southwest, has a slope of about than 3.6° whereas its gentler (stoss) flank, which faces Saint-Georges Channel to the northeast, has a slope of about 1.7°. The bank's crest is slightly sinuous and is oriented obliquely (with an angle of about 16°) to the axis of the adjacent Central Channel (MALLET *et al*., 2000).

Field observations and numerical simulations (e.g. Service Hydrographique et Oceanographique de la Marine 1968; ALLEN, 1971; Port Autonome de Bordeaux, 1980; MALLET, 1998; MALLET *et al*., 2000) have shown a complex hydrodynamic regime for the area , with Saint-Georges Bank appearing to be located close to a clockwise residual circulation cell. The bank's sediments consist mainly of fairly well sorted medium sand, which shows evidence of marine origin (LEGIGAN and CASTAING, 1981). MALLET *et al*. (2000), using trends in the statistical parameters of the bank's sediments (i.e. the Gao and Collins technique, GAO and COLLINS (1992)) as well as numerical model simulations, have found that (a) the sediment movement is ebb-dominated on the lee (southwestern) flank and flood-dominated on the stoss (northestern) flank of the bank and (b) there is a sediment transport convergence towards the bank's crest.

The estuary is characterised by a macrotidal regime, with semidiurnal tides; their amplitude ranges from 2.5 m during neap tides to > 5.5 m during spring tides, near Le Verdon (Figure 1). The tidal wave is deformed by friction and becomes asymmetrical, as it propagates landward into the upper estuary (CASTAING and ALLEN, 1981).

The average freshwater discharge into the estuary ranges between 500 and 1,000 m^3/sec. During low river flow, the estuary is well mixed and the tidal currents can be detected some 130 km upstream from the mouth. In comparison, the salinity intrusion extends 100-115 km upstream. In contrast, during river floods, the estuary is stratified, with the brackish water being restricted within the mid-estuarine funnel and up to a distance of 40 – 50 km from the inlet (ALLEN, 1991).

The bed of the estuary is supplied by two main sediment sources: the Garonne and Dordogne rivers; and the adjacent oceanic beaches and shore zone. All the fluvial sand transported as bedload remains within the estuary, as indicated by its absence within the inlet (CASTAING and ALLEN, 1981). However, a large volume of the fluvial suspended matter escapes out of the inlet, during the ebb tide; then it is deposited on the Aquitaine shelf (CASTAING, 1989; WEBER et al., 1991). To seaward, in response to coastal erosion, coarse-grained sediment is produced from Pleistocene alluvial outcrops; this is transported into the estuary inlet, by littoral drift and tidal currents. These reworked marine sand and gravel deposits penetrate into the mouth, approximately 20 km landward; they are molded into wide-scale bedforms (ALLEN and POSAMENTIER, 1993). The maximum thickness of this landward-thinning wedge is likely to be up to 25 m, including various sedimentary structures, such as parallel bedding, bi-directional cross-stratification and erosion surfaces. The sandy wedge is separated from the underlying tidal-estuarine sediments by a tidal ravinement surface (ALLEN and POSAMENTIER, 1994). Fluvial sand and mud accounts for about the 80 % of the total sediment input to the estuarine system (JOUANNEAU and LATOUCHE, 1981), whilst marine sand constitutes the remaining 20 % (HOWA, 1987).

As the Gironde is one of the largest estuaries in Europe and is of high economical importance, a large number of studies have been undertaken during the past 70 years. Of these, one of the most important early sedimentological studies was the description of the estuarine turbidity maximum, by GLANGEAUD and BONNICHON (1939). Further, the sedimentary patterns and facies have been investigated by a number of scientists, e.g. ALLEN (1972), CASTAING (1981), ALLEN (1991) and MALLET (1998). The internal stratigraphy of the estuary valley fill has been described by ALLEN and TRUILHE (1988), ALLEN and POSAMENTIER (1993, 1994) and LERICOLAIS et al. (2001).

DATA ACQUISITION AND ANALYSIS

Bathymetry

Bathymetric information has been collected in the Gironde Estuary since 1545, with the earliest reliable map dating from 1677. During the 18th and 19th centuries, the bathymetric surveys were sporadic, but since the beginning of the 20th century the Port Autonome de Bordeaux has commissioned annual detailed surveys (CASTAING, 1989). In the present study, nine bathymetric maps from 1677, 1723, 1825, 1874, 1892, 1920, 1940, 1960 and 1992, provided by the Port Authorities, have been used to reconstruct the long-term evolution of Saint-Georges Bank. The collated information has been supplemented by new observations collected in July 1999. During this survey, 20 track lines of bathymetric data with 100 m spacing and overall length of 130 km were obtained using an EK 400 Simrad (12 KHz) echosounder and a DGPS positioning system. The acquired data were reduced to the LAT level, using the real tidal curves of the survey days supplied by the Port Autonome de Bordeaux.

The maps were digitised and the digital data analysed using the TOSCA®, ArcView®, IDRISI® and SURFER® software packages. The projection system used in the analysis was the Lambert System (zone 2, ellipsoid Clark 1880) applied in France (spatial coordinates in meters). The zero level datum was set as the level of the Lowest Astronomical Tide (LAT) defined by the Port Autonome de Bordeaux.

The comparison of historical maps is a tricky exercise, requiring careful consideration of various errors, which result from the determination of the depth measurement positions by different positioning systems and cartographical methods, absence or use of different geo-reference systems, tidal datum problems and computer analysis errors (such as those introduced by the gridding procedures) (e.g. BOWYER, 1992; LIST *et al*., 1997). In order to evaluate quantitatively and correct some of the errors, standard reference points such as churches, capes, lighthouses etc have been used. Although several errors have been thus evaluated and corrected, others, particularly those related to tidal datum (see for example GUITARD, 1996), were less satisfactorily tackled.

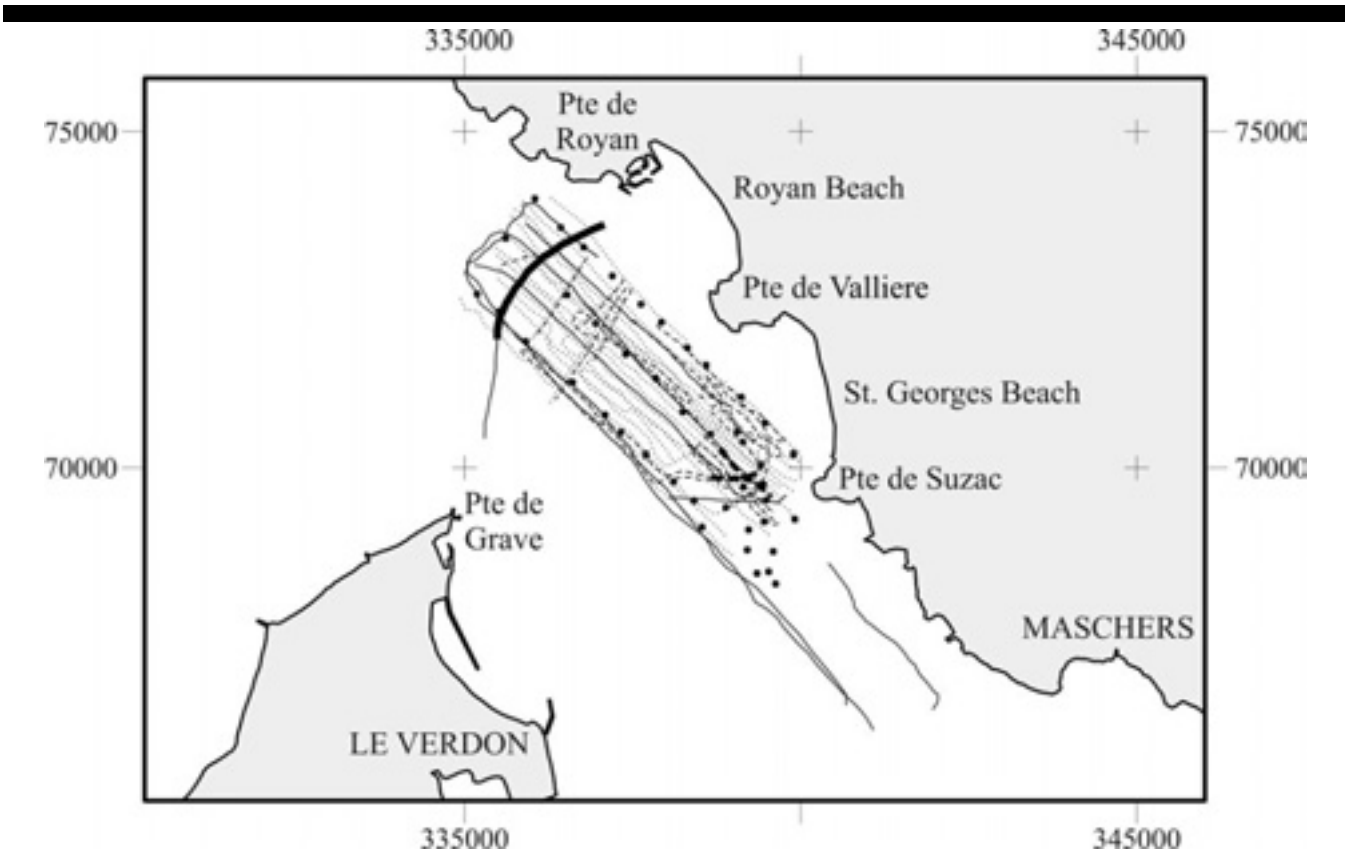

Figure 3. Location of the side scan sonar tracks of the September 1999 (broken lines) and May 2000 (dot lines) surveys. The tracks of the seismic survey (solid lines) and the surface sediment sampling positions are also shown. The bold line show the seismic track of Figure 8 and the stippled lines the side-scan sonar tracks of Figure 9.

Therefore, it is assumed that the accuracy of the comparison analysis has been in the order of 0.5 m.

The base levels for the undertaken volumetric estimations have been estimated as follows: the base level for Saint-George Bank has been assumed to be the seabed surface of 1677 (when the bathymetric information shows that there was no discernible sediment accumulation in the area), whereas the base level for Grande Barre shoal has been assumed to be the seabed surface of 1874 (when the shoal seized to exist).

Acoustic data

Side-scan sonar information was obtained during two surveys in September 1999 and May 2000 using a GeoAcoustics dual frequency side scan sonar operating at 100 or 500 kHz (Figure 3). The first survey took place during equinox spring tides with tidal coefficients (i.e. the ratios of the tidal range of the cycle to the range of the largest spring tide multiplied by 120) ranging from 97 to 106, whereas the second during a neap tide (tidal range less than 3.5 m and tidal coefficients ranging from 57 to 86). The wave conditions during the surveys varied, with those of the second survey (May 2000) being much calmer (wave heights less than 0.4 m). The spatially corrected side-scan sonar data were used to map the spatial distribution and morphological characteristics (dimensions and direction of asymmetry) of the bank's bedforms, which were classified according to ASHLEY *et al*. (1990).

Seismic profiles over the Saint George Bank (Figure 3) were obtained in a separate survey in June 2000, which covered a larger area of the inlet. The equipment used in the survey was an EdgeTech high resolution sub-bottom profiler, equipped with an X-Star acquisition and processing system. Unfortunately, the rough weather conditions, shallow water depths, the presence of thick deposits of sand-sized sediments over the bank and the high frequency nature of the signal did not allow, in most cases, sufficient penetration to detail the internal architecture of Saint George Bank.

Surficial sediments

Thirty-five bottom sediment samples were collected from the bank during the May 2000 survey using a Shipek grab (Figure 3). The samples were wet-sieved and the mud fraction was found to be less than 1% by weight in all samples. Material coarser than 4 φ (0.063 mm) was dry-sieved (at an interval of 0.5 φ between –1 (4 mm) and 4 φ (0.063 mm)) and the grain size parameters of the samples were then estimated according to FOLK (1980). Spatial relationships between the three main parameters (mean size, sorting and skewness) were then utilised to estimate grain-size trends and define "transport vectors" using the GAO and COLLINS (1992, 1994) technique (with a critical distance (D_{cr}) between neighbouring sites of 950 m) and the Dersedill software (PEDREROS et al., 1996).

Grain-size analysis was carried out in the laboratories of the University Bordeaux I, using: sieving for the coarse fractions (gravel and sand); and a Malvern 3600E laser-scattering particle size analyzer for the silt and clay (mud) fractions. Based upon

these results, the mean size, sorting, skewness, porosity and density were calculated, according to moment procedures for grain-size statistics. Data were processed with the ArcView GIS and digitized maps were created (Figure 2).

In order to identify alterations in the surficial sedimentary facies during the last 30 years, the sedimentological map published by ALLEN (1972) was digitized and compared with the new version (Figure 3), where observations on displacement of the turbidity maximum are also shown (see below).

The classification of the sedimentary facies used (Figure 3) was that defined by ALLEN (1972) and is the same for both of the maps shown: mud, when the silt and clay content is more than 80%; sand and mud, when the sand fraction exceeds 20% and the finer material ranges between 20% and 80%; sand, when the sand exceeds 80%; gravel and sand, when both coarse-grained fractions vary between 20% and 80%; gravel and mud when these fractions are not lower than 20%; and gravel, when the gravel fraction is more than 80%. The map of ALLEN was created on the basis of numerous samples collected between 1960 and 1969, under differing hydrodynamic conditions. Although this approach does not incorporate seasonal variability within the system, it provides an adequate outline of the distribution of the surficial sediments during the 1960's. In contrast, the new map is taken to be more representative of a period of high river flow and spring tides, since sampling was accomplished during these specific conditions. The comparison between the two maps provides an indication of textural changes in the sedimentary bed of the estuary.

All the cores were opened, logged visually and photographed at the University of Bordeaux I. Sections were removed for radiographic analysis, for the identification of lithological characteristics and sedimentary structures, using the SCOPIX (a new digital X-ray imaging system for core analysis (MIGEON *et al*., 1999)).

RESULTS

Morphological changes

The sequential bathymetric information (Figures 4, 5 and 6) shows that frequent and drastic morphological changes have taken place in the Gironde Estuary inlet during the past 320 years.

At the end of the 17th century (Figure 4a), Saint-Georges Bank (SGB) did not exist and the main morphological feature of the inlet was the Grande Barre (GB) shoal. The GB shoal was located in the middle of the inlet, (although its northern extremity was connected to the Palmyre coast to the north) and had an elongated shape (orientated NW-SE). The shoal was 11 km in length, 1.2 km in width and had a volume above the level of the seabed as recorded in 1874 when the shoal seized to exist, of about 48 x 10^6 m^3 (Figure 7).

In 1723, a small (1.2 km in length, 0.8 km in width), fan-shaped feature appeared for the first time offshore of the southeastern section of the beach located between Pointe de Suzac and Pointe de Vallière (Figure 4b). This feature formed probably the embryonic core of Saint-Georges Bank and had a volume (above the bed level of 1677) of about 4 x 10^6 m^3. Although the main sedimentary store of the inlet was still the Grande Barre shoal, its shape, dimensions and location had changed drastically in the period 1677-1723. The shoal had been detached from the Palmyre coast by a relatively shallow swale (the Saint-Georges Channel (SGC)) and its volume (above the bed level of 1874) had also decreased to about 36 x 10^6 m^3. Other changes in the area concern the orientation and dimensions of the Passe de l' Ouest (WP) and the formation of a wide topographic high (Banc des Marguerites (MB)) between the Saintonge (SC) and Médoc (MC) Channels (Figures 2 and 4), which contained numerous elongated estuarine shoals.

A century later (in 1825, Figure 4c), Saint-Georges Bank (SGB) had developed to a well-defined sedimentary body with a length of 2.2 km and a volume (above the bed level of 1677) of about 10 x 10^6 m^3. The bank had a NW-SE orientation, its broad southern end was connected to the Pointe de Suzac promontory and its crown depth increased offshore. In contrast, Grande Barre (GB) shoal had decreased further in dimensions and sediment volume (to about 6 x 10^6 m^3). Taking into account the proximity of the two sedimentary structures, it is likely that some of the material eroded from the Grande Barre shoal fed the growing Saint George Bank. Other changes recorded during the 1723-1825 period include (a) the loss of the connection between the Saint-Georges and Central Channels, (b) the deepening of the Central Channel (CC) to a maximum depth of 31 m, (c) the silting of the Saintonge Channel (SC), (d) changes in the position/dimensions of the Banc des Marguerites (MB), and (e) the appearance of a deep scour offshore of Pointe de Grave.

In 1874 (Figure 4d), Saint-Georges Bank (SGB) had greatly grown (to 4.8 km in length, 1.1 km in width and to a volume of about 46 x 10^6 m^3 (above the 1677 bed level)). By that time, the bank had already acquired (more or less) its present shape, whereas the last remnants of the Grande Barre shoal had disappeared. Other changes in the inlet include the deepening of the central tidal pass offshore of Pointe de Grave, the diminishing of the Saintonge Channel and further morphological changes in the Banc des Marguerites (MB).

Between 1892 and 1960 (Figures 4e, 4f, 4g, and 4h), Saint-Georges Bank retained, more or less, the same shape and orientation. The water depth over the inshore part of its crown gradually deepened (from 2.8 m in 1892, to 3.4 m in 1920, to 3.9 m in 1940, to 4.5 m in 1960), whereas the water depths over the offshore part of its crown became shallower (from 4 m in 1892, to 3.8 m in 1920, to 2.9 m in 1940, to 1 m in 1960). The overall volume of the bank (above the 1677 bed level) increased from 60 x 10^6 m^3 in 1892 to 70 x 10^6 m^3 in 1960 (Figure 7). Other changes in the area include the further deepening (to a maximum depth of 34 m) of the Central Channel (CC), the further siltation of the upstream section of the Saintonge Channel (SC) and the stabilization of the Banc des Marguerites (MB).

During the last part of the 20th Century (1960-1999) the inlet morphology has been characterized by relative stability, although morphological changes can still be detected, particularly over Saint George Bank. In 1992, Saint George Bank was about 6 km long, 1.3 km wide, its crest was 1.7 m above the MLWS (and more sinuous than before) and its volume (above the 1677 bed level) exceeded 93 x 10^6 m^3. The data of the 1999 survey showed an increase of the overall volume of the bank by about 6 x 10^6 m^3 during the period 1992-1999 as well as significant changes (e.g. an anticlockwise rotation of the bank's crest) (Figure 6). In addition, the deep offshore of Pointe de Grave was scoured further and connected with the central tidal pass by a combination of natural and anthropogenic (dredging) processes.

Figure 5 summarizes the bathymetric differences (between 1723 and 1992) over the Gironde inlet area; these are differentiated as accretionary (more than 0.5 m water depth reduction) and erosional (more than 0.5 m water depth increase).

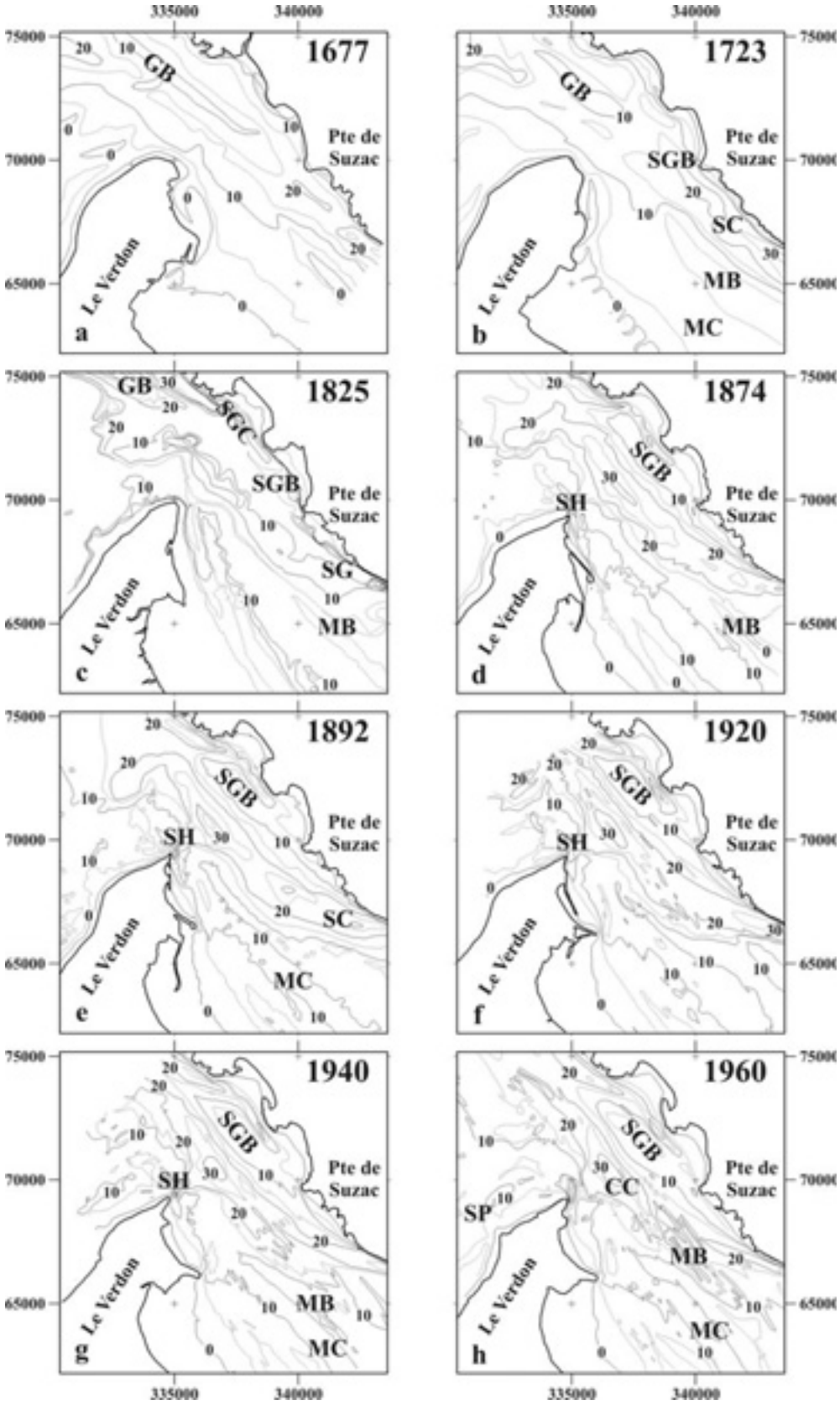

Figure 4. Historical maps of the Gironde mouth. Depths and coordinates in meters.

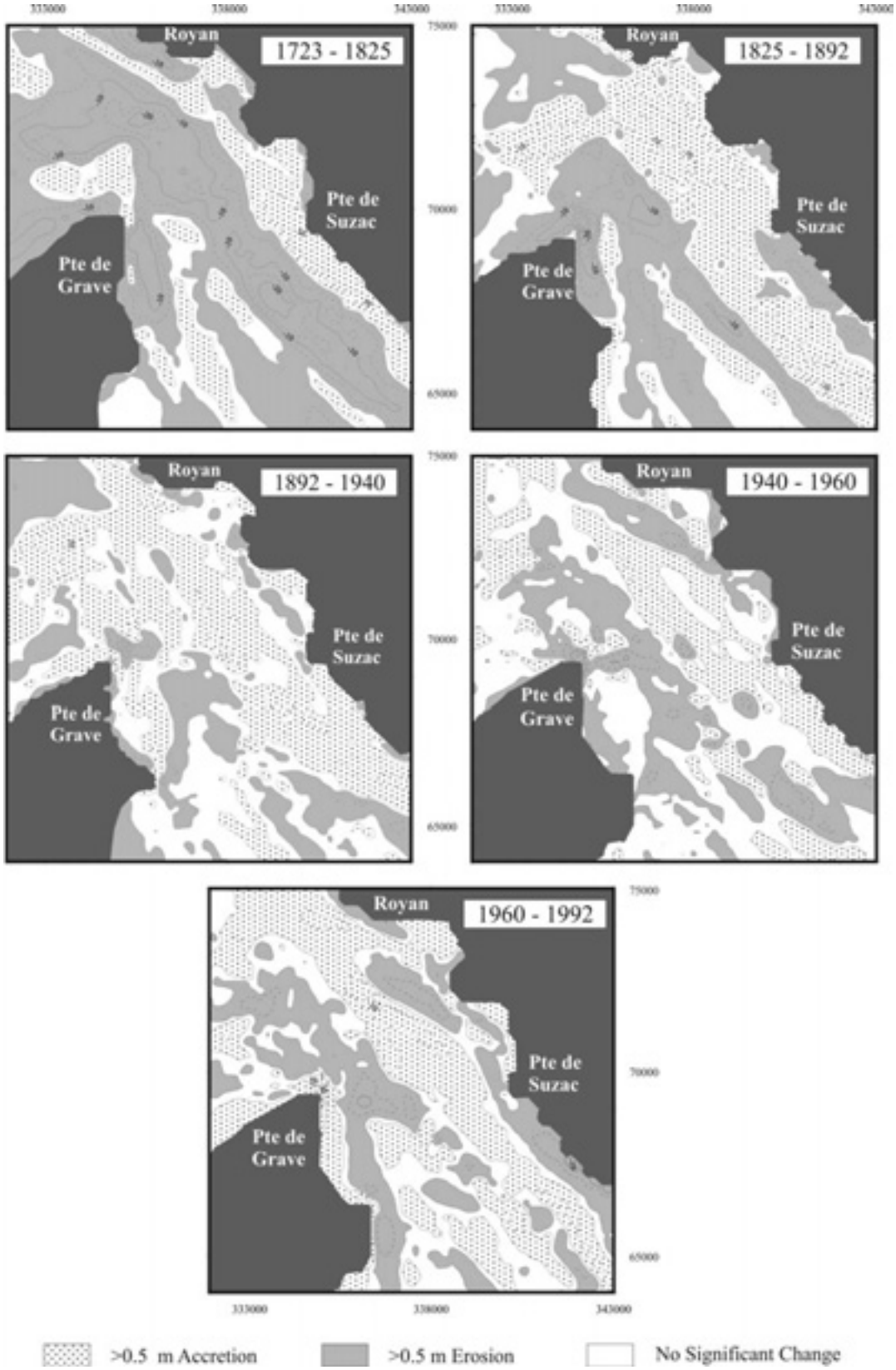

Figure 5. Accretion and erosion patterns in the Gironde Estuary mouth on the basis of the historical map comparison. Contours and coordinates in metres.

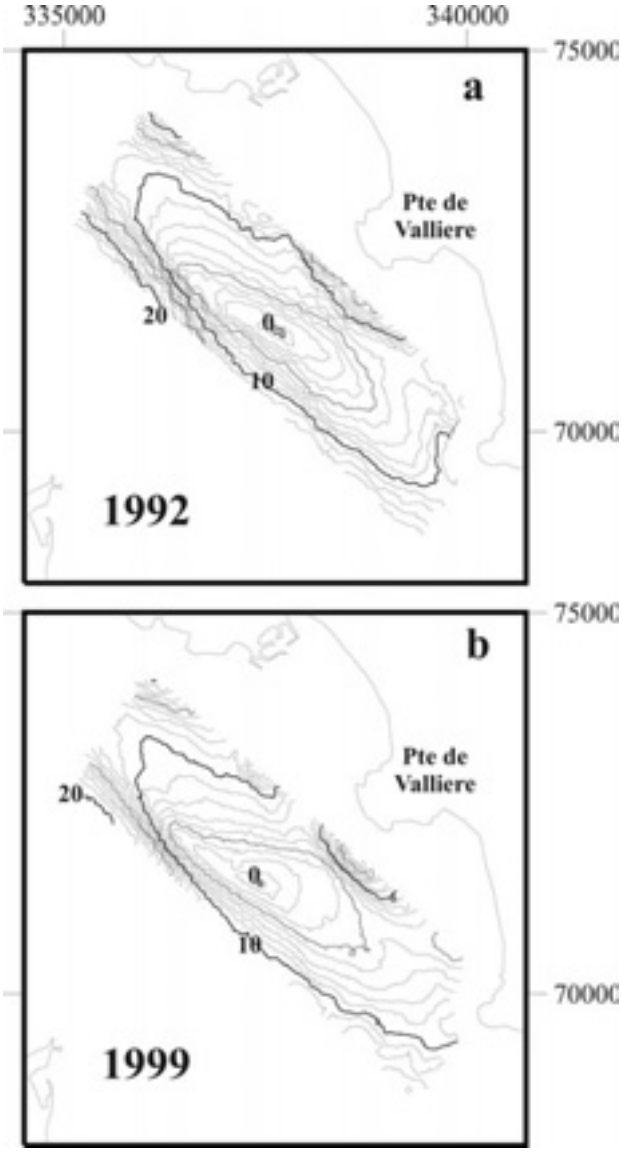

Figure 6. Morphological changes of Saint Georges Bank between a) 1992, and b) 1999.

The data show that (i) the southwestern side of the inlet as well as the main estuarine channel can be characterized mainly as erosional, whereas the northeastern side mostly as accretionary and (ii) the main changes in the area of Saint George Bank other than its formation and growth have been the destruction of Grande Barreshoal to its northwest and the development of Saint George Channel along its northeastern flank.

Internal structure

The seismic survey carried out during the present study (Figure 3) has shown the presence of an erosional surface under the surficial sedimentary deposits; in some cases, this surface shows a quite complex relief, created by the presence of local topographic highs and moderately deep-incised palaeochannels. The palaeochannels, which appear mostly in the seismic profiles obtained from the area to the south of Pointe de Suzac (Figure 3) where the relatively small thickness of the surficial sedimentary

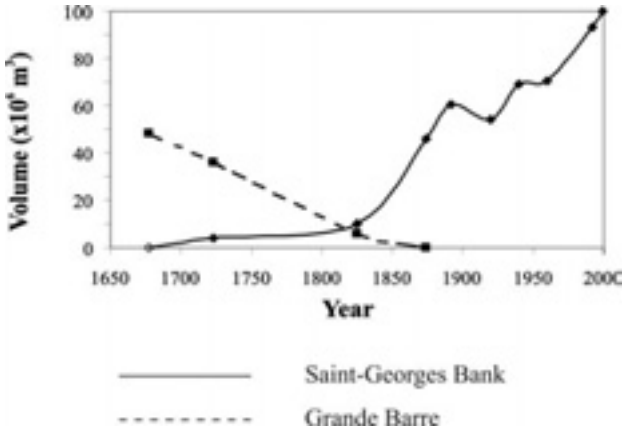

Figure 7. Volumetric changes of Saint-Georges Bank and the Grande Barre shoal between 1677 and 1999. The values shown are the mean of the envelopes which have been constructed taken into account the accuracy of the procedure (see text)..

cover allowed sufficient penetration of the high frequency signal, have mostly a NE-SW orientation. They are, probably, the now buried remnants of the small channels incised during the last lowstand to drain the Saintonge area into the main riverine channel (ALLEN and POSAMENTIER, 1993; LERICOLAIS *et al*., 2001).

Over the Saint George Bank itself, the poor penetration of the high frequency signal has not allowed the accurate mapping of the basal erosional surface and the thickness of the overlying deposits, or the imaging of internal reflectors and/or higher order bounding surfaces (BROOKFIELD, 1977; BERNE et al., 1988; BERNE et al., 1994, BASTOS et al., 2002), except where the overlying surficial sedimentary deposits pinch out (Figure 8). In these cases, it appears that the original high-relief basal erosional surface has been blanketed by a thin sedimentary cover, the upper surface of which creates a smooth pavement on which the main sedimentary body rests; such architecture is typical of hydrodynamically-controlled sedimentary bodies (e.g. COLLINS *et al*., 1995; BASTOS *et al*., 2002).

Bedforms

The sonographs showed the presence of extended fields of subaqueous dunes of different dimensions over the bank (Figure 9). The dune dimensions appear to be depth-controlled, as most of the large/very large dunes (ASHLEY *et al*., 1990) were found in the bounding channels, whereas the bank itself was covered by medium dunes.

Large/very large dunes, having a crest orientation of 60˚-240˚ N and heights and spacings ranging from 1.5 to 3 m and 80 and 160 m, respectively, were observed in the Central Channel (Figure 10); medium dunes with heights and spacings of about 0.5 and 7 m, respectively, were found superimposed upon the larger bedforms, with their crests being at oblique angles to those of the larger dunes. The direction of the cross-sectional asymmetry of the larger dunes was towards the northwest (i.e. they were ebb-oriented) and was the same on all sonographs, irrespective of the observation time; this, however, was not true for the smaller superimposed bedforms. The bed of Saint Georges Channel was also shown to be covered by sinuous-crested, regularly spaced, medium and large dunes.

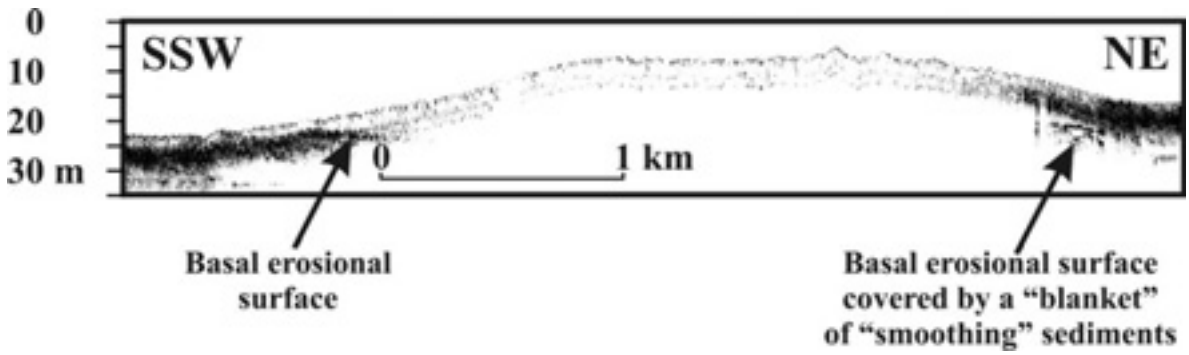

Figure 8. Seismic profile from Saint George Bank. Note that the basal reflectors show only when the sedimentary prism pinches out. For location, see Figure 3.

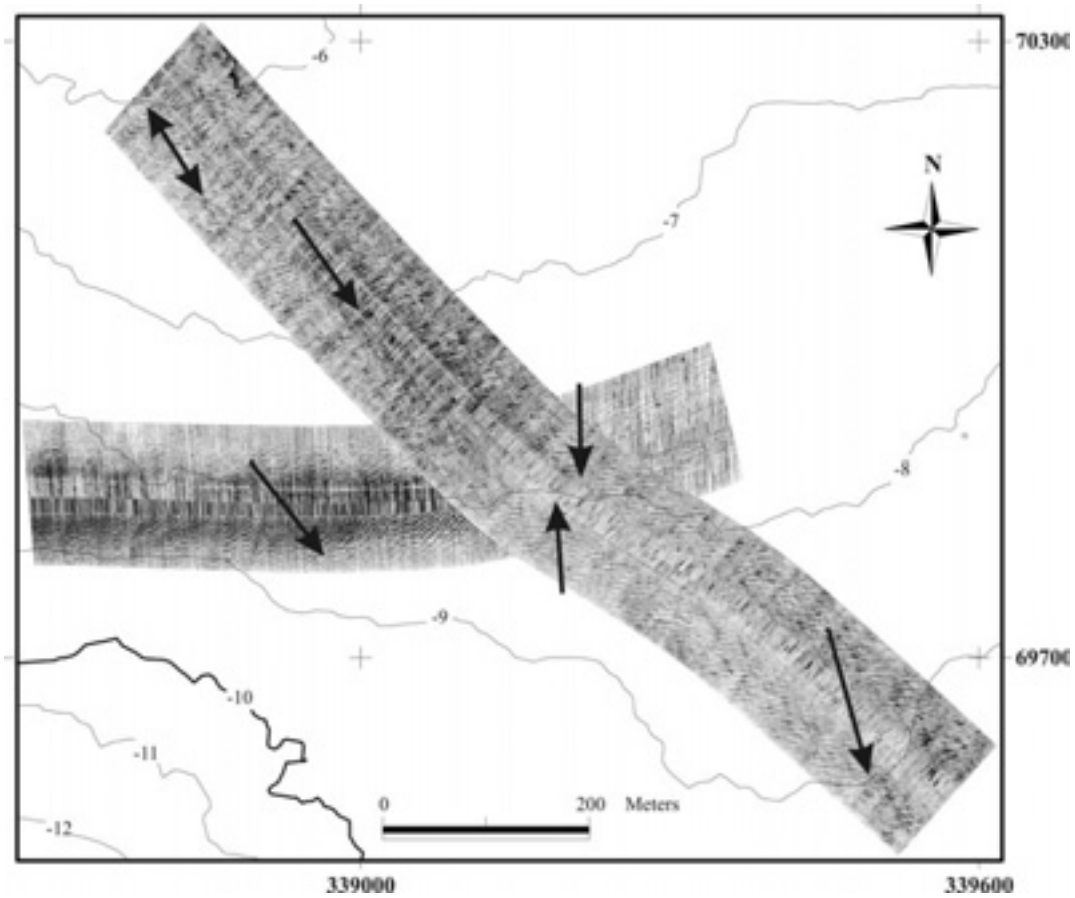

Figure 9. Side scan sonar mosaic from the bank's crown (May 2000 survey). The arrows show direction of the bedform cross-sectional asymmetry. For location, see Figure 3.

Their cross-sectional asymmetry showed to be mainly flood-dominated, although some of the smaller bedforms had in some sonographs a 'cat-back' shape showing, therefore, evidence of asymmetry reversal (BASTOS *et al*., 2003).

Over the bank itself, the bedform fields were found to consist mostly of sinuous- and/or 3D-crested, regularly-spaced medium dunes. The crest orientation of most of these bedforms showed evidence of a veering towards the crest of the bank in comparison with that of the larger bedforms within the channels (Figure 10). Their cross-sectional asymmetry was observed to be transient on sonographs obtained during different tidal stages.

The cross-sectional asymmetry of the large/very large subaqueous dunes has been used extensively as a proxy of the residual sediment transport direction (e.g. BELDERSON *et al*.,

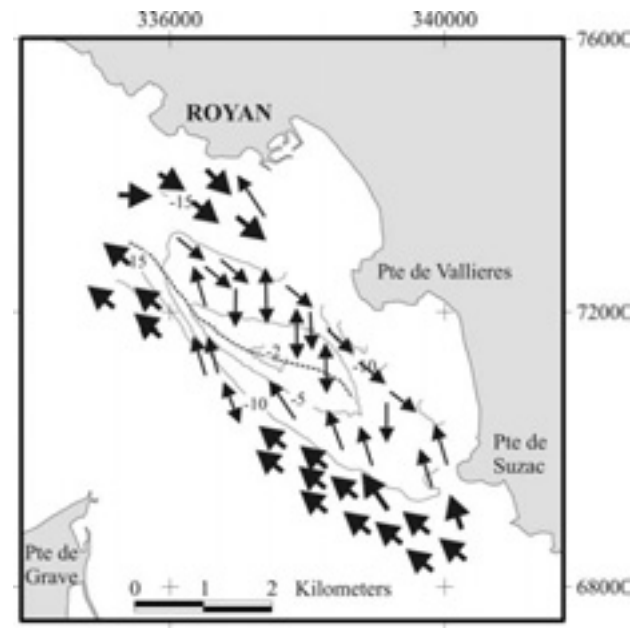

Figure 10. Location and direction of asymmetry of the subaqueous dunes of Saint George Bank. Large arrows indicate the location and direction of cross-sectional asymmetry of solitary large dunes, whereas small arrows indicate the location and direction of cross-sectional asymmetry of fields of medium dunes. Double arrows indicate symmetrical and/or cat-back forms.

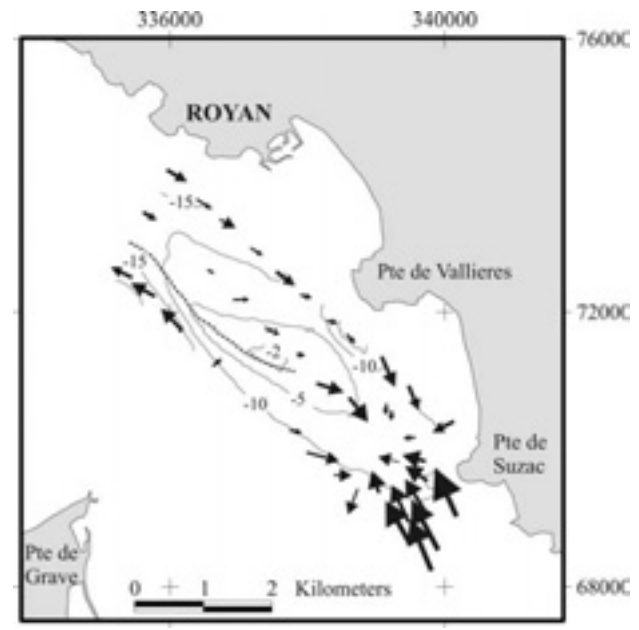

Figure 11. Patterns of surficial sediment 'transport vectors' identified according the Gao and Collins method (1992). Combined trends FB- and CB+ using the bed sediment samples collected in May 2000.

1982; GAO *et al*., 1994; LANCKNEUS and DE MOOR, 1995; VAN WESENBEECK and LANCKNEUS, 2000); in contrast, the asymmetry of the small and medium dunes can not be used to this end, as is a transient feature, rarely reflecting local current asymmetries.

As the dune cross-sectional asymmetry is hydrodynamically controlled and shallow marine and estuarine environments are influenced by various unsteady flows (i.e. tidal currents, wind and wave-induced currents, waves), it may be temporally variable (e.g. LANGHORNE, 1982; BERNE et al., 1988; BERNE et al. 1993). Tidal flow, in particular, is characterized by speed and direction variability which follows different cycles (i.e. ebb-flood, spring-neap and longer period cycles). Thus, the cross-sectional asymmetry of tidally controlled dunes may be a function of the tidal stage during which the observations have been obtained (e.g. HARRIS and COLLINS 1984; TERWINDT and BROUWER 1986; BASTOS *et al*., 2003). This is particularly true in the case of the smaller bedforms, which require smaller quantities of sediments to be transported across their crest by the reversing tidal flow in order to reverse their cross-sectional asymmetry. The geometry of the large and very large dunes, in contrast, is much more resilient, with their cross-sectional asymmetry being less sensitive to the ebb-flood and spring-neap flow modulations. If, however, wind- and wave-induced currents are superimposed on the tidal flow, then the asymmetry of the large dunes might also become unstable (LANGHORNE, 1982; HARRIS, 1991).

Therefore, it appears to be precarious to use the geometry of the bedforms as a proxy of the residual sediment transport direction, particularly that of the smaller bedforms which show a tendency to change their asymmetry according to the tidal stage. However, the spatial characteristics of the bedforms observed during the present study, particularly the cross-sectional asymmetry of the large dunes in the Central and Saint George Channels appear to be similar to those found in the same areas by MALLET *et al*. (2000). Moreover, as these areas have been surveyed during all tidal stages (both during ebb and flood) as well as during equinox spring tides (when the currents were very strong), it is safe to assume that the cross-sectional asymmetry of the large bedforms observed within the channels does not reverse with the tide. Thus, there is some evidence to suggest that the Central and Saint George Channels are characterized by opposing residual sediment transport, forming mutually evasive sediment transport pathways.

Sediments and grain-size trends

The bank's sediments consist mainly of medium (average mean size of about 1.7 ϕ (FOLK, 1980)), moderately sorted (average sorting of about 0.7 ϕ), positively skewed sand. The sediments of the southwestern flank and the northeastern extremity of the bank are coarser and more poorly sorted than those found close to the crest. Within the Central Channel, the mean sediment size increases significantly (becoming in some samples less than 0 ϕ) together with the shell fragment content.

The spatial relationships between the three main statistical parameters have been used to estimate grain size trends using the GAO and COLLINS (1992) technique. The results (Figure 11) indicate that (a) there is a convergence of transport vectors at the southeastern broad and shallow extremity of the bank and (b) there are transport vectors with opposing directions along the two flanks of the bank, indicating mutually evasive sediment transport pathways (HARRIS and COLLINS, 1991).

The comparison between the grain size trend and the dune asymmetry analyses (Figures 10 and 11) has shown that, although there is a general agreement, there are also discrepancies,

particularly over the southeastern extremity of the bank. This however is to be expected as (a) there are different sedimentary processes involved in the generation of grain-size trends and bedform asymmetry (GAO *et al*., 1994) and (b) the reversing cross-sectional asymmetry of the medium dunes which occupy most areas of the bank does not allow a reliable determination of the residual sediment transport pathways on this basis.

There are also differences between the results of the grain size trend analysis of the present study and those by MALLET *et al*. (2000), who applied the same technique in a different set of bed sediment samples from the area. MALLET *et al*. (2000) have found that (a) there is a convergence of transport vectors over the southeastern extremity of the bank and towards its crest and (b) the transport vectors over the northeastern section of the bank and along the margin of the Central Channel to its west indicate a southerly transport. These apparent differences between the results of the two studies are likely to be due to differences in the sampling spatial coverage and density. However, it appears that both results can be criticized as not being consistent. Although the relatively small density of samples used in the present study and the consequent use of a larger critical distance (D_{cr}) (D_{cr} of 950 m compared with the D_{cr} of 350 m of MALLET *et al*. (2000)) has not allowed a good resolution of transport vectors transversely to the bank, it certainly performed better in the area of the ebb-dominated Central Channel where the higher density transport vectors of MALLET *et al*. (2000) indicate a southerly (flood-dominated) residual sediment transport at some areas.

DISCUSSION

Morphological evolution of Saint George Bank

The sequential morphological data have shown that the formation and growth of the bank can be differentiated into three main evolutionary stages (Figure 12).

Stage I (late 17th century –late 19th century)

This period is characterized by the formation and rapid growth of Saint-Georges Bank. The bank appeared sometime between 1677 and 1723 and grew in a direction sub-parallel to the main tidal flow of the estuarine mouth (Figure 12a) with a mean accretion rate of about 0.35 x 10^6 m^3 yr^{-1} between 1723-1892 (but greatly accelerated after 1825 (Figure 7)). During this period, human interference (such as navigational dredging) on the estuarine morphology had been negligible compared with the natural processes (AUBIE and TASTET, 2000).

Stage II (1892–1960)

Between 1892 and 1960, Saint-Georges Bank was characterized by a rather sluggish development. The bank extended downstream (Figure 12b) with an average growth in volume of about 0.15 x 10^6 m^3 yr^{-1}. The morphological data also show that during this period the bank had a, more or less, sharp crestline. Offshore of Pointe de Vallière, the marginal Saint George Channel was deeply scoured (to a depth greater than 20 m), due probably to the action of the tidal flow. During this period, the most likely sediment sources for the bank should have been the Saint George Beach and the Saintonge coastline, as the marine sediments coming into the estuary along its northern coastline were probably trapped in beaches further downstream.

During this period, human interference increased greatly, with several coastal protection schemes (e.g. dykes, rockfills and groins) being constructed along the coast and heavy navigational dredging taking place in the estuarine channels. (AUBIE and TASTET, 2000). Since 1920s and particularly after the opening of the Western Pass Channel in 1935, there have been significant morphological changes in the area which may have also altered the tidal flow patterns (MIGNIOT, 1971).

Stage III (1960–1999)

Over the last 40 years, Saint-Georges Bank has been characterized by high accretion rates (average 0.7 x10^6 m^3 yr^{-1}) which, however, have resulted to a lateral extension of the bank (Figure 12c) and not to a vertical building up. It appears that there has been an anticlockwise rotation of the bank's crest as well as significant accretion along its offshore flank. This lateral accretion forced the local port authority to dredge twice this area removing 300 x 10^3 tons of sand each time) (Port Autonome de Bordeaux, pers. comm.). At the same period, further coastal protection works took place at the Royan Port, as well as navigational dredging (AUBIE and TASTET, 2000).

Mechanisms involved in the bank's formation-development

Although the sequential bathymetric data provide a good record of the bank's growth and development, the mechanisms involved can not be ascertained on the basis of this information alone, as contemporary hydrodynamic and sedimentological data are not available. Therefore, the discussion which follows is based on theoretical considerations as well as extrapolations from the recent data..

The sequential bathymetric data carried show that the history of Saint Georges Bank is relatively short, as its first embryonic form appeared in the beginning of the 18th century. At this point, it is interesting to note that the bank's development commenced at its southeastern section and close to the Pointe de Suzac promontory and the Saint Georges Beach. The location of its first appearance must undoubtedly have a bearing on the bank's growth mechanism.

MALLET *et al*. (2000) have studied the mechanisms involved in the maintenance of Saint Georges Bank using both *in situ* morphological and sedimentological observations and hydrodynamic model simulations. On the basis of this evidence, they found that (i) two opposing residual sediment transport paths exist along the different flanks of the bank, an ebb-oriented pathway along the margin of the steep southwestern flank that faces the Central Channel and a flood-oriented pathway along the margin of the gentler northeastern flank which faces the marginal Saint Georges Channel; (ii) there is convergence of sediment transport towards the crest of the bank; and (iii) a residual clockwise tidal current eddy exists in the area of Saint Georges Bank, centered to its west and having a flood-dominated arm along the Saint George Channel with maximum residual current velocities of 0.4 m s^{-1} and an ebb-oriented arm along the Central Channel with maximum residual current velocities of about 0.5 m s^{-1}.

The results of the present study i.e. the geometry of the bank's bedforms and the grain-size trend analysis, more or less, confirm the findings of MALLET *et al*. (2000). First, the cross-sectional asymmetry of the large dunes observed in the Central and Saint George Channels suggests that these channels may be

characterized by opposing residual sediment transport pathways, forming mutually evasive sediment transport pathways (HARRIS and COLLINS, 1991). Secondly, the veering of the orientation of the cross-sectional asymmetry of the smaller bedforms towards the bank's crest suggests a veering (and convergence) of sediment transport towards the bank's crest. Thirdly, the spatial relationships of the seabed sediment grain size parameters also indicate the presence of sediment transport pathways with opposing directions along the two flanks of the bank as well as a sediment transport convergence at the southeastern broad and shallow extremity of the bank.

MALLET *et al*. (2000) have suggested that although secondary circulation such as headland generated flow (PINGREE and

MADDOCK, 1977, 1979; PINGREE, 1978;) occurs in the area, it plays a minor role in the sandbank dynamics compared with the instantaneous tidal flow. They have proposed that the bank development and maintenance is controlled by sediment transport induced by clockwise vorticity generated from tidal flow-seabed interactions according to the theory of ZIMMERMAN (1981) and the seabed stability analysis (HUTHNANCE, 1982a, 1982b; TROWBRIDGE, 1995; HULSCHER, 1996; HULSCHER and VAN DEN BRINK, 2001)

It has been suggested elsewhere (e.g. PATTIARACHI and COLLINS, 1987; BASTOS *et al*., 2003) that the maintenance of banks close to headlands may be the result of a combination of different mechanisms such as the tidal stirring concept (PINCREE, 1978) and the bottom friction induced by the presence of bed irregularities such as the bank itself (stability model, HUTHNANCE, 1892a, 1982b). Although the proximity of the bank to the headlands of Pointe de Suzac and Pointe de Vallière suggests that their presence may have been influential to the bank's growth and maintenance and previous research over the area has identified headland associated eddies (Port Autonome de Bordeaux, 1980), we agree with the suggestion of MALLET *et al*. (2000) that promontory generated horizontal vorticity (e.g. PINGREE and MADDOCK, 1979) can not have been the primary control on the bank's development; this is because these secondary flows have been shown to be much weaker than both the instantaneous local tidal flow and the larger-scale residual flow eddy which has been identified in this area.

However, although sediment transport in accordance to the seabed stability concept (primary control) and tidal stirring (secondary control) may be the dominant mechanisms involved in the bank's growth and maintenance, they are still questions regarding the supply of the large quantities of sediments necessary for the bank's construction. Although, it is tempting to suggest that the sediments necessary for the Saint George Bank construction were mostly derived from the destruction of the downstream shoal of Grande Barre (GB) (Figure 4) and, thus, the formation and growth of Saint Georges Bank (SGB) can be viewed as an upstream migration of an estuarine mouth shoal, careful examination of the GB shoal destruction and the SGB growth rates (Figure 7) shows that most of the growth of SGB occurred after 1825, long after the GB shoal had greatly decreased in volume.

The destruction of the Grand Barre shoal is likely to have had considerable effects on the dynamics of the northwestern side of the inlet. First, the offshore depth increase resulting from the disappearance of the GB shoal increased the wave energy on the estuarine beaches of Royan and Saint George, which previously were reasonably well protected. Secondly, the detachment of the shoal from the Palmyre coast in the beginning of the 18th century (Figure 4) un-blocked the upstream wave-generated littoral drift and allowed greater quantities of marine sediments (LEGIGAN

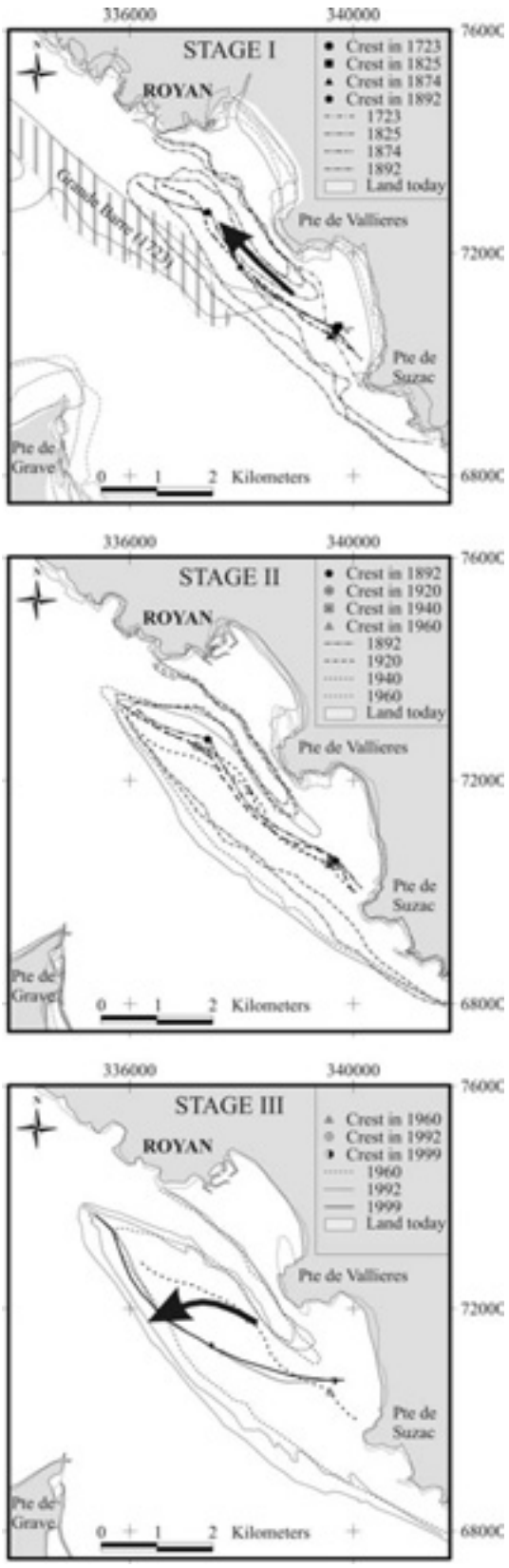

Figure 12. Evolutionary stages of Saint-Georges Bank. The arrows show the direction of the bank's lateral development.

and CASTAING, 1981; HOWA, 1987) to be transported deeper along the estuarine coast reaching the area of Saint George Bank; moreover, it allowed the easier penetration of the marginal flood tidal currents along the northeastern side of the inlet. These upstream moving sediments were then trapped in an area which (a) was characterised by the presence of mutually evasive sediment transport paths and (b) by headland associated secondary circulation.

The genesis and growth of bank is likely to be connected also to the other morphological (e.g. the shifting and scouring of the inlet's tidal channels) and related hydrodynamic changes which have taken place in the area during the last centuries. Undoubtedly, numerical experiments using the old bathymetric data would provide a valuable insight into effects of the changing bathymetry on the hydrodynamic and sedimentological regime of the estuary.

CONCLUSIONS

The results of the present study confirmed that Saint Georges Bank is maintained by a complex hydrodynamic and sediment dynamic regime consisting of a clockwise residual tidal circulation, headland associated secondary flows and trapping of sediments in a zone contained between mutually evasive sediment transport paths. There is evidence to suggest that the presence of the bank forces the veering and convergence of sediment transport pathways towards the bank's crest.

The analysis of the historical bathymetric information has shown that the initial formation of Saint-Georges Bank occurred at the end of the 17th or the beginning of the 18th century. In the absence of comparable hydrodynamic and sedimentological information the mechanisms responsible for the initial bank growth can not be ascertained. However, they might be related to the other morphological changes which took place at the estuarine inlet and particularly to the gradual destruction of the downstream estuarine shoal of Grande Barre, which (a) changed the inshore hydrodynamic regime and (b) allowed large quantities of marine sediments to move further upstream along the coast.

The Saint Georges Bank growth during the past centuries can be differentaited into 3 stages: Stage I (1723-1892), which is characterised by a rapid vertical and lateral (downsteram) growth with an average rate of 0.3 x 10^6 m^3 yr^{-1}; Stage II (1892-1960), which is characterised by a sluggish development (with an average growth of 0.15 x 10^6 m^3 yr^{-1}); and Stage III (1960-1999), during the bank's dynamics increased showing accelerated volume growth (with a rate of about 0.7 x 10^6 m^3 yr^{-1}) and a anticlockwise rotation of the crest .

Finally, it must be noted that, since the middle of the 19th century, the estuarine mouth has experienced intensive human interference (e.g. construction of coastal defences, draining of mudflats, intensive navigational dredging etc), which may also have had an impact on the morphological and sedimentological development of the estuarine mouth and, ultimately, of Saint Georges Bank itself.

ACKNOWLEDGEMENTS

This contribution was supported by the EC-TMR. Project "Sediment and Water Movement in Industrialised Estuarine Environments". Appreciation and thanks are due to the Port Autonome de Bordeaux and particularly to Mr. P. Rocco, who kindly provided the old bathymetric maps. The authors wish also to thank J. Davis (University of Southampton) for his field support during the side-scan sonar surveys. We are also grateful to Prof. P. Castaing, Dr. J.-M. Jouanneau and Dr. H. Howa (University of Bordeaux I) for their valuable discussions and comments during the preparation of the manuscript. We would also like to express our thanks to Dr. S. Poulos (University of Athens) and one anonymous reviewer for their constructive remarks.

LITERATURE CITED

ALLEN, G.P., 1971. Relationship between grain size parameter distribution and current patterns in the Gironde Estuary (France). *Journal of Sedimentary Petrology*, 41, 74-88.

ALLEN, G.P., 1972. Etude des processus sédimentaires dans l'estuaire de la Gironde. Bordeaux, France: University of Bordeaux I, Ph.D. thesis, 314 p.

ALLEN, G.P., 1991. Sedimentary processes and facies in the Gironde Estuary: a recent model for macrotidal estuarine systems. *In*: D.G. SMITH, G.E. REINSON, B.A. ZAITLIN and R.A. RAHMANI, (eds.), *Clasic Tidal Sedimentology*. Canadian Socciety of Pertoleum Geologists Memoir, 16, pp. 29-40.

ALLEN, G.P. and POSAMENTIER, H.W., 1993. Sequence stratigraphy and facies model of an incised valley fill: the Gironde Estuary, France. *Journal of Sedimentary Petrology*, 63(3), 378-391.

AMOS, C.L. and KING, E.L., 1984. Sandwaves and sand ridges of Canadian Eastern Seaboard: a comparison to global occurrences. *Marine Geology, 57,* 167-208.

ASHLEY, G.M., BOOTHROYD, J.C., BRIDGE, J.S., CLIFTON, H.E., DALRYMPLE, R.W, ELLIOT, T., FLEMMING B.W., HARMS, J.C., HARRIS, P.T., HUNTER, R.E., KRIESA, R.D., LANCASTER, N., MIDDLETON, G.V., PAOLA C., RUBIN, D.M., SMITH J.D., SOUTHARD, J.B., TERWINDT, J.H.J. AND TWITCHELL, D.C. Jr., 1990. Classification of large scale subaqueous bedforms: a new look at an old problem. *Journal of Sedimentary Petrology*, 60, 160-172

AUBIE, S. and TASTET, J.-P., 2000. Coastal erosion, processes and rates: an historical study of the Gironde coastline, Southwestern France. *Journal of Coastal Research*, 16(3), 756-767.

BELDERSON, R.H., JOHNSON, M.A. AND KENYON, N.H., 1982. Bedforms. In: A.H. STRIDE (Editor), Offshore Tidal Sands: Processes and Deposits. Chapman and Hall, London, pp. 27-57.

BASTOS, A.C., KENYON, N.H. and COLLINS, M.B., 2002. Sedimentary processes, bedforms and facies associated with a coastal headland: Portland Bill, southern UK. *Marine Geology*, 187, 235-258.

BASTOS, A.C., PAPHITIS, D.N and COLLINS, M.B., 2003. Short-term dynamics and maintenance processes of headland associated sandbanks: Shambles Bank, English Channel, UK. *Estuarine, Coastal and Shelf Science* (in press).

BERNE, G., AUFFRET, J.P. and WALKER, P., 1988. Internal structure of subtidal sandwaves revealed by high resolution seismic reflection. *Sedimentology*, 35, 5-20.

BERNE , S. CASTAING, P., LEDREZEN, E. AND LERICOLAIS, G. 1993. Morphology, internal structure and reversal of asymmetry of large subtidal dunes in the Gironde lower estuary (France). Journal of Sedimentary Petrology, 63, 780-793.

BERNE, S., TRENTESAUX, A., STOLK, A., MISSIAEN, T. and DE BATIST, M., 1994. Architecture and long-term evolution

of a tidal sandbank. The Middelkerke Bank (southern North Sea). *Marine Geology*, 121, 52-72.

BOCZAR-KARAKIEWICZ, B., AMOS, C.L. and DRAPEAU, G., 1990. The origin and stability of sand ridges on Sable Island Bank. Scotial Shelf. *Continental Shelf Research*, 10, 683-704.

BOWYER, J.K., 1992. Basin changes in Jervis Bay, New South Wales: 1894-1988. *Marine Geology,* 105, 211-224.

BRITTON, R. and BRITTON, S., 1980. Sedimentary bedforms and linear sandbanks. *In*: M.B. COLLINS, F.T. BANNER, P.A. TYLER, S.J. WAKEFIELD and A.E. JANES, AE. (eds.), *Industrial embayments and their environmental problems: a case study of Swansea Bay*. Pergamon Press, Oxford, pp. 193-214.

BROOKFIELD, M.E., 1977. The origin of bounding surfaces in ancient aeolian sequences. *Sedimentology*, 24, 303-332.

CASTAING, P., 1981. Le transfer à l'océan des suspensions estuariennes; cas de la Gironde. Bordeaux, France: University of Bordeaux I, Ph.D. thesis, 530 p.

CASTAING, P., 1989. Co-oscillating tide controls long-term sedimentation in the Gironde Estuary, France. *Marine Geology*, 89, 1-9.

CASTAING, P., FERAL, A., GAYET, J. and KLINGEBIEL, A., 1974. Centre géologique de l'embouchure de la Gironde. *C.r.som. S.G.F.*, 5, 132-134.

CASTAING, P. and FROIDEFOND, J.M., 1978. Etude morphologue et dynamique des dunes hydrauliques a l'embouchure de la Gironde. *Institut de Geologie du Bassin d' Aquitaine, Bulletin,* 24, 131-145.

CASTAING, P. and ALLEN, G.P., 1981. Mechanisms controlling seaward escape of suspended sediment from the Gironde, a macrotidal estuary in France. *Marine Geology*, 40, 101-118.

COLLINS, M.B., SHIMWELL, S.J., GAO, S., POWELL, H., HEWITSON, C. and TAYLOR, J.A., 1995. Water and sediment movement in the vicinity of linear banks: the Norfolk Banks, southern North Sea. *Marine Geology*, 123, 125-142.

CUADRADO, D.G. and PERILLO, G.M.E., 1997. Migration of intertidal sandbanks, Bahia Blanka Estuary, Argentina. *Journal of Coastal Research*, 13(1), 155-163.

DALRYMPLE, R.W and ZAITLIN, B.A., 1989. Tidal sedimentation in the in the macrotidal Cobequid Bay-Salmon River Estuary, Bay of Fundy. Field Guide, 2nd International Research Symposium on Clastic Tidal Deposition, Calgary, Alberta, Canadian Society of Petroleum Geologists. 84pp**.**

DALRYMPLE, R.W and RHODES, R.N., 1995. Estuarine dunes and bars. In: G.M.E. PERILLO (ed.) Geomorphology and Sedimentology of Estuaries. Developmnets in Sedimentology, Elsevier, Amsterdam, pp 359-422.

DALRYMPLE, R.W., ZAITLIN, B.A. and BOYD, R.J., 1992. Estuarine facies models: conceptual basis and stratigraphic implications. *Journal of Sedimentary Petrology*, 62, 1130-1146**.**

DE MOOR, G., 1989. Maintenance on the Flemish Banks, In: J.P. HENRIET and G. DE MOOR, (eds), *The Quaternary and Tertiary Geology of the Southern Bight, North Sea*, Ministry of Economic Affairs Belgian Geological Survey, pp. 185-216

DE VRIEND, H.J., 1990. Morphological processes in shallow tidal areas. *In*: CHENG, R.T. (ed.), *Residual Currents and Long-Term Transport*. Coastal and Estuarine Studies No. 38, pp. 276-301.

DOLAN, R., HAYDEN, B. and FELDER, W., 1979. Shoreline periodicities and linear offshore shoals. *Journal of Geology*, 87, 393-402.

DYER, K.R. and HUNTLEY, D.A., 1999. The origin, classification and modelling of sand banks and ridges. *Continental Shelf Research*, 19, 1285-1330.

FITZGERALD, D.M., BUYNEVICH, I.V., FENSTER, M.S. and MCKINLAY, P.A., 2000. Sand dynamics at the mouth of a rock-bound, tide-dominated estuary. *Sedimentary Geology*, 131, 25-49.

FOLK, R.L., 1980. *Petrology of the Sedimentary Rocks. (2nd Edition).* Hemphill Publishing Company, Austin, Texas, U.S.A. 182pp.

GAO, S. and COLLINS, M.B., 1992. Net sediment transport patterns inferred from grain-size trends, based upon definition of "transport vectors". *Sedimentary Geology*, 80, 47-60.

GAO, S. AND COLLINS, M.B., 1994. Analysis of grain-size trends, for defining sediment transport pathways in marine environments. *Journal of Coastal Research,* 10, 70-78.

GAO, S., COLLINS, M.B., LANCKNEUS, J., DE MOOR, G. and VAN LANCKER, V., 1994. Grain size trends associated with net sediment transport patterns: an example from the Belgian continental shelf. *Marine Geology*, 121, 171-185.

GOMEZ, E.A. and PERILLO, G.M.E., 1992. Lorgo Bank: a shoreface-connected linear shoal at the Bahia Blanca Estuary entrance, Argentina. *Marine Geology*, 104, 193-204.

GUITARD, L., 1996. Variations in the Highest High Water Springs and Lowest Low Water Springs in the Gironde Estuary over the last Century. University of Southampton and University of Bordeaux I M.Sc. Thesis, 29p.

HARRIS, P.T., 1988. Large-scale bedforms as indicators of mutually evasive sand transport and the sequential infilling of wide-mouthed estuaries. *Sedimentary Geology*, 57, 273-298**.**

HARRIS, P.T., 1991. Reversal of subtidal dune asymmetries caused by seasonally reversing wind-driven currents in Torres Strait, northeastern Australia. *Continental Shelf Research,* 11, 655-662.

HARRIS, P.T. and COLLINS, M.B., 1984. Side-scan sonar investigations into temporal variation in sand wave morphology: Helwick Sand, Bristol Channel. *Geo-Marine Letters,* 4, 91-97.

HARRIS, P.T. and COLLINS, M.B., 1991. Sand Transport: Bedload parting zone or mutually evasive transport pathways? *Marine Geology,* 101, 209-216.

HARRIS, P.T., PATTIARACHI, C.B., COLE A.R. and KEENE, J.B., 1992. Evolution of subtidal sandbanks in Moreton Bay, eastern Australia. *Marine Geology,* 103, 225-247**.**

HOUBOLT, J.J.H.C., 1968. Recent Sediments in the southern Bight of the North Sea. *Geologie Mijnb.,* 47 (4), 245-273.

HOUTHUYS, R., TRENTESAUX A. and DE WOLF, P., 1994. Storm influences on a tidal sandbank's surface (Middelkerke Bank, southern North Sea). *Marine Geology*, 121, 23-41.

HOWA, H., 1987. Le littoral du Nord Médoc (Gironde): évolution d'une côte sableuse en érosion. Bordeaux, France: University of Bordeaux I, Ph.D. thesis, 258 p.

HOWA, H., 1993. Hydrodynamique et flux sédimentaires dans une domaine d'embouchure. *Proceedings of 4ème Congrès Français de Sédimentologie*, Paris, Publication ASF, 181-182.

HULSCHER, S.J.M., 1996. Tidal and residual currents around a Norfolk sandbank. *Estuarine and Coastal Marine Science*, 19, 105-117.

HULSCHER, S.J.M and VAN DEN BRINK, G.M., 2001, Comparison between predicted and observed sand waves and sand banks in the North Sea. *Journal of Geophysical Research*, 106 (C5), 9327-9338.

HUTHNANCE, J.M., 1982a. On one mechanism forming linear sandbanks. *Estuarine and Coastal Marine Science*, 14, 79-99.

HUTHNANCE, J.M., 1982b. On the formation of sand banks of finite extent. *Estuarine and Coastal Marine Science*, 15, 277-299.

LANCKNEUS, J. and DE MOOR, G, 1995. Bedforms on the Middelkerke Bank, southern North Sea. In: B.W. FLEMMING and A. BARTHOLOMA (eds), *Tidal signatures in Modern and Ancient Sediments*, Blackwell Science, pp. 33-51.

LANGHORNE, D.N., 1982. A study of the dynamics of a marine sandwave. *Sedimentology*, 29, 571-594.

LEGIGAN, P. and CASTAING, P., 1981. La pénétration des samples marins dans les estuaries, cas de la Gironde. *Académie des Sciences, Comptes Rendus*, 292, 207-212.

LERICOLAIS, G., BERNE, S. and FENIES, H., 2001. Seaward pinching out and internal startigraphy of the Gironde incised valley on the shelf (Bay of Biscay). *Marine Geology*, 175, 183-197.

LESUEUR, P.and TASTET, J.P., 1994. Facies, internal structures and sequences of modern Gironde-derived muds on the Aquitaine inner shelf. *Marine Geology*, 120, 267-290.

LIST, J.H., JAFFE, B.E., SALLENGER, A.H. and HANSEN M.E., 1997. Bathymetric comparisons adjacent to the Louisiana barrier islands: processes of large-scale change. *Journal of Coastal Research*, 13(3), 670-678.

MALLET, C., 1998. Etude de la dynamique des sédiments non cohésifs de l'embouchure de la Gironde. Bordeaux, France: University of Bordeaux I, Ph.D. Thesis, 184 p.

MALLET, C., HOWA, H., GARLAN, T., SOTTOLICHIO, A. and Le HIR, P., 2000. Residual transport model in correlation with sedimentary dynamics over an elongate tidal sandbar in the Gironde estuary (SW France). *Journal of Sedimentary Research*, 70(5), 1005-1016.

MIGNIOT C., 1971. L'évolution de la Gironde au cours des temps. *Buletin Institut de Géologie du Bassin d'Aquitaine*, Bordeaux, 11, 221-279.

PATTIARATCHI, C.B., 1985. Hydrography and Sedimentology of a Headland Associated Linear Sandbank: Scarweather Sands, Northern Bristol Channel. Unpublished PhD Thesis, University of Wales. 128pp.

PATTIARATCHI, C. and COLLINS, M.B., 1987. Mechanisms for linear sandbanks formation and maintenance in relation to dynamical oceanographic observations. *Process in Oceanography*, 19, 117-176.

PEDREROS, R., HOWA, H.L. and MICHEL, D., 1996. Application of grain size trend analysis for the determination of sediment transport pathways in intertidal areas. *Marine Geology*, 135, 35-49.

PINGREE, R.D., 1978. The formation of the Shambles and other banks by tidal stirring of the seas. *Journal of Marine Biological Association*, 58, 211-226.

PINGREE, R.D. and MADDOCK, L., 1977. Tidal eddies and coastal discharge. *Journal of Marine Biological Association of the United Kingdom*, 57, 869-875.

PINGREE, R.D. and MADDOCK, L., 1979. The tidal physics of headland flows and offshore tidal bank formation. *Marine Geology*, 32, 269-289.

Port Autonome de Bordeaux, 1980. Etude sédimentologique des plages de Saintonge et du banc Saint-Georges. Bordeaux, France: Internal Report, 30 p.

ROBINSON, I.S., 1981. Tidal vorticity and residual circulation. *Deep-Sea Research*, 28, 195-212.

ROBINSON, I.S., 1983. Tidally induced residual flows. In: B. Johns (ed.), *Physical Oceanography of Coastal and Shelf Seas. Elsevier Oceanography Series 35,* Elsevier Amsterdam pp. 321-356.

SALOMON, J.C. and ALLEN, G.P., 1983. Rôle sédimentologique de la marée dans les estuaires à fort marnage. *Notes et mémoires de la Compagnie Francaise des Pétroles*, 18, 57-85.

Service Hydrographique et Oceanographique de la Marine, 1968. Courants de marée dans la Manche et sur les côte françaises de l'Atlantique. Bordeaux, France: Internal Report, 500 p.

SIGNELL, R.P. and GEYER, W.R., 1991. Transient eddy formation around headlands. *Journal of Geophysical Research*, 96, 2561-2575.

SIGNELL, R.P. and HARRIS, C.K., 2000. Modelling sanbank formation around tidal headlands. In: M.L. Spaulding, A.F. Blumberg (eds) *Proceedings 6th Interantional Conference Estaurine and Coastal Modelling*, New Orleans, LA, November 1999, ASCE Press.

SMITH, J.D., 1969. Geomorphology of a sand ridge. *Journal of Geology*, 77, 39-55.

SWIFT, D.J.P. and FIELD, M.E., 1981. Evolution of a classic sand ridge field: Maryland sector, North American inner shelf. *Sedimentology,* 28, 461-482.

TERWINDT, J.H.J. and BROUWER, M.J.N., 1986. The behaviour of intertidal sand waves during neap-spring tidal cycles and the relevance of palaeoflow reconstruction. *Sedimentology*, 3, 1-31.

TRENTESAUX A., STOLK, A., TESSIER, B. AND CHAMLEY, H., 1994. Surficial sedimentology of the Middelkerke Bank (southern Noth Sea). *Marine Geology*, 121, 43-55

TROWBRIDGE, J.H., 1995. A mechanism for the formation and maintenace of shore-oblique sand ridges on storm dominated shelves. *Journal of Geophysical Research*, 100 (C8), 16071-16086.

VAN WESENBEECK, V. and LANCKNEUS, J., 2000. Residual sediment transport on a tidal sand bank: A comparison between the modified McLaren model and bedform analysis. *Journal of Sedimentary Research*, 70, 470-477.

ZIMMERMAN, J.T.F., 1981. Dynamics, diffusion and geomorphological significance of tidal residual eddies. *Nature,* 290, 549-555.

Journal of Coastal Research	SI 41	43-52	STRAEE 2002	Ferrara, Italy	ISSN 0749-0208

Mixing depth experiments on an estuarine dissipative beach; St. Georges Beach, Gironde (France)

R. Gonzalez†, P. Ciavola‡*, C. Corbau‡, S. Falati‡, and Ó. Ferreira∞

†CIACOMAR/CIMA,
Universidade do Algarve
Avenidas 16 de Junho s/n
8700 - 311 Olhão, Portugal

‡Dip. Scienze della Terra
Università di Ferrara
C.so Ercole I D'Este
44100 Ferrara, Italia
*Email: cvp@dns.unife.it

∞FCMA/ CIMA
Universidade do Algarve
Campus de Gambelas
8000 Faro, Portugal

ABSTRACT

GONZALEZ, R.; CIAVOLA, P.; CORBAU, C.; FALATI, S.; and FERREIRA, Ó., 2004. Mixing depth experiments on an estuarine beach; St. Georges Beach, Gironde (France). *Journal of Coastal Research*, SI 41, 43-52. Ferrara (Italy), ISSN 0749-0208

Mixing depth experiments were carried out on the dissipative St. Georges Beach (Gironde Estuary) in September 1999 (SWAMGIR 2) and May 2000 (SWAMGIR 4). The mixing depths were found to reach maximum values of about 0.15 m during SWAMGIR 2, and 0.1 m during SWAMGIR 4. The analysis of results compares measured data with data calculated using the formula proposed by FERREIRA *et al*. (2000). Two approaches were used: a) an averaged approach, using global slope and breaking wave height at all points, and b) a non-averaged approach, considering varying breaking wave heights and slopes across the beach. Comparisons show that in general the formula works well for both approaches with calculated results within the magnitude of measured values. However, while the non-averaged approach produced significantly better results on the low-tide terrace, the standard deviation of the difference between calculated and measured values was much higher.

ADDITIONAL INDEX WORDS: *mixing depth, dissipative beaches, surf zone, foam.*

INTRODUCTION

The sediment mixing depth, defined as the layer of active sediment overlying an immobile bed (SHERMAN *et al*., 1993), is also considered to be the layer at which nearshore sediment transport occurs (e.g. SUNAMURA and KRAUS, 1985; SHERMAN *et al*., 1993, 1994; CIAVOLA *et al*., 1997). Consequently, its determination is crucial for the quantification of sediment movement, and for the understanding of nearshore processes.

The understanding of the mixing depth has made significant progress in recent years (CIAVOLA *et al*., 1997; FERREIRA *et al*., 2000). In experiments, usually the spatially averaged mixing depth of the experiment location over a certain time period is estimated. KRAUS *et al*. (1982), and KRAUS (1985) established an empirical relationship between breaker height H_b and sediment-mixing depth Z_m. However, CIAVOLA *et al*. (1997) pointed out that this relationship cannot be applied for beaches with slopes larger than 0.08. FERREIRA *et al*. (2000) were able to include the beachface slope tanβ in the formulation, establishing a more global relationship.

The main purpose of the experiments discussed here, and carried out on St. Georges Beach (Gironde Estuary, France) was to test this relationship on an extremely dissipative beach. Furthermore, as MALVAREZ and COOPER (2000) point out, most authors still utilize averaged parameters for nearshore coastal engineering and geomorphological studies, not considering temporal and spatial variations in studied areas. Consequently, it was a further aim of this study to compare averaged parameters with spatially referenced topographic and hydrodynamic data.

REGIONAL SETTING

St. Georges beach is a dissipative pocket beach located near St. Georges de Didonne, on the eastern shore of the mouth of the Gironde Estuary in SW France (Figure 1). The beach is limited to the north and the south by rocky headlands. It is sheltered from the main estuarine channel by St. Georges Bank, a linear sand bank near the Suzac headland, where the Gironde Estuary has a width of about 4.5 km. The bank is classified as a down-estuary feature (MALLET *et al*., 2000). It is elongated, 5 km long, 1.2 km wide and rises up to 1 m above the level of mean low water spring tides. The sandbar has an asymmetric cross-section, sloping gently to the northeast and more steeply to the southwest. The asymmetry is a result of an up-estuary migration of the sand bar during the past years. The bar consists of fairly well sorted medium sand, with marine characteristics. It is related to the longshore drift along the right margin of the outlet by tidal currents and wave processes, and can thus be considered a part of the "flood-tidal delta" of the Gironde estuary (LEGIGAN and CASTAING, 1981).

The semidiurnal tidal regime is macrotidal, with amplitudes of 5.3 m at spring tides (measured at Pointe de Grave opposite St. Georges across the Estuary). The mean annual fresh water discharge is around 900 m^3s^{-1}, but the mean monthly discharge varies strongly from winter months (4500 m^3s^{-1} in January) to summer ones (235 m^3s^{-1} in August), with exceptional floods reaching 7500 m^3s^{-1} (CASTAING, 1981).

The tide is semi-diurnal and almost symmetric near the mouth of the estuary, in the area of St. Georges Bank. The main central channel is ebb-dominated, whereas St. Georges Channel is flood

dominated, with maximum surface currents of about 2 ms^{-1}. The line of sediment flux convergence corresponds to the crest of the St. Georges Bank. Along-shore Counter-currents can be observed downstream of the Suzac and La Vallière headlands (see location on Figure 1), penetrating into the pocket beaches and circulating trough the St. Georges Channel, leading to anticlockwise current gyres during the flood and clockwise current gyres during the ebb tide (MALLET *et al*., 2000).

Swell waves mainly arrive from west and northwest (MALLET *et al*., 2000). The average swell within the estuary is characterised by heights of less than 1 m, and mean wave periods of 5 to 6 s (HOWA, 1993). Wave refraction generates an up-estuary drift along the right margin, where the study area is located.

METHODS

The sediment mixing depth at St. Georges beach was studied in September 1999 (SWAMGIR 2) and May 2000 (SWAMGIR 4). Four mixing depth experiments were carried out during SWAMGIR 2 and 4 each. While these were performed on consecutive low tides during SWAMGIR 2, only every second low tide was studied during SWAMGIR 4. The set-up of the experiments on the beach is sketched on Figure 2.

There are different methods to calculate sediment mixing depths, be it by inserting rods with or without washers into the sand (CLIFTON, 1969; GREENWOOD and HALE, 1980), by filling holes with marked sands (KING, 1951; WILLIAMS, 1971), or by assessing the re-distribution of previously placed sand tracers in shallow beach cores (KRAUS *et al*., 1982; KRAUS, 1985; CIAVOLA *et al*., 1997).

During SWAMGIR 2 5 columns of rods were aligned in a crosshore direction at a distance of 10 m from each other, both in long- and cross-shore direction (Figure 2). During SWAMGIR 4 4 columns were placed at a distance of 12.5 m. The first 4 rows at the top of the beach were placed at a distance of 6 m; for all other rows a distance of 10 m was used (Figure 2). The height of the portion of the rods sticking out of the sand was measured after each tide, to allow a determination of sand level variations over all tides.

For the measurement of the mixing depths, sand was removed from the beach before the experiments. The sand was washed and dried. A dark blue aniline colour dissolved in alcohol was used as dye. The sand and colour were thoroughly mixed and dried. The dried sand was dry sieved using a 250 µm mesh sieve in order to separate sand grains sticking together with dried dye.

The marked sand was placed in holes of known depth during low tides at a distance of 0.3 m from each rod. The position of the holes with marked sand was rotated by 90 degrees for each tide, in order not to mix the marked sands with the sand of previous tides. The marked sand was excavated after the tide, exposing the full vertical section of the hole. The height difference of marked sand before and after the tide gave the value of sand eroded during the tide. The height of fresh sand accumulated on top of the marked sand corresponded to the accretion. Of these two values (erosion and accretion), the higher value defines the mixing depth. Because of the high water table it was not possible to fill the two rows at the bottom of the beach rows (I, and J in Figure 2) with marked

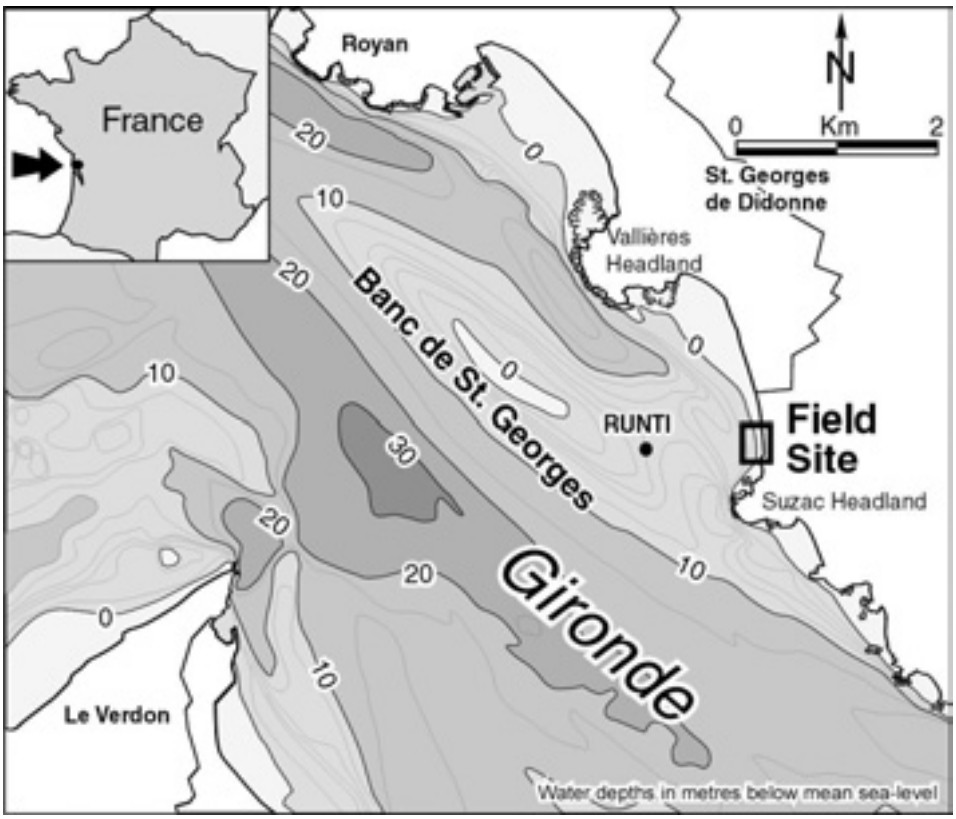

Figure 1. Study area and experiment location.

sand during any of the experiments.

One sand sample was collected at each row during SWAMGIR 2, in order to determine grain sizes, and their cross-shore variation. The samples were washed, dried at 50º C, and dry-sieved at half phi intervals. As the amount of fines was very small (<< 1%), these were not analysed separately. Mean grain size, standard deviation, and skewness of the samples were calculated using the moments method (KRUMBEIN, 1936).

Beach profiles using a theodolite were carried out every 24 hours during the first, and at every low tide during the second experiment. The theodolite was always placed at the same origin on top of the storm berm. The absolute height of this origin was later determined using a differential GPS.

The slope at each position of holes filled with marked sand was calculated using the average of slopes below and above these positions, which were known from the beach profile measurements with the theodolite. These averaged values were later used to calculate the surf scaling parameter ε (GUZA and INMAN, 1975; WRIGHT and SHORT, 1984) defined as

$$\varepsilon = (a_i \ \omega^2) / (g \tan^2\beta) \qquad (1)$$

where a_i is the incident wave amplitude (H/2; H being the wave height), ω is the angular frequency of the incident wave ($2\pi/T$; T being the wave period), and tanβ is the beach slope; and the Iribarren number ξ (BATTJES, 1974) defined as

$$\xi_b = \tan\beta / (H_b/L_0)0.5 \qquad (2)$$

where H_b is the breaking wave height, and L_0 the offshore wave length.

For SWAMGIR2 no wave data from the beach was available, due to equipment failure. Instead, refracted values from the RUNTI Lander (Remote Unit for Nearshore Transport Investigation, see CIAVOLA *et al*., 2000), positioned about 1.5 km away at a mean depth of 11 m on the eastern edge of St. Georges Bank were used (see position on Figure 1). This instrument measured 20 minute data bursts at 4 Hz every hour, generating time series of current velocity, water level, and turbidity. The processing of the time series was carried out using a suite of Matlab routines, which included the computation of the characteristics of surface waves using spectral analysis. The significant breaking wave height H_b was calculated using the following formula:

$$H_b = g \tan\beta / T \qquad (3)$$

Where g is the acceleration due to gravity, tanβ is the beach slope, and T is the wave period (GALVIN, 1968). The numerical model of CAVIGLIA (1994) was used to obtain wave characteristics in the surf zone (width of the surf zone), transferring the measured deep-water data and assuming linear wave theory.

During SWAMGIR 4 three rigs, each one equipped with a Valeport electromagnetic current meter, a pressure transducer and a flux-gate compass were set up inside the field of rods (see location on Figure 2). All sensors continuously gathered data at 2 s intervals. From these measurements only wave data relevant to the experiments will be mentioned here. For a detailed discussion of the measurements see CORBAU *et al*. (2002).

To calculate the significant breaking wave height at each position, the tidal curve was intersected with the beach profiles. This determined the time during which waves were active at each location and their breaking height. A running average of computed heights from one hour before to one hour after the determined time was created to give some allowance for the variation of the breaking position of waves on this very dissipative beach. Results are shown on Figure 3.

Predicted mean sediment mixing depths Z_m were calculated using the formula by FERREIRA *et al*., (2000):

$$Z_m = 1.86 \ H_{bs} \tan\beta \qquad (4)$$

where H_{bs} is the significant breaking weave height, and tanβ is the beach slope.

During the last tide of SWAMGIR 4 a 20 m long trench was filled with the remaining marked sand in order to obtain a

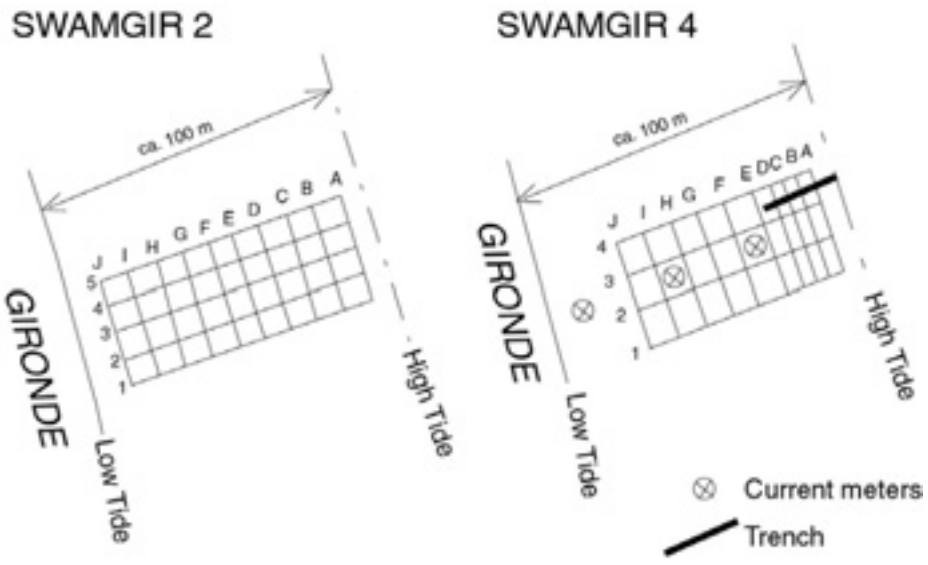

Figure 2. Experimental set-up for SWAMGIR2 and SWAMGIR 4. Both experiments were carried out at the same location. Grid-nodes indicate the injection-points of marked sand for mixing depth experiments.

continuous mixing depth profile (see location on Figure 2). To guarantee that the trench had the same known depth at all points, a slat with the dimensions 1m x 0.02 m x 0.04 m was hammered into the sand and carefully removed, creating a 4 cm deep and 2 cm wide trench. The total length of the trench was 20 m, beginning at the top of the high water mark. The trench was only in operation for one tidal cycle.

Additional observations carried out during rising tides include the semi-quantitative estimation of run-up using the rods as visual markers, and the visual estimate of breaking wave heights. These observations were carried out during both SWAMGIR 2 and 4.

RESULTS

Wave regime

Figure 3 shows the significant breaking wave heights at St. Georges Beach at each row of rods. Breaking wave heights on St. Georges Beach were found to vary with the tidal cycle as the sheltering effect of St. Georges Bank is reduced with the rising tide (Ciavola *et al*., 2002). Consequently, different areas of the beach are affected by differing breaking wave heights.

Meteorological and oceanographic conditions worsened considerably towards the end of SWAMGIR 2, as a storm developed. Breaking wave heights had heights between 1 and 2 m for the first three tides, and heights between 1.6 and 2.6 m for the last tide. These values were significantly higher than during SWAMGIR 4, where breaking wave heights were between 0.7 and 1.1 m, showing much less variation (Figure 3).

Beach characteristics

St. Georges Beach at the location the experiments were carried out has a width of approximately 120 m at low tide and about 20 m at high tide, from the dune scarp to the end of the low-tide terrace. A steep vegetated dune ridge delimits the top of the backshore. The top of the swash zone is characterised by an about 10 m wide berm (marking the top of beach profiles), and an only a few metre wide storm-berm between the dune ridge and fair-weather berm. A well-developed low tide terrace with a width of ca. 90 m dominates the foreshore morphology (Figure 4).

The sand at the locality of the experiments was found to be fine grained, with mean grain size diameters of 2.14 ϕ at the beach face and 2.00 ϕ towards the bottom of the low tide terrace. The sand was usually well sorted at the top (standard deviation 0.34 ϕ), and moderately sorted at the bottom of the beach (standard deviation 0.62 ϕ), where coarse grains skew the grain size curve negatively (skewness at the bottom -0.34 ϕ, compared to 0.06 ϕ at the top).

An analysis of the four beach profiles for SWAMGIR 2 shows that most morphological alterations occurred on the top of the foreshore and the backshore. During the course of the experiment the berm placed at the top of the low tide terrace was levelled, and the sand transferred towards the lower backshore, leading to a levelling out of the profile (Figure 4). Beach slopes were found to be very low, with typical values between 0.02 and 0.04, only showing higher values around 0.06 to 0.08 at the scarp between storm- and fair weather-berm at the beginning of the experiment.

A calculation of the surf scaling parameter ε shows that most of the beach is classified as ultra-dissipative (ε > 200), with extreme values near the crest of the fair weather-berm, where the beach slope in the near row B of rods is near 0 (Figure 4). It can be seen that while the berm is eroded, values of ε become less extreme, while backshore values increase.

All waves occurring on the beach during the course of SWAMGIR 2 were of spilling type, according to the values indicated by the Iribarren number ξ (Figure 4).

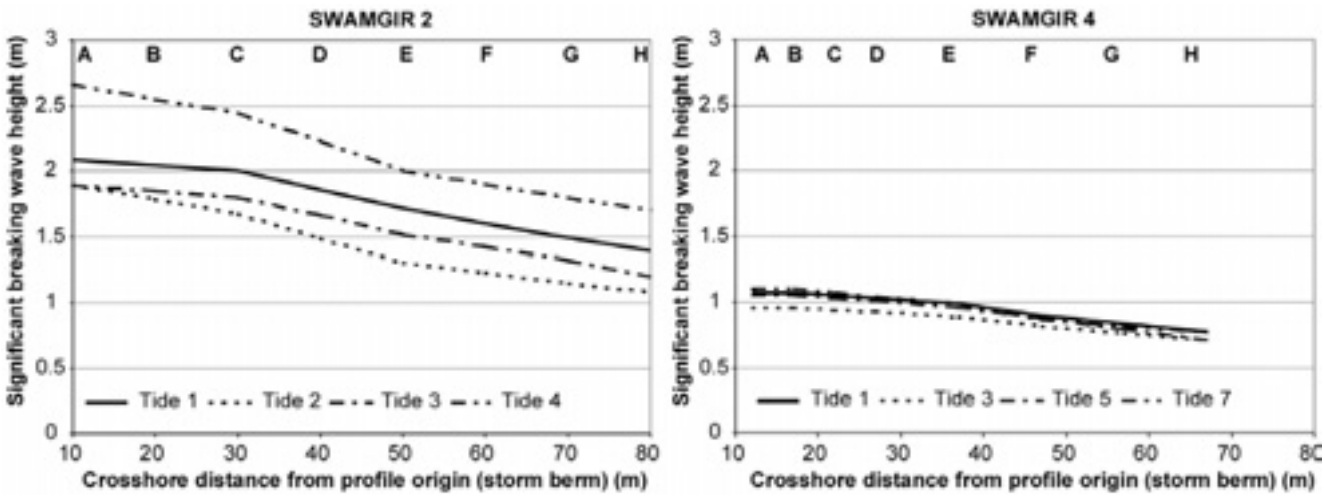

Figure 3. Computed crosshore variation of breaking wave heights during the experiments. Note the high-tide increase of significant breaking wave height, as the sheltering effect of St. Georges Bank is reduced with rising water levels (*cf*. CIAVOLA *et al*., 2002). Letters on the graph indicate the injection-points of marked sand for mixing depth experiments.

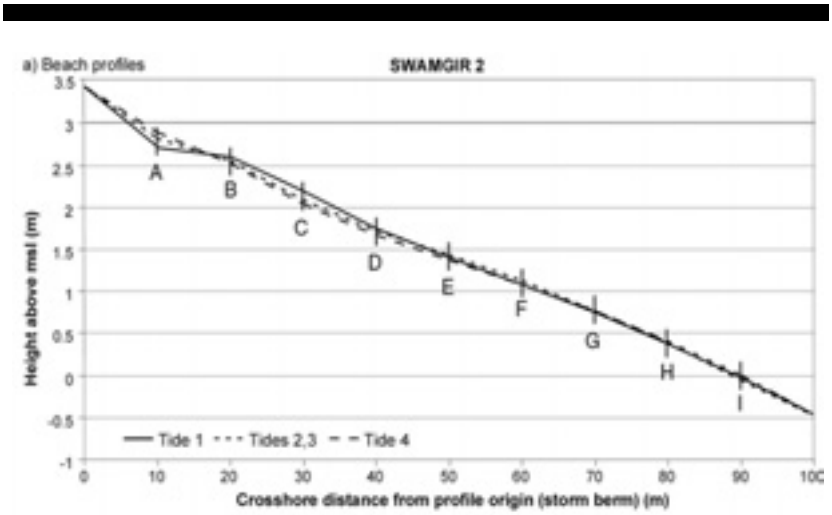

b) Surf scaling parameters

	A	B	C	D	E	F	G	H
Tide 1	75.09	3844.99	335.48	175.66	266.90	308.95	260.88	196.50
Tide 2	77.52	1091.38	166.71	161.53	251.71	241.90	188.04	149.16
Tide 3	109.59	669.02	183.96	250.65	446.18	338.83	242.97	197.89
Tide 4	136.71	548.80	251.03	322.40	512.23	445.56	341.28	267.30

Ultra-dissipative Dissipative

c) Iribarren numbers

	A	B	C	D	E	F	G	H
Tide 1	0.41	0.06	0.23	0.27	0.22	0.20	0.22	0.25
Tide 2	0.40	0.11	0.27	0.28	0.22	0.23	0.26	0.29
Tide 3	0.34	0.14	0.26	0.22	0.17	0.19	0.23	0.25
Tide 4	0.30	0.15	0.22	0.20	0.16	0.17	0.19	0.22

Spilling Plunging

Figure 4. a) Beach profile evolution during SWAMGIR 2; b) corresponding surf scaling parameters and c) Iribarren numbers for each tide and row in the experiment.

Figure 5 shows the beach profiles for low tides 1, 3, 5, and 7 for SWAMGIR 4, i.e. the low-tide periods where marked sand was placed. Note that the swash during this experiment only reached the bottom of the backshore, and the storm-berm was not affected.

The beach had a convex profile. A small depression within the low-tide terrace was filled in during the first three tides, when considerable amounts of sand accumulated on the beach. As during SWAMGIR 2 the bottom of the low tide terrace showed the smallest variations. Slopes ranged from 0.01 to 0.04, only showing slightly higher values of 0.05 at the bottom of the beach.

Similar as during SWAMGIR 2 the surf scaling parameter ε indicates that most of the central portion of the low tide terrace was ultra-dissipative during the experiment, while the top and bottom portions were dissipative (Figure 5).

In contrast to SWAMGIR 2 the calculated Iribarren numbers ξ for SWAMGIR 4 suggest that waves at the lower backshore and at the bottom of the lower terrace were of plunging type, while they were spilling on the central portion of the low-tide terrace.

Mixing depths

Mixing depths at St. Georges Beach were all found to lie between 0 and 0.1 m, with the exception of Tide 1 during SWAMGIR 2, when mixing depths between 0.05 and 0.15 m were observed (Figure 6). The standard deviation for all values was 0.028 m.

Figure 7 shows a comparison between measured and predicted values using the formulas by FERREIRA *et al*. (2000), both for parameters averaged across the entire beach, and for varying parameters. It was found that globally the predicted values are within 0.05 m of the measured ones, irrespective of the fact whether the parameters were averaged or not, although in most cases the not averaged values show a slightly better fit with measured data.

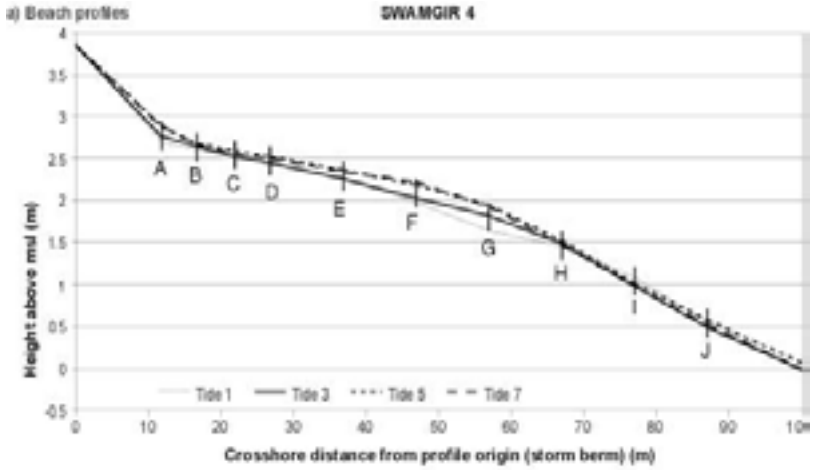

b) Surf scaling parameters

	A	B	C	D	E	F	G	H
Tide 1	219.07	780.46	381.34	413.00	139.58	121.94	175.77	47.07
Tide 3	174.16	385.72	598.46	384.73	285.39	229.42	71.47	38.94
Tide 5	102.10	966.36	994.41	618.67	661.08	214.31	67.99	53.57
Tide 7	119.06	637.68	1148.58	1990.81	1004.44	194.76	109.35	62.21

Ultra-dissipative Dissipative

c) Iribarren numbers

	A	B	C	D	E	F	G	H
Tide 1	0.52	0.28	0.40	0.38	0.65	0.70	0.58	1.13
Tide 3	0.62	0.43	0.34	0.42	0.50	0.55	1.01	1.04
Tide 5	0.84	0.28	0.27	0.35	0.35	0.61	1.09	0.89
Tide 7	0.81	0.35	0.26	0.20	0.28	0.63	0.86	1.14

Spilling Plunging

Figure 5. a) Beach profile evolution during SWAMGIR 4. Only every second beach profile is shown; b) corresponding surf scaling parameters and c) Iribarren numbers for each tide and row in the experiment.

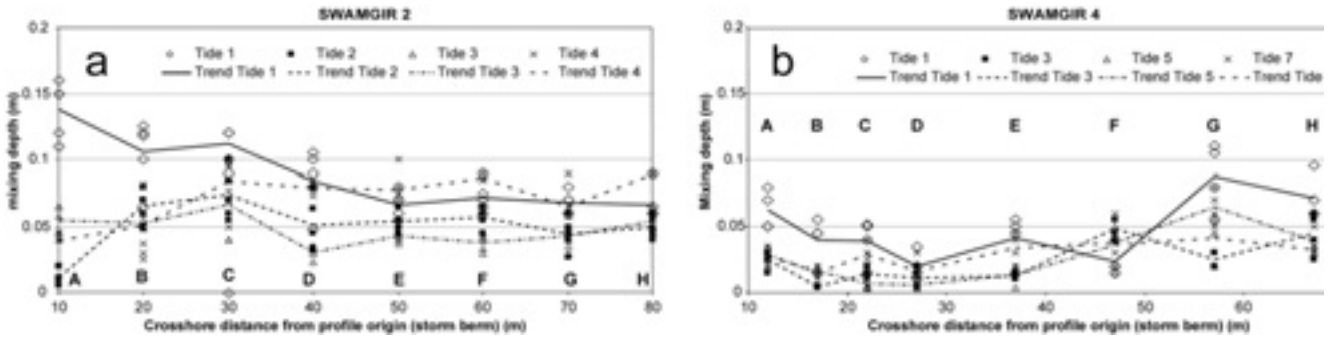

Figure 6. Observed crosshore mixing depths during SWAMGIR 2 and 4. The trend lines give the average values for each row. Letters on the graph indicate the injection-points of marked sand for mixing depth experiments.

The large majority of calculated values slightly overestimate the real values. The lowest overestimations occurred at the lower backshore and bottom of the low-tide terrace during SWAMGIR 4. Here some values, especially during tide 1, were actually slightly underestimated.

Larger differences between real and calculated values were found with increasing proximity to the top of the beach during SWAMGIR 2 (Figures 7 a, c). Not averaged and averaged calculated values show an almost identical overall difference to the observed values, with 0.056 m for non-averaged parameters compared to 0.055 m using all averaged wave height and beach slope values. The standard deviation for not averaged parameters was at 0.045 m significantly higher than for averaged parameters at 0.028 m.

However, if the data from the top 30 m of the beach is ignored, the average difference for non-averaged parameters is 0.037 m, showing a much better fit to the formula by FERREIRA *et al.* (2000) compared to 0.059 m for all averaged parameters. In both cases the standard deviation lies at 0.016 m.

The differences between prediction and observation were generally much lower during SWAMGIR 4, which featured more moderate meteorological conditions. Here, the use of non-averaged wave height and beach slope results in an average difference of just 0.015 m, while being 0.017 m for averaged parameters.

Trench analysis

Figure 8 shows the variation of mixing depth observed in the continuous trench in the top 20 m of the beach. The top of the trench was located just 0.3 m below the maximum observed run up.

With the exception of the bottom 2 m of the profile the newly deposited sand was always larger than the amount of eroded sand, thus being the determining factor for the mixing depth. In general, the mixing depth was found to be between 0.01 and 0.04 m.

Two mixing depth maxima can be observed in Figure 8. The first is between 1 and 3 m, the second approximately between 9 and 11 m from the top of the trench.

The first mixing depth maximum coincides with an area where a lot of sand was transported in the foam of waves and deposited as the run up reaches the top of the beach. Observations on the beach showed that the top 2 m of the beach were not reached by more than 10 waves during the entire tide.

The second maximum coincides approximately with the breaking point of waves at the maximum height of the tide. This is simultaneously the area where most marked sand was eroded, but also where most new sand was deposited.

DISCUSSION

In general, values predicted with the formula by FERREIRA *et al*. (2000) agreed well with the observed mixing depths. This agreement was better for SWAMGIR 4 where the average breaking wave heights were considerably lower (Figure 3). This might be related to the fact that the breaking wave heights used for SWAMGIR 2 were predicted values, derived from values measured offshore, as opposed to those of SWAMGIR 4, which were measured *in situ*. It is interesting to note that this experiment included dissipative as well as ultra-dissipative portions of the beach, and spilling as well as plunging waves. The only noticeable impact of this seems to be a slightly larger spread of observed mixing depth values for similar wave and morphological conditions (Figure 6b).

The large differences between calculated and observed mixing depth values at the backshore during SWAMGIR 2 are of particular interest. The calculated mixing depths consistently overestimate observed mixing depths. The breaking wave heights during this period exceeded breaking wave heights observed by other studies. The maximum breaking wave height observed to date were of 1.6 m, observed by SUNAMURA and KRAUS during their Hirono-1 experiment (for a full summary on breaking wave heights considered by authors see FERREIRA *et al*., 2000).

The only reasonable agreement between predictions and observations at the top of the beach during SWAMGIR 2 was for values relating to the first tide. This can possibly be explained with the observed transfer of sand from the eroding submerged berm to the top of the swash zone at the beginning of the experiment (see upper portion of beach profiles on Figure 4a). While the first profile still showed a relatively well-developed berm, the character of profiles during the following tides was increasingly homogenous, without significant morphological features.

Figure 6 shows clearly that during all tides after the first tide mixing depths decrease with increasing wave height (cf. Figure 3), contrary to the premise made since KING (1951) by several authors relating mixing depth to breaking wave height (e.g. SUNAMURA and KRAUS, 1985; KRAUS, 1985; CIAVOLA *et al*., 1997; FERREIRA *et al*., 2000). It could be speculated, that, at least on this type of highly dissipative beaches, the slope has more weight as a determinant parameter for the mixing depth than the breaking wave height; contrary to the increasing wave height the slope consistently decreased at this portion of the beach during the course of SWAMGIR 2.

The trench experiments carried out during this study indicate two other factors of importance. As already pointed out by KING (1951) and KRAUS (1985), the mixing depth is greatest around the breakpoint of waves in shallow water, which was confirmed by the observations in the trench, showing a maximum in this area, at about 10 m crosshore distance from the top of the trench (Figure 8). KRAUS (1985) attributes such a maximum to the mechanical scouring and intense turbulence generated in the region of breakers and colliding waves in the swash zone. Additionally, it could be speculated that the time during which waves are breaking over a particular location might have some influence in the mixing depth. Furthermore, as the trench analysis on Figure 8 shows, the mixing depth values decrease slightly below the maximum at 10 m crosshore distance from the top of the trench. This might indicate that even though the significant breaking wave height increases with rising tide level, the effectiveness of this increase in increasing mixing depths is reduced by the rising water level of the tide.

The second factor of relevance found in this study was the transport of significant amounts of sand by foam in the top of the swash zone, observed during run up estimations. This sand carried to the top of the beach led to unexpected large mixing depth values at the top of the beach during the trench experiments. COOPER and JACKSON (2001) identified the transport of sand by foam in the swash zone as a major agent for sand transport on dissipative beaches. Other authors point indirectly to this, although none mentions foam directly: FERREIRA *et al*. (2000) include the run up extension as an important factor in their list of factors influencing mixing depth, and KRAUS (1985) indicates a maximum mixing depth at the shoreline, creating a bi-modal distribution of mixing depth maxima.

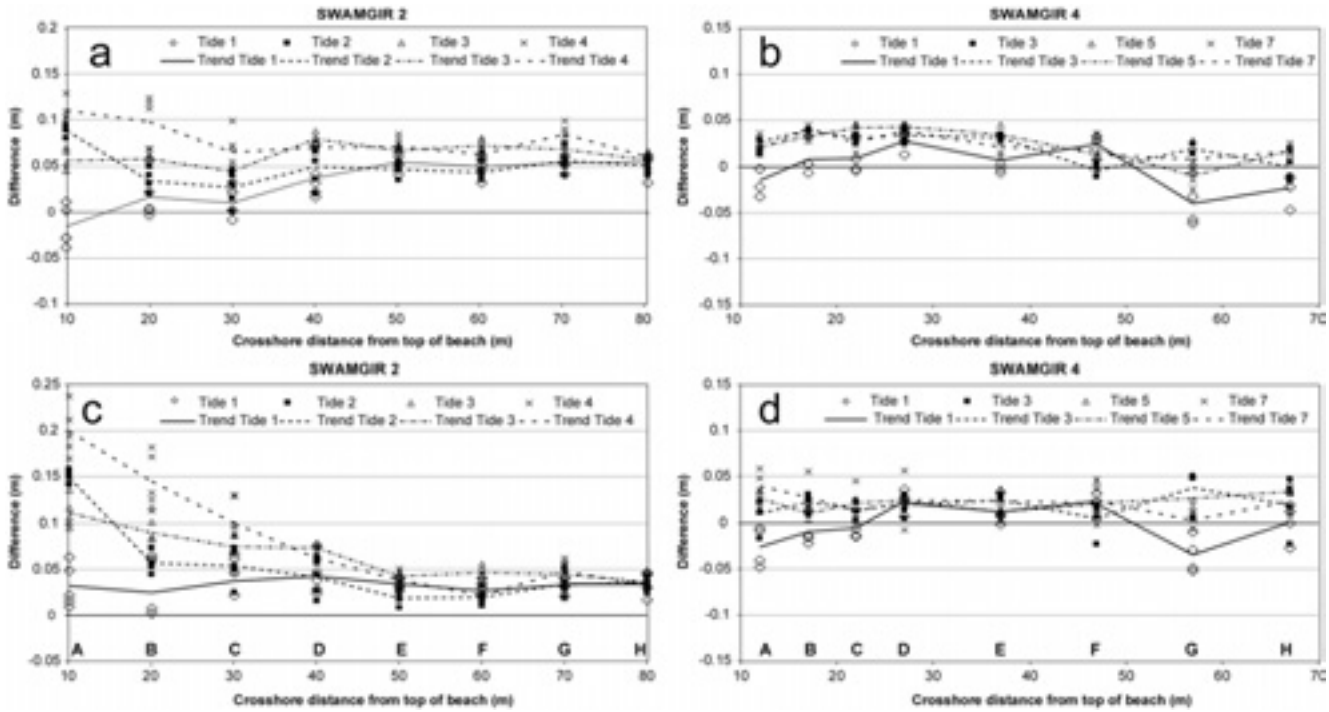

Figure 7. Crosshore differences between mixing depths calculated using the formula by Ferreira et al. (2000) and observed values. Positive differences are overestimations of the observed values, negative differences are underestimated mixing depths. The trend lines give the averages for each row. Letters on the graph indicate the injection-points of marked sand for mixing depth experiments. a) and b) were calculated using averaged breaking wave heights and beach slopes; c) and d) use varying values for each row.

As JACKSON and NORDSTROM (1993) point out, this type of bi-modal crosshore distribution probably only applies to beaches with foreshore slopes of less than 0.08. Waves on steep beaches under the described conditions are usually of plunging type. On highly dissipative beaches the areas under the direct influence of breaking waves are in most cases well separated from the zone where foam runs up the beach. On steeper beaches with plunging waves these two areas are usually not as well separated, and subsequent breakers can easily erode sand deposited by foam from previous waves.

It was not possible to verify whether the grain size had any influence on mixing depth variations, as pointed out by other authors (e.g. KING, 1951; SUNAMURA and KRAUS, 1985), since the sand on St. Georges Beach showed great uniformity. On the other

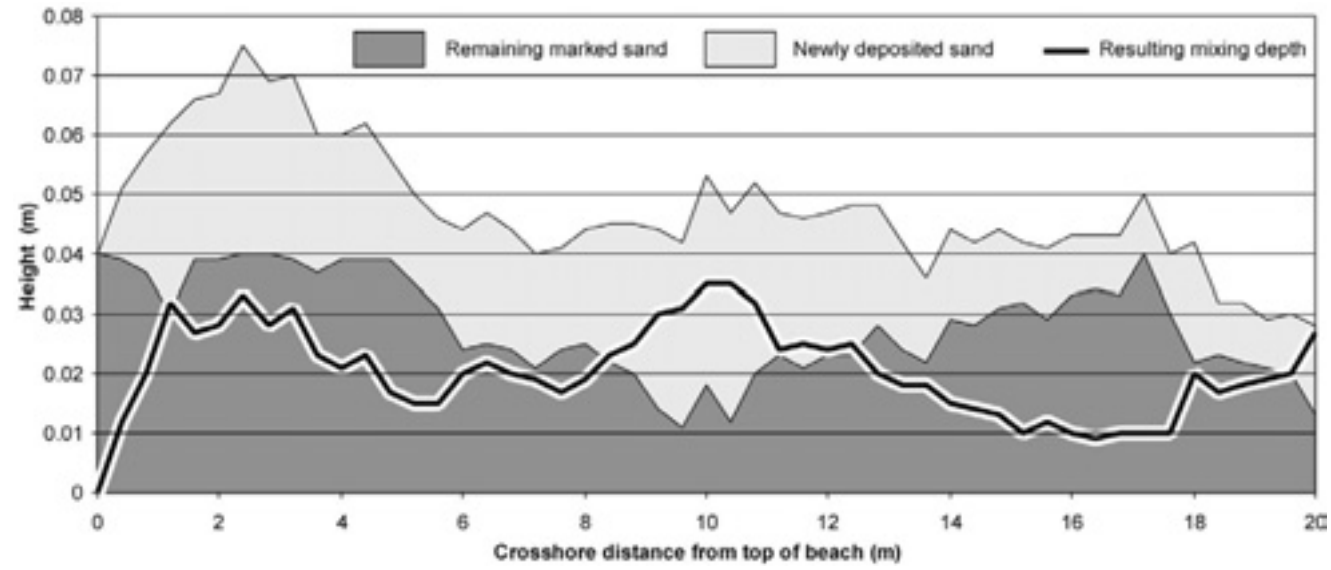

Figure 8. Crosshore variation of mixing depth obtained from a continuous trench profile.

hand, this was of advantage for the experiments carried out here, as it could be ruled out as a variable influencing mixing depth (the ultimate proof for the influence of grain size, thus, would be a beach with varying grain size, little or no variation in slope, and constant wave height).

It is interesting to observe that even on an apparently homogenous beach with few distinct morphological features, the spread of observed values at each row can be as much as plus/minus 0.05 m, with standard deviations for all values of 0.022 m and 0.028 m for, respectively SWAMGIR 2 and 4. A possible influence in this spread of values might be the occurrence of horizontal circulatory 'gyres', creating weak rip currents. These were well visible during the calmer conditions of SWAMGIR 4, with long-shore cell diameters of about 50-70 m, but may also have been present during SWAMGIR 2.

In contrast to other studies on mixing depth, this paper used non-averaged parameters to analyse mixing depth variations across the beach, and compared them to values calculated with averaged parameters. Our approach indicates that breaking wave height and slope are indeed dominant factors determining the mixing depth, particularly on the low-tide terrace. Furthermore, it is possible that other parameters such as shear stress, and the transport of particles in foam, can cause more or less large variations from expected values. Large variations from the slope/breaking wave height model occur mainly at the top of the beach. Here, the complex boundary conditions created by the influence of breaking wave height, swash, runup, morphology, shear stress, slope, and energy are no longer covered by the simple equation relating breaking wave height and slope to mixing depth. It is very likely that a high level of human activity - which was not the case on St. Georges Beach - will further alter and influence sediment mixing depths (probably increasing them), as footprints loosen the top layer of sand, and create a highly irregular and rough beach surface which can easier be remobilised by waves.

The experiments carried out on St. Georges beach show that when trying to evaluate mixing depths, it is not enough to simply consider the immediate area where mixing depths are to be determined. The non-averaged approach clearly shows how the surrounding area and external factors influence results, in this particular case offshore sand bars and tidal level influencing breaking wave heights.

CONCLUSIONS

Two mixing depth experiments were carried out on the dissipative St. Georges Beach in the Gironde Estuary in September 1999 (SWAMGIR 2) and May 2000 (SWAMGIR 4). The mixing depths were found to reach maximum values of about 0.15 m during SWAMGIR 2, and 0.1 m during SWAMGIR 4.

In general, observed mixing depth values agreed well with the values predicted using the formula by FERREIRA *et al*. (2000). However, in most cases the formula overestimated mixing depths slightly. The accuracy of predictions could be improved by using non-averaged beach parameters, predicting the local mixing depth using spatially varying topographic and hydrodynamic values.

It can be concluded that although the formula which combines breaking wave height and beach slope works well, there are other factors influencing mixing depths. Such factors include sand transport via foam in the swash, relocation of local morphological features, and bottom currents created by horizontal gyres.

ACKNOWLEDGEMENTS

The field experiments would not have been possible without the help of Miguel Castro (Universidade do Algarve), Urs Neumeier (formerly Universitá di Ferrara), John Davis and Beth (Southampton Oceanographic Centre), and Chris Waddup (Oxford University). François Pinet (Observatoire du Littoral) carried out the determination of the profile origin height. The Southampton Oceanographic Centre generously provided Electromagnetic current meters for SWAMGIR 4. The authors wish to thank an anonymous reviewer for insightful comments and suggestions. Financial support for this study was provided by the European Union project SWAMIEE (FMRX-CT97-0111). Óscar Ferreira kindly acknowledges support by the CROP Project (Cross-Shore Processes on Contrasting Environments, PDCTM/P/MAR/15265/1999).

LITERATURE CITED

BATTJES, J.A., 1974. Surf similarity. *Coastal Engineering '74*, 446-480.

CASTAING, P. 1981. Le transfert à l'océan des particules estuariennes, cas de la Gironde. *Thèse d'Etat*, n° 701, Université de Bordeaux I, 530 pp.

CAVIGLIA, F.J., 1994. Computation of longshore currents and sediment transport. *Computers and Geosciences,* 20(6), 905-917.

CIAVOLA, P.; FALATI, S.; CALDERONI, G., and TESSARI, U., 2000. RUNTI: A lightweight benthic lander for the assessment of sediment transport in lagoon environments. *Proceedings of Oceanology Internacional 2000*, 1-7 March 2000, Brighton, UK, 451-460 (CD-Rom).

CIAVOLA, P.; FALATI, S.; CORBAU, C.; PAIREAU, O., and COLLINS, M., 2002. Modulation of wave energy by a linear sand bank in the Gironde Estuary (France): Implications for Coastal Zone Management. *Littoral 2002*, EUROCOAST/EUCC, Porto, 149-153.

CIAVOLA, P.; FERREIRA, Ó.; TABORDA, R., and DIAS, A., 1997. Field observations of sand-mixing depths on steep beaches. *Marine Geology,* 141, 147-156.

CLIFTON, H.E., 1969. Beach lamination: nature and origin. *Marine Geology*, 7, 553-559.

COOPER, J.A.G. and JACKSON, D.W.T., 2001. Surficial beach structures formed by wave-generated foam. *The Journal of Geology*, 109, 780-788.

CORBAU, C.; CIAVOLA, P.; GONZALEZ, R., and FERREIRA, Ó. 2002. Measurements of cross-shore sand fluxes on a macrotidal pocket beach (Saint-Georges Beach, Atlantic Coast, SW France). *Journal of Coastal Research*, SI 36, 182-189.

FERREIRA, Ó.; CIAVOLA, P.; TABORDA, R.; BAIRROS, M., and DIAS, J.A., 2000. Sediment mixing depth determination for steep and gentle foreshores. *Journal of Coastal Research*, 16 (3), 830-839.

GALVIN, C.J., 1968. Breaker type classification on three laboratory beaches. Journal of Geophysical Research, 73 (12), 3651-3659.

GREENWOOD, B. and HALE, P.B., 1980. Depth of activity, sediment flux and morphological change in a barred nearshore environment. In: McCANN, S.B. (Ed.): *The Coastline of Canada*, Pap. 80-10, Geological Survey Canada, Halifax, 89-109.

GUZA, R.T. and INMAN, D.L., 1975. Edge waves and beach cusps. *Journal of Geophysical Research*, 80, 2997- 3012.

HOWA, H., 1993. Hydrodynamique et flux sédimentaires dans une domaine d'embouchure. *Proceedings of 4ème Congrès Français de Sédimentologie*, Paris, Publication ASF, 181-182.

JACKSON, N.L. and NORDSTROM, K.F., 1993. Depth of activation of sediment by plunging breakers on a steep sandy beach. *Marine Geology*, 115, 143-151.

KING, C.A.M., 1951. Depth of disturbance of sand on sea beaches by waves. *Journal of Sedimentary Petrology*, 21, 131-140.

KRAUS, N.C.; ISOBE, M.; IGARASHI, H.; SASAKI, T.O., and HORIKAWA, K., 1982. Field experiments on longshore sand transport in the surf zone. *Proceedings 18th International Coastal Engineering Conference*, ASCE, New York, 970-988.

KRAUS, N.C., 1985. Field experiments on vertical mixing of sand in the surf zone. *Journal of Sedimentary Petrology*, 55, 3-14.

KRUMBEIN, W.C., 1936. Application of logarithmic moments to size frequency distributions of sediments. *Journal of Sedimentary Petrology*, 6, 35-47.

LEGIGAN, P. and CASTAING, P., 1981. La penetration des sables marins dans les estuaries, cas de la Gironde. *Comptes Rendus de l'Académie des Sciences*, 292, 207-212.

MALLET, C.; HOWA, H.L.; GARLAN, T.; SOTTOLICHIO, A., and LE HIR, P., 2000. Residual transport model in correlation with sedimentary dynamics over an elongate tidal sandbar in the Gironde Estuary (Southwestern France). *Journal of Sedimentary Research*, 70 (5), 1005-1016.

MALVAREZ, G.C. and COOPER, J.A.G., 2000. A whole surf zone modelling approach as an aid to investigation of nearshore and coastal morphodynamics. *Journal of Coastal Research*, 16(3), 800-815.

SHERMAN, D.J.; SHORT, A.D., and TAKEDA, I., 1993. Sediment-mixing depth and bedform migration in rip channels. *Journal of Coastal Research*, SI 15, 39-48.

SHERMAN, D.J.; NORDSTROM, K.F.; JACKSON, N.L., and ALLEN, J.R., 1994. Sediment mixing depths on a low-energy reflective beach. *Journal of Coastal Research*, 10 (20), 297-305.

SUNAMURA, T. and KRAUS, N.C., 1985. Prediction of average mixing depth of sediment in the surf zone. *Marine Geology*, 62, 1-12.

WILLIAMS, A.T., 1971. An analysis of some factors involved in the depth of disturbance of beach sand by waves. *Marine Geology*, 11, 145-158.

WRIGHT, L.D. and SHORT, A.D., 1984. Morphodynamic variability of surf zones and beaches: a synthesis. *Marine Geology*, 56, 93-118.

Journal of Coastal Research	SI 41	53-57	STRAEE 2002	Ferrara, Italy	ISSN 0749-0208

Non-conservative behaviour of uranium in the Gironde Estuary (France) during low river discharge

K.J. Smith, C. Organo, L. León Vintró† and P.I. Mitchell

Department of Experimental Physics, University College Dublin, Belfield, Dublin 4, Ireland
† Tel: +353−1−7162221; Fax: +353−1−2837275; e-mail: luis.leon@ucd.ie

ABSTRACT

SMITH, K.J., ORGANO, C., LEÓN VINTRÓ, L. and MITCHELL, P.I., 2004. Non-conservative behaviour of uranium in the Gironde Estuary (France) during low river discharge. *Journal of Coastal Research*, SI 41, 53-57. Ferrara (Italy), ISSN 0749-0208

Data on the behaviour of dissolved (<0.45 μm) uranium isotopes in the Gironde estuary mixing zone, gathered in the course of a research campaign in summer 1999, are presented in this paper. The data clearly show uranium in the estuary to behave non-conservatively during periods of low river discharge, with removal taking place at salinities in the range 0–16‰. Results from measurements of the evolution of ^{238}U concentrations at a sampling location within the non-conservative region during a tidal cycle suggest that this removal is most pronounced at low salinities. Ultrafiltration experiments revealed that the retention of ^{238}U by a 10 kDa ultrafilter was negligible, indicating that there was little, if any, uranium associated with colloidal species in these waters. The mechanism responsible for the transport of uranium through the estuary is seasonally variable being dependent on the prevailing river discharge.

ADDITIONAL INDEX WORDS: *Gironde estuary; mixing zone; uranium; non-conservative behaviour; colloids*

INTRODUCTION

Rivers represent the main source of dissolved uranium to the oceans. The supply of this element through a particular estuary depends, however, on the lithology of the drainage basin and on the geochemical reactions taking place at the fresh water/seawater interface. Further, data from various studies show that behaviour of uranium can vary from 'conservative' to highly 'non-conservative' within the mixing zone, being functionally dependent on a number of factors including the prevailing discharge rate (BOROLE *et al*., 1982; SARIN AND CHURCH, 1994; SWARZENSKI *et al*., 1995; WINDOM *et al*., 2000).

In this paper, new data on the distribution of dissolved uranium along the Gironde estuary (SW France), including its temporal evolution during a full tidal cycle, are presented in an attempt to better understand the physical and chemical transformations controlling the fate of dissolved uranium within the estuary's mixing zone.

The Gironde estuary is the product of the confluence of the Garonne and Dordogne rivers. Mean annual water discharge is 24 $\times 10^9$ m^3 yr^{-1}, and solid discharge 2.2 $\times 10^{12}$ g yr^{-1}. The Gironde can be considered as a partially mixed, macrotidal estuary with a relatively long flushing time (ranging from 20 days in flood to 86 days during low water discharge). Hydrodynamic mechanisms in the Gironde estuary produce a well developed *turbidity maximum*, with suspended matter concentrations ranging from 0.1 to 10 g l^{-1}. During certain periods, a *fluid mud* layer, where turbidity reaches 400 g l^{-1}, accumulates on the estuary bottom. The total sediment mass of these two turbidity accumulations is twice the annual riverine solid discharge and greatly favours solid–liquid interactions (ELBAZ-POULICHET *et al*., 1984; KRAEPIEL *et al*., 1997).

MATERIALS AND METHODS

Water samples were collected in the course of a sampling campaign (SWAMGIR-1) in the Gironde estuary in late June 1999. The location of the sampling stations in the estuary are shown in Figure 1. Following retrieval, near-surface water samples (75 l) were promptly filtered through membrane filters (0.45 μm) and uranium pre-concentrated in 25 l sub-samples by co-precipitation with $Fe(OH)_3$ for total dissolved uranium determination. Measurement of colloidal uranium was carried out on the remaining 50 l of microfiltered water by tangential-flow ultrafiltration using polysulphone membrane cassettes with cut-offs corresponding to a nominal molecular weight limit (NMWL) of 10 kDa. Uranium was separated from the $Fe(OH)_3$ co-precipitate and purified using standard radiochemical techniques (LEÓN VINTRÓ AND MITCHELL, 2000; SMITH 2001). Each purified sample was then electroplated onto a polished stainless-steel disc and counted for a period of 10–20 days in a low-background alpha spectrometric system equipped with 24 independently controlled passivated ion-implanted planar silicon (PIPS) detectors.

Quality Control

Although the application of well tested analytical methods and good laboratory practices are pre-requisites for the production of high-quality data, they are not always a guarantee of their reliability, and checks on the precision and accuracy of the results should be carried out as an intrinsic part of any environmental study. In the present study, internal quality control was achieved by means of careful monitoring of reagent blank activities, regular

background determinations, and periodical re-calibration of the chemical yield monitors used.

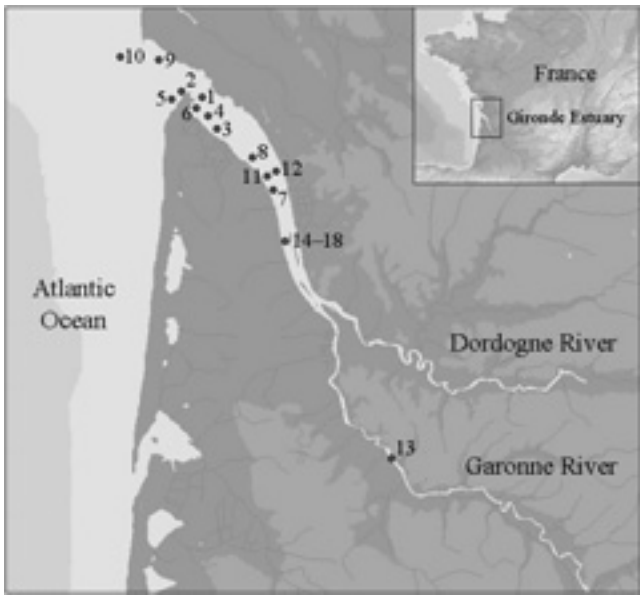

Figure 1. Sampling stations in the SWAMGIR-1 campaign (21–29 June 1999).

The accuracy of the methodology employed in this work has been tested in previous studies by comparing the results of measured uranium concentrations in seawater with the well established and widely used uranium-salinity relationship of KU *et al*. (1977), i.e. [^{238}U] = 0.07081 × Salinity (‰). Specifically, analyses were carried out in triplicate on a water sample collected in the Irish Sea, and on a large volume sample collected in the NE Atlantic. The results are summarised in Table 1. The accuracy of our measurements is evident from the consistency of the ^{234}U/^{238}U activity ratio which, at 1.14, is the expected value for seawater. Further confirmation of the validity of the method was obtained by the analysis of two samples taken in the course of the present study within the Gironde estuary mixing zone. The samples were taken at the same time in two consecutive tidal cycles and show excellent correspondence (Table 1).

RESULTS AND DISCUSSION

^{238}U and ^{234}U concentrations at each of the sampling stations, together with the corresponding ^{234}U/^{238}U activity ratios, are given in Table 2. The dissolved ^{238}U concentration measured for the Garonne River (Station 13), at 0.63 ± 0.06 dpm l^{-1} (±2σ) is within the range of various world-wide riverine 'end-members' reported by CARROLL AND MOORE (1994). The only previously reported value for the Garonne River, at 0.49 dpm l^{-1} (MARTIN *et al*., 1978), is not, strictly speaking, relevant to the present study as it was taken in springtime during a period of high river discharge. We have taken our measured value at Station 13 (significantly upstream of the known maximum saline incursion) to be representative of the zero salinity 'end-member' for the Gironde estuary during low river discharge. The open-ocean 'end-member' concentration adopted, at 2.52 ± 0.02 dpm l^{-1}, has been calculated in the conventional manner using the relationship of KU *et al.* (1977) and assuming a salinity of 35.6‰. It is consistent with the value of 2.6 ± 0.2 dpm l^{-1} (±2σ) recorded at a salinity of 34.0‰ just outside the estuary (Station 10) in the present study. It is also consistent with the value of 2.52 ± 0.26 dpm l^{-1} (±2σ) recorded in an earlier study in open waters in the North East Atlantic (Table 1).

A plot comparing ^{238}U concentrations along the Gironde salinity gradient with the theoretical dilution line obtained by joining the zero salinity and open ocean end-members, clearly shows that, at the time of sampling, dissolved uranium in the Gironde estuary behaved non-conservatively, with removal taking place at salinities in the range 0–16‰ (Figure 2). This contrasts with previous observations by MARTIN *et al*. (1978), which found uranium in the Gironde estuary to behave conservatively. It is important to note, however, that while our sampling took place during a period of relatively low river discharge (Figure 3), sampling by MARTIN *et al*. took place during late winter, when discharges are significantly greater. Indeed, other studies have shown that the non-conservative behaviour of uranium along estuaries is a seasonal feature related to the river discharge regime prevailing at the time of sampling (MAEDA AND WINDOM, 1982; SARIN AND CHURCH, 1994).

Table 1: Uranium quality assurance data (± 2σ).

Sample	Salinity	^{238}U (dpm l^{-1})		^{234}U/^{238}U
	(‰)	Measured	Calculated‡	
Irish Sea:				
#1	34.5	2.50 ± 0.12	2.44 ± 0.02	1.15 ± 0.04
#2	34.5	2.42 ± 0.08	2.44 ± 0.02	1.15 ± 0.02
#3	34.5	2.47 ± 0.08	2.44 ± 0.02	1.14 ± 0.04
Atlantic:				
#1	35.6	2.52 ± 0.26†	2.52 ± 0.02	1.14 ± 0.02
Gironde:				
#1	4	0.61 ± 0.04	-	1.14 ± 0.06
#2	4	0.63 ± 0.04	-	1.14 ± 0.04

‡ Using the relationship of KU *et al*. (1977)
† Source: SMITH (2001)

In other estuaries which exhibit non-conservative behaviour, salt-induced coagulation of riverine colloidal material has been proposed as the main mechanism responsible for the removal of uranium at low salinities (BOYLE *et al*., 1977; SWARZENSKI *et al*.,1995; SAÑUDO-WILHELMY *et al*., 1996). However, the application of tangential-flow ultrafiltration (UF) to examine the possible influence of colloids in this removal mechanism showed that there was little, if any, ^{238}U associated with colloidal matter in our samples (Table 3). Specifically, there was no discernible difference between the concentration of ^{238}U in the UF retentate (10 kDa < x < 0.45 μm) and that in the UF permeate (x < 10 kDa) at any of the 18 stations studied. Our experimental conditions (i.e., sample volume, counting time, etc.) were such that the presence of a small colloidal component (*ca.* 5–8 % or less) was unlikely to be detected.

Above a salinity of approximately 16‰, dissolved uranium concentrations are essentially indicative of conservative mixing. Such behaviour extends to open ocean salinities and has been observed in other estuarine systems (SARIN AND CHURCH, 1994; SWARZENSKI *et al*., 1995). A likely explanation for this observation lies in the 'cessation' of particle surface reactions (i.e., precipitation and coagulation) at intermediate salinities.

Table 2: ^{238}U and ^{234}U concentrations (± 2σ) in filtered water sampled along the salinity gradient of the Gironde estuary (SWAMGIR-1 campaign).

Station Code	Latitude (N)	Longitude (W)	Salinity (‰)	^{238}U (dpm l^{-1})	^{234}U (dpm l^{-1})	^{234}U / ^{238}U
13	44°39.123'	0°21.016'	0	0.63 ± 0.06	0.67 ± 0.06	1.07 ± 0.08
16	45°11.220'	0°43.156'	1.4	0.44 ± 0.03	0.49 ± 0.03	1.12 ± 0.06
15	45°11.179'	0°43.156'	1.8	0.53 ± 0.04	0.58 ± 0.04	1.08 ± 0.06
17	45°11.220'	0°43.156'	2.2	0.50 ± 0.03	0.57 ± 0.04	1.14 ± 0.06
14	45°11.179'	0°43.156'	4.0	0.61 ± 0.04	0.72 ± 0.04	1.14 ± 0.06
18	45°11.179'	0°43.156'	4.0	0.63 ± 0.04	0.70 ± 0.04	1.14 ± 0.04
07	45°19.886'	0°46.993'	7.7	0.83 ± 0.05	0.91 ± 0.06	1.10 ± 0.06
12	45°21.861'	0°45.071'	8.5	0.81 ± 0.06	0.90 ± 0.06	1.11 ± 0.04
11	45°21.342'	0°47.820'	9.5	0.95 ± 0.06	1.07 ± 0.06	1.13 ± 0.06
08	45°24.980'	0°51.475'	11.6	0.93 ± 0.06	1.10 ± 0.08	1.18 ± 0.06
03	45°30.502'	0°59.169'	14.5	1.28 ± 0.10	1.45 ± 0.12	1.13 ± 0.06
04	45°32.264'	1°01.300'	16.0	1.33 ± 0.12	1.57 ± 0.14	1.18 ± 0.06
06	45°33.455'	1°02.038'	19.0	1.77 ± 0.14	2.02 ± 0.16	1.14 ± 0.04
01	45°33.049'	1°01.006'	20.6	1.92 ± 0.12	2.18 ± 0.14	1.14 ± 0.04
02	45°34.413'	1°04.612'	22.0	1.92 ± 0.16	2.17 ± 0.18	1.13 ± 0.04
05	45°33.938'	1°06.224'	25.3	1.80 ± 0.20	2.10 ± 0.20	1.17 ± 0.06
09	45°38.830'	1°07.717'	27.9	2.05 ± 0.10	2.26 ± 0.12	1.11 ± 0.04
10	45°38.471'	1°20.106'	34.0	2.60 ± 0.20	3.0 ± 0.3	1.15 ± 0.04
-	-	-	35.6	2.52 ± 0.02	2.87 ± 0.02	1.14 ± 0.04
					Mean ratio (n = 18):	1.13 ± 0.03

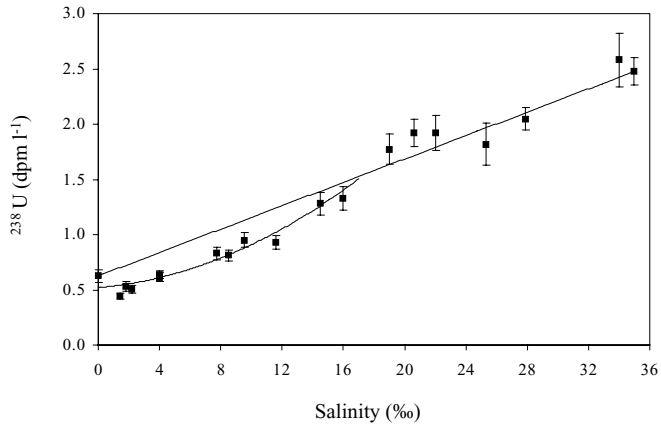

Figure 2. Dissolved ^{238}U plotted against salinity in the Gironde Estuary, illustrating non-conservative behaviour at salinities below 16‰.

Although we did not detect colloidal uranium, it is worth noting that in a period of high river discharge, KRAEPIEL *et al*. (1997) found that a significant fraction of the trace metal content in the Gironde estuary was associated with riverine derived colloidal particles (30% on average) and that this fraction passed conservatively through the estuary. Moreover, they found that iron is removed at low salinities. They, accordingly, proposed two categories of submicron particles in the Gironde: non-conservative inorganic colloids (e.g., iron oxyhydroxides) and conservative organic colloids (e.g., humic substances). Anticipating a five-fold difference in the river discharge regime between the late June sampling period of the present work (Figure 3) and the February sampling of KRAEPIEL *et al*. (1997), we would expect only about 6% association of trace metals with colloidal particles. Given also that uranium is not very particle reactive and assuming a diminished riverine colloidal input, it is not surprising that we did not detect any colloidal uranium.

To account for the observed removal under conditions of low river discharge, we suggest adsorption onto larger particles (>0.45 μm) as the concentration of suspended particles remains high in the salinity range 0 to 20‰, above which the concentration decreases (GIBBS *et al*., 1989; KRAEPIEL *et al*., 1997).

The two categories of submicron particles suggested by KRAEPIEL *et al*. (1997) may also explain the conservative behaviour of uranium in the Gironde estuary reported by MARTIN *et al*. (1978) for conditions of high river discharge. In such circumstances transport of any colloidally-bound uranium would be controlled by the presence of conservative organic colloids.In order to study the evolution of dissolved ^{238}U concentrations over a tidal cycle, samples were taken at a fixed sampling point within the turbidity maximum zone (Stations 14 – 18, inclusive) over a period of 12 hours. The results, presented in Figure 4, show a clear removal of dissolved uranium over the whole tidal cycle, with measured concentrations always inferior to those expected on the basis of the theoretical dilution line.

Table 3. ^{238}U concentrations (± 2σ) in different size fractions upon ultrafiltration of Gironde estuary water (SWAMGIR-1 campaign)

Station Code	Salinity (‰)	^{238}U (dpm l^{-1})	
		UF retentate 10 kDa < x < 0.45 μm	UF permeate x < 10 kDa
13	0	0.57 ± 0.04	0.62 ± 0.05
16	1.4	0.50 ± 0.07	0.49 ± 0.02
15	1.8	0.53 ± 0.02	0.54 ± 0.02
17	2.2	0.55 ± 0.02	0.53 ± 0.02
14	4.0	0.58 ± 0.04	0.62 ± 0.02
18	4.0	0.64 ± 0.04	0.62 ± 0.08
07	7.7	0.89 ± 0.04	0.88 ± 0.04
12	8.5	0.88 ± 0.06	0.93 ± 0.06
11	9.5	1.10 ± 0.12	1.03 ± 0.10
08	11.6	1.04 ± 0.04	1.19 ± 0.06
03	14.5	1.27 ± 0.08	1.34 ± 0.06
04	16.0	1.57 ± 0.08	1.38 ± 0.08
06	19.0	1.77 ± 0.14	2.16 ± 0.16
01	20.6	1.95 ± 0.12	1.78 ± 0.14
02	22.0	2.09 ± 0.16	2.08 ± 0.16
05	25.3	2.08 ± 0.14	2.30 ± 0.20
09	27.9	2.03 ± 0.20	2.43 ± 0.25
10	34.0	2.45 ± 0.18	2.47 ± 0.26

Comparison of measured and expected concentrations indicate that, at high tide (salinity 4‰), approximately 25% of the ^{238}U is removed from the dissolved phase. The extent of this removal is even more pronounced at low tide (salinity 1.4‰), with dissolved ^{238}U concentrations almost 40% lower than expected. These observations support the view that removal of uranium from the dissolved phase takes place preferentially at low salinities, where coagulation/flocculation processes are more active (GIBBS *et al*., 989).

CONCLUSIONS

Our data indicate that dissolved uranium in the Gironde estuary behaves non-conservatively, at least during periods of low river discharge, with preferential removal at low salinities. This contrasts with previous observations carried out during periods of high river discharge, which showed a conservative behaviour for this element (MARTIN *et al*., 1978). Together, these two sets of data reinforce the view that the non-conservative behaviour of uranium along estuaries is a seasonal feature related to the river discharge regime.

To account for the observed removal, we suggest adsorption of ^{238}U onto larger particles (> 0.45 μm) as the concentration of suspended particles remains approximately constant from 0 to 20‰, after which the concentration decreases (GIBBS *et al*., 1989; KRAEPIEL *et al*., 1997). Ultrafiltration experiments at each of the stations revealed that, during our sampling period, there was little if any colloidal ^{238}U in the Gironde estuary. It is likely that in high river discharge periods conservative organic colloids (e.g., humic substances) dominate the transport of uranium through the estuary. The non-conservative inorganic colloids (e.g., iron oxy-hydroxides) appear to be unimportant in this process.

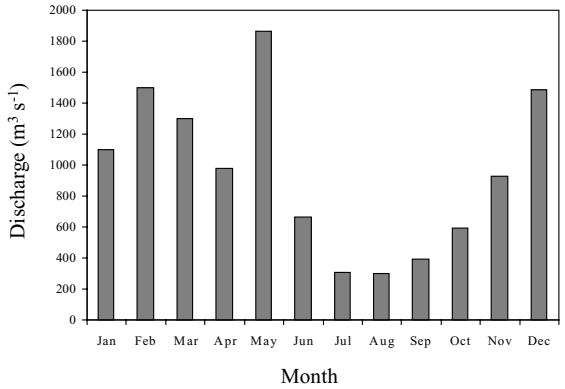

Figure 3. Fresh water discharge from the Garonne and Dordogne rivers into the Gironde estuary during 1999 (data courtesy of the Port Autonome de Bordeaux).

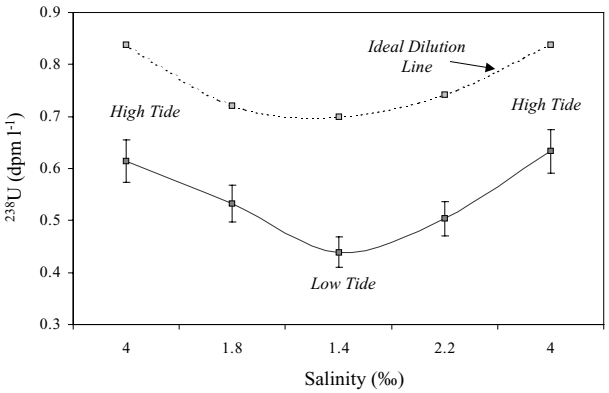

Figure 4. Evolution of dissolved (<0.45 μm) ^{238}U concentrations over a tidal cycle in the Gironde estuary (SWAMGIR-1 campaign).

ACKNOWLEDGEMENTS

This study was made possible by the generous support provided by the European Commission within the framework of the EC's Training and Mobility of Researchers Programme, 1998–2001 (SWAMIEE Project; Contract No. ERBFMRX–CT97–0111). It could not have been undertaken without the cooperation of the University of Bordeaux. We are indebted to them, to our colleagues and to the captain and crew of the R.V. Côte d'Aquitaine for their support while on station.

LITERATURE CITED

BOROLE, D.V., KRISHNASWAMI, S. and SOMAYAJULU, B.L.K., 1982. Uranium isotopes in rivers, estuaries and adjacent coastal sediments of western India: their weathering, transport and oceanic budget. *Geochimica et Cosmochimica Acta*, 46, 125–137.

BOYLE, E.A., EDMOND, J.M. and SHOLKOVITZ, E.R., 1977. The mechanism of iron removal in estuaries. *Geochimica et Cosmochimica Acta*, 41, 1313–1324.

CARROLL, J. and MOORE, W.S., 1994. Uranium removal during low discharge in the Ganges-Brahmaputra mixing zone. *Geochimica et Cosmochimica Acta*, 58, 4987–4995.

ELBAZ-POULICHET, F., HOLLIGER, P., HUANG, W.W. and MARTIN, J.-M., 1984. Lead cycling in estuaries, illustrated by the Gironde estuary, France. *Nature*, 308, 409–414.

GIBBS, R.J., TSHUDY, D.M., KONWAR, L. and MARTIN, J.-M., 1989. Coagulation and transport of sediments in the Gironde Estuary. *Sedimentology*, 36, 987–999.

KU, T.-L., KNAUSS, K.G. and MATHIEU, G.G., 1977. Uranium in open ocean: concentration and isotopic composition. *Deep Sea Research*, 24, 1005–1017.

KRAEPIEL, A.M.L., CHIFFOLEAU, J.-F., MARTIN, J.-M. and MOREL, F.M.M., 1997. Geochemistry of trace metals in the Gironde Estuary. *Geochimica et Cosmochimica Acta*, 61, 1421–1436.

LEÓN VINTRÓ, L. and MITCHELL, P.I., 2000. Determination of actinides and other alpha emitters in environmental samples. *In*: MEYERS, R.A. (ed.), *Encyclopedia of Analytical Chemistry: Instrumentation and Application*. John Wiley & Sons. pp. 12848–12884.

MAEDA, M. and WINDOM, H.L., 1982. Behaviour of uranium in two estuaries of the south-eastern United States. *Marine Chemistry*, 11, 427–436.

MARTIN, J.-M., NIJAMPURKAR, V. and SALVADORI, F., 1978. Uranium and thorium isotope behaviour in estuarine systems. *In:* GOLDBERG, E.D. (ed.), *Biogeochemistry of Estuarine Sediments*. Paris, France: UNESCO, pp. 111–127.

SAÑUDO-WILHELMY, S.A., RIVERA-DUARTE, I. and FLEGAL, A.R., 1996. Distribution of colloidal trace metals in the San Francisco Bay estuary. *Geochimica et Cosmochimica Acta*, 60, 4933–4944.

SARIN, M.M. and CHURCH, T.M., 1994. Behaviour of uranium during mixing in the Delaware and Chesapeake Estuaries. *Estuarine Coastal Shelf Science*, 39, 619–631.

SMITH, K.J. (2001). Natural radionuclides as tracers of scavenging and particulate transport processes in open ocean, coastal and estuarine environments. Dublin, Ireland: University College Dublin, PhD Thesis, 115 pp.

SWARZENSKI, P.W., MCKEE, B.A. and BOOTH, J.G., 1995. Uranium geochemistry on the Amazon shelf: chemical phase partitioning and cycling across a salinity gradient. *Geochimica et Cosmochimica Acta*, 59, 7–18.

WINDOM, H., SMITH, R., NIENCHESKI, F. and ALEXANDER, C., 2000. Uranium in rivers and estuaries of globally diverse, smaller watersheds. *Marine Chemistry*, 68, 307–321.

Journal of Coastal Research	SI 41	58-69	STRAEE 2002	Ferrara, Italy	ISSN 0749-0208

Flocculation Measured By Video Based Instruments in the Gironde Estuary During the European Commission SWAMIEE Project

A. J. Manning § ∞ K. R. Dyer §, R. Lafite † and D. Mikes †

§ School of Earth, Ocean and Environmental Sciences, University of Plymouth, Plymouth, PL4 8AA, UK. E-mail: andymanning@yahoo.com

∞ HR Wallingford, Howbery Park, Wallingford, OX10 8BA, UK

† CSIC, Institute of Earth Sciences Jaume Almera, c. Lluis Solé I Sabarí s/n E-08208, Barcelona, Spain

ABSTRACT

MANNING, A.J.; DYER, K.R.; LAFITE, R. and MIKES, D., 2004. Flocculation Measured By Video Based Instruments in the Gironde Estuary During the European Commission SWAMIEE Project. *Journal of Coastal Research*, SI 41, 58-69. Ferrara (Italy), ISSN 0749-0208

Acquisition of in-situ images of real estuarine mud flocs is a recent (during the past ten years) development. Furthermore, images coupled with the corresponding floc characteristics offer distinct advantage over previous studies. Therefore, an improved understanding of floc structure (e.g. size and shape) and composition (e.g. porosity and mass) could provide scientists with a greater insight into the flocculation of mud particles and their characteristics. Using simultaneous measurements of the distribution of floc sizes and settling velocities collected during the European Commission funded SWAMIEE project, this paper draws on a selection of visual floc images and illustrates the types of aggregates (i.e. flocs), together with their relevant floc properties, which typically comprise a floc population at various points in the tidal cycle. Measurements were carried out in the lower reaches of the Gironde estuary during neap tides, where the near bed region turbulent shear stress ranged between 0.06-0.6 N m^{-2}, but the near bed suspended particulate matter concentration did not generally exceed 200 mg l^{-1}. The floc size and settling velocity were measured primarily by the low intrusive INSSEV (In Situ Settling Velocity) instrument, with additional optical floc data provided by the Braystoke tube based VIL (Video In Laboratory) system. The study found that either very low turbidity or very high turbulence tended to produce slow settling macroflocs (floc size > 160 μm) with settling velocities of about 1-1.4 mm s^{-1}. Flow periods which generated moderate rates of turbulent shear stress between 0.4-0.47 N m^{-2} were found to produce the most productive environment for flocculation. These ambient conditions resulted in the formation of low density "comet-shaped" macroflocs about 0.5-1 mm in length and settling at a rate of 2-3 mm s^{-1}. These macroflocs displayed settling velocities up to 5-6 times greater than those typically applied in flocculation parameterisations for inclusion in vertical mass settling flux simulation modelling. When the optimum shear stress was combined with a sampling run suspended particulate matter concentration peak of 139 mg l^{-1}, the macrofloc fraction only represented 35% of the ambient suspended particulate matter. However, the resultant high macrofloc settling velocity meant that this fraction actually contributed 66% of the mass settling flux. Representation of the Gironde estuary floc characteristics in terms of a constant fractal dimension, did not adequately represent the varied distribution of flocs observed in-situ. The faster settling macroflocs and microflocs had respective fractal dimension values of 2.3 and 2.6, whilst the very porous slower settling macrofloc displayed a fractal dimension of only 2. The sample mean fractal dimensions ranged from 2.1-2.5 for all Gironde estuary floc populations.

ADDITIONAL INDEX WORDS: *Floc size, settling velocity, effective density, INSSEV instrument, flocculation, suspended particulate matter, Gironde estuary, turbulent shear stress.*

INTRODUCTION

The problems associated with mud accretion and erosion generally tend to be on a large scale, both in terms of the volume of mud being transported, and the financial costs incurred to counteract sediment movement which are often exacerbated by anthropogenic development. It is therefore some what ironic, that the underlying root of these estuarine problems tend to stem from the microscopic scale of the muds composition. Estuarine mud is composed of both individual clay minerals and organic matter (WHITEHOUSE *et al*., 1999). This makes the sediment cohesive, and in turn permits it to coagulate into aggregates called flocs, which are larger and settle faster than the individual mud particles from which they are composed. However, flocs are less dense than their primary particles. When placed in suspension, the state of flocculation continually changes in response to factors, which include: salinity, turbulent shearing (MANNING, 2004a), suspended particulate matter (SPM) concentration and the amount of biogenic adhesives (in particular mucopolysaccharides produced by bacteria, algae and higher plant species) present. Since flocs are very fragile entities, high quality site specific in-situ floc data, required for numerical sediment transport model calibration, has been very difficult to obtain.

The complex nature of estuarine systems means that there remains a number of gaps in the understanding of sediment dynamics, in particular the effect flocculation has on the vertical mass fluxes. DYER (1989) hypothesised that subtle changes in the distribution of floc properties, in particular settling velocity and density, can significantly alter the mass fluxes of the matter in

suspension. This hypothesis has been confirmed by both recent field studies (DYER *et al*., 2002; FENNESSY and DYER, 1996) and controlled laboratory simulations (MANNING and DYER, 1999; GRATIOT and MANNING, 2004). Thus, with the brief of furthering the understanding of water movement and the interaction it has with sediments within specific industrialised locations, the European Commission funded the SWAMIEE (Sediment and Water Movement in Industrialised Estuarine Environments) research project. The first SWAMIEE international field experiment (*SWAMGIR1*) was conducted in the lower reaches of the Gironde Estuary (south-west France). The aim was principally to measure how the in-situ size and settling velocity spectra of flocculated mud, in a tidal estuary, evolved in response to changes occurring in the flow velocity and SPM concentration gradients.

The acquisition of in-situ images of real estuarine mud flocs is a fairly recent development, and to obtain images coupled with the corresponding floc characteristics is a distinct advantage over previous studies which have acquired floc data by employing instruments such as: in-situ photography (e.g. EISMA *et al*., 1990), field settling tubes (e.g. OWEN, 1976) and laser particle sizers (e.g. BALE and MORRIS, 1987; LAW *et al*., 1997). An improved understanding of floc structure and composition would provide scientists with a greater insight into the agglomeration of mud particles and their resultant characteristics.

Therefore, using the floc distribution measurements made during *SWAMGIR1*, (MANNING, 2001; MANNING *et al*, 2001) it is the objective of this paper to draw on a selection of visual floc images and illustrate the types of aggregates, together with their relevant floc properties, which typically comprise a floc population at various points in the tidal cycle. Particular attention is given to how the floc characteristics are influenced by combined changes in turbulent shear stress and SPM concentration.

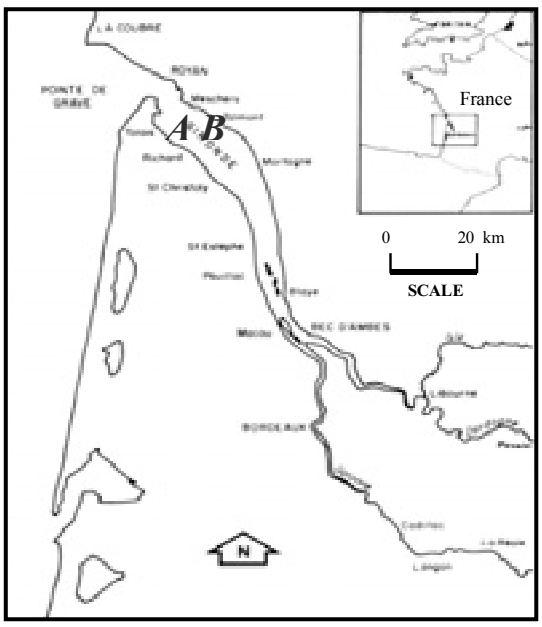

Figure 1. Location diagram of the Gironde estuary showing the positions of sampling stations at Le Verdon (*A*) and Talmont (*B*).

METHODOLOGY

Experimental Site

The Gironde estuary is the largest estuary in France, with a tidal area of 625 km^2. The estuary is generally well mixed, and it is very regular in shape, varying exponentially from the mouth to the tidal current limit, which is located 140 km upstream. The Gironde estuary drains a total catchment zone of 81,000 km^2, of which 55,000 km^2 is represented by the 580 km long River Garonne (LATOUCHE, 1971). Combined, the Rivers Garonne and Dordogne produce an annually-averaged river discharge of 760 m^3 s^{-1}. The Gironde has semi-diurnal tides and a spring tidal range at the mouth of 5.5 m, which gives the estuary a macrotidal classification (DAVIES, 1964).

From a two year observational programme, ETCHEBER (1978) estimated the mean estuary suspended concentration of particulate matter to be 1000 mg l^{-1}. Within the mouth region of the estuary the bed is predominantly covered in sand. However, the SWAMGIR1 experiment was particularly interested in the 10-20 km long deposits of mud which are found between Bordeaux and Talais (Figure 1). JOUANNEAU and LATOUCHE (1981) have stated that these 2-3 m deep patches of cohesive sediment are significant to the estuary's sediment transport regime, as they move either landward or seaward in response to the run-off. Therefore, two deployment locations were chosen in the proximity of these mud patches in the lower reaches of the Gironde estuary, where the estuary width is approximately 12.5 km. Measurements were made at site A situated 1 km from the shore at Le Verdon (see Figure 1) on the 21st and 23rd June 1999, and on the 22nd and 24th June 1999 sampling was conducted closer to the northern shoreline near Talmont (site B). At these locations throughout a typical tidal cycle, the water column would remain predominantly saline (ranging between 16-25), with the maximum water depth not exceeding 12 m.

Data Acquisition

All measurements were made from the CNRS research vessel *Cote D'Aquitaine*, which was anchored fore and aft during each sampling run. Sampling was conducted on a sub-tidal cycle time scale to focus on a range of velocities and allow frequent instrument calibration.

The flocs described in this paper were primarily examined optically using the INSSEV – IN-Situ SEttling Velocity – (FENNESSY *et al*., 1994) instrument, which is a low intrusive system and causes minimal disturbance to the flocs both during sampling and whilst being observed. The INSSEV sampling unit was mounted on a heavy metal frame which was lowered to the estuary bed by a stern mounted winch. Additional optical floc measurements were made using the Braystoke tube based VIL – Video In Laboratory system (DEFOSSEZ, 1996) developed at the University of Rouen (France).

INSSEV can obtain a representative floc population every 10-20 minutes (depending approximately on the ambient SPM concentration) from a ~3 litre sample of the water column 0.7 m above the estuary bed. Flocs, present in a volume of estuarine water, are trapped in the upper decelerator chamber by the closing of flap doors located at each end of the chamber, which shut at a rate proportional to the ambient current velocity. After allowing a period of 20-30 seconds for the turbulence in the chamber to decay, a slide door is electronically opened for a duration, which varies as a function of the SPM concentration, and this permits captured flocs to fall into a lower settling column. This column

was charged with filtered water of a salinity approximately 4-6 greater than the highest expected estuarine salinity value. During the initial development of the INSSEV instrument, FENNESSY (1994) and FENNESSY *et al*. (1994) found that the positive density contrast minimises the transfer of turbulence from the decelerator, and the formation of either secondary circulations or Rayleigh-Taylor instability occurring.

The flocs falling in the settling column were observed by an underwater monochromatic Pasecon tube video camera and were recorded in real-time using an S-VHS video recorder. This results in a lower resolution limit of 20 μm. The image quality was improved by using a built-in annulus of red LEDs to back-illuminate the flocs. This reduced image smearing by making the aggregates appear as dark objects set against a white background (i.e. a silhouetting technique). Using the optical technique described means that, unlike conventional field settling tubes or laser particle sizer instrumentation, INSSEV provides a simultaneous measurement of floc size and settling velocity (Ws) for each floc. Corresponding filtered SPM concentrations were obtained from water samples collected 0.7 m above the bed using a Niskin bottle.

To enable direct comparisons of floc properties to be made with the estuarine hydrodynamic conditions, simultaneous high frequency measurements of current velocity and turbidity were obtained using the POST - Profile Of Sediment Transport - system (CHRISTIE *et al*., 1997). This consisted of four, two-channel miniaturised electro-magnetic current meters (EMCM), five optical back-scatter (OBS) sensors, and a pressure transducer to measure the water depth. All sensors recorded continuously at 18 Hz and were low pass filtered at 5 Hz. The sensors were mounted on a vertical pole laterally off-set from the INSSEV sampling unit. The EMCM pairs measured the three orthogonal components of the flow only at the nominal INSSEV sampling height. As with the INSSEV instrument, the POST system was developed at the Institute of Marine Studies, University of Plymouth.

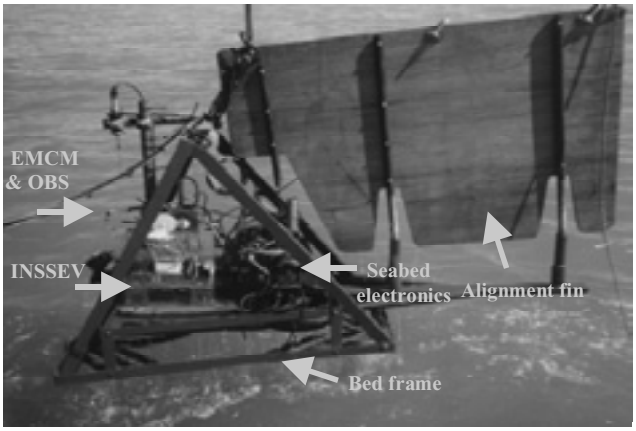

Figure 2. Instrumentation rig deployment from the stern of *Cote D'Aquitaine* during the June 1999 *SWAMGIR1* experiment (image taken from site A near Le Verdon).

The rig was aligned (+ 10o) with the ambient current flow by a fin on the rear of the rig, and the orientation was determined by a tilt / roll sensor and a fluxgate compass housed within the POST seabed electronics. The seabed electronics mounted on the rig (i.e. stepper motors which operated the INSSEV sampling apparatus, EMCMs and OBSs) were controlled by computers located onboard the surface vessel. Figure 2 illustrates the complete rig configuration.

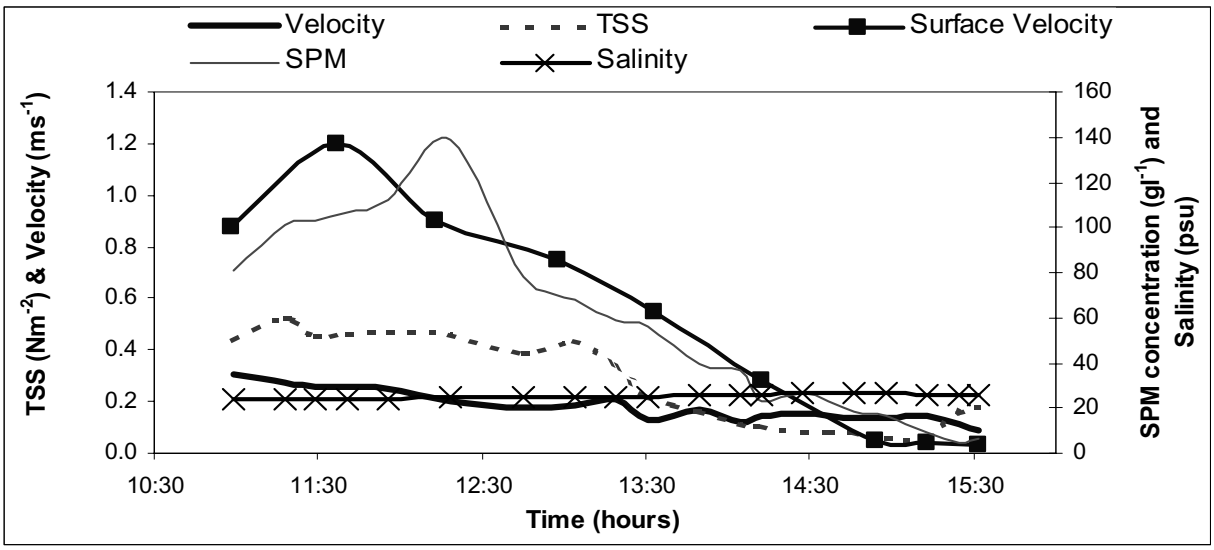

Figure 3. Time series of variations in: salinity, flow velocity, suspended particulate matter (SPM) concentration, and turbulent shear stress (TSS) for the neap tide on the 23rd June 1999. All observations were made 0.7 m above the bed (with the exception of the surface velocity), from a site A, near Le Verdon on the lower Gironde estuary (south west France).

DATA PROCESSING

Turbulence Data

The high frequency three dimensional flow velocity data measured by the EMCMs enabled the turbulent shear stress (TSS) to be calculated at the INSSEV sampling height using the Turbulent Kinetic Energy method (SOULSBY, 1983):

$$TSS = 0.19 \left(0.5\ \rho_W \left(\overline{u'^2} + \overline{v'^2} + \overline{w'^2}\right)\right) \quad (1)$$

where ρ_w is the ambient water density and $\overline{u'^2}$, $\overline{v'^2}$ and $\overline{w'^2}$ are the three turbulent variance computed from a 3 minute 47.55 second duration file.

Floc Data

All of the flocs viewed by the INSSEV video camera, for each sample, were measured. These observed flocs came from a known volume of trapped water. By implementing a sequence of algorithms developed by FENNESSY *et al*. (1997), the dry mass of a floc population could be compared with the measured estuarine SPM concentration. This gave an estimate of the efficiency of the sampling procedure, and provided corresponding rates of mass settling flux (MSF). Hence, the data obtained from INSSEV is both qualitative and quantitative.

Floc settling velocities and aggregate dimensions were obtained directly from the video recordings (manually) and translated into the real size dimensions by applying a video image calibration factor (MANNING and FENNESSY, 1997). Dimensions were measured both along the axis in the direction of settling (D_Y), and the axis normal to it (D_X), from which a height:width ratio could be determined. To aid in the interpretation of the floc size data and permit future comparisons to be made with floc size measurements made by instruments such as laser particle sizers (e.g. LAW *et al*., 1997), the two orthogonal dimensions were then converted into a spherical equivalent floc diameter, D:

$$D = (D_x \,.\, D_y)^{0.5} \quad (2)$$

The settling velocity of flocculated cohesive sediment is a function of both the floc size and effective density. The direct analysis of floc density by settling flocs in sucrose solutions is not possible, in that, even if the very fragile aggregates survive the sampling process, the floc porewater may be replaced by the sucrose solution. Therefore the effective density (ρ_e) of each floc (also referred to as density contrast), which is the difference between the floc bulk density, ρ_f) and the water density (ρ_w), was obtained by applying a Stokes' Law relationship:

$$\rho_e = (\rho_f - \rho_w) = \frac{Ws\ 18\mu}{D^2\ g} \quad (3)$$

where μ the dynamic molecular viscosity of the water and g is gravity. The water density was calculated from measured salinity and water temperature data using the International Equation of State of Sea Water, 1980 (MILLERO and POISSON, 1981). Stokes' Law has been widely used by instruments which measure only one floc component, either size or settling velocity, and apply Stokes' Law to estimate the non-measured characteristic. This requires making a very crude assumption of the floc effective density. However, the use of a Stokes' relationship for video-based instruments such as INSSEV is entirely valid as these systems provide measurements of all components of equation 3, with the only exception being the floc bulk density. Thus, Stokes' Law is the only option which is currently available to estimate ρ_e with the current technology, and has been successfully applied in numerous flocculation studies (e.g. GIBBS, 1985; BRUN-COTTAN, 1986; BURBAN et al., 1990; WEST et al., 1990; AL ANI et al., 1991; LICK et al., 1993; TEN BRINKE, 1994; FENNESSY and DYER, 1996; EISMA et al., 1997; DEARNALEY, 1997; FENNESSY et al., 1997; MANNING et al., 2001; MANNING and DYER, 2002a; GRATIOT and MANNING, 2004). Also, the settling aspects of WINTERWERP's (1998) fractal dimension floc model are based on the classic Stokes' equation.

To apply Stokes' Law, it is assumed that each sampled floc which fell through the still water enclosed within the INSSEV settling column was within the viscous Reynolds region; i.e. when the individual floc Reynolds number, Re, < 0.5-1:

$$R_e = \frac{\rho_w \cdot Ws \cdot D}{\mu} \quad (4)$$

For instances where the R_e exceeded 0.5 the Oseen modification (SCHLICHTING, 1968), as advocated by TEN BRINKE (1994), was applied to equation 3 in order to correct for the increased inertia created during settling. Stokes' also assumes that the settling particle is a small sphere, and observations have shown that flocs are often by no means spherical. Some of the large flocs have a very irregular shape, and are often joined into stringers by threads of biological matter (e.g. EISMA, 1986; MANNING and DYER, 2002b). However, by direct measurement ALLDREDGE and GOTSCHALK (1988) found that organic aggregates whose shape varied from spherical, including long comets, had settling rates very similar to those of nearly spherical particles. Similarly GIBBS (1985) showed that flocs from Chesapeake Bay had an average height:width ratios of to 1.6:1 which gave a spherical value of 0.91. Therefore, the implementation of a spherical equivalent diameter (eqn. 2) is valid.

Floc porosity (P_f) can provide an indication of the level of compactness of a floc, and was calculated by taking the ratio of the volume of interstitial water, V_{iw} (eqn. 6), contained within each floc to that of the spherical equivalent floc volume, V_f (eqn. 7):

$$P_f = \frac{V_{iw}}{V_f} \times 100 \quad (5)$$

and

$$V_{iw} = \left(\frac{1 - \rho_e}{\rho_{e\,np}}\right) V_f \quad (6)$$

$$V_f = \frac{4\pi D^2}{3} \quad (7)$$

Where $\rho_{e\,np} = \rho_{mo} - \rho_w$; ρ_{mo} is the mean dry density of the primary particles, and $\rho_{e\,np}$ is the mean effective density for solid (non-porous) aggregates. Estuarine flocs generally have a mineral to organic mass ratio of 90:10 respectively, and a mineral to organic volume ratio of 78:22 (FENNESSY, 1994). Gravimetric analysis of suspended sediment samples revealed the average

mineral dry density was 2600 kg m^{-3} and the organic matter had a mean dry density of 1030 kg m^{-3}. This means the ρ_{mo} equates to an average value of 2256 kg m^{-3}. It is assumed the interstitial fluid density is equal to ρ_w.

To aid in the interpretation of the floc data, each data set was segregated into sub-groupings of floc size. Also, in accordance with previous publication, this paper utilises the general floc size descriptive terms of macrofloc and microfloc. MANNING (2001) classifies macrofloc as those aggregates which exceed a spherically equivalent diameter of 160 μm, whilst the microflocs D < 160 μm.

RESULTS

Master Variables

Sampling near Le Verdon (Station A) on 23rd June 1999 provided a six hour record, and provides the main source of the data presented in this paper. A complete time series of the main variables measured at the nominal INSSEV sampling height of 0.7 m above the estuary bed on the 23rd June 1999 are summarised in Figure 3. The sampling programme was conducted during neap tide conditions when the bed region turbulent shear stress ranged between 0.06-0.6 N m^{-2}, but the near bed SPM concentration did not generally exceed 200 mgl^{-1}. A peak vertical turbidity gradient tended to occur in the lower water column at around the mid-tide period, where the flow velocity was ~0.15-0.2 m s^{-1}. In comparison, the corresponding surface current attained velocities ranging from 0.75-1.2 m s^{-1}. Salinity values ranged from a low of 16, through to a peak of about 25 at high water.

Floc Characteristics

A total of 35 floc population samples were collected. The original monochromatic INSSEV images were recorded on analogue S-VHS video cassette tape, and the floc images were obtained by digitisation through a PC video image capture card.

This produced a file 1216 KB in size (for a complete screen image) in an uncompressed windows bitmap (.BMP) file format, with a total screen resolution of 720 x 576 pixels.

Figure 4 shows the distribution of spherical equivalent floc size and settling velocity for sample G23-4 obtained from the Le Verdon site at 11:17 hr on the 23rd June 1999, which was mid-way through the flood (high water -3:14 hr). These conditions were a sampling run maximum TSS of 0.52 N m^{-2} at 0.7 m above the bed, and 101 mg l^{-1} of particulates were in suspension. The sample displayed a size spectrum of flocs ranging from 43 μm microflocs up to macroflocs 435 μm in diameter. However 56.8% of the dry mass (83.4% of the 79 individual flocs observed) was contained in the flocs under 160 μm in size.

The diagonal lines on Figure 4a show contours of effective density (calculated by equation 3) and indicate that there are many flocs of different size, but with the same density. Also there are flocs present with the same settling velocity, but with a wide range of sizes and densities. This point is well illustrated by the two flocs observed 34 s into the INSSEV sample G23-4 recordings. The largest floc (Figure 5a) was a low density (ρ_e = 33 kg m^{-3}) cluster-type macrofloc with a D = 399 μm and a settling velocity of 2.8 mm s^{-1}. The accompanying aggregate (Figure 5b) was a microfloc only 98 μm in size, but also had a settling velocity of 2.8 mm s^{-1} as the result of an effective density of 533 kg m^{-3}. This was an effective density difference of 500 kg m^{-3} between the two flocs. The very compact structure of the smaller microfloc was demonstrated by a porosity value of 72%. In comparison the more loosely constructed macrofloc (Figure 5a) had many more voids and was 95% porous.

Figure 6 illustrates a slower settling (Ws = 1 mm s^{-1}) macrofloc from the same sample, which was observed after an elapsed recording duration of 116 s. The macrofloc was irregular in shape, having Dx and Dy dimensions of 194 μm and 350 μm, respectively. This produced a resultant spherical equivalent diameter of 260 μm. With a porosity of 97.5% and ρ_e = 27 kg m^{-3}, this particular composition of macrofloc was presumed to be far more fragile than those observed earlier in the record.

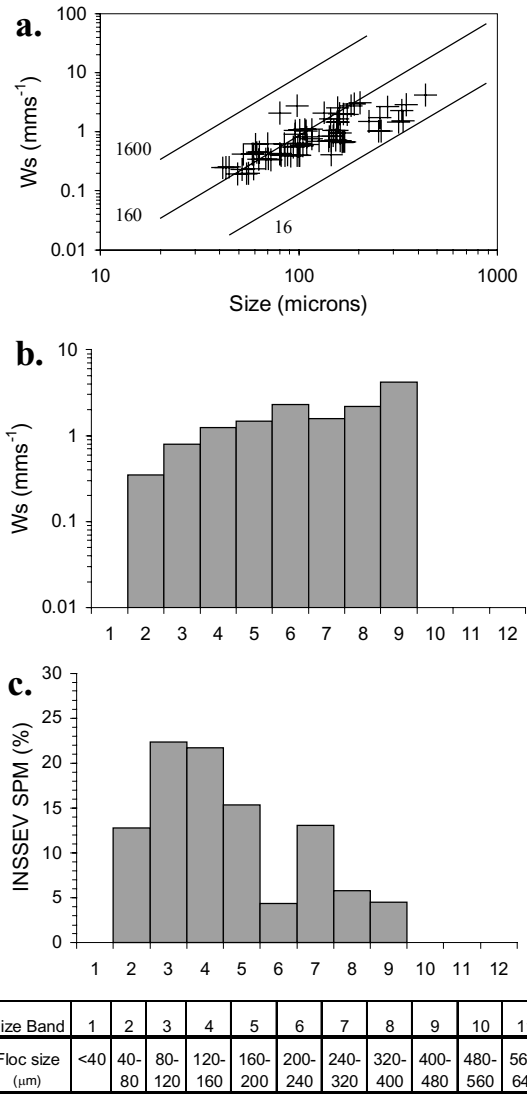

Size Band	1	2	3	4	5	6	7	8	9	10	11	12
Floc size (μm)	<40	40-80	80-120	120-160	160-200	200-240	240-320	320-400	400-480	480-560	560-640	>640

Figure 4. Summary of floc characteristics for Gironde estuary neap tide sample G23-4 obtained at high water –3:14 hr. Where (a) illustrates the relationships between floc size and settling velocities of individual flocs; (b) shows the size band distribution of settling velocity; and (c) shows the size band distribution of SPM concentration.

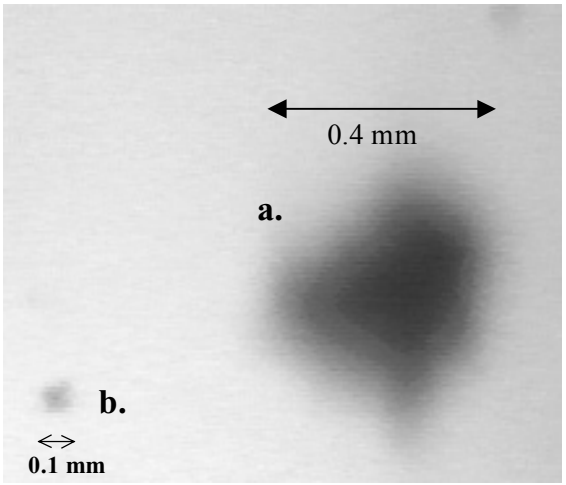

Figure 5. (a) A fast settling macrofloc and (b) a small fast settling dense non-cohesive aggregate (sample G23-4, 34 s into record).

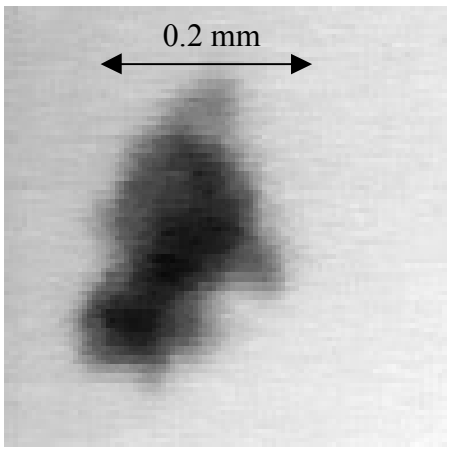

Figure 6. A slow settling, low density irregular shaped macrofloc (sample G23-4, 116 s into record).

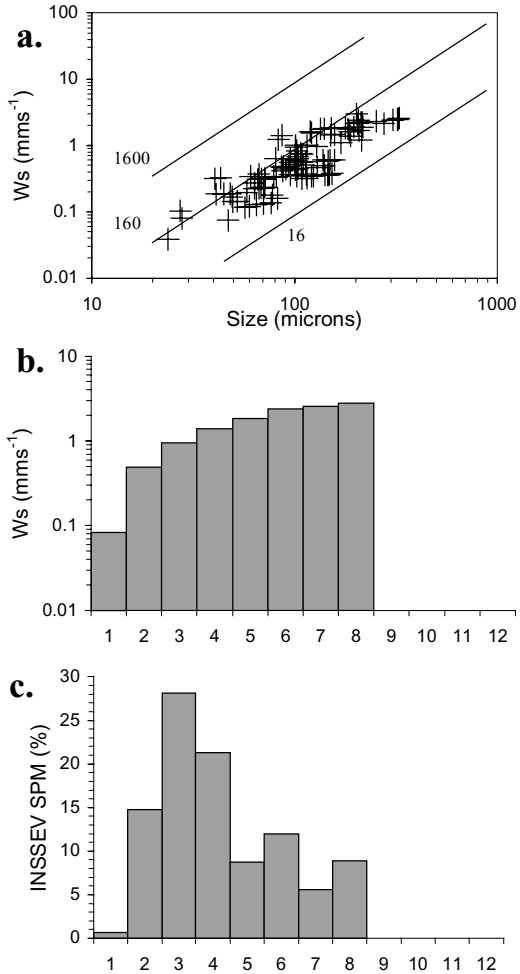

Size Band	1	2	3	4	5	6	7	8	9	10	11	12
Floc size (μm)	<40	40-80	80-120	120-160	160-200	200-240	240-320	320-400	400-480	480-560	560-640	>640

Figure 7. Summary of floc characteristics for Gironde estuary neap tide sample G23-8 obtained at high water –2:10 hr. Where (a) illustrates the relationships between floc size and settling velocities of individual flocs, with diagonal full lines showing the effective density (kg m^{-3}); (b) shows the size band distribution of settling velocity; and (c) shows the size band distribution of SPM concentration.

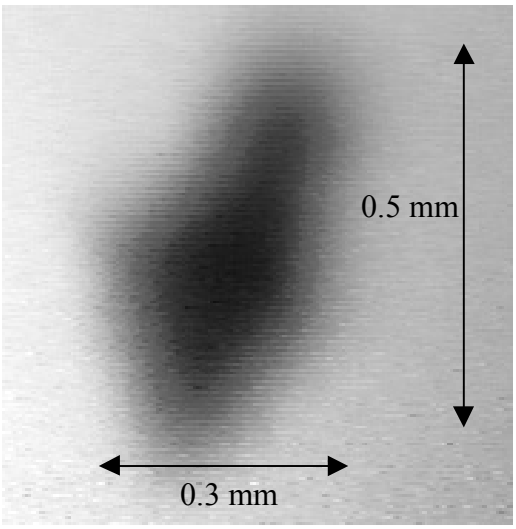

Figure 8. A large low density "comet-shaped" macroflocs (sample G23-8, 79 s into record).

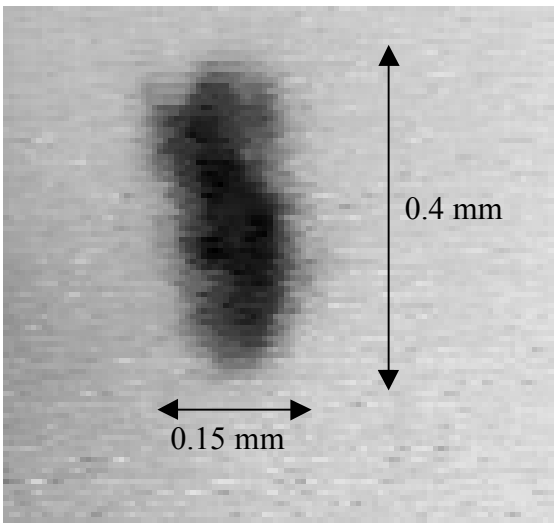

Figure 9. A slender, slow settling, low density "comet-shaped" macrofloc (sample G23-8, 125 s into record).

A further hour into the flood (high water -2:10 hr) saw the SPM increasing to a peak of 139 mgl^{-1}, whilst the TSS fell by 0.06 N m^{-2} to 0.46 N m^{-2}. At this point in the tidal cycle sample G23-8 was captured by INSSEV and the floc characteristics are summarised in Figure 7.

The individual settling velocities (Figure 7a) spanned almost three orders of magnitude from 0.05-2.85 mm s^{-1}, and the effective densities ranged between 40-812 kg m^{-3}. The largest macroflocs (D = 370 μm) had generally adopted a "comet-shaped" appearance with height to width ratios (D_y / D_x) of 1.5-2.5. An example is shown in Figure 8 by the macrofloc observed 79 s into the record (settling at 2.85 mm s^{-1}) with a Dx = 300 μm and Dy = 500 μm, and a corresponding effective density of 48 kg m^{-3}. These macroflocs displayed Ws rates up to 5-6 times greater than those values typically applied in the parameterisation for inclusion in vertical mass settling flux simulation modelling (J. Spearman, pers. com; D. Prandle, pers. com.).

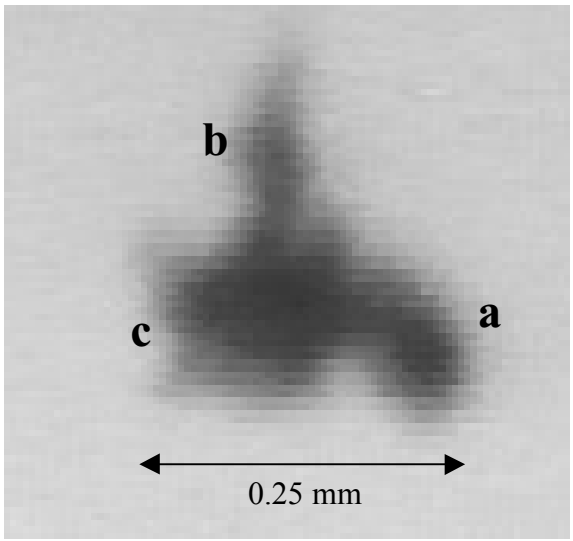

Figure 10. An irregular shaped, slow settling macrofloc composed of three key parts: (a) a high density microfloc, (b) a slender organically based floc, both attached to a (c) small near-spherical cluster-type macrofloc core (sample G23-8, 138 s into record).

Progressing a further 46 s into the record of sample G23-8, Figure 9 shows that a number of the smaller (D = 160-240 μm), slower settling (Ws ~ 1.8-2 mm s^{-1}) macroflocs also resembled comets. However, as Figure 10 illustrates, the remainder were irregular in shape. The latter of these two flocs, observed after a total elapse time of 138 s, was a composite of three principle components. By using flocs (from the G23-8 record) of a similar size as a bench mark, it was possible to estimate the individual properties of each of the three components of the larger composite aggregate. The first was an 85 μm first order (KRONE, 1963) high density (ρ_e probably greater than 600 kgm^{-3}) microfloc (Figure 10a); the second was a slender (Dx = 35 μm and Dy = 80 μm), predominantly organic-based floc (Figure 10b) possessing an effective density of probably under 15 kg m^{-3}. Both of these component flocs were attached to a core aggregate (Figure 10c) which was a near-spherical cluster-type macrofloc approximately 170 μm in diameter, and as a solitary entity it would have an effective density of about 90-100 kg m^{-3} and settling velocity of approximately 2 mm s^{-1}. The resultant irregular macrofloc had a Ws = 1.4 mm s^{-1} and ρ_e = 51 kg m^{-3}, which was distinctly different from the characteristics of the three individual component aggregates.

Sample G23-13 (Figure 11) was acquired during the period approaching high water (high water -0:42 hr). The current speed had slowed and this brought about a decrease in the turbulent shear stress (TSS = 0.16 N m^{-2}), and thus ambient SPM fell to ~40 $mg\ l^{-1}$, probably due to a cessation in bed erosion.

The majority of these flocs had reverted to a more regular shape, with height to width ratios tending to range from 0.8-1.2. Figure 12 shows an example of one of the faster settling (Ws ~5 mm s^{-1}) clustered macroflocs from the 160-200 μm size band. This particular floc had an effective density of 313 kg m^{-3} and a porosity of 62%, a structural composition more akin to that of a microfloc than a macrofloc. One can observe what appears to be a short tail of probably organic composition to the rear (in respect to the orientation of settling) of the flocs outer surface.

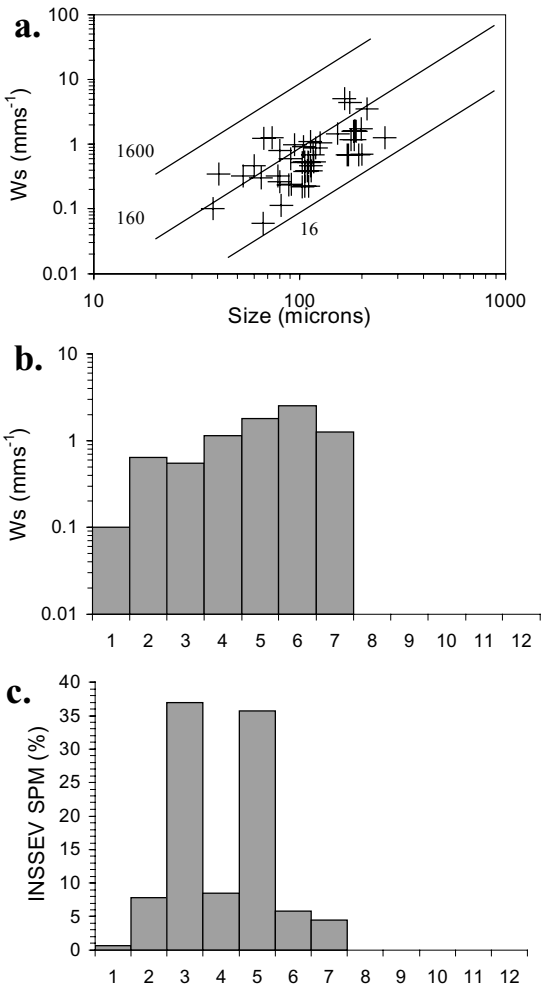

Size Band	1	2	3	4	5	6	7	8	9	10	11	12
Floc size (μm)	<40	40-80	80-120	120-160	160-200	200-240	240-320	320-400	400-480	480-560	560-640	>640

Figure 11. Summary of floc characteristics for Gironde estuary neap tide sample G23-13 obtained at high water –0:42 hr. Where (a) illustrates the relationships between floc size and settling velocities of individual flocs, with diagonal full lines showing the effective density (kg m^{-3}); (b) shows the size band distribution of settling velocity; and (c) shows the size band distribution of SPM concentration.

The scatter plot (Figure 11a) of the distribution of individual flocs shows that for the floc settling velocities, there is approximately an order of magnitude spread within each of the size band sub-divisions, although the majority of flocs are seen to favour the slower settling rates (i.e. only 21% of the floc population had Ws > 1.3 mm s^{-1}). This subsequently produces a skewness and high standard deviation for each of the calculated size band mean Ws values (Figure 11b). For this sample, SBs 3 (80-120 μm) and 5 (160-200 μm) contained 73% of the particulate matter by equal division. However with the former size band having a settling velocity of 0.54 mms^{-1} and the latter having a Ws = 1.8 mm s^{-1}, this highlights the greater contribution the macrofloc can offer to the mass settling flux.

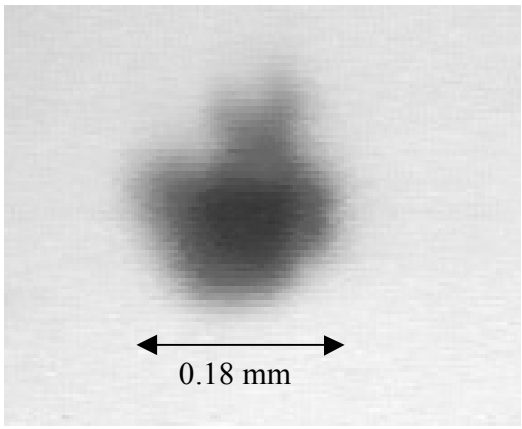

Figure 12. A small clustered macrofloc, with a short tail presumed to be composed of organic matter (sample G23-13, 53 s into record).

At local high water slack (15:13 hr), the SPM had fallen below 10 mg l^{-1} and the turbulent shear stress was only 0.06 Nm^{-2}. At this point in the tidal cycle, only 17 individual flocs were captured in sample G23-19 (Figure 13), and only two flocs had a settling speeds greater than 1.5 mm s^{-1}. This implies that most of the G23-19 flocs were probably created higher in the water column, and with their lower rates of fall, it had taken longer for them to reach the sampling height. The two large flocs (D = 270 and 277 μm) which had Ws ~ 3 mm s^{-1}, may have been the product of particle scavenging through differential settling. As they had a settling velocity of 2.85 mm s^{-1}, they were falling at a rate significantly faster than the rest of the captured population.

DISCUSSION

Flocculation is a dynamically active process which is influenced by numerous physical, chemical and biological factors. Traditionally, the floc size has been used as a parameter by which to gauge the effectiveness of mud particle flocculation. Many studies (ARGAMAN and KAUFMAN, 1970; TAMBO and HOZUMI, 1979; PANDYA and SPIELMAN, 1982) have attempted to relate modal floc size with turbulent energy dissipation rates. Unfortunately, an aggregate diameter does not provide a numerical simulation model of sediment transport within an estuarine location, with enough information about the floc dynamics, to sufficiently improve the parameterisation of the vertical concentration profile.

Since the 1970's field settling tubes (OWEN, 1971; 1976) have been widely used to collect in-situ floc samples from estuarine waters for the purpose of parameterising floc settling and calibrating estuarine numerical models. These instruments have indicated the median settling velocity to vary exponentially solely as a function of SPM concentration.
Results from a number of estuaries are summarised by DYER (1989) and show considerable differences in the exponential relationship between estuaries. DYER (1989) suggests that these variations are probably a result of floc density variations, and differences in hydrodynamic conditions (both naturally occurring and due to the floc-disruptive nature of the sampling device) at the time of data acquisition.

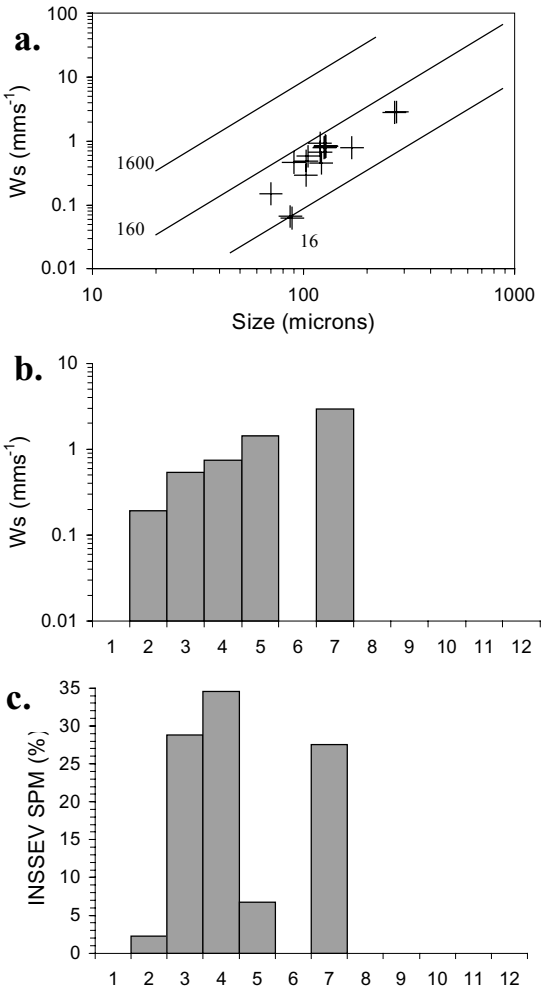

Size Band	1	2	3	4	5	6	7	8	9	10	11	12
Floc size (μm)	<40	40-80	80-120	120-160	160-200	200-240	240-320	320-400	400-480	480-560	560-640	>640

Figure 13. Summary of floc characteristics for Gironde estuary neap tide sample G23-19 obtained at high water –0:05 hr. Where (a) illustrates the relationships between floc size and settling velocities of individual flocs, with diagonal full lines showing the effective density (kg m^{-3}); (b) shows the size band distribution of settling velocity; and (c) shows the size band distribution of SPM concentration.

However, the floc size and settling velocity distributions presented in this paper have illustrated that individually neither the largest D or median Ws value can be regarded as providing a reliably accurate parameterised representation of a floc population. Also, DYER (1989) explains that the rheological properties of SPM are governed by volume concentrations, as opposed to mass concentration. Therefore, a true measure of flocculation can only be assessed by examining the combined factors which effect the mass settling flux rates. This requires initial measurements of both D and Ws, together with floc effective density variations. This point will be demonstrated by comparing sample G23-8 (acquired during peak SPM) and sample G23-4 obtained earlier in the tide during more turbulent conditions.

Although not readily apparent from the floc size vs. settling velocity plot (due to numerous flocs possessing similar size and settling characteristics; see Figure 7a), a size band analysis of the floc distribution of sample G23-8 revealed a more bi-modal distribution had developed (in comparison with sample G23-4 obtained earlier in the flood) in both the population of individual flocs and mass distributions (see Figure 7c), with the peaks in both the variables being SBs 3 (80-120 μm) and 6 (200-240 μm). By employing the microfloc:macrofloc segregation of 160 μm, this gave 86 flocs encompassing 65% of the dry floc mass in the smaller floc size group, compared to 20 flocs constituting the remaining 35% of the mass in the latter macrofloc group. This was a 4:1 population difference and a 2:1 SPM distribution ratio between the small floc group and the larger fraction. Although this indicates an SPM difference of 8.2% for the macrofloc division compared to sample G23-4, further examination shows that 66% of the mass settling flux (the product of the concentration and settling velocity) for G23-8 (compared to 54% for sample G23-4) was contained in the macrofloc groupings. This was as a result of the macrofloc settling velocities being an average of 0.5 mm s^{-1} faster for sample G23-8.

MANNING (2004b) has integrated the SWAMGIR1 floc data with floc data sets acquired from other European estuaries, to quantifiably assess how suspended matter is distributed between the microfloc and macrofloc fractions. Also, using a multiple parametric statistical technique, MANNING (2001) has produced algorithms which quantify estuarine macrofloc settling velocity distributions, with regards to SPM concentration and TSS variations, and extend the range of the SWAMIEE results obtained in the Gironde estuary. Such results provide the basis for more reliable parameterisation of flocculation and mass settling for inclusion in sediment transport mathematical modelling applications.

The wide variation in floc size and effective density present within floc samples such as G23-4, suggests that a considerable amount of aggregation and/or break-up was potentially occurring within the population. The wide range of floc properties within such a floc population was probably a consequence of the high turbulence (TSS = 0.52 N m^{-2}) creating an increased frequency of orthokinetic inter-particle collisions. This sample demonstrates the complexity of both the distribution of the floc primary characteristics (i.e. D, Ws and ρ_e) which comprise the particulate matter in suspension, and the mass settling flux dynamics at any one instance in a tidal cycle. It is difficult to represent such naturally occurring processes by purely theoretical approaches, and therefore high quality in-situ floc measurements are a prerequisite for sediment transport modelling calibration.

An interesting observation was made from sample G23-13, which was acquired in the 42 minutes prior to high water. Simple flocculation theory based on two-body collisions (GLASGOW and KIM, 1989) advocates that the lower abundance of particulates in suspension (38 mg l^{-1}), coupled with a reduction in the turbulent energy (TSS = 0.16 N m^{-2}) required to bring the particles into contact, creates a much lower inter-particular collision frequency.

However, inspection of the porosity values shows that size band average porosities ranged from 70-88% (Figure 14). This suggests that the majority of the microflocs and small macroflocs were actually created during more turbulent events earlier in the tidal cycle. These small flocs are formed from particles which are tightly packed together, instigated by a high frequency of orthokinetic inter-particular contacts. This can produce a low porous aggregate. EISMA (1986) has suggested that the reason these strongly constructed flocs can maintain their structural

integrity and retain their formation *history*, by resisting future break-up with increasing turbulent activity, is probably attributed to the presence of highly adhesive biogenic glues (in particular extra polymeric substances – EPS) which have coated the surfaces of the floc constituent particles. Therefore, these flocs would be the base components of more loosely constructed (i.e. higher porosity) larger aggregates, at a point in the tidal cycle where the turbulent stirring and concentration were more conducive for flocculation.

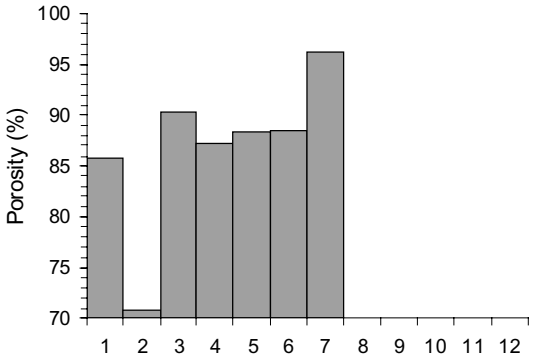

Size Band	1	2	3	4	5	6	7	8	9	10	11	12
Floc size (μm)	<40	40-80	80-120	120-160	160-200	200-240	240-320	320-400	400-480	480-560	560-640	>640

Figure 14. Size band averaged floc porosity variations for sample G23-13.

As these flocs settle into a higher shear field closer to the bed, they would be broken-up, until the individual aggregate structure that remained were in equilibrium with the estuarine shear stress, and then they would be re-entrained. MEHTA and PARTHENIADES (1975) have theorised that it is this continuous process of disruption and aggregation of mud flocs in a near bed turbulent flow, that control the maximum size of suspended estuarine mud flocs.

From a theoretical perspective, the simplest model of floc formation is derived from fractal theory. This depends on the successive aggregation of self-similar flocs producing a structure that is more or less independent of the scale considered. This is expressed as a fractal relationship between the flocs (KRONE, 1986; KRANENBURG, 1994). Many mathematical sediment dynamical models, such as those of HILL (1996) and WINTERWERP (1998), represent flocculation using fractal growth by stipulating a constant fractal dimension (nf) coefficient for all ambient conditions. However, in-situ floc data collected by the INSSEV instrument has shown that this approach very rarely applies to the diversity of a natural floc population. Using sample G23-4 as an example, the faster settling macroflocs and microflocs (see Figures 5a and 5b) had respective nf values of 2.3 and 2.6, whilst the very porous slower settling macrofloc (see Figure 6) displayed a nf of only 2. The sample mean fractal dimensions ranged from 2.1-2.5 for all Gironde estuary floc populations.

It was noticeable from the data records that there was a distinct lack of stringer type flocs at the sampling sites in the lower reaches of the Gironde estuary. Stringers comprise a number of small to medium sized macroflocs interlinked by fine organic strands (MANNING and DYER, 2002b). This has the net result of producing an aggregate with a much faster settling velocity than the component smaller macroflocs. This suggests that the organic fraction of the Gironde mud deposits in the Le Verdon and Talmont regions, which averaged at 11.4% for the floc samples acquired, was probably present primarily as a surface coating to the mineral clay fraction, as opposed to sticky fibrous strands. In turbidity maximum regions of estuaries such as the Tamar estuary (UK), where organic contents typically range from 15-30%, stringers have been shown to significantly influence and enhance the mass settling flux rates (MANNING and DYER, 2002b).

CONCLUSIONS

This study shows that either very low SPM concentration or very high turbulence tended to produce slow settling macroflocs with settling velocities of about 1-1.4 mm s^{-1}. Flow periods which generated moderate rates of turbulent shear stress between 0.4-0.47 N m^{-2}, were found to be the most productive environment for flocculation. These estuarine conditions resulted in the formation of low density "comet-shaped" macroflocs approximately 0.5-1 mm in length (Dy) and settling at a rate of 2-3 mm s^{-1}. These macroflocs displayed settling velocities up to 5-6 times greater than those values typically measured by field settling tubes, and settling rates generally used to calibrate the vertical mass settling flux component of 2-DV and full 3-D numerical estuarine sediment transport models (J. Spearman, pers. com; D. Prandle, pers. com.). When the optimum shear stress was combined with a high abundance of suspended matter, the macrofloc fraction only represented 35% of the ambient SPM. However, the resultant high macrofloc settling velocities meant that this fraction actually contributed 66% of the mass settling flux.

Representation of the Gironde estuary floc characteristics in terms of a constant fractal dimension, did not adequately represent the varied distribution of flocs observed in-situ.

ACKNOWLEDGEMENTS

The experimental programme was funded by the EC TMR SWAMIEE project under contract No. ERBFMRXCT970111. The authors would like to thank the boat crew of the CNRS *Cote D'Aquitaine* and all the technical staff who assisted during the SWAMGIR1 field experiment. The preparation of this paper was partially funded by H.R. Wallingford (UK), and the DEFRA / Environment Agency Joint Flood and Coastal Defence Research & Development Programme in Fluvial, Estuarine and Coastal Processes: Estuary Process Research (EstProc) project (under contract No.FD1905/CSA5966).

LITERATURE CITED

AL ANI, S., DYER, K.R. and HUNTLEY, D.A., 1991. Measurement of the influence of salinity on floc density and strength. *Geo-Marine Letters*, 11: 154-158.

ALLDREDGE, A.L. and GOTSCHALK, C., 1988. In-situ settling behaviour of marine snow. *Limnology and Oceanography*, 33: 339-351.

ARGAMAN, Y. and KAUFMAN, W.J., 1970. Turbulence and flocculation. *Journal of Sanitary Engineering* (ASCE), 96, 223-241.

BALE, A.J. and MORRIS, A.W., 1987. In-situ measurement of particle size in estuarine waters. *Estuarine, Coastal and Shelf Science*, 24, 253-263.

BRUN-COTTAN, J.C., 1986. Vertical transport of particles within the ocean. In: P. Buat-Menard, (ed.), *The Role of Air-*

Sea Exchange in Geochemical Cycling. D. Reidel Publishing Company, pp. 83-111.

BURBAN, P-Y., XU, Y-J., MCNEIL, J. and LICK, W., 1990. Settling speeds of flocs in fresh water and seawater. *J. Geophys. Res*., 95 (C10): 18,213-18,220.

CHRISTIE, M.C.; QUARTLEY, C.P., and DYER, K.R., 1997. The development of the POST system for in-situ intertidal measurements. *The 7th International Conference On Electrical Engineering In Oceanography*, (London, England), Publication No. 439, pp. 39-45.

DAVIES, J.H., 1964. A morphogenetic approach to world shorelines. *Zoological Geomorphology*, 8, 127-142.

DEARNALEY, M.P., 1997. Direct measurements of settling velocities in the Owen tube: a comparison with gravimetric analysis. In: N. Burt, R. Parker and J. Watts, (ed.), *Proceedings of INTERCOH Conference* (Wallingford, England), Chichester: John Wiley & Son, pp. 75-85.

DEFOSSEZ, J.P., 1996. Dynamique des macroflocs au cours de cycles tidaux, Mise au point d'un système d'observation: VIL, Video In Lab. Mémoire de DEA, Université de Rouen.

DYER, K.R., 1989. Sediment processes in estuaries: future research requirements. *Journal of Geophysical Research*, 94 (C10), 14327-14339.

DYER, K.R.; BALE, A.J.; CHRISTIE, M.C.; FEATES, N.; JONES, S., and MANNING, A.J., 2002. The turbidity maximum in a mesotidal estuary, the Tamar estuary, UK. Part II: The floc properties. In: J.C. Winterwerp and C. Kranenburg, (eds.), *Fine Sediment Dynamics in the Marine Environment - Proc. in Mar. Sci. 5.,* Amsterdam: Elsevier, pp. 219-232.

EISMA, D., 1986. Flocculation and de-flocculation of suspended matter in estuaries. *Netherlands Journal of Sea Research*, 20 (2/3), 183-199.

EISMA, D.; DYER, K.R. and VAN LEUSSEN, W., 1997. The in-situ determination of the settling velocities of suspended fine-grained sediment – a review. In: N. Burt, R. Parker and J. Watts, (ed.), *Proceedings of INTERCOH Conference* (Wallingford, England), Chichester: John Wiley & Son, pp. 17-44.

EISMA, D.; SCHUHMACHER, T.; BOEKEL, H.; VAN HEERWAARDEN, J.; FRANKEN, H.; LANN, M.; VAARS, A.; EIJGENRAAM, F. and KALF, J., 1990. A camera and image analysis system for in-situ observation of flocs in natural waters. *Netherlands Journal of Sea Research*, 27, 43-56.

ETCHEBER, H., 1978. Etude de la repartition et du comportement de quelques oligo-elements metalliques (Zn, Pb, Cu, Ni) dans le complexe fluvio-estuarien de la Gironde. Bordeaux, France: University of Bordeaux 1, B.Sc., *Report No.* 1455, 169p.

FENNESSY, M.J., 1994. Development and testing of an instrument to measure estuarine floc size and settling velocity in-situ. Ph.D. Thesis, University of Plymouth, 128 pp.

FENNESSY, M.J. and DYER, K.R., 1996. Floc population characteristics measured with INSSEV during the Elbe estuary intercalibration experiment. *Journal of Sea Research*, 36 (1-2), 55-62.

FENNESSY, M.J.; DYER, K.R. and HUNTLEY, D.A., 1994. INSSEV: an instrument to measure the size and settling velocity of flocs in-situ. *Marine Geology*, 117, 107-117.

FENNESSY, M.J.; DYER, K.R.; HUNTLEY, D.A. and BALE, A.J., 1997. Estimation of settling flux spectra in estuaries using INSSEV. In: N. Burt, R. Parker and J. Watts, (ed.), *Proceedings of INTERCOH Conference* (Wallingford, England), Chichester: John Wiley & Son, pp. 87-104.

GIBBS, R.J., 1985. Estuarine flocs: their size settling velocity and density. *J. Geophys. Res*., 90 (C2): 3249-3251.

GLASGOW, L.A. and KIM, Y.H., 1989. A review of the role of the physico-chemical environment in the production of certain floc properties. *Water, Air and Sea Pollution*, 47:153-174.

GRATIOT, N. and MANNING, A.J., 2004. An experimental investigation of floc characteristics in a diffusive turbulent flow. *Journal of Coastal Research,* SI 41 (This Volume).

HILL, P.S., 1996. Sectional and discrete representations of floc breakage in agitated suspensions. *Deep-Sea Research*, 43, 679-702.

JOUANNEAU, J.M. and LATOUCHE, C., 1981. The Gironde estuary. In: H. Fuchtbauer, A.P. Lisitzyn, J.D. Milliman and E. Seibold, (eds.), *Contributions to Sedimentology.* Stuttgart, Germany: E. Schweizerbart'sche Verlagsbuchhandlung (Nagele u. Obermiller), 10, 115p.

KRANENBURG, C., 1994. The fractal structure of cohesive sediment aggregates. *Estuarine, Coastal and Shelf Science*, 39, 451-460.

KRONE, R.B., 1963. A study of rheological properties of estuarial sediments. Hydraulic Engineering Laboratory and Sanitary Engineering Laboratory, University of California, Berkeley, *Report No. 63-68*.

KRONE, R.B., 1986. The significance of aggregate properties to transport processes. In: A.J. Mehta (ed.), *Estuarine Cohesive Sediment Dynamics*. Berlin: Springer-Verlag, pp. 66-84.

LATOUCHE, C., 1971. Les argiles des basisins alluvionnaires aquitains et des dependances oceaniques. Bordeaux, France: University of Bordeaux 1, Ph.D. thesis , 415p.

LAW, D.J.; BALE, A.J. and JONES, S.E., 1997. Adaptation of focused beam reflectance measurement to in-situ particle sizing in estuaries and coastal waters. *Marine Geology*, 140: 47-59.

LICK, W., HUANG, H. and JEPSEN, R., 1993. Flocculation of fine-grained sediments due to differential settling. *J. Geophs. Res*., 98 (C6): 10,279-10,288.

MANNING, A.J., 2001. A study of the effect of turbulence on the properties of flocculated mud. Plymouth, England: University of Plymouth, Ph.D. thesis, 282p.

MANNING, A.J., 2004a. The observed effects of turbulence on estuarine flocculation. *Journal of Coastal Research***,** SI 41 (This Volume).

MANNING, A.J., 2004b. Observations of the properties of flocculated cohesive sediment in three western European estuaries. *Journal of Coastal Research,* SI 41. (This Volume).

MANNING, A.J. and DYER, K.R., 1999. A laboratory examination of floc characteristics with regard to turbulent shearing. *Marine Geology*, 160, 147-170.

MANNING, A.J. and DYER, K.R., 2002a. A comparison of floc properties observed during neap and spring tidal conditions. In: J.C. Winterwerp and C. Kranenburg, (eds.), *Fine Sediment Dynamics in the Marine Environment - Proc. in Mar. Sci. 5.,* Amsterdam: Elsevier, pp. 233-250.

MANNING, A.J. and DYER, K.R., 2002b. The use of optics for the in-situ determination of flocculated mud characteristics. *Journal of Optics A: Pure and Applied Optics, Institute of Physics Publishing*, 4, S71-S81.

MANNING, A.J.; DYER, K.R. and CHRISTIE, M.C., 2001. Properties of macroflocs in the lower reaches of the Gironde estuary. *In*: Elbee, J. (d') and P. Prouzet, (eds.), *Actes de VIIe Colloque International Oceanographie Du Golfe De*

Gascogne (Biarritz, France), France: IFREMER, Actes de Colloques No. 31, pp. 230-235.

MANNING, A.J. and FENNESSY, M.J., 1997. INSSEV (In-Situ Settling Velocity instrument) - 1.3: Operator Manual. Plymouth, England: Institute of Marine Studies, University of Plymouth, *Internal Report*, 25p.

MEHTA, A.J. and PARTHENIADES, E., 1975. An investigation of the depositional properties of flocculated fine sediment. *Journal of Hydrological Research*, 92 (C13), 361-381.

MILLERO, F.J. and POISSON, A., 1981. International one-atmosphere equation of state seawater. *Deep-sea Research*, 28 (A), 625-629.

OWEN, M.W., 1971. The effects of turbulence on the settling velocity of silt flocs. *Proc. 14th Cong. Int. Assoc. Hydraul. Res.* (Paris), pp. D4-1 - D4-6.

OWEN, M.W., 1976. Determination of the settling velocities of cohesive muds. Hydraulics Research, Wallingford, *Report No. IT 161*, 8 pp.

PANDYA, J.D. and SPIELMAN, L.A., 1982. Floc break-up in agitated suspensions: theory and data processing strategy. *Journal of Colloid Interface Science*, 90, 517-531.

SCHLICHTING, H., 1968. *Boundary-layer theory*. New York: McGraw-Hill, 747p.

SOULSBY, R.L., 1983. The bottom boundary layer of shelf seas. In: B. Johns, (ed.), *Physical Oceanography of Coastal and Shelf Seas*. New York: Elsevier, pp. 189-266.

TAMBO, N. and HOZUMI, H., 1979. Physical characteristics of flocs – II. Strength of flocs. *Water Research*, 13, 409-419.

TEN BRINKE, W.B.M., 1994. Settling velocities of mud aggregates in the Oosterschelde Tidal basin (The Netherlands), determined by a submersible video system. *Estuarine, Coastal and Shelf Science*, 39, 549-564.

WEST, J.R.; ODUYEMI, K.O.K.; BALE, A.J. and MORRIS, A.W., 1990. The field measurement of sediment transport parameters in estuaries. *Estuarine, Coastal and Shelf Science*, 30, 167-183.

WHITEHOUSE, R.J.S.; SOULSBY, R.L.; ROBERTS, W. and MITCHENER, H.J., 1999. Dynamics of estuarine muds: a manual for practical applications. Wallingford, England: HR Wallingford, *Report No. SR 527*, 77p.

WINTERWERP, J.C., 1998. A simple model for turbulence induced flocculation of cohesive sediment. *Journal of Hydraulic Engineering*, 36 (3), 309-326.

Journal of Coastal Research	SI 41	70-81	STRAEE 2002	Ferrara, Italy	ISSN 0749-0208

Observations of the Properties of Flocculated Cohesive Sediment in Three Western European Estuaries

A. J. Manning § ∞

§ School of Earth, Ocean and Environmental Sciences, University of Plymouth, Plymouth, PL4 8AA, UK.
E-mail: andymanning@yahoo.com

∞ HR Wallingford, Howbery Park, Wallingford, OX10 8BA, UK.

ABSTRACT

MANNING, A.J., 2004. Observations of the Properties of Flocculated Cohesive Sediment in Three Western European Estuaries. *Journal of Coastal Research*, SI 41, 70-81. Ferrara (Italy), ISSN 0749-0208

The inability to adequately measure floc properties, due to their fragility, has posed a distinct problem in the understanding of the flocculation process. Therefore, within the framework of three recent European Commission funded projects – COSINUS, SWAMIEE and INTRMUD - in-situ measurements of floc size and settling velocity were made using the video-based INSSEV (In-Situ SEttling Velocity) instrument. This acquisition technique enabled the calculation of floc effective density values by using a Stokes' Law relationship. This paper utilises in-situ data collected from experiments conducted in the Tamar (UK), Gironde (France) and Dollard (The Netherlands) estuaries, with the purpose of examining how floc properties vary in tidal waters and identifying the factors which influence their resultant characteristics. Floc populations were seen to exist as combinations of macroflocs (floc size > 160 mm) and microflocs, with the macroflocs tending to represent 38-70% of the suspended particulate matter (SPM) concentration during periods of low turbidity. For higher concentration suspensions in excess of 5 g l-1, the microflocs constituted less than 10% of the SPM. The distribution of particulate matter throughout the macro- and microfloc sub-populations showed a direct correlation with the suspended solids concentration. To quantify this inter-relationship, the dimensionless SPM ratio parameter is introduced and is calculated by dividing the percentage of macrofloc SPM, in a single floc population, by the remaining percentage of microfloc SPM. An SPM ratio of unity would represent an equal apportioning of the floc mass between the two floc sub-populations. An empirical relationship representing the SPM ratio in terms of SPM (mg l-1) is: SPM ratio = 0.815 + 0.00318 SPM – 0.14x10-6 SPM2. Qualitatively, macroflocs are seen to exist as: "cluster", "stringer" or "comet" types, which collectively demonstrate effective densities of less than 90 kg m-3. Average macrofloc settling velocities ranged from 2 mm s-1 for the low SPM concentrations, such as those experienced in the Dollard estuary during neap tides, up to 4-6 mm s-1 for floc populations observed within a concentrated benthic suspension (CBS) layer in the Tamar estuary. In contrast the microflocs, from which the macroflocs are primarily composed, demonstrated effective densities ranging between 30 to 1000 kg m-3. From the data two main types of microfloc can be identified. The first is a high density microfloc fraction predominantly mineral in origin. Whilst the second microfloc type is a more organically-based, slower settling, lower density aggregate. Throughout a flocs evolution, the distribution of the two microfloc sub-classes from which macroflocs are composed would be quite different for a cluster-type, as opposed to a more organic stringer-type macrofloc.

ADDITIONAL INDEX WORDS: *Flocculation, floc size, settling velocity, effective density, INSSEV instrument, suspended particulate matter, turbulent shear stress, Tamar estuary, Gironde estuary, Dollard estuary.*

INTRODUCTION

To optimise the management and development of estuarine waterways, for purposes which include: dredge spoil removal and disposal, the construction of port and harbour infra-structure, and the reclamation of intertidal areas, the movement of the fine cohesive sediment requires accurate prediction principally through the use of computer simulation models. A major problem arises from the cohesive muds having the ability to flocculate and create flocs (i.e. aggregates), which are larger but less dense than the primary particles they are composed from. An individual floc may constitute up to 10^6 individual particulates. LICK (1994) found that the floc size can range over four orders of magnitude within any one floc population; from clay particles of 1 μm to macroflocs of several centimetres. EISMA *et al*. (1983, 1990) have observed large mud flocs in numerous European estuaries using in-situ photography. Similarly, the settling velocities can also span over four orders of magnitude, from 0.01 mm s^{-1} up to several centimetres per second (GIBBS, 1985; FENNESSY *et al*., 1994a). A factor which further complicate matters, is that flocculation is a dynamically active process which readily reacts with changes in the aquatic environmental conditions.

The inability to adequately measure floc properties, due to their fragility, has posed a distinct problem in the understanding of the flocculation process. Therefore, within the framework of three recent European Commission funded projects – COSINUS,

SWAMIEE and INTRMUD - in-situ measurements of floc size and settling velocity were made using the video-based INSSEV instrument. The type of multi-parameter aggregate data provided by such a system, is regarded as a prerequisite for improving the understanding of floc structural compositions and enables a greater insight into how mud particles agglomerate. The aim of each field experiment was principally to derive how the size and settling velocity spectra of flocculated mud evolved in response to changes occurring in both particle concentration and flow velocity gradients. The acquisition of in-situ images of real estuarine flocs is a rarity, and to obtain such images coupled with the corresponding floc characteristics, is a distinct advance on previous in-situ flocculation studies which tended to employ either field settling tube (OWEN, 1976) devices or laser particle sizer systems (e.g. BALE and MORRIS, 1987).

This paper utilised in-situ data collected from experiments conducted in the Tamar (UK), Gironde (France) and Dollard (The Netherlands) estuaries, with the purpose of examining how the distribution of floc properties, in particular: floc size, settling velocity, floc mass and fractal dimensions, varied with changing water column conditions. The aquatic environmental factors which influence the floc characteristics are identified. Examples of floc images, together with their respective floc properties, will be used to qualitatively illustrate specific floc types. The empirical relationships between some aspects of the floc settling flux are quantitatively assessed.

DATA ACQUISITION and PROCESSING

The flocs described in this paper were all examined using the INSSEV – In-Situ SEttling Velocity - instrument (FENNESSY *et al*., 1994). It comprises a sampling / deceleration chamber from which collected flocs are then allowed to fall into a lower settling column which contains still water of a higher salinity than the ambient (Figure 1).

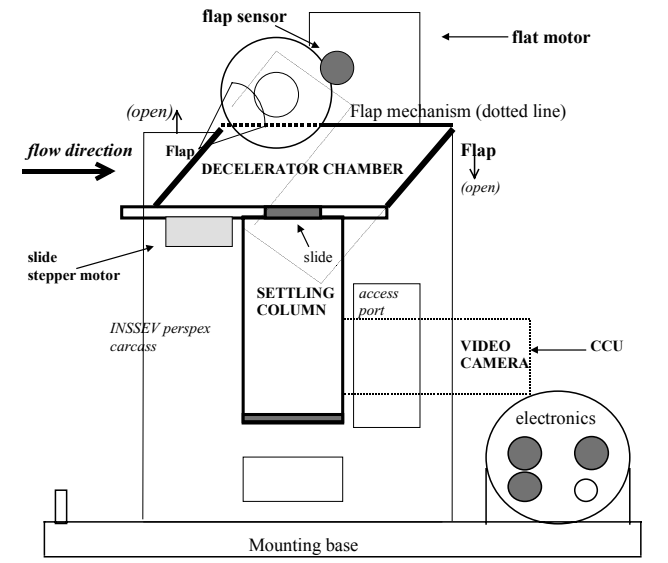

Figure 1. A schematic of the INSSEV sampling unit – version 1.3. The side elevation shown with flaps closed.

Simultaneous floc size (where Dy is the floc dimension in the vertical settling direction and Dx is the adjacent floc size dimension) and settling velocity (Ws) distributions were obtained at 10-30 minute intervals; the sampling frequency being dependent on the turbidity.

The two orthogonal floc dimensions describe the floc shape, however for comparative purposes the floc sizes referred to in this paper are predominantly spherical-equivalent sizes (D), unless otherwise stated, where:

$$D = (Dx \cdot Dy)^{0.5} \quad (1)$$

Due to the two-dimensional nature of the floc images provided by the video camera, it is assumed that the floc depth dimension, Dz, was equal to Dx.

By assuming that each floc is settling within the viscous Reynolds region (i.e. when the Reynolds number, R_e, < 0.5-1), the effective density (ρ_e) for each floc could be obtained by applying a Stokes' Law relationship:

$$\rho_e = (\rho_f - \rho_w) = \frac{Ws\ 18\mu}{D^2\ g} \quad (2)$$

where μ the dynamic molecular viscosity and g is gravity. The effective density, also referred to as density contrast, is the difference between the floc bulk density (ρ_f) and the water density (ρ_w). The water density was calculated from measured salinity and water temperature data using the International Equation of State of Sea Water, 1980 (MILLERO and POISSON, 1981). For instances where the R_e exceeded 0.5 the Oseen modification (SCHLICHTING, 1968), as advocated by TEN BRINKE (1994) and BRUN-COTTAN (1986), was applied to equation 2 in order to correct for the increased inertia created during settling.

The volume of a spherical-equivalent floc (V_f) is given by:

$$V_f = \frac{4\pi D^2}{3} \quad (3)$$

Thus, the interstitial water (V_{iw}) contained within each floc is calculated by:

$$V_{iw} = \left(\frac{1 - \rho_e}{\rho_{e\,np}}\right) V_f \quad (4)$$

where $\rho_{e\,np} = \rho_{mo} - \rho_w$; ρ_{mo} is the mean dry density of the primary particles, and $\rho_{e\,np}$ is the mean effective density for solid (non-porous) aggregates. Estuarine flocs generally have a mineral to organic mass ratio of 90:10 respectively, and a mineral to organic volume ratio of 78:22 (FENNESSY, 1994). Gravimetric analysis of suspended sediment samples revealed the average mineral dry density was 2600 kg m^{-3} and the organic matter had a mean dry density of 1030 kg m^{-3}. This meant the ρ_{mo} equates to an average value of 2256 kg m^{-3}. Assuming the interstitial fluid density to be equal to ρ_w, the dry floc mass ($M_{f\,dry}$) was calculated by:

$$M_{f\,dry} = V_f \frac{\rho_e\ \rho_{mo}}{(\rho_{mo} - \rho_w)} \quad (5)$$

The data obtained from INSSEV is both quantitative and qualitative. Quantitatively, a complete representative floc population is measured, thus allowing statistical averaging of the different floc characteristics to be calculated for the overall

population sample mean, plus average floc property values for discrete sub-population size ranges. A combination of such data provides a greater understanding of how floc populations are fundamentally composed.

The qualitative is a description of the form of the flocs and how they change in both time and space. In contrast to other floc sampling devices, INSSEV utilises an optical miniature underwater video camera to obtain the floc data from the settling column, and in turn this provides high quality visual information on the flocs directly under examination (MANNING and DYER, 2002a).

The turbulent structure and turbidity of the water column was measured using the POST – Profile Of Sediment Transport - system (CHRISTIE *et al*., 1997) which comprised four miniature electro-magnetic current meters (EMCM), and an array of up to eight optical back-scatter (OBS) sensors. The sensors were arranged on a pole mounting to give a vertical profile through the bottom 1 m of the water column. Data was recorded at a rate of 18 Hz. Flow velocity and concentration values were obtained at the INSSEV sampling height of 0.5 m above the bed (0.7 m for the Gironde experiments), by interpolation between the relevant sensors. By applying the Turbulent Kinetic Energy method (SOULSBY, 1983) to measurements of the three orthogonal components of flow, burst-average estimates of turbulent shear stress (TSS) were calculated using equation 6:

$$\mathrm{TSS} = 0.19 \left(0.5\ \rho_W \left(\overline{u'^2} + \overline{v'^2} + \overline{w'^2}\right)\right) \quad (6)$$

where $\overline{u'^2}$, $\overline{v'^2}$ and $\overline{w'^2}$ are the three turbulent variance components.

Data acquisition was typically on a sub-tidal cycle time scale. All control electronics were housed in a surface vessel, with the exception of the Dollard experiment where the data loggers were located on the BOA (Biologische Oceanografische Aardwetenschappen) project bridge which stood 5.5 m above the mudflat bed.

Additional master variable data of salinity, temperature and suspended solids were collected at regular time intervals using a profiling CTD and Downing OBS gauge. Near bed water samples were taken for OBS calibration, and INSSEV floc sample concentration referencing purposes. Bio-chemical tests for chlorophyll-a and total carbohydrate levels were performed on selected Tamar samples by the University of Plymouth's Marine Chemistry Research Group.

The original monochromatic INSSEV images were recorded on an analogue Super-VHS video cassette tape, and the floc images presented were obtained by digitisation via a PC video image capture card. This produced a file 1216 KB in size (for a complete screen image) in an uncompressed windows bitmap (.BMP) file format, with a total screen resolution of 720 x 576 pixels.

RESULTS

Tamar estuary - Turbidity Maximum

A series of deployments were conducted in the mesotidal Tamar estuary during June, August and September1998 as part of the COSINUS project (BERLAMONT, 2002). The Tamar estuary, which is topographically dendritic in shape, is located in south-west England. It has numerous meanders and wide mud flats exposed at low water, and is classified as a drowned river valley or ria (DYER, 1997). The main tributary is the River Tamar which has a 470 km^2 catchment zone, and from source to estuary mouth it is approximately 75 km in length, with tidal influence extending 31 km inland. The annual mean river discharge is approximately 20 $m^3\ s^{-1}$.

Data acquisition was conducted in a straight channel section in the upper Tamar estuary, near Calstock, within the tidal trajectory of the turbidity maximum (TM). At this site during high water at neap tides, the estuary width and depth were approximately 75 m and 4.5 m, respectively. The tidal range varied between 3.2 m (neaps) to about 4.5 m (springs). It was expected that considerable erosion and settling would occur throughout a tidal cycle, and that processes would be dominated more by vertical fluxes driven by the bed boundary conditions, rather than internal shear. The details of these COSINUS deployments are reported by DYER *et al*. (2002a).

The COSINUS experiment provided a total of 91 floc samples (i.e. complete floc population spectra) during neap and spring tidal conditions. At the sampling location, the neap tide experimental runs generally observed maximum surface current velocities of 0.6 $m\ s^{-1}$, and these conditions entrained up to 800 $mg\ l^{-1}$ of solids into suspension 0.3 m above the bed. Salinity values ranged from zero through to 9 at high water.

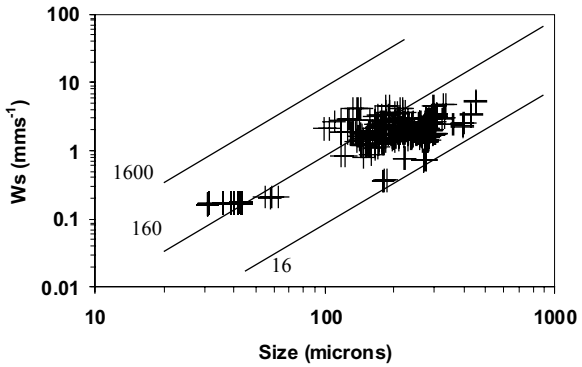

Figure 2. Relationships between floc size and settling velocities of individual flocs for Tamar estuary neap tide sample T05-9 obtained at high water –3:47 hr. The diagonal lines represent values of constant effective density (kg m^{-3}).

Figure 2 shows a scatterplot of spherical-equivalent dry mass weighted floc size against settling velocity for sample T05-9. This distribution was measured during neap tides from within the TM. The diagonal lines represent contours of constant effective density (with units of kg m^{-3}). Sample T05-9 was composed of a wide range of floc sizes, the largest being 430 μm in diameter, and settling velocities which spanned between 0.17-5.3 mms^{-1}. Closer examination of Figure 2 reveals that there are flocs of the same size, which have a wide range of settling velocities and effective densities. It is also apparent that aggregates with the same settling velocity, can display distinctly different densities and sizes. Microflocs, as defined by MANNING (2001), are those aggregates with a spherically-equivalent diameter of less than 160 μm. In this sample, the microfloc effective densities ranged from 38 kg m^{-3} through to 755 kg m^{-3}. The lower density flocs are mainly organic, whilst the later are predominantly mineral-based possessing an effective density nearly half that of a quartz particle.

Figure 3 shows a macrofloc of ~500 μm in horizontal diameter (Dx), which is representative of the faster settling macroflocs observed 45 s into the INSSEV sample T05-9 recordings. This floc was falling at a speed of 6 mm s^{-1} and was near-spherical in shape. These were closely followed by combinations of either "stringer" or "comet"-like macroflocs. The former (Figure 4a) possessed a Dy dimension of approximately 750 μm, and was composed of a single macrofloc (Dx ~310 μm) leading what appears to be a trailing organic tail (Dx ~100 μm).

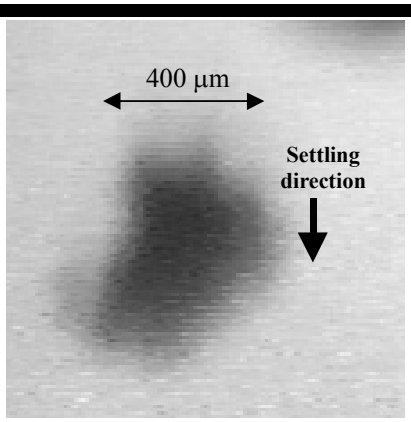

Figure 3. A large near-spherical clustered macrofloc (INSSEV sample T05-9, observed 45 seconds into record).

The latter (Figure 4b) comprised a larger rounded macrofloc nucleus (Dx ~300 μm) with a short stumpy tail (Dx ~100 μm); this floc had an overall Dy length of approximately 500 μm. These macroflocs had settling velocities of ~ 4-5 mm s^{-1}, and fell without spinning or twisting. The neap tide flocs had high organic contents (15-30%) and this organic matter was well reflected in the composition of a number of the slower settling (Ws ~2 mm s-1) and very low effective density (□e = 28 kg m-3) macroflocs observed within the TM. They had an organically linked microfloc chain preceding a trailing upper small macrofloc core. In their entirety these aggregates resemble a "seahorse" (Figure 5). In relation to the stringers and comets, these seahorse macroflocs occurred 56 seconds latter in the INSSEV sample recording.

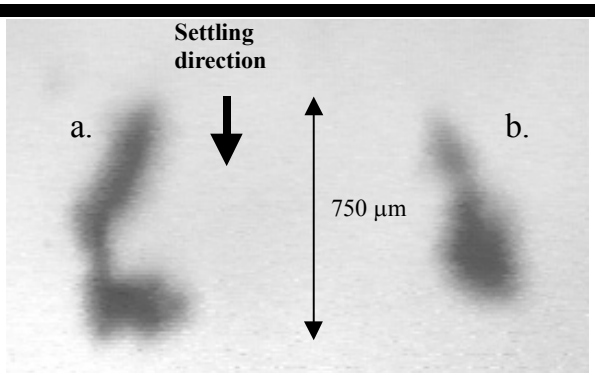

Figure 4. (a) A stringer type macrofloc composed of a single macrofloc with a trailing organic tail; (b) a comet-shaped macrofloc (INSSEV sample T05-9, observed 82 seconds into record).

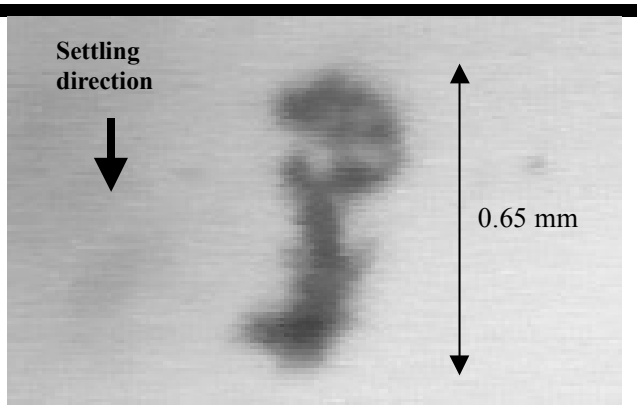

Figure 5. A small neap tide stringer which resembles a seahorse (INSSEV sample T05-9, observed 138 seconds into record).

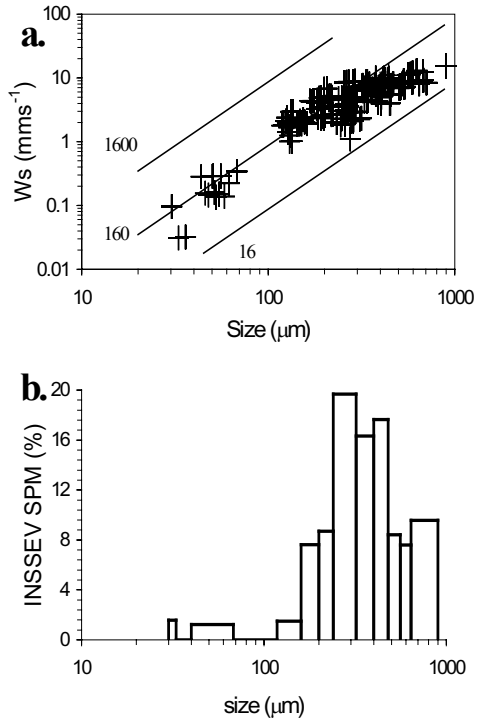

Size Band	A	B	C	D	E	F	G	H	I
Floc size (μm)	< 80	80-160	160-240	240-320	320-400	400-480	480-560	560-640	> 640

Figure 6. Summary of floc characteristics for Tamar estuary spring tide sample T24-9 obtained at high water –3:00 hr. Where (a) illustrates the relationship between floc size and settling velocities of individual flocs, with the diagonal full lines showing values of constant effective density (kg m^{-3}). The histogram (b) shows how the suspended matter is distributed across the floc size spectra, by segregating the floc population into discrete size bands. The percentage of the total SPM concentration contributed by the floc mass (as calculated from the INSSEV floc data) present within each size band is shown.

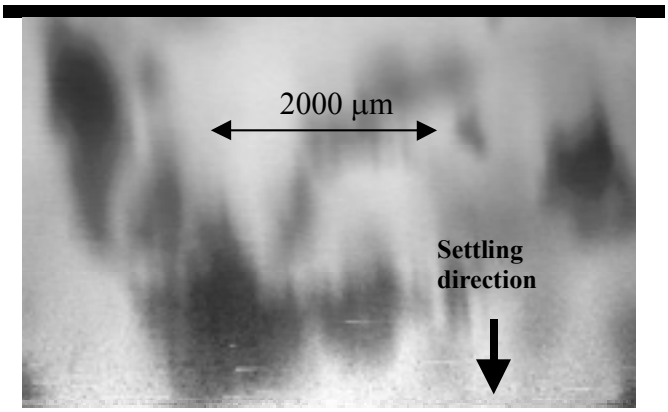

Figure 7. Numerous ragged cluster-type macroflocs settling from within a CBS sample (INSSEV sample T24-9, observed 20 seconds into record).

During spring tides the water column remained predominantly fresh throughout. Peak surface current velocities were virtually double of those experienced during neaps and the SPM concentration was an order of magnitude higher. Generally, the flocs were distinctly larger in size than those observed during neaps. Of particular interest were the mid-flood periods where a concentrated benthic suspension (CBS) layer developed in the near-bed region. A CBS is a high concentration suspension (typically up to 10 g l^{-1}) and can produce gradient Richardson numbers of 0.15-0.2, which indicate a significant level of stratification. The sediment is kept in suspension by turbulence, although the CBS layer interacts with the turbulent flow field. The CBS tends to behave in a Newtonian manner, but with increased viscosity. Unlike a fluid mud, a CBS is still transported with the main current flow. At mid-tide, the CBS layer was nominally 0.6 m thick (i.e. the distance between the estuary bed and the lutocline) and it displayed a mean concentration of ~6 g l^{-1}. CBS characteristics have been further examined by MORY *et al*. (2002).

When the concentration gradient generally exceeds 4 kg m^{-4} drag reduction can occur at the lutocline interface and this can result in the suppression of turbulent energy within a CBS. During spring tides this had the net result of producing an abundance of large macroflocs within the CBS layer. This effect was demonstrated by INSSEV sample T24-9 which was collected from within the main body of the advecting turbidity maximum, where the SPM concentration was 5.6 g l^{-1} and the TSS was restricted to 0.36 N m^{-2} at 0.5 m above the bed. The scatterplot of individual flocs (Figure 6a) reveals there are two separate modes in the floc distribution. One mode consists of a sub-group of slow settling (Ws < 0.3 mm s^{-1}) flocs in the 30-70 μm size range, however these flocs only constituted 9.5% of the total population (of individual flocs).

The distribution of the particulate matter within sample T24-9 is illustrated by Figure 6b, where each bar is representative of the percentage of the total SPM concentration contributed by the flocs present within each respective discrete floc size band (SB). Where SB.A represents flocs less than 80 μm in size, whilst SB.I are flocs greater than 640 μm in diameter. Figure 6b reveals the majority of the particulate mass, 49%, was contained within the larger sized aggregates ranging from 240-480 μm (SB.D-F). A further 25% of the dry floc mass constituted the macroflocs exceeding 480 μm. This group of large flocs had settling velocities between 4-8 mm s^{1}. The relative absence of individual microflocs indicated a high flocculation efficiency occurring within the CBS layer. This concurs with the findings of field studies reported by DYER *et al*. (2002b), and laboratory experiments by MORY *et al*. (2002).

An inspection of the most commonly occurring flocs, indicated that the CBS environment cultivated mainly large, fast settling, "cluster"-type macroflocs which were ragged in appearance (Figure 7). Visual enlargements of numerous flocs encountered early in the sample T24-9 record revealed that a high proportion of the macroflocs had been flattened (height:width ratios of 0.8-0.9) as a result of non-destructive inter-macrofloc contacts, which possibly occurred during settling within the CBS layer. These very porous (porosity > 96%) macroflocs had effective densities of only 40-60 kg m^{-3} and resultant fast settling velocities ranging between 10-15 mm s^{-1}.

In contrast, within less turbid spring tide conditions, which are a step on the way to the more fully saturated situation described previously, smaller macroflocs could still further increase their settling rate potential by combining with other flocs to form a more linear floc configuration. This is illustrated by INSSEV sample T21-5, which was acquired at a period in the tidal cycle when the concentration was 1.1 g l^{-1} and the shear stress was 0.42 N m^{-2} (at the INSSEV sampling height). The fastest settling flocs which occurred most commonly during spring tide sample T21-5 were the ragged, cluster-type (Figure 8a) displaying Dx and Dy of 1000 μm and 1250 μm, respectively.

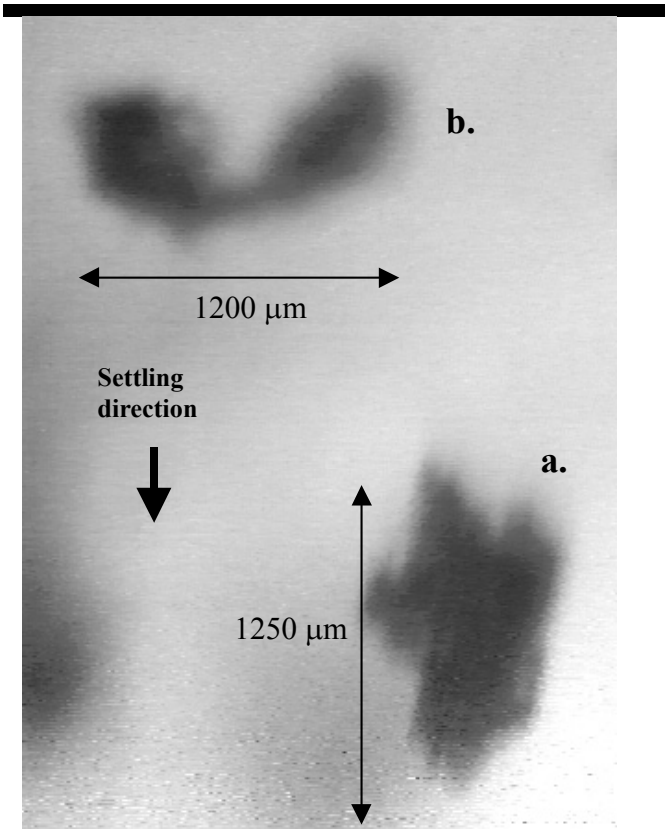

Figure 8. (a) A ragged cluster-type macrofloc and (b) a simple stringer composed of two macroflocs possibly bonded by sticky organic fibres (INSSEV sample T21-5, observed 30.7 seconds into record).

These macroflocs fell at a rate of 12 mm s^{-1}. However, the other macrofloc captured in the same frame (Figure 8b) shows that the

joining of two aggregates only 500 μm in diameter, produced a floc with similar settling characteristics to those of the single large cluster macrofloc (Figure 8a).

The process of floc capturing is taken to an even greater extreme by the very unusual stringer-type floc which is illustrated in Figure 9. Possessing an overall length of 2 mm, its construction of five small spherically clustered macroflocs (individual D ranging between 350-420 μm) interlinked in-line by fine organic strands, make it resemble a "string of pearls" configuration. By interconnecting small macroflocs of moderate settling velocity (Ws ~ 2-3 mm s^{-1}) in this manner to act as a single entity, the stringer produced a significantly higher net settling velocity (Ws ~ 10 mm s^{-1}), and in turn increased the mass settling flux displayed by the matter in suspension. The empirical results imply that there is the fine balance between the abundance of SPM concentration and turbulent mixing activity, which create the ideal environmental conditions to permit this high level of flocculation.

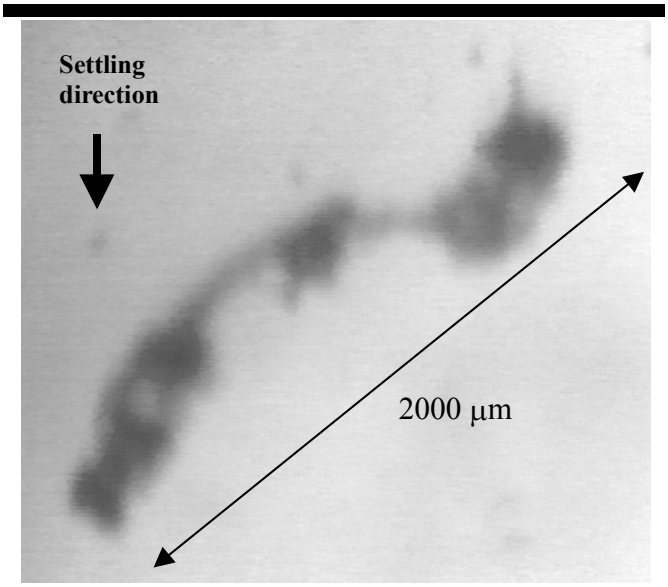

Figure 9. A string of pearls configuration macrofloc (INSSEV sample T21-5, observed 42 seconds into record).

Gironde estuary - Lower Reaches

The first SWAMIEE international field experiment, referred to as *SWAMGIR1*, was conducted in the lower reaches of the Gironde estuary (south-west France). Possessing a tidal area of 625 km^2, the Gironde is the largest estuary in France. The Gironde estuary is generally partially stratified, with the water column salinity profile becoming more vertically homogeneous towards the mouth. It is topographically very regular in shape and the outline varies exponentially from the mouth through to the tidal current limit, which is located 140 km upstream. The Gironde estuary has a total catchment of 81,000 km^2 (LATOUCHE, 1971), which is one hundred times greater than the Tamar estuary. Together the Rivers Garonne and Dordogne produce an annually-averaged river discharge of 760 m^3 s^{-1}. The Gironde has a semi-diurnal tidal regime and a spring tidal range of 5.5 m, which gives the estuary a macrotidal classification. SWAMGIR1 measurements were made from a surface vessel moored at two separate locations. The first site was situated 1 km from the shore at Le Verdon, whilst the second was a location closer to the northern shoreline near Talmont. This placed the data acquisition within the vicinity of one of the localised mud deposits situated between Bordeaux and Talais (JOUANNEAU and LATOUCHE, 1981). These 2-3 m deep patches of cohesive sediment are significant to the estuary's sediment transport regime, as they move either landward or seaward in response to the run-off.

The SWAMIEE sampling programme was conducted during neap tides, where the near bed turbulent shear stress ranged between 0.09-1.94 N m^{-2} (MANNING *et al*., 2004). However, the near bed SPM was much lower than experienced within the Tamar, with concentrations rarely exceeding 300 mg l^{-1}. In comparison, the corresponding surface current attained velocities ranging from 0.75-1.2 m s^{-1} which were faster than the Tamar estuary during neap tides. The downstream sampling locations in the Gironde meant the water column remained predominantly saline throughout a tidal cycle, with salinity values ranging from lows of 16, through to peaks of 25.5 at high water. The maximum water depth did not exceed 12 m.

Figure 10 shows the floc characteristics for sample G23-8 which was acquired near Le Verdon 2 hours 10 minutes before local high water. The peak concentration was 139 mg l^{-1} and the TSS was 0.46 N m^{-2}. The settling velocities spanned three orders of magnitude from 0.05-3.43 mm s^{-1}, and the effective densities ranged between 38-483 kg m^{-3}. The largest macroflocs observed at this period of the tide were low density "comet-shaped" aggregates (Figure 11) 1 mm in length (Dy).

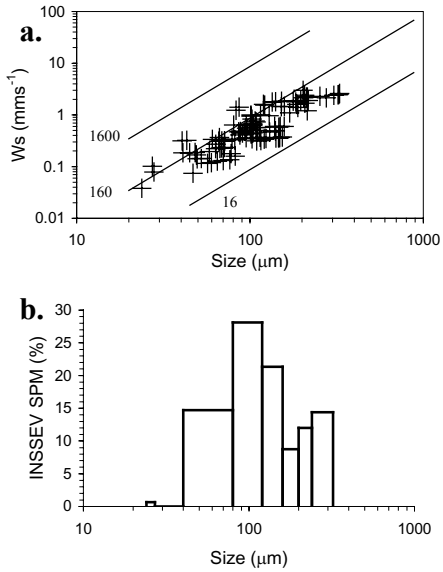

Size Band	A	B	C	D	E	F	G	H	I
Floc size (μm)	< 80	80-160	160-240	240-320	320-400	400-480	480-560	560-640	> 640

Figure 10. Summary of floc characteristics for Gironde estuary neap tide sample G23-8 obtained at high water –2:10 hr. Where (a) illustrates the relationship between floc size and settling velocities of individual flocs, with the diagonal full lines showing values of constant effective density (kg m^{-3}). The histogram (b) shows how the suspended matter is distributed across the floc size spectra, by segregating the floc population into discrete size bands. The percentage of the total SPM concentration contributed by the floc mass (as calculated from the INSSEV floc data) present within each size band is shown.

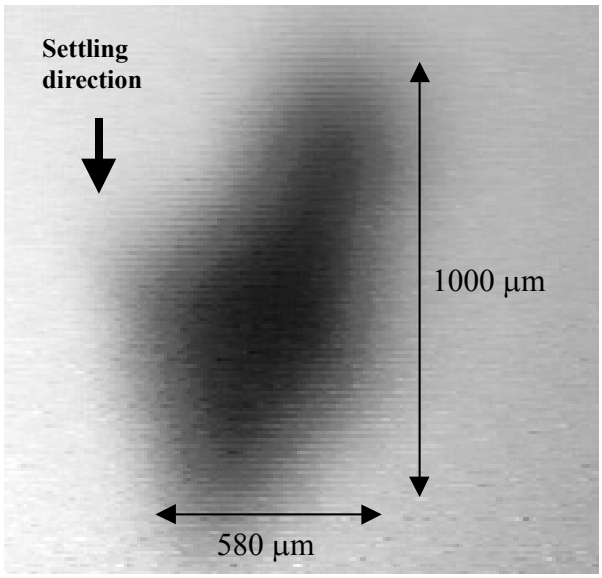

Figure 11. A large low density comet-shaped macrofloc (INSSEV sample G23-8, observed 80 seconds into record).

These flocs were composed of approximately 12% organic matter, which was less than half the organic content observed for the comparative Tamar estuary neap tide flocs. MANNING et al. (2001) reports similar observations for Gironde estuary macroflocs.

When comparing the microfloc and macrofloc subgroups for sample G23-8, it revealed that 86 flocs encompassed 65% of the dry floc mass in the microfloc subgroup (i.e. SB.A-B), compared to just 20 flocs constituting the remaining 35% of the dry mass in the latter group. This was a 4:1 population difference and a 2:1 SPM distribution ratio between the small floc group and the larger fraction. However 66% of the mass settling flux (MSF), which is defined as the product of the SPM concentration and the settling velocity, was contained in the larger floc size grouping of 160-400 μm, as a result of their significantly faster settling velocities.

Dollard estuary – Intertidal Mudflats

The Dollard estuary is a well mixed semi-diurnal mesotidal estuary embayment fringing the southern part of the Ems estuary. It is located in the north-eastern part of the Dutch Wadden Sea on the border with Germany. The Dollard comprises a surface area of 112 km^2 (76 km^2 are the intertidal flats) of the total 500 km^2 Ems system (DANKERS *et al*., 1984). The main freshwater input comes from the Ems River which has an annual mean discharge of 20 m^3s^{-1}, although seasonally this can vary from 25 $m^3 s^{-1}$ to 390 $m^3 s^{-1}$ (DE JONGE, 1992). In contrast to the Tamar and Gironde, the Dollard is an ebb dominant estuary.

The INTRMUD interdisciplinary experiment (DYER *et al*., 2000) was conducted on the Heringsplaat intertidal mudflats, at a position approximately 200 m from the Groote Gat channel. At this location the mudflat was dry for nearly half the tidal cycle and the maximum water depth at high tide was about 1.5 m. A total of eleven samples were obtained. Figure 12 shows the floc sizes, settling velocities and effective density values obtained for sample D31-2 collected 1.5 hours prior to high water. At this point in the tidal cycle, the near bed SPM was 664 mg l^{-1} and TSS = 0.32 N m^{-2}. It is evident that there are two separate modes in the floc distribution. There is a very tight group of microflocs about 20-30 μm in diameter and with a mean settling velocity of ~ 0.3 mm s^{-1} and effective density of 450 kg m^{-3}. This group is quite distinctly different from the macroflocs, which had lower effective densities ~ 60 kg m^{-3}, a size range of about 120 to 490 μm and a mean settling velocity of approximately 2.8 mm s^{-1}. Many of the macroflocs appeared as complex stringer configurations measuring up to 5 mm in length. Whereby smaller flocs were attached to each other by thread-like connections. With only a few flocs observed between the two groups, implies that the sediment in suspension could be defined as being very unstable (VAN LEUSSEN, 1994), i.e. it was nearing its optimum level of flocculation with only limited intermediate aggregation or disaggregation occurring.

DISCUSSION

For the duration of a complete tidal cycle, an average macrofloc settling velocity of 2 mm s^{-1} was calculated for the Dollard estuary samples acquired during neap conditions. This value rose as high as 3.3 mm s^{-1} for a Tamar estuary spring tide. On a sub-tidal cycle time scale, periods of high SPM concentration (such as within a CBS layer) coupled with a moderate level of turbulent shear, created a water column environment very conducive to flocculation by producing a high percentage of constructive inter-particular collisions. This was reflected in the macrofloc size fraction settling velocities of 4-6 mm s^{-1}.

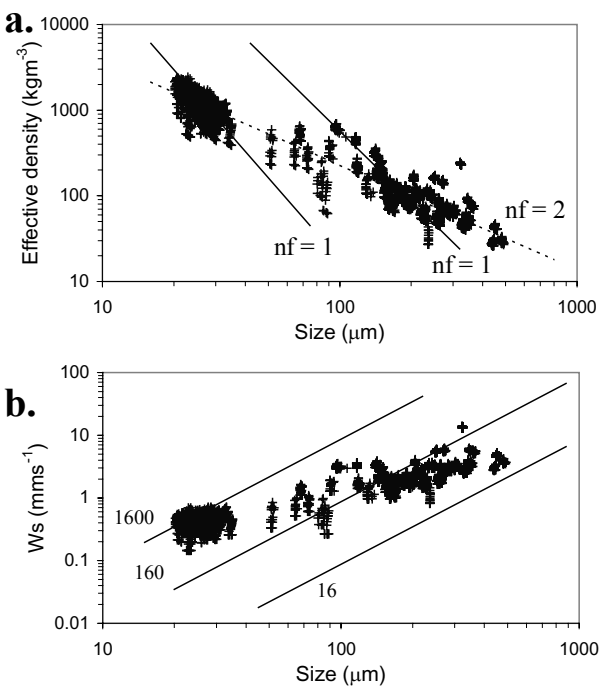

Figure 12. Relationships between floc size and (a) effective density and (b) settling velocity for sample D31-2 from the Dollard estuary. This sample was acquired during the early part of the flood tide (high water -1:35 hr) when the total water depth was 0.95 m. For plot (a) the continuous line illustrates fractal dimensions (nf) = 1 and the dashed lines nf = 2. For plot (b) the contours represent values of constant effective density (kg m^{-3}).

These empirical findings confirm the long established hypothesis which advocates that the macrofloc settling velocity is a function of particle concentration. However, the presence of a moderate degree of turbulent stirring is also necessary to successfully generate large flocs, and this important flocculation mechanism has quite often been completely ignored in many flocculation studies and parameterisations. The requirement of both turbulence and SPM to achieve optimum flocculation has been independently confirmed by recent controlled laboratory investigations conducted by MANNING and DYER (1999), GRATIOT (2000) and MORY *et al.* (2002).

Settling rates in computer simulation models have commonly been parameterised using data collected by sampling instruments which have more recently been revealed as floc-disruptive, in particular field settling tubes (OWEN, 1976). These devices tended to produce sample mean Ws of 0.5-1 mm s^{-1}, which are substantially slower than those demonstrated by the macrofloc sub-populations observed in European estuaries by the INSSEV instrument. It is evident from the INSSEV results that these slower Owen tube derived settling rates are representative of the more structurally robust microfloc fractions. One could postulate that using Ws values in the 0.5-1 mm s^{-1} range, as opposed to those more representative of typical macrofloc settling dynamics, would significantly effect the predictive output from a numerical sediment transport simulation.

Both KRONE (1986) and EISMA (1986) have hypothesised that the consistently lower effective density, fast settling macrofloc fractions are constructed from the smaller microflocs. This is the order of aggregation theory and is discussed later in this section. The floc distribution scattergraphs of each estuary show that the individual microflocs can exhibit effective densities spanning from 30 kg m^{-3} up to 1000 kg m^{-3}. This suggests that it is possible that each macrofloc could be composed from a combination of microflocs which display a variety of floc characteristics. However, from the experimental results presented in this paper, one can deduce that there are two main types of microfloc. The first type of microfloc is predominantly mineral in origin and probably formed during very turbulent events, by a high frequency of orthokinetic inter-particular contacts. EISMA (1986) found that these microflocs are commonly formed in combination with the presence of strong biogenic glues on the particle surfaces, which in turn produces a compact, very dense (ρ_e of 350- 900 kg m^{-3}), fast settling microfloc. The second lower density type is a slower settling, more organically based, microfloc (DYER *et al*., 1996). During aggregate evolution, the distribution of the two microfloc types within a macrofloc, would be quite different for a cluster-type, as opposed to a more organic stringer-type macrofloc, and this could partly account for the contrasting floc properties demonstrated by each macrofloc type.

Salinity was seen to have little influence on floc formation. The more turbulent environment of the highly saline (salinity up to 25.5) Gironde estuary actually made it less conducive for macrofloc production. This was reflected in a mean floc size which ranged between 89-176 μm, in contrast to the Tamar neaps where the average floc size was as high as 309 μm, for comparative ambient TSS and concentration conditions.

Based on the results of a statistical analysis (for the data from the Gironde and Tamar estuaries), MANNING (2004) has identified a TSS region between 0.32-0.42 N m^{-2} as providing the optimum level of turbulent intensity which most effectively stimulates the macrofloc settling velocity, for concentrations up to 8 g l^{-1}. On many occasions (e.g. Dollard sample D31-2 and Tamar sample T24-9) these turbulent conditions tended to produce dual modes in the size-settling velocity distributions of specific floc populations. Whereby a separate clustering of macroflocs and microflocs develop, and these are separated by only a minor number of transitional aggregates. One can hypothesise that the particles in suspension have flocculated into their most efficient spectral distribution. This observation is not to be confused with the flocs being permitted to attain a state of equilibrium with the controlling shear stress, i.e. the flocculation time (WINTERWERP, 1999). A floc population can be in equilibrium with the surrounding turbulence, but the shear stress may never permit the flocs to attain a higher level of aggregation. For example, VAN LEUSSEN (1994) has shown that, depending upon the SPM concentration, a TSS of 0.35 N m^{-2} would typically require 30-100 seconds to equilibrate a suspension of particulates.

Flocculation has a dual influence on the vertical sediment flux. As well as governing the rate at which the suspended matter settles, it also controls how the matter is distributed across the size spectrum. By implementing a sequence of algorithms developed by FENNESSY *et al*. (1997), the dry mass of a floc population observed by the INSSEV instrument can be referenced with the SPM concentration. This in turn provides corresponding rates of mass settling flux.

When comparing estuarine neap tide conditions at times of peak SPM concentrations, macroflocs constituted 65-75% of the suspended matter in the Tamar, whereas this was only 38-52% for the Gironde macroflocs. The difference could be attributed to variations in the mineralogical composition, the adhesive properties of organic coatings, and / or the greater turbulent activity present within the Gironde estuary water column. The corresponding values of SPM distribution for the Dollard macroflocs fell mid-way between the other two estuaries. For the higher concentration Tamar spring tides, over 90% of the floc dry mass comprises macroflocs. Therefore, when considering the combined effects of the Ws and floc mass distribution, high concentration spring tides can produce a MSF rate which are one or two orders of magnitude greater than neap conditions.

The most effective parameter which compares the distribution of particulate matter throughout the macrofloc and microfloc sub-populations, is the dimensionless SPM ratio. This is calculated by dividing the percentage of macrofloc SPM by the percentage of microfloc SPM. An SPM ratio of unity would represent an equal apportioning of the floc mass between the two floc sub-populations. It must be stressed that this type of computation is unique to data obtained from instruments such as INSSEV, which can accurately estimate floc effective density and hence permit the determination of the dry floc mass for each individual floc throughout an entire floc size spectrum. A parametric regression analysis was conducted on the SPM ratio values of all three estuaries by combining them into a single data set, and a correlation (R-square = 0.732) with SPM concentration (units are mg l^{-1}) was revealed. This indicated that the empirical algorithm (eqn. 7) was a realistic representation of the Tamar, Gironde and Dollard estuary floc mass distribution. The regression curve is shown in Figure 13.

$$\text{SPM ratio} = 0.815 + 0.00318\ \text{SPM} - 0.14\text{x}10^{-6}\ \text{SPM}^2 \qquad (7)$$

The scatter in SPM ratio data points is greatest for concentrations under 200 mg l^{-1}. However when applying such a division of the floc particulate matter for predictive modelling purposes, particularly those which attempt to simulate sediment transport over numerous consecutive tidal cycles, this would have a minimal effect. This is because the more significant mass settling fluxes develop during the periods of higher SPM concentration.

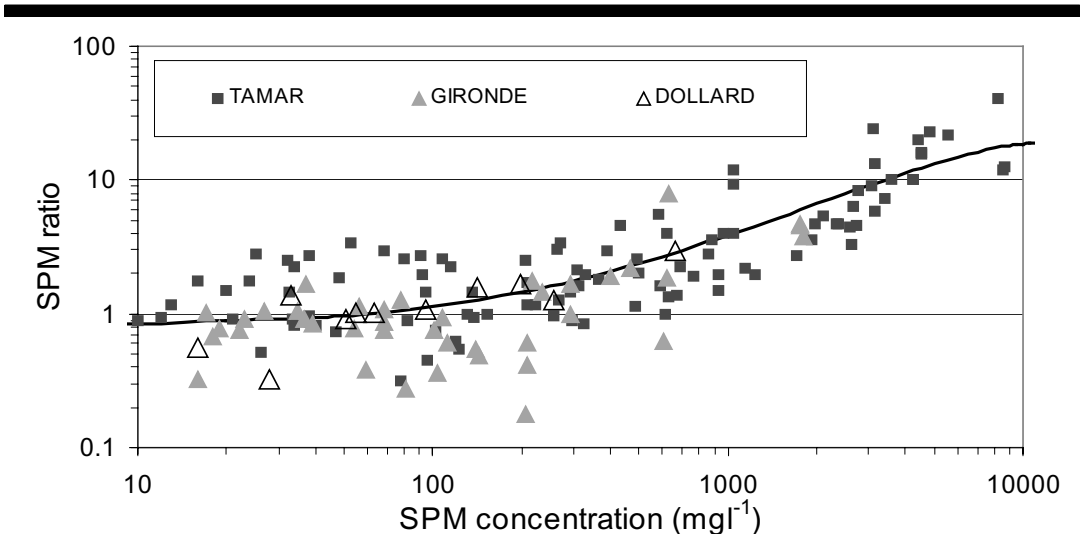

Figure 13. A plot of the SPM ratio against suspended particulate matter concentration. Data points for the Tamar, Gironde and Dollard estuaries are shown. The best fit regression line ($R^2 = 0.732$) is representative of equation 7.

The organic matter content varied quite considerably, from lows of 12% for the Gironde through to peaks of 35% for the Dollard mudflats. However, EISMA (1986) has deduced from data collected during previous field studies conducted in both the Ems and Rhine estuaries (EISMA *et al*., 1982; 1983), that it is not just the overall organic content of the mud which inevitably influences flocculation, but more importantly the stickiness of the organics within the mud which increases the inter-particular cohesion. This can be inferred by the level of sugars or carbohydrates present, in particular extra-cellular polymeric substances (EPS). During Tamar neap tides in August 1998, near bed SPM ranged between 50-500 mg l^{-1}, with an organic content of between 14.5-28%. These relatively low SPM conditions coincided with a mean carbohydrate per mass of sediment of up to 34 mg per g of SPM. This compares with up to 5.9 mg per g of SPM during spring tides, where the organic levels were significantly reduced (i.e. 10-14%). The lower organic levels observed throughout spring tides were attributed to the stronger bed shear stresses which eroded deeper into the more compact bed substrate, and suspended bed sediment which was in various stages of decomposition (MANNING and DYER, 2002b). However, with a significantly higher abundance of particulate matter placed into suspension during spring tides (at times two orders of magnitude greater than neaps), the overall effective carbohydrate concentrations were seen to be up to seven times greater during the spring tidal conditions compared with neaps; i.e. maximum values of carbohydrate concentration of 2.5 mg l^{-1} at neap tides, compared to 17.5 mg l^{-1} during spring tides.

Tamar and Dollard estuary results have suggested that the transformation of smaller macroflocs into stringer configurations have a significant effect on the effective settling velocity. If one assumes that estuarine stringers are of a similar composition to the delicate marine snow observed by divers or submersibles in the open sea (NISHIZAWA *et al*., 1954; SHANKS and TRENT, 1979; ALLDREDGE, 1979), it would infer that estuarine stringers have a very low shear stress threshold, beyond which aggregate break-up readily occurs. However, further investigation has revealed that during Tamar spring tides, the presence of a high carbohydrate concentration appears to optimise the production of numerous fast settling stringers throughout highly turbulent episodes of the tidal cycle. Floc sample T21-4 from a Tamar spring tide deployment on the ebb illustrates the above phenomena. Although the TSS was 0.68 N m^{-2}, i.e. which is beyond what is regarded as the optimum turbulence region for flocculation, and the organic content was only 5.3%, a high total carbohydrate concentration of 10.3 mg l^{-1} aided in the coagulation of the particulates (SPM concentration ~ 2 g l^{-1}) by producing what appeared to be numerous delicate stringer configurations. In fact, stringers (floc with H:W ratio > 2.5) were found to represent up to 12% of the individual floc numbers composing a single population at periods of the tide when the above ambient condition occurred. It is likely that the dissolved carbohydrates were present within the flocs as sticky mucopolysaccharides and these are produced by bacteria, algae and higher plant species (CORPE, 1980; LEPPARD and BURNISON, 1983). This has the net result of transforming 40% of the SPM into fast settling (Ws ranging from 1.8-3.7 mm s^{-1}) macroflocs with spherically equivalent diameters of 240-480 μm. With height:width ratios ranging between 1.8-6, these long stringers had a very loose structure possessing effective densities of only 18-70 kg m^{-3} and they were up to 98.6% porous. The only way these flocs could retain their structural integrity in such turbulent conditions was by having interconnecting joints which were strongly bonded.

Many mathematical flocculation models, such as those of HILL (1996) and WINTERWERP (1997), represent flocculation using fractal growth and this requires the stipulation of a constant fractal dimension coefficient (nf). Floc fractal theory is based on KRONE'S (1963, 1986) order of aggregation and can be regarded as a hierarchical process, whereby primary particles stick together to form zero order flocs, these then coagulate to transform them into first order flocs, etc. However, this approach does not take into account any of the variability in the organic constituents from which estuarine muds are partly composed, and thus may very rarely apply to the diversity of natural estuarine floc populations. This was demonstrated by DYER and MANNING (1999) who, using Dollard estuary floc sample D31-2 as an example, found it was possible to fit lines with slopes appropriate to fractal dimensions of unity (see Figure 12a), indicating a constant settling velocity, through each of the two modes. Thus, it seems likely that the flocs are composed of two different elements with limited flocculation occurring between each aggregate group. Alternatively, a line for the fractal number of 2 can be drawn through both modes. In summary, the former (nf = 1) indicates two sub-populations both composed of very weak marine snow

type flocs, whereas the latter suggests self-similar particles or microflocs which can progressively coagulate into macroflocs. Therefore, with other Dollard, Gironde and Tamar estuary floc samples showing similar patterns, the fractal approach appears to provide only a first order representation of a floc spectrum.

CONCLUSIONS

The INSSEV instrument has successfully measured both quantitative and qualitative floc characteristics in-situ for floc populations observed in the Tamar, Gironde and Dollard estuaries. INSSEV measurements of complete floc spectra revealed average settling velocities for the larger macrofloc (D > 160 μm) fraction ranged between 2 mm s^{-1} for the low concentrations experienced in the Dollard estuary, and 4-6 mm s^{-1} for floc populations observed within a CBS layer in the Tamar estuary. These settling velocity values were 4-10 times faster than both those measured by more disruptive instruments (such as field settling tubes), and settling velocities typically implemented in numerical sediment transport simulation models.

Qualitatively, macroflocs are seen to exist as: cluster, stringer or comet types. Most fast settling macroflocs had effective densities of less than 90 kg m^{-3}. Particulates which aggregated into a stringer formation were particularly noted as significantly improving the settling characteristics of small macroflocs; from the simple articulation of two flocs, through to the formation of complex string-of-pearls configurations. During neap tides macroflocs represented 38-70% of the SPM concentration, whilst during more turbid spring tides this rose to in excess of 90%. Flocculation was potentially enhanced during spring tides by the presence of high carbohydrate concentrations which had the effect of raising inter-particle cohesion.

In contrast, the microflocs observed in each estuary (from which the macroflocs are principally composed), demonstrated effective densities spanning from 30 to 1000 kg m^{-3}. The high density fraction are predominantly mineral in origin and are probably formed during very turbulent events by a high frequency of orthokinetic interparticular contacts. Whilst the slower settling, lower density, microflocs are more organic. During floc evolution, the distribution of the two microfloc types within a macrofloc, would be quite different for a cluster-type when compared to a more organic stringer-type configuration.

The division of particulate matter present within the macrofloc and microfloc fractions for samples obtained in the Tamar, Gironde and Dollard estuaries, showed a close correlation with the SPM concentration. The ability to be able to apportion particulate mass between the two key floc sub-populations is a distinct advancement when parameterising flocculation for inclusion in sediment transport models.

ACKNOWLEDGEMENTS

The Tamar estuary experimental programme was funded by the EC MAST as part of contract MAS3-CT97-0082 COSINUS (Prediction of cohesive sediment transport and bed dynamics in estuaries and coastal zones with integrated numerical simulation models). The Gironde estuary experiments were funded by the EC TMR SWAMIEE (Sediment and water movement in industrialised estuarine environments) project under contract No. ERBFMRXCT970111. The Dollard estuary experimental programme was funded by the EC MAST project INTRMUD (The Morphological Development of Intertidal Mudflats) under contract MAS3-CT95-0022. The author would like to thank the boat crews and all the technical staff who assisted during all the field experiments. The preparation of this paper was partially funded by H.R. Wallingford (UK), and the DEFRA / Environment Agency Joint Flood and Coastal Defence Research & Development Programme in Fluvial, Estuarine and Coastal Processes: Estuary Process Research (EstProc) project (under contract No.FD1905/CSA5966).

LITERATURE CITED

ALLDREDGE, L.L., 1979. The chemical composition of macroscopic aggregates in two neritic seas. *Limnol. Oceanogr*., 24, 855-866.

BALE, A.J. and MORRIS, A.W., 1987. In-situ measurement of particle size in estuarine waters. *Estuarine, Coastal and Shelf Science*, 24, 253-263.

BERLAMONT, J.E., 2002. Prediction of cohesive sediment transport and bed dynamics in estuaries and coastal zones with integrated numerical simulation models. In: J.C. Winterwerp and C. Kranenburg, (eds.), *Fine Sediment Dynamics in the Marine Environment - Proc. in Mar. Sci. 5.,* Amsterdam: Elsevier, pp. 1-4.

BRUN-COTTAN, J.C., 1986. Vertical transport of particles within the ocean. In: P. Buat-Menard, (ed), *The Role of Air-Sea Exchange in Geochemical Cycling*. D. Reidel Publishing Company, pp. 83-111.

CHRISTIE, M.C.; QUARTLEY, C.P., and DYER, K.R., 1997. The development of the POST system for in-situ intertidal measurements. *The 7th International Conference On Electrical Engineering In Oceanography*, (London, England), Publication No. 439, pp. 39-45.

CORPE, W.A.,1980. Microbial surface components involved in adsorption of microorganisms onto surfaces. In: G. Bitton and K.C. Marshall (eds.), *Adsorption of microorganisms to surfaces*. London: John Wiley and Son, pp.105-144.

DANKERS, N.; BINSBERGEN, M.; ZEGERS, K.; LAANE, R. and VAN DE LOEFF, R.M., 1984. Transportation of water, particulate and dissolved organic and inorganic matter between a salt marsh and the Ems-Dollard estuary, The Netherlands. *Estuarine, Coastal and Shelf Science*, 19, 143-165.

DE JONGE, V.N., 1992. Physical processes and dynamics of microphytobenthos in the Ems estuary. Groningen, The Netherlands: University of Groningen, Ph.D. Thesis.

DYER, K.R., 1997. *Estuaries: A physical introduction (2nd Edition)*, Chichester, England: Wiley & Sons Ltd., 195p.

DYER, K.R. and MANNING, A.J., 1999. Observation of the size, settling velocity and effective density of flocs, and their fractal dimensions. *Journal of Sea Research*, 41, 87-95.

DYER, K.R.; BALE, A.J.; CHRISTIE, M.C.; FEATES, N.; JONES, S., and MANNING, A.J., 2002a. The turbidity maximum in a mesotidal estuary, the Tamar estuary, UK. Part I: Dynamics of suspended sediment. In: J.C. Winterwerp and C. Kranenburg, (eds.), *Fine Sediment Dynamics in the Marine Environment - Proc. in Mar. Sci. 5.,* Amsterdam: Elsevier, pp. 203-218.

DYER, K.R.; BALE, A.J.; CHRISTIE, M.C.; FEATES, N.; JONES, S., and MANNING, A.J., 2002b. The turbidity maximum in a mesotidal estuary, the Tamar estuary, UK. Part II: The floc properties. In: J.C. Winterwerp and C. Kranenburg, (eds.), *Fine Sediment Dynamics in the Marine Environment - Proc. in Mar. Sci. 5.,* Amsterdam: Elsevier, pp. 219-232.

DYER, K.R.; CHRISTIE, M.C.; FEATES, N.; FENNESSY, M.J.; PEJRUP, M. and VAN DER LEE, W., 2000. An investigation into processes influencing the morphodynamics of an intertidal mudflat, the Dollard estuary, The Netherlands: I. Hydrodynamics and suspended sediment. *Estuarine, Coastal and Shelf Science*, 50, 607-625.

DYER, K.R.; CORNELISSE, J.; DEARNALEY, M.P.; FENNESSY, M.J.; JONES, S.E.; KAPPENBERG, J.; McCAVE, I.N.; PEJRUP, M.; PULS, W.; VAN LEUSSEN, W. and WOLFSTEIN, K., 1996. A comparison of in-situ techniques for estuarine floc settling velocity measurements. Netherlands Journal of Sea Research, 36 (1-2), 15-29.

EISMA, D., 1986. Flocculation and de-flocculation of suspended matter in estuaries. *Netherlands Journal of Sea Research*, 20 (2/3), 183-199.

EISMA, D.; CADEE, R.; LAANE, R. and KALF, J., 1982. Preliminary results of AURELIA and NAVICULA cruises in the Rhine and Ems estuaries, January-February, 1982. *Mitt. Geol.-Palaontol. Inst. niv. Hamburg*, SCOPE/UNEP Sonderbereich, 52, 633-654.

EISMA, D.; BOON, J.; GROENEWEGEN, R.; ITTEKKOT, V.; KALF, J. and MOOK, W.G., 1983. Observations on macro-aggregates, particle size and organic composition of suspended matter in the Ems estuary. *Mitt. Geol.-Palaontol. Inst. niv. Hamburg*, SCOPE/UNEP Sonderbereich, 55, 295-314.

EISMA, D.; SCHUHMACHER, T.; BOEKEL, H.; VAN HEERWAARDEN, J.; FRANKEN, H.; LANN, M.; VAARS, A.; EIJGENRAAM, F. and KALF, J., 1990. A camera and image analysis system for in-situ observation of flocs in natural waters. *Netherlands Journal of Sea Research*, 27, 43-56.

FENNESSY, M.J., 1994. Development and testing of an instrument to measure estuarine floc size and settling velocity in-situ. Ph.D. Thesis, University of Plymouth, 128 pp.

FENNESSY, M.J.; DYER, K.R. and HUNTLEY, D.A., 1994a. Size and settling velocity distributions of flocs in the Tamar estuary during a tidal cycle. *Netherlands Journal of Acquatic Ecology*, 28(3-4), 275-282.

FENNESSY, M.J.; DYER, K.R. and HUNTLEY, D.A., 1994b. INSSEV: an instrument to measure the size and settling velocity of flocs in-situ. *Marine Geology*, 117, 107-117.

FENNESSY, M.J.; DYER, K.R.; HUNTLEY, D.A. and BALE, A.J., 1997. Estimation of settling flux spectra in estuaries using INSSEV. In: N. Burt, R. Parker and J. Watts, (eds.), *Proceedings of INTERCOH Conference* (Wallingford, England), Chichester: John Wiley & Son, pp. 87-104.

GIBBS, R.J., 1985. Estuarine flocs: their size settling velocity and density. Journal of Geophysical Research, 90 (C2), 3249-3251.

HILL, P.S., 1996. Sectional and discrete representations of floc breakage in agitated suspensions. *Deep-Sea Research*, 43, 679-702.

JOUANNEAU, J.M. and LATOUCHE, C., 1981. The Gironde estuary. In: H. Fuchtbauer, A.P. Lisitzyn, J.D. Milliman and E. Seibold, (eds.), *Contributions to Sedimentology*. Stuttgart, Germany: E. Schweizerbart'sche Verlagsbuchhandlung (Nagele u. Obermiller), 10, 115p.

KRONE, R.B., 1963. A study of rheological properties of estuarial sediments. Hydraulic Engineering Laboratory and Sanitary Engineering Laboratory, University of California, Berkeley, *Report No. 63-68*.

KRONE, R.B., 1986. The significance of aggregate properties to transport processes. In: A.J. Mehta (ed.), *Estuarine Cohesive Sediment Dynamics*. Berlin: Springer-Verlag, pp. 66-84.

LATOUCHE, C., 1971. Les argiles des baisins alluvionnaires Aquitains et des dependances oceaniques. Bordeaux, France: University of Bordeaux 1, Ph.D. thesis , 415p.

LEPPARD, G.G. and BURNISON, B.K., 1983. Bioavailability, trace element associations with colloids and an emerging interest in colloidal organic fibrils. In: G.G. LEPPARD, (ed.), *Trace element speciation in surface waters and its ecological implications*. New York: Plenum Press, pp. 105-122

LICK, W., 1994. Modelling the transport of sediment and hydrophobic contaminants in surface waters. *U.S.A. / Israel Workshop on monitoring and modelling water quality*, (Haifa, Israel).

LICK, W.; HUANG, H. and JEPSEN, R., 1993. Flocculation of fine-grained sediments due to differential settling. *Journal of Geophysical Research*, 98 (C6), 10279-10288.

MANNING, A.J., 2001. A study of the effect of turbulence on the properties of flocculated mud. Plymouth, England: University of Plymouth, Ph.D. thesis, 282p.

MANNING, A.J., 2004. The observed effects of turbulence on estuarine flocculation. *Journal of Coastal Research,* SI 41. (This Volume).

MANNING, A.J. and DYER, K.R., 1999. A laboratory examination of floc characteristics with regard to turbulent shearing. *Marine Geology*, 160, 147-170.

MANNING, A.J. and DYER, K.R., 2002a. The use of optics for the in-situ determination of flocculated mud characteristics. *Journal of Optics A: Pure and Applied Optics, Institute of Physics Publishing*, 4, S71-S81.

MANNING, A.J. and DYER, K.R., 2002b. A comparison of floc properties observed during neap and spring tidal conditions. In: J.C. Winterwerp and C. Kranenburg, (eds.), *Fine Sediment Dynamics in the Marine Environment - Proc. in Mar. Sci. 5.,* Amsterdam: Elsevier, pp. 233-250.

MANNING, A.J.; DYER, K.R.; LAFITE, R. and MIKES, D., 2004. Flocculation measured by video based instruments in the Gironde estuary during the European Commission SWAMIEE project. *Journal of Coastal Research,* SI 41. (This Volume).

MANNING, A.J.; DYER, K.R. and CHRISTIE, M.C., 2001. Properties of macroflocs in the lower reaches of the Gironde estuary. *In*: Elbee, J. (d') and P. Prouzet, (eds.), *Actes de VII^e Colloque International Oceanographie Du Golfe De Gascogne* (Biarritz, France), France: IFREMER, Actes de Colloques No. 31, pp. 230-235.

MANNING, A.J. and FENNESSY, M.J., 1997. INSSEV (In-Situ SEttling Velocity instrument) - 1.3: Operator Manual. Internal Report for Institute of Marine Studies, University of Plymouth, 25 pp.

MEHTA, A.J. and PARTHENIADES, E., 1975. An investigation of the depositional properties of flocculated fine sediment. *Journal of Hydrological Research*, 92 (C13), 361-381.

MILLERO, F.J. and POISSON, A., 1981. International one-atmosphere equation of state seawater. *Deep-sea Research*, 28 (A): 625-629.

MORY, M.; GRATIOT, N.; MANNING, A.J. and MICHALLET, H., 2002. CBS layers in a diffusive turbulence grid oscillation experiment. In: J.C. Winterwerp and C. Kranenburg, (eds.), *Fine Sediment Dynamics in the Marine Environment - Proc. in Mar. Sci. 5.,* Amsterdam: Elsevier, pp.139-154.

NISHIZAWA, S.; FUKUDA, M. and INQUE, H., 1954. Photographic study of suspended matter and plankton in the sea. *Bull. Fac. Fish.*, Hokkaido Univ., 5, 36-40.

OWEN, M.W., 1976. Determination of the settling velocities of cohesive muds. Wallingford, England: HR Wallingford, *Report No. IT 161*, 8 pp.

SCHLICHTING, H., 1968. *Boundary-layer theory*. New York: McGraw-Hill, 747p.

SHANKS, A.L. and TRENT, J.D., 1979. Marine snow: microscale nutrient patches. *Limnol. Oceanogr.*, 24, 850-854.

SOULSBY, R.L., 1983. The bottom boundary layer of shelf seas. In: B. Johns, (ed.), *Physical Oceanography of Coastal and Shelf Seas*. New York: Elsevier, pp. 189-266.

TEN BRINKE, W.B.M., 1994. Settling velocities of mud aggregates in the Oosterschelde Tidal basin (The Netherlands), determined by a submersible video system. *Estuarine, Coastal and Shelf Science*, 39, 549-564.

VAN LEUSSEN, W., 1994. Estuarine macroflocs and their role in fine-grained sediment transport. Utrecht, The Netherlands: University of Utrecht, Ph.D. thesis, 488p.

WINTERWERP, J.C., 1998. A simple model for turbulence induced flocculation of cohesive sediment. *Journal of Hydraulic Engineering*, 36 (3), 309-326.

WINTERWERP, J.C., 1999. On the dynamics of high-concentrated mud suspensions. Delft, The Netherlands: Delft University of Technology, Faculty of Civil Engineering and Geosciences, Ph.D. thesis, 172p.

Journal of Coastal Research	SI 41	82-89	STRAEE 2002	Ferrara, Italy	ISSN 0749-0208

Controlling factors in estuarine flocculation processes: experimental results with material from the Seine Estuary, Northwestern France

D. Mikes† ‡, R. Verney ‡, R. Lafite‡ and M. Belorgey∞

† CSIC, Institute of Earth Sciences Jaume Almera, c. Lluís Solé i Sabarís s/n, E-08028, Barcelona, Spain

‡ UMR CNRS 6143 M2C, Université de Rouen 10 Bd de Broglie, 76821 Mont Saint Aignan Cedex, France email : romaric.verney@etu.univ-rouen.fr robert.lafite@univ-rouen.fr

∞ UMR CNRS 6143 M2C, Université de Caen 15 Avenue des Tilleuls, 14000 Caen, France

ABSTRACT

MIKES, A.; VERNEY, R.; LAFITE, R. and BELORGEY, M., 2004. Controlling factors in estuarine flocculation. Experimental results with material from the Seine estuary, Northwestern France. *Journal of Coastal Research*, SI 41, 82-89. Ferrara (Italy), ISSN 0749-0208

Flocculation is one of the main process of sedimentation which modifies suspended particulate matter (SPM) characteristics, i.e. size and settling velocity. A combination of physical, chemical and biological parameters control coagulation and fragmentation of natural samples. A newly developed instrument, the Video In Lab, was used to monitor the kinetics of flocculation. Flocculation tests were carried out on natural freshwater samples collected at multiples sites along the Seine estuary, spanning a variety of seasons. Testing was aimed at quantifying the influence of three main parameters: turbulence, SPM concentration and salinity. The tests show that weak turbulence favours flocculation, whereas strong turbulence limits the maximum floc size. Presence of available organic matter and high SPM concentration enhances kinetics efficiency and floc size. Salinity induces flocculation throughout a threshold action, controlled by SPM concentration, organic matter quality and floc density. These preliminary results emphasise the complexity involved in the understanding of natural flocculation. These processes are controlled by key parameters depending themselves upon the composition of the samples.

ADDITIONAL INDEX WORDS: *Macroflocs, Turbulence, Salinity, SPM concentration, Planktonic bloom*

INTRODUCTION

Estuarine sediments are from miscellaneous sources: fluvial, erosion, re-entrainment, emissaries discharge, organic production and the atmosphere (EISMA, 1993). Once in estuaries these sediments are influenced by several time-variable hydrodynamic forcing parameters such as tide, swell and currents. Estuarine sediments are also influenced by strong spatial gradients of salinity, suspended particulate matter concentration (SPM) and currents, this last parameter inducing turbulence (FENNESSY et al., 1994). Sediment transport processes are controlled by a well known cycle involving the presence of SPM in the water column, settling, deposition, packing, erosion, re-entrainment (DYER, 1994). During this cycle, flocculation and deflocculation mechanisms play a key role. The basic material are microflocs (EISMA, 1993): particulate aggregates whose sizes are generally inferior to 100µm (LAFITE, 2001), and which are comprised of elementary particles such as clays, minerals and organic matter of fluvial origin (DUPONT and LAFITE, 1986; DUPONT et al., 1994). They are relatively dense, resistant to high levels of turbulence and represent the main part of particulate matter present in estuaries. When these microflocs are exposed to favourable hydrodynamic, physico-chemical and environmental conditions, aggregation occurs to form macroflocs. Aggregation influences the shape and size of macroflocs, and consequently their settling velocity (MANNING and DYER, 1999). In estuaries and especially in the turbidity maximum zone, SPM concentration ranges from 100 mg l^{-1} to several g l^{-1}. Work by MIGNIOT (1968) shows that flocculation processes occur at high SPM concentrations (from 10 to 100 g l^{-1}). Beyond these levels of SPM concentration flocs become hampered in their movement preventing them from moving freely. Little work has been conducted to quantify flocculation processes at low SPM concentration in the water column (from 10 to 250 mg l^{-1}).

The parameters identified by EISMA (1993) and VAN LEUSSEN (1994) as being the most important in estuarine zones, are grouped in four main classes:

- Statistical parameters : SPM concentration (EISMA, 1993),
- Hydrodynamical parameters : Turbulence, differential settling velocity (CHEN et al., 1994; MILLIGAN and HILL, 1998),
- Constituting parameters : Organic matter, sticking material (LARTIGES et al., 2001),
- Physicochemical parameters : ionic charged water , i.e. salinity (THILL et al., 2001; MIGNIOT, 1968).

This study aims at scaling the influence of key parameters in low SPM concentrated environments (from 10 mg l^{-1} to 1 g l^{-1}). Because of the wide range of parameters acting upon flocculation and the difficulty to isolate each parameter from the other, only

three main parameters have been selected to be investigated: SPM concentration, salinity and turbulence.

MATERIAL AND METHODS

Instrumentation : Video In Lab

Flocculation processes can be well monitored *in-situ* by a variety of instruments, such as the INSSEV instrument (FENNESSY *et al.*, 1994), the VIS (VAN LEUSSEN, 1994) and an *in-situ* suspended matter camera system (EISMA et al., 1990). The Video In Lab instrument (VIL) was developed for *in-vitro* tests to measure flocs greater than 100µm. The VIL visualises flocs in a glass bowl of 13 cm diameter and 20 cm height. It measures their characteristic sizes and then displays the floc size distribution. The instrument consists of a backlight, a CCD camera and image processing software. A variable speed agitator controls the turbulent nature of the flow circulating inside the bowl. The backlight generates a uniform white background upon which flocs appear as dark forms. The Microvision image software Replay® records 2D floc pictures during 40s at 2Hz. The image quality mainly depends on the flow velocity, i.e. the slower the flow, the better the picture. Therefore, the agitator was stopped before each recording and a half-transparent-cylinder was immersed around the recording window to quickly reduce the flow velocity. Pictures were then processed by the Microvision Ellix® image analysis software to measure floc sizes using the contrast between the white background and the dark silhouettes of flocs. Ellix® fits an ellipse to each form (Fig. 1), displaying numerous parameters of each 2D floc silhouettes and its corresponding ellipse, e.g. major and minor axis, ellipse surface, floc surface, and perimeter of ellipses and flocs. A minimum of 300 flocs was sampled to yield the sample's floc size distribution. The highest resolution, using this system is around 50 µm, therefore, microflocs are partially excluded from measurements.

VIL calibration – level of turbulence

VAN LEUSSEN (1997) characterises turbulence by the presence of eddies of various sizes. In this study, the size of the largest eddies equals the diameter of the bowl. The eddies are very energetic and split up cascade-like into smaller ones of weaker energy until all energy is dissipated by means of viscous forces. The minimum size of eddies depends upon the fluid viscosity and the initial energy given to the largest eddies. This smallest size is used to define a characteristic size of turbulence : the Kolmogorov microscale. VAN LEUSSEN (1997) suggests that turbulence, and more precisely eddies, tear apart flocs whose sizes exceed that of the eddies. Hence, every floc larger than the smallest eddy present in the bowl is eventually split up. This leads to the conclusion that turbulence controls the maximum size of macroflocs. Therefore, we use the Kolmogorov microscale to describe the levels of turbulence because of its strong relationship with characteristic floc sizes. Calibrating the VIL requires an accurate cartography of the various levels of turbulence present inside the bowl. This is realised by measuring punctually the horizontal velocity (u) and vertical velocity (v) with a Laser Doppler Velocimeter. According to the Reynolds formulation, these velocities are expressed as the sum of an average velocity ($\overline{u}$, $\overline{v}$) and a fluctuating velocity (u', v'). From u' and v' the turbulent kinetic energy (k) is deduced according to equation 1:

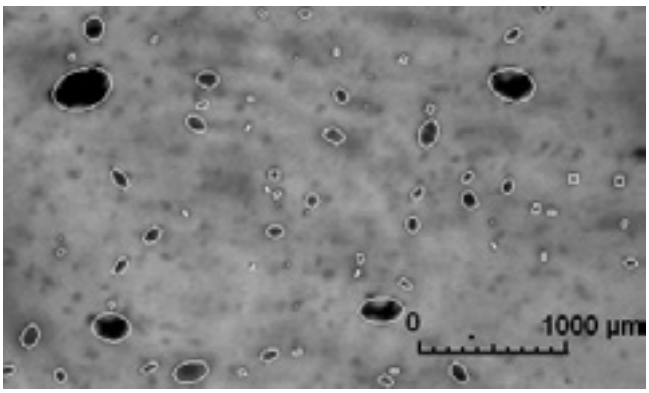

Figure 1. Flocs characteristics measured by Ellix® (Microvision). Measurements are based on ellipse patterns.

$$k = \frac{1}{2}\left(\overline{u'^2} + \overline{v'^2} \right) \qquad (1)$$

Next the k-ε closure relationship (2) is used to approximate the dissipation energy in spite of the non homogeneity and anisotropy of the flow.

$$\varepsilon = c_v \frac{k^{\frac{3}{2}}}{l} \qquad (2)$$

Here c_v is a k-ε closure constant evaluated at 0.09 (MATSUNAGA et al., 1999). l is the mixing length and corresponds here to the diameter of the bowl, i.e. 0.1m. The transition between epsilon and the Kolmogorov microscale (η) is made by using the following relationship (3) :

$$\eta = \left(\frac{\upsilon^3}{\varepsilon} \right)^{\frac{1}{4}} \qquad (3)$$

where ν is the water kinematic viscosity ($\nu = 1.15\ 10^{-6}\ m^2\ s^{-1}$). This approximation of the Kolmogorov microscale is used as the unit of turbulence in this paper. A calibration of turbulence is carried out for each stirring velocity from this relationship between u', v' and η. According to *in-situ* turbulence measurements conducted by MANNING and DYER (1999) during the slack water period, all flocculation tests will be carried out with a turbulent level characterised by a Kolmogorov microscale around 1000 µm.

Representative sizes

The best floc representation would be to capture them in three dimensions, which still remains technically difficult. However two physical sizes determined from the 2D floc pictures have been chosen to characterise floc distribution: the floc length and the floc diameter. The floc length is deduced from the main axis of the ellipse. This size is used to compare flocs and turbulence represented by the Kolmogorov microscale. However the floc length leads to overestimate the flocculated state of samples because it only considers flocs as one dimension objects. The floc diameter that is the diameter of the circle with a surface equivalent to the floc surface measured by Ellix®, is the size chosen to describe precisely flocculation mechanisms. This size does not include the porosity but allows a better approximation of the true

3D size of flocs. All distributions displayed in this paper will be surface percentage distributions.

Flocculation experimental protocol

In estuarine systems, sedimentary particles are subjected to waves and tides, therefore the duration of the slack water period during which turbulence in estuaries is favourable for flocculation can be estimated at 120 min (LE HIR et al., 2001). This characteristic time size was chosen as the maximum time period for the flocculation tests.

For each new test, a sample is introduced into the bowl, at a salinity of 0. Then the sample is subjected to the highest stirring velocity generating a turbulence level of 200 µm. The objective is to begin each test with approximately the same initial floc size distribution. Next the agitator is set to the appropriate level of turbulence (1000µm) and the test starts. Flocculation is monitored for all the duration of the test by recording series of pictures at specific time steps : every 1 min for the first 10 min of test, every 2 min for 10 min till 20 min, every 5 min till 60 min and every 10 min for the last 60 min. This should allow to accurately monitor flocculation for the first 20 minutes which appears to be the critical period for flocculation. Figure 2 shows typical floc pictures and grain-size distributions obtained at the start and end of tests. Next, the salinity is increased and a new test starts. Tests were carried out until a salinity of 30. A specific protocol was used to show the impact of turbulence on flocculation. A single test was undertaken, under optimum conditions in term of salinity and concentration, for 20 min at the lowest level of turbulence (flocculation tests conditions), and a measure of the grain-size distribution was performed. Next turbulence was increased and another measure was taken after 5 min. This is repeated until the highest level of turbulence.

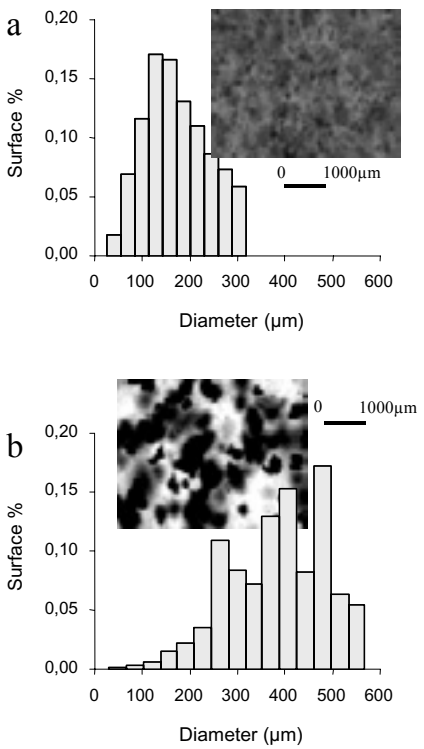

Figure 2. Typical grain-size distribution and VIL pictures at t_0 (a : η=200µm) and t_{120} (b : η =1000µm).

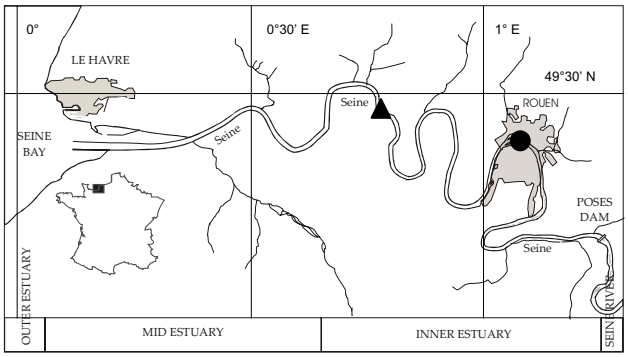

Figure 3. Location of the sampling sites along the Seine Estuary (France); ● : Rouen; ▲ : Le Trait.

Sampling strategy

Two different sites have been chosen for sampling. Both are located in the fluvial freshwater part of the Seine estuary (GUEZENNEC et al., 1999). This choice is motivated by our intention to characterise sediments with different densities and compositions. Station 1 is located in Rouen (Fig. 3) in the water column (Samples A, B and C). Here, flocs have not settled recently, contrary to the water sample collected in March 2000 at station 2, located on a tidal mudflat (Sample D, Le Trait, Fig. 3). There, particles have settled and may be consolidated before re-entrainment. Samples from station 1 were collected in different seasons to monitor flocculation at specific hydrodynamical and environmental conditions : end of winter (March 2000, flood period - Sample A), spring (April 2002, planktonic activity, end of flood period - Sample B) and fall (September 2000, low discharge - Sample C). During all experiments, samples were stored in a dark room at a constant ambient temperature, without notable pH variation. Microflocs grain-size analysis using a Coulter Counter has been done for each sample. Due to the short time required and the high agitation in the bowl during a Coulter Counter analysis, macroflocculation is assumed to be negligible. Scanning electron microscope (SEM) observations and X-ray analysis supplied global information on structure and composition of samples.

RESULTS

Turbulence

Figure 4 represents the maximum floc length that is the upper limit size for flocs under specific hydrodynamics conditions, at the end of a kinetic test as a function of the Kolmogorov microscale calculated for the corresponding stirring velocity. Data appear to correlate reasonably well with the unity line y=x. This result enforces the idea that turbulence strongly controls flocculation by limiting the floc size to the Kolmogorov microscale (VAN LEUSSEN, 1997; MILLIGAN and HILL, 1998).

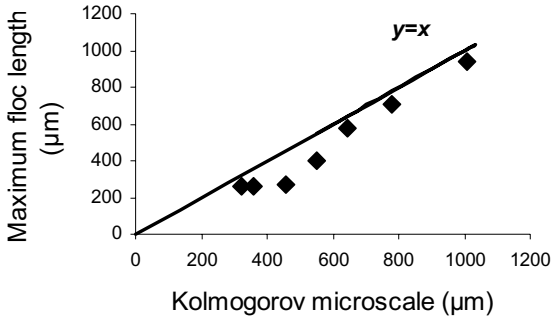

Figure 4. Comparison between the Kolmogorov microscale and the maximum floc length, size determined from the ellipse length measured by Ellix®.

Samples characteristics

Results from mineralogical analyses carried out on samples A and C collected from station 1 are given in Table 1. Compared to the existing database (LESOURD, 2000), these results are of the order of the common mineralogical composition of SPM globally present in the Seine estuary along the year. Grain-size measurements were carried out on samples collected at station 1 (Fig. 5). Grain-size distributions are similar in March and September, characterised by a single mode as observed previously in this system (DUPONT et al., 1995). In sample A, the mode is around 10 µm and SEM pictures show a low organic matter availability. The mode is around 20 µm in sample C, composed mostly of little aggregates. A peak of planktonic bloom of diatoms was present at the sampling station 1 in April 2002. Because of the strong temporal variability of diatom populations, analyses by Coulter Counter have been carried out for all the duration of the experiments. These show that initially microflocs are characterised by diatoms (Fig. 5 - sample B_1 - mode around 15 µm) and the large amount of fresh organic matter directly available (Fig. 5 - see black patches on SEM pictures). During the storage period, particles settled and created second order microflocs from diatoms and organic matter as demonstrated by granulometric spectra in samples B_2 and B_3: the 15 µm mode disappeared and larger flocs were created, size greater than 30 µm. In this situation, organic matter is trapped in these second order microflocs (Fig 5. - see SEM pictures) and remains less available in the system (Fig. 5 - samples B_2 and B_3), which inhibits macroflocculation at a later stage.

Table 1 : Mineralogical composition for Samples A and C (water column system, low organic matter availability)

Sample	Kaolinite (+/- 5%)	Illite (+/- 5%)	Smectite (+/- 5%)	Chlorite (+/- 5%)
A	45	20	30	5
C	45	20	25	10

Flocculation tests

Six configurations are studied for flocculation tests. All tests are carried out at the weakest turbulence level obtained in the bowl, i.e. η= 1000µm. Origin and characteristics of all samples are summarised in Table 2. For each sample influence of the salinity gradient is monitored. From these results, three main trends are observed on Figure 6:

- For samples B_2, B_3 and C, only the mechanical action of the stirring velocity influences flocculation. The salinity gradient seems to have no effect on the flocculation processes: at every time step, the same average floc size is measured independently of the salinity. A difference exists on sizes reached at the end of each test: diameters are of 300 µm for samples B_2 and B_3 on the contrary to sample C where diameters are under 200 µm.

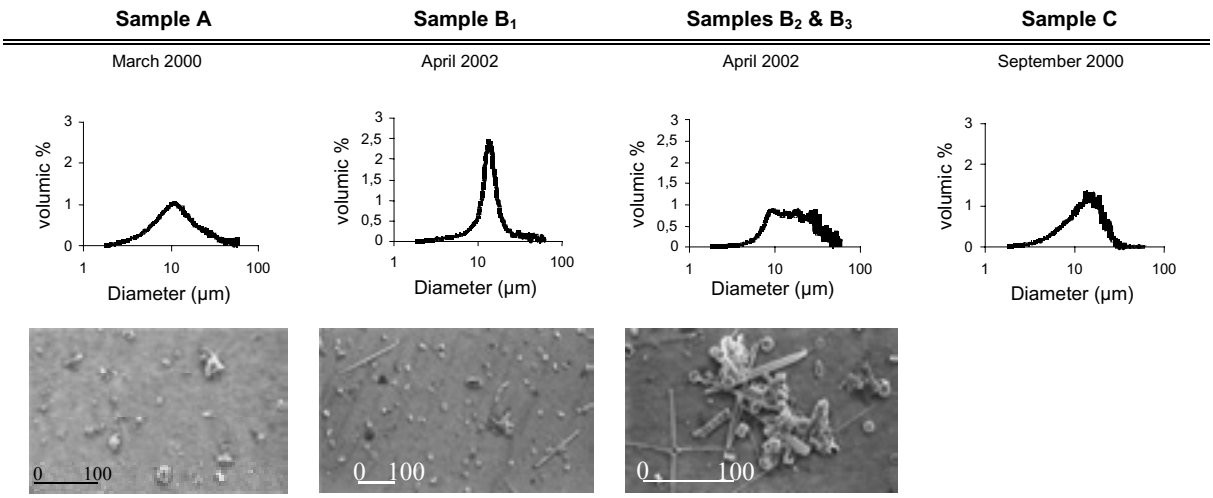

Figure 5. Grain-size distributions and SEM pictures for samples collected at station 1 (freshwater zone) in the water column, during the annual survey (SEM scale : 100 µm).

Table 2. Main characteristics of samples studied.

Sample	Station	Date	System	Characteristics
A	1	March 2000	Water Column	C_{SPM} = 70 mg l^{-1} ; low OM availability
B_1	1	April 2002	Water Column	C_{SPM} = 28 mg l^{-1} ; diatoms bloom & OM availability
B_2	1	April 2002	Water Column	C_{SPM} = 28 mg l^{-1} ; diatoms & OM aggregated, low OM availability
B_3	1	April 2002	Water Column	C_{SPM} = 138 mg l^{-1} ; diatoms & OM aggregated, low OM availability
C	1	September 2000	Water Column	C_{SPM} = 50 mg l^{-1} ; low OM availability
D	2	March 2000	Mudflats	C_{SPM} = 87 mg l^{-1} ; settled material

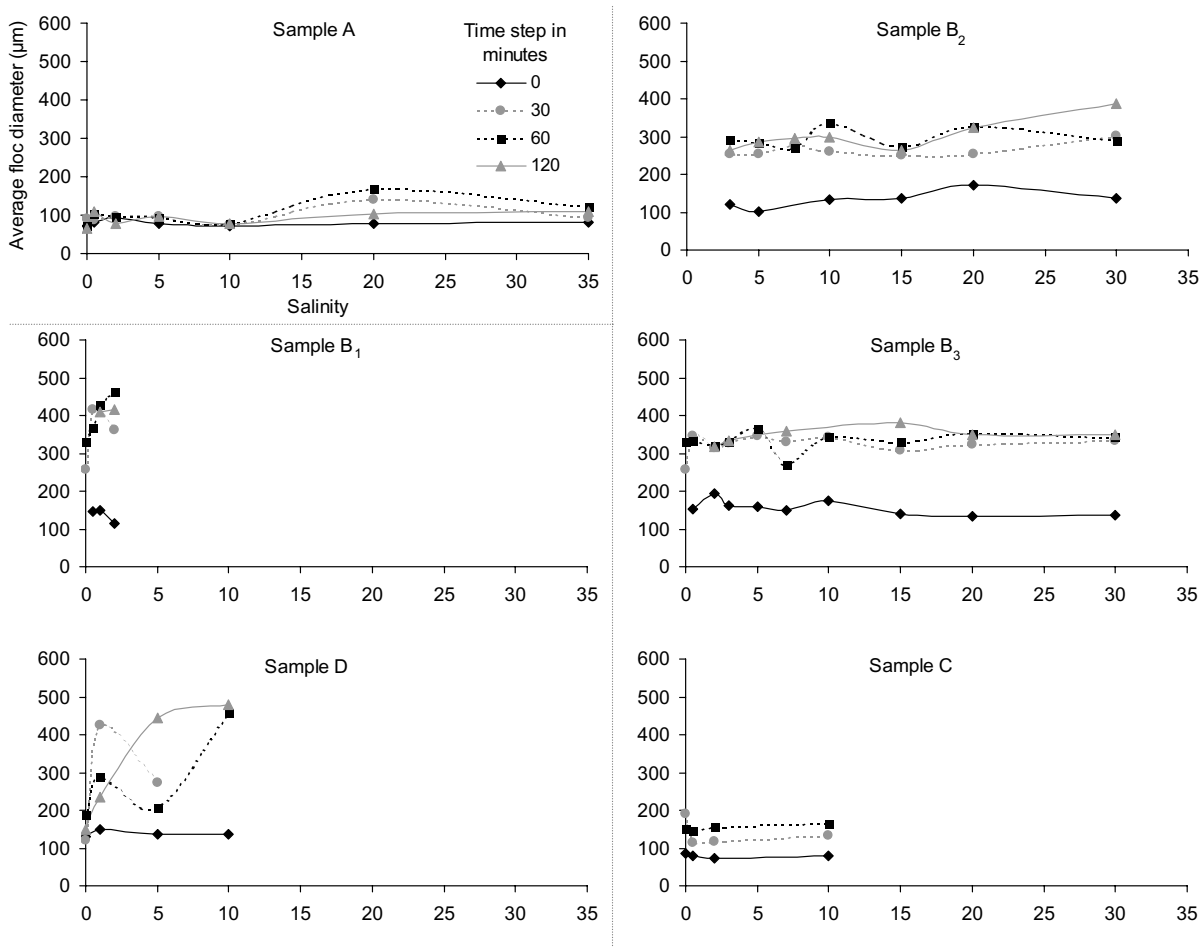

Figure 6. Salinity gradient action on flocculation at different time steps during the tests. Sample A : water column system, low OM availability, low SPM concentration; Sample B_1 : water column system, high OM availability, low SPM concentration; Sample B_2 : Settled particles, low OM availability, low SPM concentration; Sample B_3 : settled particles, low OM availability, SPM concentration high; Sample C : water column system, low OM availability, low SPM concentration; Sample D : mudflats system, low OM availability, low SPM concentration; OM : Organic matter.

- For samples B_1 and D, flocculation is enhanced by salinity, with a rapid increase of floc sizes at low salinity, and with a maximum floc size over 400 µm for sample B_1 and around 600 µm for sample D.
- For sample A, flocculation is favoured by salinity above 10. Flocs have sizes around 200 µm.

Deflocculation tests

Deflocculation tests have been carried out on samples A, C (water column system, low organic matter availability), B_3 (water column system, organic matter trapped) and D (mudflat system) see Figure 7. Contrary to results presented on turbulence (Fig. 4), not the maximum floc length but the average floc length is represented as a function of the Kolmogorov microscale, due to the better representation of the average operator of the floc population. The straight line representing the Kolmogorov microscale in Figure 7 shows the upper limit, above which flocs are destroyed by the smallest eddies. Results show that the behaviour of aggregates is described by two main trends. In sample D, the size of macroflocs issued from mudflat sediment increases with turbulence until this upper limit. Once this limit is reached, average floc length decreases with the Kolmogorov microscale. On the other hand, macroflocs in samples A, B_3 and C do not reach this limit. They are destroyed as soon as the turbulence is increased and well before the limit of Kolgomorov microscale: their resistance seems to be less important. During the increase of turbulence, the size of macroflocs decreases until it reaches the lowest admissible size of SPM, i.e. the microfloc size. The sample B_3, which is more concentrated, has the highest macrofloc size.

DISCUSSION

The *in-vitro* system Video In Lab, developed for flocculation tests has proved to be efficient at low SPM concentrations up to 500 mg l^{-1}. This system produces reliable floc sizes estimations, as a result of the high quality image processing. The experimental protocol allows the visualisation and quantification of the flocculation processes, by carrying out reproducible experiments. From these tests it is shown that key parameters control the flocculation at different scales.

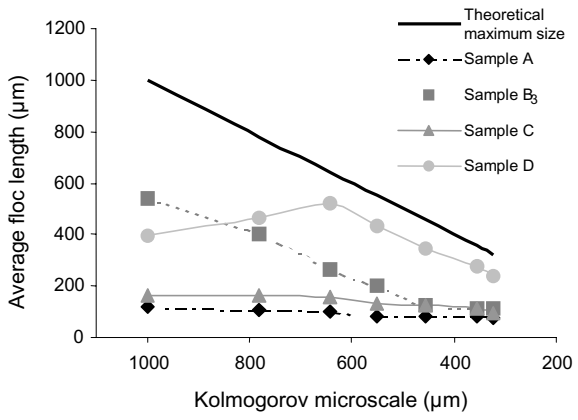

Figure 7. Deflocculation tests for samples A (water column system) B_3 (settled particles) C (water column system) and D (mudflats system). These cases are characterized by their organic matter availability.

Microflocs vs. Macroflocs

As mentioned previously, microflocs and macroflocs are fundamentally different and consequently, their behaviour is significantly different. Microflocs are omnipresent in estuaries and they are the macroflocs building blocks. They are always present in the strongest turbulence conditions of our experiments. Their bonds are strong enough (DUPONT and LAFITE, 1986) to withstand the most aggressive ambient physical parameters, including the highest turbulent shear close to the bed. Microfloc size is controlled by the origin and 3D structure of microflocs. They are larger and denser when they originate from a mud sediment or in presence of planktonic or benthic blooms (see SEM pictures and grain size distributions, Fig. 5). In contrast macroflocs react strongly on the ambient conditions, and their destiny is much less stable.

Turbulence control

Turbulence plays a dual role on flocculation : in a first stage, turbulence favours flocculation by increasing collision rate between particles (EISMA, 1993). In a second stage, when particle sizes are in the order of the Kolmogorov microscale, eddies tear macroflocs apart and consequently limit maximum floc size, as shown in Figure 4 (VAN LEUSSEN, 1997). This control exercised by turbulence on floc size is confirmed by results obtained from the deflocculation tests (Figure 7). The control by turbulence is quite important, when turbulence variations are considered during tidal cycles (FENNESSY et al., 1994; MANNING and DYER, 1999). This parameter has to be known for any extrapolation of results.

Salinity control by a threshold effect

Salinity plays an evident role in estuarine zone, because particles issued from the catchment areas or fluvial particles must go through the salinity gradient of the estuary. Salinity is usually given as a key parameter influencing flocculation through a threshold action (MIGNIOT, 1968; THILL et al., 2001). However, these results using material from the Seine estuary (Fig. 6), show that this threshold is variable in salinity and can be not present under specific conditions. Considering the results shown Figure 6, a conceptual model can be drawn (Fig. 8). This model is based on the variations of the floc population at the end of the 120 min test throughout the salinity gradient. This conceptual model is characterised by three stages: the unflocculated stage, the dynamical stage and the final flocculated stage.

The initial stage represents the unflocculated particles, that is the microflocs. Particles could not flocculate under mechanical stress when organic matter is not available, or without any planktonic or bacterial activities which could generate gluing material such as polysaccharides (Fig. 6 – Sample A). This stage may be transitory until a specific salinity value is attained, above which flocculation is favoured by a rise of salinity (Sample A).

The dynamical stage is parameterised by two strongly variable parameters : the flocculation onset and the flocculation efficiency. The flocculation onset can occur at very low salinity (Fig. 6 - around 0.5 – Sample B_1 and D), at a salinity of 10 (Fig. 6 - Sample A) or never occur (Fig. 6 - Samples B_2, B_3 and C). The threshold can be characterised by a steep slope (Fig. 6 - Sample B_1) or a gentle slope (Fig. 6 - Sample A and D). It is possible that these two parameters are controlled by a variability in organic matter quality and availability, a variable structure and content of

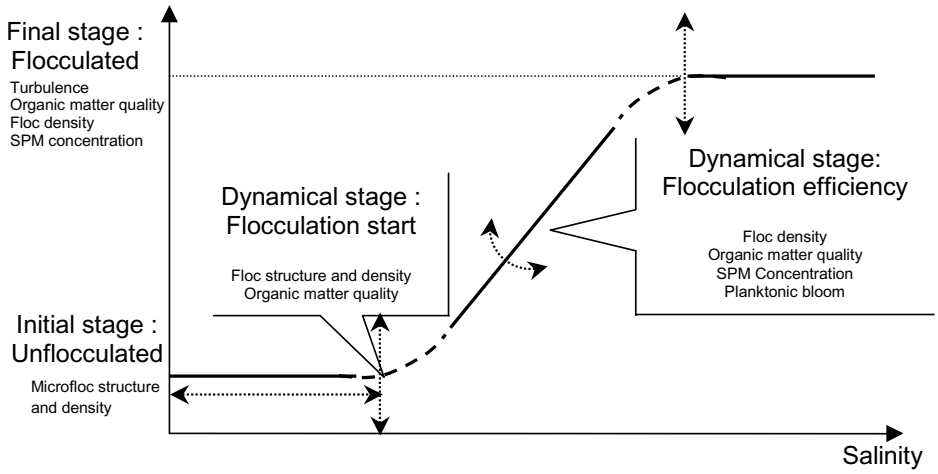

Figure 8. Schematic representation of the salinity influence on flocculation processes : stages and controlling parameters.

microflocs and the presence or absence of planktonic blooms and polysaccharides. These results agree with LARTIGES et al. (2001) and MOUCHEL (1998) who demonstrated that the organic matter content, polysaccharides originated from bacteria or diatoms, or organic inputs from human activities, can enlarge flocculation processes in river systems, and in some cases override the salinity action (Fig. 6 - Samples B_2, B_3 and C).

The final flocculated stage represents the maximum average floc size reached during flocculation episodes carried out throughout the salinity gradient. As was shown in Figure 7, turbulence limits floc size. However, not all samples reached this limited size. Firstly, the maximum floc size depends on SPM concentration. Here only samples B_2 and B_3 can be compared due to their similar organic matter content and microflocs structure. It results that the maximum floc size is 100 µm higher when SPM concentration rises from 28 mg l^{-1} (Fig. 6 - sample B_2) to 138 mg l^{-1} (Fig. 6 - sample B_3). Secondly, similarly to the dynamical stage the flocculated stable stage is also enhanced by the organic matter availability, the presence of diatoms and the probable presence of polysaccharides. Indeed, maximum diameter in sample B_1 (fresh diatoms and high organic matter availability) is twice as large as the maximum diameter reached in sample B_2, where organic matter is trapped in by diatoms aggregates and three times larger than in sample A, where organic matter presence is low. Finally, sediment 3D structure and density influence the maximum floc length : the final floc size in sample D (collected on mudflats) is above 600 µm whereas all the other samples collected in the water column reached a lower flocculated state, with a maximum diameter under 400 µm (Fig. 6).

CONCLUSIONS

These experiments carried out with sediment from the macrotidal Seine estuary demonstrate that controlling parameters variably influence flocculation. Turbulence automatically limits the flocculation state and SPM concentration increases the final floc diameter. These two parameters influence flocculation whatever the SPM content is, contrary to salinity. The conceptual model permits a visualisation of how salinity influences the flocculation processes. It clearly highlights that the salinity threshold action is controlled by the SPM quality and content. Under specific conditions, this control leads to completely override the salinity threshold. This is clearly observed in the Seine river from the upper river to the estuary mouth along the year because of the high polysaccharides and organic matter variations (TEXIER et al., 1993).

Future extensive investigations on organic matter quality and planktonic and benthic blooms are scheduled, in order to refine knowledge on the influence of SPM content and quality on the flocculation processes and their main controlling parameters.

ACKNOWLEDGEMENTS

The authors thank Irene Zimmerlin for her work on the Scanning Electron Microscopy, as well as Heidi Burgess, Frederic Murzyn, Mohammad Movahedan. Daniel Mikes was supported by the European TMR SWAMIEE programme and Romaric Verney is financially supported by the Conseil Régional de Haute Normandie, France.

LITERATURE CITED

CHEN, S.; EISMA, D. and KALF, J., 1994. In situ distribution of suspended particulate matter during a tidal cycle in the Elbe estuary. *Netherlands Journal of Sea Research*, 32 (1) 37-48.

DUPONT, J.P. and LAFITE, R., 1986. Importance et rôle du matériel organique vivant et inerte dans les suspensions de la Baie de Seine. In: La Baie de Seine (GRECO-MANCHE) – Université de Caen, 24-26 Avril 1985, Actes de Colloques n. 4 155-162.

DUPONT, J.P.; LAFITE, R.; HUAULT, M.F.; HOMMERIL, P. and MEYER, R., 1994. Continental / Marine ratio changes in suspended and settled matter across a macrotidal estuary (the Seine estuary, northwestern France). *Marine Geology,* 120, 27-40.

DUPONT, J.P.; WANG, H.Q.; LAFITE, R.; MEYER, R. and TEXIER, H., 1995. Granulométrie et vitesse de chute des matières en suspension en estuaire de Seine. *Comptes Rendus de l'Académie des Sciences*, 320, 961-968.

DYER, K.H., 1994. Estuarine sediment transport. In: PYE, K. (ed.), *Sediment transport and depositional processes.* Blackwell Scientific Publications, pp 193-218.

EISMA, D.; SCHUMACHER, T.; BOEKEL, H.; VAN HEERWAARDEN, J.; FRANKEN, H.; LAAN, M.; VAARS, A.;

EIJGENRAAM, F. and KALF, J., 1990. A camera and image-analysis system for in situ observation of flocs in natural waters. *Netherlands Journal of Sea Research*, 27 (1) : 43-56.

EISMA, D., 1993. *Suspended mater in the aquatic environment*. Springer-Verlag, 315p.

FENNESSY, M.J.; DYER, K.R. and HUNTLEY, D.A., 1994. INSSEV : An instrument to measure the size and settling velocity of flocs in-situ. *Marine Geology*, 117, 107-117.

GUEZENNEC, L.; LAFITE, R.; DUPONT, J.P. and MEYER, R., 1999. Hydrodynamics of suspended particulate matter in the tidal freshwater zone of a macrotidal estuary (the Seine estuary, France). *Estuaries*, 22 (3A), 717-727.

LAFITE, R., 2001. Impact de la dynamique tidale sur le transfert de sédiments fins. Thèse HDR, France, Université de Rouen, 80p.

LARTIGES, B.S.; DENEUX-MUSTIN, S.; VILLEMIN, G.; BARRES, O.; CHAMEROIS, M.; GERARD, B. and BABUT, M., 2001. Composition, structure and size distribution of suspended particulates from the Rhine river. *Water Research,* 35 (3) 808-816.

LE HIR, P.; FICHT, A.; SILVA JACINTO, R.; LESUEUR, P.; DUPONT, J.P.; LAFITE, R.; BRENON, I.; THOUVENIN, B. and CUGIER, P., 2001. Fine sediment transport and accumulation at the mouth of the Seine estuary (France) , *Estuaries*, 24 (6B) 950-963.

LESOURD, S., 2000. Processus d'envasement d'un estuaire macrotidal : zoom temporel du siècle à l'heure. Application à l'estuaire de la Seine. PhD thesis, France, Université de Caen, 280p.

MANNING, A.J. and DYER, K.R., 1999. A laboratory examination of floc characteristics with regard to turbulent shearing. *Marine Geology* 160, 147-170.

MATSUNAGA, N.; SUGIHARA, Y.; KOMATSU, T. and MASUDA, A., 1999. Quantitative properties of oscillating-grid turbulence in homogeneous fluid. *Fluid Dynamics Research*, 25, 147-165

MIGNIOT, C., 1968. Etude des propriétés physiques de différents sédiments très fins et de leur comportement sous des actions hydrodynamiques. *La houille blanche,* 7, 591-620.

MILLIGAN, T.G. and HILL, P.S., 1998. A laboratory assessment of the relative importance of turbulence, particle composition, and concentration in limiting maximum floc size and settling velocity. *Journal of Sea Research,* 39**,** 227-241.

MOUCHEL J.M., 1998. Floculation et sédimentation dans l'estuaire de la Seine. In Rapport Seine Aval 1997 / FIN-173

TEXIER, H.; LAFITE, R.; DUPONT, J.P.; FIRMIN, V.; GADEL, F.; SERVE, L. and CHARRIERE, B., 1993. Organic matter transport across a macrotidal estuary gradient : the Seine estuary, France. *Netherlands Journal of Aquatic Ecology*, 27 (2-4) 405-413.

THILL, A.; MOUSTIER, S.; GARNIER, J.M.; ESTOURNEL, C.; NAUDIN, J.J. and BOTTERO, J.Y., 2001. Evolution of particle size and concentration in the Rhône river mixing zone : influence of salt flocculation. *Continental Shelf Research*, 21, 2127-2140.

VAN LEUSSEN, W., 1994. Estuarine macroflocs, their role in fine-grained sediment transport. PhD Thesis, University of Utrecht (The Netherlands), 488p.

VAN LEUSSEN, W., 1997. The Kolmogorov microscale as a limiting value for the floc sizes of suspended fine grained sediments in estuaries. In BURT, N.; PARKER, R. and WATTS, J. (eds.): *Cohesive sediment*. Wiley & Sons, pp 45-62.

Journal of Coastal Research	SI 41	90-104	STRAEE 2002	Ferrara, Italy	ISSN 0749-0208

The Observed Effects of Turbulence on Estuarine Flocculation

A. J. Manning § ∞

§ School of Earth, Ocean and Environmental Sciences, University of Plymouth, Plymouth, PL4 8AA, UK.
E-mail: andymanning@yahoo.com

∞ HR Wallingford, Howbery Park, Wallingford, OX10 8BA, UK.

ABSTRACT

MANNING, A.J., 2004. The Observed effects of turbulence on estuarine flocculation. *Journal of Coastal Research*, SI 41, 90-104. Ferrara (Italy), ISSN 0749-0208

Turbulent shear generated in estuarine water columns is recognised as having an influence on both the formation of cohesive sediment flocs, and aggregate break-up. By drawing on examples of floc spectra obtained during recent European Commission funded experiments, this paper assesses how floc properties and the vertical mass flux are influenced by changes in turbulent shear stress intensity. Initially, a series of simultaneous turbulence and floc property measurements made from within the turbidity maximum in the Tamar estuary (UK), during neap and spring tidal conditions, are presented. The ambient conditions produced a suspended concentration and turbulent shear stress range of 10-8000 g cm^{-3} and 0.04-0.7 N m^{-2}, respectively. The flocs were observed using the INSSEV (In-Situ Settling Velocity) instrument, which provides measurements of floc size, settling velocity and effective density. These field experiments showed that within the turbidity maximum there was an increase in the mean floc size from about 90 μm to about 350 μm, which in general matched the changing suspended particulate concentrations. There was also an increase in mean settling velocity through the turbidity maxima following the changes in size and concentration. This was generally in the range 0.5-6 mm s^{-1}. The changes in floc size and settling velocity indicated a subsequent decrease occurring in the macrofloc (floc size > 160 μm) effective densities, which at times fell from 715 kg m^{-3} to less than 100 kg m^{-3} within the turbidity maximum. In terms of mass settling flux, the fast settling macroflocs from the more turbid spring tides accounted for a continuous tidal time series average of 89% of the mass settling flux, which was 20% greater than for a comparative neap tide time series. A statistical regression analysis of the Tamar estuary macrofloc settling velocity values (Ws_{MACRO}), together with values obtained from similar measurements made in the Gironde estuary (France) and Dollard estuary (The Netherlands), showed that Ws_{MACRO}, is dependent on both turbulent shear stress and suspended particulate matter concentration terms. The best fit relationship representing Ws_{MACRO} had a highly significant R^2 of 90.6%. Quantifiably, the empirically derived model of Ws_{MACRO} displayed an increase in settling velocity at low shear stresses due to flocculation enhanced by shear, and floc disruption at higher stresses for the same concentration; the transition being a turbulent shear stress of about 0.36 N m^{-2}. This critical shear region for macrofloc flocculation was also confirmed by complementary laboratory experiments. A statistical analysis of the Ws_{micro} fraction indicated a closer correlation with just the turbulent shear. As with the macroflocs, the microfloc settling velocity rose with increasing shear stress until a limiting turbulent shear stress of about 0.42 N m^{-2} was reached. At this point the regression model predicted a peak Ws_{micro} of about 1 mm s^{-1}; this was significantly slower than the comparative macroflocs.

ADDITIONAL INDEX WORDS: *Flocculation, turbulence, turbulent shear stress, floc size, settling velocity, effective density, INSSEV instrument, suspended particulate matter..*

INTRODUCTION

Suspended particulate matter concentration in estuarine waters exists as flocculated aggregates whose properties of size and density, are continually changing in response to the ambient conditions. Mud flocs are composed of a combination of clay mineral and organic constituent particles. In order for these particles to flocculate into larger aggregates, the particulates must be brought into close proximity and then stick together. The efficiency with which the particles coagulate is a reflection of the stability of the suspension (VAN LEUSSEN, 1994). A suspension is classified as unstable when it becomes fully flocculated, and is stable when all particles remain as individual entities. The most effective interactions are between large and small flocs, which allows the flocculation process to progressively remove the finer particles from suspension (KRANCK, 1973).

There are three principle particle collision mechanisms, which are: Brownian motion, turbulent shear and differential settling. By using the simple aggregation models of FRIEDLANDER (1977), and assuming decreasing floc density with increasing diameter according to McCAVE (1984a), for particles of diameter: 0.5 μm, 5 μm 50 μm and 500 μm, colliding with particles ranging from: 0.01μm to 1 cm, VAN LEUSSEN (1988) assessed the relevant importance of the three collision mechanisms. VAN LEUSSEN (1988) found that turbulent shear stress was the dominant flocculation mechanism for shear rate values of 1-10 s^{-1}, which corresponds with a turbulent shear stress range of 0.035-0.76 N m^{-2}. These turbulent shear rates are representative of those typically experienced in the near bed region of many European tidal

estuaries. The probability of collision is further increased as the abundance of particles in suspension rises.

The turbulent shear which promotes floc growth, is also the primary source for instigating floc break-up. McCAVE (1984b) advocated that turbulence determines the maximum floc size in tidal waters. The energy for turbulent mixing is derived from the kinetic energy dissipated by the water flowing across a rigid rough boundary. The frictional force exerted by the flow per unit area of the bed is known as the shear stress (turbulent shear stress during turbulent flow conditions). The velocity gradients are largest in the lower 10-20% of the water column and approximately 80% of the turbulent energy generated by the flow occurs within this zone. It is here that the strongest lift and shear forces occur, and MEHTA and PARTHENIADES (1975) have suggested that it is these forces which control the maximum size of the flocs in suspension. As turbulent activity increases - both turbulent pressure differences and turbulent shear stresses in the flow rise. If the floc integrity is less than the ambient turbulent shear stress, the floc will fracture. Hence the turbulent shear stress can impose a maximum floc size restriction on the floc population. EISMA (1986) observed the maximum floc size generally agrees with the smallest turbulent eddies. This was observed experimentally by PANDYA and SPIELMAN (1982), and TAMBO and HOZUMI (1979) who related the maximum floc size to the turbulent dissipation rate, ε, and the Kolmogorov microscale of turbulence. KOLMOGOROV (1941) proposed a cascade of turbulent energy from energy-containing eddies down to energy-dissipating eddies. TAMBO and HOZUMI (1979) showed that when the floc diameter was larger than the lengthscale of the energy dissipating eddies, the aggregate would break-up.

The way in which the flocs break-up should dictate the size of the fragments. Both ARGAMAN and KAUFMAN (1970) and PARKER *et al*. (1972) suggested that flocs may decrease in size by gradual break-up through surface erosion induced on the floc through turbulent drag. The rate at which this takes place is proportional to the floc surface area and the surface shearing stress. These processes of floc break-up are more significant at low concentrations.

The act of an aggregate breaking-up requires a force to be exerted by the surrounding turbulent shear field. The floc structure model of VAN DE VEN and HUNTER (1977) studied various sources of energy loss due to break-up. It identified that to cause a floc to rupture, energy is dissipated in stretching the internal bonds to the limit of their tensile strength. Also viscous dissipation occurs as a result of the interstitial water moving to accommodate the change in floc shape as it is distorted.

PULS *et al*., (1988), and KRANCK and MILLIGAN (1992) have hypothesised that both concentration and turbulence are thought to have an effect on the maximum floc size, and the resulting spectra. As concentrations increase, the influence of particle collisions can also act as a floc break-up mechanism. BURBAN *et al.* (1989) proposed a general formula, based on research by LICK and LICK (1988), which described the change in particle size distribution with time. The formula utilised the collision frequency components from a simple flocculation theory based on two-body collisions (GLASGOW and KIM, 1989), and was employed to examine the various aspects involved with disaggregation. BURBAN *et al.* (1989) found that if initially it was assumed that floc break-up did not occur and the presence of shear resulted solely in flocculation, the median floc size would be proportional to the square of the particle concentration, because the particle collisions increased with concentration.

Furthermore, if the floc model conditions were altered to allow for aggregate break-up, floc break-up by fluid shear would be seen to be proportional to the concentration, and break-up due to inter-particular collisions would be proportional to the square of the concentration. Thus, if turbulent shear was the dominant process in the break-up of flocs, the model indicated that the median diameter would also increase with concentration, and if particle collisions due to velocity gradients was the dominant mechanism - the median diameter would remain approximately the same at increasing concentrations. However, if it was assumed that three-particle collisions (as opposed to two-particle collisions) were the dominant process in aggregate break-up, the median floc diameter would decrease with particle concentration. BURBAN *et al.* (1989) found from laboratory experiments a marked decrease in the floc size with increasing concentration (at steady state), which indicated that floc break-up by three-particle collisions was the dominant process.

A key factor in both flocculation and floc break-up is the strength of the interparticle floc bonds. The surface cohesion of the particulates will also have a significant impact on the shear forces required to break down the floc integrity, as well as influencing the probability of particles adhering when collisions occur during the aggregation process. For estuarine sediments, this cohesion has classically been attributed to the physio-chemical process of salt flocculation. Measurements by EISMA (1991) conducted in the Zaire River estuary indicated that salt flocculation did not appear to be an important cohesion mechanism for the formation of in-situ flocs, principally due to the weak nature of the electrostatic bonds. This observation was also reported by MANNING (2004) for the Tamar, Dollard and Gironde estuaries.

Of greater significance, is organically enhanced "bioflocculation". Within estuaries, the organic coatings on the particles contain long-chain types of molecules (i.e. natural polymers) that stick out through the water mantle around the individual particulates. In estuarine waters these polymers are mostly polysaccharides (e.g. mucus) produced by mud-dwelling micro-organisms, such as diatoms and bacteria. When particles come close to each other, these chains attract to those on the other particle. Experiments by KRANCK (1984) have shown that the flocculation of mineral particles which contained some organic matter, greatly enhanced the settling velocity of the aggregates. Both KRANCK and MILLIGAN (1988) reported enhanced flocculation following diatom and coccolith blooms at the entrance of tidal inlets, and coccolithophorids may also act as nuclei around which flocs are created. JACKSON (1990) modelled flocculation during a diatom bloom by considering both aggregation processes and algal growth. It was concluded that the important parameters were: turbulent shear, the algal (particle) concentration, and the size and stickiness of the algae.

It has been generalised that there are two distinct component groups of flocs: *macroflocs* and *microflocs* (EISMA, 1986). Macroflocs are large, highly porous (> 90%), fast settling aggregates which are typically the same size as the turbulent Kolmogorov microscale. Although floc density generally decreases as the macroflocs grow larger, the overall settling velocities tend to increase significantly. However, these low densities mean that the macroflocs are very fragile, and can be easily progressively broken down when passing through regions of higher turbulent shear stress and reduced to their component microfloc sub-structure (GLASGOW and LUCKE, 1980). The smaller microflocs are much more resistant to break-up by turbulent shear; they tend to have slower settling velocities, but exhibit a much wider range in effective densities (MANNING, 2004) than the macroflocs. Microflocs are formed in a similar way to macroflocs (by inter-particle collisions), but EISMA (1986)

attributes the strong bonding of their constituent particles to the biogenic "glues" produced by organisms. However, KRANCK (1975) suggests there is a linear relationship between the primary grain size and the microfloc size. MANNING (2001) defines microflocs as those aggregates with a spherically equivalent diameter of less than 160 μm. Macroflocs are those with a diameter > 160 μm.

At present the influence and occurrence of flocculation, as well as floc break-up, on in-situ floc size and settling velocity distributions is largely unknown, apart from the general fact that suspended particulate matter flocculates and flocculation typically dominates over break-up. A conceptual model illustrating expected trends (Figure 1), was proposed by DYER (1989). Still, relatively little quantitative data has been obtained to clarify these inter-relationships.

Fractal dimensions provide an alternative approach to describing flocculation and floc behaviour in turbulent waters (WINTERWERP, 1998; HILL, 1996). KRANENBURG, (1994) made the assumption that flocculated mud could be represented by a self-similar fractal structure. Floc fractal theory is similar to KRONE'S (1978) order of aggregation and can be regarded as a hierarchical process, whereby primary particles stick together to form zero order flocs, these then coagulate to transform them into first order flocs, etc. Thus, when larger flocs coagulate to form an even larger floc, this new larger floc has the same structure and geometry as the smaller floc, but on a larger size scale, and it contains the same number of *building blocks* as on the smaller size scale. Fractal dimensions generally range between 1.4 (for very fragile flocs) and 2.6 (for strong estuarine flocs). Fractal floc models, together with a number of useful theoretical approaches (e.g. VAN LEUSSEN, 1994; McANALLY and MEHTA, 2001)

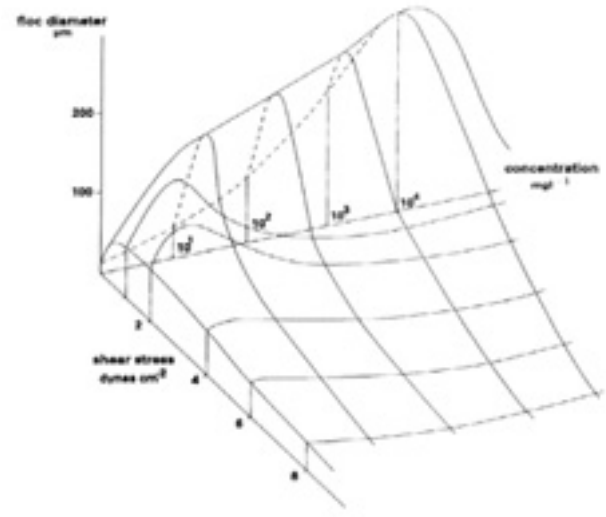

Figure 1. Conceptual diagram showing the relationship between floc modal diameter, suspended sediment concentration and shear stress (DYER, 1989).

would all benefit from simultaneous measurements of size and settling velocity.

To fully understand how flocs behave in a turbulent flow requires their direct measurement. However the largest and fastest settling flocs, which tend to contain most of the particulate mass (MEHTA and LOTT, 1987), are very fragile and easily broken-up upon sampling. Early attempts to sample flocs in-situ with devices such as Owen tubes (OWEN, 1976), led to under-estimation of floc size and settling velocity as they were very disruptive to the floc populations. Similarly, instruments such as Niskin bottles (GIBBS and KONWAR, 1983) and pipettes were also found to be potentially destructive to the sampled flocs (GIBBS, 1985; VAN LEUSSEN, 1988). This could be the reason that previous studies tended to show a much lower floc size range than is now known; i.e. the disruptive nature of the instrument was returning sampled macroflocs back to their stronger microfloc sub-structure.

The presence of large estuarine macroflocs was observed by in-situ photography (EISMA *et al*., 1983, 1990), and in-situ laser particle sizer measurements (BALE and MORRIS, 1987). KINEKE and STERNBERG (1989) observed the properties of suspended sediment in San Pablo Bay and found that it was dominated by flocs as large as 450 μm. Whilst EISMA *et al*. (1991) found the maximum floc size in three European estuaries (Ems, Rhine and Gironde) were 600 to 800 μm. In fact estuarine floc sizes can range over four orders of magnitude, from individual clay particles of 1 μm to stringer-type flocs of several centimetres in length. However, these sizing techniques still provided no indication of settling velocity. LICK (1994) found that like floc size, their settling velocities could also range over four orders of magnitude, from 0.01 mms^{-1} up to several centimetres per second. These non-intrusive instruments only measured floc size, and then used Stokes' Law to predict the settling velocity. This requires making an assumption of the floc effective density (also known as density contrast, density difference or excess density). However, the settling velocity of a floc is the function of both its floc size and effective density.

Optical devices to measure concentration profiles by SPINRAD *et al*. (1985), KINEKE *et al*. (1989), and McCAVE and GROSS (1991) have sought to quantify the rate of water clearance, but they are unable, like all earlier instrumentation, to measure particle size and settling velocity spectra directly. Also, most of these systems can not claim to be obtaining their data from undisturbed in-situ conditions.

The development of recent video floc sampling devices such as the INSSEV - IN-Situ Settling Velocity - (FENNESSY *et al*., 1994) instrument has provided a tool with which both floc sizes and settling velocities can all be measured within a naturally turbulent flow, whilst causing minimal de-flocculation. Floc effective densities can then be accurately estimated from a Stokes' Law relationship. Furthermore, provided the flocs are obtained from a known volume of fluid, the distribution of concentration throughout the floc population can be calculated (FENNESSY *et al*., 1997).

A series of in-situ field experiments and a laboratory based study have been conducted within the framework of recent research projects funded by the European Commission MAST III programme, whereby the floc characteristics were measured using low intrusive video techniques. By drawing on examples of floc spectra obtained during these experiments, it is the purpose of this paper is to assess how floc properties and the vertical mass flux are influenced by changes in turbulent shear stress intensity. Both the generalised variations in mean floc properties and changes occurring within individual aggregate fractions, at specific points in a tide, will be examined.

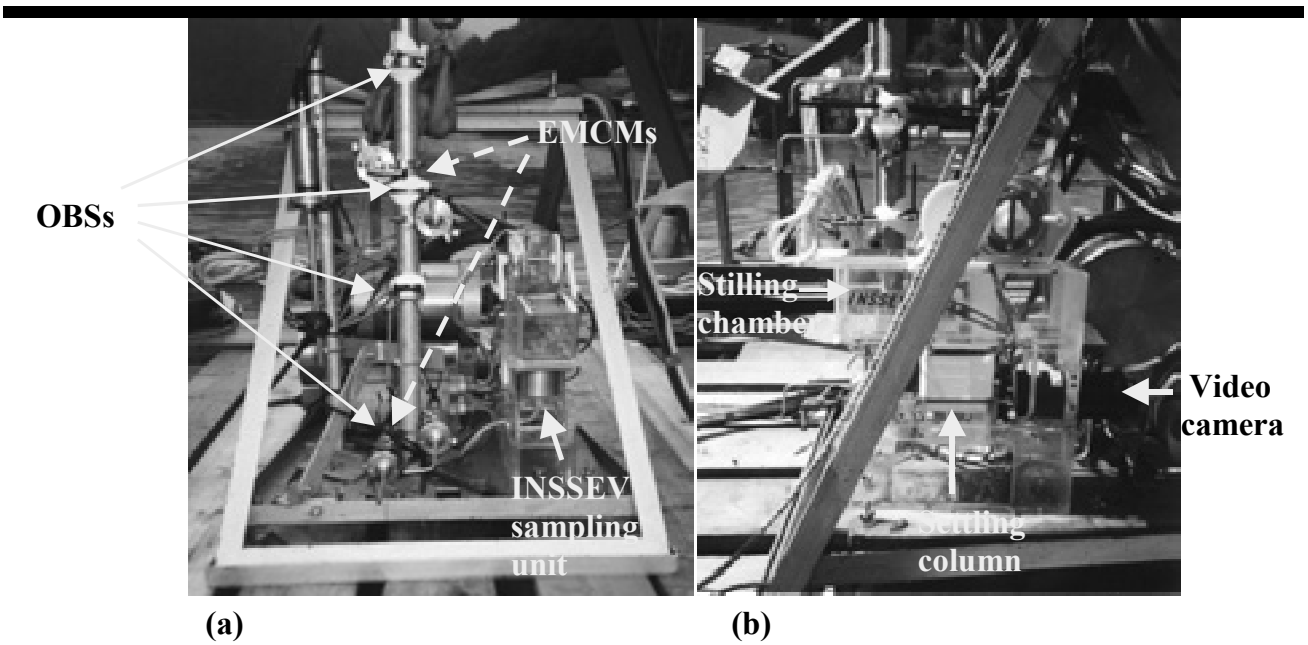

Figure 2. INSSEV and POST sensors mounted on the estuarine bed frame – (a) front view and (b) side view.

FIELD STUDY INSTRUMENTATION & METHODOLOGY

The in-situ field experiment floc data described in this paper was acquired using the INSSEV instrument which was developed at the Institute of Marine Studies, University of Plymouth by FENNESSY *et al*. (1994a). It has the distinct advantage of permitting the simultaneous measurement of both size and settling velocity of a characteristic sample of flocs in-situ. The sampling apparatus comprises a two chamber device, whereby a volume of flowing suspension is trapped in the upper stilling chamber. After a short period to allow the turbulence in the chamber to decay, a sliding door (situated in the floor of the stilling chamber) opens for a predetermined duration (estimated as a function of the estuarine concentration at the time of sampling) to allow a representative number of flocs to settle into a settling column located directly beneath. The column is filled with clear water of a pre-determined salinity, which is marginally higher than that of the ambient; this helps to reduce secondary currents developing.

As the flocs settle they are observed as silhouettes by a miniature underwater video camera (positioned in the settling column wall), which has an integral low heat backlighting array. The recorded images provided individual floc dimensions and settling velocity (both manually measured directly from the video monitor), from which the floc effective density, ρ_e, (floc bulk density minus the density of water) could be determined by Stokes' Law. All floc sizes reported in this paper are spherical equivalent, unless otherwise stated. This standardised format permits comparisons to be made with other flocculation studies. The recording S-VHS video system gives INSSEV a practical lower resolution limit of 20 μm. To obtain the distribution of floc dry mass and floc porosity, the flocs are referenced with a 400 mm^3 volume of fluid as prescribed by: the nominal video image width (4 mm), depth of field (1 mm), and the height of the stilling chamber (100 mm). Fractal dimensions were calculated by a formula offered by WINTERWERP (1998).

The INSSEV apparatus requires physical stability in order to capture a floc sample of good integrity, and also to allow the camera to view the flocs precisely. Thus, to prevent any vertical and horizontal motion during a sampling deployment, it was secured to a heavy bed frame, which sat on the estuary bed throughout the entire duration of the sampling procedure.

Turbulence and turbidity values were obtained from high frequency (18 Hz) measurements made using the POST – Profile Of Sediment Transport - system (CHRISTIE *et al*., 1997). This included four miniature discoidal electro-magnetic current meters, and an array of up to eight optical back-scatter sensors. The POST sensors were mounted on a vertical pole, which was positioned adjacent to the INSSEV sampling unit, on the bed frame. The current meter heads were positioned in pairs at 25 cm and 75 cm above the estuary bed, and were carefully aligned to measure all three orthogonal components of the flow. Figure 2 illustrates the complete instrumentation bed frame configuration.

The *turbulent kinetic energy* was the preferred method for calculating the turbulent shear stress, as opposed to the logarithmic profile or Reynolds stress approaches, which are more sensitive to sensor misalignment errors. Burst-averaged values of turbulent kinetic energy (STAPLETON and HUNTLEY, 1995), E, were calculated for each 3 minute 47.55 second duration data file by equation 1:

$$E = 0.5\ \rho_W \left(\overline{u'^2} + \overline{v'^2} + \overline{w'^2}\right) \qquad (1)$$

where ρ_w is the estuarine water density and $\overline{u'^2}$, $\overline{v'^2}$ and $\overline{w'^2}$ are the three turbulent variance components.

The turbulent shear stress (τ) is proportional to the turbulent kinetic energy (SOULSBY, 1983), assuming the energy production equals the energy dissipation and was calculated by:

$$\tau = 0.19 \cdot E \qquad (2)$$

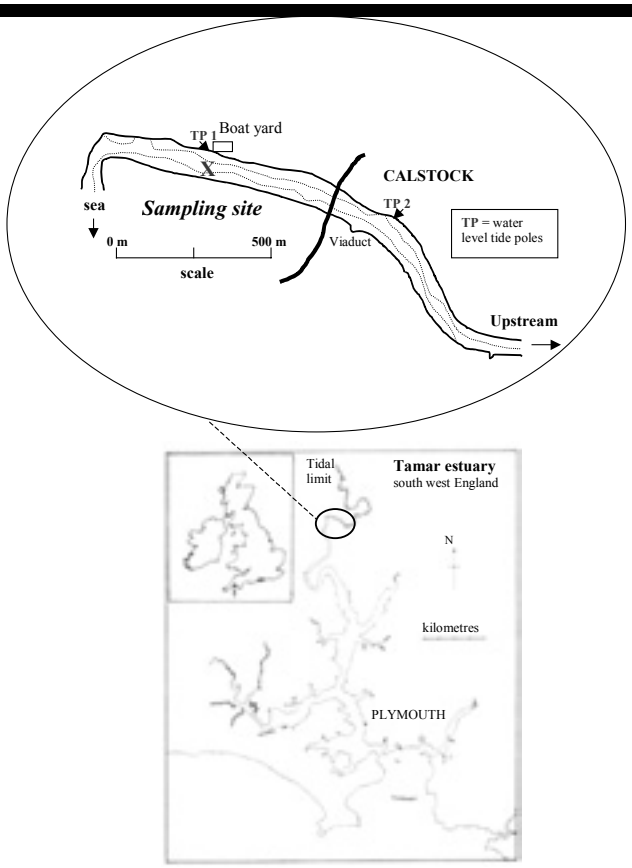

Figure 3. Location diagram of the Tamar estuary showing the position of the sampling site; X indicates where the research vessels were moored.

A Seabird Systems CTD was used to obtain water column profiles of salinity and temperature at 15 minute intervals. To compensate for the sub 20 μm fraction not observed by the INSSEV camera, a correction was applied to the total calculated INSSEV dry mass for each floc spectrum by making a direct comparison with the concentration obtained from water samples collected simultaneously with each INSSEV sample. The gravimetric analysis of the water samples was also used to calibrate the optical back-scatter sensors. Loss-on-ignition tests were conducted on filtered sediment samples to provide an indication of the organic content of the mud in suspension. Further details of the field experiment sampling protocols are reported by MANNING and DYER. (2002a).

FIELD STUDY RESULTS

A series of deployments were conducted from a mid-channel location (which was 75 m wide at high water) in the upper reaches of the mesotidal (DAVIES, 1964) Tamar estuary (near Calstock) during June, August and September 1998, as part of the EC MAST III funded COSINUS project (BERLAMONT, 2002). Located in south-west England, the Tamar estuary is topographically dendritic in shape, has numerous meanders and wide mud flats exposed at low water (Figure 3). It is classified as a coastal plain, flood dominant estuary (DYER, 1997), and the annual mean river discharge is about 20 $m^3 s^{-1}$. The Tamar has a semi-diurnal tidal regime, and the sampling programme experienced both neap and spring tidal conditions, where the average tidal range was 3.2 m and 4.5 m, respectively.

The Calstock site placed the instrumentation bed frame in the path of the turbidity maximum, which meant that a wide range of turbulent and particle concentration conditions would be experienced, from which the flocculation response could be examined. The neap tide experiments observed maximum surface current velocities of 0.6 m s^{-1}, and these conditions entrained up to 800 g cm^{-3} of solids into suspension 30 cm above the bed. The water column water partially stratified with salinity values ranging from zero, through to 9 at high water. During spring tide sampling, the water column at the Calstock location remained predominantly fresh throughout. Suspended particle concentrations were an order of magnitude greater than those experienced during neaps and the peak surface flow velocities were twice as fast.

The detailed aims of the fieldwork programmes were to obtain in-situ data on the distribution of floc size, settling velocity and effective density in relation to salinity, concentration and turbulence characteristics. Measurements were made during deployments conducted on a sub-tidal cycle time scale for a duration of approximately 3 hours, at times when the flow conditions were either reasonably steady or gradually changing. This provided regular intervals for instrument servicing and calibration. More details of these COSINUS deployments are reported by DYER *et al*. (2002a).

A selection of floc data will be initially presented from a low energy and low concentration neap tides deployment. This will be followed by examples of data obtained from the contrasting more turbulent and higher ambient concentrations experienced during spring tides. It is not the intention of this paper to solely compare tidal conditions, but to compare how the variations in levels of turbulent energy and concentration influence the physical properties of estuarine floc populations.

Neap Tides

Figure 4a shows the time series for variations in concentration and turbulent shear stress, both at the INSSEV sampling height of 0.5 m above the bed, for an ebb deployment during a neap tide. The corresponding distribution of sample mean mass weighted spherical equivalent floc size and mean mass weighted settling velocity are illustrated in Figure 4b. The Tamar is a flood dominant estuary, therefore an ebb run during a neap tide would typically produce low turbulent energy mixing conditions. The concentration started to rise when the stress exceeded a value of about 0.15 N m^{-2}, from a background concentration of about 40 g cm^{-3} to reach a maximum of 280 g cm^{-3} within the turbidity maximum. The mean size of the flocs also rose from about 150 μm to almost 220 μm. The smaller sized flocs in the clearer water prior to the turbidity maximum had settling velocities of almost 10 mm s^{-1}. These flocs had a very high effective density. The mean settling velocity reduced to 1-2 mm s^{-1} within the turbidity maximum. However, the mean settling velocity was at its slowest at the beginning of the turbidity maximum when stress and concentration were relatively low, but increased as shear stress and concentration rose. The increase in size and subsequent decrease in settling velocity within the turbidity maximum, implies a drastic decrease in macrofloc effective density, which fell from 715 kg m^{-3} to less than 100 kg m^{-3} (Figure 4c).

Figure 5a shows the distribution of spherical equivalent floc size and settling velocity for INSSEV sample T15-6. This sample was acquired at 16:41 hr, which was 2 hours and 3 minutes after local high water (HW+2:03 hr).

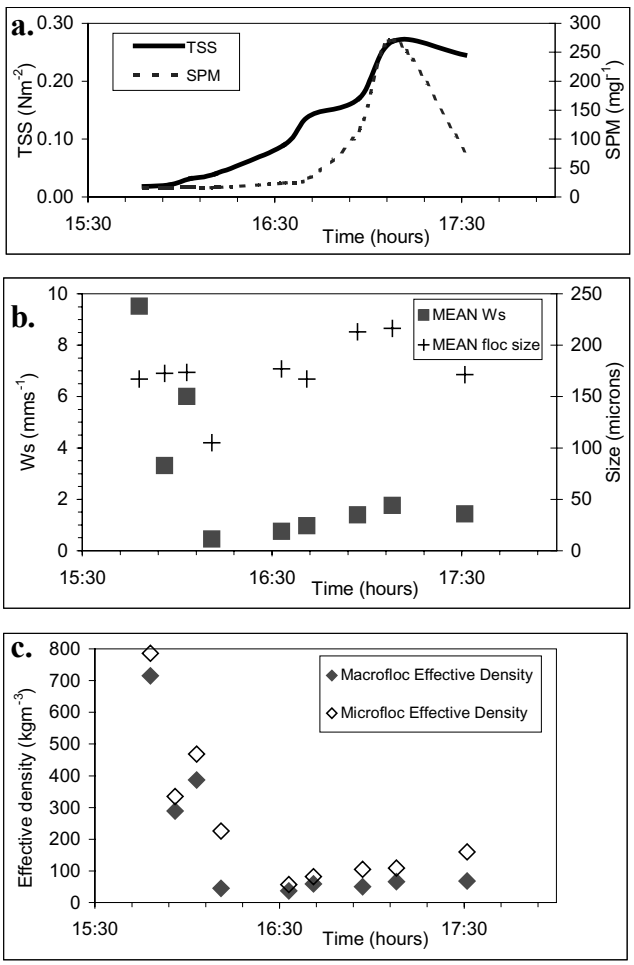

Figure 4. Time series for measurements made in the Tamar estuary turbidity maximum during the ebb on a neap tide showing the variations of: (a) turbulent shear stress (TSS) and suspended particulate matter (SPM) concentration; (b) mean floc and mean settling velocity size; and (c) macrofloc and microfloc effective density values.

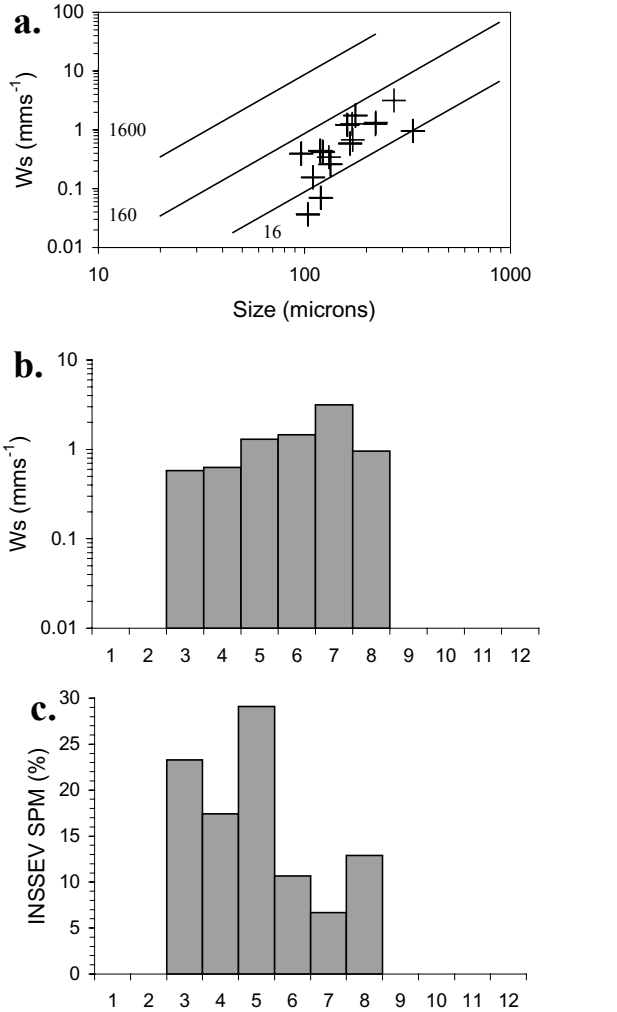

Size Band	1	2	3	4	5	6	7	8	9	10	11	12
Floc size (μm)	<40	40-80	80-120	120-160	160-200	200-240	240-320	320-400	400-480	480-560	560-640	>640

Figure 5. Summary of floc characteristics for Tamar estuary neap tide sample T15-6 obtained at 16:41 hr (high water +2:03 hr). Where (a) illustrates the relationships between floc size and settling velocities of individual flocs, with diagonal full lines showing the effective density (kg m^{-3}); (b) shows the size band distribution of settling velocity; and (c) shows the size band distribution of suspended concentration.

By then the salt wedge had receded downstream and the water column was left fresh. The floc size spectra increased towards the larger sizes in response to the increasing concentration. The diagonal lines are contours of effective density. To assist in the interpretation of the varying floc properties, the spectrum has been divided into twelve size bands. Where size band 1 represents flocs less than 40 μm in size, whilst size band 12 constitutes flocs greater than 640 μm in diameter.

Sample T15-6 had two flocs in the 320-400 μm size range (size band 8), and these constituted 13% of the overall ambient concentration (Figure 5c), which was 32 g cm^{-3}. By then the low turbulent (~ 0.14 N m^{-2}) conditions permitted the moderately organic-rich (suspended concentration was approximately 20% organic content at that time) cohesive sediment to flocculate, and this is reflected in the flocs throughout size bands 3-8 (80-400 μm) being predominantly high in porosity, and possessing effective densities all under 105 kg m^{-3}.

The high organic content contributed to the formation of a number of stringer type flocs (MANNING and DYER, 2002b). Stringers consist of small clustered aggregates inter-connected as a chain by fine organic matter. The size band 1-4 (20-160 μm) flocs which had settling velocities of 0.2-0.3 mm s^{-1}, and fractal dimensions of 1.85-1.95.

The latter indicates that these were poorly bonded flocs and very susceptible to disaggregation under an increase in turbulent shear (DYER and MANNING, 1999). Although the flocs greater than 160 μm in diameter sampled from 16:30 hr onwards tended to have settling velocities predominantly in the 1-3 mm s^{-1} range, a greater portion of the particulate mass was seen to occur within the macrofloc sub-population. This was demonstrated by floc sample 15-7 acquired at 16:55 hr (Figure 6), where 69% of the

concentration was contained by the flocs exceeding 160 μm in size, when the stress and concentration were 0.17 N m^{-2} and 115 g cm^{-3}, respectively.

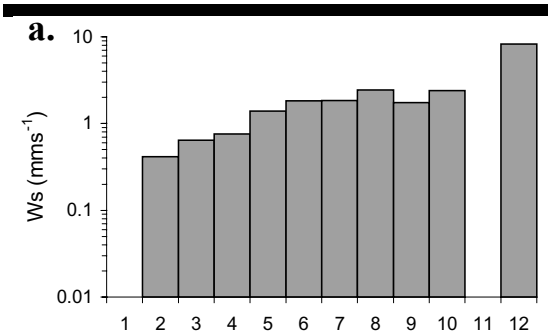

Size Band	1	2	3	4	5	6	7	8	9	10	11	12
Floc size (μm)	<40	40-80	80-120	120-160	160-200	200-240	240-320	320-400	400-480	480-560	560-640	>640

Figure 6. Summary of floc characteristics for Tamar estuary neap tide sample T15-7 obtained at 16:55 hr (high water +2:17 hr). Where (a) shows the size band distribution of settling velocity, and (b) illustrates the size band distribution of suspended concentration.

By 17:08 hr (HW +2:39 hr) both the shear stress and concentration had risen to their maximum values of 0.27 N m^{-2} and 271 g cm^{-3}, respectively. Examination of INSSEV sample T15-8 (Figure 7), which was collected at that time, showed that the amount of suspended matter constituting the floc sub-population greater than 160 μm had risen to an ebb peak of 77.4%. This suggests that the combined rise in particle abundance and turbulent shear stimulated floc growth.

Figure 8 shows a time series illustrating the relative changes in the percentage contribution of the macrofloc (D > 160 μm) and microfloc to the mass concentration, for the neap tide flocs on the ebb. Generally, the first few samples show a higher percentage of mass in the microfloc sizes. However, subsequent samples show increasing mass in the macrofloc and decreasing mass in the microfloc with increasing stress values. Outside of the turbidity maximum the proportions of both fractions approach 50%, and then cross over at a stress value of about 0.1 N m^{-2}.

Spring Tides

The more dynamic estuarine water column associated with the increased tidal range of spring conditions, produced a significantly higher range in turbidity and a more turbulent water column than observed during the more sedate neap conditions, and thus an even greater variety in floc characteristics. On the flood (as the Tamar is a flood dominant estuary) peak surface current velocities were virtually double those recorded during neap tides, and the concentration was also one or two orders of magnitude higher.

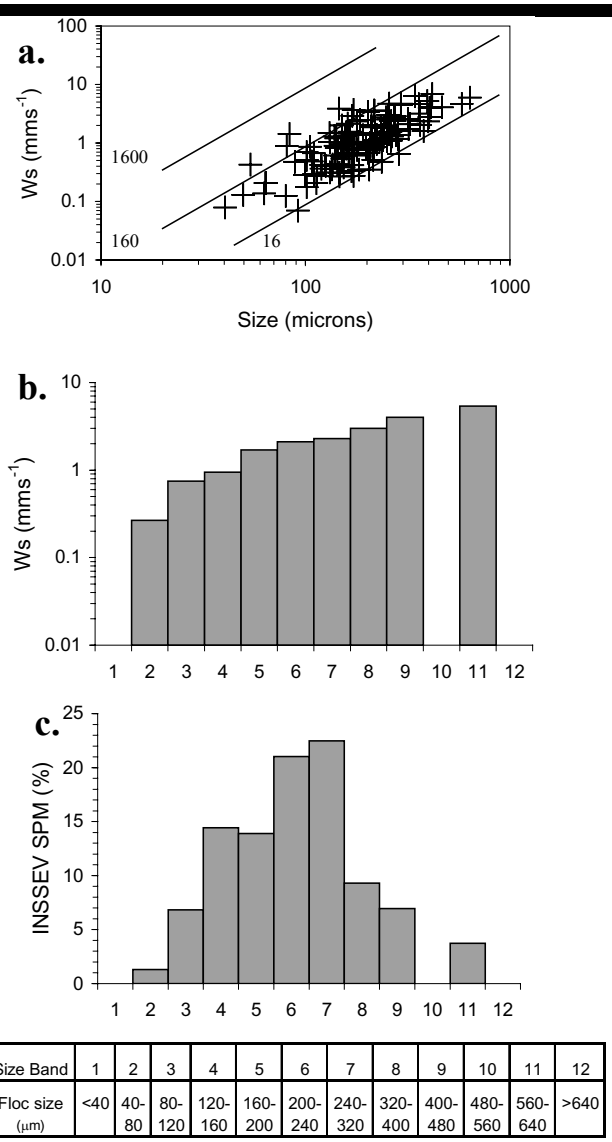

Size Band	1	2	3	4	5	6	7	8	9	10	11	12
Floc size (μm)	<40	40-80	80-120	120-160	160-200	200-240	240-320	320-400	400-480	480-560	560-640	>640

Figure 7. Summary of floc characteristics for Tamar estuary neap tide sample T15-8 obtained at 17:08 hr (high water +2:39 hr). Where (a) illustrates the relationships between floc size and settling velocities of individual flocs, with diagonal full lines showing the effective density (kg m^{-3}); (b) shows the size band distribution of settling velocity; and (c) shows the size band distribution of suspended concentration.

The concentrations on a typical flood sampling run, at 0.5 m above the bed, reached in excess of 8 kg cm^{-3} (Figure 9a), and the corresponding mean floc size was greater than 300 μm (Figure 9b). The most distinctive effect was that of the high concentrations on the turbulence. For the period between 16:20-17:40 hr. Figure 9a shows the shear stress commences to fall as the concentration rises. This is due to the formation of a concentrated benthic suspension (CBS) layer in the near bed region, and turbulence damping occurred within the CBS as a result of density stratification. Unlike a fluid mud, which acts independently from

the main flow, a CBS is still transported with the dominant current. The solids forming the CBS were kept in suspension by turbulence, although the CBS layer can interact with the turbulent flow field. The CBS behaves in a Newtonian manner, but with increased viscosity. The optical back-scatter array indicated that the CBS layer was nominally 0.6m high (i.e. the distance between the estuary bed and the lutocline) and it displayed a mean concentration of about 5 kg cm^{-3} at 0.5 m above the bed. CBS layer dynamics have been examined by both DYER *et al*. (2003) and MORY *et al*. (2002). The turbulent shear stress was drastically affected by drag reduction (DYER *et al*., 2002b; BEST and LEEDER, 1993; LI and GUST, 2000) once the concentration gradients exceeded ~ 4 kg m^{-4} (DYER *et al*., 2002b), and the shear stress values decreased across the turbidity maximum. Drag reduction is the phenomenon of shear stress reduction at the boundary and turbulent shear being temporarily shifted to a higher level in the water column, i.e. the lutocline interface.

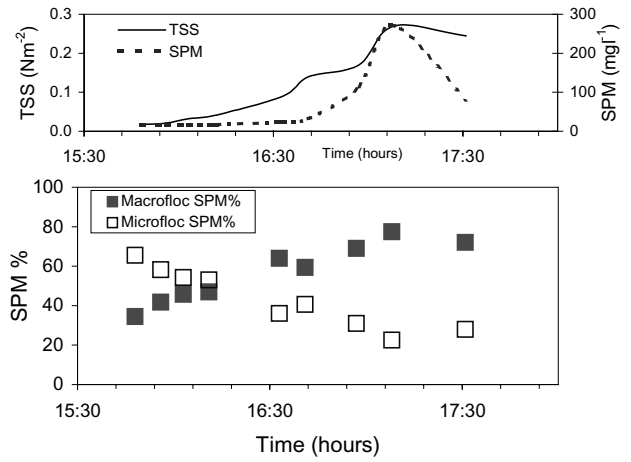

Figure 8. Time series for measurements made in the Tamar estuary turbidity maximum during the ebb on a neap tide showing the variations of: (top) turbulent shear stress (TSS) and suspended particulate matter (SPM) concentration; and (bottom) the percentage division of macrofloc and microfloc suspended particulate matter concentration (SPM%).

At the tail end of the turbidity maximum, once concentrations started reducing, the mean floc size decreased to about 150 µm. Once the concentration fell below ~ 4 kg cm^{-3}, the turbulent shear stress increased rapidly as turbulence became more active, causing a further size reduction to about 100 µm. The settling velocity reached almost 6 mms^{-1}, but reduced to about 0.5 mm s^{-1} towards the end of the turbidity maximum. The macrofloc effective density was under 95 kg m^{-3} for all samples within the turbidity maximum (Figure 9c).

Figure 10 shows the floc characteristics for sample T22-7, which was collected at 16:10 hr (HW -3:58 hr). This was just prior to the turbidity maximum reaching the sampling station, which accounted for a low ambient concentration of 858 g cm^{-3}. Although early into the flood, an already fast flowing surface current had created a stress of 0.44 N m^{-2} at the INSSEV sampling height. The floc size population spanned from 36 up to 523 µm in diameter. Although the larger flocs displayed higher settling velocities, the smaller sized aggregates showed a more varied settling rate. Nearly 86% of the dry floc mass was held by flocs 120-400 µm (size bands 4-8) in diameter.

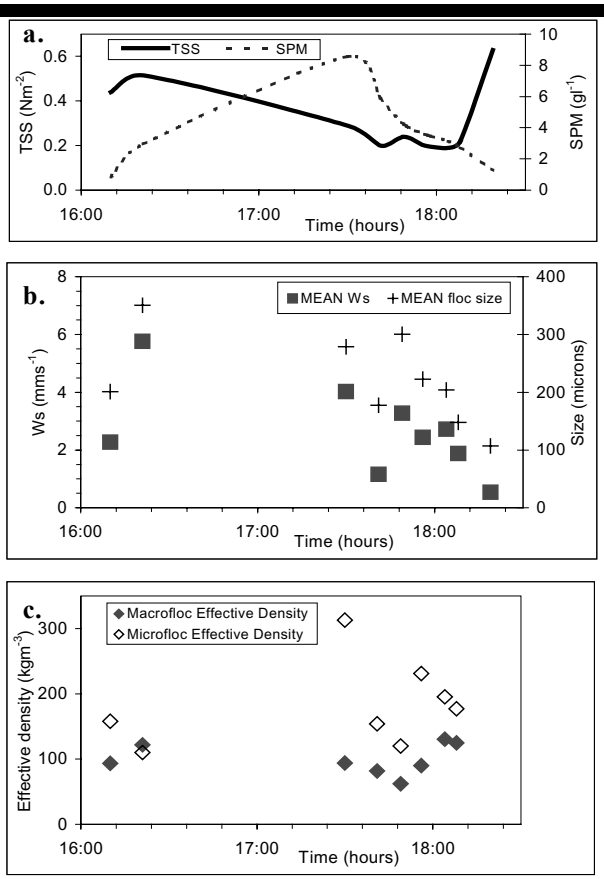

Figure 9. Time series for measurements made in the Tamar estuary turbidity maximum during the flood on a spring tide showing the variations of: (a) turbulent shear stress (TSS) and suspended particulate matter (SPM) concentration; (b) mean floc and mean settling velocity size; and (c) macrofloc and microfloc effective density values..

However, further analysis revealed that the ratio of macrofloc to microfloc concentration was close to unity, indicating an equal apportioning of the particulate mass between these two key floc sub-populations. The majority of the flocs under 240 □m in diameter had effective density values in excess of 200 kg m-3. These dense flocs had corresponding mean porosity and fractal dimensions of 80% and 2.45, respectively.

Sample T22-9 (Figure 11) was obtained at 17:30 hr (HW -2:38 hr) from within the CBS layer, which had formed close to the bed during the advection of the main body of the turbidity maximum. The estuarine concentration was 8.5 kg cm^{-3} at 0.5 m above the bed, and the turbulent energy damping associated with this high concentration level suppressed the turbulent shear stress to only 0.29 N m^{-2}. A very distinctive change had occurred within the floc population. The earlier unimodal floc distribution, had been replaced by a very bi-modal population; both modes demonstrating very different floc characteristics. The first mode was composed of both microflocs and macroflocs up to 232 µm in diameter. This was a total of 1672 individual flocs representing 80% of the total floc population. However in terms of dry floc mass, this only constituted 41% of the total content.

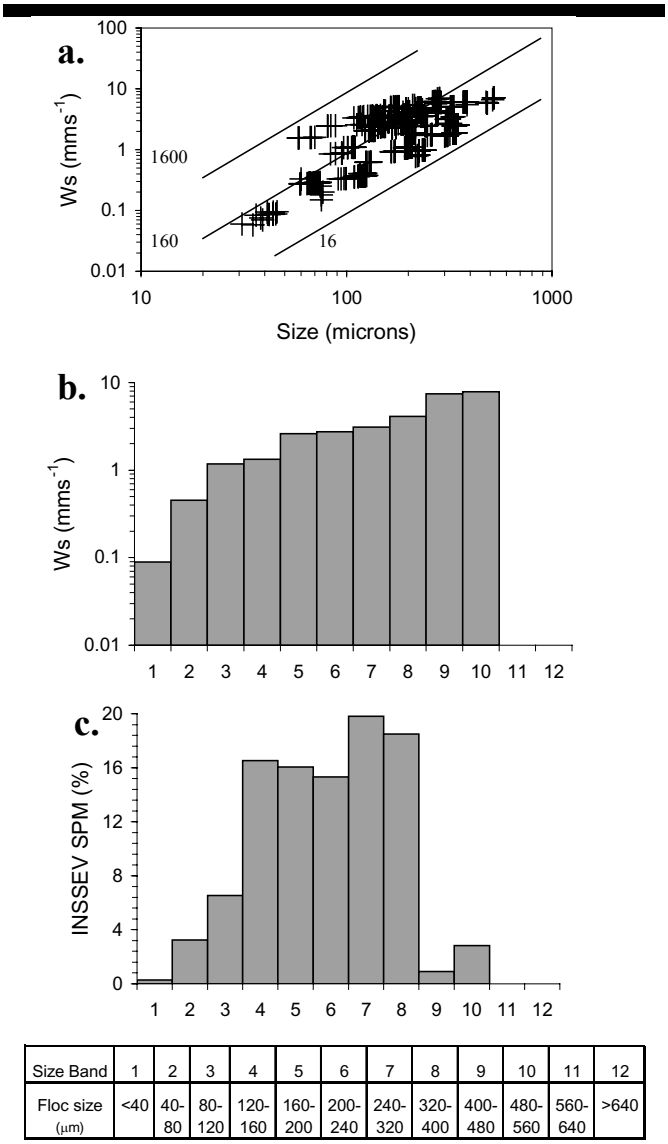

Size Band	1	2	3	4	5	6	7	8	9	10	11	12
Floc size (μm)	<40	40-80	80-120	120-160	160-200	200-240	240-320	320-400	400-480	480-560	560-640	>640

Figure 10. Summary of floc characteristics for Tamar estuary spring tide sample T22-7 obtained at 16:10 hr (high water -3:58 hr). Where (a) illustrates the relationships between floc size and settling velocities of individual flocs, with diagonal full lines showing the effective density (kg m^{-3}); (b) shows the size band distribution of settling velocity; and (c) shows the size band distribution of suspended concentration

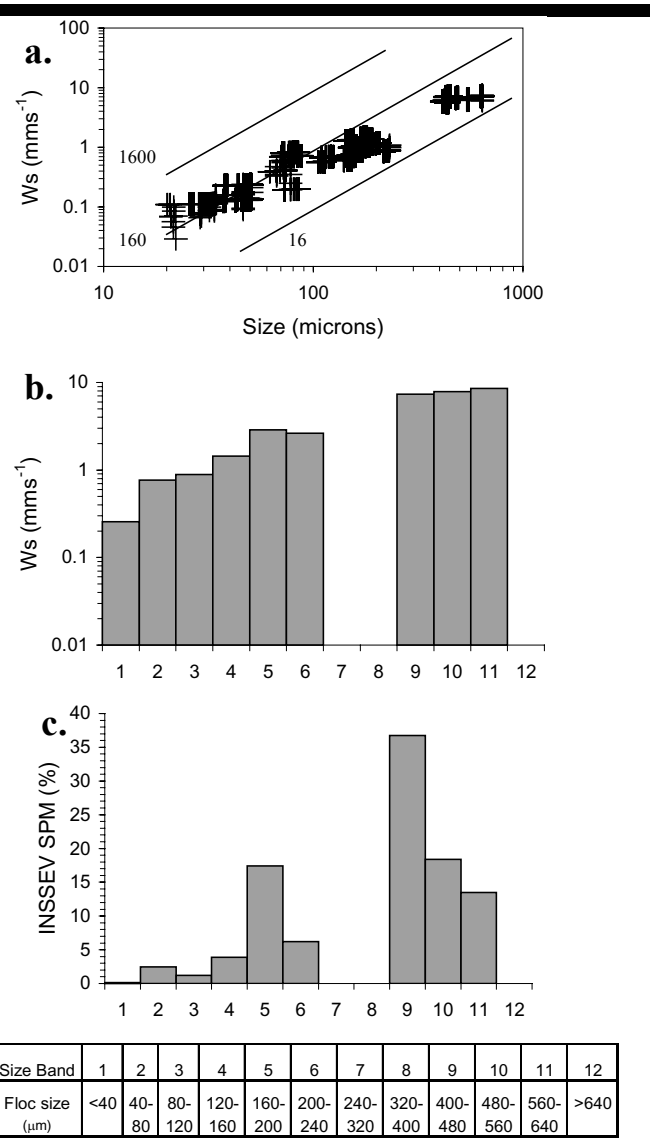

Size Band	1	2	3	4	5	6	7	8	9	10	11	12
Floc size (μm)	<40	40-80	80-120	120-160	160-200	200-240	240-320	320-400	400-480	480-560	560-640	>640

Figure 11. Summary of floc characteristics for Tamar estuary spring tide sample T22-9 obtained at 17:30 hr (high water -2:38 hr). Where (a) illustrates the relationships between floc size and settling velocities of individual flocs, with diagonal full lines showing the effective density (kg m^{-3}); (b) shows the size band distribution of settling velocity; and (c) shows the size band distribution of suspended concentration.

The microflocs had typical effective density values of 200-320 kg m^{-3}, and their settling velocities ranging from 0.2-0.8 mm s^{-1}. The remaining 20% of the floc population, which accounted for 59% of the floc dry mass, were large macroflocs ranging from 410-640 μm in diameter and possessed settling velocities between 5-7 mm s^{-1}. This translated into this larger floc size fraction contributing 91% of the total mass settling flux (31.7 g.m^{-2} s^{-1}). It may be hypothesised that the reduction in shear stress, due to turbulence damping within the CBS, produced a rate of orthokinetic (i.e. shear induced) inter-particular contacts which promoted a greater degree of flocculation as the concentration level rose.

By 17:49 hr (HW -2:19 hr), the CBS layer had started to decrease in thickness and the concentration had fallen to 4.2 kg cm^{-3}. This 50% reduction in concentration, from that observed only 20 minutes previously, together with a further reduction in shear stress to 0.24 N m^{-2}, brought a return to a definite negative skewness to the floc population, as shown by sample T22-11 (Figure 12). The 80-160 μm sized flocs constituted 54% of the total flocs, and 32% of the particulate mass. This cluster of small slow settling flocs represents a portion of the population which had not been incorporated into higher order flocs at that point in the tidal cycle. The microflocs are most probably a fraction that would not aggregate. It is unlikely that they were the result of break-up as the stress was low.

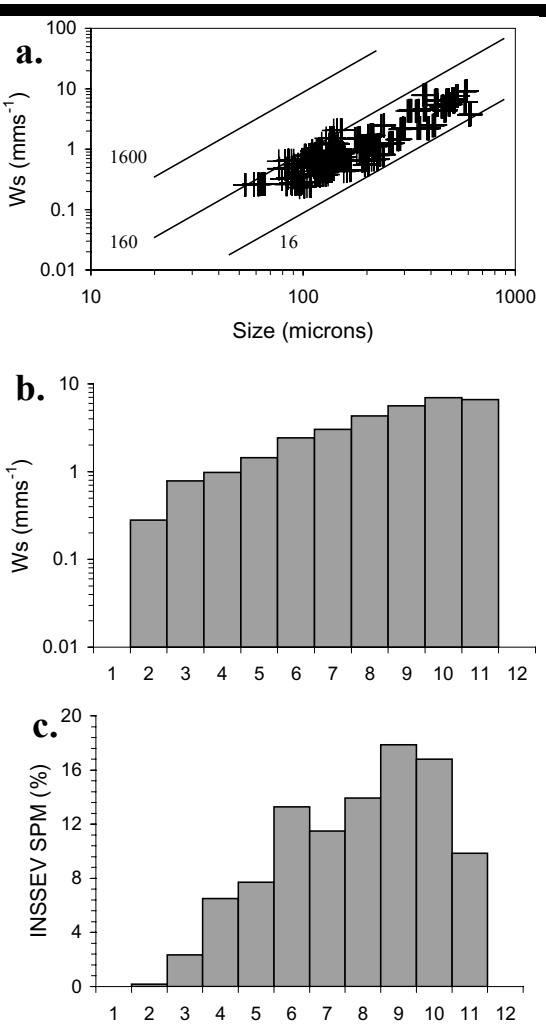

Size Band	1	2	3	4	5	6	7	8	9	10	11	12
Floc size (μm)	<40	40-80	80-120	120-160	160-200	200-240	240-320	320-400	400-480	480-560	560-640	>640

Figure 12. Summary of floc characteristics for Tamar estuary spring tide sample T22-11 obtained at 17:49 hr (high water -2:19 hr). Where (a) illustrates the relationships between floc size and settling velocities of individual flocs, with diagonal full lines showing the effective density (kg m^{-3}); (b) shows the size band distribution of settling velocity; and (c) shows the size band distribution of suspended concentration.

The remaining particulate matter was relatively evenly distributed through near-spherical macrofloc, which reached up to 616 μm in diameter. These macrofloc had size band mean settling velocities which increased progressively with each successive size band. The respective mean settling rates of size bands 5 (160-200 μm) and 11 (560-640 μm), were 0.9 mm s^{-1} and 6.2 mm s^{-1}. This gave the fraction over 160 μm a mean settling velocity of 4.2 mm s^{-1}, and 92% of the settling flux.

In summary, at the beginning of the turbidity maximum the proportion of macroflocs was 73-85% (by mass) (Figure 13), and this exceeded 90% for most of the remainder of the turbidity maximum.

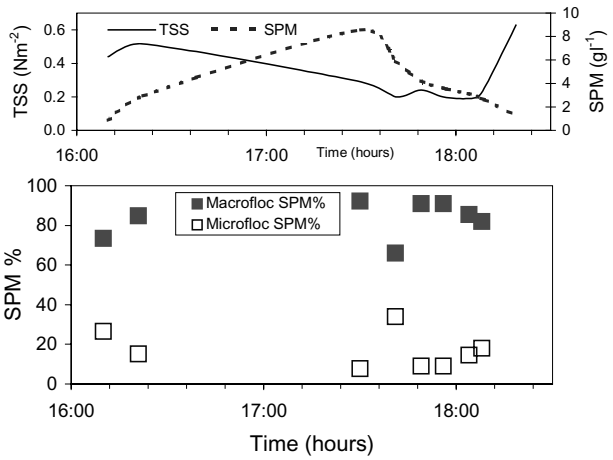

Figure 13. Time series for measurements made in the Tamar estuary turbidity maximum during the flood on a spring tide showing the variations of: (top) turbulent shear stress (TSS) and suspended particulate matter (SPM) concentration; and (bottom) the percentage division of macrofloc and microfloc suspended particulate matter concentration (SPM%).

Although there was indication that the proportion might have been decreasing towards the end of the high concentration period.

LABORATORY EXPERIMENTAL STUDY

There is a long history, particularly in the sanitation industry (ARGAMAN and KAUFMAN, 1970), of using laboratory hydraulic simulation models to study flocculation. However, the laboratory experiments reported in this paper were among the first to use video technology to monitor floc behaviour within an artificially created turbulent flow environment. Controlled laboratory conditions allow keeping pre-selected individual processes constant, which permits specific phenomena to be studied (on a repeatable basis) in greater detail.

Method

Laboratory measurements were carried out by MANNING and DYER (1999) to investigate the inter-relationships between floc size and settling distributions with increasing turbidity (80-200 g cm^{-3}) and turbulent shear stress (0.1-0.6 N m^{-2}). Suspensions of natural Tamar estuary mud of known concentration were placed in an annular flume. Each suspension was sheared at a high rate for half an hour, and then the shear stress was reduced (in 0.1 N m^{-2} increments) and the flocs were allowed to equilibrate at the new stress level for a further half an hour. This procedure was used to mimic the variation of natural shearing experienced by flocs in a tidal flow and ensure the initial distribution was composed of microflocs. The resultant distributions of floc size and settling velocity were measured, at each shear stress increment, by the INSSEV underwater miniature video camera. This was mounted in a viewing port on the flume channel wall. Floc measurements were made 120 seconds after the induced turbulence had ceased.

Results

The relationship between the floc size of the largest four flocs in each sample, and the corresponding shear stress and

concentrations are shown in Figure 14a. Qualitatively the results were similar to those of TSAI *et al*. (1987) and BURBAN *et al*. (1989). At low shear stresses the size of the flocs at the lowest concentration was smaller than those at the higher concentrations. With regards to the floc settling velocities, these were fastest for high concentrations when the applied shear stress was low (Figure 14b). Whereas for the higher stress region, the fastest settling rates occurred within the lower concentrations. This is similar to the in-situ field observations.

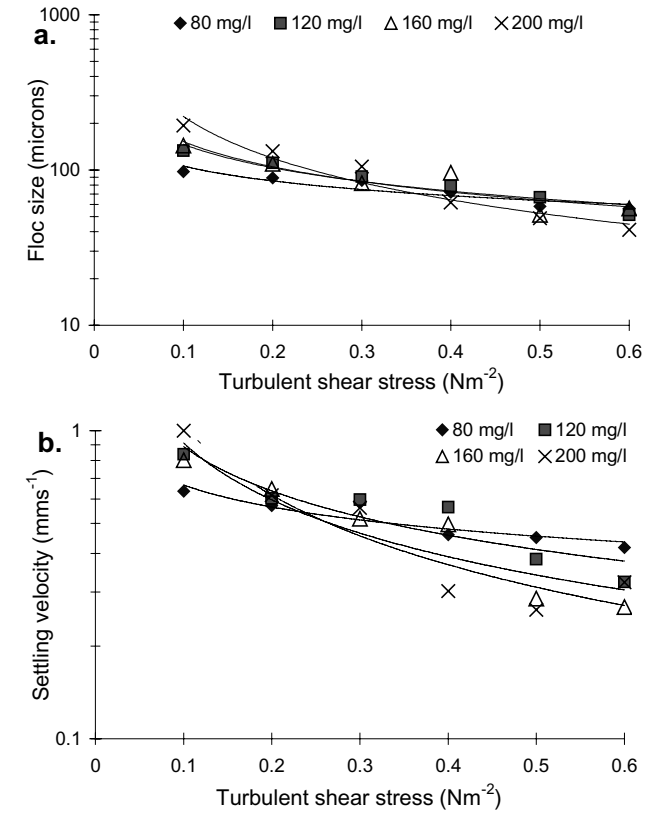

Figure 14. Variations in both (a) floc size and (b) settling velocity for various concentration (different symbols) against turbulent shear stress, derived from laboratory annular flume experiments. Power regression lines have been added (from Manning and Dyer, 1999).

DISCUSSION

The Tamar estuary field experiments showed that within the turbidity maximum there was an increase in the mean floc size, which in general, matched the changing concentrations. There was also an increase in mean settling velocity through the turbidity maximum following the changes in size and concentration. These mean settling velocities were in the region of 0.5-6 mm s^{-1}. The changes in size and settling velocity imply that the effective density must decrease within the turbidity maximum.

The proportion of macroflocs changed significantly across the turbidity maximum. Before the passage of the turbidity maximum, the macroflocs contributed about 50% of the total floc mass on neaps and 60-70% on springs. Within the turbidity maximum the macrofloc proportion rose rapidly until they contributed at least 75% of the floc dry mass during neap conditions, and at spring tides this reached in excess of 90-95%. A similar concentration distribution was observed by FENNESSY and DYER (1996) for an in-situ floc spectrum acquired in the Elbe estuary. These observations concur with the findings of EISMA *et al.* (1991), who measured large floc sizes in the bottom water of several estuaries, where particle concentrations were at a higher level. EISMA *et al.* (1991) explains this effect by suggesting that the increase in near bed suspended concentration, such as the CBS layer formation during the passage of the main body of the turbidity maximum in the upper Tamar estuary, as having the net effect of reducing turbulence to a level which produced an increasing frequency of constructive particle collisions, and hence causing enhanced macrofloc growth.

The variations in the relative proportions of macrofloc and microfloc dry mass in several European estuaries has been statistically analysed by MANNING (2004), who found a strong correlation with the estuarine concentration. In terms of mass settling flux, the fast settling macroflocs observed during the high energy and high concentration flood throughout spring tide conditions accounted for a flood average of 89% of the flux. Whereas during the less turbulent and less turbid ebb during neap tides, the macroflocs contributed nearly 20% less to the settling flux rate. This can be mainly accredited to a time series averaged macrofloc settling velocity of 4.6 mm s^{-1} for the spring tides sampling run, which was 2.8 mm s^{-1} faster than the corresponding settling velocity computed for neap conditions.

An assessment of the complete Tamar estuary macrofloc and microfloc data sets, has revealed that the rate at which the microflocs are permitted to coagulate into macroflocs is dependent on the combination of the shear stress and concentration. This indicates that the basic mechanism controlling the rate of flocculation is likely to be the number of successful inter-particle collisions that occur. This agrees with the findings of numerous laboratory studies (LICK *et al*., 1993; MANNING and DYER, 1999; GRATIOT and MANNING, 2004). However, WINTERWERP (1999) suggests that that the floc size and settling velocity are both inversely proportional to the turbulent shear when the residence time of the flocs in the shear field is unlimited. This means that a limitation in residence time can restrict floc growth when both the turbulent activity and particle concentrations are very low; i.e. at low shear stresses and concentrations, there are insufficient collisions to fully initiate flocculation.

From the in-situ observations it is possible to examine the relationships between the variables and to produce quantifiable empirical algorithms. A conclusion drawn from an Intercomparison Experiment of various floc measuring devices conducted in the Elbe estuary (DYER *et al*., 1996), was that a mean or median settling velocity did not adequately represent an entire floc spectrum, especially in considerations of a flux to the bed. DYER *et al*. (1996) recommended that the best approach for accurately representing the settling characteristics of a floc population for the modelling of fine sediment dynamics, is to split a floc distribution into two components, each with their own median settling velocity. Therefore, to quantitatively assess the settling velocity data reported in this paper, the macrofloc and microfloc sub-fractions were chosen.

The statistical package *Minitab for Windows - version 10.1* was used to perform a multiple regression analysis on the settling velocity data, with a default statistical confidence level of 95%. To provide a more rigorous and less site-specific assessment, the Tamar estuary data was extended by the inclusion of INSSEV floc settling data acquired from two addition sources.

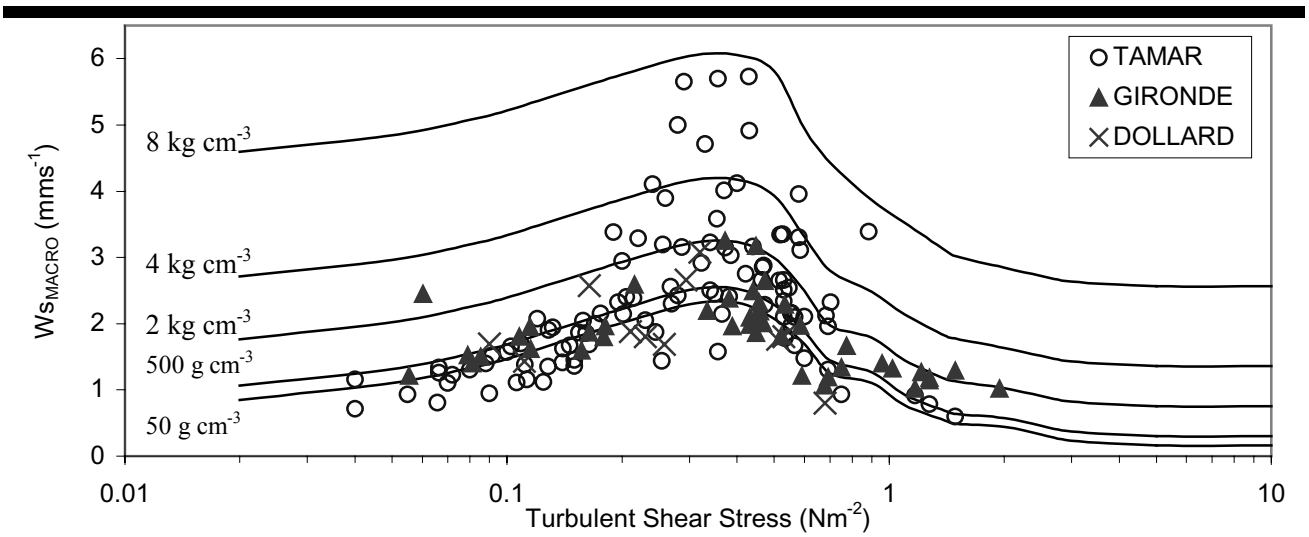

Figure 15. A statistical representation of the mass weighted macrofloc settling velocity (Ws_{MACRO}), based on equation 3, at various levels of suspended concentration plotted against turbulent shear stress. Experimental Ws_{MACRO} values obtained from the Tamar, Gironde and Dollard estuaries are added to the plot..

These were from a series of deployments conducted in lower reaches of the Gironde estuary in south-west France (MANNING *et al*., 2004), and on the intertidal mudflats of the Dollard estuary situated in The Netherlands (DYER *et al*., 2000). The data matrix constituted a total of 145 macrofloc (Ws_{MACRO}; units = mm s^{-1}) and microfloc (Ws_{micro}; units = mm s^{-1}) settling velocity pairings, all measured in-situ. Corresponding values of concentration (C; units = g cm^{-3}) and turbulent shear stress (τ; units = N m^{-2}) were included in the analysis. To produce an accurate representation of the macrofloc settling velocity over the entire shear stress range, required separating the shear stress scale into three zones, which overlapped to produce continuity. The best fit relationship for the lower stress region (equation 3) had a highly significant R-square value of 0.91.

$$Ws_{MACRO} = 0.718 + 8.33\,\tau - 12\,\tau^2 + 0.000938\,C \qquad (3)$$

Equation 3 is valid for the shear stress region ranging from 0.04-0.7 N m^{-2} and concentrations up to 8.5 kg cm^{-3}. The combined influence of concentration and turbulent shear on the control of the macrofloc properties agrees with hypotheses offered by both PULS *et al*., (1988), and KRANCK and MILLIGAN (1992). To justify the representation of Ws_{MACRO} described by equation 3, there must be no direct correlation between the independent variables. A linear regression of the turbulence values plotted against the corresponding concentration observations resulted in an R-square fit of 0.12 (MANNING, 2001), which indicates no correlation and hence the multiple regressions presented in this paper are valid.

The complete series of Ws_{MACRO} curves are shown graphically in Figure 15. Figure 15 displays a similar relationship to that proposed by DYER (1989, see Figure 1), with an increase in settling velocity at low shear stresses due to flocculation enhanced by shear, or due to residence time constraints (WINTERWERP, 1999), and a decrease in settling velocity due to floc disruption at higher stresses for the same concentration. A shear stress between 0.3-0.42 N m^{-2} is identified from the regression as providing the optimum level of turbulent intensity which most effectively stimulates flocculation at most concentration levels. Turbulent shear stresses of less than 0.1 N m^{-2} and greater than 1 N m^{-2} generally produced Ws_{MACRO} values of less than 1.5 mm s^{-1}. The optimum turbulent shear stress range identified from the regression produced Ws_{MACRO} values approaching 6 mm s^{-1} for concentrations of 8 kg cm^{-3}.

In contrast a multiple regression analysis of the settling velocities of the smaller microflocs (Ws_{micro}), revealed a correlation solely with turbulent shear stress (Figure 16). As with the macroflocs, the microfloc settling velocity rose with increasing shear stress until a limiting stress of about 0.45 N m^{-2} was reached, whereby the regression model predicted a peak Ws_{micro} of just under 1 mm s^{-1}. This was significantly slower than the comparative macroflocs. The higher limiting shear stress for the microflocs can possibly be attributed to their stronger inter-connective bondings, together with their residence time history. The influence of turbulent shear stress (together with biogenic glue strength) as a main factor in the formation of natural mud microflocs, agrees with the findings of EISMA (1986). The lack of correlation with concentration probably comes from them being the building blocks from which the larger macroflocs are formed. There were a number of the Ws_{MACRO} values which were smaller than the microfloc settling velocities. This was due to a contrast in effective densities; the very slow settling macrofloc fraction being of a low effective density, whereas the fast Ws_{micro} values were the product of a more densely constructed microfloc.

An important feature highlighted from the laboratory data were the cross-over points (see Figures 14a and 14b) on the regression lines between shear stresses of about 0.25-0.4 N m^{-2}. These are conjectured to mark the stress magnitudes where the effect of the increasing turbulent shear on the floc size and settling velocity, together with the higher concentrations, causes disruption rather than enhancing the flocculation process. Thus, the higher concentrations resulted in larger flocs for low shear stresses, and the lowest concentration produced the larger mean floc size for the higher shear stress. A similar pattern was observed for the settling velocities. These cross-over points were not directly observed from the field experimental data, primarily because in a natural environment the concentration is constantly varying in response to the flow generated turbulent shear stress, and time is not so limiting. However, the in-situ results indicate that the region between 0.3-0.45 N m^{-2} signifies a point whereby, if the stress was increased, disruption to the macroflocs would occur and hence the mean macrofloc settling velocities would progressively reduce.

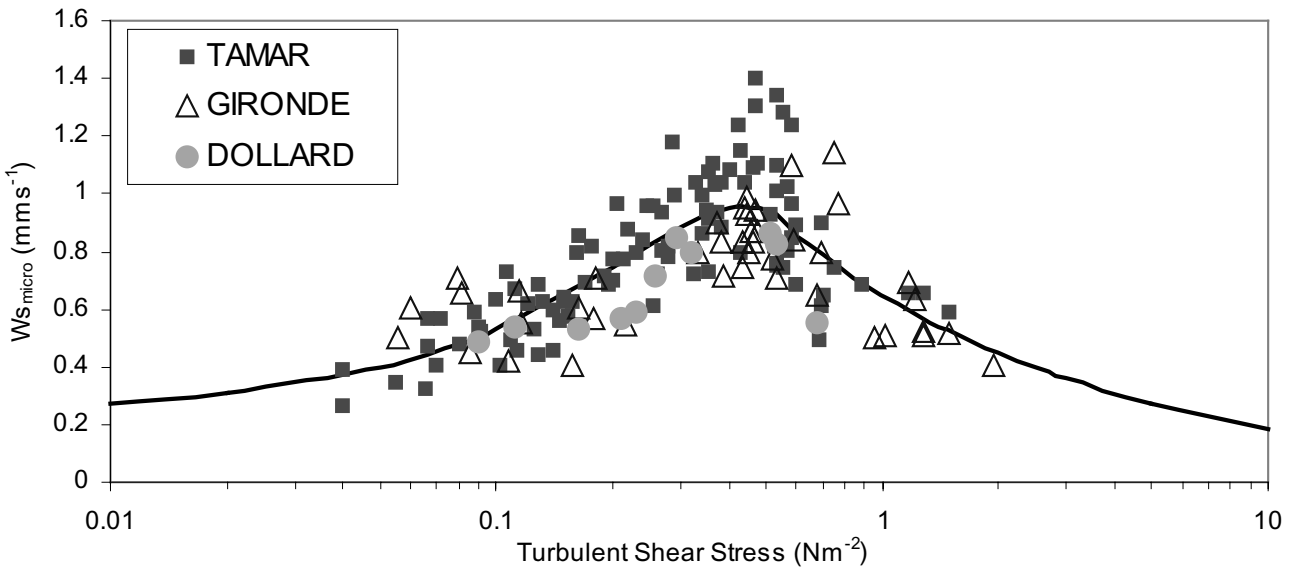

Figure 16. A statistical representation of the mass weighted microfloc settling velocity (Ws_{micro}), based on a multiple regression analysis, plotted against turbulent shear stress. Experimental Ws_{micro} values obtained from the Tamar, Gironde and Dollard estuaries are added to the plot.

CONCLUSIONS

The results presented in this paper have shown that turbulent shear stress, together with concentration, has a significant controlling influence over estuarine mud flocculation. Quantitatively, the macrofloc settling velocity, Ws_{MACRO}, is dependent on both turbulent shear stress and suspended particle concentration terms. A quantified empirically derived model of Ws_{MACRO} displays a similar relationship to that proposed by DYER (1989), with an increase in settling velocity at low shear stresses due to flocculation enhanced by stress, followed by floc disruption occurring at higher stresses (for the same concentration). The transition being a turbulent shear stress of about 0.36 N m^{-2}. Complementary laboratory experiments have also identified 0.25-0.4 N m^{-2} as a critical shear stress region for macrofloc flocculation.

In contrast, a statistical analysis of in-situ Ws_{micro} values indicated a close correlation only with the turbulent shear stress. As with the macroflocs, the microfloc settling velocity rose with increasing shear stress until a limiting stress of about 0.42 N m^{-2} was reached. At this point the regression model predicted a peak Ws_{micro} of about 1 mm s^{-1}; this was significantly slower than the comparative settling rate demonstrated by the macroflocs.

In terms of mass settling, the changes in floc size and settling velocity distributions observed in the upper Tamar estuary, imply that the effective density must decrease within the turbidity maximum. This means that there is a continual redistribution of the particulate mass between the macrofloc and microfloc portions. When comparing a typical tidal cycle, the fast settling macroflocs accounted for nearly 90% of the mass settling flux during high concentration spring tides, compared to 70% during the less turbulent and less turbid neap conditions.

ACKNOWLEDGEMENTS

The Tamar estuary experimental programme was funded by the EC MAST as part of contract MAS3-CT97-0082 COSINUS (Prediction of cohesive sediment transport and bed dynamics in estuaries and coastal zones with integrated numerical simulation models). The Gironde estuary experiments were funded by the EC TMR SWAMIEE (Sediment and water movement in industrialised estuarine environments) project under contract No. ERBFMRXCT970111. The Dollard estuary experimental programme was funded by the EC MAST project INTRMUD (The Morphological Development of Intertidal Mudflats) under contract MAS3-CT95-0022. The preparation of this paper was partially funded by H.R. Wallingford (UK), and the DEFRA / Environment Agency Joint Flood and Coastal Defence Research & Development Programme in Fluvial, Estuarine and Coastal Processes: Estuary Process Research (EstProc) project (under contract No.FD1905/CSA5966).

LITERATURE CITED

ARGAMAN, Y. and KAUFMAN, W.J., 1970. Turbulence and flocculation. *Journal of Sanitary Engineering* (ASCE), 96, 223-241.

BALE, A.J. and MORRIS, A.W., 1987. In-situ measurement of particle size in estuarine waters. *Estuarine, Coastal and Shelf Science*, 24: 253-263.

BERLAMONT, J.E., 2002. Prediction of cohesive sediment transport and bed dynamics in estuaries and coastal zones with integrated numerical simulation models. In: J.C. Winterwerp and C. Kranenburg, (eds.), *Fine Sediment Dynamics in the Marine Environment - Proc. in Mar. Sci. 5.,* Amsterdam: Elsevier, pp. 1-4.

BEST, J.L. and LEEDER, M.R., 1993. Drag reduction in turbulent muddy seawater flows and some sedimentary consequences. *Sedimentology*, 40, 1129-1137.

BURBAN, P-Y.; LICK, W. and LICK, J., 1989. The flocculation of fine-grained sediments in estuarine waters. *Journal of Geophysical Research*, 94 (C6), 8323-8330.

CHRISTIE, M.C.; QUARTLEY, C.P., and DYER, K.R., 1997. The development of the POST system for in-situ intertidal measurements. *The 7th International Conference On Electrical Engineering In Oceanography*, (London, England), Publication No. 439, pp. 39-45.

DAVIES, J.H., 1964. A morphogenetic approach to world shorelines. *Zoological Geomorphology*, 8, 127-142.

DYER, K.R., 1989. Sediment processes in estuaries: future research requirements. *Journal of Geophysical Research*, 94 (C10), 14327-14339.

DYER, K.R., 1997. *Estuaries: A physical introduction (2nd Edition)*, Chichester, England: Wiley & Sons Ltd., 195p.

DYER, K.R., CORNELISSE, J., DEARNALEY, M.P., FENNESSY, M.J., JONES, S.E., KAPPENBERG, J., McCAVE, I.N., PEJRUP, M., PULS, W., VAN LEUSSEN, W., and WOLFSTEIN, K., 1996. A comparison of in-situ techniques for estuarine floc settling velocity measurements. *Journal of Sea Research*, 36 (1-2): 15-29.

DYER, K.R. and MANNING, A.J., 1999. Observation of the size, settling velocity and effective density of flocs, and their fractal dimensions. *Journal of Sea Research*, 41, 87-95.

DYER, K.R.; CHRISTIE, M.C.; FEATES, N.; FENNESSY, M.J.; PEJRUP, M. and VAN DER LEE, W., 2000. An investigation into processes influencing the morphodynamics of an intertidal mudflat, the Dollard estuary, The Netherlands: I. Hydrodynamics and suspended sediment. *Estuarine, Coastal and Shelf Science*, 50, 607-625.

DYER, K.R.; BALE, A.J.; CHRISTIE, M.C.; FEATES, N.; JONES, S., and MANNING, A.J., 2002a. The turbidity maximum in a mesotidal estuary, the Tamar estuary, UK. Part II: The floc properties. In: J.C. Winterwerp and C. Kranenburg, (eds.), *Fine Sediment Dynamics in the Marine Environment - Proc. in Mar. Sci. 5.*, Amsterdam: Elsevier, pp. 219-232.

DYER, K.R.; BALE, A.J.; CHRISTIE, M.C.; FEATES, N.; JONES, S., and MANNING, A.J., 2002b. The turbidity maximum in a mesotidal estuary, the Tamar estuary, UK. Part I: Dynamics of suspended sediment. In: J.C. Winterwerp and C. Kranenburg, (eds.), *Fine Sediment Dynamics in the Marine Environment - Proc. in Mar. Sci. 5.,* Amsterdam: Elsevier, pp. 203-218.

DYER, K.R.; CHRISTIE, M.C., and MANNING, A.J., 2004. The effects of suspended sediment on turbulence within an estuarine turbidity maximum *Estuarine, Coastal and Shelf Science*, 59, 237-248.

EISMA, D., 1986. Flocculation and de-flocculation of suspended matter in estuaries. *Netherlands Journal of Sea Research*, 20 (2/3), 183-199.

EISMA, D., 1991. Particle size of suspended matter in estuaries. *Geo-Mar. Letters*, 11: 147-153.

EISMA, D.; BOON, J.; GROENEWEGEN, R.; ITTEKKOT, V.; KALF, J. and MOOK, W.G., 1983. Observations on macro-aggregates, particle size and organic composition of suspended matter in the Ems estuary. *Mitt. Geol.-Palaontol. Inst. niv. Hamburg*, SCOPE/UNEP Sonderbereich, 55: 295-314.

EISMA, D.; SCHUHMACHER, T.; BOEKEL, H.; VAN HEERWAARDEN, J.; FRANKEN, H.; LANN, M.; VAARS, A.; EIJGENRAAM, F. and KALF, J., 1990. A camera and image analysis system for in situ observation of flocs in natural waters. *Netherlands Journal of Sea Research*, 27, 43-56.

EISMA, D.; BERNARD, P.; CADEE, G.C.; ITTEKKOT, V.; KALF, J.; LAANE, R.; MARTIN, J.M.; MOOK, W.G.; VAN PUT, A. and SCHUHMACHER, T., 1991. Suspended matter particle size in some west European estuaries. *Neth. J. Sea Res*., 28 (3): 193-220.

FENNESSY, M.J. and DYER, K.R., 1996. Floc population characteristics measured with INSSEV during the Elbe estuary intercalibration experiment. *Journal of Sea Research*, 36 (1-2): 55-62.

FENNESSY, M.J.; DYER, K.R. and HUNTLEY, D.A., 1994a. INSSEV: an instrument to measure the size and settling velocity of flocs in-situ. *Marine Geology*, 117, 107-117.

FENNESSY, M.J.; DYER, K.R. and HUNTLEY, D.A., 1994b. Size and settling velocity distributions of flocs in the Tamar Estuary during a tidal cycle. *Netherlands Journal of Aquatic Ecology*, 28, 275-282.

FENNESSY, M.J.; DYER, K.R.; HUNTLEY, D.A. and BALE, A.J., 1997. Estimation of settling flux spectra in estuaries using INSSEV. In: N. Burt, R. Parker and J. Watts, (ed.), *Proceedings of INTERCOH Conference* (Wallingford, England), Chichester: John Wiley & Son, pp. 87-104.

FRIEDLANDER, S.K., 1977. Smoke, dust and haze. In: *Fundamentals of Aerosol Behaviour*, New York: Wiley, 317p.

GIBBS, R.J. and KONWAR, L.N., 1983. Sampling of mineral flocs using Niskin bottles*. Environ. Sci. Technol*., 17 (6): 374-375.

GLASGOW, L.A. and LUCKE, R.H., 1980. Mechanisms of deaggregation for clay-polymer flocs in turbulent systems. *Industrial Engineering Chemistry Fundamental*, 19, 148-156.

GRATIOT, N. and MANNING, A.J., 2004. An experimental investigation of floc characteristics in a diffusive turbulent flow. *Journal of Coastal Research,* SI 41. (This Volume).

HILL, P.S., 1996. Sectional and discrete representations of floc breakage in agitated suspensions. *Deep-Sea Research*, 43, 679-702.

JACKSON, G.A., 1990. A model of the formation of marine algal flocs by physical coagulation processes. *Deep Sea Research*, 37: 1197-1211.

KINEKE, G.C.; STERNBERG, R.W. and JOHNSON, R., 1989. A new instrument for measuring settling velocity in-situ. *Marine Geology*, 90, 149-158.

KINEKE, G.C. and STERNBERG, R.W., 1989. The effect of particle settling velocity on computed suspended sediment concentration profiles. *Marine Geology*, 90, 159-174.

KOLMOGOROV, A.N., 1941. The local structure of turbulence in incompressible viscous fluid for very large Reynolds numbers. CR Academic Science, URSS, 30, 16p.

KRANENBURG, C., 1994. The fractal structure of cohesive sediment aggregates. *Estuarine, Coastal and Shelf Science*, 39, 451-460.

KRANCK, K., 1973. Flocculation of suspended sediment in the sea. Nature, 246: 348-350.

KRANCK, K., 1975. Sediment deposition from flocculated suspensions. Sedimentology, 22: 111-123.

KRANCK, K., 1984. The role of flocculation in the filtering of particulate matter in estuaries. In: V. Kennedy (ed.), *The Estuary as a Filter*, Academic Press, Orlando Inc, 159-175.

KRANCK, K. and MILLIGAN, T.G., 1988. Macroflocs from diatoms: in-situ photography of particles in Bedford Basin, Nova Scotia. *Mar. Ecology. Prog. Ser*., 4: 183-189.

KRANCK, K and MILLIGAN, T.G., 1992. Characteristics of suspended particles at an 11-hour anchor station in San Francisco Bay, California. *J. Geophys. Res*., 97 (C7), 11373-11382.

KRONE, R.B., 1978. Aggregation of suspended particles in estuaries. In: B. Kjerfve (Ed.), *Estuarine Transport Processes*. Univ. South Carolina Press, Columbia, SC, pp. 177-190.

LI, M.Z. and GUST, G., 2000. Boundary layer dynamics and drag reduction in flows of high cohesive sediment suspensions. *Sedimentology*, 47, 71-86.

LICK, W., 1994. Modelling the transport of sediment and hydrophobic contaminants in surface waters. In: *U. S. / Israel*

Workshop on monitoring and modelling water quality, May 8-13, 1994, Haifa, Israel.

LICK, W.; HUANG, H. and JEPSEN, R., 1993. Flocculation of fine-grained sediments due to differential settling. *Journal of Geophys. Res.*, 98 (C6), 10279-10288.

LICK, W. and LICK, J., 1988. On aggregation and disaggregation of fine grained lake sediments. *Journal of Great Lakes Research*, 14 (4): 514-523.

MANNING, A.J., 2001. A study of the effect of turbulence on the properties of flocculated mud. Plymouth, England: University of Plymouth, Ph.D. thesis, 282p.

MANNING, A.J., 2004. Observations of the properties of flocculated cohesive sediment in three western European estuaries. *Journal of Coastal Research,* SI 41. (This Volume).

MANNING, A.J. and DYER, K.R., 1999. A laboratory examination of floc characteristics with regard to turbulent shearing. *Marine Geology*, 160, 147-170.

MANNING, A.J. and DYER, K.R., 2002a. A comparison of floc properties observed during neap and spring tidal conditions. In: J.C. Winterwerp and C. Kranenburg, (eds.), *Fine Sediment Dynamics in the Marine Environment - Proc. in Mar. Sci. 5.,* Amsterdam: Elsevier, pp. 233-250.

MANNING, A.J. and DYER, K.R., 2002b. The use of optics for the in-situ determination of flocculated mud characteristics. *Journal of Optics A: Pure and Applied Optics, Institute of Physics Publishing*, 4, S71-S81.

MANNING, A.J.; DYER, K.R.; LAFITE, R. and MIKES, D., 2004. Flocculation measured by video based instruments in the Gironde estuary during the European Commission SWAMIEE project. *Journal of Coastal Research,* SI 41. (This Volume).

McANALLY, W.H. and MEHTA, A.J., 2001. Collisional aggregation of fine estuarial sediment. In: J.C. McAnally and C. Mehta, (eds.), *Coastal and Estuarine Fine Sediment Processes – Proc. in Mar. Sci. 3.*, Amsterdam: Elsevier, pp. 19-39.

McCAVE, I.N., 1984a. Size spectra and aggregation of suspended particles in the deep ocean. *Deep-Sea Res*., 31: 329-352.

McCAVE, I.N., 1984b. Erosion, transport and deposition of fine-grained marine sediments. In: D.A.V Stow and DJ.W. Piper (eds), *Fine-Grained Sediments: Deep Water Processes and Facies*, pp. 35-69.

McCAVE, I.N. and GROSS, T.F., 1991. In-situ measurements of particle settling velocity in the deep sea. *Marine Geology*, 99, 403-411.

MEHTA, A.J. and LOTT, J.W., 1987. Sorting of fine sediment during deposition. *Speciality Conference for Advances in Understanding Coastal Sediment Processes*, (New York). New York: ASCE publishing, pp. 348-362.

MEHTA, A.J. and PARTHENIADES, E., 1975. An investigation of the depositional properties of flocculated fine sediment. *Journal of Hydrological Research*, 92 (C13), 361-381.

MORY, M.; GRATIOT, N.; MANNING, A.J. and MICHALLET, H., 2002. CBS layers in a diffusive turbulence grid oscillation experiment. In: J.C. Winterwerp and C. Kranenburg, (eds.), *Fine Sediment Dynamics in the Marine Environment - Proc. in Mar. Sci. 5.,* Amsterdam: Elsevier, pp.139-154.

OWEN, M.W., 1976. Determination of the settling velocities of cohesive muds. Wallingford, England: HR Wallingford, *Report No. IT 161*, 8 pp.

PANDYA, J.D. and SPIELMAN, L.A., 1982. Floc break-up in agitated suspensions: theory and data processing strategy. *Journal of Colloid Interface Science*, 90, 517-531.

PARKER, D.S.; KAUFMAN, W.J. and JENKINS, D., 1972. Floc break-up in turbulent flocculation processes. *Journal of Sanitary Engineering* (ASCE), 98 (SA1), 79-97.

PULS, W.; KUEHL, H. and HEYMANN, K., 1988. Settling velocity of mud flocs: results of field measurements in the Elbe and the Weser Estuary. *In*: J. Dronkers, and W. van Leussen, (eds), *Physical Processes in Estuaries*. Berlin: Springer-Verlag, pp. 404-424.

SOULSBY, R.L., 1983. The bottom boundary layer of shelf seas. In: B. Johns, (ed.), *Physical Oceanography of Coastal and Shelf Seas*. New York: Elsevier, pp. 189-266.

SPINRAD, R.W.; BARTZ, R. and KITCHEN, J.C., 1989. In-situ measurements of marine particle settling velocity and size distributions using the remote optical settling tube. *J. Geophys. Res*., 94 (C1), 931-938.

STAPLETON, K.R. and HUNTLEY, D.A., 1995. Sea bed stress determinations using the inertial dissipation method and the turbulent kinetic energy method. *Earth Surface Processes and Landforms*, 20: 807-815.

TAMBO, N. and HOZUMI, H., 1979. Physical characteristics of flocs – II. Strength of flocs. *Water Research*, 13, 409-419.

TSAI, C.H.; IACOBELLIS, S. and LICK, W., 1987. Flocculation of fine-grained sediments due to a uniform shear stress. *Journal of Great Lakes Research*, 13, 135-146.

VAN DE VEN, T.G. and HUNTER, R.J., 1977. The energy dissipation in sheared coagulated soils. *Rheologica Acta*, 16, 534-543.

VAN LEUSSEN, W., 1988. Aggregation of particles, settling velocity of mud flocs : A review. *In*: J. Dronkers, and W. van Leussen, (eds), *Physical Processes in Estuaries*. Berlin: Springer-Verlag, pp. 347-403.

VAN LEUSSEN, W., 1994. Estuarine macroflocs and their role in fine-grained sediment transport. Utrecht, The Netherlands: University of Utrecht, Ph.D. thesis, 488p.

WINTERWERP, J.C., 1998. A simple model for turbulence induced flocculation of cohesive sediment. *Journal of Hydraulic Engineering*, 36 (3), 309-326.

WINTERWERP, J.C., 1999. On the dynamics of high-concentrated mud suspensions. Delft, The Netherlands: Delft University of Technology, Faculty of Civil Engineering and Geosciences, Ph.D. thesis, 172p.

Journal of Coastal Research	SI 41	105-113	STRAEE 2002	Ferrara, Italy	ISSN 0749-0208

An experimental investigation of floc characteristics in a diffusive turbulent flow

N. Gratiot† and A.J. Manning‡∞

† Laboratoire d'écologie littorale,
Unité ELISA, IRD Guyane,
BP 165, Rte de Montabo, Cayenne
97323, Guyane Francaise, France
gratiot@cayenne.ird.fr

‡ School of Earth, Ocean and Environmental Sciences,
Institute of Marine Studies, University of Plymouth, Drake
Circus, Plymouth, Devon, UK. PL4 8AA.

∞ HR Wallingford, Howbery Park, Wallingford, OX10 8BA, UK

ABSTRACT

GRATIOT, N., and MANNING, A.J., 2004. An experimental investigation of floc characteristics in a diffusive turbulent flow. *Journal of Coastal Research*, SI 41, 105-113. Ferrara (Italy), ISSN 0749-0208

The work presented aimed at investigating the influence of the physical processes effecting mud flocculation in a grid stirred experiment. Two natural muds from the Gironde estuary (organic and another with the organic content removed) and mud from the Tamar estuary (organic) were used to examine the influence of the biological and chemical compositions on interparticular collision efficiency (i.e. stickiness). For every experiment, the mean sediment concentration were deduced from extracted water samples and by optical methods. The turbulent shearing was estimated from high frequency measurements of the velocity profile. Floc size and settling velocity were obtained by high resolution video observational techniques. The study showed that particles are advected with the large scale turbulent eddies from low to high turbulent shearing regions. It does not imply an instantaneous response and floc properties remained predominantly homogeneous in the water column of the experimental tank. From the measurements made, it is therefore possible to conclude that time scales associated to the turbulent transport are much smaller than the ones associated to flocculation processes. As sediment concentrations increased up to 8 $g.l^{-1}$, the increase in particle collision frequency enhanced the flocculation process to such a high degree that only a small percentage of the total floc population fell within the microfloc (< 120 μm) size range. Flocculation is especially significant for trials with organic muds and the effect of floc break-up by inter-particular collisions was not observed, at all shear and concentration levels, during our study. The Gironde mud with the organic components neutralised produced only a minor number of flocs, at all shear and suspended concentration combinations, which exceeded the pre-sieving mesh size of 125 μm. This highlights the important role organic matter plays in the flocculation of natural cohesive sediments. This paper compares the distribution of size and settling velocity of macroflocs and microflocs and mean floc properties for the different sediment types under the various experimental concentration and shear ranges. The findings highlight how floc properties change in response to their ambient environment.

ADDITIONAL INDEX WORDS: *cohesive sediments, floc size, settling velocity, turbulent shear, grid stirred experiment*

INTRODUCTION

The understanding of fine sediment transport in rivers and estuaries is an important issue for many managerial problems, such as coastal protection, dredging and dredged spoil relocation, the survey of contaminant transport and deposition. Their dynamics depend on a complex set of interactions between sediment, fluid and flow within which the particles aggregation plays a major role. As a result of interparticle collisions, floc growth implies large variations in the sediment settling flux with direct implications on the vertical distribution of sediment loading. Hence, strong stratifications may appear and in turn have a feed back effect on the flocculation process.

A first examination of this complex interaction is best attained under laboratory conditions, because the evolution of floc properties can be examined under controlled hydrodynamic forcings. This study aims at measuring and quantifying the effect of turbulent shearing with the resultant floc characteristics. This agent of flocculation is indeed very important for the modelling and prediction of fine sediment transport in estuarine and coastal environments. Experiments were carried out in a water column agitated by a stirring grid, and particular attention was addressed to the measurement of turbulence properties.

The analytical model of collisional flocculation of MCANALLY and MEHTA (2001) and more simple approaches are first introduced to point out the relevant physical and chemical parameters of the problem. Section 3 underlines the interest of grid stirred experiments to the examination of flocculation process in the light of previous works and recent instrumental developments. Details of the facility are given in section 4 and the experimental results are presented in section 5. The near bottom floc segregation effects, the influence of organic content on flocculation and others considerations are then discussed with regards to the experimental results.

In this study, the term "flocculation" is used to express both processes of particles aggregation and breakage. The term "floc" is employed in a general sense and is associated to all the aggregates present in the suspension. Micro-flocs and macro

flocs denominations are introduced to discriminate flocs that do not correspond to the same order of aggregation.

TURBULENCE INDUCED FLOCCULATION

The rate of natural fine sediment aggregation depends on the fluid, flow and sediment properties, plus the number concentration of particles in suspension. The collisions of sediment particles are governed by three physical mechanisms which are: Brownian motion, differential settling and turbulent shearing. Following MANNING (2001) and WINTERWERP (2002), this later agent is identified as the most significant for flocculation in natural estuarine and coastal environment. Consequently, Brownian motion and differential settling are not considered in this work.

The rate of flocculation between two flocs in shear dominated environments can be expressed by (MCANALLY and MEHTA, 2001):

$$N_{im}=\alpha'\left(\frac{\beta_{im}}{F_c^2}\right)n_i n_m \tag{1}$$

which is a rearranged form of the SMOLUCHOWSKI (1917) equation. In (1), N_{im} is the number of efficient collision between *i* and *m* class flocs per unit time and per unit volume, α' is the collision efficiency function, and F_c is the collision diameter function. These two functions can vary between 0 and 1. β_{im} is the flow shear collision frequency function and n_i and n_m are the number concentration of *i* and *m* class flocs.

In the case of isotropic turbulence, the flow shear collision frequency function β_{im} is simply given by :

$$\beta_{im}=\left[\frac{\pi F_c^2}{4}\sqrt{\frac{2}{15\pi}}\right]\sqrt{\frac{\varepsilon}{\nu}}(D_i+D_m)^3 \tag{2}$$

with ε : turbulent energy dissipation rate, ν : kinematic viscosity of the fluid and D_i, D_m : diameter of the *i* and *m* class flocs.

MCANALLY and MEHTA (2001) pointed out that the major difficulty to establish a model of collisional flocculation from (1) results in the determination of the collision efficiency function α' and the collision diameter function F_c. From the examination of 40 data sets found in the literature, they have proposed a formulation of α' and F_c that partition the role of fluid, flow and sediment properties in seven non dimensional numbers :

$$\left[\left(\frac{\Delta\rho_i D_i^3}{\Delta\rho_m D_m^3}\right),\left(\frac{u_i(D_i+D_m)}{\nu}\right),\left(\frac{D_g}{D_1}\right),\left(\frac{S}{S_0}\right),\left(\frac{T_c}{T_0}\right),\left(\frac{CEC}{CEC_0}\right),\left(\frac{\tau_m}{\tau_{im,m}+\tau_u}\right)\right] \tag{3}$$

where $\Delta\rho$ is the floc excess density ; u_i is the relative velocity between class flocs *i* and *m* ; D_g is the diameter of primary grain ; D_1 is the reference particle size ; *S*, T_c , are fluid salinity and temperature respectively ; *CEC* is the mineral cation exchange capacity ; τ_m is the floc strength ; $\tau_{im,m}$ is the collisional shear stress and τ_u is the flow induced shear stress. The last non-dimensional number concerns the disaggregation process by flow shearing or interparticular collisions.

The set of physical and chemical parameters introduced in equations (1), (2) and (3) yield a good overview of all the parameters that have to be considered when examining turbulent induced flocculation. For a more complete examination of orthokinetic flocculation, the role of organic content on particle cohesion should be considered, as it is generally ignored. MCANALLY and MEHTA (2001) indeed pointed out a poor correlation of the collision efficiency function α' with the mineral cation exchange capacity *CEC* and argued the important role of organic matter and oxide coatings on floc surface charge, when considering real sediments in estuarial waters.

The application of the turbulence induced flocculation model of MCANNALLY and MEHTA (2001) is mainly restricted by instrumental limitation. It is indeed very difficult to achieve direct measurements of the above mentioned parameters. For example, the estimate of the collisional shear stress $\tau_{im,m}$, the floc strength τ_m and the floc density ρ_i can not be measured directly. They are usually derived from physical expressions in which empirical parameters are fitted to experimental data on a case-by-case basis.

Because of these instrumental limitations, many authors have looked for semi-empirical formulation based on more easily measured parameters (DYER, 1989, VAN LEUSSEN, 1994, TEETER, 2001, among others). DYER (1989) first proposed a conceptual model to describe the simultaneous influence of the sediment concentration *C* and turbulence shear rate on floc size D_f. Later, VAN LEUSSEN (1994) derived a simple formulae that describes the global effect of turbulence and concentration on the flocs settling velocity :

$$w_s=w_{s0}\frac{1+aG}{1+bG^2} \tag{4}$$

where *G* is the dissipation parameter, w_{s0} *(C)* is the reference settling velocity in still water, *a* and *b* are empirically determined constants.

It can be noticed that from the measurements of w_s, D_f, *G*, and *C*, various physical models can be applied to deduce *n*, $\Delta\rho$, τ_m, $\tau_{im,m}$ and τ_u (KRANENBURG, 1994 ; DYER and MANNING, 1999, WINTERWERP, 1999) so that these four parameters give a relevant framework for the examination of turbulence induced flocculation as introduced in equations (1), (2) and (3).

FLOCCULATION IN THE GRID STIRRED EXPERIMENT

The role of turbulence on the flocculation processes has been investigated in the so called “grid stirred” experiment. In such systems, the turbulence is generated by the vertical oscillation of one or several grids at a given frequency. This device has already been used by VAN LEUSSEN (1994, 1997) who described the influence of turbulence on floc settling velocities as presented in equation (4). Unfortunately, no measurements of the turbulence with sufficient details were available and the author expected the distribution of turbulent zones to conform to those in stirred reactors. The present study aims at reinforcing the examination of flocculation in grid stirred experiments with the benefits of recent instrumental developments.

The turbulence field is generated by the stirring of a unique grid located in the lower part of the column. The spatial distribution of the turbulence field is determined with a recently developed ADV (GRATIOT ET AL., 2000). The measurement facility is presented in Figure 1 and all technical specifications

are reported in the next section. The turbulence is advected upward by a diffusive process; its intensity decreases with the distance from the grid. The turbulence field is nearly isotropic except at the direct vicinity of the grid and consequently, the rate of turbulent energy dissipation can be related to the energy input at large scales by (TENNEKES and LUMLEY, 1972) :

$$\varepsilon = A\frac{u^3}{\ell} \tag{5}$$

where A is a constant close to the unity and ℓ is the integral length scale of the turbulence.

As a result of previous investigations (HOPFINGER and TOLY, 1976 ; MORY et al., 2002), the turbulent integral length scale was chosen to increase linearly with distance to the grid. The best empirical fit was given by :

$$\ell = 0.2z \tag{6}$$

The decrease of the turbulence shear rate with the distance to the grid is then estimated from the formulation of the dissipation parameter proposed by CAMP and STEIN (1943) :

$$G(z) = \sqrt{\frac{\varepsilon}{\nu}} \tag{7}$$

The possible effect of salinity (S/S_0) and temperature (T_c/T_0) expressed in equation (3) was not examined. Each experiment was performed with fluid mud mixtures possessing a salinity value of 16.5±0.1 ppt. The fluid mud temperature measured during experiments varied slightly in the range 21.4 to 24.6°C and its effect was considered negligible. The kinematic viscosity (ν) of the water was considered constant and equal to 10^{-6} $m^2.s^{-1}$. Hence, at the exception of *CEC*, all of the input parameters of the turbulence-induced flocculation model aforementioned were implicitly measured in this study. The effect of organic content and clay mineral sediment composition on the aggregational efficiency were qualitatively examined by an intercomparison of the behaviour of three natural muds submitted to a similar hydrodynamic forcing.

EXPERIMENTAL SET-UP, INSTRUMENTATION

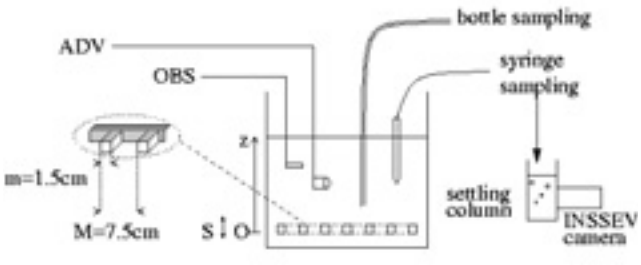

Figure 1. Schematic view of the experimental set-up. For clarity, the vertical steel bar that serves as guidance for the grid stirring has not been represented.

The tank consists of a square Plexiglas box of 53 cm wide and 90 cm high. For all experiments, the water depth was H=40 cm. The grid was fixed horizontally on a vertical steel bar which served as guidance for the stirring. The mean grid position was located at 5 cm above the bottom of the tank. It oscillates at a frequency F= 4 Hz with a stroke (twice the amplitude) S=4.5 cm. The grid is made of seven square bars in the two horizontal directions. The thickness of square bars is m=1.5 cm with a mesh size M=7.5 cm. This geometry agrees with the standard ratio M/m=5. It corresponds to a grid porosity of nearly 65% which has been proven to be the most efficient to reduce secondary flows forming (THOMPSON and TURNER, 1975, HOPFINGER and TOLY, 1976). For a reason of geometry, the field of turbulence is considered 1DV. The z-axis origin is chosen at the mean grid position and is counted positively upward.

The two natural muds with organics used during the survey were bottom sediments extracted from the Gironde estuary (France) and from the Tamar estuary (UK). These natural mud were sampled in 1999 in the framework of MASTIII COSINUS (BERLAMONT, 2002) and SWAMIEE (MANNING and DYER, 2003) projects, respectively. The third sample was previously extracted from the Gironde estuary and was treated chemically to inhibit the efficiency of its organic content. Therefore, the cohesion efficiency of this mud only results from the Cation Exchange Capacity of its clay fraction. The sediment analysis performed by DE CROUTTE et al. (1996) indicated that the sample comprised: 27% kaolinite, 35% illite, 24% smectite and the remaining 14% was chlorite. The three types of mud were pre sieved at 125 µm and stored in a hermetic dark tank. The particle size distributions and the total organic contents are presented in table 1.

Table 1. Mineral composition of the muds used (DE CROUTTE et al., 1996 ; FEATES et al., 1999 ; present study).

symbol		T	Gi	G n.o.
mud type		natural	natural	treated
estuary		Tamar	Gironde	Gironde
particle size distribution	D_{50} (µm)	15	13.1	12
	very fine sand (<125 µm)	7.8	5.3	3
	silts and clays (<63 µm)	92.2	93.4	97
total organic content (% by mass)		15.2	11.4	0

The turbulent shearing was characterised from an Acoustic Doppler Velocimeter (ADV) system dedicated to the measurement of turbulent properties in highly concentrated fluid mud layers (GRATIOT et al., 2000). The ADV system provides the measurement of the one component horizontal fluctuating velocity for 1 to 16 locations in the window 4-8 cm in front of the probe. The distance between two successive measurement volumes was 3 mm. The rms velocity u was calculated by averaging arithmetically all the time series acquired simultaneously at the same elevation above the grid. Each value of u was deduced from about 4000 turbulent velocity measurements. The turbulent integral lengthscale ℓ was deduced from pair by pair longitudinal correlation of all of the time series acquired simultaneously. For more details on the measurements

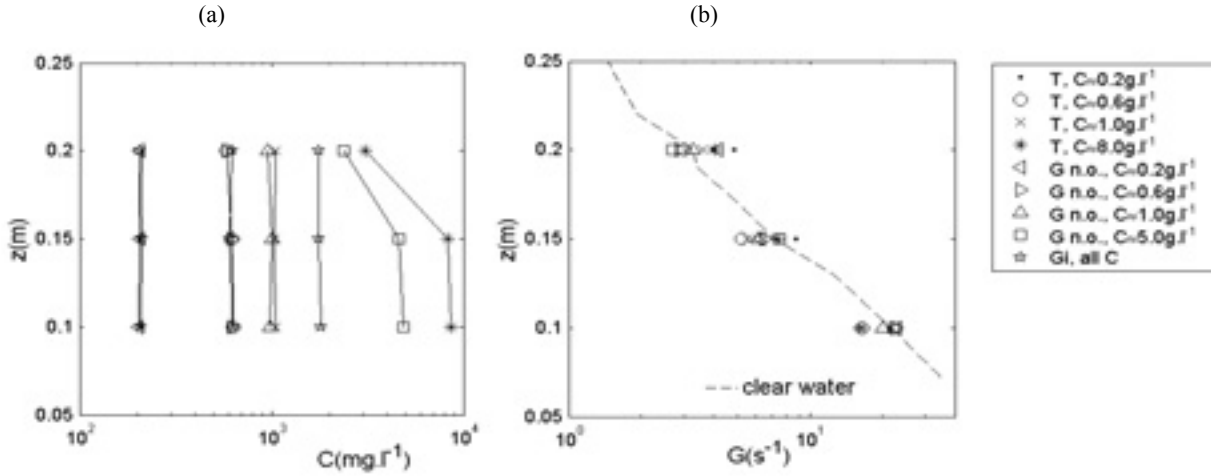

Figure 2. Vertical profiles of the sediment concentration (2a) and of the dissipation parameter (2b).

of u and ℓ in grid stirred experiments, the reader can refers to MORY et al. (2002).

The vertical profile of temporally averaged sediment concentration was deduced from both water sampling and optical methods. The sampling method consists on the extraction of a measured volume (≈100 ml) of fluid mud by tube pumping over a duration of 5-10 s. After decanting and drying, the solid fraction was obtained by weighing. Data acquired with the Optical Backscatter System (OBS) were recorded over 30 s at a frequency of 10 Hz. Sampling and OBS methods presented a good agreement and in every case, the precision was better than 5%.

The INSSEV - In Situ SEttling Velocity – (FENNESSY et al., 1994) system was used in a simplified version for the application to the grid stirred experiment. Flocs were extracted from the tank by syringe sampling and were slowly introduced into the settling column of the INSSEV camera. The duration of transfer was sufficiently short (about 10-20 s) and it could be assumed that flocculation remain limited within the syringe. Furthermore, the syringe orifice is sufficiently large (internal diameter of 6.5mm) to restrict floc breakage by shearing during the suction. The method of syringe sampling was validated in extensive preliminary testing and a good agreement was obtained between the floc properties measured from syringe sampling and from *in-situ* floc observations. The floc video recordings obtained from INSSEV provided a direct measurement of each individual floc diameter and settling velocity. The video system resolution permitted the measurement of the aggregate properties of all flocs exhibiting a diameter above 20µm. The interpretation of floc data is based on the following assumptions: a) each syringe sampling contains a sufficient number of flocs to ensure a statistical representation (between 186 and 6700 flocs were measured for each sampling run); b) flocculation and breakage remain small for the duration of floc's transfer; c) cloud formation and settling convection are negligible in the settling column. The reader can refer to FENNESSY et al., 1994; FENNESSY et al., 1997; GRATIOT, 2000) to get a detailed review on these measurement techniques.

The experimental programme had eleven runs for increasing sediment loading in the range of 200 to 8000 mg.l^{-1}. An individual run comprises first filling the tank with a premixed fluid mud mixture and then agitating the suspension for a duration of 30 minutes before making any measurements. This duration was assumed to be sufficient to reach the dynamic equilibrium between the rates of flocculation and breakage. The variation of floc properties with the hydrodynamic conditions was then examined from the measurements of the turbulent shearing, the mass sediment concentration and the distribution of flocs size and settling velocity at three distances above the mean grid position: 0.10, 0.15 and 0.20 m.

RESULTS

The dissipation parameter G for height individual runs and for the three positions above the grid was calculated from the measurement of $u(z)$ and the application of equations (5), (6) and (7). The results in terms of vertical profiles of sediment concentration $C(z)$ and dissipation parameter $G(z)$ for steady conditions are reported on Figure 2a and 2b, respectively. The vertical profile $G(z)$ for a clear water experiment is also reported for comparison in Figure 2b.

Figure 2a shows that the sediment concentration is uniformly distributed for a mean sediment loading up to 2000 mg.l^{-1}. For higher sediment concentrations, stratification effects become more effective, whilst turbulence is not sufficiently efficient to fully mix sediment up to the highest position of measurement (z=0.2m). In Figure 2b, the dissipation parameter G decreases with z without a significant difference between runs. Hence, sediment loading has no significant effect on the diffusion of turbulence even for the higher concentrations. This point is underlined by the fact that all runs fit reasonably well with the clear water measurements. The ADV system suffered technical problems and no measure of the turbulence properties where performed for trials with the natural mud from the Gironde estuary (Gi). It is assumed that the natural mud from Gironde has also no effect on the turbulence field. The mean value of the dissipation parameter decreases from 19 to 7 to 3 s^{-1} when z increases from 0.10 to 0.15 and through to 0.20 m.

Since the sediment concentration is roughly uniformly distributed up to 2000 mg.l^{-1}, flocs located at various depths will only experience a variation of flow shear. The influence of the turbulent shear on flocs size and settling velocity distributions have been investigated for each run and depth increment. The graphs presented in Figure 3 recover the three runs conducted to a

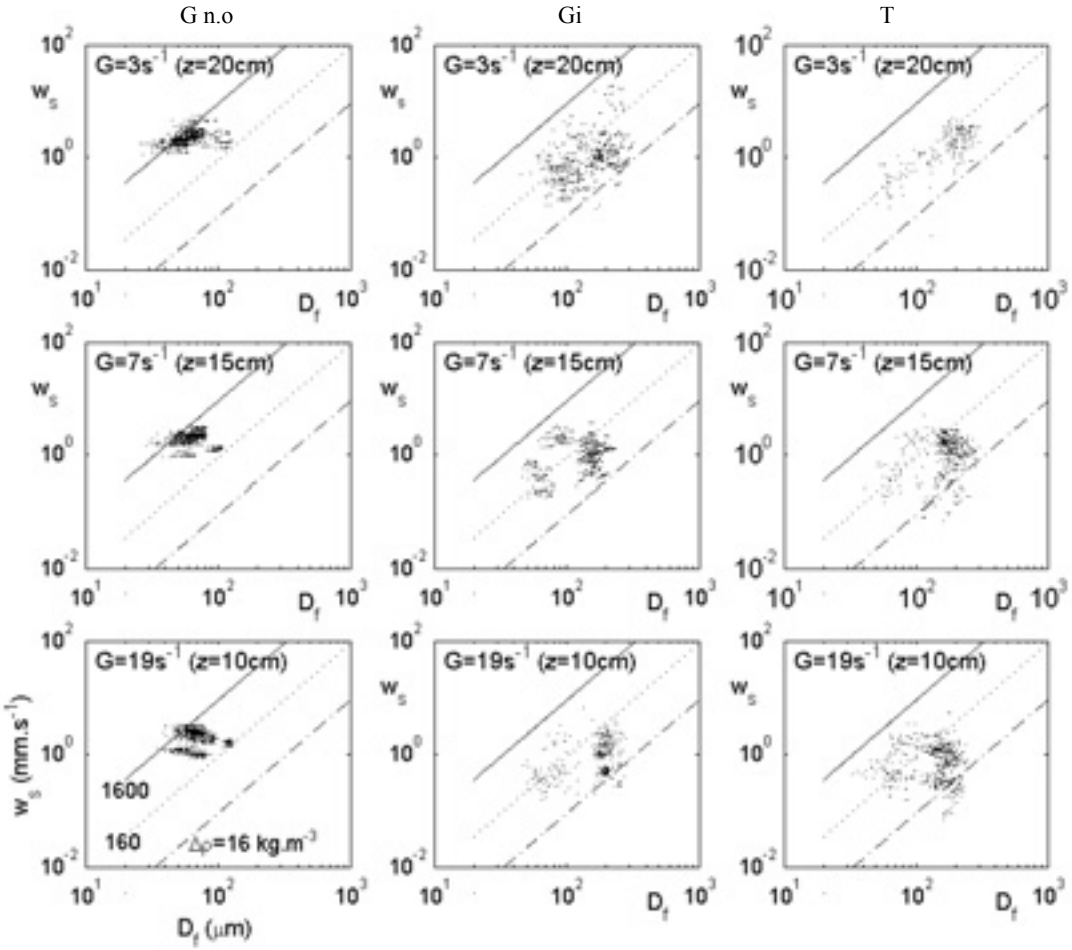

Figure 3. Influence of the dissipation parameter G on floc properties for three types of natural mud (G n.o., Gi, T). For all graphs, the sediment loading corresponds to a mean sediment concentration C=600 mg.l^{-1}.

mean sediment concentration of 600 mg.l^{-1}. Each column corresponds to an individual run i.e. a mud type, while each row corresponds to a position of measurement above the grid i.e. a level of turbulent shearing. Hence, each graph yields the measured distribution of size and settling velocity of flocs for a given mud and for a given elevation. Each dot of a graph represents the size and settling velocity of a single floc; the diagonal lines show contours of effective density calculated from Stokes' law.

A row by row analysis of the graphs reveal no clear correlation between the floc properties and turbulent shear intensity. The cloudy distribution of settling velocity vs. floc diameter remains more or less similar for low (G=3 s^{-1}), medium (G=7 s^{-1}) and high (G=19 s^{-1}) turbulent shear levels. Similar analyses were conducted for all of the remaining sediment loadings (C=200 to 8000 mg.l^{-1}) investigated during this work. Consequently, it is coherent to consider that floc properties measured at various positions above the grid correspond to a unique set of data in equilibrium with the mean spatial distribution of the flow shear.

It is interesting to discuss the experimental results in light of previous works. Typical values for the dissipation parameter G range from 1 to 100 s^{-1} in an estuarine environment (VAN LEUSSEN, 1994 ; BERHANE et al., 1997 ; WINTERWERP, 1999 ; MANNING and DYER, 1999 among others). This is consistent with the range of variation of G obtained in the grid stirred experiment. Furthermore, according to the experimental and theoretical proposals of NEZU and NAKAGAWA (1993), the mean vertical gradient of the turbulent shear occurring in the lower 10% of the water column of a typical open channel flow is about: $dG/dz=O(100)$ s^{-1}.m^{-1}. In our experiment, the mean gradient of turbulence is in the range 40-120 s^{-1}.m^{-1} and is in good agreement with the proposal of NEZU and NAKAGAWA (1993). Thus, both the level of turbulent shearing and its vertical gradient are representative of natural conditions.

Following the analytical proposal of WINTERWERP (2002), the large vertical gradients of turbulent shear that occur in the grid stirred experiment or in the near bed proximity of a natural channel imply large variations of both the flocculation time and the equilibrium floc size. Consequently, a considerable segregation effect should be observed. In contrast, VAN LEUSSEN (1997) advocated that the nature of near bed flocculation processes is governed by a continuous advection of flocs by the large scale turbulent eddies through regions of low and high turbulent activity. By consequence, floc properties are a result of the mean turbulence levels that flocs experience during their path through the water column due to a cycle of continual deposition

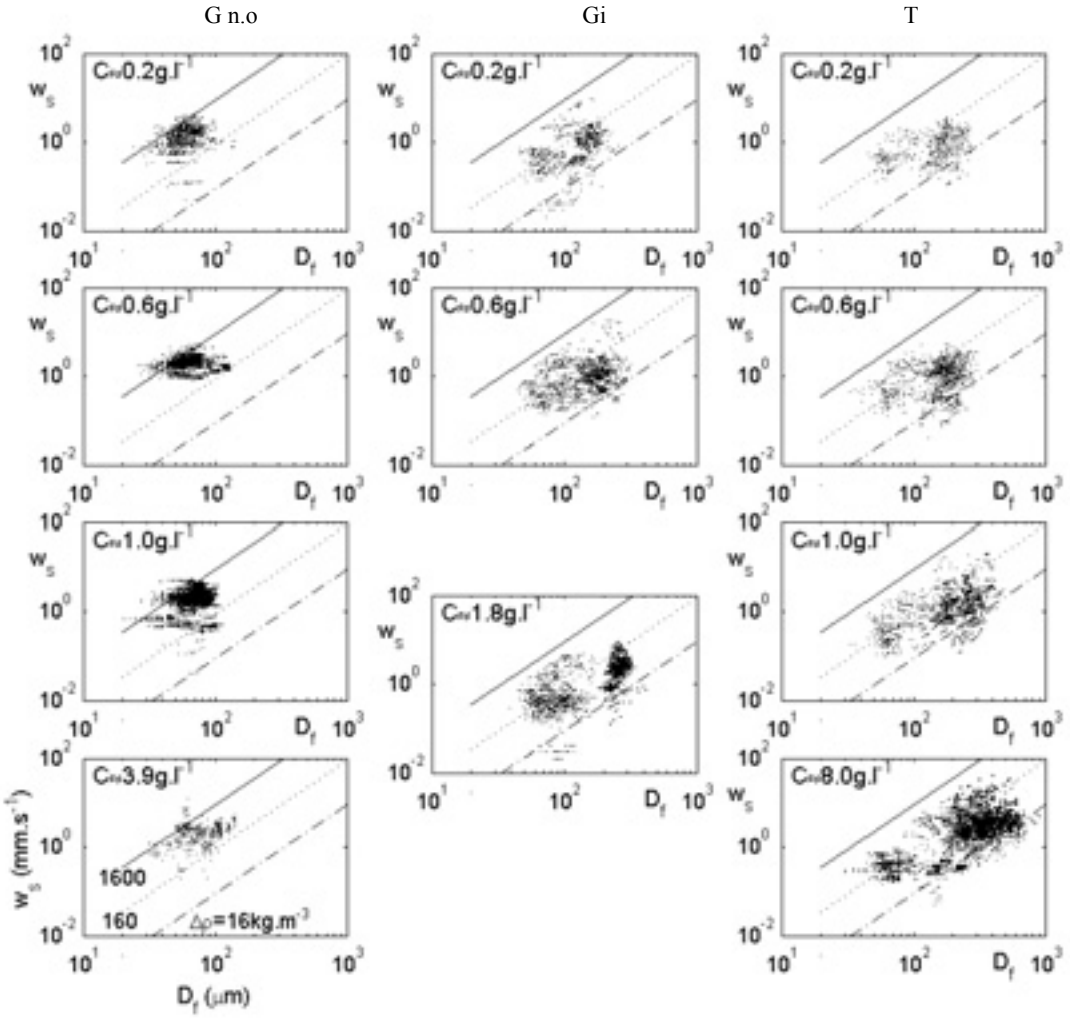

Figure 4. Influence of sediment concentration on floc properties for three type of estuarine mud (G n.o., Gi, T).

and re-entrainment of the bed sediments. Our experimental results support this second hypothesis.

In fact, segregational effects can be examined by comparing the time of residence of flocs to a specific shear level (T_r) in relation to the flocculation time (T_f). As the floc settling velocity remains small when compared to the rms turbulent velocity, it is assumed that flocs are moving with the time scale of turbulent eddies turn over: $T_r \approx T_e = \ell / u$. For all depth increments, T_e never exceeds 8 seconds during this study. The actual time of flocculation T_f in natural environment has typical values ranging from several minutes within high concentration benthic suspensions close to the near bed, to several hours in the proximity of the free surface. As previously indicated, both the level of turbulence and the vertical gradient of the turbulent shear rates measured during this study present a good agreement with values observed *in-situ* in the lower 10% region of the water column. This led us to consider that $T_f = O(100\text{s})$ and consequently,

$$\frac{T_f}{T_r} \approx \frac{T_f}{T_e} = O(10) \tag{8}$$

As $T_r << T_f$, the nature of the flow acts in favour of a well mixed situation and it is coherent to measure no significant evolution of floc properties within the tank. The fact that suspended sediment concentrations were rather homogeneously distributed underlines this expectation.

The effect of sediment concentration and mud characteristics on floc properties are demonstrated on Figure 4. The graphs illustrate all experimental runs and sampling depths investigated during this work. Each column corresponds to a specific mud type, while each row corresponds to a sediment concentration.

The Gironde mud with no organics (G n.o.) displays a mono-distributed floc population. Its poorly scattered population is characterised by a floc size ranging from 30 to 100 µm and a settling velocity distributed over only one order of magnitude which centred about a fall rate of approximately 1 mm.s^{-1}. The mean excess density is rather high and characteristic of a densely packed floc structure. The influence of concentration on floc

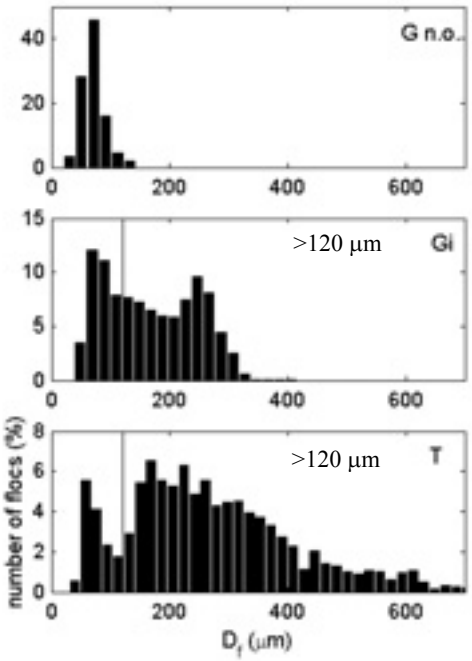

Figure 5. Floc size distribution for three type of natural mud (G n.o., Gi, T).

properties is not clearly identified as the floc distributions appear similar for all graphs in the first column. The non-treated mud from the Gironde and Tamar estuaries (Gi and T) exhibit a radically different floc distribution under similar hydrodynamic forcing. Floc properties display a bi-modal and scattered distribution with low excess densities. It is indicative of a loose aggregate structure. The increase in concentration considerably enhanced the flocculation process. This is particularly obvious for the runs with the Tamar mud. For the highest concentration considered (8000 mg.l^{-1}), the distribution covers more than one order of magnitude in size and nearly two orders of magnitude in settling velocity.

For a quantitative analysis, it is interesting to discriminate the aggregates between microflocs and macroflocs. The critical diameter D_{crit} that distinguishes micro flocs from macro flocs is deduced from the floc diameter distribution presented on Figure 5. The single value D_{crit}=120µm was considered to be well representative of the cut of between micro- and macrofloc populations for both organic mud from Gironde and Tamar estuaries (Gi and T). D_{crit} was not consider for the Gironde mud with no organic (G n.o.) because its distribution is not bimodal.

The influence of concentration on microfloc and macrofloc sub-classes are presented in Figure 6. Figure 6a shows the proportion of microflocs relative to the total number of flocs. The general trend consists of a decrease in the microflocs population density with concentration. This is especially clear for the experiments with the Tamar mud where the microflocs comprised 27.6% of the aggregate population when the sediment concentration averaged 200 mg.l^{-1}, and no more than 11.0% for a suspended particulate concentration of 8000 mg.l^{-1}. Figure 6b reports the evolution of the mean floc size $\overline{D_f}$ and settling velocity $\overline{w_s}$ for both micro- and macroflocs. It can be considered as a statistical representation of data presented on Figure 4. For the mono-distributed non-organic Gironde mud (G n.o.,'○'), the mean floc diameter increased from 61 to 82 µm, while the mean settling velocity increased from 1.50 to 2.54 mm.s^{-1}. The evolution of the floc properties are significant, but remain small when compared to the two muds with organic content (Gi,'Δ' and T,'•'). Hence, Tamar mud macroflocs doubled their mean diameter (181 to 348 µm) and quadruple their mean settling velocity (1.04 to 4.22 mm.s^{-1}) when sediment concentration rises from 200 to 8000 mg.l^{-1}. At the same time, the microfloc population is not affected by sediment loading. The non-treated Gironde mud (Gi,'Δ') exhibits a very similar behaviour to the Tamar mud which brings a qualitative indication of the dominant role of organic content in the flocculation process. The mean effective density is very different for mud with or without organic content. By considering Stokes' law, the mean effective density of the Tamar microflocs is $\Delta\rho$=221kg.m^{-3} and reduces to $\Delta\rho$=69 kg.m^{-3} for the macroflocs. The values calculated for the non-organic Gironde mud were as high as $\Delta\rho$=742 kg.m^{-3}.

The measurements achieved during this study showed that high concentrations promoted floc growth at all depths and all tested concentrations. If we refer to BURBAN et al. (1989), these experimental results indicate that the turbulent shearing is the dominant mechanism for floc growth limitation in the grid stirred experiment. In a two-body collision dominated environment, the mean floc diameter would have remained approximately constant as concentration increases. In such an environment, the rates of flocculation and disaggregation are indeed both proportional to the square of the number concentration. A three-body collision dominated environment would promote the rate of disaggregation and consequently would have resulted in a decrease in the mean floc diameter as the particulate concentration increases.

For the three mud types employed during this experimental work, the mean floc diameter growth fits nicely to Stokes' law (Figure 6b). Hence, both microflocs and macroflocs satisfy the relationship:

$$\overline{w_s} \propto \overline{D_f}^2 \tag{9}$$

Following the analytical proposal of WINTERWERP (2002), equation (9) is characteristic of populations of aggregates having a constant floc density and a fractal dimension close to 3. This is coherent with the conclusions of CHEN and EISMA (1995), reporting that flocs generated in a fluid shear dominated environment are likely to be characterised by high fractal dimension.

Another interesting result is that the microfloc properties of the two organic muds are not noticeably modified by sediment loading. This supports the "Order of aggregation" theory, first advocated by KRONE (1963), whereby the primary particles (or flocculus) flocculate to form microflocs and an equivalent process happens at the upper scale. Therefore, microflocs aggregate to form macroflocs. Floc densities ρ_i and floc strength τ_m decrease rapidly with the order of aggregation. For the experiments with C≈200 mg.l^{-1}, Gironde (Gi) and Tamar (T) microflocs have ever reached a maturated stage of aggregation. Hence, the pursuit of flocculation processes for higher concentrations goes through a change of the order of aggregation with the formation of macroflocs. In this study, no upper order of aggregation is reached, which indicates that macroflocs have not yet reached their maturated stage of aggregation, even for the highest suspended concentration tested. High levels of shear

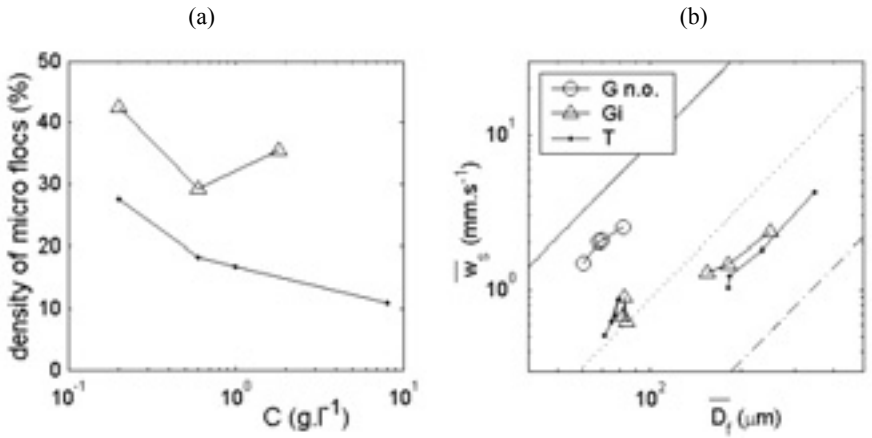

Figure 6. Influence of concentration on the statistical floc properties for three natural mud. A bi-modal distribution is consider for the two organic muds (Gi and T).

generated close to the grid are undoubtedly a limiting factor for the occurrence of an upper order of aggregates. The evolution of mean floc properties for the non-organic Gironde mud present a similar trend to the one observed for the organic Gironde and Tamar macroflocs. In light of the order of aggregate theory, it may be associated to the growth of flocs by colliding primary particles or flocculus. The 20µm resolution of the video system was not sufficient to provide a detailed analysis of flocculation process at this order of aggregate. The macrofloc order of aggregation was not attained for this mud and consequently, we may assume that the organic content is a major agent for the flocculation at this scale.

CONCLUSIONS

An experimental study has been conducted to get quantitative measurements of the evolution of floc properties under a controlled hydrodynamic forcing. The analysis was restricted to the examination of directly measured floc data, together with the simultaneous measurement of the vertical profile of the dissipation parameter *G(z)*.

The turbulent shear intensity occurring in the grid stirred experiment and its vertical gradient were set-up to be equivalent to the ones existing in the 10% near bed region of a water column in open channel flows. The important gradient of the dissipation parameter measured does not necessarily result in a vertical segregation of floc diameter and settling velocity. For sediment loading up to 2000 mg.l^{-1}, the sediment properties were almost homogeneous for all type of mud tested. The effect of scalar diffusion by turbulent mixing was a dominant agent acting in favour of a mean level of flocculation. For all experiments, the non dimensional time scale T_r/T_f always exceeded the unity. This non-dimensional number is certainly a good indicator of the existence or non-existence of segregation.

The grid stirred experiment generated a diffusive turbulent flow that always promoted flocculation for increasing concentration. This result was anticipated for flocs which evolve in a predominantly fluid shear environment, as turbulent shear stress τ_u typically constitutes the main limiting parameter (BURBAN, 1989, VAN LEUSSEN, 1997). For any kind of mud, the distribution of floc size and settling velocity is well representative of the order of aggregate theory with a clear distinction between the microfloc and macrofloc sub-populations. The observed flocs tended to grow with a constant effective density as sediment concentration increased. This supports a high fractal dimension and is in agreement with previous observations in similar environments (CHEN and EISMA, 1995). Some qualitative conclusions can be addressed by comparing the floc properties of the different types of mud. Gironde mud with and without active organic contents exhibit a very different response to the hydrodynamic forcings. The macrofloc order of aggregate was not reached for trials with the inorganic Gironde mud. In contrast, the naturally organic-rich muds always contained a majority of macroflocs. Gironde and Tamar muds with organic content demonstrated a similar evolution of their mean floc properties with respect to increasing sediment loading. This point is more remarkable as the study covers a wide range of concentration from 200 to 8000 mg.l^{-1}. It highlights the major role that the organic content plays in the flocculation process of natural estuarine mud. In future, an effort has to be made to take into account the increase of flocculation by organic content in numerical modelling. As pointed out by many authors, this agent supersedes the mineral cohesion effect in most environmental applications.

ACKNOWLEDGEMENTS

This work was carried as part of the COSINUS Program, which is funded by the European Commission (contract MAS3-CT97-0082). We express our gratitude to E. HOPFINGER, who made the grid tank facility available, and J.M. BARNOUD for his continuous technical assistance. K.R. DYER, H. MICHALLET and M. MORY are thanked for their support during the collaboration at the origin of the present work. A.J. MANNING's contribution to this paper was partially funded by H.R. Wallingford (UK), and the DEFRA / Environment Agency Joint Flood and Coastal Defence Research & Development Programme in Fluvial, Estuarine and Coastal Processes: Estuary Process Research (EstProc) project (under contract No.FD1905/CSA5966).

LITERATURE CITED

BERHANE, I., STERNBERG, R.W., GAIL, C., KINEKE, T.G. and KRANK, K., 1997. The variability of suspended aggregates on the Amazon Continental Shelf. *Continental Shelf Research*, 17(3), 267-285.

BERLAMONT, J.E. Prediction of cohesive sediment transport and bed dynamics in estuaries and coastal zones with integrated numerical simulation models. In: J.C. Winterwerp and C. Kranenburg, (eds.), *Coastal and Estuarine Fine Sediment Processes*. Amsterdam: Elsevier, pp. 1-4.

BURBAN, P.Y., LICK, W. and LICK, J., 1989. The flocculation of fine-grained sediments in estuarine waters. *Journal of Geophysical Research*, 94(C6), 8323-8330.

CAMP, T.R. and STEIN, P.C., 1943. Velocity gradients and internal work in fluid motion. *Journal of Boston Society of Civil Engineers,* 219-237.

CHEN, S. and EISMA, D., 1995. Fractal geometry of in situ flocs in the estuarine and coastal environments. *Netherlands Journal of Sea Research*, 32, 173-182.

DE CROUTTE, E., GALLISSAIRE, J.M. and HAMM, L., 1996. Flume measurements of mud processes over a flat bottom under steady and unsteady currents. *Report n°R3.* Sogréah Ingénieurie.

DYER, K.R. 1989. Sediment processes in estuaries: furture research requirements. *Journal of Geophysical Research*, 94(C10), 14327-14339.

DYER, K.R. and MANNING, A.J., 1999. Observation of the size, settling velocity and effective density of flocs, and their fractal dimensions. *Journal of Sea Research*, 41, 87-95.

EISMA, D., 1986. Flocculation and de-flocculation of suspended matter in estuaries. *Netherlands Journal of Sea Research*, 20, 183-199.

FEATES, N.G., HALL, J.R., MITCHENER, H.J. and ROBERTS, W., 1999. COSINUS field experiment, Tamar estuary measurement of properties of suspended sediment flocs and bed properties. *Report TR 82*. HR Wallingford.

FENNESSY, M.J., DYER K.R. and HUNTLEY, D.A. , 1994. INSSEV: an instrument to measure the size and settling velocity of flocs in situ. *Marine Geology*, 117, 107-117.

FENNESSY, M.J., DYER K.R. and HUNTLEY, D.A. , Bale, A.J., 1997. Estimation of settling flux spectra in estuaries using INSSEV. *In :* Burt, N., Parker, R. and Watts, J., *eds.*, Cohesive Sediments, John Wiley & Sons, Chichester, UK, 87-104.

GRATIOT, N., 2000. Etude expérimentale de la formation des couches de crèmes de vases turbulentes. *Ph. D. thesis*, Université de Grenoble (*in french*). France.

GRATIOT, N., MORY, M. and AUCHÈRE, D., 2000. An acoustic Doppler velocimeter (ADV) for the characterisation of turbulence in concentrated fluid mud. *Continental Shelf Research*, 20, 1551-1567.

HOPFINGER, E.J. and TOLY, J.A., 1976. Spatially decaying turbulence and its relation to mixing across density interfaces. *Journal of fluid mechanics*, 78, 155-175.

KRANENBURG, C., 1994. On the fractal structure of cohesive sediment aggregates. *Estuarine, Coastal and Shelf Science,* 39, 451-460.

KRONE, R.B., 1963. A study of rheologic properties of estuarial sediments. Tech. Bull 7, Committee of tidal hydraulics, hydraulic engineering laboratory and sanitary engineering research laboratory, University of California, Berkeley.

MANNING, A.J., 2001. A study of the effect of turbulence on the properties of flocculated mud. Plymouth, England: University of Plymouth, Ph.D. thesis, 282p.

MANNING, A.J. and DYER, K.R., 1999. A laboratory examination of floc characteristics with regard to turbulent shearing. *Marine Geology*, 160, 147-170.

MANNING, A.J.; DYER, K.R.; LAFITE, R. AND MIKES, D., 2004. Flocculation measured by video based instruments in the Gironde estuary during the European Commission SWAMIEE project. This volume.

MCANALLY, W.H. and MEHTA, A.J., 2001. Collisional aggregation of fine estuarial sediment. *In :* MCANALLY, W.H. and MEHTA, A.J., eds., Coastal and Estuarine Fine Sediment Processes, Elsevier Science B.V., 19-39.

MORY, M., GRATIOT, N., MANNING, A.J. and MICHALLET, H., 2002. CBS layers in a diffusive turbulence grid oscillation experiment. *In :* Winterwerp, J.C. and Kranenburg, C., eds., Fine sediment dynamics in the marine environment, Elsevier Science B.V., 139-154.

NEZU, I. and NAKAGAWA, H., 1993. Turbulence in open-channel flows. *International Association for Hydraulic Research*, Monograph Series, Balkema, Rotterdam.

SMOLUCHOWSI, M.Z., 1917. Versuch einer mathematischen theorie der koagulations-kinetic kolloider losungen. *Zietschrift für Physicalische Chemime,* 92-99.

TEETER, A.M., 2001. Clay-silt sediment modelling using multiple grain classes. Part I: Settling and deposition. *In :* MCANALLY, W.H. and MEHTA, A.J., eds., Coastal and Estuarine Fine Sediment Processes, Elsevier Science B.V., 157-171.

TENNEKES, H. and LUMLEY, J.L., 1972. A first course in turbulence. MIT Press.

THOMPSON, S.M. AND TURNER, J., 1975. Mixing across an interface due to turbulence generated by an oscillating grid. *J. Fluid. Mech.,* 67, 349-368.

VAN LEUSSEN, W., 1994. Estuarine macroflocs and their role in fine-grained sediment transport. *Ph.D. thesis,* University of Utrecht, The Netherlands.

VAN LEUSSEN, W., 1997. The Kolmogorov microscale as a limiting value for the floc sizes of suspended fine-grained sediments in estuaries. *In :* Burt, N., Parker, R. and Watts, J., *eds.*, Cohesive Sediments, John Wiley & Sons, Chichester, UK, 45-62.

WINTERWERP, J.C., 1999. On the dynamics of high-concentrated mud suspension. *Ph.D. thesis,* Delft University of Technology, The Netherlands.

WINTERWERP, J.C., 2002. On the flocculation and settling velocity of estuarine mud. *Continental Shelf Research*, 22, 1339-1360.

Journal of Coastal Research	SI 41	114-123	STRAEE 2002	Ferrara, Italy	ISSN 0749-0208

Cohesive sediment transport modelling – application to the Lister Dyb tidal area in the Danish Wadden Sea

U. Lumborg

DHI- Institute for Water and Environment
Agern Allé 5
DK-2970 Hørsholm
Denmark
ulu@dhi.dk

ABSTRACT

LUMBORG, U., 2004. Cohesive sediment transport modelling – application to the Lister Dyb tidal area in the Danish Wadden Sea. *Journal of Coastal Research*, SI 41,114-123. Ferrara (Italy), ISSN 0749-0208

A numerical 2D one-layer cohesive sediment transport model has been set up for the Lister Dyb tidal area in the Danish Wadden Sea. The applied modelling system MIKE 21 consists of several separate modules. The modules used in this study are a hydrodynamic module (MIKE 21 HD) calculating the water movements in the area, a near shore waves module (MIKE 21 NSW) for calculating a number of wave fields, and a mud transport module (MIKE 21 MT) for calculating the cohesive sediment dynamics in the area. The simulated suspended sediment concentrations are compared to measured time series during a six-week period. It shows that the suspended sediment concentration (SSC) phase is in accordance with the observed patterns showing relatively low concentrations at high water and high concentrations at low water. The magnitude of the concentrations also to a high degree correlate with the observed values, although the lowest concentration levels around high water may be too high. Further, the bed level change has been validated on the time scale of a few tidal periods. This shows that the model is capable of creating the correct pattern of bed level change. However, on longer time scales (months), the net deposition pattern and hence the calculated sediment budget may not be realistic. As the cohesive sediment transport model is well calibrated, it has been possible to calculate the distances of the settling and scour lags individually. The combined lag effects amount to distances of around 1500 m, with the scour lag being of greatest importance. Through this study, it has been shown that it is possible to use numerical modelling to simulate suspended sediment concentrations that fit well with observed values. In addition, it is possible to recreate measured patterns of relative bed level change. This leads to the assumption that cohesive sediment transport models in the future can be used to elaborate on cohesive sediment transport problems with a high degree of reliability.

ADDITIONAL INDEX WORDS: *Cohesive sediment; modelling; bed level change; settling/scour lag; Lister Dyb tidal area; Denmark*

INTRODUCTION

Cohesive sediment transport patterns in estuarine areas are an important research topic, since large amounts of sediment are transported to and deposited in these areas every year. The siltation of navigation channels is a major problem due to expensive dredging costs and contamination problems when dumping the dredged sediment. Further, the estuarine areas are feeding place for a large number of micro and macro faunal species, thus making estuaries and intertidal areas important ecological habitats.

Since the middle of the 20th century, research on cohesive sediment transport has been carried out in order to understand the processes leading to erosion, transport, and deposition of cohesive sediment (e.g. POSTMA, 1954; VAN STRAATEN and KUENEN, 1958; KRONE, 1962; MIGNIOT, 1968). This research has also led to establishment of qualitative equations that describe some of these processes (e.g. PARCHURE and MEHTA, 1985; PEJRUP, 1986; MEHTA *et al.*, 1989; TEISSON, 1991; VAN LEUSSEN, 1994; VAN DER LEE, 2000). During the last decade, such equations have been incorporated in numerical models that describe the erosion, transport, flocculation, and deposition of cohesive sediments (e.g. CANCINO and NEVES, 1999; LE NORMANT, 2000). However, presented models often have lack of significance when the modelled suspended sediment concentrations are compared to measured values. Even when a fair significance is obtained, usually only very short time series (few tidal periods) are presented.

Detailed description of the bed level change in tidally influenced estuaries and the processes of settling and scour lag is a highly complicated task, and modelling of these features has not yet been published. In this research project, it is attempted to use an existing model and by using, a careful calibration and fitting site-specific algorithms, to obtain significant results during a longer period. The bed level change is described over a shorter period and the importance of the settling and scour lag effects are estimated. In this paper, the functionality of an existing cohesive

sediment transport model will be described. A calibration of the model will be presented and results from a modelling period of six weeks and comparisons with measured time series from the same period will be discussed and evaluated.

STUDY AREA

The study was carried out in the Lister Dyb tidal area situated in the southern part of the Danish Wadden Sea (figure 1); the basin is protected from the North Sea by the two barrier islands Rømø and Sylt. The tidal basin covers an area of app. 400 km^2 of which the intertidal flats comprises about 45%. The area has semidiurnal tides with an average height of 1.8 m, which classifies the area as microtidal (DAVIES, 1964). Two small rivers Brede Å and Vidå are fresh water sources to the tidal area. However, these only contribute to 0.2% of the tidal prism, which has been calculated to 620×10^6 m^3 (LUMBORG and WINDELIN, 2003). The bottom sediment of the area is classified into sand flats, mixed mud flats, mud flats, and marsh (figure 1) (PEJRUP *et al.*, 1997). Furthermore, PEJRUP *et al.* (1997) established a sediment budget for the intertidal areas, showing that approximately 58 000 t of cohesive sediment is deposited in the area every year. The input from the rivers contributes to 14% of the deposited sediment, primary production 15%, salt marsh erosion 5%, atmospheric deposition 2%, and input from the North Sea (calculated as residual value) amounts to 64% of the total deposition at the intertidal areas.

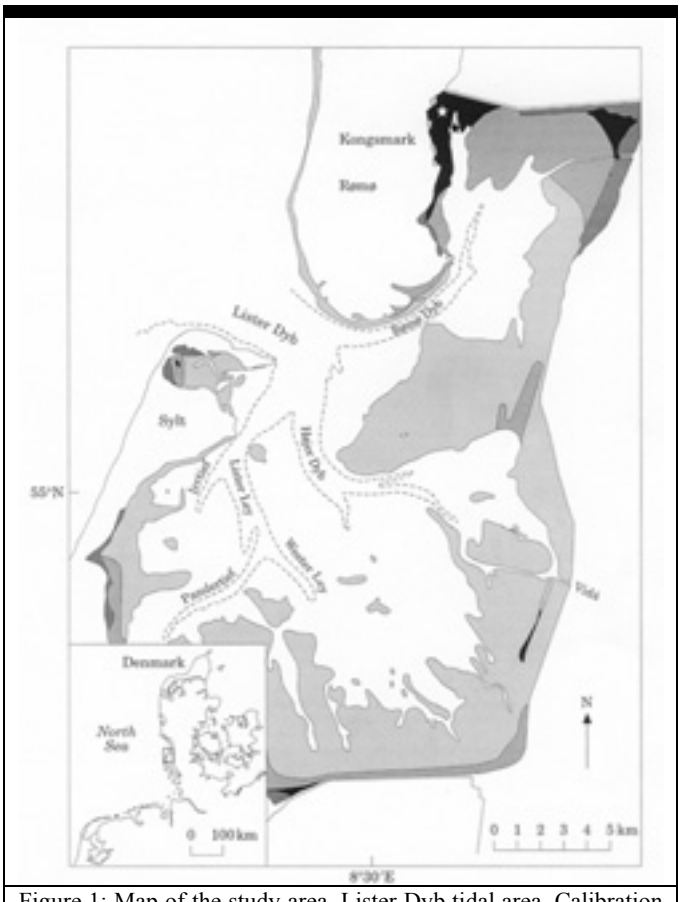

Figure 1: Map of the study area, Lister Dyb tidal area. Calibration points are indicated (A: Kongsmark tidal flat; B: Fuglegrøft tidal channel). The map is based on PEJRUP *et al.* (1997).

METHODS

Description of the Model

The model applied to the Lister Dyb tidal area is the MIKE 21 modelling system, comprising of several modules, of which three are applied here. MIKE 21 HD is the hydrodynamic module that calculates the water levels and fluxes in the area (DHI, 2000). The setup of the hydrodynamic model uses a very detailed bathymetry, six tidal constituents, measured time series of water levels, and a bottom roughness measured in the area. MIKE 21 NSW is a module for modelling near shore waves. In this context, the module is used for calculating a number of wave fields in the specific area. The wave modelling has resulted in 36 sketches of wave fields. The algorithms behind and assumptions for using the MIKE 21 NSW module are presented in JOHNSON (1998). The MIKE 21 MT module is the cohesive sediment transport module. The module is used for calculating the erosion, transport, and deposition of cohesive sediment in the area. The structure of the model is presented as a flow diagram in figure 2 and an exposition of the basic algorithms is given in the following.

In the sediment transport model (MIKE 21 MT), the bottom is described using a layer structure following the principle presented in PARCHURE and MEHTA (1985). Each bottom layer is described using the density of the sediment, the critical shear stress for erosion, the erodibility, and the α-coefficient. In addition, each layer should have an initial thickness. By using this model, it is possible to describe the increase of resistance to erosion down through the bottom layers, and the settling scour lag processes will quantitatively be included in the model.

Transport of the suspended sediment is calculated using the advection-dispersion equation, which is classically written (e.g. TEISSON, 1991):

$$\frac{\partial \bar{c}}{\partial t} + V_X \frac{\partial \bar{c}}{\partial x} + V_Y \frac{\partial \bar{c}}{\partial y} = \frac{1}{h}\frac{\partial}{\partial x}\left(hD_X \frac{\partial \bar{c}}{\partial x} \right) + \frac{1}{h}\frac{\partial}{\partial y}\left(hD_Y \frac{\partial \bar{c}}{\partial y} \right) + \sum_{i=1}^{n} \frac{S_i}{h} \qquad (1)$$

where c is the depth averaged suspended sediment concentration (g m^{-3}), V_X and V_Y are depth averaged flow velocities (m s^{-1}) (calculated in the hydrodynamic module), D_X and D_Y are dispersion coefficients (m^2 s^{-1}), h is water depth (m) (calculated in the hydrodynamic module), and S_i is the source/sink term (g m^{-2} s^{-1}) taking into account the erosion or deposition of sediment.

The bottom shear stress (τ_b in N m^{-2}) is calculated with respect to currents and waves using the following equation:

$$\tau_b = \tfrac{1}{2}\rho_w f_w \left(U_b^2 + U_\delta^2 + 2U_b U_\delta \cos\beta \right) \qquad (2)$$

where ρ_w is the density of water (kg m^{-3}), f_w is the wave friction factor, U_b is the horizontal mean wave orbital velocity at the bed (m s^{-1}), U_δ is the current velocity at top of wave boundary layer (m s^{-1}), and β is the angle between the mean current direction and the direction of wave propagation.

The formula of deposition (eqn. 3) was originally proposed by KRONE (1962) and has a stochastic element incorporated, since the

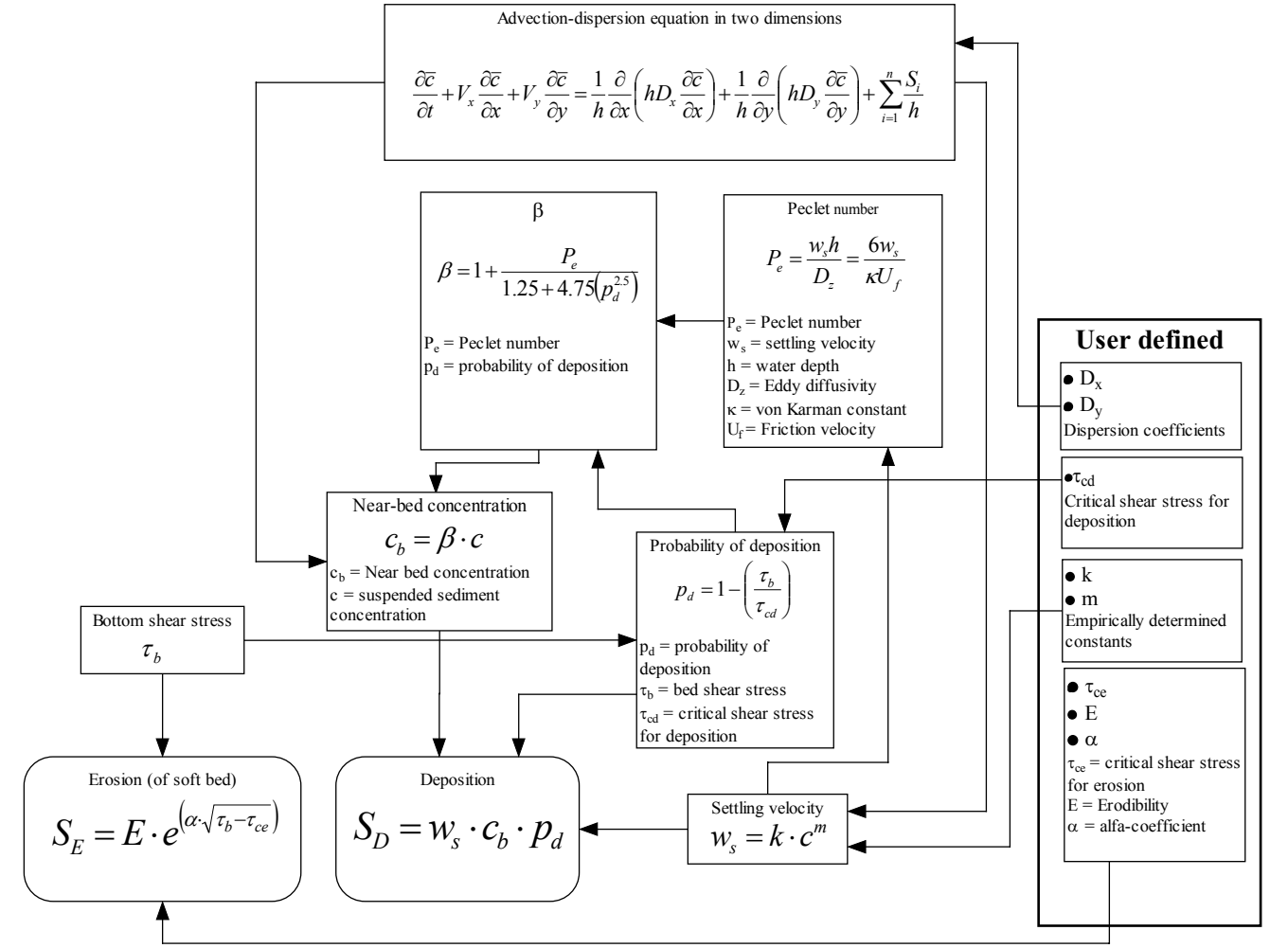

Figure 2: Flow diagram showing the structure of the cohesive sediment transport model MIKE 21 MT, and the interdependency of the variables included in the model.

p_d part is the probability of deposition which is dependent on the ratio between the bottom shear stress (τ_b) and the critical shear stress of deposition (τ_{cd}) (figure 2). The near bottom concentration (c_b (g m^{-3})) is dependent on the depth averaged sediment concentrations as described in TEETER (1986) (figure 2).

$$S_D = w_s c_b p_d \tag{3}$$

where S_D is the deposition rate in g m^{-2}.

The settling velocity in m s^{-1} (w_s) is described by the well-known exponential relationship with the suspended sediment concentration (e.g. BURT, 1986; PEJRUP, 1988).

$$w_s = kc^m \tag{4}$$

where k and m are site-specific constants that have to be determined empirically.

Erosion from the sediment bed is described using an expression originally proposed by PARCHURE and MEHTA (1985). The expression for erosion is as follows:

$$S_E = E \cdot e^{\left[\alpha\sqrt{\tau_b-\tau_{ce}}\right]} \tag{5}$$

where S_E is the erosion rate in g m^{-2}, E is the erodibility of the bed (g m^{-2} s^{-1}), τ_{ce} is the critical shear stress for erosion (N m^{-2}), and α is termed the α-coefficient (m N$^{-0.5}$). This formula can be calibrated very specifically to a given site due to the erodibility and α-coefficient.

Field Survey

A field survey was carried out in order to collect calibration data for the hydrodynamic and the cohesive sediment transport model. Two self-recording Aanderaa RCM-9 current meters (TENGBERG *et al.*, 2001) were deployed in the northern part of the study area. One on the tidal flat near the village Kongsmark on Rømø (A on figure 1) and one in a nearby small tidal channel named Fuglegrøft (B on figure 1). The meters recorded water depth, current velocities, and suspended sediment concentrations every 10 minutes during the investigated period.

Table 1: Values of all parameters used in the cohesive sediment transport model

Parameter		Value
D_X, D_Y		$D_X = D_Y = 25$ m^2 s^{-1}
w_s	$0 \le c \le 6$ mg l^{-1}	0.00042 m s^{-1}
	$50<c\le1000$ mg l^{-1}	$3.96\times10^{-6}*c^{1.19}$ m s^{-1}
	$c > 1000$ mg l^{-1}	0.015 m s^{-1}
τ_{cd} (spatially varied)		0.04, 0.03, 0.02 N m^{-2}
ρ_{sed} (bottom layers 1–5)		90, 129, 225, 600, 1000 kg m^{-3}
τ_{ce} (bottom layers 1–5)		0.1, 0.2, 0.3, 0.5, 0.7, 2 N m^{-2}
E (bottom layers 1–5)		0.0005, 0.005, 0.005, 0.005, 0.005 g m^{-2} s^{-1}
α (bottom layers 1–5)		6.5, 6.5, 6.5, 6.5, 6.5 m N$^{-0.5}$

The suspended sediment concentrations were measured using an OBS sensor, which was calibrated using water samples taken at known times. The water samples were filtered, dried, and weighted so that exact

concentrations were obtained. The instrument has earlier been found ideal for monitoring sediment concentrations at the site (ANDERSEN, 1999).

The water depth and current velocities were used for calibration of the hydrodynamic model. This calibration is presented in LUMBORG and WINDELIN (2003). The suspended sediment concentrations were used for calibration and validation of the cohesive sediment transport model. The calibration period for the model lasted for three weeks (October 20, 1999 – November 12, 1999), as did the validation period (November 12, 1999 – December 4, 1999).

Modelling Procedure

One of the most important parts of a hydrodynamic modelling study is to obtain a bathymetry of high quality, describing the bottom topography of the area. The bathymetry used in this study is provided by the Danish Coastal Authorities, who made a high quality measurement of the Danish part of the Wadden Sea in 1992. The data set is of high accuracy and is therefore a good basis for the modelling work. The grid resolution of the bathymetry was selected to 150×150 m. Due to the sensitivity of the model to abrupt bathymetric changes, the bathymetry was slightly smoothed using an averaging moving window function.

At the model boundaries, time series of water levels is applied. In order to obtain a precise description of the water level the time series is calculated in two steps. First the astronomical tide is calculated using the six main tidal constituents following the Admiralty Method (ADMIRALTY TIDE TABLES, 1999). Afterwards, a 12-hour running average of measured water levels is added to the astronomical tide in order to include the meteorological alterations of the water levels. The model is subsequently fine-tuned using the bottom roughness parameter, resulting in a fine reproduction of the measured water levels. A more detailed description of the hydrodynamic modelling can be found in LUMBORG and WINDELIN (2003).

By using the near shore waves module, 36 momentary wave fields have been calculated, each using unique values of wind velocity, wind direction, and water level. The wave fields are organised in a three dimensional wave database. When the bottom shear stress is calculated (eqn. 2), the model carries out an interpolation in the database.

The calibration process focused on providing a good description of the bottom, for which several parameters should be specified, for each bottom layer, including sediment density, critical shear stress for erosion, erodibility (E in eqn. 5), and the α-coefficient. A site-specific description of the settling velocity also had to be established. The dispersion coefficients and the critical shear stress for deposition have mainly been used as calibration parameters. In the following, the motivation for the size of different parameters is described. A complete overview of the values of all input parameters to the cohesive sediment transport model is given in table 1.

Dispersion Factors

The dispersion factors included in the advection-dispersion equation (eqn. 1) determine the net amount of sediment the model is capable of moving through a grid cell boundary each time-step. The values therefore determine the size of the advective component. The size of the factors is dependent on the size of the grid cells. The dispersion factors are calibrated to 25 m^2 s^{-1}.

Settling Velocity of the Suspended Sediment

The settling velocity is in MIKE 21 MT related to the suspended sediment concentration and significant relationships following equation 4 are often seen in the literature (e.g. BURT, 1986; PEJRUP, 1988; BARTON *et al.*, 1991; DYER *et al.*, 1996; PEJRUP and EDELVANG, 1996). In the present study, a large dataset of settling velocities analysed by the settling tube method in the study area has been analysed and a site- and season specific description that yields $w_s = 3.96\times10^{-6} * c^{1.19}$, is used in the model. The description is held constant at concentrations below 50 mg l^{-1} due to data uncertainties related to insignificance in the settling tube measurements (PEJRUP, 1988). At sediment concentrations over 1000 mg l^{-1} the settling velocity is also held constant in order to prevent too high deposition rates as the settling velocity is included in the formula of deposition (eqn. 3).

Critical Shear Stress for Deposition

The critical bottom shear stress for deposition determines when the suspended sediment will start to deposit in relation to the calculated bottom shear stress. The value of the critical shear stress for deposition is site-specific and to a high degree influenced by biological processes (ANDERSEN, 1999). However, no measurements of the critical shear stress for deposition are made in the study area and the parameter is therefore used for calibration. The selected values are 0.04, 0.03, and 0.02 N m^{-2}. The highest values are used for the tidal flats where the largest amount of sediment is actually deposited, while the lowest values are used for the tidal channels and for the North Sea area. The used values are consistent with earlier given general values, e.g. 0.06 N m^{-2} (KRONE, 1962) or 0.18–1.1 N m^{-2} (MEHTA and PARTHENIADES, 1975).

Density of Bottom Sediment

Densities of the sediment from the upper layers at different sites in the northern part of the study area are reported have values varying from 90 kg m^{-3} to 225 kg m^{-3} (AUSTEN *et al.*, 1999). These values are in accordance with general values reported by VAN RIJN (1989). ANDERSEN (1999) reports a sediment profile, from Rømø Dyb, which has densities varying from 450 kg m^{-3} (upper 40 cm)

to 1 000 kg m^{-3} (40–80 cm). In this study, different density values are selected for each bottom layer as shown in table 1. The values are consistent with the above mentioned studies.

Critical Shear Stress for Erosion

The critical shear stress for erosion has been measured in the study area. An overview of results can be found in AUSTEN *et al.* (1999) and ANDERSEN (2001). The values vary between 0.16 N m^{-2} at the upper sediment layers that are easily eroded to 3 N m^{-2} in the lower and more sandy and consolidated layers. PARCHURE and MEHTA (1985) reported critical erosion values at 0.04–0.62 N m^{-2}, but these values account only for upper layers. For this model setup, values at 0.1–0.7 N m^{-2} are used. A value of 2 N m^{-2} is artificially used to prevent erosion from the lowest bottom layer.

Erodibility

The erodibility is used as a calibration factor and values of 0.0067 to 0.3 g m^{-2} s^{-1} (PARCHURE and MEHTA, 1985) and of 0.0005–0.005 g m^{-2} s^{-1} (VAN RIJN, 1989) have been reported. From erosion experiments made in the northern part of the Rømø Dyb tidal area by ANDERSEN (2001) approximate values of the erodibility has been derived. In this study, a value of 0.0005 g m^{-2} s^{-1} is used for the uppermost bottom layer and 0.005 g m^{-2} s^{-1} for the four underlying layers.

α-coefficient

The α-coefficient is the factor that steers the exponential rise in erosion when the bottom shear stress rises and strongly varying values have been given (4.6–25.6 m $N^{-0.5}$ (PARCHURE and MEHTA, 1985) and 10–20 m $N^{-0.5}$ (VAN RIJN, 1989)). Several model runs using values of the α-coefficient between 2 and 15 m $N^{-0.5}$ has been carried out in order to obtain as much erosion needed to establish a concentration pattern that fits the observations. Finally, a value of 6.5 m $N^{-0.5}$ is used for all layers. This value gives some amount of erosion and at the same time preventing very high erosion rates when the bottom shear stress rise due to the influence of wind waves.

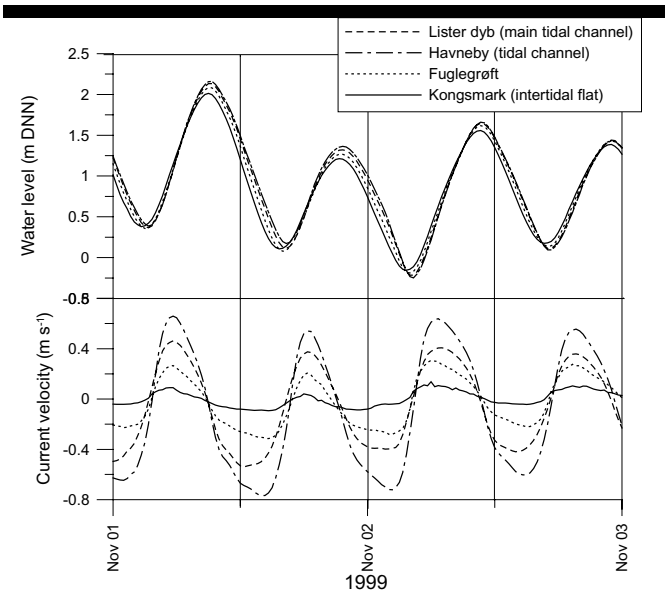

Figure 3: Deformation of the tidal wave in the Lister Dyb tidal area.

RESULTS

The calibration and validation of the cohesive sediment transport model is based on six weeks time series from two self-recording Aanderaa RCM-9 current meters, placed in the northern part of the study area. One is placed in the tidal channel Fuglegrøft and another is placed on a tidal mudflat near the village Kongsmark (figure 1).

The hydrodynamic simulation was calibrated and validated, using water levels and current velocities from the two current meters and the simulation is found to be in accordance with the observed values (LUMBORG and WINDELIN, 2003). By subtraction of simulated values and observed values the water heights do not show much discrepancy. The difference between the measured and the modelled water levels is below 0.2 m at 62.3% of the time. The corresponding percentage for 0.5 m is 95.0%. A difference of more than 1 m only occurs at 0.6% of the time connected to an extreme storm event in December 1999.

The deformation of the tidal wave is a characteristic feature of tidally influenced shallow estuaries. The deformation occurs when the propagating wave is slowed down because of the bottom friction. This makes the tidal wave crest to travel faster than the wave trough. Consequently, the tide rises quickly and falls slowly. This will extend the ebb period and produce a characteristic saw-tooth shaped water level curve (e.g. DYER, 1986). As the deformation of the tidal wave is very important for cohesive sediment dynamics, it is essential that the hydrodynamic model simulate the deformation satisfactorily. In figure 3, the modelling of this feature is shown. The wave is symmetrical in the main tidal channel (Lister Dyb). The wave deforms and becomes successively asymmetric as it enters the inner parts of the lagoon. The curve for the Lister Dyb point shows lower current velocities than that for the Havneby point, due to the narrowing of the channel after the dividing point is reached.

In figure 4, the result of a MIKE 21 MT simulation is shown. The figure includes time series of observed and simulated suspended sediment concentrations from the two calibration sites and the measured wind statistics. In the tidal channel (Fuglegrøft) the simulated sediment concentrations as an overall observation follows the theories of cohesive sediment dynamics in an estuary (DYER, 1986), showing the highest concentrations around low water and lower sediment concentrations in the flood period. When the current slows down toward high water slack the sediment falls out of the water column and the lowest sediment concentrations thus appear around high water slack. This phase of sediment concentrations closely follows the observed pattern and the peaks show up at exactly the same time in the observed and the simulated time series.

The levels of the simulated sediment concentrations at most times follow the measured levels, which is satisfactory. However, at some occasions the simulated concentrations lies an order of magnitude below or above the observed concentrations, showing that the model is not always capable of reproducing the exact levels of sediment concentrations. The model only gives an indication about cohesive sediment dynamics over a longer period. As a further consequence of this, it is not immediately possible to simulate cohesive sediment dynamics on yearly or decadal time scales.

At the tidal mudflat at the Kongsmark site the modelled sediment concentrations are generally overestimated, originating from instabilities in the hydrodynamic model.

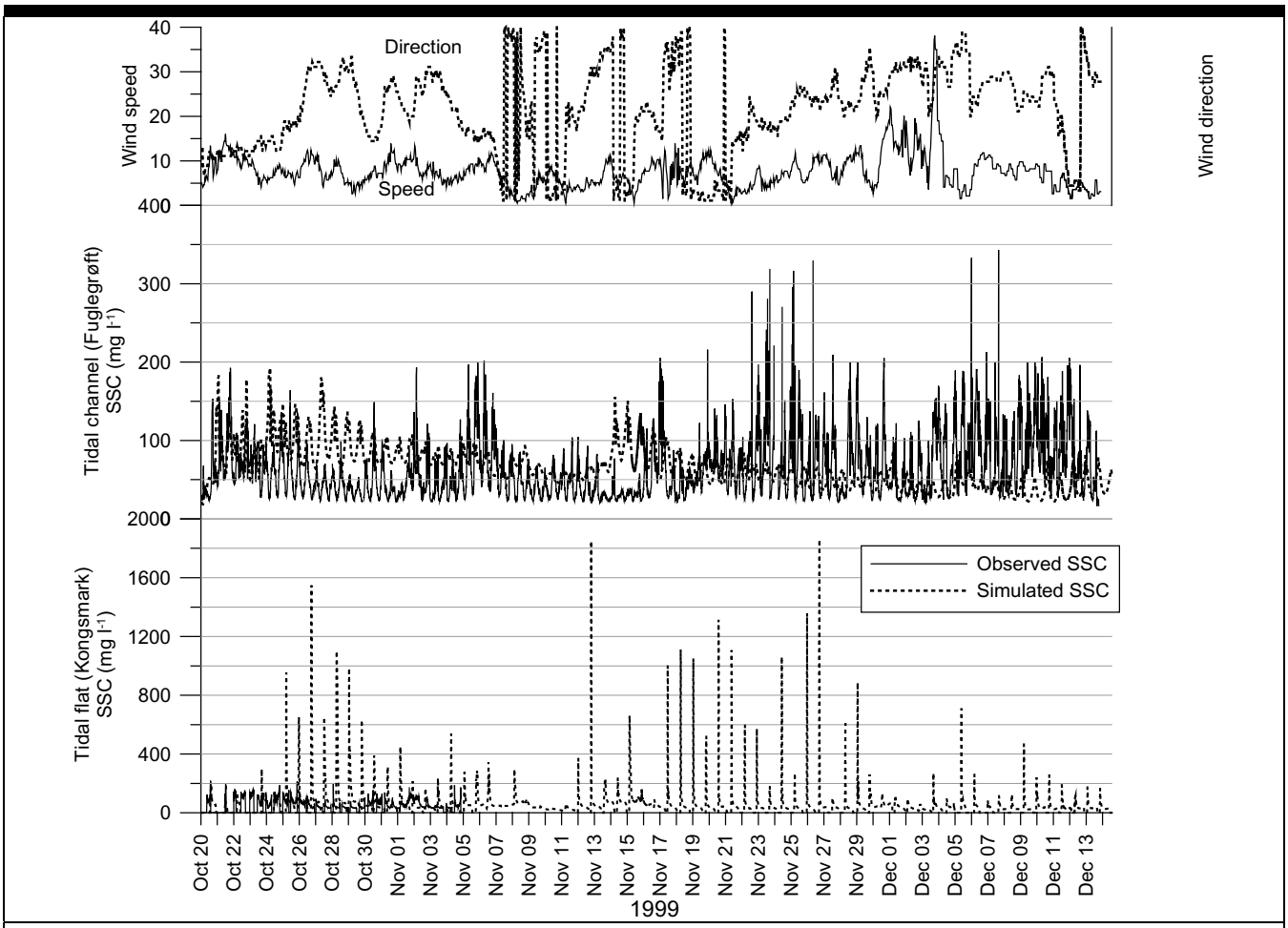

Figure 4: Example of results from a cohesive sediment transport simulation. Suspended sediment concentrations during a six-week period compared to measured values are presented.

When the water level gets below app. 10 cm there is a possibility that the continuity equation becomes unstable and therefore producing unrealistically high bottom shear stresses.

This results in high erosion rates and following high suspended sediment concentrations. These unrealistically high sediment concentrations are artefacts in the results. However, if the scale on the y-axis is diminished (figure 5) and the instabilities left out, the concentrations show the asymmetrical pattern that is observed at tidally influenced mudflats in general (WHITEHOUSE and MITCHENER, 1998) and at the Kongsmark tidal flat in particular (ANDERSEN, 1999).

When looking at the sediment concentrations at shorter time scales such as a couple of tidal periods (figure 6) it can be seen that the modelling results are very close to the measurements. Even the very short drop in concentration at low water slack is modelled with a high accuracy. This shows that numerical models can be used to give very significant information about cohesive sediment dynamics in a specific area at a specific period.

DISCUSSION

As the sediment concentrations at the calibration points have been modelled satisfactorily, it is believed that the modelled sediment concentrations over the whole area are representative for the actual occurring concentrations.

From the model simulations, it can be seen that in the Lister Dyb tidal area the sediment concentrations reach the highest levels when onshore winds are prevailing. Further, it is recognized that even during wind situations the sediment concentrations on sheltered sites (e.g. the Kongsmark site during westerly winds) will not reach high values as is seen around the period October 26 to October 30 (figure 4). Only when wind velocities higher than app. 18 m s^{-1} occur (e.g. December 1 to December 5) the concentrations in the tidal channel rise, while on the tidal flat the concentrations still remain at a relatively low level.

The suspended sediment over the tidal flats mostly comes from local resuspension while the suspended sediment occurring in the tidal channels often is transported from the tidal flats and the North Sea to the channels and only limited erosion occurs in spite of high concentrations in the tidal channels. In some situations concentrations of several hundreds mg l^{-1} exist in the channels while the concentrations over the tidal flats only amounts to around 30 mg l^{-1}, resulting in strong horizontal concentration gradients.

In figure 7, a time series of two days, showing current velocities, suspended sediment concentrations, and bed level change at the calibration site in the tidal channel are presented. The figure illustrates several features characteristic for the specific

site and for many shallow estuaries in general. The settling and scour lag processes, originally defined and described by VAN STRAATEN and KUENEN (1958) are here treated individually.

When a sediment particle settles from a slackening flood current, the particle will not deposit directly below the place where it has started to settle but at a place longer landwards. When the water parcel which originally carried the particle passes the place of deposition again (now as an ebb current) it will not travel fast enough to erode the particle. The particle will therefore be eroded by water situated further inwards. This water parcel will not be able to transport the particle as long seaward as it originally was eroded. The consequence of this is that the particle each tidal period is brought further inward and finally it will be deposited so close to the coast that it cannot be eroded by a tidal current again. This process is referred to as settling lag.

It is found that it requires higher current velocities to erode a particle from the bottom than it requires depositing it. By this, it follows that if a flood current deposit a particle, an ebb current with a higher velocity is required to resuspend it. This process, which results in an inward transport of sediment, is referred to as scour lag. The scour lag is included in the model by choosing different critical shear stress values for erosion (τ_{ce}) and deposition (τ_{cd}) (higher critical values for erosion).

The importance of these two processes for the study area is illustrated in figure 7. The settling lag (figure 7, letter A) is measured as the time lag between high water slack and the time of minimum suspended sediment concentration. The settling lag in this tidal period is app. 1 hour. The average current velocity during that period is app. 0.2 m s^{-1}, which means that the sediment can be transported app. 700 m landwards during this settling lag period.

The scour lag is illustrated for the next tidal period (figure 7, letter B). The first vertical line defines the starting point of deposition and it is seen that the flood current velocity is app. 0.1 m s^{-1}. The second vertical line shows when the ebb current reaches the same current velocity. However, the resuspension does not start until app 1.5 hour after this time (at the third vertical line). This 1.5 hour is defined as the scour lag. The average current velocity is app. 0.2 m s^{-1}, which means that due to the scour lag the sediment is prevented from being brought more than 1 km seawards. These values are consistent with calculated lag effects in Ho Bight, also located in the Danish Wadden Sea (BARTHOLDY, 2000).

In figure 7, it is further seen that the maximum current velocities in the flood periods and the maximum current velocities in the ebb periods often are slightly different. However, it is different which one is highest. This means that the system at the site of investigation is neither flood nor ebb dominated. Because of this, the sediment transport solely connected to current velocity will alternate in favouring landward and seaward sediment transport. In the three tidal periods presented in figure 7, it is seen that the highest sediment concentrations occur at low water slack. Immediately after this point, a marked drop in SSC is seen (figure 7, letters C) and is also observed in measured data. When the sediment concentrations increase towards low water slack the settling velocities of the sediment rise accordingly and when low water is approaching and the current velocity is slowing down, the sediment can no longer stay in suspension and begins to fall out and the concentration drops. However, shortly after the current velocity has again reached a point where it can hold sediment in suspension and the concentration again rises until the maximum ebb current velocity is reached. Hereafter the concentration falls slowly until high water slack.

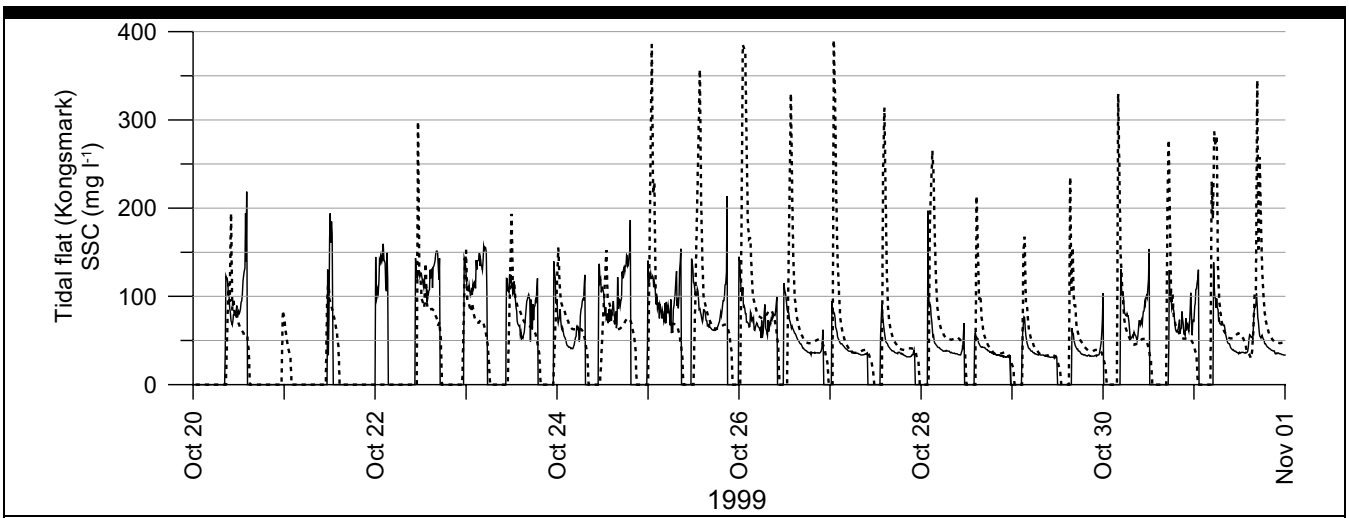

Figure 5: Simulated suspended sediment concentrations at the Kongsmark tidal flat compared to measured values. Due to instabilities leading to unrealistically high concentrations, the y-axis is diminished in order show the concentration pattern.

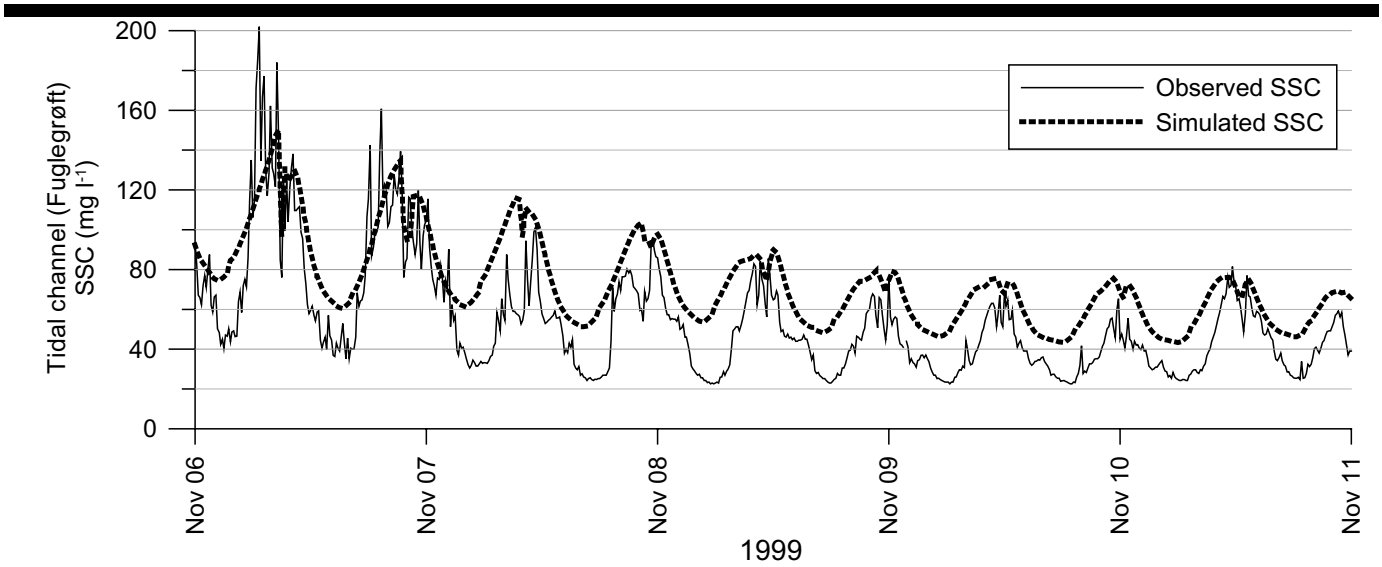

Figure 6: Simulated suspended sediment concentrations at the calibration site in Fuglegrøft compared to measured values.

The pattern of the bed level change is different during the periods of high water and low water. The deposition around high water generally shows a flat profile (around 0.25 mm). Due to the low sediment concentrations, the settling velocities are low and not much deposition is possible.

The sediment is deposited for around 2 hours before the current reaches velocities high enough to cause resuspension. Then the sediment is eroded relatively fast (around 0.5 hours) resulting in an asymmetric net deposition profile. In the period around low water, a more marked peak is simulated, due to the higher

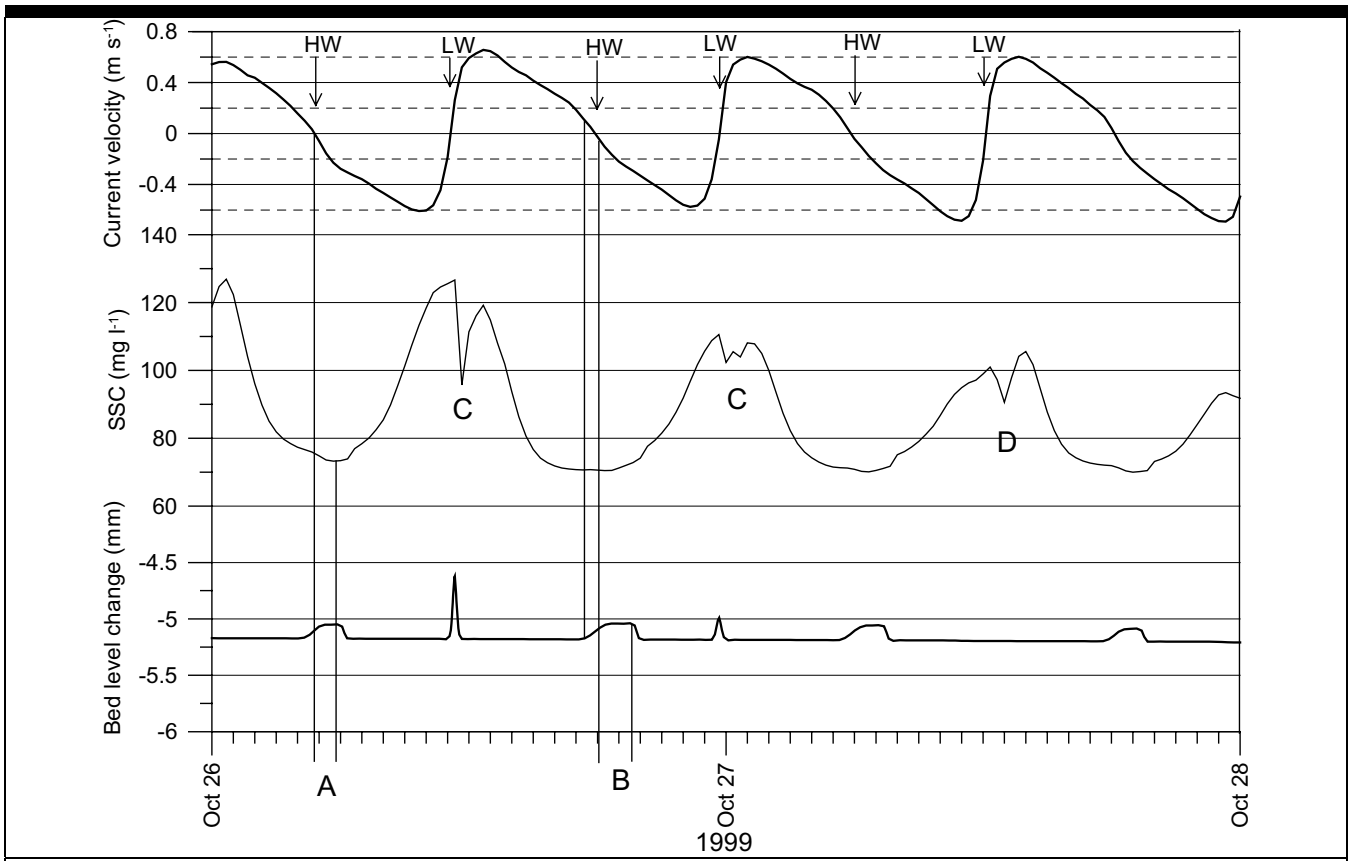

Figure 7: Current velocities, suspended sediment concentrations, and relative bed level change at the calibration site in Fuglegrøft. The letters A – D refer to specific discussion elements in the text.

suspended sediment concentrations and settling velocities. The deposition profile is generally so high (around 0.5 mm) that it can actually be noticed as a drop in the suspended sediment concentration as described above. However, due to the deformation of the tidal wave, the current velocities rise quickly after slack water and the deposition phase only lasts for about 0.5 hours and the suspended sediment concentration rises again. The net deposition phase lasts for app. 1 hour.

At the last high water period showed in figure 7 the suspended sediment concentrations do not reach a level high enough to cause high settling velocities during the very short period of low current velocities. Because of this, no deposition occurs during this low water period (figure 7, letter D).

Over a longer time span (six weeks) at a typical autumn situation in Denmark the model results suggest that deposition and erosion are approximately in equilibrium. The system has a little export of sediment during the period.

CONCLUSIONS

The model set-up is capable of reproducing an overall pattern of cohesive sediment dynamics in the Lister Dyb tidal area and can therefore be used to elaborate on the dynamics in the area. The sediment concentrations in the tidal channel vary between app. 20 mg l^{-1} and up to 400 mg l^{-1}. The highest concentrations appear around low water but with a slight lowering of concentrations at low water slack. At high water slack, the concentrations generally show the lowest values. On the tidal flat, the concentrations follow a typical pattern with high concentrations just when the flat is inundated, lower concentrations during high water, and high concentrations again just before the tidal flat dries out towards low water.

The investigation of the net deposition shows that several millimetres of sediment can be deposited and eroded again during one tidal period. The deposition pattern during the high water period shows a slight asymmetry towards low water, showing that the scour lag process is active in the inner parts of the estuary. Further, the settling lag defined as the time lag between slack water and the minimum concentration is modelled satisfactorily, generating an inward sediment transport and a net deposition, as long as the sediment is not eroded for example by large waves.

The results presented in this study show that it is possible to use cohesive sediment transport models to describe suspended sediment concentrations and relative bed level changes over a relatively long time period (here six weeks). However, a model setup requires a long time of calibration and collection of site-specific values is necessary. This is especially true for parameters concerning settling velocity and erosion.

By this, it follows that cohesive sediment transport models have great potential when it comes to model the effects of dredging plans or larger construction works. Numerical model can also be applied when analyzing different parameters effects to a smaller area over a shorter period. However, more research is needed in order to use cohesive sediment transport models for predicting the evaluation of intertidal areas over a time span of years or decades. This research must in particular address the settling velocity and erosion formulations and their seasonal variation.

ACKNOWLEDGEMENTS

The author would like to thank Klavs Bundgaard from "DHI – Institute for Water and Environment" for technical assistance during the model setup. Morten Pejrup, Thorbjørn Joest Andersen, and Niels Vinther are thanked for helpful discussions during completion of this manuscript. Thanks also go to my former fellow student Anders Windelin, with whom I made the initial modelling work. I would also like to thank an anonymous reviewer for constructive comments.

LITERATURE CITED

ADMIRALTY TIDE TABLES, 1999. Volume 2, Europe. Published by the Hydrographer of the Navy.

ANDERSEN, T. J., 1999. Suspended Sediment Transport and Sediment Reworking at an Intertidal Mudflat, the Danish Wadden Sea. *Meddelelser fra Skalling-Laboratoriet*, 37, 1-72.

ANDERSEN, T. J., 2001. Seasonal variation in erodibility of two temperate, microtidal mudflats. *Estuarine, Coastal and Shelf Science*, 53, 1-12.

AUSTEN, I., ANDERSEN, T. J., and EDELVANG, K., 1999. The Influence of Benthic Diatoms and Invertebrates on the Erodibility of an Intertidal Mudflat, the Danish Wadden Sea. *Estuarine, Coastal and Shelf Science*, 49, 99-111.

BARTHOLDY, J., 2000. Processes controlling import of fine-grained sediment to tidal areas: a simulation model. *In*: PYE, K. and ALLEN, J. R. L. (Editors), *Coastal and Estuarine Environments: sedimentology, geomorphology and geoarchaeology*, Geological Society, London, Special publications, 175, pp. 13-29.

BARTON, M. L., J. A. STEPHENS, R. J. UNCLES, and J. R. WEST, 1991. Particle fall velocities and related variables in the Tamar Estuary. *In*: ELLIOT, M. and DUCROTOY, J. P. (Editors), *Estuaries and Coasts: Spatial and Temporal Intercomparisons*, Olsen & Olsen, pp. 31-36.

BURT, N., 1986. Field Settling Velocities of Estuary Muds. *In*: MEHTA, A. J. (Editor), *Estuarine Cohesive Sediment Dynamics*, Vol. 14, Chap. 7. Springer-Verlag, Berlin, Heidelberg, NewYork, Tokyo, pp. 126-150.

CANCINO, L. and NEVES, R., 1999. Hydrodynamic and sediment suspension modelling in estuarine systems Part II: Application to the Western Scheldt and Gironde estuaries. *Journal of Marine Systems*, 22, 117-131.

DAVIES, J. L. H., 1964. A morphogenetic approach to world shorelines. *Zeitschrift der Geomorphologie*, 8, 127-142.

DHI, 2000. *MIKE 21 hydrodynamic module. User guide and reference manual, Release 2000.*

DYER, K. (1986). *Coastal and Estuarine Sediment Dynamics*. John Wiley & Sons.

DYER, K., CORNELLISSE, J. M., DEARNALEY, M. P., FENNESEY, M. J., JONES, S. E., KAPPENBERG, J., MCCAVE, I. N., PEJRUP, M., VAN LEUSSEN, W., and WOLFSTEIN, K., 1996. A comparison of in situ techniques for estuarine floc settling velocity measurements. *Journal of Sea Research*, 36, 15-29.

JOHNSON, H. K., 1998. On modelling wind-waves in shallow and fetch limited areas using the method of Holthuijsen, Booij and Herbes. *Journal of Coastal Research*, 14, 917-932.

KRONE, R. B., 1962: Flume Studies of the Transport of Sediment in Estuarine Shoaling Processes. *Final Report to San Francisco District U. S. Army Corps of Engineers*, Washington D.C. University of California, Berkeley.

LE NORMANT, C., 2000. Three-dimensional modelling of cohesive sediment transport in the Loire estuary. *Hydrological Processes*, 14, 2231-2243.

LUMBORG, U. and WINDELIN, A., 2003. Hydrography and cohesive sediment modelling: application to the Rømø Dyb tidal area. *Journal of Marine Systems*, 38, 287-303.

MEHTA, A. J., HAYTER, E. J., PARKER, W. R., KRONE, R. B., and TEETER, A. M., 1989. Cohesive Sediment Transport. I: Process Description. *Journal of Hydraulic Engineering-ASCE*, 115, 1076-1093.

MEHTA, A. J. and PARTHENIADES, E., 1975. An Investigation of the depositional properties of flocculated fine sediments. *Journal of Hydraulic Research*, 12, 361-609.

MIGNIOT, C., 1968. A Study of the physical parameters of different very fine sediments and their behaviour under hydrodynamic action. *La Houille Blanche*, 7, 591-609.

PARCHURE, T. M. and MEHTA, A. J., 1985. Erosion of Soft Cohesive Sediment Deposits. *Journal of Hydraulic Engineering-ASCE*, 111, 1308-1326.

PEJRUP, M., 1986. Parameters affecting fine-grained suspended sediment concentrations in a shallow micro-tidal estuary, Ho Bugt, Denmark. *Estuarine, Coastal and Shelf Science*, 22, 241-254.

PEJRUP, M., 1988. Flocculated suspended sediment in a micro-tidal environment. *Sedimentary Geology*, 57, 249-256.

PEJRUP, M. and EDELVANG, K., 1996. Measurements of in situ settling velocities in the Elbe estuary. *Journal of Sea Research*, 36, 109-113.

PEJRUP, M., LARSEN, M., and EDELVANG, K., 1997. A fine-grained sediment budget for the Sylt-Rømø tidal basin. *Helgoländer Meeresuntersuchungen*, 51, 253-268.

POSTMA, H., 1954. Hydrography of the Dutch Wadden Sea. A study of the relations between water movement, the transport of suspended materials and the production of organic matter. *Archives Neerlandaises de Zoologie*, 10, 405-511.

TEETER, A. M., 1986. Vertical Transport in Fine-Grained Suspension and Newly Deposited Sediment. *In*: MEHTA, A. J. (Editor), *Estuarine Cohesive Sediment Dynamics*, Vol. 14, Chap. 9. Springer-Verlag, Berlin, Heidelberg, NewYork, Tokyo, pp. 170-191.

TEISSON, C., 1991. Cohesive suspended sediment transport: feasibility and limitations of numerical modelling. *Journal of Hydraulic Research*, 29, 755-769.

TENGBERG, A., PEJRUP, M., ANDERSEN, T. J., GUILLEN, J., PALANQUES, A., HOVDENES, J., MINKEN, H., INGVALDSEN, R., LOENG, H., JOZSA, J., and SARKKULA, J., 2001. Use of current meters in aquatic research & engineering. *Sea Technology*, 42, 10-18.

VAN DER LEE, W. T. B., 2000. The settling of mud flocs in the Dollard estuary, The Netherlands. *Netherlands Geographical Studies*, 274, 15-121.

VAN LEUSSEN, W., 1994. *Estuarine macroflocs and their role in Fine-grained sediment transport*. Utrecht University.

VAN RIJN, L. C., 1989: *Transport of Cohesive Materials*. Report H 461, pp. 12.1-12.27. Delft Hydraulics.

VAN STRAATEN, L. M. J. U. and KUENEN, PH. H., 1958. Tidal action as a cause of clay accumulation. *Journal of Sedimentary Petrology*, 28, 406-413.

WHITEHOUSE, R. J. S. and H. J. MITCHENER, 1998. Observations of the morphodynamic behaviour of an intertidal mudflat at different timescales. *In*: BLACK, K. S., PATERSON, D. M. and CRAMP, A. (Editors), *Sedimentary Processes in the Intertidal Zone, Geological Society, Special Publication*, London, pp. 255-271.

Journal of Coastal Research	SI 41	124-129	STRAEE 2002	Ferrara, Italy	ISSN 0749-0208

Drogue-based measurements of estuarine suspended sediment characteristics: a new approach

C. Schacht and C. Lemckert

School of Engineering
Griffith University, Gold Coast campus
Queensland, 9726 Australia
c.schacht@griffith.edu.au, c.lemckert@griffith.edu.au

ABSTRACT

SCHACHT, C. and LEMCKERT, C., 2004. Drogue-based measurements of estuarine suspended sediment characteristics: a new approach. *Journal of Coastal Research*, SI 41, 124-129. Ferrara (Italy), ISSN 0749-0208

In situ measurements of estuarine parameters are usually made at fixed sites, strategically chosen to best represent the system. However, this method does not accurately evaluate phenomena occurring between these stationary points (such as the flocculation and deflocculation of suspended sediments). To alleviate this problem, a new drogue was developed so that a specified parcel of estuarine surface water could be followed and its properties monitored over time. The drogue was equipped with a Global Positioning system (GPS) for monitoring the drogues position, an ASM-IV sediment staff for measuring optical backscatterance levels every 1 cm at 6 second intervals, within the top 2 m of the water column, and a Greenspan CTD sensor for monitoring temperature and conductivity of the water parcel at 20 cm depth. Data collected from a trial experiment showed that while the device was beneficial for studying estuarine sediment dynamics, the horizontal scale of estuaries (~100 m) poses limitations on the drogue's use.

ADDITIONAL INDEX WORDS: *Drogue-based instrument, Insitu measurements, Brisbane River, flocculation*

INTRODUCTION

Sediment transport dynamics within estuarine systems have received a lot of attention in the past due to their association with the transportation of pollutants and fine-grained natural elements. The fine-grained particles or Suspended Particulate Matter (SPM) are significant carriers of pollutants due to their ability to adsorb chemicals (MCCAVE, 1979 and VAN LEUSSEN, 1998). SPM often results from natural erosion or anthropogenic inputs such as dredging, agricultural activities, industrial activities and urbanization of upland basins (MOSS, 1992 and HOSSAIN, *et al*., 2001). Suspended sediments in estuaries also pose both economical and environmental problems on the surrounding community due to their inherent ability to be deposited in navigable entrances, thus interfering with the surrounding ecosystems.

Suspended sediments in lakes and estuarine systems can exist in the form of flocs (EISMA, 1986). The term '*floc*' is used to describe an agglomeration of finer primary particles that have joined or 'flocculated' together to form larger secondary particles. KRANENBURG (1994) noted that the findings of KRONE (1963, 1986) and PARTHENIADES (1965) had significantly contributed to our present understanding of a floc structure. One of the most obvious effects of flocculation occurrence is observed within estuaries of high primary particle concentration, whereby the appearance of water can actually 'clean up' due to the agglomeration process. This is because it is the finer particles that scatter light, causing the estuary to appear turbid.

To accurately predict certain processes and phenomena, one must obtain quantitative data derived from in-situ investigations for use in predictive computer modelling. Especially in the field of estuarine sediment dynamics, laboratory-based research is limited due to the difficulty of reproduction or calculation of all necessary parameters. That is, there will always be factors of ambiguity. The quantification of SPM in estuarine systems and coastal waters has been extensively studied especially since MCCAVE, (1979) and DOWNING, *et al*., (1981) documented the potential of Optical Backscatter sensors. Since then, non-obtrusive in situ instruments such as optical instruments, video cameras and drogues (as in this study) have been used (see also the review paper by WREN et al, 2000 for further details of suspended monitoring instrumentation).

Numerous suspended sediment studies conducted in rivers, estuaries and related catchment areas have been conducted throughout the world, the majority being investigated at fixed sites, chosen to best represent the system. A common study is that conducted on established traverses approximately 5 km apart within a tidally influenced river (COX, 1998). But what happens between these sites? Although one is left to assume there is a constant relationship between them, this isn't always the case. Drogues and drifters have been used for years to track and monitor surface currents (RICHARDSON, 1981; KERY and FOLEY, 1995; CRISP and GRIFFITHS, 1995). Drifters (measuring platforms developed to follow the same parcel of water) are ideally designed to provide estimates of changes along the trajectory of the water parcel (RIGHI and STRUB, 2001). The principle of a drogue is adopted in this study to measure the suspended sediment in a constant parcel of water for the duration of a complete tidal cycle.

The objective of this paper is to introduce a novel drogue-based instrument and present some of the preliminary results. These results have indicated that despite the limitations due to the changing water masses in estuaries, the use of this instrument will improve our understanding of sediment dynamics.

DESCRIPTION OF INSTRUMENT

The most effective method of obtaining conclusive data is to combine and synchronise an array of instruments so that different measurements are made in similar water parcels on similar time scales (STERNBERG, 1989). This was adopted when designing the drogue. In its trial experiment (reported here) the drogue carried three self-contained battery-operated instruments. These instruments were the Argus ASM-IV (optical backscatterance) Sediment staff, a Greenspan CTD probe and a portable Global Positioning System.

The drogue-based instrument was primarily designed to track a parcel of upper estuarine water (depths~1 m). This was achieved by attaching a series of four (4) stainless steel vanes to the buoyant portion of the structure (consisting of a resin coated block of high-density foam), which allowed the drogue to flow with the current(see Figure 1.)

The size of the vanes was primarily limited to 500 mm deep, which was sufficient to track the upper water column without interfering with the sample volume of water below. The 5 mm thick detachable vanes can be replaced with longer depth vanes if required. One of the main concerns in designing the whole system was to ensure that the instrument was not directly influenced by the wind. For this reason, the top of the float sat flush with the water surface, while the vanes were placed away from the center in order to minimise influences on the parcel's sediment dynamics

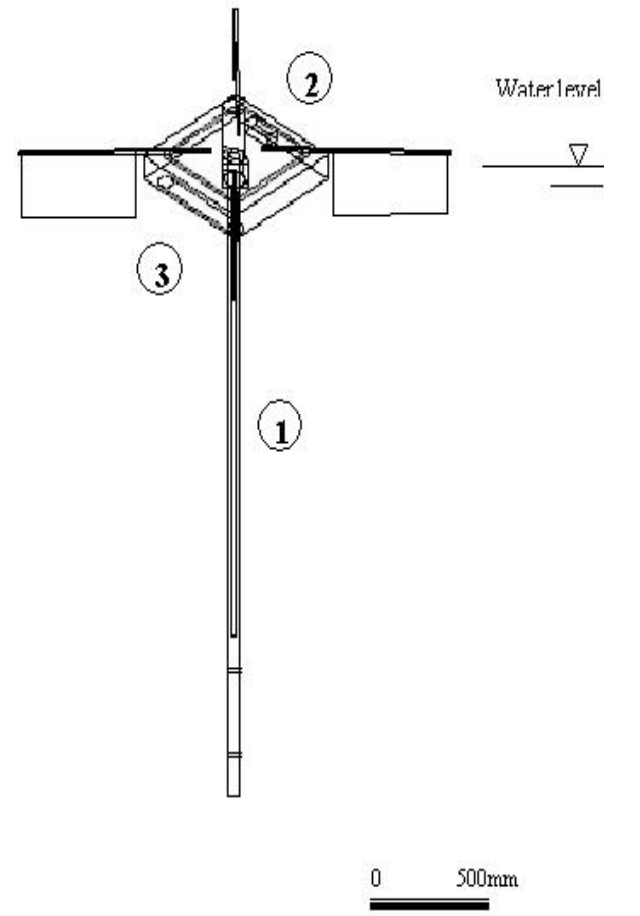

Figure 1. Schematic drawing of drogue-based instrument. (1) ASM-IV Sediment Staff, (2) Lowrance Globalmap-100 GPS and housing, (3) Greenspan CTD350 Multiparameter Sensor.

Sediment staff

The 2-meter Argus Surface Meter, ASM IV (a high-resolution sediment staff) operates with 100 infrared sensors (central optical frequency of 900 nm) per meter. These sensors are located on an active board protected by a clear epoxy resin and embedded in a stainless steel rod. Each sensor samples a fixed volume of approximately 0.5 cm^3, at a fixed distance between 5 and 10mm from the rod. Data from all sensors were logged internally every 6 seconds, with the time stamp synchronised with the other sensors (based on the programming PC clock).

This study documents the first time the ASM-IV Optical Backscatterance Sediment Staff has been used to track a parcel of water; the ASM IV instrument was developed primarily for high-resolution measurements at the bottom of moving water (in a fixed position). The sensors embedded in the Optical Backscatterance staff measure the reflected and refracted light scattered by the suspended particles (MCCAVE, 1979). The advantage of measuring suspended sediment characteristics with a non-obtrusive instrument is that the aggregates or flocs will not be broken up by routine methods of sampling and testing (GIBBS, 1981, 1982; GIBBS and KONWAR 1982, 1983).

GPS – Tracking device

AS WILSON (1999) predicted, the emergence of more advanced telemetry technologies has led to increased usage by drifter designers and researchers. Additionally, the recent advent of the Selective Availability ending in May 2000 has seen the accuracy of the civilian GPS increase threefold. Accuracy has changed from +/- 200m to +/-10m (MELDRUM, 1999). The Lowrance Globalmap-100 Global Positioning System (GPS) was adopted in this study with accuracy between 5-10m. The internal GPS data logger was programmed to update the trail every 10 seconds (maximum capacity of 3000 track points per trail) which allows a running time of approximately five hours. The default GPS setting outputs NMEA 0183 $GPRMC data sentences through a computer serial port using RS232 protocols. The GPS was attached to the top of the drogue in an airtight container; a weatherproof GPS receiver antenna was then connected to the GPS to heighten its receiver results. The principal function of the GPS was to determine the path and relative velocity of the drogue as a function of the time.

Greenspan smart sensors

The Greenspan CTD350 sensor combines the functions of Conductivity, Temperature and Pressure (Depth). This non-cabled sensor (with fully-sealed RS232 connector between the data logger and PC) was fixed to the base of the float (depth 20 cm) and remained submerged at all times. Pressure is measured using a ceramic-faced pressure sensor with a sensing range of 0-10 m and an accuracy of ± 0.07% FS (over temp range ~25ºC). Conductivity is obtained using an integrated toroidal sensor with a range of 0-60000 μS and an accuracy of ± 0.7% FS (over temp range 0-

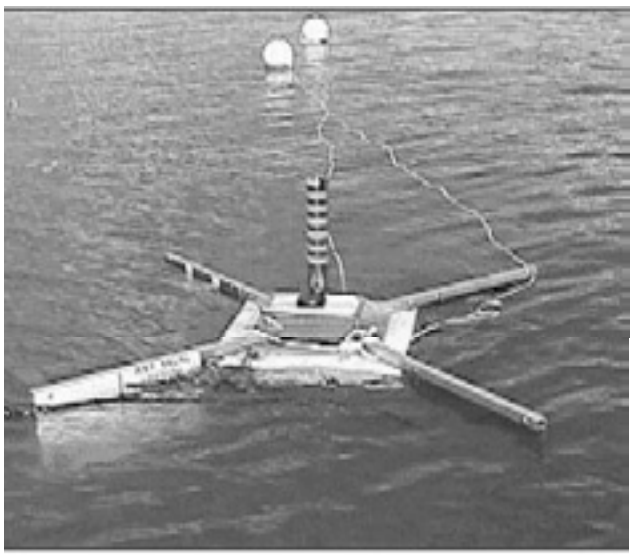

Figure 2. Photograph of Drogue prototype deployed in Brisbane River on 23 August 2002.

50ºC). Temperature was derived from an embedded sensor with a range of 0-50ºC and an accuracy of ± 0.2ºC.

A Greenspan PS310 pressure sensor was deployed separately to monitor the tidal elevation of the estuarine system near the drogue deployment site. The onboard microprocessor converts the output voltage to a 16 bit digital signal so that the software program, SmartCom® can display in real units, i.e. meters of depth.

Both probes use a total of nine Li/Mn02, Lithium Thionyl Chloride 3.6V AA cells. This configuration supplies 10.8 volts at 5.2A/Hr. Whilst sampling, the PS310 and CTD350 have a current draw of 32mA and 70mA respectively. All sensors were sampled and stored every 5 seconds.

METHODOLOGY

Site Description

The unique deep morphology of the Brisbane River and its associated high-concentration of SPM makes it an ideal location to deploy and study the nature of the drogue (see photograph of drogue, Figure 2). The site selection within the Brisbane River was guided by the need to find a convenient location with little or no boat traffic, and which was nominally deeper than 2.3m.

The sub-tropical Brisbane River (Figure 3), one of Moreton Bay's major tributaries, is located in South East Queensland and has a catchment of 13560 km^2 (EYRE, *et al*., 1998). The region is generally dominated by two (2) climatic patterns - summer and winter. The summer months are controlled by heavy rainfall and thunderstorms that result from the moist and unstable subtropical maritime airflows. Conversely, the winter months bring forth the stable anticyclonic air pressure systems with perfect clear skies and light winds (AULICEIMS, 1990).

Several studies have made considerable contribution to the understanding of the Brisbane River (e.g. BENNETT, 1986; MOSS, 1987; ODD and BAXTER, 1980; and RANKIN and MILFORD, 1979). The water quality and physico-chemical parameters associated with the lower reaches of the river were studied by STRAUGHAN(1967) and MOSS (1979 and 1987). A study on the suspended sediment budget (EYRE, *et al*., 1998) found the enhanced sediment trapping ability and turbidity of the river has resulted from years of dredging and anthropogenic modifications of the morphology of the river.

More recently, HOLLYWOOD *et al.,* (2001) conducted an extended study on the sediment dynamics within the Brisbane River. They discovered this highly-modified microtidal estuary experienced a turbidity maximum in the mid-reaches, which was driven by a combination of tidal asymmetry and tidal straining. This persistent feature was the driving force behind the drogue development as it was necessary to design a system that could follow the behaviour of the turbidity maximum during the ebb and flood tide (where turbidity levels were observed to drop significantly).

Trial experiment

A trial experiment to test the drogue was undertaken on 23 August 2002. The weather conditions were generally calm and sunny, although some showers had occurred in the region, prior to the experiment (no gauging data was available). The drogue was deployed approximately two hours before the flood tide and recovered approximately four hours later. The short duration of deployment was necessary as after this time the drogue would have moved into an area of high boat traffic, with significant risk of damage and/or loss.

For this preliminary study a Greenspan PS310 Pressure Sensor, as previously detailed (which utilises a ceramic-based capacitive element as the transducer) was deployed close to the river's edge to monitor the tidal response over a half tidal cycle. The location of the sensor is marked by the number 1 and can be observed in Figure 4.

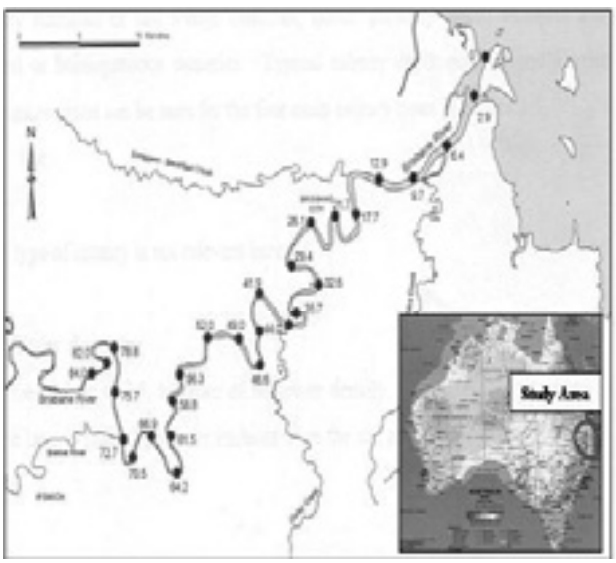

Figure 3. Location of Brisbane River, Queensland with respect to Australia.

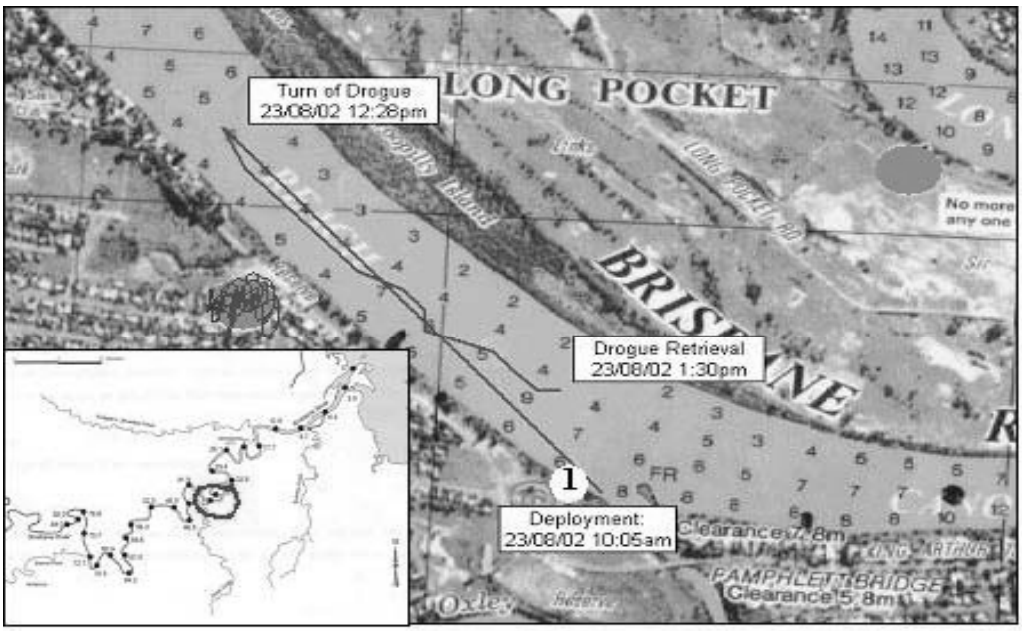

Figure 4: Track of drogue given by GPS unit. Deployment time 10:05 am, turn of tide 12:28 pm and retrieval of drogue 1:30 pm. (1)-Location where the PS310 Pressure sensor was fixed (near the entrance of the Oxley Creek inlet).

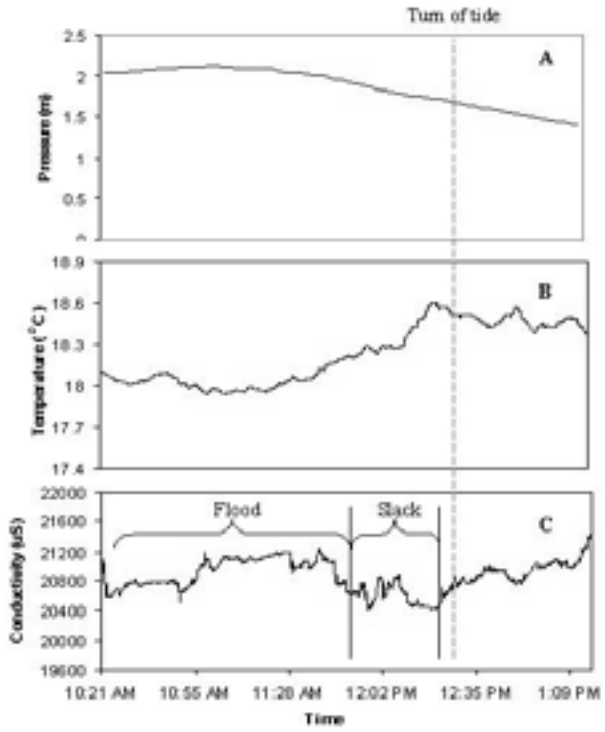

Figure 5. Results from the CTD probe and Pressure Probe. (A) Tidal pressure over stipulated drogue deployment time; (B) Temperature of the water parcel at the drogue; (C) Conductivity readings from the water parcel at the drogue. Slack tide starting at ~11:50 am and finishing at ~11:17 am with the commencement of the ebbing tide.

RESULTS AND DISCUSSION

The results from the preliminary deployment of the drogue-based instrument quantify some of the main governing physical attributes of the Brisbane River. As previously discussed, the recording of the drogue's trajectory in the Brisbane River was achieved by the GPS. Figure 4 shows that the drogue (deployed at 10:05 am) changed its direction from proceeding upstream to downstream at 12:28 pm. This correlates with Figure 5, which suggested that at the change of tide, the drogue started to follow another water parcel of different temperature and conductivity.

As can be seen from Figure 5, the flooding tide reached its peak at 11:20 am on 23 August 2002 and, after this point in time the tide started to reach its slack period at ~11:50 am. The GPS data revealed (see Figure 4) the drogue did not change direction until 12-12:30 am, leaving a time lag between that of the drogue and the actual tide. HOLLYWOOD *et al.,* (2001) also observed a similar tidal velocity lag in the Brisbane River. Figure 5 also presents the conductivity and temperature data derived from the CTD. The data reveals that there was a gradual warming of the surface water until about 12:20 am, when a more rapid change occurred. This warming may have been the result of solar radiation. The conductivity signal varied throughout the deployment, this may have been a result of the tidal straining processes encountered in the estuary. Tidal straining is the name given to the process, which can lead to a decrease in vertical salinity stratification during the ebbing tide. It is caused by an interaction between the vertical sheared tidal currents and the along-channel salinity gradient (SIMPSON *et al.,* 1990).

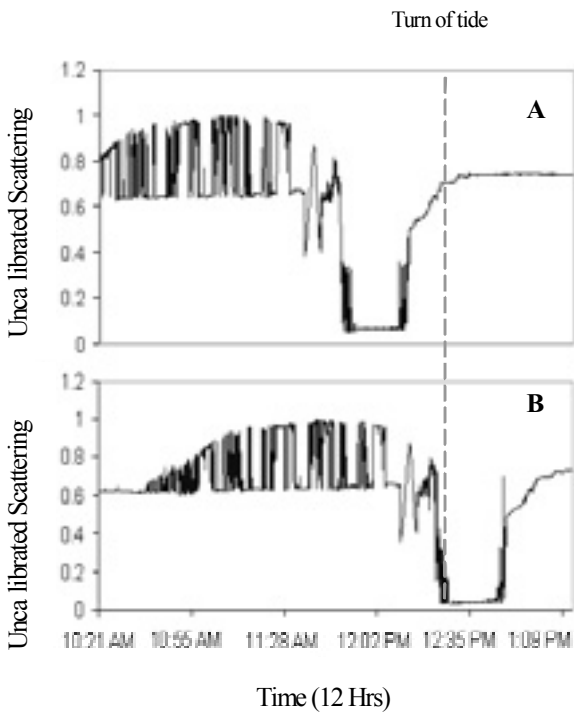

Figure 6. Normalised ASM-IV (Sediment staff) graphs of Backscatter. (A)-Sensor 2 at depth of 22 cm and (B)- Sensor 100 at depth of 122 cm below the water surface. NB: The sensors are numbered ascending from the top of the staff, near the head unit.

Examples of the backscatter data derived from the ASM-IV are graphed in Figure 6. The data presented from sensors 2 and 100 (at depths of 22 cm and 122 cm below the water surface, respectively) were normalised by dividing the recorded values by the maximum recorded by that sensor during deployment. The data reveals that the reflectivity values measured by sensor 2 initially increased until 11:10 am, before decreasing to extremely low values at 11:50 am. At 12:10 pm a dramatic increase in backscatter was observed until 12:15 pm, when it reached and maintained a nearly constant value. Sensor 100 followed a similar trend although the signal lagged that of sensor 2 by approximately 30 minutes. It is likely the unsteady nature observed in the early stages of deployment resulted from tidal straining, which has been shown to cause rapid changes in SPM levels (HOLLYWOOD *et al.,* 2001). The lag indicates the water column was probably stratified, and that the parcel of water that SPM was initially at the surface moved downward through the water column with time; in time suggesting a very complex settling/mixing process was active. This may have been caused by a frontal structure resulting from the inflow of Oxley Creek (location shown in Figure 4), observed during the field trip.

These results suggest that, in addition to the scattering profile data, it is also necessary to determine the vertical salinity/temperature distribution so that vertical changes in these (resulting from different mixing processes) can be quantified. Additionally, determination of the in situ vertical particle size distributions will help distinguish between flocculation and settling, both of which can lead to reduced backscatter, and deflocculation and vertical advection of material, which can lead to enhanced backscatter.

CONCLUSIONS

This paper has presented a unique method for the investigation of sediment dynamics within an estuary; albeit with some limitations. Future deployments will be carried out with simultaneous traverses of the LISST-100 (Laser Insitu Scattering and Transmissometry) sediment-sizer, so the ASMIV-derived turbidity levels can be related to particle distribution (obtained by the LISST-100) as in HOLLYWOOD, *et al*., (2001). One of the major shortcomings of the LISST-100 is its limitation to measure flocs exceeding 250µm. This can pose a problem in estuaries such as the Halifax Inlet where the large flocs or marine snow (>250µm) account for 36-100% of the total suspended particle matter concentrations (SYVITSKI *et al*., 1995). Therefore the use of other methods of obtaining concentration levels and size distributions (such as the AGC Floc Camera Assembly (HEFFLER *et al*., 1991) and the high-resolution video camera (STERNBERG *et al*., 1999) is recommended. The latter method comprises a sediment trap attached to a video camera where time-lapse images of the settling aggregates are taken through the water column.

The LISST (which is also equipped with a Seabird SBE 37i CTD) will also be used to investigate any changes in vertical structure that may arise from tidal straining, or by the drogue encountering and estuarine front. Additionally, a Nortek Vector current meter for recording the background turbulence levels when dissipation rates exceed 10^{-4} m^2/s^3, will be attached to the base of the sediment staff. This will give details of the turbulent levels near the drogue, which will help to quantify the influence of tidal straining and the importance of turbulence in any settling and/or flocculation process. The LISST will assist in determining whether the process is resuspension and/or flocculation, as it will permit the determination of particle size distribution.

It is evident from this investigation that careful considerations must be made when selecting a suitable drogue deployment location. Ideally the site ideally must have no external inputs (including wind and freshwater inflows). While this limits the study sites to some extent, it will certainly enhance our understanding of the water within the upper depths of an estuary.

ACKNOWLEDGEMENTS

The authors would like to thank Charles Allport for his assistance in the construction and deployment of the drogue. The project was financially supported by the CRC for Coastal Zone Estuary and Waterway Management. Special thanks also to the School of Engineering Griffith University for the utilization of their facilities and equipment.

LITERATURE CITED

AULICIEMS, A., 1990. Climates of the Brisbane Valley. *In*: DAVIE., P.; STOCK, E. and LOW CHOY, D. (eds.), *The Brisbane River, a source-book for the future*, Queensland Museum, Brisbane, pp.7-16.

BENNETT, J.C., 1986. Use of Mathematical Modelling in Water Quality Management of the Brisbane River*, Proceedings Hydrology and Water Resources Seminar* (Griffith University, Brisbane).

COX, M.E., 1998. Distribution of Salinity and Other Physico-Chemical Parameters in the Brisbane River Estuary, Moreton Bay. *In*: TIBBETTS, I.R.; HALL, N.J. and DENNISON, W.C. (eds.), *Moreton Bay and Catchment. School of Marine*

Science, The University of Queensland, Brisbane, pp. 185-202.

CRISP, N. and GRIFFITHS, G., 1995. Observations of tidal and wind-driven currents, and acoustic backscatter using an acoustic Doppler current profiler on a surface-following buoy. *In*: ANDERSON, S.P.; APPELL, G.F. and WILLAMS, A.J. (eds.), *Proceedings of the IEEE Fifth Working Conference on Current Measurement*, St. Petersburg, Florida, pp. 30-34.

DOWNING, J.P.; STERNBERG, R.W. and LISTER, C.R.B., 1981. New instrumentation for the investigation of sediment suspension processes in the shallow marine environment. *Marine Geology*, 42, 19-34.

EISMA, D., 1986. Flocculation and de-flocculation of suspended matter in estuaries. *Netherlands Journal of Sea Research*, 20(2/3), 183-199.

EYRE, B.; HOSSAIN, S. and MCKEE, L., 1998. A Suspended Sediment Budget for the Modified Subtropical Brisbane River Estuary, Australia. *Estuarine and Coastal Shelf Science*, 47, 513-522.

GIBBS, R.J., 1981. Floc breakage by pumps. *Journal of Sedimentary Petrology*, 51, 670-672.

GIBBS, R.J., 1982. Floc breakage during HIAC light-blocking analysis. *Environmental Science Technology*, 16, 298-299.

GIBBS, R.J. and KONWAR, L.N., 1982. Effect of pipetting on mineral flocs. *Environmental Science Technology*, 16L, 119-121.

GIBBS, R.J. and KONWAR, L.N., 1983. Sampling of mineral flocs using Niskin bottles. *Environmental Science Technology,* 17, 371-375.

HOLLYWOOD, S.; LEMCKERT, C.; HOWES, T. and NEUMANN, L., 2001. Suspended sediment dynamics in a highly modified microtidal estuary, *Proceedings of Coasts and Ports 2001* (Gold Coast, Queensland, Australia), pp. 517-522.

HOSSAIN, S.; EYRE, B. and MCCONCHIE, D., 2001. Suspended Sediment Transport Dynamics in the Sub-tropical Micro-tidal Richmond River Estuary, Australia. *Estuarine, Coastal and Shelf Science*, 52, 529-541.

KERY, S. and FOLEY, J., 1995. Low Drag Subsurface Buoy with Integral Acoustic Doppler Current. *In:* ANDERSON, S.P.; APPELL, G.F. and WILLIAMS, A.J. (eds.), *Proceedings of the IEEE Fifth Working Conference on Current Measurement* (St. Petersburg, Florida), pp. 30-34.

KRANENBURG, C., 1994. The Fractal Structure of Cohesive Sediemnt Aggregates. *Estuarine, Coastal and Shelf Science*, 39, 451-460.

KRONE, R.B., 1963. A study of the rheological properties of estuarial sediments. *Hydraulic Engineering Laboratory and Sanitary Engineering Laboratory* (University of California, Berkeley), pp. 63-68.

KRONE, R.B., 1986. The significance of aggregate properties to transport processes. *In*: MEHTA, A.J., (ed.), *Estuarine Cohesive Sediment Dynamics.* Springer-Verlag, Berlin, pp. 66-84.

MCCAVE, I.N., 1979. Suspended Sediment. *In:* DYER, K.R. (ed.), *Estuarine Hydrography and Sedimentation*. Cambridge Univ. Press, pp. 131-185.

MELDRUM, D., 1999. Recent Developments at Dunstaffnage: the GPS-Argos Drifter, the Smart Buoy and the Mini Drifter. *In*: ANDERSON, S. P.; TERRAY, E.A.; WHITE, J.A.R. and Williams, A.J. (eds.), *Proceedings of the IEEE Sixth Working Conference on Current Measurement* (Bahia Hotel, San Diego, CA), pp. 75-81.

MOSS, A.J., 1979. Report on a special survey of pesticides and heavy metals in the Brisbane River Estuary in 1978, *Unpublished Report*, Water Quality Council of Queensland.

MOSS, A.J., 1987. Studies of the Trophic Status of the Brisbane River Estuary. *Water*, March 87.

MOSS, A.J.; RAYMENT, G.E.; REILLY, N. and BEST, E.K., 1992. A primary assessment of sediment and nutrient exports from Queensland Coastal catchments.

ODD, N.V.M. and BAXTER, T., 1980. Port of Brisbane Siltation Study, *Proceeding of the International Conference of Coastal Engineering.*

PARTHENIADES, E., 1965. Erosion and deposition of cohesive soils. *Journal of Hydraulics Division,* American Society of Civil Engineers, 91, 105-139.

RANKIN, S.N. and MILLFORD, S.N., 1979. Computer Simulation of Brisbane River - Part 1 Salinity. *Journal of Australian Water and Wastewater Association,* 6 (1), 9-16.

RICHARDSON, P.L., 1981. Gulf stream trajectories measured with free-drifting buoys. *Journal of Physical Oceanography*, 11, 999-1010.

RIGHI, D.D., and STRUB, P.T., 2001. The use of simulated drifters to estimate vorticity. *Journal of Marine Systems*, 29, 125-140.

SIMPSON, J.H., BROWN, J., MATTHEWS, J. and ALLEN, G., 1990. Tidal Straining, Density Currents, and Stirring in the Control of Estuarine Stratification. *Estuaries*, 13(2), 125-132.

STERNBERG, R.W.; SHI, N.C. and DOWNING, J.P., 1989. Suspended Sediment Measurements. *Nearshore Sediment Transport* (Plenum, New York), pp. 231-257.

STERNBERG, R.W.; BERHANE, I. and OGSTON, A.S., 1999. Measurement of size and settling velocity of suspended aggregates on the northern California continental shelf. *Marine Geology,* 154, 43-53.

STRAUGHAN, D., 1967. Intertidal fouling in the Brisbane River, Queensland, *Proceeding of the Royal Soc.* (Queensland), pp. 25-40.

SYVITSKI, J.P.M.; ASPREY, K.L. and LEBLANC, K.W.G., 1995. In-situ characteristics of particles within a deep-water estuary. *Deep-Sea Research 2*, 42(1), 223-256.

VAN LEUSSEN, W., 1988. Aggregation of Particles, Settling Velocity of Mud Flocs: A Review. *In*: DRONKERS, J. and VAN LEUSSEN, W. (eds.), *Physical Processes in Estuaries.* Springer-Verlag, Netherlands, pp. 348-403.

WILSON, T.C.J., 1999. Current and Emerging Satellite Technologies: Implications for Drifting Buoy Design. *In*: ANDERSON, S.P.; TERRAY, E.A.; WHITE, J.A.R. and WILLIAMS, A.J. (eds.), *Proceedings of the IEEE Sixth Working Conference on Current Measurement* (Bahia Hotel, San Diego, CA.), pp. 95-100.

WREN, D.G.; BARKDOLL, B.D.; KUHNLE, R.A. and DERROW, R.W., 2000. Field Techniques for suspended-Sediment Measurement. *Journal of Hydraulic Engineering*, 126(2), 97-104.

Journal of Coastal Research	SI 41	130-140	STRAEE 2002	Ferrara, Italy	ISSN 0749-0208

Circulation and suspended matter distribution in a microtidal deltaic system: the Isonzo river mouth (northern Adriatic Sea)

S. Covelli†, R. Piani†, J. Faganeli‡ and A. Brambati†

† Dip. di Scienze Geologiche, Ambientali e Marine
Università di Trieste
Via Weiss, 2
34127 Trieste, Italia
email: covelli@univ.trieste.it; piani@univ.trieste.it

‡ Marine Biological Station
Fornace 41
6330 Piran, Slovenia
email: jadran.faganeli@uni-lj.si

ABSTRACT

COVELLI, S., PIANI, R., FAGANELI, J. and BRAMBATI, A. 2004. Circulation and suspended matter distribution in a microtidal deltaic system: the Isonzo river mouth (northern Adriatic Sea). *Journal of Coastal Research*, SI 41, 130-140. Ferrara (Italy), ISSN 0749-0208

Two field investigations, under low river flow regime, were conducted in the Isonzo River mouth, Gulf of Trieste, to examine effluent dynamics and suspended sediment characteristics through the water column. The well-marked stratification influences particle size distribution. Multivariate statistical analysis was successfully utilized to define the characteristics and mutual relationships of the water masses in the estuarine zone. The results allow the Isonzo River mouth to be identified as a microtidal, low-energy, fine-grained deltaic system. The highly stratified water column and related hypopycnal flux prevail in the dynamic regime within the lower reach of the distributary mouth. This type of circulation is interrupted during extreme river floods, when the salt-wedge is pushed out of the river mouth.

ADDITIONAL INDEX WORDS: *salt-wedge, mixing zone, statistical analysis*

INTRODUCTION

The evolution of river mouths depends on several factors acting on sediment dispersal and accumulation pattern at different time and space scales. The most important are hydrodynamic parameters, such as tidal motion, river discharge and wave motion. Estuaries develop in coastal areas drowned by postglacial sea-level rise, subjected to daily tidal action, and where the fluvial sedimentary load is relatively small in relation to the dynamic forces that redistribute the terrigenous material. Deltas, on the contrary, are located in areas where these conditions are reversed, although single distributary channels may behave as estuaries themselves (PERILLO, 1995). Several studies have been conducted on river-mouth processes (e.g. WRIGHT and COLEMAN, 1974; WRIGHT, 1977) and focused on modelling the dynamics of river plumes (POULOS and COLLINS, 1994) and water circulation, sediment transport and deposition in estuaries (MEADE, 1972; PAULSON et al. 1989; DYER, 1991; BOLDRIN et al., 1992; KOSTASHUCK et al. 1992; SONDI et al., 1995). River mouths, especially estuaries, are sedimentary traps due to the rapid decrease in flow velocities and fine particle aggregation as consequence of sharp changes in physico-chemical conditions (MENON et al. 1998). Trace metals and contaminants are generally associated with fluvial suspended matter. An understanding of the dynamics of an estuarine system is thus important in the identification of the factors determining accumulation/desorption and to the prediction of the fate of contaminants in these environments (VERLAAN et al. 1998; ZWOLSMAN and VAN ECK, 1999). Following recent investigations into mercury contamination in the Gulf of Trieste (COVELLI et al. 2001; FAGANELI et al. 2003), the Isonzo River has been recognized as the main source of dissolved and particulate heavy metals in this area. However, information on estuarine physico-chemical processes affecting the Isonzo River suspended matter is still scarce.

The aim of this paper is to describe the physico-chemical

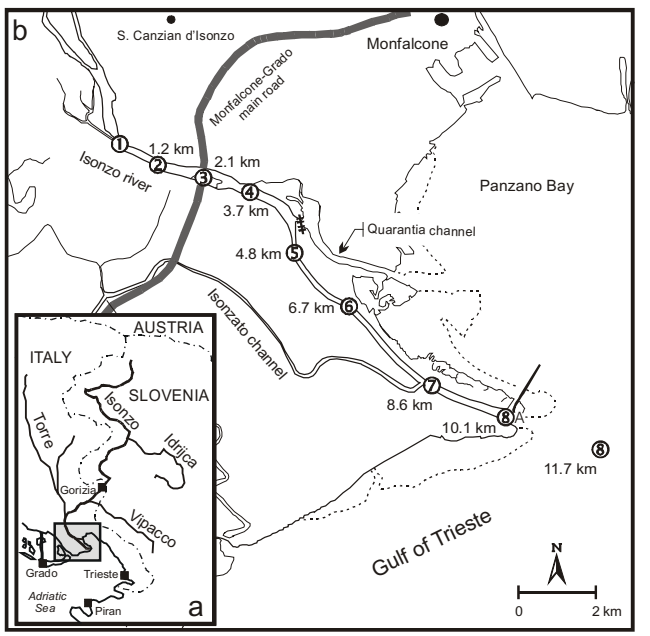

Figure 1: a): The Isonzo River drainage basin; b) the lower river course and location of sampling stations with related distances from the first sampling point.

characteristics of water masses within the Isonzo River channel, and outflow dynamics under relatively low water discharge, in order to identify the presence and extent of the salt-wedge and its influence on suspended matter concentration and grain-size distribution.

ENVIRONMENTAL SETTING

The Isonzo River is the main freshwater input to the Gulf of Trieste, a semi-enclosed marine basin located in the north-eastern Adriatic Sea (Fig. 1a). The surface area of the Gulf is about 600 km^2 and the water depth is generally shallow, reaching a maximum of about 25 m only in the central part of the Gulf. The catchment area of the Isonzo River covers about 3300 km^2, of which 2235 km^2 are located in Slovenia (where its name is Soča River) and the remainder in Italy.

The total river discharge depends in part on the water supply from its major tributaries (Idrijca, Torre-Natisone and Vipacco) and from the spring line located about 15 km upstream of the mouth. The average annual flow rate at the river mouth was estimated to be 80-110 $m^3\ s^{-1}$ (or 3.9 x $10^8\ m^3\ month^{-1}$) by OLIVOTTI et al. (1986), 170 $m^3\ s^{-1}$ by ŠIRCA et al. (1999) and 196.8 $m^3\ s^{-1}$ (43.1-665.9 $m^3\ s^{-1}$) based on more recent daily data (INTERREG II, 2001; Fig. 2). The river discharge shows significant seasonal variations, with two typical flood events governed by snowmelt and rainfall: a relatively long spring maximum (March-May) and a shorter, but more intensive, early autumn maximum (September-November), when the rate of flow can exceed 2500 $m^3\ s^{-1}$ (RAFVG, 1986). According to MOSETTI (1983), the mean annual solid discharge is 150 g m^3, with peaks of 1000 g m^3 during extreme events. Construction of artificial reservoirs for hydroelectric purposes is presumed to have reduced the sediment supply to the delta in the last eighty years. The estimated average sedimentation rate obtained by ^{210}Pb determination amounts to 1.84 mm yr^{-1} in the mid-Gulf (COVELLI et al., 2001), and 2.5 mm yr^{-1} in the coastal area in front of the river mouth (OGORELEC et al., 1991). Fluvial inputs

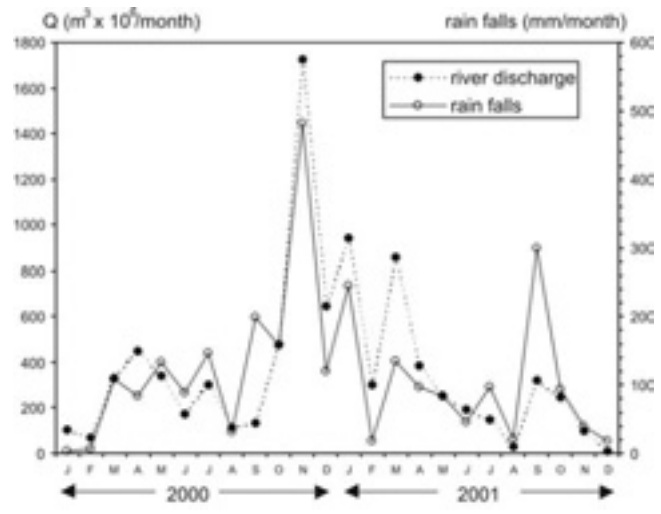

Figure 2: Comparison between average monthly rate of flow estimated at 15 km from the river mouth (INTERREG II, 2001) and mean monthly rainfall near Gorizia (data from ARPA FVG).

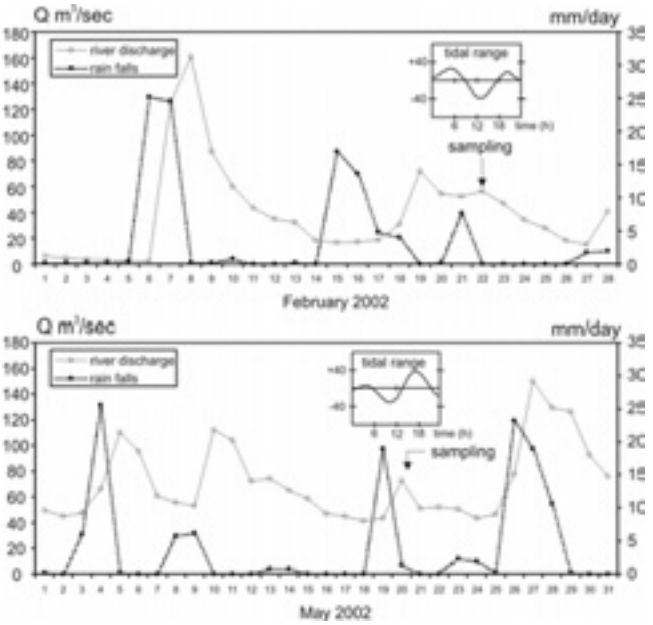

Figure 3. Comparison between average daily river discharge estimated at 15 km from the river mouth (data from RFVG, pers. comm.) and daily rainfall near Gorizia (data from ARPA FVG) in the sampling periods.

appear to control primary production throughout the coastal marine system, as high contents of nutrients, especially nitrate, which determine phytoplankton blooms, are associated with the highest river discharges (MALEJ et al., 1995; SALVI et al., 1998).

Currently, the Isonzo River mouth can be considered a stable straight and finger-like river-dominated delta (BRAMBATI, 1970) with river banks built up to prevent floods in the surrounding reclaimed areas. A delta bar crest faces the main distributary channel, which extends into the shallow waters of the Gulf of Trieste. A secondary river branch, the Quarantia channel, was active from the beginning of the 20th century until 1937, when a barrage was built to avoid transport and settling of sediments in Panzano Bay and, especially, into the navigation channel towards Monfalcone harbour. Medium to fine sands and pelitic sands prevail along the littoral zone on both sides of the river delta. The distribution pattern of fine deposits in the prodelta zone is related to the expansion of the fluvial plume in the Gulf and is characterized by grain-size decrease, from very sandy pelites near the river mouth, to pelites in the mid-Gulf and at depths greater than 6-7 m in Panzano Bay (BRAMBATI et al., 1983). The prodeltaic sediments are primarily carbonates, originating from Mesozoic limestone and dolomite, with secondary quartzo-feldspathic material derived from Eocene flysch, all of which are exposed in the Isonzo river drainage basin (STEFANINI, 1968). The water circulation system in the Gulf is affected by the action of winds (E-NE) and tides (average and spring ranges of 0.5 and 1 m, respectively).

The main circulation is anticlockwise and affects the whole northern Adriatic, acting on deep water layers flowing permanently at 2-3 cm s^{-1}. Wind-driven superficial currents characterize the uppermost water mass, to a depth of about 5 m, flowing anticlockwise with easterly winds and clockwise with westerly winds (STRAVISI, 1983; MALACIC, 1991).

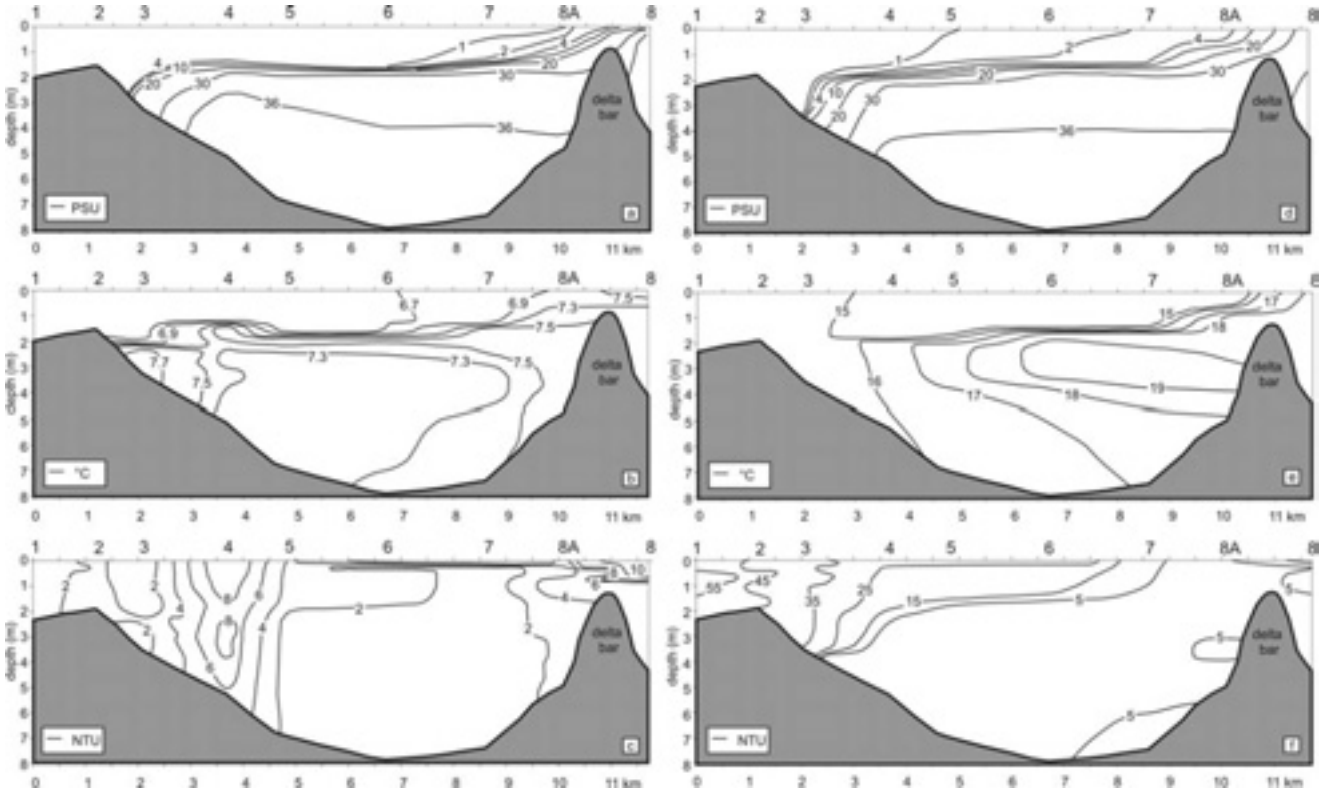

Figure 4. Schematic representation of salinity (PSU, Practical Salinity Unit), temperature (°C) and turbidity (NTU, Nephelometric Turbidity Units) in the lower river course in February (a, b, c) and in May (d, e, f) 2002.

EXPERIMENTAL METHODS

Field activities were carried out in two campaigns, both of them under low hydrodynamic flow regime (Fig. 3): the first one following a period of lower water discharge in February 2002 (56 m^3 s^{-1} during the sampling day) and the second, during a period of relatively higher water discharge (73 m^3 s^{-1} during the sampling day), in May 2002, after one day of heavy rains. Nine sampling stations were selected along the lower Isonzo river course (Fig. 1b), the first one about 11 km upstream from the mouth. Sampling was conducted from a boat along the main axis of the river channel starting from the sea (station 8), in both cases during neap flood-tide conditions. It is important to point out that in May, river flood flow reached station 6 while sampling operations were still in progress. Basic hydrographic parameters (pressure, temperature, salinity, turbidity) were recorded by CTD Hydrolab H_2O Multiprobe with a 0.1 dbar pressure step. Water samples were collected by means of a Niskin bottle (5 liters capacity) at the surface (i.e. 5-s; s=surface), at the bottom (i.e. 5-b; b=bottom) and at variable depths, according to the salinity profiles (i.e. 5-m; m=intermediate). Oxygen concentrations in water samples were determined using the Winkler method (GRASSHOFF et al., 1983). Along with salinity profiles reported in PSU (Practical Salinity Unit), the salinity was also measured (in ‰) on Niskin bottle samples using the Mohr-Knudsen titrimetrical method (STRICKLAND and PARSONS, 1972). To determine total suspended matter (TSM) concentrations, water samples were filtered on Whatman fibreglass GF/F (diameter 47 mm, 0.8 µm pore size) filters, pre-treated at 450 °C (STRICKLAND and PARSONS, 1972). Particulate organic carbon (POC) and total nitrogen (PN) contents, expressed as percentage of total solid and concentration (mg l^{-1}) in filtered water samples, were determined after acidification with 1 N HCl (HEDGES and STERN, 1984), using a Perkin Elmer CHN Elemental Analyser. Particle size analysis in the range 9-4 phi (1.95-62.5 µm) was performed by using a Coulter Multisizer II (Coulter Electronics Ltd., 1972). The Accucomp programme was used to acquire and process grain-size spectra.

RESULTS AND DISCUSSION

Hydrography and suspended matter

Spatial variability for salinity, temperature and turbidity in the river mouth section is shown schematically in Fig. 4a-e for lower (February) and higher (May) river discharges. At stations 1, 2 and 3 the temperature (averaging 6 and 15 °C, respectively) and salinity (< 1 ‰, < 2 PSU) values are homogenous through the water column and typical of riverine waters. Only in February, at the bottom of station 3, were intermediate salinity waters (16 ‰) detected (Fig. 5). These are formed by mixing of riverine and marine waters at the salt-wedge tip, always present in the river during low river discharge and shifting its position landward according to tidal range (RAFVG, 1995). In the central sector of the river mouth (stations 4, 5, 6 and 7), vertical salinity profiles allow a very sharp halocline between the surficial freshwaters and the bottom saltwaters to be distinguished. At station 8A, just before the delta bar, the trend of the vertical salinity profile

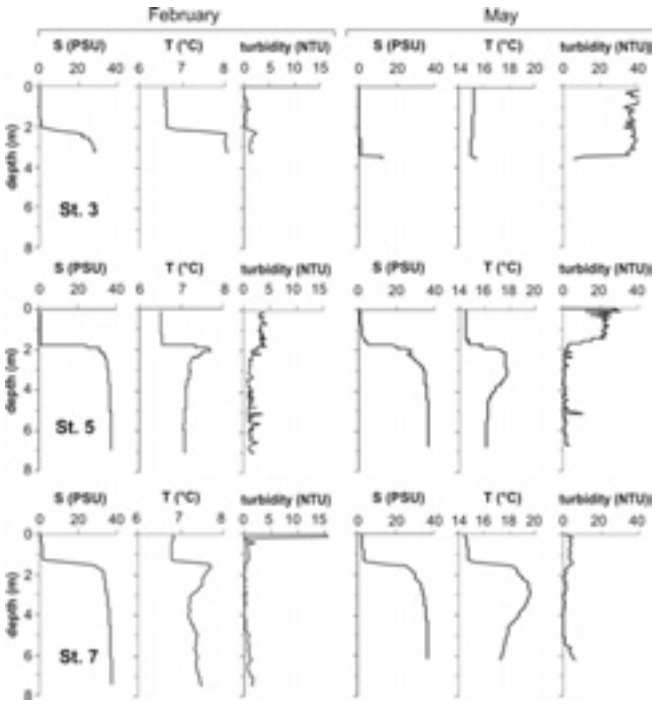

Figure 5. Vertical profiles of salinity (PSU, Practical Salinity Unit), temperature (°C) and turbidity (NTU, Nephelometric Turbidity Units) in sampling stations 3, 5 and 7 (February and May 2002).

suggests an increase in mixing between the fresh and salt water layers as the delta bar is approached. This intensified vertical mixing and entrainment can be explained in terms of breaking of internal waves (WRIGHT and COLEMAN, 1974; DYER, 1991), which also causes turbulence and an increase in turbidity values (Fig. 4c).

Temperature variability in the water column is small in winter (6.5-8.3 °C), whereas in spring, the range is much larger (14.3-19.6 °C). In comparison with February, the May data show a clear thermal stratification in the saline water mass, with a warmer layer at the top of the salt-wedge, just below the freshwater interface. Such a layer is restricted to a maximum of 30-40 cm vertical thickness (Fig. 5).

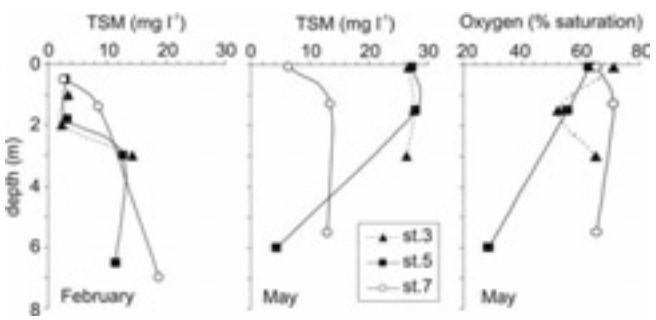

Figure 6. Vertical profiles of suspended load (TSM, mg l^{-1}) and dissolved Oxygen (% saturation) in stations 3, 5 and 7 (February and May 2002).

Turbidity values are generally very low in February (2-4 NTU, Nephelometric Turbidity Units), although maxima at sampling points 4 and 5 (6-8 NTU) characterize the interaction between fluvial and salt waters (Fig. 5). In May, this parameter is clearly related to the moderate flood event, showing the highest values (up to 55 NTU) in stations 1 and 2.

Dissolved oxygen concentration, measured only in May, exhibits a general decrease from the surface throughout the water column (Fig. 6). Undersaturated values at the bottom decrease from the sea (81.3 %, station 8) upstream to the salt-wedge tip (24.5 %, station 4). Oxygen depletion is due to respiration processes and consequent mineralization of organic matter in the salt-wedge. The low rate of exchange across the halocline implies that the residence time of the saline bottom water in the fluvial channel is probably long. The water can be renewed during the spring tide period of high current velocities or following intense floods which completely flush the sea water from the river mouth (DYER, 1991).

In February, TSM concentrations show a rapid increase from the surface to the riverbed (Fig. 6). The freshwaters layer is characterized by low TSM values (2 mg l^{-1}) in comparison with the intermediate depths (3-12 mg l^{-1}) and the saline bottom layer, where values are at a maximum (about 19 mg l^{-1}). An opposite vertical trend can be recognized in the data from the May sampling campaign, between station 4 and 6, where flood waters flow over the salt-wedge. Suspended loads at the surface reach up to 28 mg l^{-1}.

In February, particulate organic carbon (POC) and nitrogen (PN) varied within the ranges 0.7-14.6 % and 0.1-2.2 %, respectively. A general decrease of these parameters from the surface to the bottom layer was observed. In May, the corresponding POC and PN ranges were 1.1 %-11.8 % and 0.2-2.5 % respectively and intermediate depth samples showed higher percentages than both surface and bottom samples. The values for the Isonzo River are very close to the results obtained for the Adige (BOLDRIN et al., 1992) and Po (PETTINE et al., 1998) Rivers, the main water courses draining into the Adriatic Sea. POC and PN values are highly correlated (Fig. 7a), confirming that organically bound nitrogen was dominant in the estuarine suspended matter.

Significant inverse relationships between percentage values of POC and PN and suspended matter load were observed (Fig. 7b), similar to those reported for the Po River by PETTINE et al. (1998), and for most rivers in the world by MYBECK (1982). According to the last author, this is because autochthonous particulate matter is mixed with land-derived particles poor in organic content. This theory is supported by the marked positive linear relationship between carbonate contents and TSM (Fig. 7c). The distribution of POC (Fig. 7d) and PN (mg l^{-1} and %) as a function of salinity show similar relationships, thus indicating that physical processes such as advection and turbulent mixing control organic matter concentration. The POC/PN ratios varied between 4.4 and 8.7 in February, and between 5.1 and 7.3 in May. These values denote a freshwater and/or marine phytoplankton contribution (WAFAR et al., 1989; SULLIVAN et al., 2001).

The well marked stratification also affects particle size distributions of suspended matter along the river course and, vertically, in the water column in low discharge conditions (Fig 8). Grain-size spectra in the freshwater layer are usually skewed, poorly sorted and dominated by fine particles, with the mode ranging from 6.6 to 14.7 μm. In the mixing zone, particle size distributions show an abrupt increase in the fine fraction when compared with surface samples.

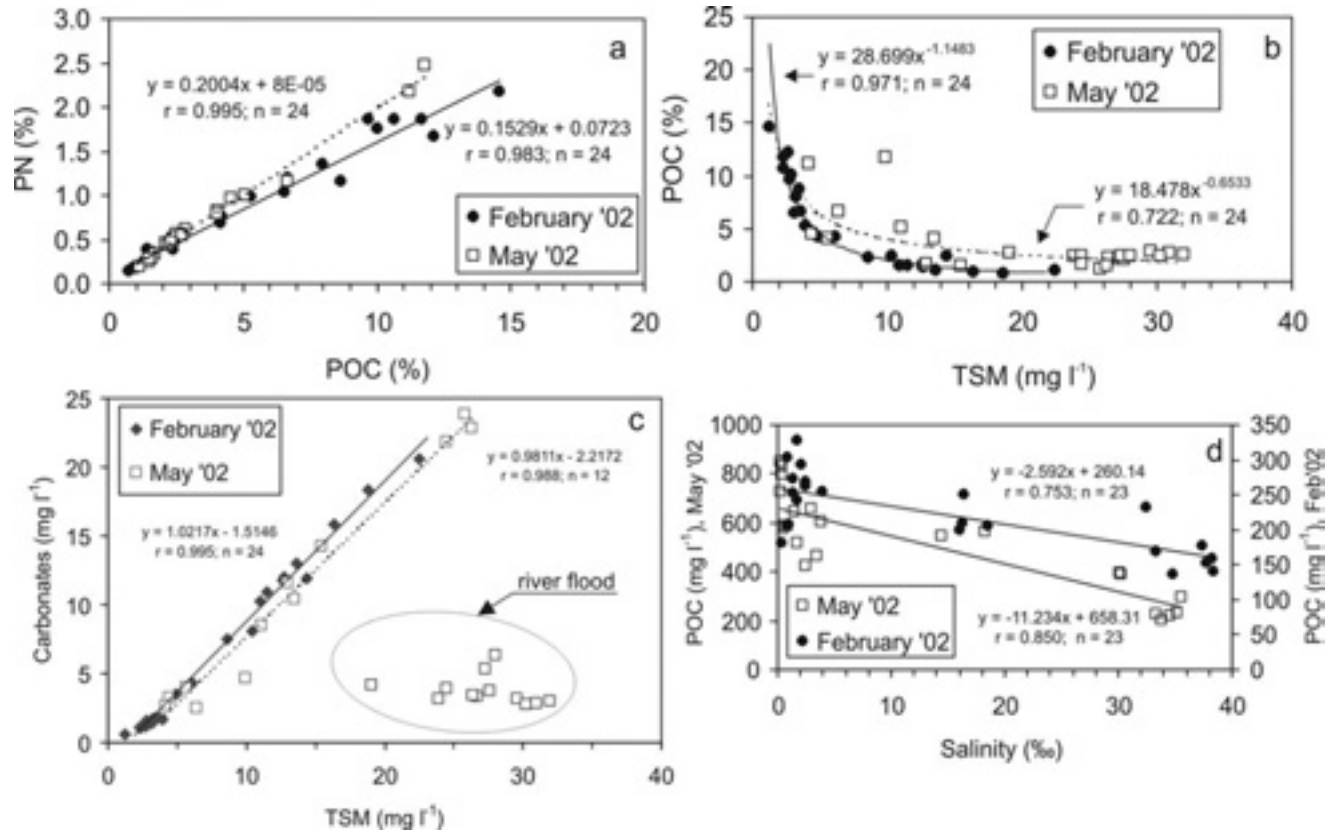

Figure 7. Relationship between POC and PN (a), POC and TSM (b), carbonate content and TSM (c) and POC and salinity (d) in the two sampling periods.

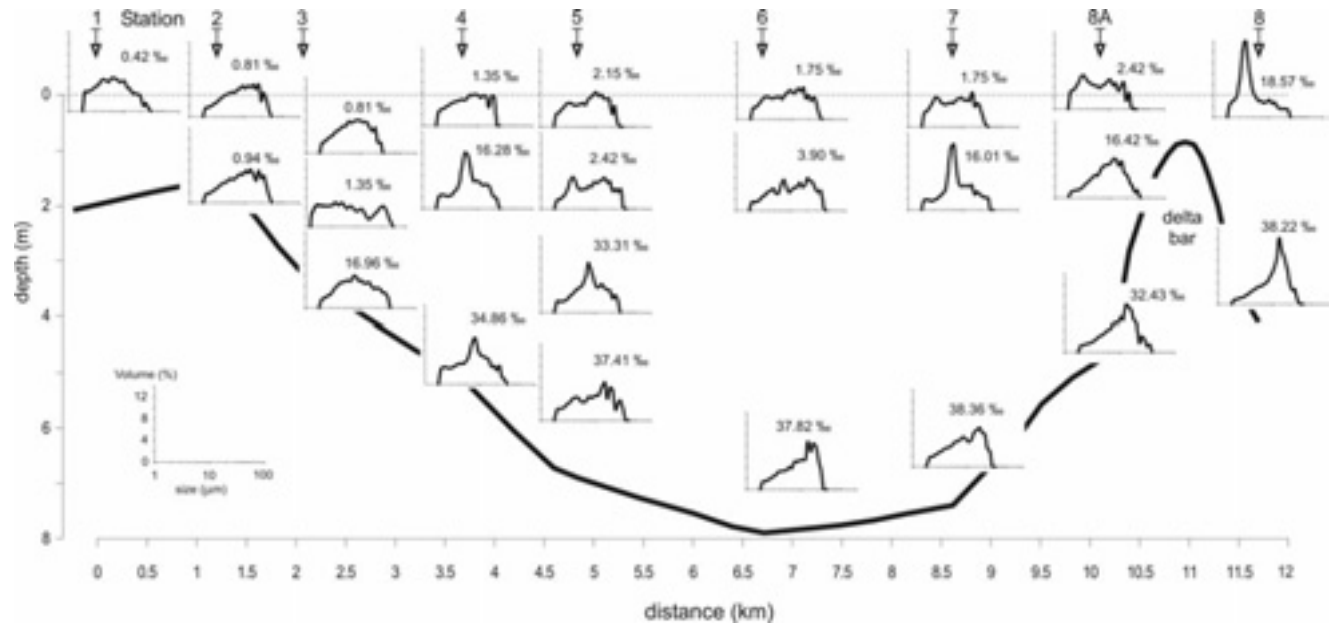

Figure 8. Grain-size spectra (volume %) of suspended matter in the Isonzo river mouth at low stage (February 2002). Salinity values (‰) for each sample are reported.

This typical sharp peak could be due to phytoplankton predominance and, particularly, to the aggregation of diatom cells influenced by low salinities (EISMA, 1993), water column stratification, low rainfall and nutrient availability (JONES et al. 1998, ORIVE et al., 1998).

Microscopic analyses confirmed the abundance of phytoplankton (mainly *Thalassionema nitzschioides, Pseudo-nitzschia seriata, Chaetoceros affinis*) in the mixing layer.

In this layer, the relative abundance is four times higher than at the surface and twice higher than at the river bottom, respectively (CABRINI, pers. comm.). In the bottom layer of the salt-wedge, the size spectra are positively skewed with coarser modal class between 12.8 and 16.0 µm. This particle size distribution is also evident in front of the river mouth (station 8), thus indicating that the source of particles does not seem to be the fresh layer across the halocline, but a slow inflow of seawater intruding the lower river course at the bottom.

Statistical analysis

The variability of the two data sets has been systematically examined using factor analysis, in order to provide information on the dynamics of particulate matter and water bodies in the river mouth. This multivariate statistical technique has been widely and successfully utilized in studies of coastal (IMBRIE and VAN ANDEL, 1964; KLOVAN, 1966) and estuarine (VASCONCELOS et al., 1995; VERLAAN et al., 1998) environments. Q-mode factor analysis was applied to suspended matter (grain-size, TSM, POC and PN) and physico-chemical parameters (T and S) in order to discriminate the main sample populations for each sampling. Varimax rotation was used as a best-fit procedure on the original data matrix. For the February sampling, factor loadings along with communalities, Eigenvalues, and percent of total variance accounted for are reported in Table 1a. Two factors account for the 95.69 % of the total variance. The first rotated factor, contributing 58.16 % of total variance, is related to freshwater samples, whereas the second factor is associated with seawater samples. The surficial sample of station 1 (1-s) and the bottom sample of station 7 (7-b) are the two end-members (Fig. 9a). Three main groups of samples are clearly distinguished from the binary relationship of the two factor loadings (Fig 9b). They reflect the characteristics of the main water bodies and their vertical stratification in the river mouth. The first group identifies fluvial samples (0.42-2.42, 1.84 ‰ avg salinity), collected at the surface along the whole river course from station 1 to station 8A, just before the river bar, and at the depth between 1.5-2 m at sampling points 2, 3, 5 and 6.

Table 1a: Q-mode Varimax rotated factor matrix for samples from February 2002

Variables	Factor 1	Factor 2	Communality
1-s (0.2m)	0.993	0.091	0.994
3-m (2.0m)	0.993	0.091	0.994
4-s (0.5m)	0.992	0.105	0.995
7-s (0.5m)	0.992	0.107	0.996
6-s (0.5m)	0.992	0.110	0.996
5-s (0.5m)	0.992	0.112	0.997
3-s (1.0m)	0.992	0.113	0.997
8A-s (0.2m)	0.991	0.104	0.993
5-ms (1.8m)	0.991	0.115	0.995
2-b (1.5m)	0.990	0.111	0.992
2-s (0.2m)	0.987	0.115	0.987
6-m (1.8m)	0.969	0.169	0.968
8-s (0.2m)	0.810	0.400	0.816
8A-m (1.0m)	0.670	0.710	0.953
3-b (3.0m)	0.653	0.726	0.953
7-m (1.4m)	0.639	0.656	0.839
4-m (1.5m)	0.447	0.780	0.808
5-b (6.5m)	0.159	0.956	0.939
5-mb (3.0m)	0.143	0.976	0.973
8-b (3.5m)	0.131	0.949	0.918
4-b (5.0m)	0.035	0.981	0.964
8A-b (4.0m)	0.028	0.969	0.940
6-b (7.0m)	-0.006	0.987	0.974
7-b (7.0m)	-0.061	0.990	0.984
Eigenvalues	*13.957*	*9.007*	
Total Variance	*58.16%*	*37.53%*	

Table 1b: Q-mode Varimax rotated factor matrix for samples from May 2002

Variables	Factor 1	Factor 21	Factor 3	Comm.
3-m (1.5m)	0.946	0.237	0.214	0.997
2-s (0.1m)	0.945	0.226	0.235	0.999
3-s (0.1m)	0.944	0.228	0.231	0.996
2-b (2.0m)	0.942	0.230	0.236	0.996
3-b (3.0m)	0.937	0.229	0.257	0.996
5-s (0.1m)	0.926	0.249	0.270	0.992
5-m (1.5m)	0.919	0.287	0.259	0.994
1-b (0.5m)	0.915	0.216	0.299	0.973
4-s (0.1m)	0.908	0.203	0.335	0.978
1-s (0.1m)	0.896	0.204	0.357	0.972
4-m (1.8m)	0.877	0.296	0.367	0.991
6-s (0.1m)	0.839	0.206	0.486	0.983
6-b (6.5m)	0.141	0.950	0.251	0.985
8-b (3.0m)	0.344	0.933	0.051	0.991
7-b (5.5m)	0.138	0.931	0.321	0.989
8A-b (3.0m)	0.45	0.880	0.120	0.991
8-s (0.1m)	0.442	0.877	0.164	0.991
4-b (4.0m)	0.144	0.631	0.758	0.993
5-b (6.0m)	0.156	0.580	0.797	0.996
7-m (1.3m)	0.523	0.383	0.758	0.995
8A-m (0.5m)	0.432	0.363	0.819	0.989
6-m (1.5m)	0.344	0.168	0.916	0.986
7-s (0.1m)	0.457	0.044	0.886	0.996
8A-s (0.2m)	0.381	0.012	0.923	0.997
Eigenvalues	*11.613*	*5.896*	*6.256*	
Total Variance	*48.39%*	*24.57%*	*26.07%*	

These samples (Table 2a) show, on average, low contents of TSM (3.16 mg l^{-1}) and low T (6.82 °C), whereas high contents of POC (90.07 µg mg^{-1}), PN (14.63 µg mg^{-1}) and high POC/PN ratios (7.17) were observed in comparison with bottom samples recovered from station 4 to station 8, and belonging to the third "saltwater" group (32.43-38.36, 36.06 ‰ avg salinity). In fact, for this group, the minimum POC and PN contents (11.48 and 2.19 µg mg^{-1}, respectively) and POC/PN ratio (6.35) are associated to maximum TSM values (15.21 mg l^{-1}) and higher temperature (7.30 °C), although the highest value for this parameter affects the mixing layer (7.68 °C). Only five samples, belonging to the second group, show intermediate salinity values (16.01-18.57, 16.85 ‰ avg), thus representing the freshwater-seawater mixing zone. Interfacial shear stress causes some entrainment of saltwater in the river water and an upward exchange of mass from the salt layer to the fresh layer (WRIGHT and COLEMAN, 1974). However, because of the stable density gradient, outlined by the sharp halocline revealed from CTD profiles and due to the relatively low velocity of the river current, mixing and turbulence are considerably reduced at the interface between the two water masses.

The Q-mode procedure, applied to the data matrix of late spring sampling, gave three factors accounting for 99.03 % of the total variance (Table 1b). The "end-member" samples are 3-m, 6-b and 8A-s, respectively, corresponding to three distinct groups of samples (Fig. 10a): freshwater samples, which belong to the moderate flood event, falling close to Factor 1; saltwater samples occurring near Factor 2; and freshwater and moderately salty samples identifying Factor 3. The last are found within the lower river course, which had not been reached by the flood event while sampling was in progress. Table 2b summarizes the average values of single parameters for each group. At the beginning of the flood event, fresh waters tend to be highly stratified and limited to the surface, filling the whole channel as river discharge increases. In May, flood waters had reached station 6 at the surface while the salt-wedge was still present upstream, at the bottom of station 4. During flood events, it was estimated, through in situ current-meter measurements, that freshwater takes from four to eight hours to reach the river bed (RAFVG, 1995). The same study showed that the value of the surface current speed (more than 120 cm sec^{-1}) is twice that recorded at the bottom. The salt wedge can be pushed completely seaward, to a position just outside the bar crest, during peak fluvial discharges. After a flood event, marine waters enter the river and move upstream depending on river flow and tidal fluxes. Tidal current speed is approximately 10-15 cm sec^{-1} in flood tide conditions (RAFVG, 1995).

For the May flood event, three distinct water masses interact along the estuarine section, as shown schematically in Fig. 10b.

Table 2a: Mean values (±std) of hydrographical parameters, TSM and the main compositional parameters for the three groups of samples recognised by factor analysis (February 2002).

parameter	unit	freshwaters (n=12)		mixing zone (n=5)		saltwaters (n=7)	
TSM	mg l^{-1}	3.16	±1.17	10.19	±3.68	15.21	±4.23
POC	µg mg^{-1}	90.07	±30.58	25.96	±9.51	11.48	±2.93
PN	µg mg^{-1}	14.63	±4.55	4.77	±1.60	2.19	±0.84
POC	µg l^{-1}	255.79	±42.49	242.08	±60.72	166.78	±32.26
PN	µg l^{-1}	41.91	±6.86	44.91	±11.26	31.09	±6.68
C/N		7.17	±0.84	6.31	±0.63	6.35	±0.92
T	°C	6.82	±0.35	7.68	±0.32	7.30	±0.12
S	‰	1.67	±0.96	16.85	±1.02	36.06	±2.49
turbidity	NTU	2.43	±2.55	8.72	±11.22	2.81	±2.09

Table 2b: Mean values (±std) of hydrographical parameters, TSM and the main compositional parameters for the four groups of samples recognised by factor analysis (May 2002).

parameter	unit	river flood n=12		saltwedge-upper limit n=2		fluvial waters n=5		saltwaters n=5	
TSM	mg l^{-1}	27.17	±3.54	5.01	±0.87	9.02	±3.73	20.99	±6.29
POC	µg mg^{-1}	24.46	±2.29	43.28	±3.61	77.49	±35.36	14.87	±2.11
PN	µg mg^{-1}	5.12	±0.56	8.96	±1.10	15.22	±7.51	2.65	±0.49
POC	µg l^{-1}	665	±111	215	±20	634	±305	306	±83
PN	µg l^{-1}	139	±27	44	±2	126	±69	54	±15
C/N		5.59	±0.22	5.65	±0.22	6.02	±0.41	6.60	±0.51
T	°C	15.07	±0.48	16.14	±0.03	15.24	±0.86	18.11	±0.99
S	‰	1.15	±1.17	33.53	±0.34	12.07	±8.71	33.15	±2.73
turbidity	NTU	36.35	±13.37	1.00	0.00	4.31	±1.69	5.24	±6.35
O_2	µmol l^{-1}	203.10	±29.91	66.38	±6.65	198.18	±10.69	163.03	±31.11
O_2	%	65.13	±9.69	26.52	±2.79	68.22	±3.76	67.58	±13.46

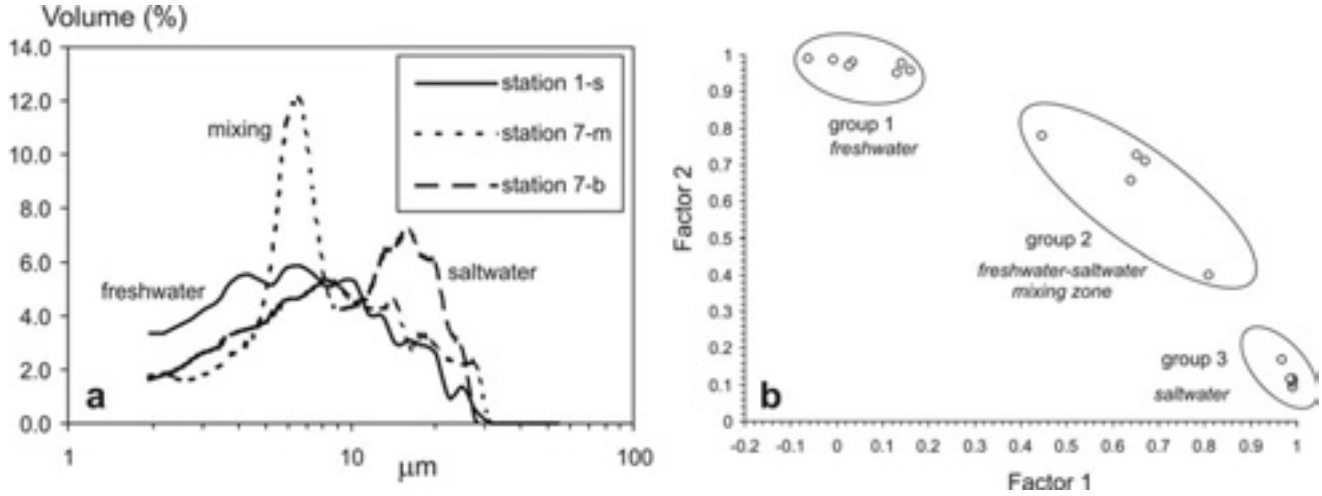

Figure 9. a) Typical grain-size spectra of suspended matter in freshwater (station 1-s), saltwater (station 7-b) and the mixing layer (station 7-m) in February 2002. b) Plot of factor loadings on the two factor axes for samples collected during the February 2002 campaign.

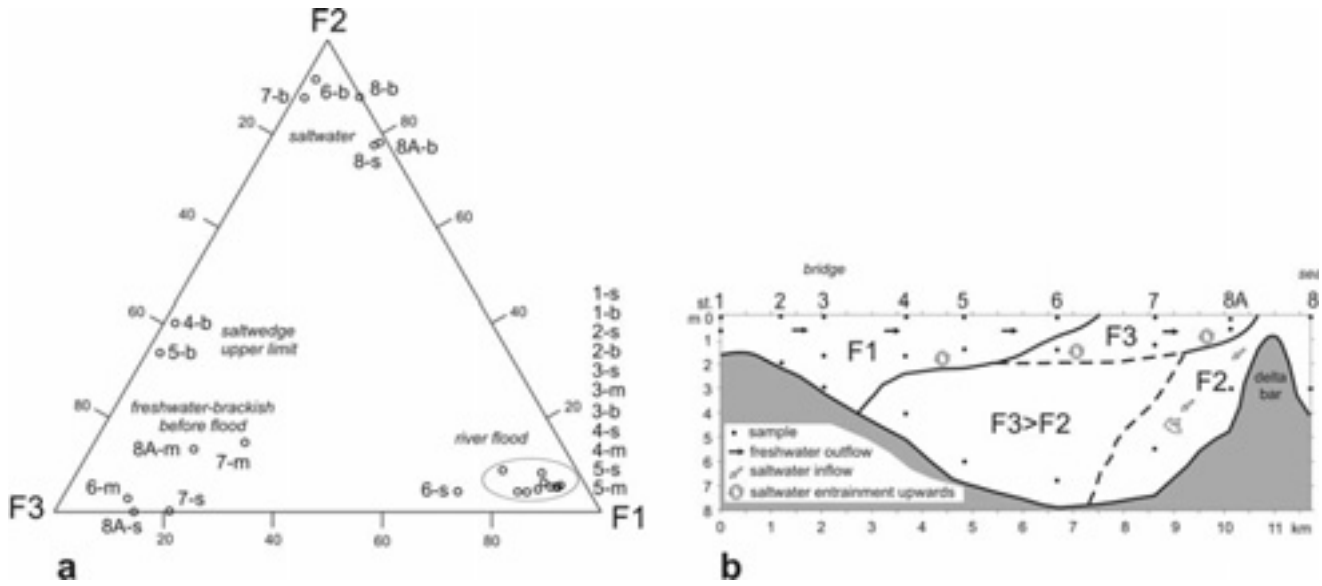

Figure 10. a) Plot of normalized factor components for samples collected during the May 2002 campaign. b) Schematic representation of the relationship between water masses and the three main factors in the lower river course (May 2002).

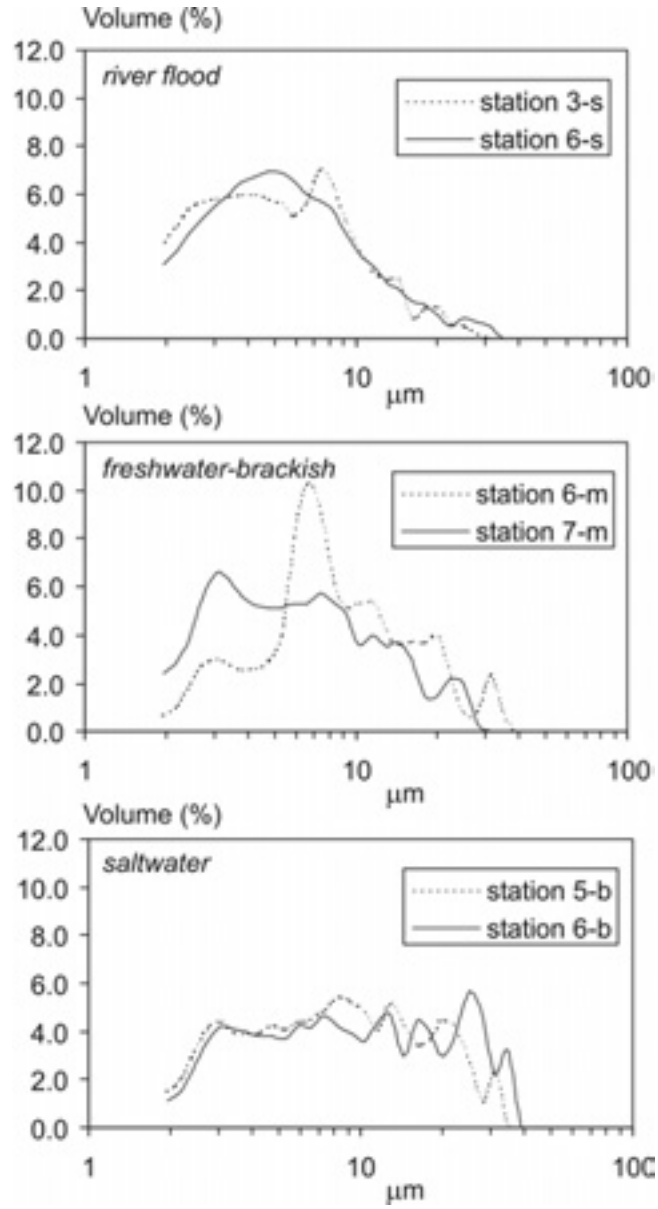

Figure 11. Representative grain-size spectra of suspended matter samples collected during the May 2002 campaign.

Grain-size spectra of TSM along the estuary (Fig. 11) are marked by two main sources, very fine river-borne and coarser marine particles. Particle size distributions are similar through the water column (mode 7.4 μm) in stations 1, 2 and 3, indicating homogenous transport conditions.

At low stage, although fluvial particles are partly affected by aggregation/flocculation in the mixing layer, it seems that fluvial suspended sediments do not settle in the channel. Because of the higher surficial river flow and the stratification, they are transported seaward of the mouth bar to the prodelta area and over even longer distances during flood periods (WRIGHT and COLEMAN, 1974). As demonstrated by the similarity of particle spectra of TSM above the bottom in front of the river mouth and in the channel, wave energy would contribute to resuspension of particles in the water column and tidal flux would provide the necessary energy for transporting suspended material in the salt-wedge.

CONCLUSIONS

The Isonzo River mouth is a microtidal, low-energy and fine-grained deltaic system. It is affected by long periods of low-medium discharges and short peaks of intense riverine flow, associated with high suspended sediment load, following heavy rainfall.

Systematic measurements of physico-chemical parameters along the water column in the lower course of the river allowed a salt-wedge intrusion to be distinguished, its extension in neap tide conditions to be defined, and the recognition of the freshwater-seawater mixing layer. The thickness of the freshwater layer above the saline intrusion decreases with distance seaward of the salt wedge tip whereas salinity increases. Suspended matter concentrations during low river discharge are higher at the bottom of the salt-wedge, the reverse being observed during a moderate flood event. In addition, grain-size spectra at the salt-wedge bottom are similar to those found outside the bar crest, suggesting a common marine source. Suspended particles are prevalently inorganic, and this component increases with high TSM concentrations. The organic fraction is bound to the finest particles and low POC/PN values indicate a contribution from freshwater and/or seawater phytoplankton. Multivariate statistical analyses helped to define the characteristics of the water masses in the estuarine zone, especially during moderate flood events, and their mutual relationships.

The Isonzo River mouth is rather deep in relation to fluvial discharge rate, and it is fronted by moderately deep water. Most of the year, the highly stratified water column and related hypopycnal flux prevail in the dynamic regime within the lower reach of the distributary mouth. This type of circulation, and the consequent buoyancy-dominated depositional pattern, is interrupted during extreme river floods. The salt-wedge is pushed out of the river mouth, turbulent bed friction becomes dominant and the coarser bed load is transported to the bar crest, where it accumulates following the rapid deceleration of the flow. The outflow spreads as a plume above the underlying marine water, transporting fine river borne material seaward to the prodelta zone. Further research should focus on sediment transport and deposition in front of the river mouth during real flood events and in the river channel during spring tide conditions.

ACKNOWLEDGEMENTS

This study was part of the project “Il sistema deltizio isontino: aspetti morfologici, sedimentologici e geochimici”, supported by the Italian Ministry for University and Research (research grant MIUR 60%, 2001 to Prof. A. Brambati). Thanks are due to Ecothema (Mr. D. Gasparo) and the personnel of the Regional Reserve of the Isonzo River mouth for help during sampling operations. The staff of Laboratorio di Biologia Marina of Trieste is acknowledged for dissolved oxygen analyses. The authors are also grateful to Dr. G. Fontolan and the anonymous reviewers for their constructive comments about the manuscript. Acknowledgements are also due to Direzione Regionale dell’Ambiente del Friuli-Venezia Giulia for making available data on river discharge at Pieris (GO) and to ARPA FVG OSMER for meteorological data from the Gradisca d’Isonzo (GO) station.

LITERATURE CITED

BOLDRIN, A.; JURACIC, M.; MENEGAZZO VITTURI, L.; RABITTI, S. and RAMPAZZO, G., 1992. Sedimentation of riverborne material in a shallow shelf sea: Adige River, Adriatic Sea. *Marine Geology*, 103, 473-485.

BRAMBATI, A., 1970. Provenienza, trasporto e accumulo dei sedimenti recenti nelle lagune di Marano e di Grado e nei litorali tra i fiumi Isonzo e Tagliamento. *Memorie Società Geologica Italiana,* 9, 281-329.

BRAMBATI, A.; CIABATTI, M.; FANZUTTI, G.P.; MARABINI, F. and MAROCCO, R., 1983. A new sedimentological textural map of the Northern and Central Adriatic Sea. *Bollettino di Oceanologia Teorica ed Applicata*, 1, 267-271.

COVELLI, S.; FAGANELI, J.; HORVAT, M. and BRAMBATI, A., 2001. Mercury contamination of coastal sediments as the result of long term cinnabar mining activity (Gulf of Trieste, Northern Adriatic sea). *Applied Geochemistry,* 16, 541-558.

DYER, K.R., 1991. Circulation and mixing in stratified estuaries. *Marine Chemistry*, 32, 111-120.

EISMA, D., 1993. Particle Size. *In:* EISMA., D. (ed.), *Suspended matter in the aquatic environment*. Springer Verlag, pp. 131-166.

FAGANELI, J.; HORVAT, M.; COVELLI, S.; FAJON, V.; LOGAR, M.; LIPEJ, L. and CERMELJ, B., 2003. Mercury and methylmercury in the Gulf of Trieste (northern Adriatic Sea). *Science of the Total Environment,* 304: 315-326.

GRASSHOFF, K.; EHRHARDT, M. and KREMLING, K., 1983. *Methods of seawater analysis*. Verlag Chemie, Wenheim, 419p.

HEDGES, J.I., and STERN, J.H., 1984. Carbon and nitrogen determinations in carbonate-containing solids. *Limnology and Oceanography*, 29, 657-663.

INTERREG II, 2001. *Progetto di monitoraggio dell'Alto-Adriatico – Relazione Conclusiva*, Luglio 1998 – Giugno 2001. Direzione Regionale dell'Ambiente, Laboratorio di Biologia Marina, Trieste, Italia, 112p.

IMBRIE, J., and VAN ANDEL, T.H., 1964. Vector analysis of heavy mineral data. *Geological Society of American Bulletin*, 75, 1131-1156.

JONES, S.E.; JAGO, C.F.; BALE, A.J.; CHAPMAN, D.; HOWLAND, R.J.M. and JACKSON, J., 1998. Aggregation and resuspension of suspended particulate matter at a seasonally stratified site in the southern North Sea: physical and biological controls. *Continental Shelf Research*, 18, 1283-1309.

KOSTASHUCK, R.A.; CHURCH, M.A. and LUTERNAUER, J.L., 1992. Sediment transport over salt-wedge intrusions: Fraser River estuary, Canada. *Sedimentology*, 39, 305-317.

KLOVAN, J.E., 1966. The use of factor analysis in determining depositional environments from grain-size distributions. *Journal of Sedimentary Petrology*, 36, 115-125.

MALACIC, V., 1991. Estimation of the vertical eddy diffusion coefficient of heat in the Gulf of Trieste (Northern Adriatic). *Oceanologica Acta,* 14, 23-32.

MALEJ, A.; MOZETIC, P.; MALACIC, V.; TERZIC, S., and AHEL, M., 1995. Phytoplankton responses to freshwater inputs in a small semi-enclosed gulf (Gulf of Trieste, Adriatic sea). *Marine Ecology Progress Series*, 120, 111-121.

MEADE, R.H., 1972. Transport and deposition of sediments in estuaries. *Memory Geological Society of America*, 133, 91-120.

MENON, M.G.; GIBBS, R.J. and PHILLIPS, A., 1998. Accumulation of muds and metals in the Hudson River estuary turbidity maximum. *Environmental Geology*, 34, 214-222.

MOSETTI, F., 1983. Sintesi sull'idrologia del Friuli-Venezia Giulia. *Quaderni dell'Ente Tutela Pesca*, 6, 1-295.

MYBECK, M., 1982. Carbon, nitrogen and phosphorus transport by world rivers. *American Journal of Science*, 282, 401-450.

OGORELEC, B.; MISIC, M., and FAGANELI, J., 1991. Marine geology of the Gulf of Trieste (northern Adriatic): sedimentological aspects. *Marine Geology*, 99, 79-92.

OLIVOTTI, R.; FAGANELI, J. and MALEJ, A., 1986. Impact of 'organic' pollutants on coastal waters, Gulf of Trieste. *Water Science and Technology*, 18, 57-68.

ORIVE, E.; IRIARTE, A.; DE MADARIAGA, I. and REVILLA, M., 1998. Phytoplankton blooms in the Urdaibai estuary during summer: physico-chemical conditions and taxa involved. *Oceanologica Acta*, 21, 293-305.

PAULSON, A.J.; FEELY, R.A.; CURL, H.C. and TENNANT, D.A., 1989. Estuarine transport of trace metals in a buoyant riverine plume. *Estuarine, Coastal and Shelf Science*, 28, 231-248.

PERILLO, G.M.E., 1995. Geomorphology and sedimentology of estuaries: an introduction. *In:* PERILLO, G.M.E. (ed.), *Geomorphology and Sedimentology of Estuaries*. Elsevier Amsterdam, The Netherlands: Developments in Sedimentology 53, pp. 1-16.

PETTINE, M.; PATROLECCO, L.; CAMUSSO, M. and CRESCENZIO, S. 1998. Transport of carbon and nitrogen to the northern Adriatic Sea by the Po river. *Estuarine, Coastal and Shelf Science*, 46, 127-142.

POULOS, S.E. and COLLINS M.B., 1994. Effluent diffusion and sediment dispersion at microtidal river mouths, predicted using mathematical models. *Estuarine, Coastal and Shelf Science*, 38, 189-206.

RAFVG (Regione Autonoma Friuli-Venezia Giulia), 1995. Studio idrologico per la determinazione delle scale delle portate dei corsi d'acqua in sinistra Tagliamento. Relazione finale, Osservatorio Geofisico Sperimentale, Direzione Regionale dell'Ambiente, 107p.

RAFVG (Regione Autonoma Friuli-Venezia Giulia), 1986. Piano di risanamento del bacino idrografico del fiume Isonzo. Rapporto conclusivo. Cappella & C. s.a.s., Trieste, 6-13.

SALVI, C.; MELIS, R.; CELIO M., and FAGANELI, J., 1998. Suspended matter in the Gulf of Trieste (Northern Adriatic Sea) during the occurrence of macroaggregates in 1991. *Bollettino di Geofisica Teorica ed Applicata*, 39, 219-241.

ŠIRCA, A.; HORVAT, M.; RAJAR, R.; COVELLI, S.; ZAGAR, D., and FAGANELI, J., 1999. Estimation of mercury mass balance in the Gulf of Trieste. *Acta Adriatica*, 40, 75-85.

SONDI, I.; JURAČIĆ, M and PRAVDIĆ, V., 1995. Sedimentation in a disequilibrium river-dominated estuary. The Raša River Estuary (Adriatic Sea-Croatia). *Sedimentology*, 42, 769-782.

STEFANINI, S., 1968. Distribuzione dei carbonati di Ca e Mg nelle sabbie dei fiumi tributari dell'Adriatico settentrionale tra Venezia e Trieste e dei loro principali affluenti. *Studi Trentini di Scienze Naturali*, 45, 101-124.

STRAVISI, F., 1983. The vertical structure annual cycle of the mass field parameters in the Gulf of Trieste. *Bollettino di Oceanologia Teorica e Applicata*, 1, 239-250.

STRICKLAND, J.D.H. and PARSONS, T.R., 1972. A practical handbook for seawater analysis. Second ed., *Bulletin Fishery Research Board of Canada*, 167p.

SULLIVAN, B.E.; PRAHL, F.G.; SMALL, L.F. and COVERT, P.A., 2001. Seasonality of phytoplancton production in the Columbia River: A natural or anthropogenic pattern? *Geochimica et Cosmochimica Acta*, 65, 1125-1139.

VASCONCELOS, F.P.; PIRON-FRENET, M.; PERTHUISOT, J.P.; BEN HAJ, S. and ALLIOT, A., 1995. Trace-metal dynamics in tidal estuaries (Bay of Pen Bé, Brittany, France). *Journal of Coastal Research*, 11, 763-775.

VERLAAN, P.A.J.; DONZE, M. and KUIK, P., 1998. Marine vs fluvial suspended matter in the Scheldt estuary. *Estuarine, Coastal and Shelf Science*, 46, 873-883.

WAFAR, M.V.M.; LE CORRE, P.; BIRRIEN, J.L., 1989. Transport of carbon, nitrogen and phosphorus in a Brittany River, France. *Estuarine, Coastal and Shelf Science*, 29, 489-500.

WRIGHT, L.D., 1977. Sediment transport and deposition at river mouths: a synthesis. *Geological Society of American Bulletin*, 88, 857-868.

WRIGHT, L.D. and COLEMAN, J.M., 1974. Mississippi river mouth processes: effluent dynamics and morphologic development. *Journal of Geology*, 82, 751-778.

ZWOLSMAN, J.J.G. and VAN ECK, G.T.M., 1999. Geochemistry of major elements and trace metals in suspended matter of the Scheldt estuary, southwest Netherlands. *Marine Chemistry*, 66, 91-111.

Journal of Coastal Research	SI 41	141-147	STRAEE 2002	Ferrara, Italy	ISSN 0749-0208

Observations of fine-sediment transport in a semi-enclosed sheltered natural harbour (Pagham Harbour, UK)

S. B. Mitchell, H. M. Burgess* and D. J. Pope

School of the Environment, University of Brighton
Lewes Road, Brighton, BN2 4GJ, UK
E-mail: S.B.Mitchell@bton.ac.uk

*Halcrow Group Ltd, Martlett House
St John's Street, Chichester, West Sussex, PO19 1UH, UK,
E-mail: BurgessHM@Halcrow.com

ABSTRACT

MITCHELL, S. B.; BURGESS, H. M. and POPE, D J., 2004. Observations of fine-sediment transport in a semi-enclosed sheltered natural harbour (Pagham Harbour, UK). *Journal of Coastal Research*, SI 41, 141-147. Ferrara (Italy), ISSN 0749-0208

Preliminary analysis of results from a series of studies of fine sediment transport in the macrotidal Pagham Harbour (U.K.) have revealed patterns of sediment transport which are related to tidal range and wind speed. This paper will present an analysis of some preliminary results from continuous monitors from two sites, which logged turbidity, salinity, water level and wind speed/direction at a frequency of 10 minutes or less. At one site in particular (the Ferry Pool site), detailed results of the variation in salinity and suspended sediment concentration with depth, and near-bed flow velocity, are presented. In general, shorter, faster flood-tide currents lead to concentrations of suspended sediment which are highest during the first 90 minutes of the flood tide. These decrease rapidly due to settling, during the relatively low velocities around the time of high slack water. The magnitude of the peak flood-tide suspended sediment concentrations appear to correlate more with tidal range, than with wind speed, pointing to a greater sediment mobility during spring tides. Further analysis of the variation in salinity and suspended sediment concentration with depth reveal that these high flood tide suspended solids concentrations are related to short-lived local peaks, both of near-bed velocity and of vertical salinity gradient. Rapid settling of sediment occurs following flow deceleration and vertical mixing of the water with respect to salinity. It is suggested that this mechanism is of great importance in describing the landward transport of fine sediment in harbours of this kind.

ADDITIONAL INDEX WORDS: *Estuaries, cohesive sediment transport, macrotidal, tidal range, stratification, salinity, lagoon*

INTRODUCTION

The management of semi-enclosed natural harbours around the UK coastline relies amongst other things on a quantitative understanding of the processes of fine sediment transport within these systems. Several such systems, generally characterised by a narrow harbour entrance and relatively low fresh water input, exist along the heavily populated areas of the Southern and East Anglian coastlines. At present, there is concern that rising sea levels and increased incidence of storms, coupled with a general ever-increasing demand for land development at some coastal sites, has implications for the balance of fine sediment transport processes occurring in and around these harbours. In order to investigate these issues, high resolution, good quality field data describing existing sediment budgets and transport mechanisms within natural harbours are required. Field data are also essential for the design and calibration of numerical models used to predict the effects of any natural or artificial changes imposed on the system.

Hydraulic and meteorological conditions are well known to influence sediment erosion/deposition rates within estuarine systems (DYER, 1997). The transport of material under the action of tides, river flow, wind and wave action, and thus the distribution of suspended material throughout the estuarine system, is governed by the interaction of tides, river flow and wind-induced wave action.

Field studies of estuary systems of this type have focused mainly on larger estuaries where fluvial influence from a single major point source is important (e.g. MITCHELL *et al.*, 1998). Relatively few investigations have been made focusing on cohesive sediment transport in natural harbours. Given the influence of fluvial flow on the formation and maintenance of turbidity maxima in estuaries, there is a need to identify sediment cycling mechanisms of systems with less fresh water input. In common with other systems (e.g. KE and COLLINS, 2000), it is known that Pagham Harbour is accreting at its landward limits (CUNDY *et al*., 2002). While suggestions have been made as to the overall accretion rates in response to local sea level rise, only limited progress has thus far been made in identifying and quantifying the mechanisms by which this accretion takes place. In many estuaries (MITCHELL *et al*., 1998; FETTWEIS *et al*., 1998; GUEZENNEC *et al*., 1999), asymmetry of the tidal wave can result in higher velocity during the flood tide, leading to greater sediment transport than during the subsequent ebb tide. As the floodwaters rise out of the creeks to cover the mudflats, the velocities decrease as the relative cross-sectional area increases, resulting in a settling out of the sediment on the mudflats (LE HIR *et al*., 2000). On a larger time scale, 'tidal pumping' (DYER, 1997) has been proved to be a major contributor to sediment movement in estuaries (e.g. GRABEMANN and KRAUSE, 2001).

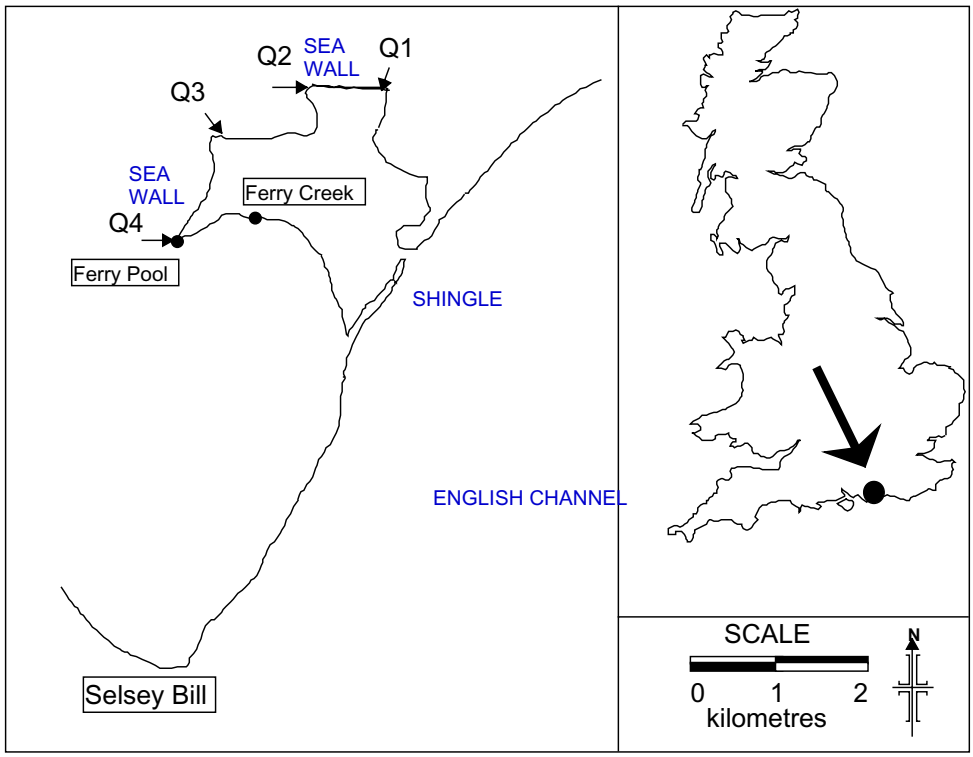

Figure 1. Pagham Harbour location and site plan.

A preliminary analysis of an initial quasi-continuous monitoring data set obtained from Pagham Harbour, a semi-enclosed harbour on the Southern English coast, over a 70-day monitoring period between 11 October and 18 December, 2001, is presented. In addition, results are described showing the variation of salinity and suspended sediment-turbidity with depth, for a single tidal cycle on 11 July 2002.

STUDY SITE AND METHODS

Pagham Harbour (0˚ 45´ W, 50˚ 48´ N), with an area 2.8 km^2 (measured at high water level on spring tides, GEODATA INSTITUTE, 1994), is one of a series of semi-enclosed natural harbours situated on the central south coast of England (Figure 1). Fresh water input is low (<1 m^3/s in total) and occurs via a small network of small streams or 'rifes' which drain the surrounding agricultural land (the principal locations of these are indicated as Q1-Q4 on Figure 1). A system of inner sea walls protects the surrounding low lying reclaimed land, with tidal flaps preventing saline intrusion upstream. The harbour is connected to the English Channel via a 100 m wide entrance, and protected by an artificially replenished shingle spit. Local tides (predicted for Pagham) are semi-diurnal with a mean tidal range of between approximately 2.0 m (Neaps) and 5.5 m (Springs), but owing to its relatively high elevation, the tidal cycle within the harbour is asymmetrical, with seawater only entering the harbour during the upper parts of the tide.

Turbidity, water level and salinity were measured remotely by the deployment of a moored Seabird Instruments SBE-19 CTD with internal data logger and an additional Optical Backscatter (OBS) sensor attached for monitoring turbidity. The CTD was situated at Ferry Creek (Figure 1) in a narrow side channel near a freshwater input controlled by a tidal flap gate, recording values of water depth, conductivity, temperature and turbidity at 10 minute intervals. The instrument was suspended so that its sensors were 0.25 m from the bed of the creek, by attaching it to a scaffold tube mounted onto the concrete apron surrounding the tidal flap gate. Correlation between suspended solid concentration (SSC) and recorded turbidity was determined by gravimetric analysis of samples taken at the same time. While direct comparison between optically measured NTU and grams-per-litre suspended sediment concentration is problematic (BUNT *et al*., 1999), calibration for this site (Figure 2) reveals an approximately linear relationship. A standard algorithm was employed to determine salinity from conductivity and temperature measurements. Hourly wind speed and direction data were obtained by a basic Campbell Scientific Ltd. Automatic Weather Station, situated 500 m north of the Ferry Creek. Further details of experimental procedure may be found in BURGESS *et al*. (2002).

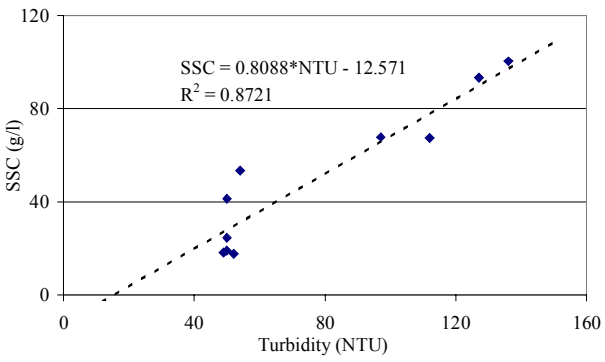

Figure 2. Calibration of SSC (g/l) against turbidity (NTU).

The CTD was also used to measure the variations of turbidity and salinity with depth and time on 11 July 2002 (predicted tidal range = 4.8 m) in another narrow channel at the Ferry Pool site (Figure 1). At this site, fresh water is periodically pumped into the harbour for a period of a few minutes, approximately every 30-40 minutes throughout the tide. The CTD was suspended from a point above the water level and raised and lowered repeatedly throughout the sampling period. In addition, near bed velocity was measured using a Braystoke impeller connected to a counting device, and near-bed turbidity, using a Partech IR15C transmissometer connected to a voltmeter.

RESULTS

To illustrate typical behaviour over a single tidal cycle at the study site, observed water level, salinity and turbidity on two days are shown in Figure 3. Water levels have been multiplied by a factor of 10 for increased clarity. Although both graphs depict measured conditions for a similar, neap, tidal condition, the predominant wind conditions are different between the two tides. For the first case (26 October 2001 second tide; predicted maximum tidal height above local chart datum for Shoreham = 4.6 m; Admiralty Tide Tables, 2000) the mean 6-hour wind condition is relatively high (4.2 m/s from direction 207º). In the second case (9 December 2001 second tide, predicted maximum tidal height = 5.3 m; ADMIRALTY TIDE TABLES, 2000), the mean 6-hour wind condition is lower (1.7 m/s from direction 36º). In both cases, the rise in water level at the start of the flood tide coincides with a sharp rise in turbidity, which continues until saline water arrives when turbidity levels reach their peak. Towards the end of the ebb tide there is a second peak in turbidity that coincides with the drop in salinity levels and the opening of the tidal flap gate. In both cases, the salinity peaks at a level of around 30, and for much of the ebb tide, the salinity remains above 10, even when the incoming water is from land drainage. This is probably due to the presence of a lens of salinity that remains behind until flushed away by the next flood tide.

Comparing the two cases suggests that the larger waves produced by higher wind conditions on 26 October may have re-suspended greater quantities of sediment than for the similar tide on 9 December. Observations of turbidity in other enclosed tidal lagoons for different degrees of storminess add credence to this theory (SANTAMARINA CUNEO and FLEMING, 2000). In addition to the observed higher peak turbidity observed, it can be seen that there is also a greater variability in concentrations of suspended sediment for the more windy conditions of 26 October. In determining the factors leading to the landward movement of sediment at this site, it is important to explore further the nature of the flood-tide turbidity peak. To investigate the relationship between the magnitude of the observed turbidity peak and forcing factors of tidal range and wind speed, analysis was carried out for the entire data set, in which the peak turbidity during the flood tide was obtained for each tide. In an attempt to smooth out unrepresentative 'spikes', an average of three values centred on the peak was calculated for each tide. The complete time series of these may be found in BURGESS *et al*. (2002). Correlation of the magnitude of this peak was carried out against both peak tidal water level and mean wind speed (during the flood tide). Although the resulting graphs (Figure 4) both show a large amount of scatter, a greater dependence of this peak on tidal range than on wind speed (BURGESS *et al*., 2002), is suggested.

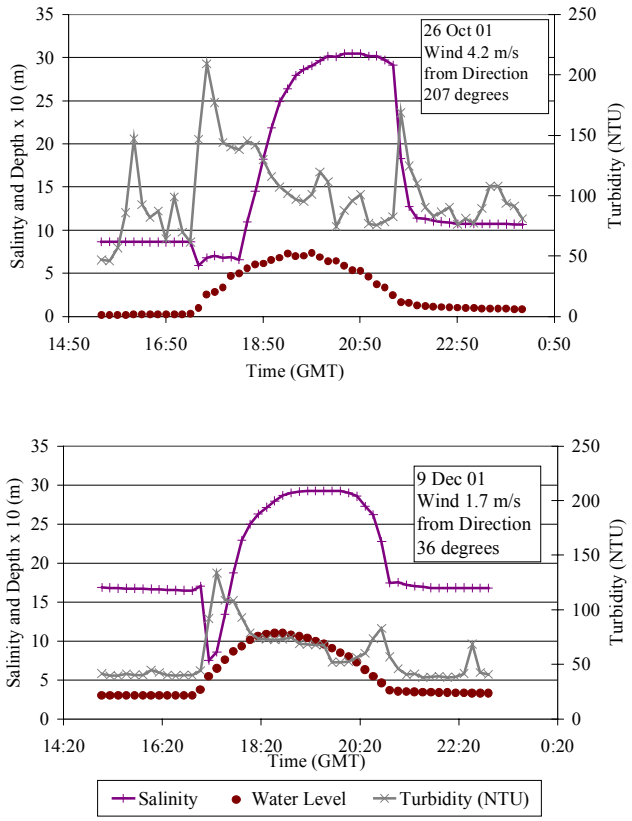

Figure 3. Time Series water level, turbidity and salinity 26 October 2001 (upper panel); 9 December 2001 (lower panel).

DISCUSSION

In order to better understand the mechanisms of formation of the peaks in turbidity that occur near the beginning of each flood tide, some detail of the depth variations in turbidity and salinity is required. Observations of salinity and turbidity variation with depth made at intervals during a single tide (11 July 2002; Figure 5) reveal that the degree of stratification with respect to salinity and turbidity varies significantly during the flood tide. This in turn helps to explain the variation in near-bed turbidity and velocity (Figure 6). It can be seen (Figure 5) that a brief peak in turbidity at approximately 11.45 BST coincides with a high vertical salinity gradient, brought about by a seaward surface flow of fresh water at this time. This vertical salinity gradient is symptomatic of a high degree of vertical stratification in the channel. In order to preserve continuity of flow, this causes a further increase in the near bed velocity at this time, and limits the mixing of suspended sediment into surface layers by inhibition of vertical turbulent transport (GEYER, 1993). Thus the combination of stratified flow and high flood tide velocity can help explain the peak in suspended sediment concentration at the early flood tide. Flow stratification is also periodically enhanced by the influx of pumped fresh water as described above, which also helps to explain the sudden decrease in measured flow velocity at 12.00 (Figure 5).

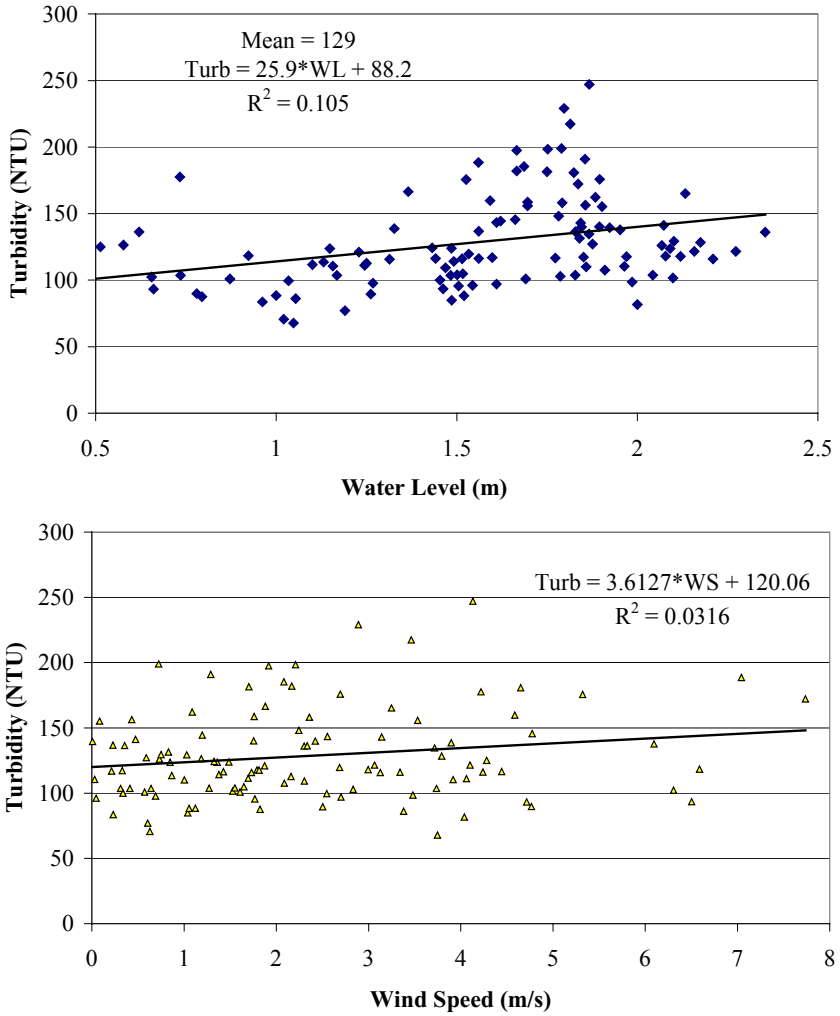

Figure 4. Peak flood tide turbidity vs. peak tidal water level (upper) and wind speed (lower panel), Ferry Creek, 11 Oct - 18 Dec 2001.

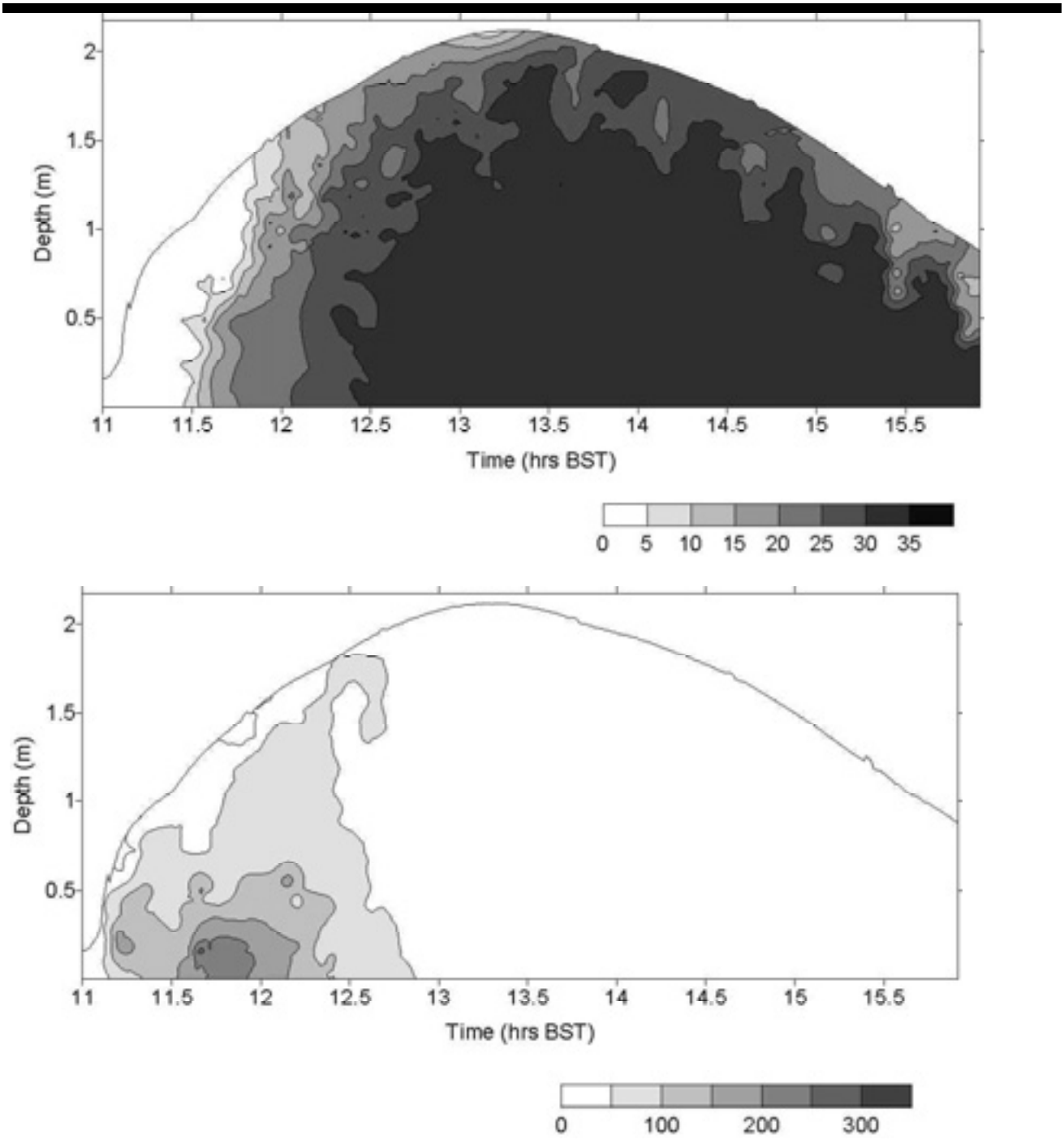

Figure 5. Vertical Profiles of Salinity (upper panel) and Turbidity (NTU; lower panel), 11 July 2002, Ferry Pool Site, Pagham Harbour. Note near-bed turbidity peak at 11.75 (11:45), high water 13.25 (13:15).

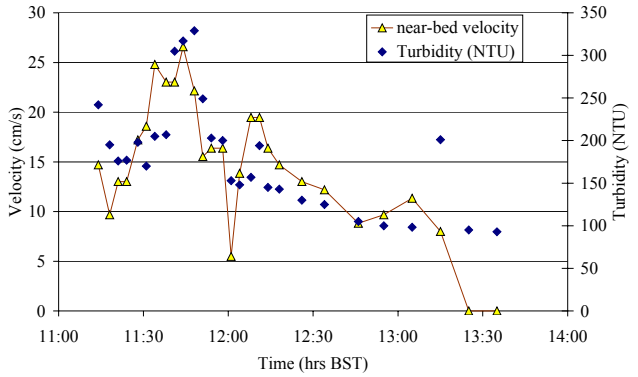

Figure 6. Near-bed velocity and turbidity, Ferry Pool Site, 11 July 2002. High water 13:15.

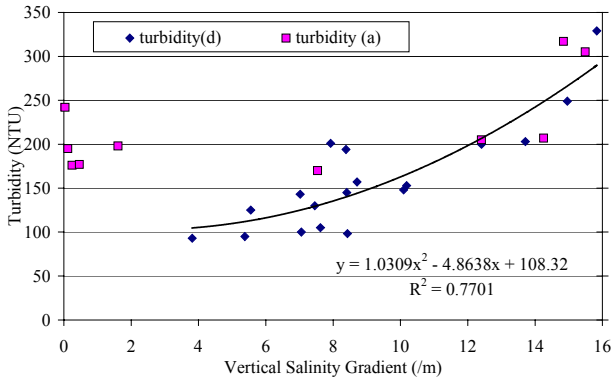

Figure 7. Near-bed turbidity plotted against vertical salinity gradient. Symbols separated into accelerating (a) and decelerating (d) velocities, Ferry Pool Site, 11 July 2002.

The effect of stratification on suspended sediment concentration is further illustrated in Figure 7. For this analysis, salinity stratification is taken as the difference between the salinity in the top and bottom 0.1 m of the flow, divided by the distance between these two points. In general, a quadratic relationship of the form shown on Figure 7 is suggested, with a particularly steep increase in observed turbidity at values of salinity stratification above 15 m^{-1}. However, there exist also a cluster of points on the left hand side of the graph for which the stratification is observed to be very low or zero, but the turbidity is high, at around 200 NTU. These points do not conform to the same quadratic relationship described above, and coincide with the early part of the flood tide when the rate of water level rise was at its steepest.

CONCLUSIONS

Preliminary analysis of continuously monitored turbidity, salinity, water level, wind speed and wind direction at the tidal limits of Pagham Harbour, UK has yielded the following useful conclusions in relation to the hydrodynamic and sediment transport characteristics:

1. Relatively fast flood-tide currents (>0.25 m/s) generally coincide with a short-lived turbidity peak at the observation point, which is at a landward extreme in the harbour. At the same instant, fresh water is forced landwards by the incoming tidal waters. It is suggested that this action re-suspends loosely bound sediments and transports them landwards.

2. Although a considerable degree of scatter is observed in both cases, the magnitude of these turbidity peaks appears to correlate more closely with peak tidal water level ($R^2 = 0.105$) than with wind speed ($R^2 = 0.032$).

3. Detailed observations of depth profiles of salinity and turbidity over time for a single tidal cycle have revealed that a short-lived, significant peak in turbidity occurs near the beginning of the flood tide. This is brought about by a high near-bed velocity that is enhanced by vertical salinity stratification as fresh water moves seawards. This stratification may also be observed to restrict the transport of fine sediment vertically upwards by inhibition of vertical turbulent transport.

4. Further work is needed to identify the spatial distribution of this observed distribution of suspended sediment, by re-deployment of the CTD logger to other sites within the harbour, as well as repeating the same measurements for a more extensive range of hydrological and meteorological conditions.

ACKNOWLEDGEMENTS

This research is funded by the UK Engineering and Physical Science Research Council (EPSRC) grant no. GR/47516/01. The authors thank Bob Gayler (University of Brighton) and Rob Carver (West Sussex County Council) for their valuable assistance.

LITERATURE CITED

ADMIRALTY TIDE TABLES 2001, Vol. 1, 2000. Hydrographer of the Navy, UK.

BUNT, J.A.C., LARCOMBE, P., and JAGO, C.F., 1999. Quantifying the response of optical backscatter devices and transmissometers to variations in suspended particulate matter. *Continental Shelf Research* 19, 1199-1220.

BURGESS, H.M., MITCHELL, S.B. and POPE, D.J., 2002. The influence of tides and wind speed on fine-sediment transport in a semi-enclosed natural harbour (Pagham Harbour, UK). In: Brebbia, C.A., (ed.), Coastal Environment. Southampton, UK: WIT Press, pp.193-202.

CUNDY, A.B., LONG, A.J., HILL, C.T., SPENCER, C., and CROUDACE, I.W., 2002. Sedimentary Response of Pagham Harbour, southern England to barrier breaching in AD 1910. *Geomorphology* 46, 163-176.

DYER, K.R., 1997. *Estuaries: a physical introduction*, 2nd edition. Chichester: Wiley, 156p.

FETTWEIS, M., SAS, M. and MONBALIU, J., 1998. Seasonal, neap-spring and tidal variation of cohesive sediment concentration in the Scheldt estuary, Belgium. *Estuarine Coastal Shelf Sci*., 47, 21-36.

GEODATA INSTITUTE, 1994 *Pagham Harbour: Review of Physical and Biological Processes*. Report for West Sussex CC, English Nature & National Rivers Authority, University of Southampton, 92p.

GEYER, W.R., 1993. The importance of suppression of turbulence by stratification on the estuarine turbidity maximum. *Estuaries*, 16(1), 113-125.

GRABEMANN, I. and KRAUSE, G., 2001. On different time scales of suspended matter dynamics in the Weser estuary. *Estuaries*, 24, 688-698.

GUEZENNEC L., LAFITE R., DUPONT J-P., MEYER R. and BOUST D., 1999. Hydrodynamics of suspended particulate matter in the tidal freshwater zone of a macrotidal estuary (the Seine estuary, France). *Estuaries*, 22, 717-727.

KE, X. and COLLINS, M., 2000. Tidal Characteristics of an accretional tidal flat (The Wash UK). In: Flemming, B.W., Delafontaine, M.T. and Liebezeit, G. (eds.), Muddy coast dynamics and resource management, Amsterdam: Elsevier, pp.13-38.

LE HIR, P., ROBERTS, W., CAZAILLET, O., CHRISTIE, M., BASSOULET, P. and BACHER, C., 2000. Characterization of intertidal flat hydrodynamics. *Continental Shelf Research*, 20, 1433-1459.

MITCHELL, S.B., WEST, J.R., ARUNDALE, A.M.W., GUYMER, I. and COUPERTHWAITE, J.S., 1998. Dynamics of the turbidity maxima in the upper Humber estuary system. *Marine Pollution Bulletin*, 37, 190-205.

SANTAMARINA CUNEO, P. and FLEMMING, B W., 2000. Quantifying concentration and flux of suspended particulate matter through a tidal inlet of the East Frisian Wadden Sea by acoustic doppler current profiling. In: Flemming, B.W., Delafontaine, M.T. and Liebezeit, G. (eds.), Muddy coast dynamics and resource management, Amsterdam: Elsevier, pp.39-54.

Journal of Coastal Research	SI 41	148-159	STRAEE 2002	Ferrara, Italy	ISSN 0749-0208

Morphology and historical evolution of north-east Atlantic coastal deposits: the west Donegal estuaries, north-west Ireland.

H. Burningham† and J. A. G. Cooper‡

†Coastal & Estuarine Research Unit
Department of Geography,
University College London,
Chandler House, 2 Wakefield Street,
London, WC1N 1PF, UK
h.burningham@geog.ucl.ac.uk

‡ Coastal Studies Research Group
School of Biological &
Environmental Sciences ,
University of Ulster, Coleraine,
BT52 1SA, Northern Ireland
JAG.Cooper@ulster.ac.uk

ABSTRACT

BURNINGHAM, H. and COOPER, J. A. G., 2004. Morphology and historical evolution of north-east Atlantic coastal deposits: the west Donegal estuaries, north-west Ireland. *Journal of Coastal Research*, SI 41, 148-159. Ferrara (Italy), ISSN 0749-0208

Estuaries on the north-west coast of Ireland exhibit varying scales of morphological change, both temporally and spatially. Morphological changes in the west Donegal estuaries over the last 200 years (historical/meso-scale) determined from maps and aerial photographs provide a regional assessment of coastal evolution over this medium-term scale. A conceptual model of estuarine morphodynamics is presented. This is supported by estimations of sediment budgets associated with channel migration and dune erosion within the inlet regions, which occur in rock-bounded discrete coastal cells. Significant shifts in morphology, particularly inlet configuration and dune character, appear to have occurred at specific times or during certain decadal periods within the last 200 years. Potential forcing mechanisms, such as the occurrence of high-energy events or changing wind and wave climate associated with changes in the North Atlantic Oscillation are discussed.

ADDITIONAL INDEX WORDS: *meso-scale, inlets, dunes, storms, antecedent morphology, topographical and geological controls*

INTRODUCTION

The importance of meso-scale coastal evolution (order 10^1-10^3 years) in the understanding of contemporary behaviour and future development of coastlines is becoming increasingly recognised. For example, although the impact of one storm often leaves an immediate signature on a coastline (e.g. MORTON *et al.*, 1995), its influence may continue for several decades as the system responds to the various morphological changes and associated interference in process dynamics (e.g. ORFORD *et al.*, 1999), and its mark may persist in the sediment record for centuries or millennia (e.g. DELANEY & DEVOY, 1995).

The process-dominance approach to the understanding of coastal, particularly estuarine, behaviour has emphasised the relative importance of the wave, tidal and fluvial regimes (ROY, 1984; DALRYMPLE *et al.*, 1992; COOPER, 1993), but it is clear that the geological history and evolutionary path of such systems generates specific antecedent conditions which morphodynamically dictate process and future change (RIGGS *et al.*, 1995; HEAP & NICHOL, 1997).

The north-west coast of Ireland has been the focus of several studies examining Holocene sea levels (CARTER *et al.*, 1989) and aeolian deposits (CARTER & WILSON, 1991; CARTER & WILSON, 1993), but the contemporary coastal geomorphology of the region has been relatively neglected. Furthermore, whilst understanding of macro-scale (10^3+ years) coastal behaviour is evolving (Shaw, 1985; CARTER & WILSON, 1993; SHAW & CARTER, 1994), meso-scale (historical) changes are poorly documented. This contribution addresses this deficiency through an examination of west Donegal coastal morphology, in order; to describe the historical (decadal-century scale) evolution of this environment; to examine the regional coherence of geomorphological change; and to present a preliminary statement on the controls on meso-scale coastal behaviour.

REGIONAL SETTING

The bedrock-framed, west coast of Ireland is highly indented, with considerable variation in shoreline orientation. In County Donegal, in the far north-west of Ireland, are 25 estuarine systems, including Loughros Beg, Loughros More, Gweebarra and Trawenagh estuaries that border the north-east Atlantic (Figure 1). The present estuarine systems are sediment-rich, having infilled via onshore transport of glacigenic shelf deposits (mainly sand) during the Holocene marine transgression (SHAW & CARTER, 1994).

The estuaries experience ocean spring tidal ranges of over 3.5 m and receive small fluvial inputs. Estuarine basins are typically characterised by extensive intertidal sand flats, sinuous low-tide ebb-channels, and inlet regions variably constrained by dune barriers or rock headlands. The terrestrial landscape is dominated by bedrock outcrop and blanket peat, with less than a third of the region suitable for agriculture (FOSSITT, 1994).

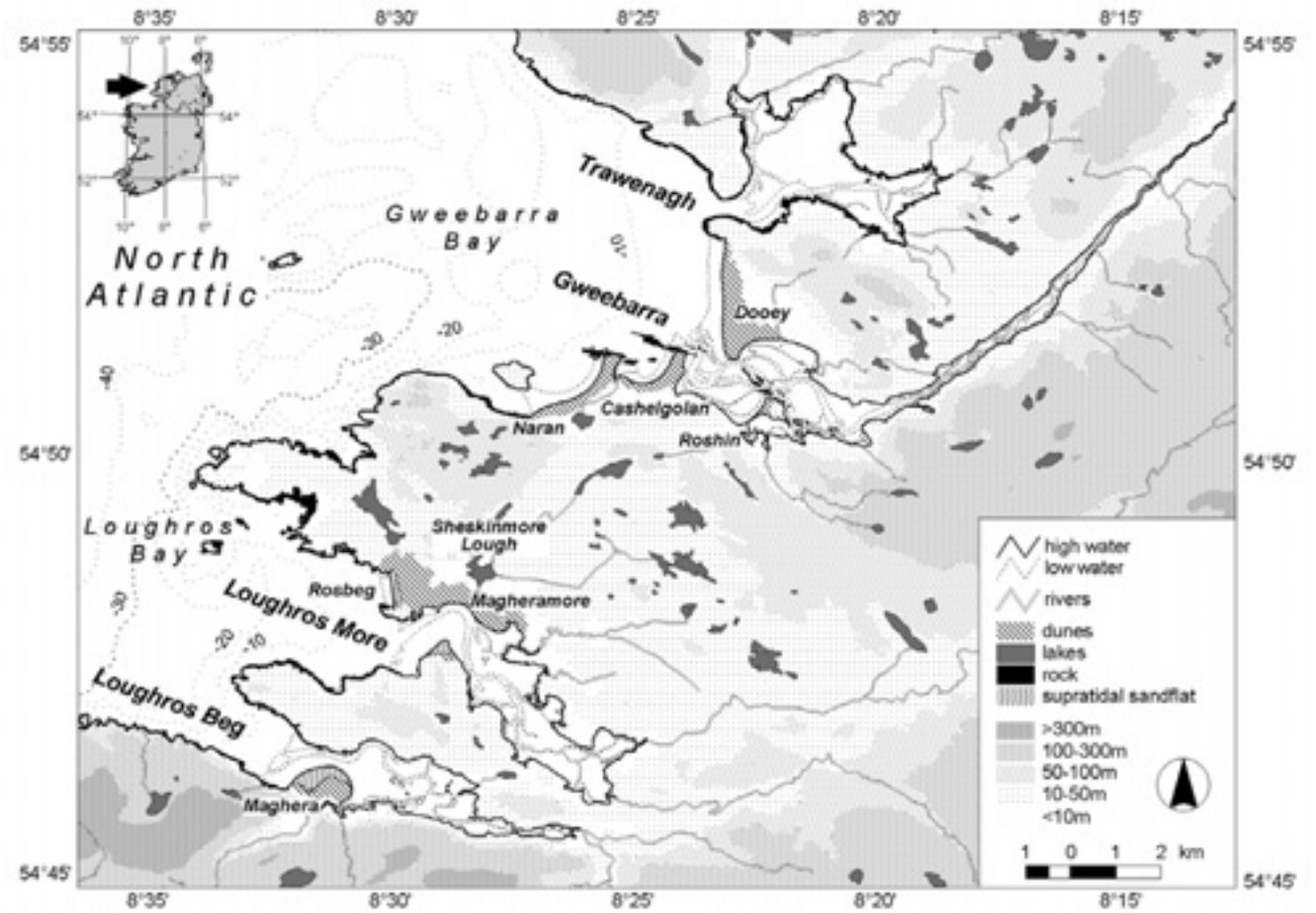

Figure 1. The west Donegal coastline, north-west Ireland, showing the location of the Trawenagh, Gweebarra, Loughros More and Loughros Beg estuaries.

The north-east Atlantic is windy and stormy. The average annual wind speed at Malin Head, in north-west of Donegal is 8ms^{-1}, with gales recorded on 46 days of the year (1956-1996 average): 70% of gales have a westerly wind direction. The climate is seasonal, wherein 60% of winds at Force 6 or above (≥11ms^{-1}) and 77% gale force winds (≥17ms^{-1}) occur between November and March. Offshore data from the UK Meteorological Office ocean weather buoy RARH, 240km north-west of Malin Head, provide an annual average wind speed of 8.5ms^{-1} and significant wave height of 3.3m (August 2001-2002).

METHODS

Estuary morphology was examined from published maps, aerial photographs and field observations. Ordnance Survey (OS) maps (1:10,560) from 1835, 1853 and 1907, and aerial photographs from 1951, 1977 and 1995 were digitised and geo-referenced within ARC-INFO and ArcView. Full map and aerial photograph records were available for the Gweebarra, Loughros More and Loughros Beg estuaries, but due to limited resources, consideration of the Trawenagh system is presently limited to 1907, 1977 and 1995.

Geo-rectified maps representing sedimentary environments and morphological character were derived from the various map and photograph resources within a GIS, allowing simple visual comparisons and spatial analysis. Delimitation and classification of environments was aided by detailed field observations, which incorporated morphological and sedimentological surveying and analysis (BURNINGHAM, 1999).

RESULTS

Contemporary Coastal Morphology

The west Donegal coastline comprises two distinct bays, Gweebarra Bay and Loughros Bay, each of which is occupied by two estuarine systems (Figure 1). Gweebarra Bay has a relatively shallow offshore slope (0.18^{o} (1:318) average) that is interrupted in places by several small islands and sub-tidal rock outcrops. The 30m depth contour is >10km west of the Trawenagh estuary, but to the south of Gweebarra Bay, a narrow valley, extends the 30m contour to within 6km of the Gweebarra estuary. The coastline bordering Gweebarra Bay comprises low-relief (<100m) bedrock cliffs to the north and south: coastal sediment deposits are restricted to the estuaries of Gweebarra and Trawenagh and the adjacent beach systems of Dooey, Cashelgolan and Naran. The Gweebarra estuary drains a catchment area of ~155km^2 via a trellis drainage network to the principal river (Gweebarra). The high tide area of the estuary is ~8.4km^2 and its tidal limit is 15km

inland from the coastline. The Trawenagh catchment is ~65km^2 and several small rivers drain into the expansive estuarine system (high tide area 8.5km^2).

Loughros Bay, south-west of the Gweebarra Bay (Figure 1) is distinctly narrower and deeper. The 30m depth contour defines the western extent of the Bay. To the east, the Loughros More and Loughros Beg estuaries occupy elongate valleys, separated by a bedrock peninsula.. The average offshore slope from Loughros More is 0.34^o, steepening to 0.46^o in the vicinity of Loughros Beg. The low-relief rocky shoreline to the north is replaced to the south by steep (>200m) cliffs. As in Gweebarra Bay, shoreline sediment deposits are limited to the estuarine systems. Loughros Beg occupies a glacially elongate valley, with a high tide area of 5.4km^2, and drains a ~48km^2 catchment. Drumlins are present fringing the lower slopes of the valley. The Loughros More catchment is ~207km^2 and the estuary has a high tide area of ~7.5km^2.

Estuarine Systems

The contemporary estuarine systems on the west Donegal coast can be conceptualised as a series of morphological *zones* that reflect changes in inherited topography and varying wave-tide-fluvial influence. In general, the *upper estuary* region corresponds to a relatively narrow valley or valleys, that accommodates the initial tidal stages of the main river(s). The system then expands, in terms of the bedrock valley, into an *estuarine basin* where the main low tide channel divides, meanders and re-unites before exiting the estuary through a narrow *inlet*, which in some systems is often associated with an extensive dune-beach barrier.

Upper Estuary

Sediments at the head of the estuaries are predominately sandy, but contain significant mud and gravel components, and are generally poorly sorted (BURNINGHAM, 1999). Gweebarra and Loughros Beg have distinct narrow upper estuary valleys. In Gweebarra, this fluvio-tidal zone extends for 10km and the floor width varies from 50 to 400m. The surrounding topography rises to 100m within 0.5km of the valley floor and borders the valley as low relief hills for its entire tidal length. At the estuary head, salt and reed marshes fringe the valley for ~1.5km. The valley floor is occupied by a succession of small intertidal lobate sand shoals and a braided low tide channel that merges as the valley narrows to 160m at the junction with the estuarine basin. Within Loughros Beg, the Bracky River enters the head of the estuary through a confined saltmarsh. Further small and localised saltmarsh units exist on some of the intertidal flats, east of the constriction. The valley tapers further, creating a significant constriction halfway along the 2.5km valley. Low tide channels initially meander and bifurcate around shoals, and then west of the constriction, unite to form a relatively linear course. Distinct narrow upper estuary valleys are absent from the generally broader Trawenagh and Loughros More estuaries. Several small streams provide a small fluvial input to these estuaries: small saltmarsh systems are associated with most of the fluvial inputs.

Estuarine Basin

The transition from the narrow valley to the basin in Gweebarra and Loughros Beg relates to a marked change in geological structure. In Gweebarra, a change from fractured granite to a complex of pelites, limestones, granodiorite and appinite (MENEILLY, 1982) that have been preferentially eroded, allow the estuarine basin region to expand from 500m to a maximum width of 2km. In Loughros Beg, the tillite of the upper estuary is replaced, at the junction with the estuarine basin, with quartzite to the south and pelite to the north. From the narrow valley, the channel enters the south side of the estuarine basin and meanders northward to occupy a position favouring the northern bedrock margin. Geological structure is also a fundamental feature of the Loughros More and Trawenagh estuaries. The estuarine basin of Loughros More exploits the diorite fringe to the southwest of the Ardara Pluton. The extensive granite to the north, however, imposes no significant controls on the shape of the Trawenagh estuarine basin, which has a significantly broader body.

The distribution of sedimentary environments in the estuarine basin is largely dependent on the proximity of tidal channels or stream inputs. The intertidal flats throughout these estuaries are sandy: minor coarser and finer fractions are only present in discrete pockets close to sheltered estuarine margins. The intertidal sand bodies closer to the inlet, which comprise the main components of flood-tidal deltas (HAYES, 1975), are especially dynamic and are characterised by broad shoals of megaripples. Throughout the basins, several meandering channels exist at low water. Within Gweebarra, a single dominant tidal channel extends from the valley into the basin and to the mouth of the estuary, although the overall low tide channel network is notably more complex than the other estuaries (Figure 1). Tidal channels in Loughros More meander and coalesce, but tend to favour the bedrock south-west margin. The Trawenagh basin is the least complex. Here, tidal channels are generally associated with specific fluvial sources and they do not coalesce until close to the inlet.

In Loughros Beg, the Owenwee River enters through a small saltmarsh close to the inlet, but its low tide course is eastward until its confluence with the low tide channel sourced by the Bracky River. This channel position appears to be maintained by the presence of Sand Island (bedrock based, dune covered). Geological controls within the estuarine basin are also present within Gweebarra. The position and orientation of a number of rock outcrops and a large island (Roshin) located in the centre of the estuarine basin, influence the flow of tidal and river waters, resulting in braiding of the main channel. A notable feature of the Gweebarra estuary is the presence of a narrow (~25m at high tide) and low (crest 5m above MWL) cobble barrier that connects the bedrock-based Roshin island to the southern estuarine margin; it is partly covered by limited inter- and supratidal sand deposits.

Inlet

Estuarine inlets on this coastline are generally constricted, particularly at low tide. At Trawenagh, the ~400m wide inlet is clearly constrained by rocky headlands (Figure 2A), and sediment deposits are limited to the intertidal shoals within the estuarine basin. The channel through the inlet is deep (8m below MWL), but shallows rapidly within the estuary. The Gweebarra inlet has a high tide width of ~900m, defined by the Dooey and Cashelgolan dune systems. Inlet-associated sediment shoals which extend seaward (ebb-tidal delta) and landward (flood-tidal delta) of the inlet, constrict the low tide channel, and the main tidal flow is confined between two rock outcrops less than 100m apart. In Trawenagh, the flood-tidal delta appears to control the position of the ebb channel, against the south margin of the system, within the inlet region; ebb-tidal deposits are limited to a small subtidal shoal seaward of the bedrock inlet.

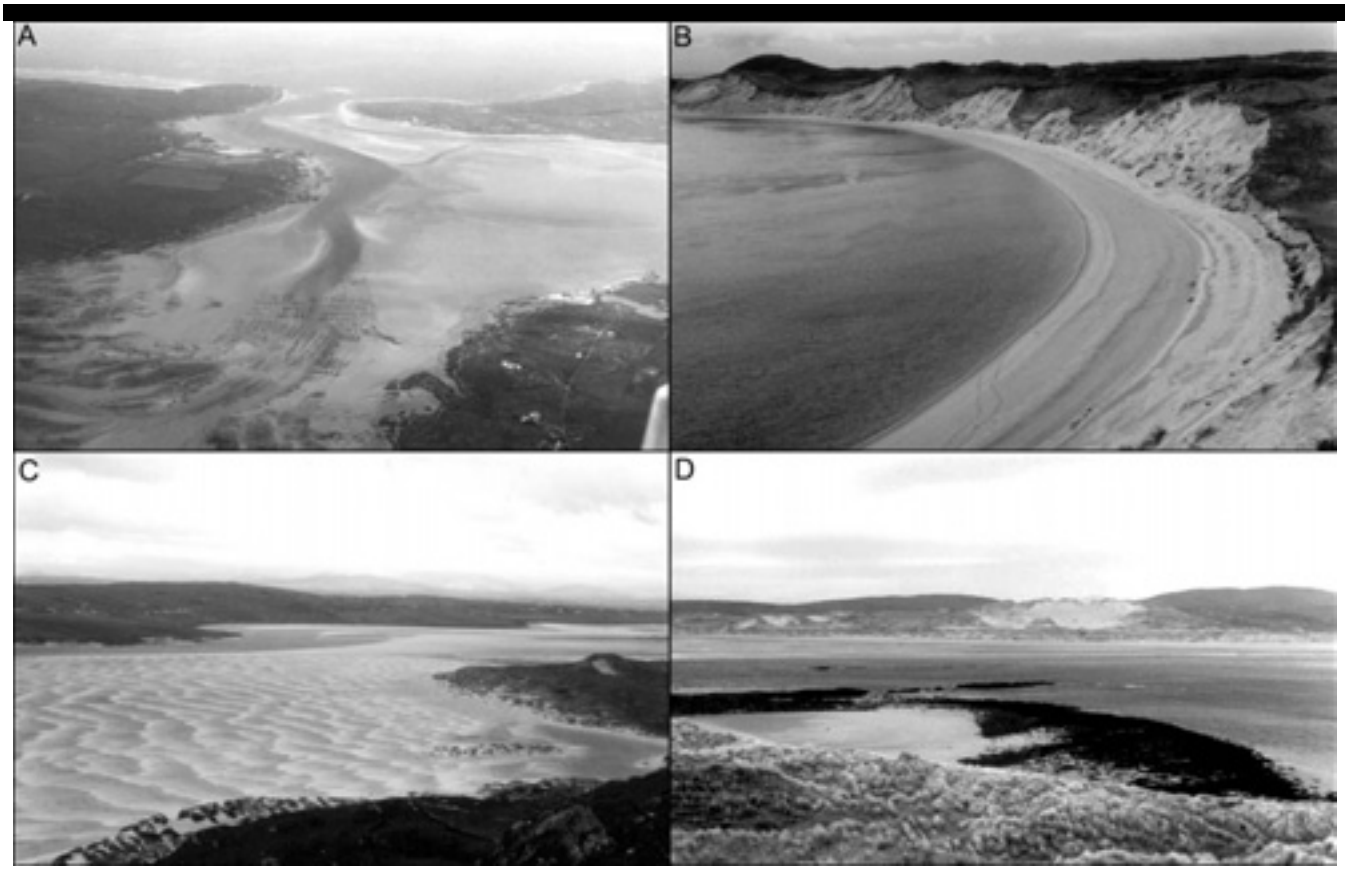

Figure 2. A) Oblique aerial photograph of the Trawenagh estuary; B) Ebb channel meander at the mouth of Loughros More; C) Supratidal strand at the mouth of Loughros Beg; D) Large blowout in the Dooey dune system in Gweebarra (photograph taken from the Cashelgolan dune system).

The two Loughros inlets are dominated by large supratidal beach and dune barrier systems. The high tide width of the Loughros More inlet (~1km) is characterised by a large tidal channel meander (Figure 2B). The two Loughros inlets are dominated by large supratidal beach and dune barrier systems. The high tide width of the Loughros More inlet (~1km) is characterised by a large tidal channel meander (Figure 2B). From the southern margin, a supratidal and intertidal sand flat diverts the low tide channel northward into the large Magheramore dune system on the northern margin. The low tide channel is less than 200m wide. Seaward of the meander, both high tide shorelines are bedrock, and the channel exits the system through intertidal sand shoals. Similarly, the Maghera inter- and supratidal sand body on the southern margin of the Loughros Beg inlet constrains the position of the low water channel which is formed against the northern bedrock margin.(Figure 2C). At this point, the high tide inlet is reduced to a width of 400m, and the ebb channel has a width of only 150m. The low water channel exits the system through intertidal sand shoals seaward of Maghera. Both Loughros inlets comprise these seaward intertidal deposits, which are wave-sculpted ebb-tidal shoals. Flood-tidal deposits define the transition from basin to inlet, and the change in ebb-channel character from multiple/braided to single meander.

Inlet-Margin Sediment Bodies

The inlet-margin dune environments of the Gweebarra, Loughros More and Loughros Beg estuaries are significant components of the estuarine system, particularly in terms of sediment volume. The Trawenagh system is distinctly different in this manner as it lacks any supratidal depositional component.

The Maghera supratidal system covers ~0.75km^2 at the mouth of Loughros Beg: small ramp dunes fringe the bedrock cliffs to the west (CARTER & WILSON, 1993), but the system is dominated by the north-eastward extending dunes and supratidal sand flat (Figure 2C). The main dune field is scattered with blowouts, most of which are inactive and have been re-colonised to a certain extent by grasses. To the west, foredune hummocks grade into a supratidal strand, which is covered in a variety of transient aeolian bedforms. The elevation of the strand varies from extreme high water to the west (the intersection with the foreshore), to mean high water springs (MHWS) closer to the dunes. The landward/southern extent tends to flood during extended periods of wet weather. Due to the high wind speeds and large waves experienced on this coastline, the transition between supra- and intertidal zones within the inlet is a changeable feature. Intertidal processes often encroach over the supra-tidal environment and similarly, aeolian processes continue over the intertidal zone at low tide.

The Magheramore dune system within the Loughros More inlet is considerably more expansive (~2.1km^2), and extends north-westward to back the Tramore beach system at Rosbeg. Several blowouts are present across the dune surface. The dune shoreline of Magheramore is not continuous, however, due to the presence of a large pelite outcrop that bounds the system to the south-west. These divide the Rosbeg and Loughros More intertidal systems. Dunes also occupy a small area (~0.07km^2) on the south margin of the inlet.

The inlet shoals of Gweebarra merge to the north with an extensive (2km long, >300m intertidal width) surf-dominated beach, backed by the steep (5–15m high) dune front of the Dooey barrier. This is one of three dune barrier systems close to the mouth of the Gweebarra, estuary. The Dooey system to the north is the most substantial, covering ~1.3km^2, and is dominated by a large blowout (~0.07km^2) toward the southern extent. This also corresponds to the broadest and highest point of the system (Figure 2D). Several other significantly smaller blowouts are present within the dune system. Spatially, the dune systems of Cashelgolan and Naran cover ~0.45km^2 and ~0.5km^2 respectively and both correspond to crescentic embayments, delimited by rock outcrops toward the north.

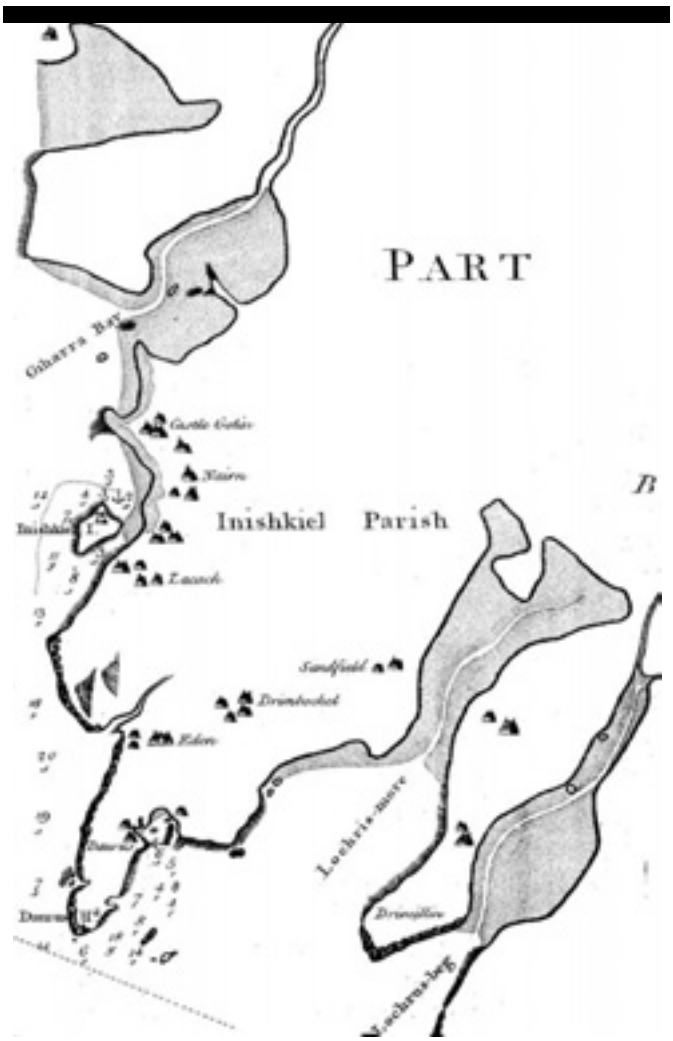

Figure 3. Charted map of the west Donegal coast as surveyed by MACKENZIE (1775).

Meso-scale Evolution and Behaviour

From archaeological evidence (KNOWLES, 1901; BRUNICARDI, 1914; D'EVELYN, 1933; O'RIORDAIN & RYNNE, 1959; CARTER & WILSON, 1991; O'FLOINN, 1995), it is clear that the estuary-associated dune systems have experienced periodic destabilisation and re-organisation over the last 1000 years. Backbarrier deposits show that some areas of the dune barriers were still forming 800 years ago (Naran), however, these seaward elements of the coastal system reveal very little about the evolving estuarine basins. Map evidence can delimit the development over the last 200 years, but the intervening period remains poorly understood.

Navigation charts in the 18th century (MACKENZIE, 1775) provide a broad view of coastal morphology (Figure 3), but their simplicity precludes detailed comparison with the more recent Ordnance Survey maps and aerial photographic resources. The fundamental elements of the systems, such as presence of dune barriers and dominant channel position, typify the contemporary morphology, but also present a coarse-resolution depiction of the suite of morphologies exhibited over the 1835-1995 period (map and aerial photograph) (Figures 4-7).

Morphological changes since 1835 are predominantly expressed within two elements of the estuarine system: the channel network throughout the systems and the supratidal bodies within the inlet regions. In terms of ebb channel position and configuration, there have been distinct cycles of migration, and a suggestion of increased sinuosity over the 160-year period. This is evidenced at Gweebarra (Figure 4) in the lateral extension of meanders west of Roshin and the shift between two dominant ebb channel positions (e.g. 1853 is equivalent to 1977, 1951 is equivalent to 1995) east of Roshin. In Loughros More (Figure 5), the ebb channel meander within the inlet region has laterally extended and migrated northward, and now occupies a position 650m north of its position in 1835 (BURNINGHAM, 2002). Further increases in sinuosity are exhibited throughout the estuarine basin. At the mouth of Loughros Beg (Figure 6), the ebb channel has switched between a diagonal course across the mouth (e.g. 1835) to a position directly next to the north shoreline (e.g. 1951): a swathe of over 800m (BURNINGHAM, *in press*). Within the estuarine basin, the channel course from south to north margin has become increasingly sinuous since 1835, despite maintaining a relatively fixed position elsewhere. Trawenagh, the morphology of which is only illustrated for the years 1907, 1977 and 1995 (Figure 7), presents considerable inactivity in comparison with the other three systems and channel position has shifted by only small amounts (10s metres).

It is clear that significant shifts in ebb channel position occurred in the 1907-1951 period. Examination of ebb channel sinuosity within the inlet region of the Gweebarra and Loughros estuaries (Figure 8) shows some consistency in the timing of specific changes in inlet configuration. Despite the correlation in period of initial change, the subsequent behaviour of the inlet channels is distinct in each estuary. At Loughros Beg, the channel ultimately tends back toward a comparable 1907 position. In Loughros More, the meander extension continues to advance north, resulting in considerable migration by 1995. Gweebarra represents a further variance, where the channel configuration of 1977 closely resembles that of 1907 and is then followed by a more progressive lateral extension comparable to the post- 1907-1951 behaviour. Again, examination of the available resources for the Trawenagh system shows that this system does not significantly reflect the changes shown in the other estuaries. Considering the similarity of the 1907 and 1977 inlet configuration at Gweebarra, currently

there is no evidence to support or refute the possibility that Trawenagh changed between 1907 and 1951.

A stronger link between the behaviour of the Trawenagh and Gweebarra systems, and to a lesser extent the Loughros systems, is the apparent increase in intertidal sediment volume within the inlet regions, as discerned from comparison of the 1951/1977 morphologies. This is particularly clear in the 1951 Gweebarra inlet (Figure 4), where channel position appears constrained by sediment surplus within the flood-tidal delta deposits. By 1977, the channel appears to have reworked sediment to provide a more hydraulically efficient configuration. At this point, the correspondence with Trawenagh is most evident, as the 1977 morphology is very similar to that of 1907, although the lack of data from 1951 precludes any judgement on morphological change (or not) between 1907 and 1951. Excess sediment deposition within the inlet region could also explain the mechanism by which the Loughros More inlet meander commenced its northward migration: valley orientation and the inlet structure are thought to provide the differentiating controls on the subsequent continued channel migration, when compared to Gweebarra and Loughros Beg.

The supratidal sediment systems that dominate the estuarine inlets (except Trawenagh), also display signs of progressive adjustment and what appear to be intermittent changes. Most dune systems on this coastline appear to have experienced a period of surface degradation. Aerial photographs from 1951 clearly show dune surfaces that have suffered from an intensive period of denudation: numerous shore-normal blowouts are present and the vegetated regions are covered in thin deposits of wind blown sand. These demonstrate the importance of the high-energy wind climate on the morphological behaviour of these coastal systems. Magheramore and Dooey dunes appear to have suffered the most extensive degradation, whereas the intra-estuarine system of Roshin exhibits minimal morphological change. The large blowout within the Dooey dunes, which formed at this time (between 1907 and 1951), has changed very little since, and most other blowouts have become visibly inactive during the same period.

The dune environments also respond directly to the changes in ebb channel position. This is most evident in Loughros More, where northward migration of the ebb channel has resulted in considerable erosion of the dune system. Lateral shifts in the inlet ebb channels also influence the dune environments by allowing supratidal sedimentation elsewhere in the estuarine system. In Loughros More, this is clearly evident on the south margin of the inlet, where a small dune system and expansive supratidal sand flat have prograded northward in association with the northward migrating ebb channel. A more pronounced area of dune progradation is present to the east of Magheramore, where a small dune lobe has advanced south-east of the main dune system.

Smaller scale reorganisation of the dune shoreline is exhibited in the Dooey dunes in Gweebarra. Over the 1835-1995 period, the southern tip of Dooey recurved eastward. This is particularly clear when comparing the 1853 and 1907 morphologies. However, dune front erosion of the western aspect of the system since 1907 has also been accompanied by a southward extension in the form of dune ridges. The short-term contemporary (1996-1998) behaviour suggests a link between dune front recession and backbarrier accretion, whereby the shoreline of the southernmost tip of Dooey has shifted further eastward (BURNINGHAM, 2000). Within the Loughros More system, the Rosbeg environment also exhibits a recessive dune front. Between 1907 and 1951, the dune shoreline retreated 130m, but has since made a slight recovery with the advancement of a 50m wide supratidal zone and growth of embryo dunes (BURNINGHAM, 2002).

Examination of sediment budgets is somewhat difficult when dealing with non-topographical data, but field observations of contemporary foredunes at Maghera and Dooey provide a basic topographical model to infer approximate sediment losses and gains within the overall dune systems (BURNINGHAM, 1999). It is estimated that the erosion of the Magheramore dunes by ebb channel migration alone has released ~$1.8 \times 10^6 m^3$ of sediment over the 1835-1995 period. Approximately 25% of this volume is thought to be contained within the prograding lobe to the east of the system, and a further 30% in the supratidal flat and dune environment extending from the southern margin (BURNINGHAM, 1999). In addition, it is estimated that a net ~$1.0 \times 10^6 m^3$ of sand has been released from the Maghera dune system, whilst the discrete changes at Dooey, in Gweebarra, suggest that approximately half of the $0.5 \times 10^6 m^3$ sediment lost from the dune front has been re-deposited in the south and east progradational foredunes.

Whilst these are crude estimates, it is clear that sediment removed from the dune environments, via dune front recession or ebb channel migration, has contributed to the development of smaller supratidal systems elsewhere in the systems. The estimates also infer that considerable quantities of sediment have either been transported out of the system (offshore) or have contributed to progressive intertidal sedimentation within the estuarine basins.

Driving Mechanisms and System Controls

Analysis of historical change and contemporary processes in sandy coastal environments has delimited mechanisms behind specific morphological behaviour. For example, ebb channel migration within inlet regions is generally attributed to longshore sediment transport (e.g. FINLEY, 1978) and marine or fluvial flooding and breaching events (e.g. CONLEY, 1999; COOPER, 2002). In terms of supratidal environments, ORFORD *et al.* (1999) concluded that extreme storms triggered large-scale erosion of foredunes in south-west Ireland, whilst storminess and sea level variability were important in reworking the eroded material. In the absence of sea level change, dune front erosion is usually associated with high-energy wave attack and positive surges (CARTER & STONE, 1989), whereas dune surfaces become degraded as a consequence of high energy wind events or human (e.g. grazing, agriculture) pressures. The recognition of several processes operating over varying timescales and spatial extents on the west Donegal coast indicates a particularly complex pattern of coastal behaviour.

Whilst an attempt has been made to identify conformity and distinction in the morphological development of the west Donegal coastal systems, it is also necessary to acknowledge meso-scale controls and place this historical evolution in an appropriate context. This can be based on the known evolution of the systems, where sedimentary sequences reflect the influence of sea level changes, coastal habitation and the north-east Atlantic storm climate. It should also be noted that this coastline is considered to be sediment starved, in that there are no longer any significant land or shelf based sediment deposits supplying the coastal systems (CARTER *et al.*, 1989). As a consequence, morphological change involves reworking of a finite sediment volume.

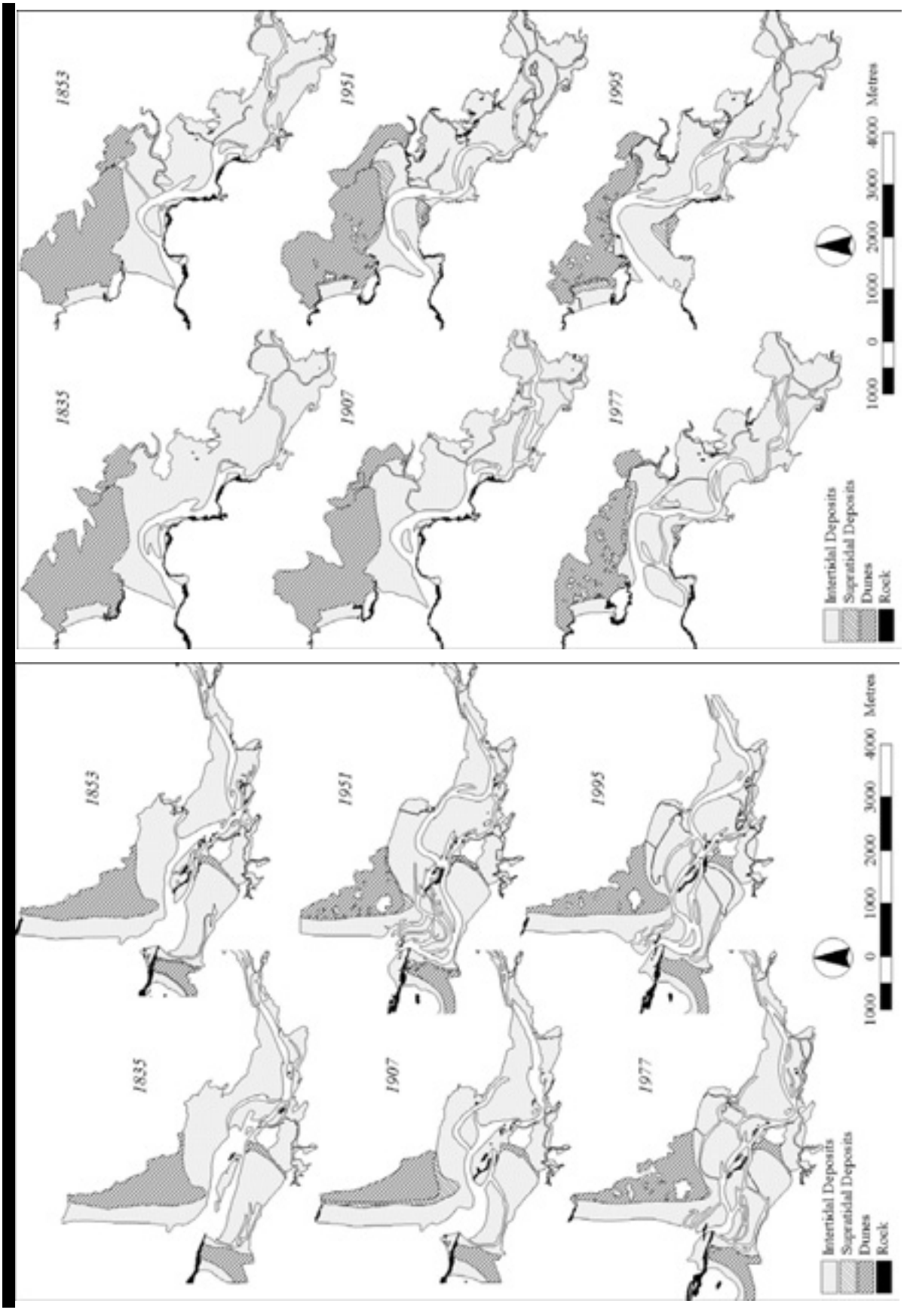

Figure 4. Morphological changes in the Gweebarra estuary

Figure 5. Morphological changes in the Loughros More estuary

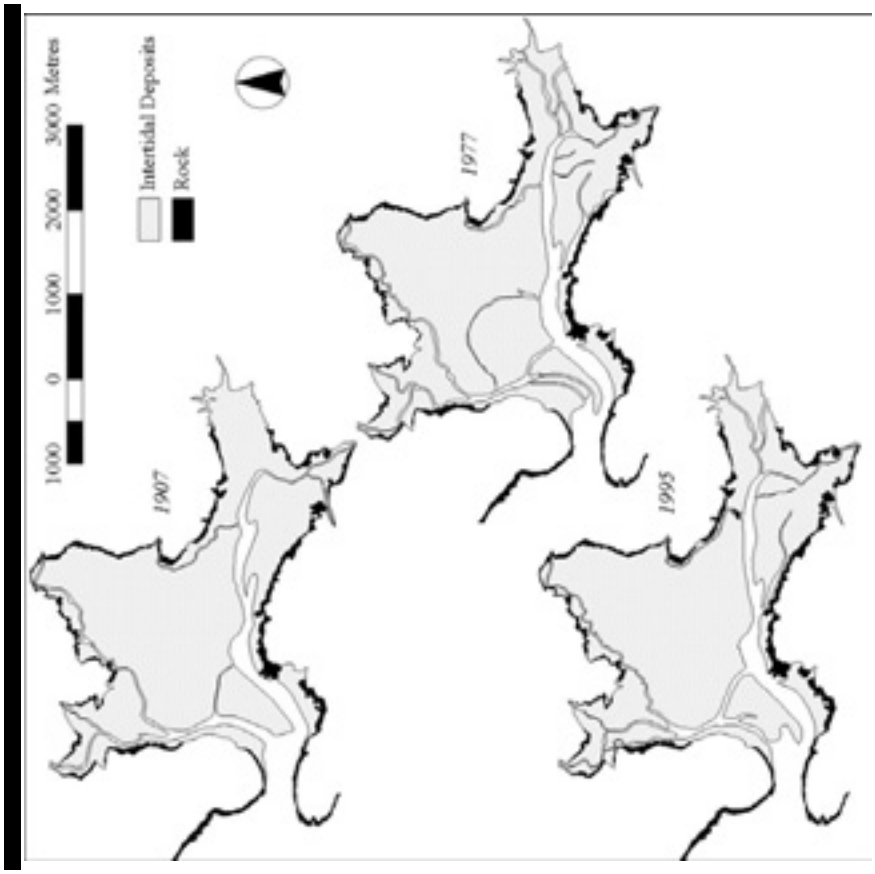

Figure 7. Morphological changes in the Trawenagh estuary.

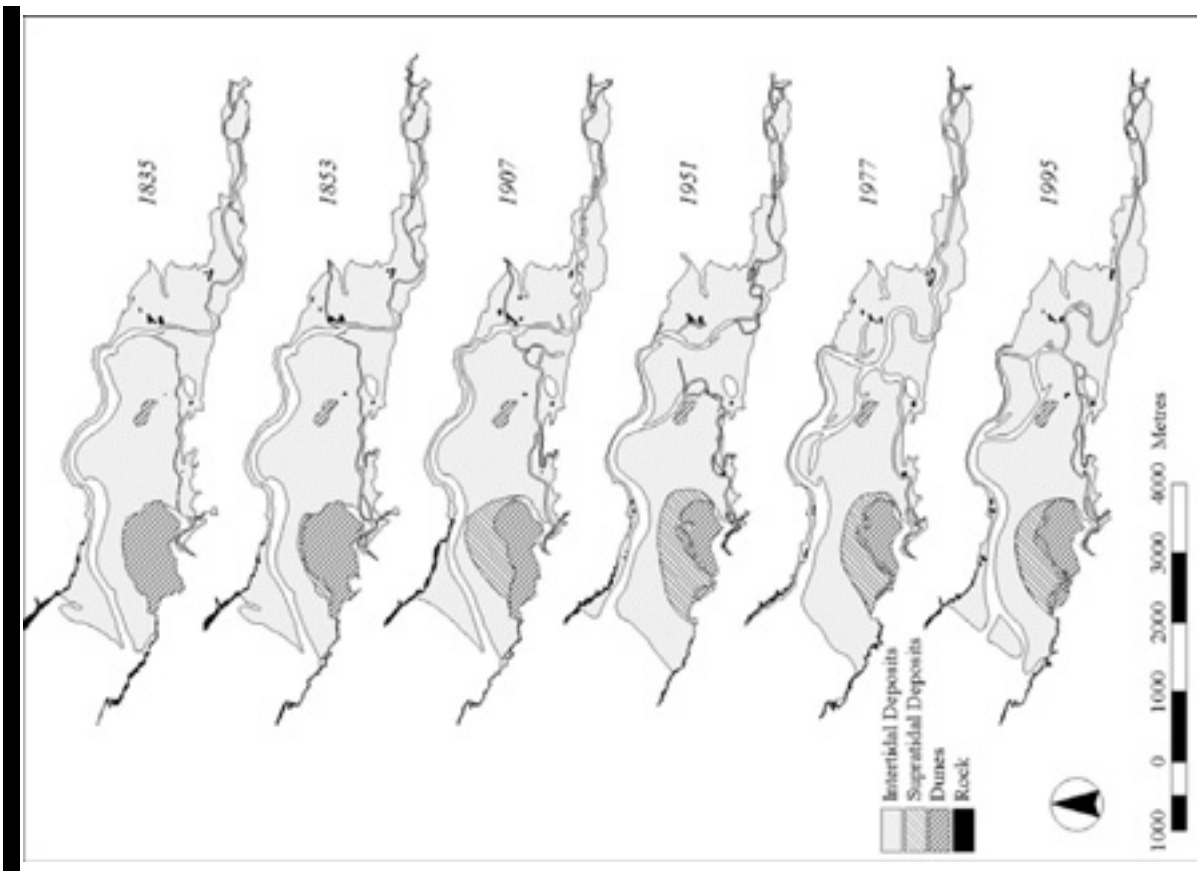

Figure 6. Morphological changes in the Loughros Beg estuary.

Although the west Donegal estuaries have evolved in response to sea level rise throughout the Holocene, their meso-scale behaviour is not primarily driven by sea level change. Historical sea level records in the north-west of Ireland are scarce. Although the long record from Newlyn, Cornwall, which shows a 20th century sea level rise of 1.6mmyr^{-1}, has been used in the examination of coastal evolution in the south-west of Ireland (ORFORD *et al.*, 1999), regional variations in post-glacial isostatic readjustment lessen its relevance to the Donegal coast. Tide-gauge records from Malin Head, in the north of Donegal, exhibit a rise of 0.18mmyr^{-1} (1960-1991) (SCOTT, 1996) whilst more extensive records (1845-1980) available from the north-east of Ireland suggest a rise of 0.6mmyr^{-1} (PUGH, 1982). Late-Holocene sea level curves are significantly different between the north-east and north-west of Ireland (SHAW & CARTER, 1994) and these discrete regional differences are likely to persist as the landscape continues to respond to glacial unloading. It is therefore doubtful that sea level has risen by more than 8cm in the last 150 years; and at the maximum rate of 0.6mmy^{-1}, the rise is considered to be relatively unimportant.

The west Donegal estuaries have not suffered from the industrial, agricultural and recreational pressures of some of their north-west European counterparts. Small-scale farming has impinged only slightly on the landward fringes of the dune environments, but has not impacted on the more dynamic estuarine and open coast margins. Terrestrial low-lying backbarrier areas have been partially drained over the last 50 years to improve agriculture, and ditches provide drainage through the limited saltmarshes into the estuary. In places, such as Gweebarra, this diversion and channelling of land-derived water has resulted in the development of small tributaries draining toward the main channel at low tide. Although this appears to be associated with the extension of ebb meanders into the backbarrier intertidal flats, the progressive change between 1835 and 1907 in Gweebarra suggests that channel migration was a natural consequence of widespread sedimentation throughout the system. This is also true of the upper reaches of Loughros' More and Beg, where increased sinuosity and braiding is evident.

In common with most west Irish coastal systems in the 17th and early 18th centuries, the introduction and 'farming' of rabbits has been a primary factor in the destabilisation of dunes, via grazing and burrowing (QUINN, 1977; CARTER & WILSON, 1991; CONVIE, 1995). Anecdotal reports suggest that this pressure did not have a fundamental effect on dune behaviour in west Donegal as rabbit population control mechanisms (e.g. infection with the myxomatosis virus) were employed in the early to mid 20th Century.

West coast palaeoenvironments show evidence of extreme event controls on coastal development, generally in terms of stratigraphical switches between biogenic and minerogenic sediments. The sharp contact between peat and overlying sand from Mayo, on the west Irish coast, is thought to be indicative of

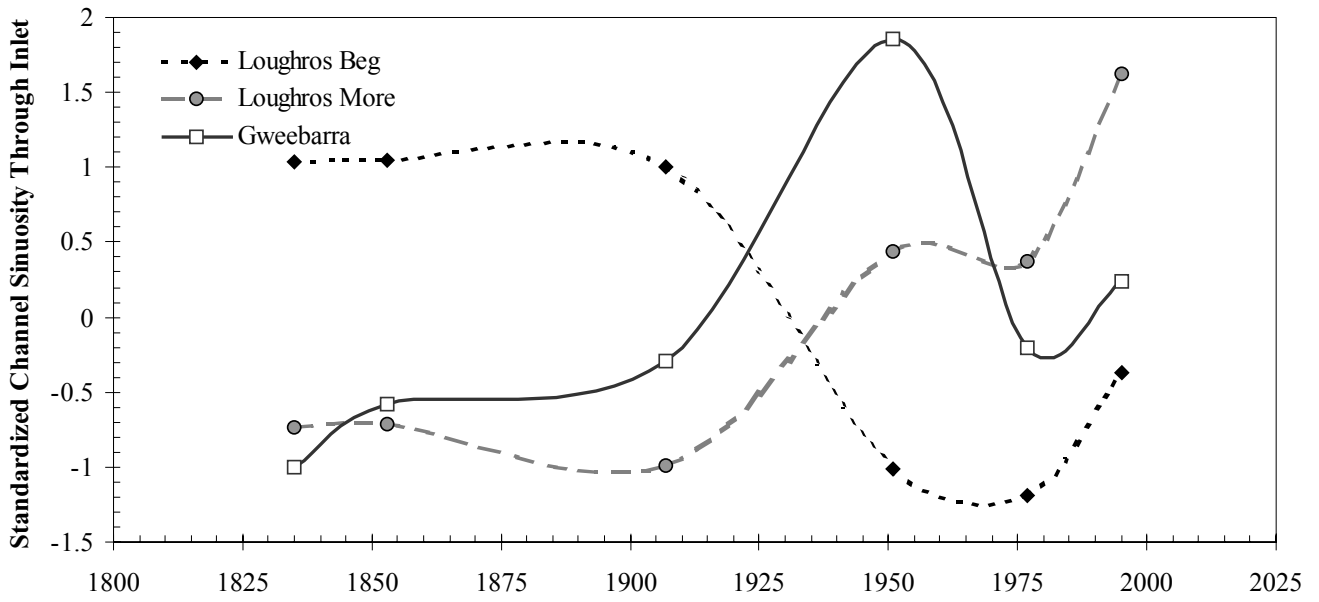

Loughros Beg	*1907-1951*: switch in channel position from south to bedrock margin on north side of inlet *subsequent changes*: channel stays in 1951 position until the 1990s, when it starts to migrate southward
Loughros More	*1907-1951*: lateral extension of ebb channel meander toward dune margin on north side of inlet *subsequent changes*: channel stays in ~1951 position until the 1980s, when it continues to migrate further north
Gweebarra	*1907-1951*: lateral extension of ebb channel meander toward bedrock margin on south side of inlet *subsequent changes*: channel migrates back to ~1907 by 1977, but has migrated slightly southward by 1995

[*Dating constraints supported by oblique aerial photographs (Gweebarra and Loughros Beg, 1965) and a SPOT image (west Donegal, 1980s).*]

Figure 8. Temporal changes in channel sinuosity within the Gweebarra and Loughros estuarine inlets, with supporting morphological observations. Positive change corresponds to meander extension; negative change to meander shortening.

sudden sediment deposition into a back-barrier area and is further suggestive of barrier overwash during storm surge events (DELANEY & DEVOY, 1995). SHAW (1985) demonstrated how similar controls on coastal development in Donegal have contributed to the present-day estuaries and their stratigraphical history. The development and reorganisation of coastal dune sediments over the Holocene has maintained a significant control on coastal dynamics, especially in terms of marine–estuarine–freshwater environmental transitions.

DISCUSSION

The results presented above show a variety of forms of coastal change at the historical timescale. While a generic model of estuarine sedimentation has been presented, there is significant inter-estuary variability in the detail in each sedimentary zone. This is ascribed to differing physical controls on estuary morphology. Against this background, there is an apparent consistency in the timing of initiation or increased rates of morphological change in the1907-1951 period in the west Donegal estuaries which suggests a possible regional conformity in the forcing mechanisms. Although the instrumental wind climate record does not precede the 1950s, the North Atlantic Oscillation (NAO) winter (November-March) index (Figure 9), as an expression of north-east Atlantic storminess (HURRELL, 1995; JONES *et al.*, 1997), provides an important signature of historical climate change on this coast (BURNINGHAM, *in press*).

Between 1907 and 1951, surface degradation of the dune systems in the Gweebarra and Loughros estuaries was accompanied by dune front erosion at Rosbeg in Loughros More (BURNINGHAM, 2002), and channel switching at Loughros Beg (BURNINGHAM, *in press*). The position of the channel within the Loughros Beg inlet has only moved between 1907 and 1951 and between 1977 and present, and saltmarsh sedimentation sequences at the head of the Loughros Beg estuary show marked peaks in deposition rate in the early 1940s and mid-1980s, which are thought to be associated with storm surge sedimentation (WHEELER *et al.*, 1999). While the possibility of aliasing over this long time period cannot be definitively ruled out at this stage, the comparable timing of these diverse geomorphological signatures and the NAO-derived representation of climate forcing, suggest a potential regional-scale morphological response to enhanced storm climate.

The period of these marked morphological changes correlates well with the sustained positive phase of the NAO in the early 20th century and the more recent positive phase over the last 20 years (BURNINGHAM, *in press*). Although it is not clear whether the 1907-1951 period was marked by one or more extreme events, the dune environments had clearly suffered considerable erosion by 1951. The concurrent and subsequent behaviour of the estuarine systems is considered to represent a range of morphodynamic responses to this period of extensive erosion. Whilst the 1907-1951 switch in channel position at Loughros Beg is attributed to storm surge flooding (BURNINGHAM, *in press*), the changes within the Gweebarra inlet are thought to be directly associated with sediment released from the 1907-1951 storm event(s). The presently sand-choked inlet is indicative of excess flood-tidal delta deposition here, and at Trawenagh may be indicative of sediment release during periods of increased storminess. Although there are no dunes within the Trawenagh system, the inlet is sufficiently close to the nearshore and dune environment of Dooey that, in the event of storm-related erosion, some sediment may be partitioned to the Trawenagh environment. At Loughros More, flood-tidal delta deposition may have initiated the northward migration of the inlet meander: dune destabilisation of Magheramore at that time is thought to have contributed to the erosivity of the meander extension.

Since 1951, dune surfaces have recovered to some extent, and the estuarine environments have exhibited behaviour associated with infilling: tidal flat sedimentation is often accompanied by a change from flood to ebb-dominated hydrodynamics (CARTER *et al.*, 1992), increased channelling of tidal flow and hence enhanced sinuosity (ROY, 1984). In Loughros Beg, the increased sinuosity of the main ebb channel within the estuarine basin correlates well with a post-1951 period of sediment redistribution, which is also evident in Gweebarra and Loughros More. Elsewhere, reworking of sediment is reflected in the progradation of small areas of estuarine foredunes.

The morphological behaviour recognised in the west Donegal estuaries over the historical scale is comparable to an erosional

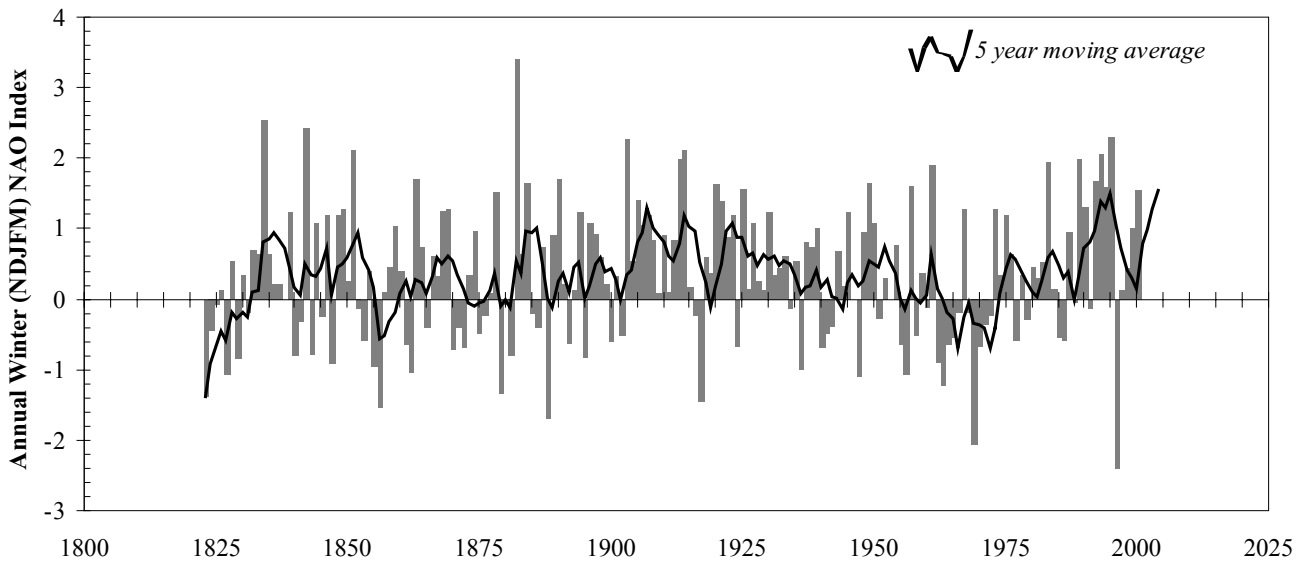

Figure 9. North Atlantic Oscillation winter (November-March: NDJFM) index (1823-2000) [Source: JONES (2002)].

front whereby sediment eroded from one area contributes to deposition elsewhere on the coastline, resulting in a landward translation of coastal deposits (ORFORD *et al.,* 1991). In those systems that have supratidal bodies in the inlet region, sediment released from the dunes is reworked and re-deposited elsewhere in the estuarine basin. At Trawenagh, morphological changes are more discrete because the lack of supratidal sediment bodies has reduced the sediment availability required for the estuary to behave in a similar way to the Gweebarra and Loughros estuaries. Although there is some suggestion that flood-tidal deposition has occurred, sedimentation volumes are considerably smaller due to the lack of site-specific sediment sources.

Changes in relative sea level over the period in question are minimal, and are thought to be secondary to the dominant storm climate controls on coastal morphology on the north-west coast. It is therefore tentatively suggested that these systems are exhibiting behaviour associated with an erosional front, but under negligible sea level rise. The importance of this recessional signature is in the role of the supratidal systems in supplying the estuarine systems with sediment. In the absence of significant fluvial deposition, marine forcing appears to drive coastal sediments into the estuarine systems through marginal dune erosion, flood-tidal deposition and intertidal flat sedimentation. Similar behaviour has been observed over a shorter time-scale in south Wales (JAGO, 1980), where the Taf estuarine environment is infilling from a storm-wave delivered marine source.

It is also apparent that meso-scale morphological behaviour is dependent on the genetic properties and evolutionary trajectory of each system. Geological controls strongly influence inter-estuary variability. Tidal currents in Gweebarra are deflected by rock outcrops throughout the system, which have contributed to the sinuous nature of the ebb channel. In Loughros More, the presence of a headland divides the dune shoreline between the Rosbeg and Magheramore systems, which otherwise might have the characteristics of the Dooey barrier in Gweebarra. Unlike Loughros More, the bedrock shoreline of Loughros Beg has constrained meander migration to a natural swathe between north and south margins. In Trawenagh, bedrock has an even greater influence to the narrow nature of the inlet, where no significant intertidal forms are able to develop.

The presence of coastal dune deposits is also intrinsically linked to inherited geological constraints. Aeolian sediments have preferentially accumulated where the regional topography has provided broad low-lying valleys, notably Gweebarra and Loughros More (Figure 1).

At Loughros Beg, the local physiography provides a partial explanation for the position and size of the Maghera system. A narrow valley projecting south-west of Maghera corresponds to the only low-lying margin of the estuarine basin, which presents the accommodation space and an appropriate aeolian-related orientation to allow the development of a discrete dune deposit. It is clear that the dominant topographical control, in terms of the constricted bedrock inlet, has prevented supratidal deposition at Trawenagh, and this has continued to influence the behaviour of the system throughout the Holocene to the present day.

CONCLUSIONS

The coastal systems of west Donegal exhibit both conformity and variance in behaviour, despite evolving under the same regional climate. The morphodynamic behaviour of both estuaries and dune systems continues to be controlled by the inherited structural framework and the legacy of post-glacial sea level rise that has influenced the type, size and location of sediment deposits within the systems.

The main changes in estuarine morphology are associated with the inlet supratidal sediment bodies and ebb channels throughout the systems. Storm-related dune erosion appears provides the main sediment source to the estuarine environment. Intra-estuarine sediment reworking and recycling within the inlet, and through the tidal-delta shoals, contributes to small-scale dune progradation and intertidal flat sedimentation, representative of behaviour associated with an erosional front.

The major conclusions are as follows:

(1) the west Donegal estuaries exhibit behaviour associated with an erosional front in the absence of significant sea level rise: the primary forcing mechanism is, instead, considered to be the north-east Atlantic storm climate.

(2) geological controls have an important role in the evolution of estuarine systems, particularly as a determinant of accommodation space for inter- and supratidal sediment bodies

(3) coastal dune deposits provide an essential source of sediment on low drift, sediment-starved coastlines.

ACKNOWLEDGEMENTS

This research was funded by a Department of Education for Northern Ireland Distinction Award. Thanks to Jon French, Joanne Millington and an anonymous reviewer for their valuable comments on the original draft. We also thank Colin Burningham for the use of his photograph (Figure 2A).

LITERATURE CITED

BRUNICARDI. 1914. The shore-dwellers of ancient Ireland. *Journal of the Royal Society of Antiquaries of Ireland*, 44, 185-213.

BURNINGHAM, H. 1999. *Morphodynamics of West Donegal Estuaries*. Unpublished D.Phil. Thesis, University of Ulster, 281pp.

BURNINGHAM, H. 2000. Short-term changes at an inlet margin dune barrier: Dooey Spit, Gweebarra Estuary, north-west Ireland. *Periodicum Biologorum*, 102, 505-512.

BURNINGHAM, H. 2002. Meso-scale morphological changes in the Loughros More estuary. *Proceedings of Littoral 2002: The Changing Coast*, 3, 265-270.

BURNINGHAM, H. *in press*. Morphodynamic Behaviour of a High-Energy Coastal Inlet: Loughros Beg, Donegal, Ireland. In: FITZGERALD, D. M. & KNIGHT, J. (eds.) *Morphodynamics and Sedimentary Evolution of Estuaries*.

CARTER, R. W. G. & STONE, G. W. 1989. Mechanisms associated with the erosion of sand dune cliffs, Magilligan, Northern Ireland. *Earth Surface Processes and Landforms*, 41, 1-10.

CARTER, R. W. G. & WILSON, P. 1991. Chronology and Geomorphology of the Irish Dunes. *In*: M. B. QUIGLEY (ed.), *A Guide to the Sand Dunes of Ireland*. 18-41.

CARTER, R. W. G. & Wilson, P. 1993. Aeolian Processes and Deposits in Northwest Ireland. *In*: K. PYE (ed.), *The Dynamics and Environmental Context of Aeolian Sedimentary Systems*. Geological Society Special Publication No. 72, 173-190.

CARTER, R. W. G., DEVOY, R. J. N. & SHAW, J. 1989. Late Holocene sea levels in Ireland. *Journal of Quaternary Science*, 4, 7-24.

CARTER, R. W. G., ORFORD, J. D., JENNINGS, S. C., SHAW, J. & SMITH, J. P. 1992. Recent evolution of a paraglacial estuary under conditions of rapid sea level rise: Chezzetcook Inlet, Nova Scotia. *Proceedings of Geologists' Association*, 103, 167-185.

CONLEY, D. C. 1999. Observations on the impact of a developing inlet in a bar built estuary. *Continental Shelf Research*, 19, 1733-1754.

CONVIE, G. 1995. *A regional assessment of dune/machair systems management in County Donegal*. Unpub. MSc Thesis, University of Ulster, 213pp.

COOPER, J. A. G. 1993. Sedimentation in a river dominated estuary. *Sedimentology*, 40, 979-1017.

COOPER, J. A. G. 2002. The role of extreme floods in estuary-coastal behaviour: contrasts between river- and tide-dominated microtidal estuaries. *Sedimentary Geology*, 150, 123-137.

DALRYMPLE, R. W., ZAITLIN, B. A. & BOYD, R. 1992. Estuarine facies model: Conceptual basis and stratigraphic implications. *Journal of Sedimentary Petrology*, 62, 1130-1146.

DELANEY, C. & DEVOY, R. 1995. Evidence from sites in Western Ireland of late Holocene changes in coastal environments. *Marine Geology*, 124, 273-287.

D'EVELYN, A. M. 1933. A sandhill settlement, Maghera, Co. Donegal. *Journal of the Royal Society of Antiquaries of Ireland*, 63, 88-100.

FINLEY, R. J. 1978. Ebb-tidal delta morphology and sediment supply in relation to seasonal wave energy flux, North Inlet, South Carolina. *Journal of Sedimentary Petrology*, 48, 227-238.

FOSSITT, J. A. 1994. Late-glacial and Holocene vegetation history of western Donegal, Ireland. *Proceedings of the Royal Irish Academy*, 94B, 1-31.

HAYES, M. O. 1975. Morphology of sand accumulation in estuaries: an introduction to the symposium. *In*: L. E. CRONIN (ed.), *Estuarine Research*, Academic Press, New York, 2, 3-22.

HEAP, A. D. & NICHOL, S. L. 1997. The influence of limited accommodation space on the stratigraphy of an incised-valley succession: Weiti River estuary, New Zealand. *Marine Geology*, 144, 229-252.

HURRELL, J. W. 1995: Decadal trends in the North Atlantic Oscillation and relationships to regional temperature and precipitation. *Science*, 269, 676-679.

JAGO, C. F. 1980. Contemporary accumulation of marine sand in a macrotidal estuary, southwest Wales. *Sedimentary Geology*, 26, 21-49.

JONES, P. D., JÓNSSON, T. & WHEELER, D. 1997: Extension to the North Atlantic Oscillation using early instrumental pressure observations from Gibraltar and South-West Iceland. *International Journal of Climatology*. 17, 1433-1450.

JONES, P. D. 2002. North Atlantic Oscillation Index Data: UEA Climate Research Unit (accessed June 2002) http://www.cru.uea.ac.uk/cru/data/nao.htm.

KNOWLES, W. J. 1901. Prehistoric remains from the sandhills of the coast of Ireland. *Proceedings of the Royal Irish Academy*, 22, 331-389.

MACKENZIE, M. 1775. A Maritime Study of Ireland and the West Coast of Britain.

MENEILLY, A. W. 1982. Regional structure and syntectonic granite intrusion in the Dalradian of the Gweebarra Bay area, Donegal. *Journal of Geological Society London*, 139, 633-646.

MORTON, R. A., GIBEAUT, J. C. & PAINE, J. G. 1995. Meso-scale transfer of sand during and after storms: implications for prediction of shoreline movement. *Marine Geology*, 126, 161-179.

O'FLOINN, R. 1995. Sandhills, silver and shrines - Fine metalwork of the Medieval Period from Donegal. *In*: W. NOLAN, L. RONAYNE & M. DUNLEVY (eds.), *Donegal; History and Society*. Geography Publications, Dublin,

ORFORD, J. D., CARTER, R. W. G. & JENNINGS, S. C. 1991. Coarse clastic barrier environments: evolution and implications for Quaternary sea level interpretations. *Quaternary International*, 9, 87-104.

ORFORD, J. D., COOPER, J. A. G. & MCKENNA, J. M. 1999. Mesoscale temporal changes to foredunes at Inch Spit, south-west Ireland. *Zeitschrift für Geomorphologie*, 43, 439-461.

O'RIORDAIN, A. B. & RYNNE, E. 1959. A settlement in the sandhills at Dooey, Co. Donegal. *Journal of the Royal Society of Antiquities in Ireland*, 91, 58-64.

PUGH, D. T. 1982. A comparison of recent and historical tides and mean sea levels of Ireland. *Geophysical Journal of the Royal Astronomical Society*, 71, 809-815.

QUINN, A. C. M. 1977. *Sand Dunes: Formation, Erosion and Management*. An Foras Forbartha, Dublin,

RIGGS, S. R., CLEARY, W. J. & SNYDER, S. W. 1995. Influence of inherited geologic framework on barrier shoreface morphology and dynamics. *Marine Geology*, 126, 213-234.

ROY, P. S. 1984. New South Wales Estuaries: Their origin and evolution. *In*: B. G. THOM (ed.), *Coastal Geomorphology in Australia*. Academic Press Australia, 99-122.

SCOTT, B. 1996. *The morphodynamics of coarse clastic beaches: Examples from North Donegal, Ireland*. Unpublished D.Phil. Thesis, University of Ulster.

SHAW, J. & CARTER, R. W. G. 1994. Coastal peats from northwest Ireland: implications for late-Holocene relative sea level change and shoreline evolution. *Boreas*, 23, 74-91.

SHAW, J. 1985. *Holocene Coastal Evolution, Co. Donegal, Ireland*. Unpub. D.Phil. Thesis, University of Ulster, 278pp.

WHEELER, A. J., ORFORD, J. D. & DARDIS, O. 1999. Saltmarsh deposition and its relationship to coastal forcing over the last century on the north-west coast of Ireland. *Geologie en Mijnbouw*, 77, 295-310.

Journal of Coastal Research	SI 41	160-167	STRAEE 2002	Ferrara, Italy	ISSN 0749-0208

Sandy Tidal Flat Morphodynamics? Examples from Strangford Lough in Northern Ireland

Gonzalo C. Malvárez†, Fatima Navas†† Javier Alcántara††† and Derek W. T. Jackson‡

† Geografia Fisica ,
Universidad Pablo de Olavide
Sevilla, Spain
Email: gcmalgar@dhuma.upo.es

†† Coastal Management and
Information Systems Res. Group
Universidad de Sevilla, Spain

††† Facultad de Ciencias
Experimentales
Universidad C. de
Valencia, Spain

‡ Coastal Studies Research
Group
University of Ulster,
Coleraine, N. Ireland

ABSTRACT

GONZALO C. MALVAREZ, FATIMA NAVAS, JAVIER ALCÁNTARA and DEREK W. T. JACKSON, 2004. Sandy Tidal Flat Morphodynamics? Examples from Strangford Lough in Northern Ireland. *Journal of Coastal Research*, SI 41, 160-167. Ferrara (Italy), ISSN 0749-0208

In coastal research tidal flats are often classified and investigated in the context of estuarine dynamics due to the widely accepted view that tidal forces are the main responsible for their geomorphological evolution and that biological variables need to play a major role in its evolution. On the other hand coastal morphodyanmics deals mostly with geomorphological evolution of beaches taking a purely geological view on sediment dynamics. In this paper, a discussion is presented in relation to the adequate treatment of tidal flat research by illustrating various numerical and empirical methods used to address morphodynamics on the sandy tidal flats of Newtownards. Common to other sandy tidal flats, the intertidal shores of Newtownards in Strangford Lough (Northern Ireland) are affected by tidal flows (c 0.1 ms^{-1}) given the average tidal range of 3.5 m and the action of wind generated waves over the fine grained siliciclastic sediments which frequently shows rippled surfaces. The results from a wide range of investigations (previously published) that utilized mainly numerical modeling indicated that the flats of Newtownards characterized by a RTR (relative tidal range) factor of 2.3 to 7, are very sensitive to sediment redistribution due to combined water level / wave height effects which implies that wave energy dissipation due to bottom friction the primarily shoaling process during relative high energy events. Using empirical methods designed for beach morphodynamics research, it was found that (i) waves exceeded predicted values given short fetch under westerly winds, (ii) wave penetration was a parameter that proved extremely sensitive for sediment entrainment and was not sufficient to generate bedload sediment transport and (iii) further numerical simulations need to be conducted to achieve further understanding on the role of shoaling and spatial distribution of wave energy dissipation on the translating surf and nearshore zones to achieve a complete morphodynamic classification of these ultra-mega dissipative wave dominated environments.

ADDITIONAL INDEX WORDS: *ultra dissipative beaches, surf zone migration, wave height sensitivity.*

INTRODUCTION

Coastal geomorphologists have moved from simplistic classification schemes to rather complex and fine tuned morphological and dynamical expressions that are able to characterize most littoral settings. However, at the very extreme of the morphodynamic classifications of ultra dissipative beaches, sandy tidal flats are commonly ignored in the literature of beach science as the result of the complexity of investigating wave shoaling, breaking and swash on a high spatial resolution. Whilst open ocean beaches have been the subject of a tremendous variety of empirical and numerical studies and three morphodynamic zones (the swash zone, the surf zone and the zone of shoaling waves) are considered, tidal flats have consistently been the focus of separate research efforts. Dominance of cohesive sediments, extreme flatness of its morphology, higher degree of biological bioturbation and variable strength of tidal flows as main hydrodynamic force built a strong case for the isolation of tidal flats in morphodynamic approaches, especially in the case of muddy tidal flats. Sandy tidal flats are dominated by hydrodynamic forcing factors and morphologic settings that get them closer to open ocean beaches and thus a morphodynamic approach seems justified since wave induced sediment entrainment and combined wave-current interactions are expressed in complex assemblages of sedimentary spatial distributions.

Empirical relationship between the equilibrium gradient of morphodynamic zoning and wave and sediment conditions have been assumed for open ocean beach nearshores, but as zones shift up and down the intertidal flat with the tide, relative occurrences of each of these zones (morphodynamic zones) over the profile during a tidal cycle may be assumed to have a wide and mobile morphological imprint on tidal flats evolution. Sandy tidal flats can be also be included alongside the most extreme of tidal beaches.

Although tidal flats generally occur in low energetic settings, features may be encountered that suggest that the relative levels of energy could be high. CARTER (1988) approached a preliminary classification of tidal beaches from an energetic stand point and described the features to be expected as energy levels decreased from washed out profiles to mixed current ripple environments where sinusoidal forces are sometime superceded by the laminar

flow associated with tidal currents. The lowest energy environments in macrotidal beaches are supposed to be characterized by ridge and runnel morphologies as mobile shoaling, surf and swash zones operated on varying water depths (KING and WILLIAMS, 1949; MASSELINK and SHORT, 1993; NAVAS et al., 2001). Following this argument, most sandy flats would be morphologically dominated by ridge and runnel topographies; this, however, seems not always to be the case and instead a variety of wave and tide associated forms develop upon the extreme low gradients of the mega intertidal extents.

Several studies have demonstrated a broad link between wave energy and tidal flat morphology (BOYD et al., 1992; RYAN & COOPER, 1998). At a local scale, CARLING (1982) investigated the role of waves by the deployment of a wave pole at a single location and using time-averaged results as a measure of wave intensity. While the results apparently showed a link between wave action and tidal flat behavior at the scale of the whole tidal flat, these results were based on data from a single point and cannot explain adequately, variability within a tidal flat.

What seems clear is that the rates of wave energy dissipation (due to shoaling and not breaking) must affect tidal flats in the same fashion as nearshore regions of beaches despite the morphological adjustments. Tidal currents are a constant feature on the ultra dissipative environments of tidal flats but the hydrodynamic effects of them are most acute when combined wave/tide currents are present. In macrotidal environments, however, it is generally accepted that the influence of waves is diminished, mainly because tidal translation over the intertidal region results in rapid movement of surf and swash zones over the active area and thus tidal currents should play a greater role both in absolute terms and relative to local waves (NORDSTROM, 1992).

The complex interaction of the two forcing factors have been analysed by many authors but it appears that it is accepted that tidal forces have little influence on beach morphodynamics (MASSELINK and TURNER, 1999). However, these authors explain that as tidal range increases tidal flows and coupling tide/wave interaction plays a significant role particularly affecting the directional component of sediment transport.

Inside estuaries waves may occur as the result of filtering through its seaward entrance and, mostly, as result of wind generation inside the estuary. The types of waves generated this way are typically short crested, high frequency and steep and their geometry reflects the fetch available given constant wind conditions. Under steady wind, waves are highest at high tide because fetch is generally longer (in onshore wind conditions) but wave induced stress on the bottom surface may be small because under short period waves wave orbital motions cannot penetrate to the bed. GREEN and MACDONALD (2001) illustrated that at some optimum combination of wave/water depth, wave penetration under steep choppy waves influences resuspension of bottom sediments. Changing wind conditions and stable water levels are responsible for sediment resuspension in lakes given that wind generated waves are the only force in play that induces water column deep stresses (JIN and JI, 2001). Wave sensitivity to water level (induced by tidal effects) appears to be a crucial element in shoaling processes associated with waves acting across tidal flats. As is the case on macrotidal beaches, tidal stage determines how waves affect the bed sediments and also where. The duration of the effects of shoaling waves on the mobile "nearshore" dictates potential morphodynamical stages (MASSELINK and TURNER, 1999). Whereas beach profiles seem relatively insensitive to wave height across the dissipation zone, tidal flats appear to respond sedimentologically to variations in wave energy dissipation and wave orbital velocity. The combined effect of water level variation, fetch and tidal prism dynamics and related wave penetration presents a very complex scenario for characterization of morphodynamic criteria for tidal flats resulting in greatly fine-tuned models of waves, current, morphology and sediment grain sizes interactions.

The aim of this paper is to contribute in the discussion on weather tidal flat research should be placed in the context of coastal morphodynamics or estuarine research through an example from Newtownards in Strangford Lough, Northern Ireland. The flats are studied using concepts applicable to macrotidal beaches to establish whether some types of tidal flats could be addressed as extreme dissipative environments in a morphodynamic context. Drawing on results from numerical simulations previously published by the authors in the same line of work in this paper the results of an experiment are presented in the context of in situ measurements of hydrodynamic and sediment activation and transport during continuous recording sessions.

ENVIRONMENTAL SETTING

The intertidal sandy flats of Newtownards are located on the northern most confines of Strangford Lough (Figure 1). The Lough is an elongate embayment with an N-S traveling axis. It is bordered by bedrock topped by glacial sediments and contains many drowned drumlins within its margins. Average tidal range is 3.5m throughout and little amplification of the tidal wave is evident in the Lough. The bathymetric configuration of the Lough in the central regions exceeds 40m in depth whereas the margins of the system are characterized by a variety of intertidal flats, bedrock and glacial shorelines.

The intertidal areas are characterized by a flat or gently sloping sandy surface intersected by one major drainage channel and a number of temporally variable tributary channels. These display a characteristic morphology around the embayment. Examination of tidal flat cross sections shows that the intertidal area between high tide and low tide is about 1000-1200m along the western shore and only about 300-500m along the Eastern shore. Cross sections of the tidal flat generally have a marked break in slope that separates a gently inclined upper tidal flat from a steeper lower section leading to the low tide mark at the margin of the tidal and storm channel that drains from Newtownards.

Silici-clastic sediments on the flats are generally fine sands ranging from 0.10mm to 0.25mm. The wave climate is dominated by wind waves within the Lough with limited fetch distance and narrow entrance from the Irish Sea. Wind directions affecting the wave climate at Newtownards are typically from the SE.

The extensive intertidal regions for shoaling of wind generated waves on Newtownards tidal flats are characterized by extensive intertidal profiles with an extension that varies from the western to eastern shores.

Methods utilized for the investigation of this kind of environments often present shortcomings in addressing wave related information. Several authors have taken the empirical approach to the limit but in situ measurement is never capable to resolve wave propagation, shoaling etc. on a satisfactory level given the impracticability of deployment of an adequate number of probes and pressure transducers. As background to the experiment described in this article results from numerical simulation from previous research have been used (MALVAREZ et al. 2001a). These simulations were conducted to overcome the spatial resolution problem and illustrated a variety of issues. Amongst the main findings of this previous work was that location of sediment grain sizes appeared to be related to wave action as

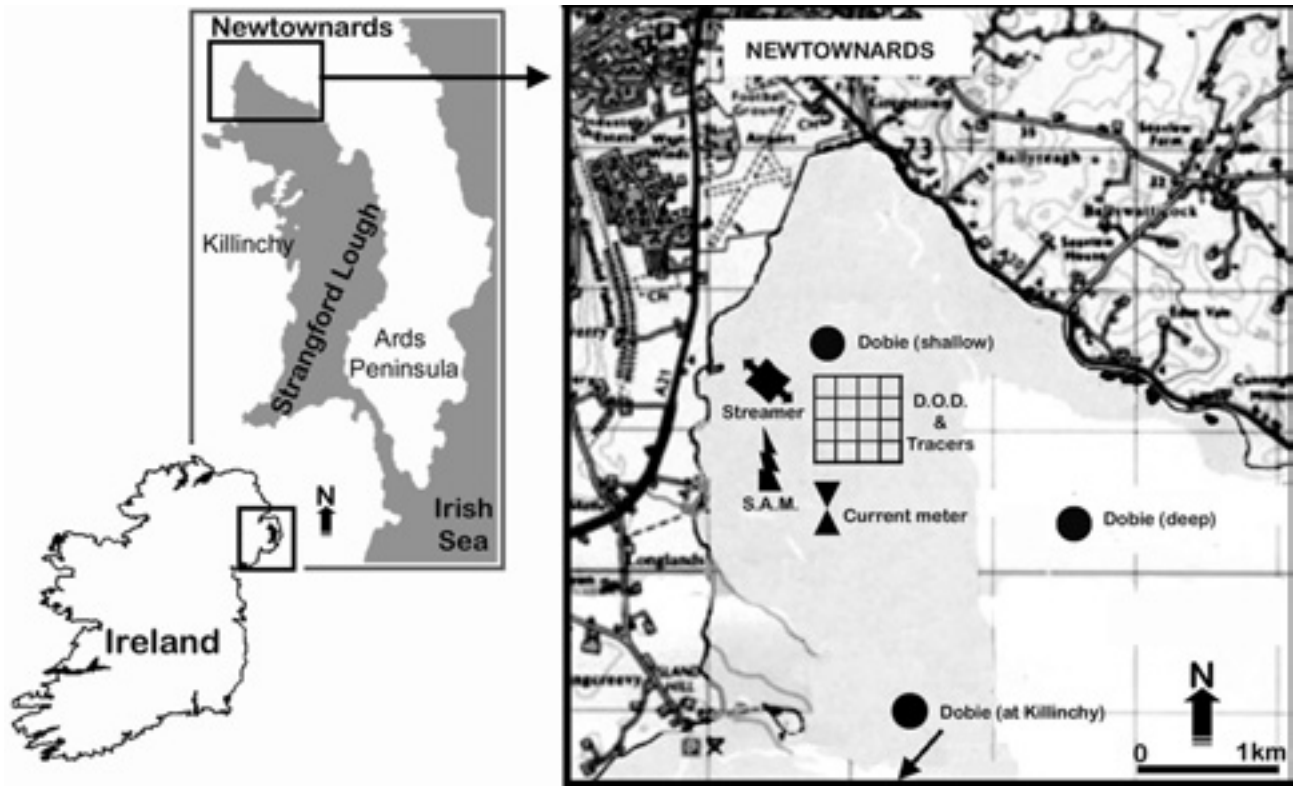

Figure 1. Location of sample area

indicated by significant correlations between wave orbital velocity and mean grain size of sediment (Figure 2).

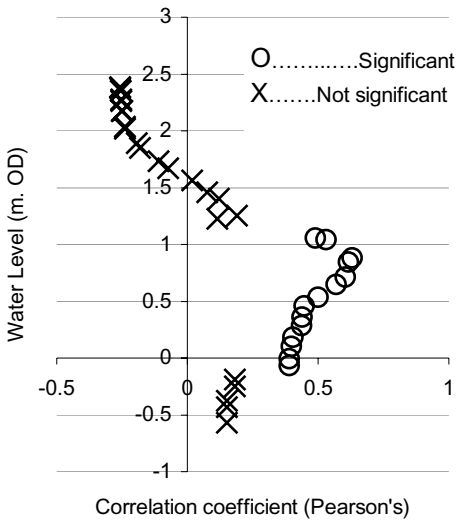

Figure 2. Relationship between recorded water level and statistical coefficient (relating wave action and sediment grain size).

The combined hydrodynamic and morpho-sedimentary data sets provided input for statistical analysis yielding significant correlations to determine optimum water levels that affected wave penetration on the sandy tidal flats. Multidirectional simulations upon the optimum water level from MALVAREZ et al. (2001b) also identified that wind records could be added to the high resolution approach, although results demonstrated that further control was needed on water level under variable wave geometries generated by real wind conditions.

Single point empirical approach

An empirical measurement campaign was planned after the optimum water level had been identified (MALVAREZ et al 2001a and b) which suggested that further control was necessary over the water level wave sensitivity relationships. A single point morphological and hydrodynamic experiment was organized to cover three events largest tidal events during the month of June 2002. In all, sediment transport was measured by a specially design streamer trap and fluorescent tracers, depth of disturbance and sediment bed change, tidal currents, wave height, period and orbital velocities in two sites and water levels in three sites (Figure 1). All the measurements were recorded in high temporal resolution over the three high tidal events.

The rational behind the experiment was to measure simultaneously tides, waves and sediment transport (bed load and suspended) to establish relationships between the morphodynamic variables. Three time slots, coinciding with predicted optimum water levels and tidal current velocities were targeted for short duration streamer trap measuring periods. Divers would open sequentially the streamer trap at given times for given duration.

The rest of the instrumentation (described below) was to record continuous time series and/or depth of disturbance during the three tides under investigation.

Hydrodynamics

A Valeport Ltd. Electromagnetic current meter (Series 800-2 axis) was deployed across the flood-ebb tidal current path to record flow velocities during the experiment. A Squirrel Grant data logger and battery pack was assembled into a stainless steel water-tight casing constructed for immersion deployment beside the probe. The interrogation period for the data logger was set at 5 minutes. The measuring probe was fixed to a stainless steel frame held in position at 1.0 m height.

Three Dobie wave and tide gauges (GREEN, 1998) were deployed at three locations to record waves and water levels. Hydrostatic pressure was recorded as time series of 2048 samples at 10 minutes intervals during the three events pressure is then processed through the PEDP software which uses semi-empirical formulae to establish wave height, period, significant orbital speed at the bed, wave penetration through the column of water, etc. Water levels were recorded at Killinchy for temporal meso scale tidal reference. One of the wave recorders was deployed in the center of the instrument array to establish local wave hydrodynamics and the third wave/water level recorder was deployed 1.2 kilometers south of the experimental site to record deeper water wave conditions. Data was recorded simultaneously on all wave recorders to enable synchronous post experiment analysis.

Sediment Transport

A stainless steel sediment transport Streamer Trap (Figure 3) was constructed based on a modified design from KRAUS (1987). The trap was located in the instrument array site facing the incoming flood tide in the first instance and was then rotated after the first tide to measure ebb related sediment transport. The trap had 12 inlets that were covered with individual shutters for selective release by divers. Each column of inlets was coded identifying a water level within the experiment. The "socks" (1.2m bags of 63mm mesh) were placed semi-horizontally to retain sediments in low velocity flow conditions.

Depth of disturbance, sea bed position or active mixing layer was measured using three methods: A Sediment Activity Meter (JACKSON and MALVAREZ, 2002) was deployed in the experiment array site to measure sea bed motion during the tide at 124 seconds intervals (Figure 3). Depth of disturbance was measured using a 100m X 100m D-GPS referenced grid of rods and washer combination. Relative to this grid, 50kg of dyed sand were injected beside the main experimental site over. Dyed sand was prepared in the laboratory, using sediment previously extracted from the experimental site and fluorescent orange paint. Grain sizes were tested in the settling tube to check relationship between native (non-colored sand) and dyed sand, and results were satisfactory (native sand: Median 2.78, Mean 0.154, Sorting 0.76, Skewness -1.42; and dyed sand: Median 2.75, Mean 0.155, Sorting 0.53, Skewness -1.85).

Wind data was also recorded simultaneously at 30 minutes interval from a Davies Weather Wizard III weather station linked to PCLink software. Wind direction and speed were logged during the three-day experiment.

RESULTS

All recorded data was downloaded and entered onto a database for analyses.

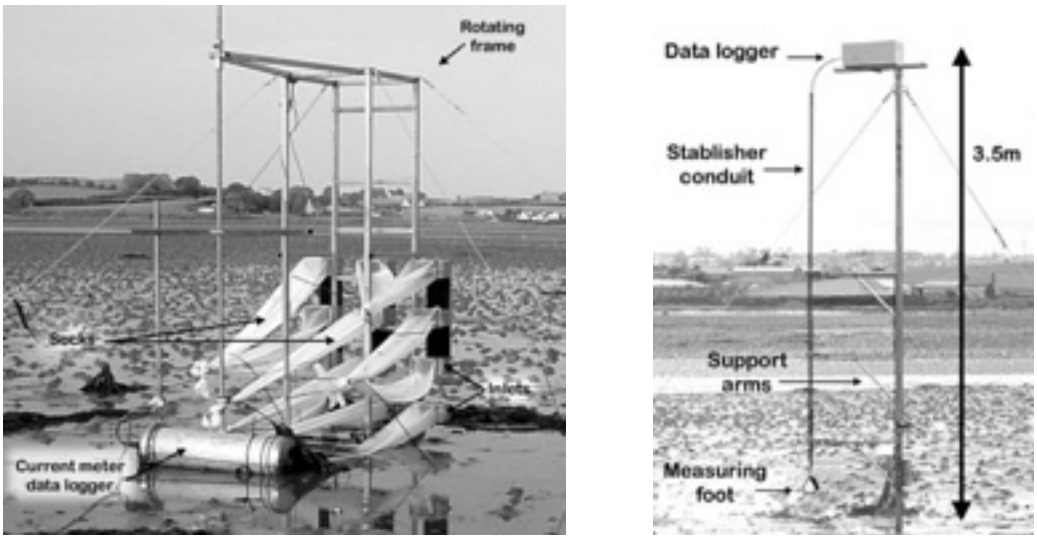

Figure 3. Sediment transport Streamer Trap, current meter data logger (left photograph) and Sediment Activity Meter (S.A.M.) (right photograph) deployed on the sandy tidal flats.

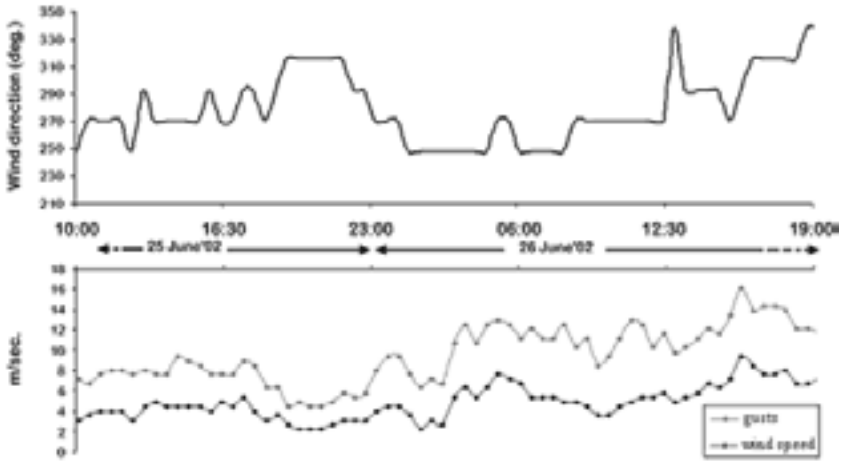

Figure 4. Wind speed and direction recorded at Newtownards meteorological station during the experiment at 30 minute interval.

Wind data (speed and direction) was also recorded during the experiment. The partial record over the experimental period (Figure 4) shows an increasing wind velocity towards the third tidal event coinciding with a change in direction to take a full WNW approach during this high wind period. This resulted in the generation of steep waves during the latter part of the experiment.

Hydrodynamics

Water levels and wave records are shown in Figure 5a for the duration of the experiment. The three tides recorded can be identified and an asymmetry in the flood/ebb recognized. The relative tidal envelope on the site was small reaching a maximum of 2m. during high tide. Waves reacted to the expansion of the tidal prism (and fetch) achieving maximum wave height during the high tide of the third tide of the experiment. Values for orbital velocity (Figure 5b) also peaked during the third high tide. Wave period remained stable during most of the experiment but with very low values (high frequency waves), which would be expected under locally, generated waves. The significant short periods combined with relatively high waves depicts geometry of very steep and irregular waves inducing high orbital velocities but penetrating very little in the column of water as a result of short wave lengths.

Tidal currents were low during the three tidal events despite Spring tide conditions. The current meter recorded values outside the main drainage channels to portray realistic currents on the flats. The two vector components of the recorded currents were added to establish the overall flow (Figure 5c). During the second tide the data logger was set to off by the integrated timer thus recording no currents. However, during the third tide, values for the ebbing tide peaked under the combined effects of Northwesterly winds and falling tide. Waves recorded during that period also showed greater values and coupling of wind induced currents plus hydrodynamic forces may had occurred.

Sediment transport

The most significant result of the experiment was related to the sediment transport elements. Despite underwater evidence (as divers opened the inlets for the streamer traps) of existence suspended sediment no significant volume of sediment was trapped by the streamer trap, measured by Sediment Activity Meter (SAM), recorded as depth of disturbance nor inflicted on the injected dyed sand. This notable result was consistent throughout the three tides recorded in the experiment.

There was no evidence of any morphological change along the depth of disturbance grid either (as measured by D-GPS which recorded exact same positions within the error band of the apparatus).

The focus of the experiment presented in this article was to empirically measure how high tidal flow velocities (Spring tides in the area) and strong winds could be used to illustrate the forcing factors in play upon the macrotidal beach using a suit of equipment designed for surf zone investigations. Although wind speeds and current velocities reached as high values as expected and relatively high and steep waves were generated locally under very limited fetch, no morphological or sedimentological response was noted at any point (despite measuring at theoretically optimum water levels).

Northwesterly winds dominated the recording period which produced extremely steep waves that grew (developed) offshore rather than propagate onshore. The tidal prism was blown from the NW quadrant and the effects on tidal current velocities were also noted during the third ebbing tide. The coupling of optimum wave penetration (combination of high orbital velocities and water levels within closure depth) did not appear to affect the decisive role indicated in previous research, perhaps because the limited fetch controlled wave generation and development above water depth.

Resuspension was visible during diving although very clear waters throughout the experiment indicate that sediment concentration was low, flocculation nil and suspended sediment was deposited over the source area. This was radically documented by the lack of motion on the dyed sands deployed over the study area. CIAVOLA et al., (1997) documented the effect of breaking wave height on activation of sediments as documented by measurements of depth of disturbance. Using this framework the SAM apparatus, which had been tested on open beaches in the North of Ireland yielding results that were

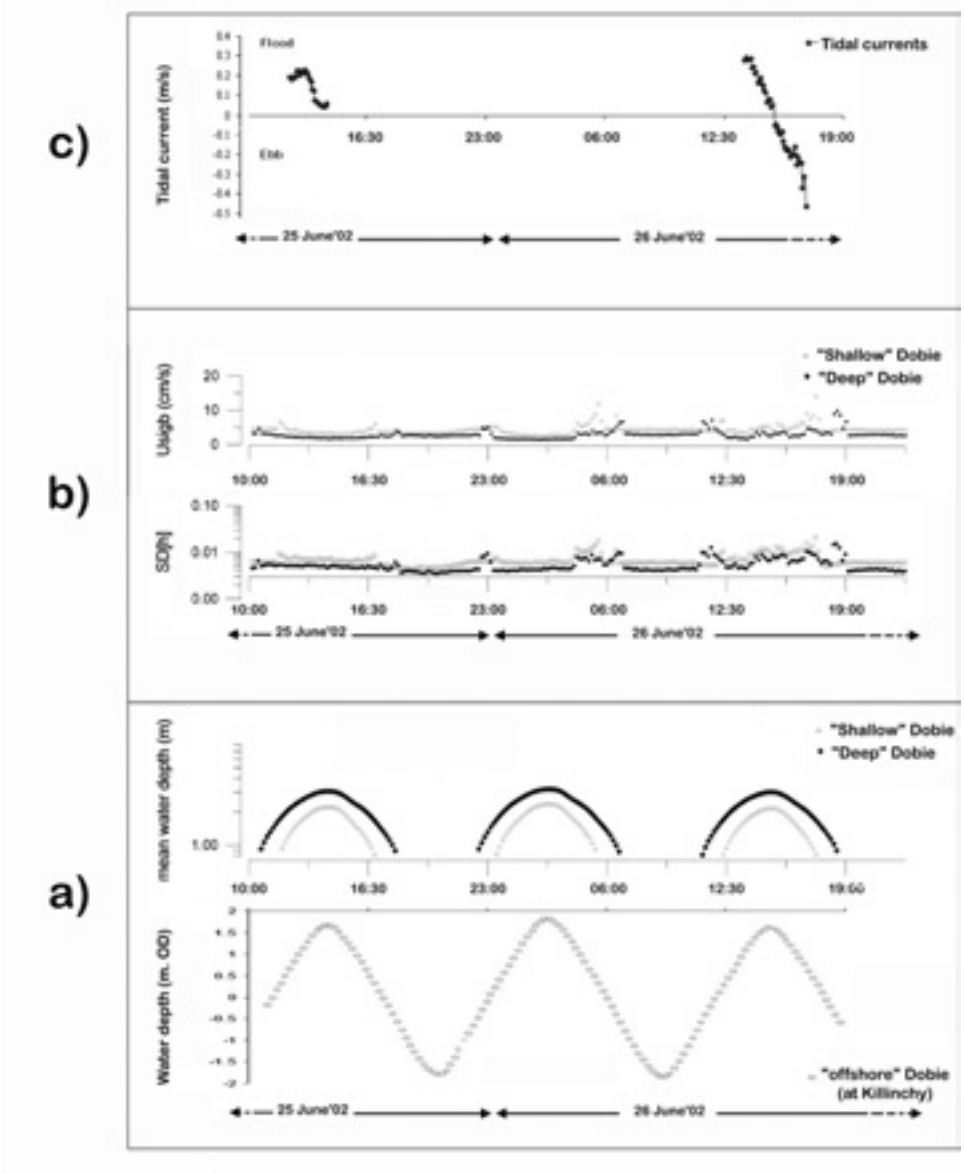

Figure 5. Hydrodynamic data recorded during the experiment: a) water levels, b) wave orbital velocity and c) tidal current velocity.

comparable but used shoaling rather than breaking wave height (JACKSON and MALVAREZ, 2002), proved inefficient on the tidal flat. Within the framework of morphodynamic research measurements of depth of disturbance should have yielded results despite the fact that the slope (as a controlling factor) was much lower than on beaches. Thus the lack of sedimentation under waves of significant potential for activation shows that the temporal scales under which beaches operate may not be comparable to that of tidal flats.

DISCUSSION

The definitive results of these experiments are interpreted here in the light that if tidal flats are investigated utilizing equipment that is designed to study beaches no significant sediment motion or topographic change would be measured. If physical processes affecting tidal flats and beaches are the same, why theoretical predictions (such as interpreted from numerical simulations) did not match expected results in real empirical conditions? Conceptually, however, the mega dissipative environments found in tidal flats could be classified under morphodynamic classification due to expected dominance of tidal flows over wave-induced morphodynamics. This approach may be the most effective to go forward in tidal flat research. In macrotidal environments in particular, the extent of beaches can dictate that the flat morphology dissipate wave and tidal energy generating a shift by which the tide may be regarded as a water level controller rather than a dynamic forcing factor. Tidal current alone may not be sufficient in these conditions to exert entrainment velocities on sea bed sediments and thus deposition dominates (extremely fine sediments and muds).

Therefore to introduce tidal flat research into beach morphodynamics it is proposed to place the tidal flats of Newtownards along with open ocean macrotidal beach

morphodynamic parameters. First the extent of tidal flats can be characterized by the expression:

XIT = TR / tanb

where XIT is the lateral extent of the intertidal area, TR is the tidal range and tanb is the beach gradient. For Newtownards the tidal flats can then be calculated as intertidal extents of 1230 and 520 m for the western and eastern shores respectively. To refine this concept and further into a morphodynamic classification a definition of the morphodynamic states are described by the parametric factor RTR (MASSELINK and TURNER, 1999):

RTR = TR / H

where RTR is the relative tidal range, TR is the tidal range and H is wave height. Table 1 shows a classification of morphodynamic environments based on the above RTR index. Using this index for Newtownards the tidal flats may be characterized as wave dominated to mixed wave-tide dominated (index 2.5 using local measured H and TR on the intertidal, 2.3 using storm H and 7 on average conditions) clearly placing the study of these tidal flats in the context of other macrotidal beaches.

Given then the classification of these environments as mixed wave-tide dominated, it follows that the approach taken to the investigation of such environments could be marked within empirical and numerical investigations on macrotidal beaches. Sandy tidal flats have, however, never been viewed in this way. There is little research done from this standpoint and has to our knowledge has always coincided with understated reflection on the role of wave action on tidal flats sedimentation.

An analysis of the variables involved can also help understanding tidal flats as macrotidal beaches. Wave energy distribution across sandy tidal flats varies according to the state of the tide and, is most effective across the tidal flat at about mid-tide. At lower tidal levels high orbital velocities occur in narrowly defined zones that represent a narrow surf-zone towards the seaward margins of the intertidal flat. At lower tidal levels (between 0 and 1m OD in Newtownards with storm waves), wave orbital velocities are less intense but are above sediment transport thresholds capable of work across a much greater area of the tidal flat. At elevations greater than 1m OD, wave bottom orbital velocities decrease across most of the tidal flat and a narrow zone of high orbital velocity develops at high-tide margin of the tidal flat. Under these conditions penetration of wave energy through the water column is impeded by the increased water depth, and wave action on the sea bed does not produce sediment movement.

Spatial variations in wave energy levels can explain much of the observed variability in sediment grain size (MALVAREZ et al., 2001a). Rather than a rapidly migrating zone of intense activity of breaking waves acting as main control on sediments grain size on such a sandy tidal flat (such as exists at the margin of the advancing or retreating tide), prolonged activity at a slightly lower energy level may have a more significant role on the distribution of sediment texture. Wave shoaling processes are active across a broad area of the tidal flat; the strongest relationship is found between wave velocities and sediment texture.

The issue of water level and wave penetration is however, particularly sensitive in these mega dissipative tidal flats. Previous research has also shown how wave penetration through the column of water and the variability of shoaling and surf zones lead to the sandy tidal flat sedimentation in the context of generic coastal morphodynamics. GREEN and MCDONALD (2001) indicated that some optimum water level appeared to occur during their experiments in New Zealand that affected sedimentation under the effects of waves.

Table 1. Classification of morphodynamic environments based on the RTR index. After MASSELINK and TURNER, 1999.

Relative Tide Range	Group	Beach type
RTR < 3	Wave-dominated	1. Reflective
		2. Barred
		3. Dissipative
3 < RTR < 15	Mixed wave-tide	4. Low tide terrace
3 RTR < 7		5. Low tide bar/rip
3 RTR < 15		6. Ultra-dissipative
RTR > 15	Tide-dominated	7. Transitional (beach to tidal flat)

The effects of combined wave and tidal action is being considered the focus of a variety of research projects currently (e.g. some work published in this volume) but further research is needed to document the complex scenario presented on sandy tidal flat sedimentation. The decisive role of biological factors in sedimentation processes may be more significant than anticipated and certainly than it is considered in beach science. The sensitive balance of tidal and wave interaction may also need to be reflected in the manner in which sea bed morphology is described. A great amount of fine tuning is needed to illustrate the potential role of sea grass (e.g. zoostera marina) on physical sedimentation processes as well a the topographic effect that worm mounts may have on wave propagation over extreme shallow environments.

It is proposed that given the unpredictability of morphodynamic conditions to design a more successful empirical experiment and the large uncertainty that is intrinsic to numerical modeling in these environments, in situ measurements could be the way to better our knowledge on sandy tidal flat morphodynamics. Research carried out on tidal flats using in situ flumes deployed on the surface of the (exposed) tidal flats has documented the validity of such an approach. An in situ wave simulator could be proved a useful addition to the state of the art in the context of morphodyncmics of tidal flats.

CONCLUSIONS

In this paper a review of the context of macrotidal beaches has been presented in view to considering sandy tidal flats as mega-macrotidal beaches. Measurements and calculation showed that using existing morphodynamic indicators, the sandy tidal flats of Newtownards in Strangford Lough, Northern Ireland should be classified as wave-tide dominated intermediate environments and thus its investigation could be approached from the stand point of beach science rather than a more traditional estuarine one.

Previous research illustrated how water level combined with numerically simulated wave energy could be used to document potential dominance of wave induced processes over tidal currents on sandy tidal flats. A new experiment was then carried out using the knowledge gathered from this previous research. The deployment of various apparatus to measure hydrodynamic (tide and waves) as well as sedimentation processes (bed load, depth of disturbance and suspended sediment transport) was carried out on a selected portion of the sandy tidal flats of Newtownards. Results illustrated that although the hydrodynamic conditions during the high energy events recorded in the experiment should have been

sufficient to entrain sediment, traps and other devised deployed for the experiment recorded negligible quantities.

These results illustrate that the combination of factors affecting sedimentation on tidal flats are more complex than measured and that further research needs to be conducted to document further the relationships between water level, wave orbital velocity and penetration, tidal current velocities and direction and its integration with morphologic change.

A discussion is presented opening a variety of possibilities for taking tidal flat research further. A series of recommended lines of work are proposed including the development of in situ wave simulators to develop more controlled experiments in the field including oscillatory motions for the first time in the simulation of hydrodynamic forces.

ACKNOWLEDGEMENTS

The authors would like to thank the staff of the mechanical workshop and the personnel of the electronic workshop of the Faculty of Life and Health Sciences of the University of Ulster at Coleraine, in particular Nigel MacAuley and Terry Griffin, for capturing our ideas and transforming them into scientifically sound instrumentation.

LITERATURE CITED

BOYD, R., DALRYMPLE, R., and ZAITLIN, B.A., 1992. Classification of clastic coastal depositional environments. *Sedimentary Geology*, v. 80, p. 139-150.

CARLING, P.A., 1982. Temporal and spatial variation in intertidal sedimentation rates. *Sedimentology*, v. 29, p. 17-23.

CARTER, R.W.G., 1988. *Coastal Environments*. Academic Press, Cambridge, 617pp.

CIAVOLA P., TABORDA R., FERREIRA Ó. and ALVEIRINHO DIAS J., 1997. Field observations of sand-mixing depths on steep beaches. *Marine Geology*, 141, 147-156.

GREEN, M.O., 1998. DOBIE the intelligent wave gauge, Operator Manual, NIWA (National Institute of Water and Atmospheric Research Ltd.), Manufactured by NIWA Instrument Systems, Christchurch, New Zealand.

GREEN, M.O. and MACDONALD, I. T., 2001. Processes driving estuary infilling by marine sands on an embayed coast. *Marine Geology*, 178(1 – 4), 11-37.

JACKSON D.W.T. and MALVAREZ, G., 2002. A new, high-resolution 'depth of disturbance' instrument (SAM) for use in the surf zone. *Journal of Coastal Research* , SI, ICS2002.

JIN, K.R. and JI, Z.G., 2001. Calibration and verification of a spectral wind-wave model for Lake Okeechobee. *Ocean Engineering*, Vol. 28, pp. 571-584.

KING, C.A.M. and WILLIAMS, W.E., 1949. The formation and movement of sand bars by wave action. *Geographical Journal*, 113, pp. 70-85.

KRAUS, S. C., 1987. "Application of Portable Traps for Obtaining Point Measurements of Sediment Transport Rates in the Surf Zone," *Journal of Coastal Research*, Vol 3, No. 2, pp. 139-152.

MALVAREZ, G. and COOPER, J.A.G., 2000. A whole-surf zone approach to modelling nearshore circulations. *Journal of Coastal Research* ,16: 800-815.

MALVAREZ, G., COOPER, J.A.G. and J.A.G., JACKSON, D.W.T., 2001a. Relationship between waves and tidal flat sedimentation *Journal of Sedimentary Research*, Vol. 71, 5, pp. 705-712

MALVAREZ, G., COOPER, J.A.G., JACKSON, D.W.T. and NAVAS, F., 2001b. The role of wave action on sedimentation of tidal flats: application of high spatial resolution numerical modelling in Strangford Lough, Northern Ireland. *Journal of Coastal Research*, S.I. 34, pp.172-182.

MASSELINK, G. and SHORT, A.D., 1993. The influence of tide range on beach morphodynamics: a conceptual model. *Journal of Coastal Research*, 9, 785–800.

MASSELINK, G. and TURNER, I. 1999. The effect of tides on beach morphodynamics. In *Handbook of beach and shoreface morphodynamics*. Ed. A.D. Short. Pub. John Wiley & Sons Ltd.

NAVAS, F., COOPER, J.A.G., MALVAREZ, G. and JACKSON, D.W.T., 2001. Theoretical approach to the investigation of ridge and runnel topography of a macrotidal beach: Dundrum Bay, Northern Ireland. *Journal of Coastal Research*, S.I. 34, pp.183-193.

NORDSTROM, K. F., 1992. *Estuarine Beaches: An Introduction to the Physical and Human Factors Affecting Use and Management of Beaches in Estuaries, Lagoons, Bays, and Fjords*. Elsevier Science Pubs.

RYAN, N.M., and COOPER, J.A.G., 1998. Spatial variability of tidal flats in response to wave exposure: examples from Strangford Lough, Northern Ireland. In *Sedimentary Processes in the Intertidal Zone.* Black, K.S., Paterson, D. M., and Cramp, A. eds. Geological Society of London Special Publication 139, p. 221-230.

LIST OF REVIEWERS

The editors are grateful to the reviewers for their dedication during the reviewing process.

Amos C.L., Southampton, UK

Bass S.J., Plymouth, UK.

Bernè S., Plouzanè, France

Bilbao I.A., Las Palmas, Spain

Brun-Cottan J. C., Caen, France

Dyer K., Plymouth, UK.

Friend P., Southampton, UK

Gracia F. J., Càdiz, Spain

Hardisty J., Hull, UK

Hill P.S., Halifax, Canada

Jackson D., Coleraine, UK

Juracic M., Zagreb, Croatia

Klein A.H.F., Itajaì, Brazil

Langone L., Bologna,Italy

Masselink G., Loughborough, UK

McCave I.N., Cambridge, UK

Medina R., Santander, Spain

Neumeier U., Southampton, UK

Orford J., Belfast, UK

Paterson D.M., St. Andrews, UK

Pejrup M., Copenhagen, Denmark

Ridgway J., Keyworth, UK

Schettini C., Itajaì, Brazil

Silva A., Lisbon, Portugal

Spearman, J.R., Oxford, UK

Spencer T., Cambridge, UK

Sternberg R., Seattle, USA

Taborda R., Lisbon, Portugal

Trentesaux A., Villeneuve d'Ascq,France

Voulgaris G., Columbia, USA

Williams D.J.A., Swansea, UK

Journal of Coastal Research	SI 41	Abstracts	STRAEE 2002	Ferrara, Italy	ISSN 0749-0208

Measurements of Erodibility and Settling Velocity of Intertidal and Subtidal Cohesive Sediments in a Coastal Lagoon, The Danish Wadden Sea.

T.J. Andersen[1], K.T. Jensen[2], L. Lund-Hansen[2], K.N. Mouritsen[2], M. Pejrup[1]

[1] Institute of Geography, University of Copenhagen, Øster Voldgade 10, 1350 Copenhagen K, Denmark
[2] Department of Marine Ecology, Institute of Biological Sciences, University of Aarhus, Finlandsgade 14, 8200 Aarhus, Denmark.

ABSTRACT

The erodibility and settling velocity of cohesive sediments are key-parameters for the erosion, transport and deposition of mud in the estuarine environment. However, the parameters are not easily predicted on the basis of, e.g. primary grain-size, water content or organic content and in situ field-measurements are generally needed.
The purpose of the present work was to examine the spatial variation of erodibility (erosion thresholds and erosion rates) and settling velocity in a microtidal coastal lagoon in the Danish

Wadden Sea. The portable EROMES erosion-equipment was deployed on an intertidal transect and on box-core samples taken from the bed of a nearby tidal channel. Both erosion thresholds, erosion rates and settling velocities of the eroded material were determined and the surface sediment was analysed for organic content, chl a, grain size, fecal pellet content and macrozoobenthos.

The sediment at the mudflat is very fine-grained whereas a slightly higher sand content is found at the tidal channel station. The erodibility at the transect was mainly determined by the presence or absence of the deposit-feeding mud-snail Hydrobia ulvae and at places also by biofilms formed by benthic diatoms. H. ulvae destabilizes the surface due to its surface tracking and fecal pellet production whereas biofilms were observed to stabilize the bed. The erodibility of the bed in the tidal channel seemed to be less affected by biological effects, primarily due to the much smaller macrozoobenthic population. The mudflat sediments are easily eroded (low erosion thresholds and high erosion rates) at stations with a large population of H. ulvae. At stations with small macrozoobenthic populations, the erodibility is low, primarily due to the stronger cohesive behaviour in the absence of intense aggregation. The channel bed show intermediate erodibility with relatively high erosion thresholds and low erosion rates.

The settling velocity of the eroded material is slightly but significantly higher at the intertidal mudflat than in the tidal channel, despite the fact that the sediment is sandier in the channel. The reason for the higher settling velocity of material eroded at the mudflat is that the sediment generally consists of aggregates which are larger and more numerous than the aggregates found in the tidal channel. The aggregation is mainly due to the fecal pellet production by Hydrobia ulvae and faeces and pseudo-faeces production by other invertebrate macrozoobenthos. The aggregation is significantly lower in the winter and early spring and much higher settling velocities are found at the mudflat during the warmer months. Consequently, the difference between the settling velocities at the mudflat and in the tidal channel is expected to be more pronounced in the warmer seasons.

The net-effect of the differences in erodibility and settling of eroded material is likely to be a landward directed net-transport of suspended sediments as sediment settling to the bed at the mudflats gets incorporated in larger aggregates which are less likely to disappear from the area.

Journal of Coastal Research	SI 41	Abstracts	STRAEE 2002	Ferrara, Italy	ISSN 0749-0208

A Multidisciplinary Study of Mudflat in Venice Lagoon, Italy.

Cappucci S.[1], Amos C.L.[1], Hosoe T.[1] & Umgiesser G.[2]

[1] School of Ocean and Earth Science, Southampton Oceanography Centre, Empress Dock, Southampton, UK SO14 3ZH , e-mail: sc14@soc.soton.ac.uk
[2] ISDGM, National Research Council, S. Polo 1364, 30125 Venice, Italy.

ABSTRACT

A multidisciplinary study was undertaken in order to determine the factors controlling the stability and the evolution of Palude della Centrega, a fine-grained intertidal mudflat in Venice Lagoon, Italy. Venice Lagoon is the largest (1m spring tidal range) microtidal estuary in the Mediterranean Sea and is suffering from a loss of about 1 million m^3/a of sediment to the sea. The consequence of such a deficit in the sediment budget is the progressive destruction of salt marshes and tidal flats. By 2050 all the salt marshes will have disappeared if this trend continues.

An investigation of temporal and spatial variation of the surface sediment properties, stability and of environmental data was undertaken on August 1998 and February-March 1999 in Venice Lagoon. 8 sites were studied in order to determine the characteristics and the erosive behaviour within a range of different habitats (subtidal and intertidal). During these field campaigns a new version of the Mini Flume erosive device was deployed for the first time in-situ. The purpose was to determine the critical shear stress of erosion under controlled flows. Relationships between erosion threshold and biological properties revealed that a complex feed-back mechanism enhance the accretion of the intertidal areas in the northern part of the Lagoon.

Palude della Centrega (one of the investigated site) is a well preserved intertidal mudflat located in the northern part of the Lagoon. Its sediment stability, sediment properties, elevation, habitat changes have been monitored over a period of about 15 months (from August 1998 and December 1999). Erosion threshold and sediment strength were derived by using the Cohesive Strength Meter and a Tor Shear Vane. Sediment stability of Palude della Centrega is influenced by changes of the sediment physical properties. The evolution of the area is in contrast with the general trend of the intertidal mudflats in Venice Lagoon as it is accreting at a constant rate of 1.6cm/a. This trend is confirmed by investigations of the long-term morphological changes and sediment dating carried out in the area.

A 0D model called SLIM (Simulation of LIttoral Morphodynamics) was constructed in order to predict which factors were responsible for the accretion of Palude della Centrega. The sensitivity analysis of SLIM showed that the accretion of the mudflat appears controlled by sediment input through the erosion of the surrounded areas and biostabilisation of sediment by micro and macro-phytobenthos (which increase the erosion threshold and decrease the bed shear stresses, resulting from wind generated waves).

Journal of Coastal Research	SI 41	Abstracts	STRAEE 2002	Ferrara, Italy	ISSN 0749-0208

Evaluation of Suspended Particulate Matter, for the Venice Lagoon Waters, by using Landsat7 ETM+ Data

F. Corbani[1], S. Silvestri[2, 3] & P. Ciavola[1]

[1] Università degli Studi di Ferrara - Dipartimento di Scienze della Terra, Corso Ercole I° d'Este 32, 44100, Ferrara, cbf@unife.it
[2] Consorzio Venezia Nuova - Servizio Informativo, San Marco 2949, 30124, Venezia
[3] Università degli Studi di Padova - Dipartimento I.M.A.G.E., Via Loredan 20, 35131, Padova

ABSTRACT

Suspended Particulate Matter (S.P.M.) is an important index for the quality of coastal waters, being also a factor that influences benthos activity. In the Lagoon of Venice the understanding of sediment transport pathways is also linked to a series of environmental, civil engineering and navigation problems.

Remote sensing methods to estimate S.P.M. in complex environments have greater potential than punctual measurements. Indeed, while punctual measurements are restricted by the number of samples, imagery techniques can have as many samples as their number of pixels.

A first test of the method's capability was undertaken processing a Landsat 7 ETM+ scene, which tipically has a spatial resolution of 30x30 meters.

On the 20th of September 2001, in a time period of ± 2 hours with respect to the Landsat TM 7 overpass, 14 water samples were collected at 10 stations located in the central and northern part of the lagoon.

The sample sites were selected to account for the different physiographic features of the lagoon: bassofondo (shallow), velma (shoal) and tidal or navigation channel.

The samples were analysed to obtain S.P.M. values, which range at the surface from 10.1 to 56.5 mg/l and the concentrations were used as ground truth data for image processing.

The full scene of the lagoon, at the Level 1G, was processed using the ENVI® software. Different algorithms were tested in order to find the best correlation coefficient between image reflectance and measured values.
This study represents just the first step of a research strategy aimed at integrating in-situ measurements with image-generated maps and a diffusive module of a finite-element hydraulic model.

The authors wish to thank Thetis S.p.A. (Venice), for the support during sample analysis, and the Ministero delle Infrastrutture e dei Trasporti - Magistrato alle Acque di Venezia, through its operative branch Consorzio Venezia Nuova (Venice), for providing the Landsat imagery.

Journal of Coastal Research	SI 41	Abstracts	STRAEE 2002	Ferrara, Italy	ISSN 0749-0208

Monitoring of a Beach-Barrier-Lagoon System Located at the Mouth of a Ria.

S. Costas[1], I. Alejo[1], J. Alcántara-Carrió[1] and I. Alonso[2]

[1] Dpto. of Xeociencias Mariñas e O.T., Univ. of Vigo, 36200 Vigo. Pontevedra, Spain.
[2] Dpto. of Física, Univ. of Las Palmas de Gran Canaria, 35080 Las Palmas, Spain.
sucostas@uvigo.es; ialejo@uvigo.es; carrio@uvigo.es; ignacio.alonso@física.ulpgc.es

ABSTRACT

A monitoring using different techniques was carried out, during one year and half period, in order to determine the morphodynamic behaviour of a beach-barrier-lagoon developed at Islas Cíes. This archipelago is located at the mouth of the Ría de Vigo (NW Spain) with a N-S orientation, acting as a natural barrier for the waves, swell and sea, arriving from the open ocean. The general pattern of the ría circulation, tidal currents and their interaction with the incoming waves, is controlled by the presence of these islands (Fraga, 1991; Souto, 2000).

The archipelago is formed by three islands. The two northern ones are joined, at its eastern margin, by a 1 km long sand barrier system (Rodas Beach), which confines a shallow lagoon. The western margin constitutes a narrow permanent connection with the open sea, widely restricted by an artificial path constructed to link the islands since the last decades. The sand barrier is developed between two tombolos, which show a established dune complex. During high energy events a channel is stabilised through the northern extreme, connecting the lagoon with the ría system.

Several methods have been used in order to determine the sediment transport pattern through the short and medium term evolution study of this sedimentary environment. The techniques used were: beach and dune survey profiles, fluorescent sands tracers (Ciavola et al. 1998), grain size trends (Gao, 1996) and wave propagation (Taborda, 1993) numerical models.

Results showed that the northern zone of the beach presents a seasonal behaviour with an erosive net trend, while the southern zone does not present significative changes during the study period, nevertheless showed an erosive net trend. This morphodynamic behaviour was agreed with the trend observed by aerial photograph analysis at a longer period. This trend is related to the human activities developed at the islands during the last decades.

In order to prove this preliminary long term evolution hypothesis is necessary the continuation of the monitoring during a longer period.

This work is a contribution to the projects REN2000-1102 MAR, PGIDIT00MAR30103PR, PGIDT00PX130105PR, BTE2000-0877 and EVK2-CT-2000-00060.

REFERENCES

Ciavola, P., Dias, N., Ferreira, O. , Taborda, R. and Dias, J.M.A. (1998). Fluorescent sands for measurements of longshore transport rates: a case study from Praia de Faro in southern Portugal. Geo-Marine Letters, 18: 49-57.

Fraga, F. 1991. El afloramiento costero en la costa Atlántica de la peninsula ibérica. Revista Académica Galega de Ciencias, 10: 144-152.

Gao, S. (1996). A fortram program for grain-size trend analysis to define net sediment transport pathways. Computers and geociences, 22(4): 449-452.

Souto, C. 2000. Predicción numérica y contraste experimental de al circulación en la Ría de Vigo. Tesis Doctoral. Universidade de Vigo, 173 pp, inédita.

Taborda, R. (1993). Modelaçao da Dinamica Sedimentar Induzida pela Ondulaçao na Plataforma Continental Portuguesa, Universidade de Lisboa. Lisboa, 126 pp.

Journal of Coastal Research	SI 41	Abstracts	STRAEE 2002	Ferrara, Italy	ISSN 0749-0208

Sediment Transport Pathways in the Ría de Vigo (NW Spain): Evidences from Benthic Foraminifera and Physical Processes.

P. Diz; S. Costas; J. Alcántara-Carrió; I. Alejo; G. Francés and F. Vilas

Dep. of de Geociencias Marinas y O.T. Universidad de Vigo, 36200 Vigo, Spain.

ABSTRACT

Foraminifera can be used to determine the sources of carbonate sediment and the directions of sediment transport (Li et al., 1998; Alejo et al., 1999) in shallow marine embayments such as the external area of the Ría de Vigo.

The Ría de Vigo consists of an elongated funnel-shaped embayment of 33 km long and 10 km wide at its mouth, which is partially closed by a group of islands. The most important bathymetric feature is the presence of a central channel with a maximum depth of 43 m. Surface sediments mainly consist of organic rich mud in the deepest areas, around the central axis, while sandy bottoms are often found near the margins and contouring the mud. Gravel, mainly bioclastic, is restricted to the northern edge close to the coastline and to the southern mouth.

Two surveys were carried out in January and September 1998 according to contrasted energetic conditions. During both periods, eleven boxcore sediment samples were collected at the most active hydrodynamic areas of the Ría, ranging from gravel to fine sand. Each box core was sampled at 1-cm interval from the top to 5 cm. Subsamples of 50 cm^3 were taken to work out living faunal assemblages (Rose Bengal stained). For living foraminifera analyses the >63 μm fraction was used, while the dead assemblages from the >63 μm fraction were analysed separately in 1 phi interval. The spatial distribution of live and dead benthic foraminiferal assemblages determinates the transport pathways. The comparison between grain size distributions of live and dead fauna at each boxcore allows us to determinate accumulation areas and infer transport mechanisms. Moreover, the disturbance depth of the sediment is inferred from the downcore live benthic distribution.

Other techniques were used to check the foraminifera results. Analysis of grain size trends was performed to define sediment transport pathways (Gao, 1996) using a boxcore regular network of samples at the outer and middle zones of the Ria. A wave propagation numerical model (Taborda, 1993) fed by extreme wave data recorded during the surveys (Puertos del Estado; http://www.puertos.es/clima.html), considering the two dominant wave approach directions (NW and SW). The results obtained from these two techniques provide both complementary and confirming evidence about the transport processes inferred from benthic foraminifera.

This work is a contribution to the projects REN2000-1102 MAR, PGIDIT00MAR30103PR, PGIDT00PX130105PR.

REFERENCES:

Alejo, I., Austin, W.E.N., Francés, G. & Vilas, F. 1999: Preliminary investigations of the recent foraminifera of Baiona Bay, N.W. Spain. Journal of Coastal Research 15, 413-427.

Gao, S. 1996: A fortram program for grain-size trend analysis to define net sediment transport pathways. Computers and Geosciencies 22, 449-452.

Li, C., Jones, B. and Kalsbleisch, W.B.C. 1998. Carbonate sediment transport pathways based on foraminifera: case study from Frank Sound, Grand Cayman, British West Indies. Sedimentology 45, 109-120.

Taborda, R. 1993: Modelaçao da Dinamica Sedimentar Induzida pela ondulaçao na plataforma continental portuguesa. Tesis Doctoral. Universidade de Lisboa, Lisboa, 126 pp.

Sediment Movement Patterns in a Small Macrotidal, Wave-Exposed Estuary Mouth : the Authie, Northern France.

Christine Dobroniak

Coastal Geomorphology and Shoreline Management Unit, Université du Littoral Côte d'Opale, 2 Chaussée des Darses, 59140 Dunkerque.
christine.dobroniak@univ-littoral.fr

ABSTRACT

The Authie is a small macrotidal estuary largely infilled by marine sand affected by flood dominant tides and waves. The shallow estuary mouth exhibits on the south bank a massive sand spit platform, that confine the main Authie channel towards the north bank.

The meso-scale morphodynamic variability of the shoreline was analysed from scale-rectified aerial photographs taken between 1947 and 2000. The data highlighted a recycling of sand, eroded from coastal dunes lining the estuary, into the intertidal inner estuarine sink.

The south bank of the estuary is bounded by a rectilinear shore that functions as a longshore drift corridor. The drift terminus is characterised by successive longitudinal dune ridges that highlight progressive northward extension of this shoreline. The sand deposits are also introduced by flood tidal asymmetry within estuarine sink.

The north bank differs markedly in that it is dominated by erosion. Rates of erosion since 1947 have varied spatially and temporally as a result of variable shoreline exposure to waves and tidal currents and of the influence of engineering structures to protect the health and seaside resort of Berck. Sand eroded from this north bank is progressively deposited within the inner of the estuary by the sediment alongshore drift. Finally, it contributes in the estuarine infill.

However, topographic survey and field measurement show that the beach serves as an important temporary storage zone for the sand released by dune erosion or driven onshore by combined storm-tidal currents, and may show substantial short-term accretion.

This example shows that the sand released during storm wave attack of the dune on both bank of the Authie estuary is recycled successively as beach, dune, transported by tidal current drift and finally estuarine deposits.

Flood Induced Sediment Transport to the Inner and Middle Shelf in the Vicinity of the Guadiana Estuary (Gulf of Cadiz, Southwestern Iberia Peninsula)

Gonzalez, R.[1], Lobo, F.[2], Mendes, I.[1], Dias, J.M.A.[2], Santos, A.I.[3] & Silva, A.J.[3]

[1] CIACOMAR, Universidade do Algarve, Avenidas 16 de Junho s/n, 8700 - 311 Olhão, Portugal, rgonzale@ualg.pt
[2] FCMA/CIACOMAR, Universidade do Algarve, Campus de Gambelas, 8000 Faro, Portugal
[3] Instituto Hidrográfico, Rua das Trinas, 49, 1249-093 Lisboa, Portugal

ABSTRACT

The coastline and shelf adjacent to the Guadiana Estuary in the northern Gulf of Cadiz are highly dynamic areas. Particularly the Guadiana estuary itself, the adjacent coastline, infralittoral, and inner shelf have experiencend a high degree of sedimentation and infilling in historic times, with offshore sediment accumulation rates that are estimated to be as high as 0.02-0.03 m/a in some areas of the shelf.

The sedimentary dynamics in the estuary and shelf are influenced by several factors, such as river volume, tides, wave regime, storms, and shelf current patterns. The wave regime results in a net littoral drift from west to east. The interaction between tidal flow and fair weather low river volume generally results in an accumulation of sand inside the estuary, and, most prominently, in the vicinity of the estuarine mouth.

In particular river volume can be highly variable, with values as low as 6 m3/s during dry summer months, and as high as 3000 m3/s (and higher) during winter floods. During such flood events large amounts of sediment are cleared out from the estuary to the shelf, contributing to the build up of the Guadiana prodelta.

Data collected during several field surveys between September 1999 and November 2001 sheds some light on the sediment export mechanisms, particularly the survey of February 2001 carried out during a high river volume period in the winter of 2000/2001.

Sediment grab samples (sampling the same locations near the Guadiana Estuary mouth up to four times) show a significant change in the sand:clay ratio in samples, which give values around 10:1 in 1999 and 2000, and change to a ratio of 160:1 at depths of around 20m in February 2001. This alteration can be seen in samples down to a depth of 35-40m. A re-sampling of the sites in November 2001 shows a reduction in sand:clay ratios at the same sites, indicating a post-flood redistribution of sediment.

During the same February 2001 flood period, water samples taken across the entire northern Gulf of Cadiz show a body of elevated suspended particulate matter with concentrations of up to 10-15 mg/l extending from the vicinity of the Guadiana mouth to a 35 km long shore-parallel lense at the southward limit of the inner shelf. The formation of this lense may be related to bottom currents flowing along the inner shelf limit and an increase in slope in this area from 0.14-0.17º to 0.29-0.42º.

This area of the shelf coincides with the northern limit of large deposits of fine-grained material dominating the sediment cover throughout the middle shelf at depths between approximately 50 and 100 m in the northern Gulf of Cadiz. These bodies of very fine-grained sediment (mean grain-sizes are generally between 7-8 phi) probably represent the sink for suspended material exported from regional river basins to the shelf during flood events.

Journal of Coastal Research	SI 41	Abstracts	STRAEE 2002	Ferrara, Italy	ISSN 0749-0208

Wave Action on Tidal Flats - A Seine Estuary Application

Ricardo Silva Jacinto[1], Hervé Jestin[1] and Christophe Bessineton[2]

[1] Ifremer – French Research Institute for Exploitation of the Sea, Department of Coastal Ecologie, BP 70, 29280 Plouzané, France. rsilva@ifremer.fr or hjestin@ifremer.fr .
[2] Maison de l'Estuaire, 16 quai Casimir Delavigne, 76600 Le Havre.
Maison.estuaire@wanadoo.fr

ABSTRACT

In the Seine estuary, a macrotidal estuary localised in the north-western coast of France (English channel), fine sediment dynamics is mainly driven by tides at short term and modulated by river flow at seasonal time scales. Its morphology is characterised by a relatively extended tidalflats, mainly muddy, which reveals a marked characteristic of the morphodynamic equilibrium of macrotidal estuaries. Considering the extent of these shallow areas and of the mudflats, gravity waves can play a significant part in the overall fine sediments dynamics of the estuary. Hence, the aim of this study is to examine the wave action on the tidal flats of the Seine estuary and to deduce their impact on the estuarine fine sediment dynamics.

Short crested waves in the Seine estuary are shown to be generated by local winds mainly blowing from the west sector toward which the estuary is exposed. Therefore, the wave climate in the estuary presents a co-relation with river runoffs, i.e. after storms and relevant waves on the mudflat, river runoff tends to increase as well.

The wave impact on the Northern mudflat of the Seine estuary was studied at different time scales. Field measurements realised during a storm event showed that waves present a linear dependence to water depth that limits the wave energy over the tidalflat. This limitation or "saturation" of wave energy results from the balance between wave shoaling and bed friction. However, large erosions of 10 to 20 cm thickness are shown to occur after storm events. Complete and sudden erosion of both consolidating layers, which are liquefied and entrained, and consolidated layers is observed. The erosion of consolidated layers consists in mass or bulk erosion and muddy pebbles are dispersed over the tidal flat.

A monthly survey of seasonal variability over the mudflat shows that events of large erosion are followed by progressive sedimentation, so that yearly variations are weak in comparison with meteorological-induced changes. When extrapolated to the area of the mudflat, the sediment resuspended during storm events is of the order of the estuary turbidity maximum.

These results demonstrate that even in sheltered areas like estuaries wave action is an important forcing for the sediment budget. Furthermore, the discussion based on these results allow us to provide a conceptual model of fine sediment dynamics near the Northern mudflat of the Seine estuary.

Journal of Coastal Research	SI 41	Abstracts	STRAEE 2002	Ferrara, Italy	ISSN 0749-0208

KEY NOTE LECTURE

A New Approach To The Determination of Cohesive Sediment Resuspension Below Waves

Charles Lemckert

School of Engineering, Griffith University Gold Coast Campus,
PMB50 Gold Coast Mail Centre, 9726, Qld, Australia
c.lemckert@mailbox.gu.edu.au

ABSTRACT

The resuspension of cohesive sediments plays an important role in the dynamics of coastal systems, including the transportation of sediment-associated pollutants, the erosion of banks and channels, and water column turbidity levels (which in turn influences water quality). Presently, it is nearly impossible to use mathematical models to predict the critical velocity required to achieve cohesive sediment resuspension and the subsequent rate of erosion from the bed. Consequently, experimental investigations are required to quantify these important sediment related values. However, while a number of devices have been developed to quantify these sediment related values they have distinct and substantial limitations, especially when waves are the dominant resuspension mechanism.

This paper will review existing methodologies presently used for determining the critical velocity to initiate resuspension and the subsequent erosion rate. Particular emphasis will be placed upon emphasising their advantages and disadvantages, and the possible misinterpretation of data that can be achieved. The paper will then present new methods (based on existing devices) that could be used to determine the critical velocity and resuspension rates (in-situ) in tidal wave dominated environments. Also presented will be a new in-situ instrument that has been specially developed to determine the critical resuspension parameters for cohesive sediments subjected to wave like motions.

Journal of Coastal Research	SI 41	Abstracts	STRAEE 2002	Ferrara, Italy	ISSN 0749-0208

Numerical Simulation of the Salinity Stratification in the Guadiana Estuary

Lígia Pinto, André B. Fortunato, Anabela Oliveira

National Laboratory of Civil Engineering, Hydraulics Department, Av. do Brasil, 101, 1700-066 Lisboa. Phone:+351-218443613; fax: +351-218443016. email: llpinto@lnec.pt

ABSTRACT

In many estuaries, salinity stratification strongly affects the hydrodynamics, salinity distribution and several biogeochemical processes. In the Guadiana estuary, which constitutes the southern border between Portugal and Spain, high stratification is known to occur for strong river flows. However, previous analyses of tidal propagation and salinity intrusion were based on depth-averaged models and limited data (e.g. Fortunato et al., 2002). Motivated by the construction of a large dam in the Guadiana River, which may severely affect the estuarine dynamics, we analysed the hydrodynamics of the estuary under strong river flows. The main objectives were:
to characterize in detail the hydrodynamics and salinity of estuary, under stratified conditions;
to determine under which combinations of river flow and tidal conditions stratification occurs;
to analyse the response time of the stratification with changes in river flow.

This study is conducted through a combination of numerical modelling and data analysis. High-resolution numerical simulations are performed with a state-of-the-art, three-dimensional baroclinic model using unstructured grids (Baptista et al., 2002). This model is based on finite volumes for mass conservation, and uses Eulerian-Lagrangian concepts for efficiency and high accuracy. A level 2.5 Mellor and Yamada turbulence closure scheme is used to adequately represent vertical mixing.

Field data are used both to validate the model and to complement the analyses of the estuarine behaviour. Given the limitations of historical data, two research cruises were performed, in February and October 2001. Measurements included two-week vertical profiles of velocity with an ADCP, and 14-hour velocity and conductivity profiles with an RCM at several locations in the estuary. In addition, water levels were measured during one year at selected locations.

Model results will also be used to verify existing empirical criteria to determine estuarine stratification (e.g., based on the ratio between river flow and the tidal prism).

REFERENCES:

Fortunato, AB., A. Oliveira and E. Alves, 2002. Circulation and Salinity Intrusion in the Guadiana Estuary, Thalassas, submitted.

Baptista et al., 2002. A Finite Volume Model of Coastal Circulation, with application to Plumes and River-Dominated Estuaries, in preparation.

Acknowledgments

The authors would like to thank Drs. A.M. Baptista, E. Myers and J. Zhang for the model ELCIRC.
This work was sponsored by the Fundação para a Ciência e a Tecnologia, project Protecção e Valorização da Zona Costeira Portuguesa and by Laboratório Nacional de Engenharia Civil.

Journal of Coastal Research	SI 41	Abstracts	STRAEE 2002	Ferrara, Italy	ISSN 0749-0208

Long Term Relationships between River Sediment Input and Bathymetric Change along the Rhone Delta Shoreline, Mediterranean Sea, France

François Sabatier[1], Grégoire Maillet[1], Serge Suanez[2], Mireille Provansal[1]

[1] CEREGE, UMR CNRS 6635, Europôle de l'Arbois, B.P.80, 13545 Aix-en-Provence Cedex 04, FRANCE
[2] Géolittomer Brest, UMR 6554 CNRS, IUEM, Technopôle Brest Iroise Place Nicolas Copernic, 29280 Plouzané, FRANCE

ABSTRACT

Since the beginning of the 20th century, the Rhone delta comprises two fluvial branches, the Grand and Petit Rhone. During the last millennia, deltaïc progradation was controlled by successive avulsion phases and mouth shifts. In the front of the mouths, river sediments input have built submarine prodeltas, whose fossil deposits control today's bathymetry.

Here, we evaluate and quantify the relations between the shoreface evolution, the Rhone sediment input and erosion of the fossil prodeltas over the last century. The secular bathymetric change is investigated using four bathymetric surveys: 1841,1872,1895 and 1974. The data cover the entire deltaïc coastline (90 km) and extend from the shoreline to –25 m depth. After numerisation of the bathymetric data points, geodetic corrections and gridding operations using a Geographic Information System software, digital elevation models (DEM) are computed to describe submarine morphology and quantify secular sediment budgets.

A simple model of sediment transport between –5 m and –20 m depth is run on the 1974 bathymetric survey to test whether fossil prodeltas, removed by wave asymmetric transport, can feed the surf zone. The model uses wave refraction diagram and the Bagnold bed load transport equation. A typical year storm with Hs = 3.5 m, T = 7s from SSE sector is simulated. Two-grain sizes (0.1 and 0.2 mm) are selected to check whether coarser and finer sediments can have different cross-shore movements during storms. As no field measurements are available, the results should rather be considered as qualitative.

The bathymetric comparisons between 1841 and 1974 show a contrasted evolution on the two current mouths and a long-term submarine erosion of the fossil mouths and associated prodeltas.

The current prodelta of the Petit Rhone is destroyed by wave action in relation to a river flow and sediment input decrease during the 20th century. The Grand Rhone mouth prograded up to 2.5 km to the south, but sedimentation on the prodelta has decreased (3×10^6 m^3 yr^{-1} to 1.8×10^6 m^3 yr^{-1}) and is restricted to the mouth (3-4 km along shore). This trend is explained by natural evolution (flow reduction) and human action (engineering works and construction of dams) and correlated with the river bed incision described by previous works over the same time scale. The secular rate of prodelta erosion decreases with time because these features are slowly deepening by wave destruction.

Sedimentation is confined in three spits, which are interpreted as sink areas for a littoral cell organisation. Modelling shoreface sediment transport indicates that the surf zone is potentially fed by the old prodeltas. Our results suggest that after a mouth shift, the fossil deposits start to be removed by wave action, to feed the spits and the offshore area. The model shows that coarser sediments of the fossil prodeltas can move onshore during storms while finer sediments move offshore.

The present work argues for a secular negative sediment budget of the shoreface of the Rhone delta in relation to a decrease in river sediment input.

Journal of Coastal Research	SI 41	Abstracts	STRAEE 2002	Ferrara, Italy	ISSN 0749-0208

Acoustic doppler current observations of tidal and subtidal circulation in the vicinity of the Saint Georges Bank, Gironde estuary

Aldo Sottolichio[1], Cyril Mallet[2] & François Bourrin[3]

[1] Département de Géologie et Océanographie, UMR CNRS 5805 EPOC, Université Bordeaux I - France

[2] Bureau de Recherches Géologiques et Minières, Parc Technologique Europarc 33600 Pessac - France

ABSTRACT

The Gironde estuary is a well known meso to macrotidal estuary, where hydrodynamics results from the combined effects of gravitational and barotropic tidal circulation. Depending on the tidal range and on the river runoff, the estuary behaves either as a well-mixed estuary or as a stratified estuary. In the mouth, circulation and sediment fluxes are also dependent on the rate of stratification. A set of Acoustic Doppler Current Profiles was obtained in the narrower pass of the mouth, in the vicinity of the Saint-Georges Bank. This is a sandbar which belongs to the of the flood-tidal delta of the estuary. Current velocity and water density profiles were recorded through cross-channel, along-channel transects and loops around the bank. Results are discussed in terms of vertical structure of currents with respect to density stratification and bottom topography. In situ measurements of suspended matter concentrations were used to calibrate the backscatter echo intensity recorded by the ADCP, with the purpose of providing sediment concentration profiles over the studied zone. Combining these data with simultaneous current profiles leads to more comprehensive interpretation of instantaneous and residual sediment fluxes in the mouth.

List of Participants

Thorbjoern Joest Andersen
Institute of Geography
University of Copenhagen
Øster Voldgade 10, 1350 Copenhagen K-
Denmark
tja@geogr.ku.dk

Ing. Viviana Ardone
Consorzio Venezia Nuova
San Marco, 2803
30124 Venezia
Italy

Paolo Billi
Dip. di Scienze della Terra
Università di Ferrara
Corso Ercole I d'Este, 32
44100 Ferrara
Italy

Heidi Burgess
Halcrow Group Ltd, Martlett HouseSt John's
Street, Chichester, West Sussex, PO19 1UH
UK
BurgessHM@Halcrow.com

Helene Burningham
Coastal and Estuarine Res. Unit,
Department of Geography
University College London
Chandler House
2 Wakefield Street,
London WC1N 1PF
UK
h.burningham@geog.ucl.ac.uk

Sergio Cappucci
ICRAM, Via di Casalotti 300 00166 Roma
Italy
s.cappucci@icram.org

Paolo Ciavola
Dip. di Scienze della Terra
Università di Ferrara
Corso Ercole I d'Este, 32
44100 Ferrara
Italy
cvp@dns.unife.it

Mike Collins
School of Ocean and Earth Science
Southampton Oceanography Centre,
Empress Dock, Southampton
SO14 3ZH
UK
mbc@soton.ac.uk

Fabio Corbani
Università di Parma
Dipartimento di Scienze della Terra
Parco Area delle Scienze, 157A - "Campus"
43100, Parma
Italy
fcorbani@nemo.unipr.it

Corinne Corbau
Dip. di Scienze della Terra
Università di Ferrara
Corso Ercole I d'Este, 32
44100 Ferrara
Italy
corinne.corbau@unife.it

Susana Costas
Dpto. of Xeociencias Mariñas e
O.T.,
Univ. of Vigo,
36200 Vigo. Pontevedra
Spain
sucostas@uvigo.es

Nicolas Delsinne
Centre M2C
CNRS/Univ. de Caen/UMR 6143
24 rue des Tilleuls
14000 Caen
France.
delsinne@geos.unicaen.fr

Christine Dobroniak
Coastal Geomorphology and
Shoreline Management Unit
Univ. du Littoral Côte d'Opale
2 Chaussée des Darses,
F-59140 Dunkerque
France
christine.dobroniak@univ-littoral.fr

Karen Edelvang
DHI – Water and Environment
Agern Allé 11
Dk-2370 Hoersholm
Denmark
kae@dhi.dk

Ricardo Silva Jacinto
Ifremer – French Research Institute
for Exploitation of the Sea
Department of Coastal Ecologie
BP 70
29280 Plouzané
France
rsilva@ifremer.fr

Vasilis Kapsimalis
National Centre for Marine
Research (NCMR)
Agios Kosmas
166 04 Hellinikon
Greece
kapsim@erato.fl.ncmr.gr

Ramon Gonzales
Vivel 737482 Bergun
Switzerland

Nicolas Gratiot
IRD – French Guiana
BP 165, Rte de Montabo
97 323 Cayenne
France
gratiot@cayenne.ird.fr

Robert Lafitte
UMR 6143 M2C
University of Rouen,
10 bd De Broglie
76821 Mont Saint Aignan Cedex France

Charles Lemckert
School of Engineering Griffith
University Gold Coast Campus,
PMB50 Gold Coast Mail Centre
9726, Qld
Australia
c.lemckert@mailbox.gu.edu.au

Francisco Lobo
Instituto Andaluz de Ciencias de la Tierra
(IACT), Universidad de Granada, Faculdad de
Ciencias, Campus de Fuentenueva, s/n18002
Granada
Spain
pacolobo@ugr.es

Ulrik Lumborg
DHI- Institute for Water and
Environment, Agern Allé 5DK-2970
Hørsholm
Denmark
ulu@dhi.dk

Cyril Mallet
BRGM (SGR/AQUI)
24 avenue Léonard de Vinci
33600 Passac
France
c.mallet@brgm.fr

Gonzalo Malvarez
Geografia Fisica, Universidad Pablo de
Olavide
Sevilla
Spain
gcmalgar@dhuma.upo.es

Andrew Manning
Institute of Marine Studies
University of Plymouth
Drake Circus, Plymouth, Devon
PL4 8AA
UK
andymanning@yahoo.com

Laurent Masse
Dept. De Géologie et Océanographie
UMR CNRS 5805 EPOC
Univ. de Bordeaux I
Avenue des Facultés
33045 Talence
France

Daniel Mikes
CSIC, Institute of Earth Sciences Jaume
Almera, c. Lluís Solé i Sabarís s/n, E-08028,
Barcelona
Spain

Luis Neumann
Dept. of Chemical Engineering
The University of Queensland
St. Lucia 4072 Qld
Australia
luisn@cheque.uq.edu.au

Catherine Organo
Radiological Protection Institute of Ireland,
3 Clonskeagh Square, Clonskeagh Road
Dublin, 14
Ireland
corgano@rpii.ie

Raffaella Piani
Dept of Geological
Environmental & Marine Sciences
Via E. Weiss 2, I-34127 Trieste
Italy
piani@univ.trieste.it

Ligia Pinto
National Laboratory of Civil Engineering
Hydraulics department
Av. Do Brasil, 101
1700-066 Lisboa
Portugal
llpinto@lnec.pt

François Sabatier
CEREGE, UMR 6635
Europôle de l'Arbois, B.P.
80 F-13 545 Aix-en-Provence
France
sabatier@cerege.fr

Christie Schacht
Griffith University
School of Engineering
Gold Coast Campus
Queensland
Australia
c.schacht@mailbox.gu.edu.au

Aldo Sottolichio
Dept. De Géologie et
Océanographie
UMR CNRS 5805 EPOC
Univ. de Bordeaux I
Avenue des Facultés
33045 Talence
France
a.sottolichio@epoc.u-bordeaux.fr

Romaric Verney
UMR 6143 M2C, University of
Rouen,
10 bd De Broglie
76821 Mont Saint Aignan Cedex
France
Romaric.verney@wanadoo.fr

THE COASTAL EDUCATION AND RESEARCH FOUNDATION

Post Office Box 210187
Royal Palm Beach, FL 33421, USA

1656 Cypress Row Drive
West Palm Beach, FL 33411, USA

The Coastal Education and Research Foundation *[CERF]* is a nonprofit corporation dedicated to the advancement of the coastal sciences. The Foundation is devoted to the multi-disciplinary study of the complex problems of the coastal zone. The purpose of *CERF* is to help translate and interpret coastal issues for the public and to assist professional research and public information programs. The Foundation specifically supports and encourages field and laboratory studies on a local, national, and international basis. Through the medium of scientific publications, television, and radio *CERF* brings accurate information to the public and coastal specialists on all aspects of coastal issues in an effort to maintain or improve the quality of shoreline resources.

Because CERF is concerned with broad environmental issues, our efforts concentrate on significant problems such as maintenance of good quality (potable) water with adequate supply, and hazards associated with potential beach erosion, flooding, and susceptibility of developed shorelines to storm surge and wave attack. By focusing attention on these potential man-made and natural hazards, it is hoped that our research efforts will help others improve the quality of life in diverse coastal areas. CERF thus aims to stimulate awareness of coastal (marine and freshwater shorelines) land and water problems; initiate and foster research and innovation to promote long-term coastal productivity; establish an educational forum for the debate of contentious coastal issues; and develop new principles and approaches for enlightened coastal management, and encourage their adoption and use.

CERF is associated with the Department of Geography and Geology at Florida Atlantic University in Boca Raton, Florida 33431. This association provides a basis for cooperative investigation of biophysical resources found in open and naturally protected coastal regions, estuaries, large inland bodies of water bounded by shorelines, wetlands, and other coastal environments. Joint investigative efforts by faculty, students, and staff at various institutions span a wide and diversified range of interrelated topics that are relevant to solutions of today's dynamic problems. It is hoped that these combined attempts to better understand the nature of coastal processes will help forestall what may become contentious issues of tomorrow.

☐ CERF MEMBERSHIP ☐

Members are individuals, institutions, and corporations that support the aims of the foundation through personal and group efforts or by donations. Memberships are available in different categories with privileges.

Publications of the Foundation:

CERF Quarterly Journal:
Journal of Coastal Research (JCR) (ISSN 0749-0208).

JCR Special Issues and Reports:

No. 1 (1986): Late Quaternary Sea-Level Changes and Coastal Evolution (out of print)
No. 2 (1986): Annotated Bibliography of Quaternary Shorelines, Fourth Supplement 1978–1983 (out of print)
No. 3 (1988): Dune/Beach Interaction, Norbert P. Psuty (ed.). [$US 45.00]
No. 4 (1988): The Effects of Seawalls on the Beach, N. C. Kraus and O. H. Pilkey (eds.). [$US 45.00]
No. 5 (1989): High Concentration Cohesive Sediment Transport, A. J. Mehta and E. J. Hayter [$US 45.00]
No. 6 (1990): Artificial Beaches, M. L. Schwartz and E. C. F. Bird (eds.). [out of print]
No. 7 (1990): Rational Design of Mound Structures, N. Kobayashi and M.A. Losada (eds.). [$US 45.00]
No. 8 (1991): Impacts of Hurricane Hugo: September 10–22, 1989, C. W. Finkl and O. H. Pilkey (eds.). [$US 45.00]
No. 9 (1990): Proceedings of the Skagen Symposium (September 1990) [out of print]
No. 10 (1992): Simplified Technical Summary of the Complete Delta Works [out of print]
No. 11 (1991): Geology of Long Island Sound, P. T. Gayes, R. S. Lewis, and H. J. Bokuniewicz (eds.). [$US 45.00]
No. 12 (1994): Coastal Hazards, C. W. Finkl (ed.). [$US 45.00]
No. 13 (1995): Atlas of Coastal Geomorphology and Zonality, D. Kelletat [$US 45.00]
No. 14 (1995): Impacts of Sea-Level Rise on Developing Countries, R. Nicholls and S. P. Leatherman [$US 45.00]
No. 15 (1993): Beach and Surf Zone Morphodynamics, A. D. Short (ed.). [$US 45.00]
No. 16 (1992): International Bibliography of Coastal Geomorphology, D. Sherman (ed.). [$US 45.00]
No. 17 (1995): Holocene Cycles: Climate, Sea Level, and Coastal Sedimentation, C. W. Finkl (ed.). [$US 45.00]
No. 18 (1993): Beach/Inlet Processes and Management, A. J. Mehta (ed.). [$US 45.00]
No. 19 (1996): International Bibliography of Coastal Geomorphology, 1991–1994, D. Kelletat (ed.). [out of print]
No. 20 (1994): Coastal Wetland Loss in Louisiana, D. F. Boesch (ed.). [$US 45.00]
No. 21 (1995): Impacts of Hurricane Andrew (1992), G. W. Stone and C. W. Finkl (eds.). [$US 45.00]
No. 22 (1995): The Polish Coast: Past, Present & Future, K. Rotmicki (ed.). [$US 45.00]
No. 23 (1996): Understanding Physical Processes at Inlets, A. J. Mehta (ed.). [$US 45.00]
No. 24 (1998): Island States at Risk, S. P. Leatherman (ed.). [$US 45.00]
No. 25 (1997): Sediment Transport and Buoyancy in Estuaries, D. G. Aubrey (ed.). [$US 45.00]
No. 26 (1998): Proceedings of the International Coastal Symposium (ICS '98), C.W. Finkl and P. Bruun (eds.). [$US 60.00]
No. 27 (2000): Tidal Wetlands: Physical and Ecological Processes, P. Goodwin and A. J. Mehta (eds.). [$US 45.00]
No. 28 (1999): Coastal Erosion Mapping and Management, S. P. Leatherman and M. Crowell (eds.). [$US 45.00]
No. 29 (2001): Natural and Artificial Reefs for Surfing and Coastal Protection, K. Black *et al*. (eds.). [$US 45.00]
No. 30 (2001): Tidal Dynamics: Vol. 1, Theory and Analysis of Tidal Forces, F. G. Wood [$US 120.00]
No. 31 (2001): Tidal Dynamics: Vol. 2, Extreme Tidal Peaks and Coastal Flooding, F. G. Wood [$US 120.00]
No. 34 (2002): Proceedings of the International Coastal Symposium (ICS 2000), T. R. Healy (ed.) [$US 120.00]
No. 38 (2003): Shoreline Mapping and Change Analysis, M. R. Byrnes, M. Crowell, and C. Fowler (eds.), [$US 45.00]
No. 43 (2004): Tidal Dynamics and Environment, T. Healy (ed). [$US 45.00]

Contributions, bequests, and gifts to the Foundation are deductible for Federal income, estate and gift tax purposes.